

Geology

of the
Prince Charles Mountains,
ANTARCTICA



BMR
S55(94)
BUL.45
v.247
copy 3

BMR
\$55(94)
BUL. 45
v. 247
copy 3

AGSO – Geoscience Australia Bulletin 247

**Geology of the Prince Charles
Mountains, Antarctica**



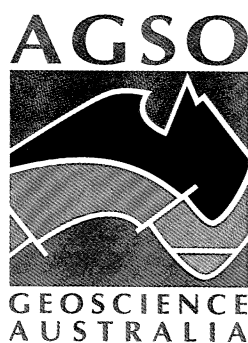


Australian and Russian Antarctic scientists have been involved in collaborative studies for many years. This picture was taken during the visit of an Australian National Antarctic Research Expedition (ANARE) party to a Soviet Antarctic Expedition (SAE) geological field camp near Mount McCauley in January 1973. Bob Tingey (left) is admiring a geological hammer presented to him by Leonid Fedorov (centre).

AGSO – Geoscience Australia Bulletin 247

**Geology of the
Prince Charles Mountains, Antarctica**

E.V. Mikhalsky¹, J.W. Sheraton^{2,4}, A.A. Laiba⁵, R.J. Tingey^{2,6}, D.E. Thost^{2,7},
E.N. Kamenev¹ & L.V. Fedorov⁵



AGSO – Geoscience Australia
Canberra

Department of Industry, Science and Resources

Minister: Senator the Hon. Nick Minchin
Parliamentary Secretary: The Hon. Warren Entsch

AGSO – Geoscience Australia

Chief Executive Officer: Dr Neil Williams

All-Russian Research Institute for Geology & Mineral Resources of the World Ocean (VNIIO)

Director: Academician I.S. Gramberg

Polar Marine Geological Research Expedition

Director: Dr V.D. Kryukov

© Commonwealth of Australia 2001

Apart from any use permitted under the *Copyright Act 1968*, no part of this bulletin is to be reproduced by any process without written permission. Requests and inquiries should be addressed to the Chief Executive Officer, AGSO – Geoscience Australia, GPO Box 378, Canberra ACT 2601.

The authors have tried to make the information in this bulletin as accurate as possible, but they do not guarantee that the information is totally accurate or complete. Readers therefore are advised not to rely solely on this information when making a commercial decision.

ISSN 0084-7089

ISBN 0 642 39858 5

Executive producer: John Bain

Technical editor: Julie Wissmann

Cover designer: Karin Weiss

Layout: National Capital Printing

Printed in Canberra by: National Capital Printing

Author contact details:

- ¹ VNIIOkeangeologia, Angliiskiy Avenue 1, St Petersburg 190121, Russia
- ² AGSO – Geoscience Australia
- ³ Department of Geology, Australian National University, Canberra, ACT 0200, Australia
- ⁴ Present address: Stoneacre, Bream Road, St Briavels, Gloucestershire GL15 6TL, United Kingdom
- ⁵ Polar Marine Geological Research Expedition, Pobedy Street 24, Lomonosov 189510, Russia
- ⁶ Present address: 67 Wybalena Grove, Cook, ACT 2614
- ⁷ Australian Antarctic Division, Channel Highway, Kingston, Tas 7050, Australia

Front cover: Southern Mawson Escarpment, looking north towards Harbour Headland (extreme left), with the Lambert Glacier to the left. Cliffs are up to 800 metres high, and comprise interfolded Archaean granitic basement rocks and Menzies Series metasediments cut by metadolerite dykes (middle distance).

Back cover: Part of the Athos Range, looking east from Mount Bechervaise. Hunt Nunataks, Mount Dovers and Mount Peter are in the middle distance. These outcrops consist mainly of paragneiss and garnet-bearing granitic leucogneiss.

Recommended citation:

Mikhalsky E.V., Sheraton J.W., Laiba A.A., et al. 2001. Geology of the Prince Charles Mountains, Antarctica. AGSO – Geoscience Australia, Canberra; bulletin 247.

Copies of bulletin 247 can be bought from the AGSO – Geoscience Australia Sales Centre, GPO Box 378, Canberra ACT 2601, Australia. Tel. +61 2 6249 9519, fax +61 2 6249 9982, e-mail sales@agso.gov.au

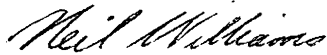
FOREWORD

With its harsh, majestic landscape Antarctica has long been a destination for explorers and a target for the research efforts of geoscientists. Today it is even a destination for tourists. Antarctica is a source of valuable information that can help us understand the dynamic geological processes of our planet and the consequences of those processes for our societies.

This publication is the culmination of over thirty years of survey work in the Prince Charles Mountains, Antarctica, and represents unprecedented cooperation between Australia and Russia in the pursuit of

geoscientific knowledge and excellence. It consolidates the very large body of field and laboratory data that has been collected over the years and outlines the major geological features of the region.

I believe that this bulletin is a significant addition to the literature on Antarctic geoscience; indeed, it is a milestone. I am confident it will contribute to a greater understanding of the geological evolution of the Prince Charles Mountains and I hope that it will be a stimulus for further work in the area.



Dr Neil Williams
Chief Executive Officer
AGSO – Geoscience Australia
October 2001

CONTENTS

Acknowledgments	vii	Neoproterozoic mafic igneous rocks	108
Abstract	viii	Mafic granulite dykes	108
Introduction	1	Ultramafic dykes	108
Ruker Terrane	9	Metadolerite dykes	108
Archaeon granitic rocks	9	Phanerozoic igneous rocks	111
Felsic orthogneiss (Mawson Orthogneiss)	10	Early Palaeozoic granitoids	111
Granitic plutons	14	Hornblende–biotite granite of eastern Amery	
Archaeon–Palaeoproterozoic pegmatite	17	Ice Shelf	111
Archaeon–?Palaeoproterozoic mainly		Muscovite–biotite granite stocks	112
metasedimentary rocks (Menzi Series)	17	Minor intrusions	114
Pelitic metasediments	20	Palaeozoic mafic dykes	117
Psammitic metasediments	23	Lamproite dykes	117
Calcareous metasediments	24	Mafic dykes of the Jetty Peninsula area	119
Metaconglomerate	25	Mafic dykes of the Radok Lake area	127
Mafic and ultramafic schists of the southern		Other mafic dykes	129
Mawson Escarpment	25	Mesozoic alkaline ultramafic rocks	130
Late Archaeon–Palaeoproterozoic(?) metavolcanic		Jetty Peninsula intrusions	130
and metasedimentary rocks (Ruker Series)	25	Kimberlites of the Fisher Massif area	138
Metavolcanic rocks	27	Eocene tephritic phonolite lava of Manning	
Pelitic metasediments	32	Massif	138
Psammitic metasediments	32	Permo–Triassic sedimentary rocks (Amery	
Calcareous metasediments	32	Group)	140
Banded ironstone	32	Radok Conglomerate	141
Late Archaeon–Mesoproterozoic mafic intrusive		Bainmedart Coal Measures	141
rocks	36	Flagstone Bench Formation	142
Amphibolite	36	Palaeoenvironment	143
Metadolerite sills of Mount Ruker	38	Cainozoic glacial–marine and glacial sediments	144
Mafic dykes	38	Cainozoic glacial–marine sediments (Pagodroma	
Proterozoic metasedimentary rocks (Sodruzhestvo		Group)	144
Series)	47	Quaternary glacial sediments	146
Pelitic metasediments	49	Structural geology	148
Psammitic metasediments	49	Ruker Terrane	148
Calcareous metasediments	49	Fisher Terrane	151
Metaconglomerate	49	Beaver–Lambert Terrane	154
Fisher Terrane	50	D ₁ deformation	154
Mesoproterozoic metavolcanic and subvolcanic		D ₂ deformation	154
rocks	54	D ₃ deformation	154
Fisher Massif	54	D ₄ deformation	154
Mount Willing	63	D ₅ deformation	155
Nilsson Rocks	66	D ₆ deformation	156
Mesoproterozoic metasedimentary rocks	67	D ₇ deformation	158
Mesoproterozoic metagabbro	67	D ₈ deformation	158
Mount Willing	67	Late brittle structures	160
Fisher Massif	74	Metamorphism	161
Nilsson Rocks	75	Ruker Terrane	161
Mesoproterozoic–Neoproterozoic granitoids	76	Early high-grade metamorphism (M ₁)	161
Mesoproterozoic–Neoproterozoic mafic dykes	81	Late Mesoproterozoic to early	
Beaver–Lambert Terrane	86	Neoproterozoic(?) metamorphism (M ₂)	163
Mesoproterozoic metasedimentary rocks	86	Cambrian metamorphism (M ₃)	165
Pelitic metasediments	87	Fisher Terrane	167
Psammitic metasediments	88	Beaver–Lambert Terrane	169
Calcareous metasediments	90	Late Mesoproterozoic–Early Neoproterozoic	
Mesoproterozoic felsic orthogneiss	91	peak metamorphism	169
Mesoproterozoic mafic to ultramafic rocks	95	Retrograde metamorphism	172
Amphibolite	95	Discussion	175
Mafic granulite	96	Geological history	175
Ultramafic granulite and serpentinite	98	Ruker Terrane	175
Neoproterozoic felsic igneous rocks	100	Beaver–Lambert and Fisher Terranes	183
Orthopyroxene granitoids	100	Regional correlations	187
Syenitic and granitic rocks of Mount Collins	104	Nature of the c.1000 and c.500 Ma events	191
Garnet granitoids	106	References	197
Minor intrusions	107		

TABLES

1. Mineral abbreviations.	8
2. Chemical analyses of Archaean granitic rocks.	15
3. Chemical analyses of Menzies Series metasedimentary rocks.	21
4. Comparison of quartzite and average sandstone.	24
5. Chemical analyses of Ruker Series metavolcanic rocks and ultramafic schists from the southern Mawson Escarpment.	28
6. Chemical analyses of Ruker Series metasedimentary rocks.	33
7. Chemical analyses of mafic igneous rocks from the Ruker Terrane.	34
8. Chemical analyses of Sodruzhestvo Series metasedimentary rocks.	48
9. Chemical analyses of metavolcanic and subvolcanic rocks from the Fisher Terrane.	58
10. Chemical analyses of metasedimentary rocks from Fisher Massif.	67
11. Chemical analyses of gabbroic rocks from the Fisher Terrane.	72
12. Chemical analyses of granitic intrusive rocks from the Fisher Terrane.	80
13. Chemical analyses of mafic dykes and ultramafic intrusives from the Fisher and Beaver-Lambert Terranes.	84
14. Chemical analyses of metapelites from the Beaver-Lambert Terrane.	89
15. Chemical analyses of felsic gneisses from the Beaver-Lambert Terrane.	94
16. Chemical analyses of amphibolites and mafic granulites from the Beaver-Lambert Terrane.	97
17. Chemical analyses of Neoproterozoic granitic intrusive rocks from the Beaver-Lambert Terrane.	103
18. Chemical analyses of early Palaeozoic granitic intrusive rocks.	113
19. Chemical analyses of Phanerozoic mafic igneous rocks.	120
20. Chemical analyses of Mesozoic alkaline ultramafic rocks.	136
21. Summary of the geological history of the Prince Charles Mountains area.	176
22. U–Pb ages.	178
23. Sm–Nd isotopic data.	179
24. Rb–Sr isotopic data.	180
25. K–Ar ages.	181
26. Correlation of major events in the Prince Charles Mountains area with those in adjacent parts of the East Antarctic Shield.	186

4. Part of the Athos Range, looking east from Mount Bechervaise.	3
5. Beaver Lake, looking northeast from near Radok Lake.	4
6. Northeastern face of Mount Stinear.	4
7. Southern Mawson Escarpment, looking south.	5
8. Eastern part of Mount Ruker, looking southeast.	5
9. Moat or 'wind scour' near Mount Cresswell.	6
10. Mount Menzies, looking east from Mount Mather.	6
11. Archaean basement felsic orthogneiss and locally discordant amphibolite dykes cut by Cambrian biotite granite and pegmatite veins; northeastern tip of Mount Scherger.	10
12. Migmatitic biotite–quartz–feldspar gneiss with minor interlayered metapelite and amphibolite cut by pegmatites of probable Cambrian age; northwestern Mount Twigg.	11
13. Normative Q–Ab–Or and Ab–Or–An diagrams for Archaean granitic rocks of the Ruker Terrane.	12
14. Spidergrams for Archaean granitic rocks.	12
15. Chondrite-normalised REE plots for Archaean granitic rocks.	13
16. Archaean granitic rocks.	14
17. Staurolite–garnet schist and massive white quartzite of the Menzies Series; southwestern Mount Stinear.	17
18. Schematic geological cross section of Mount McCauley.	18
19. Geological sketch map of Mount Rymill.	19
20. Probable Menzies Series metasediments; northern Mount Maguire.	19
21. AFM diagram (after Winkler 1974) for Menzies Series metapelites.	22
22. AFM diagram for contact metamorphosed metapelites from Mount McCauley.	23
23. Cr–Zr–Ba plot for Menzies Series quartzites.	23
24. Contact of Menzies Series metaconglomerate with mica–staurolite–quartz schist; Mount Stinear.	25
25. Geological sketch map of Mount Ruker.	26
26. U–Pb concordia diagram for zircons from biotite granite and metasedimentary rocks from Mount Ruker.	27
27. Alkalies–SiO ₂ plot for metavolcanic rocks of the Ruker Series and ultramafic schists from the southern Mawson Escarpment.	29
28. AFM diagram for metavolcanic rocks of the Ruker Series and ultramafic schists from the southern Mawson Escarpment.	29
29. MgO variation diagrams for metavolcanic rocks of the Ruker Series and ultramafic schists from the southern Mawson Escarpment.	29
30. Logarithmic plots of various incompatible elements against Zr for metavolcanic rocks of the Ruker Series and ultramafic schists from the southern Mawson Escarpment.	30
31. Spidergrams for metavolcanic rocks of the Ruker Series.	31
32. Chondrite-normalised REE plots for metavolcanic rocks of the Ruker Series.	31

FIGURES

1. Part of East Antarctica, showing major metamorphic complexes and outcrops.	1
2. Generalised geological map of the Prince Charles Mountains–Amery Ice Shelf area.	2
3. Lambert Glacier, looking north.	3

33. Atomic Al – (Fe+Ti) – Mg plot for metavolcanic rocks of the Ruker Series and ultramafic schists from the southern Mawson Escarpment.	31	65. AFM diagram for volcanic and subvolcanic rocks and metagabbros from Fisher Massif.	57
34. Banded ironstone (jaspilite) dipping beneath greyish-green slate and metagreywacke; northwestern side of Mount Ruker.	32	66. Spidergrams for basalts from Fisher Massif.	60
35. Alkalies–SiO ₂ plot for amphibolites, metadolerite dykes and metadolerite sills from the Ruker Terrane.	36	67. N-MORB-normalised spidergrams for basalts from Fisher Massif.	60
36. AFM diagram for amphibolites, metadolerite dykes and metadolerite sills.	37	68. SiO ₂ variation diagrams for volcanic and subvolcanic rocks and metagabbros from Fisher Massif.	61
37. Logarithmic plots of various incompatible elements against Zr for amphibolites, metadolerite dykes and metadolerite sills.	37	69. Spidergrams for andesitic volcanic rocks from Fisher Massif.	62
38. Spidergrams for metadolerite sills from Mount Ruker.	38	70. Spidergrams for felsic volcanic rocks and subvolcanic rocks from Fisher Massif.	62
39. Chondrite-normalised REE plots for metadolerite sills from Mount Ruker.	38	71. Mafic rocks from Mount Willing.	63
40. Metadolerite dykes cutting Archaean granitic rocks and subordinate metasediments; southern Mawson Escarpment.	39	72. Alkalies–SiO ₂ plot for metavolcanic rocks from Mount Willing and Nilsson Rocks.	64
41. Metadolerite dykes cutting Archaean felsic orthogneiss; western side of Cumpston Massif.	39	73. AFM diagram for metavolcanic rocks from Mount Willing and Nilsson Rocks.	65
42. Stages in the metamorphism of dolerite dykes.	41	74. SiO ₂ variation diagrams for metavolcanic rocks from Mount Willing and Nilsson Rocks.	65
43. Alkalies–SiO ₂ plots for mafic dykes from the Ruker, Fisher and Beaver-Lambert Terranes.	42	75. Spidergrams for metavolcanic rocks from Mount Willing.	66
44. AFM diagram for mafic dykes.	42	76. Chondrite-normalised REE plots for metabasaltic rocks from Mount Willing.	66
45. <i>mg*</i> variation diagrams for mafic dykes.	43	77. Layered metagabbro intrusion; northern side of Mount Willing.	68
46. Logarithmic plots of various incompatible elements against Zr for mafic dykes.	44	78. Tonalite and gabbro separated by a granite body; southern side of Mount Willing.	68
47. Ce–Y plots for mafic dykes.	45	79. Olivine gabbro, showing olivine grain with rims of cumingtonite and green amphibole; Mount Willing.	69
48. Spidergrams for mafic dykes from the Ruker Terrane.	45	80. Mineral compositional variations with stratigraphic height in the Mount Willing layered gabbro intrusion.	69
49. Chondrite-normalised REE plots for mafic dykes from the Ruker Terrane.	45	81. Generalised major-element geochemical variations with stratigraphic height in the Mount Willing layered gabbro intrusion.	71
50. Sodruzhestvo Series metasediments, showing tight concentric folds; northern side of Mount Rubin.	46	82. Plots of major and trace elements against stratigraphic height for the Mount Willing layered gabbro intrusion.	74
51. Cross-bedding in psammitic schist; Goodspeed Nunataks.	46	83. AFM diagram for gabbroic rocks from the Fisher Terrane.	74
52. Schematic geological cross-section along the northern slope of Mount Rubin.	47	84. <i>mg*</i> variation diagrams for gabbroic rocks from the Fisher Terrane.	75
53. Schematic geological cross-section of Mount Dummett.	48	85. Spidergrams for gabbroic rocks from Mount Willing and Fisher Massif.	76
54. Metaconglomerate; Goodspeed Nunataks.	49	86. Contact between melagabbro and leucogabbro; southwestern Fisher Massif.	76
55. Geological map of Fisher Massif.	51	87. Layered gabbro intruded by tonalite bodies; western Mount Willing.	77
56. Geological map of Mount Willing.	52	88. Metabasaltic xenoliths in granite near the contact zone; northern Fisher Massif.	77
57. Geological map of Nilsson Rocks.	53	89. Layered gabbro intruded by two generations of tonalite vein; western Mount Willing.	78
58. Central part of the southeastern slope of Fisher Massif, showing outcrops of metavolcanic rocks and glacial sediments.	54	90. Normative Q–Ab–Or and Ab–Or–An diagrams for granitic and subvolcanic rocks from the Fisher Terrane.	78
59. Schematic measured sections of metavolcanic sequences at Fisher Massif.	55	91. Alkalies–SiO ₂ plot for granitic and subvolcanic rocks from the Fisher Terrane.	79
60. Tight folds in marble bed; northeastern Fisher Massif.	55	92. SiO ₂ variation diagrams for granitic and subvolcanic rocks from Fisher Massif and Mount Willing.	79
61. Minor folds in marble–schist bed; northeastern Fisher Massif.	56	93. Plot of ASI against SiO ₂ for granitic and subvolcanic rocks from the Fisher Terrane.	81
62. Slightly layered marble inclusion in metabasalt; northeastern Fisher Massif.	56		
63. Metavolcanic rocks from Fisher Massif.	56		
64. Alkalies–SiO ₂ plot for volcanic and subvolcanic rocks and metagabbros from Fisher Massif.	57		

94. Spidergrams for granitic rocks from Fisher Massif.	82	122. Spidergrams for Neoproterozoic syenitic and granitic rocks from Mount Collins.	106
95. Chondrite-normalised REE plots for granitic rocks from Fisher Massif.	82	123. Chondrite-normalised REE plots for Neoproterozoic syenitic rocks from Mount Collins.	106
96. Spidergrams for granitic rocks from Mount Willing.	82	124. K-feldspar megacrystic garnet–biotite granite gneiss cut by aplite vein; Else Platform.	107
97. Plot of Y against Sr/Sr* for granitic and subvolcanic rocks from Fisher Massif and Mount Willing.	83	125. Spidergrams for Neoproterozoic garnet–biotite granitoids and Jetty Peninsula leucogranites.	108
98. Spidergrams for metadolerite dykes from Fisher Massif and Mount Willing.	83	126. Mafic granulite dyke with parasitic F_6 folds in a D_6 low-strain zone; Mount Kirkby.	109
99. Granulite-facies metasediments and garnet-bearing granitic leucogneiss; Zebra Peak.	87	127. Spidergrams for mafic dykes from the Beaver-Lambert Terrane.	109
100. Modified A'FM diagram (Winkler 1974) for Mesoproterozoic high-grade metapelites from the Beaver-Lambert Terrane.	88	128. Metadolerite dykes.	110
101. Plot of ASI against SiO_2 for Mesoproterozoic felsic gneisses from the Beaver-Lambert Terrane.	92	129. Normative Q–Ab–Or and Ab–Or–An diagrams for early Palaeozoic granitic rocks.	111
102. Normative Q–Ab–Or and Ab–Or–An diagrams for Mesoproterozoic orthopyroxene and biotite-bearing felsic gneisses.	92	130. Plot of ASI against SiO_2 for early Palaeozoic granitic rocks.	112
103. Y– SiO_2 plots for Mesoproterozoic orthopyroxene, biotite and garnet-bearing felsic gneisses.	93	131. SiO_2 variation diagrams for early Palaeozoic granitic rocks.	112
104. Plot of Y against Sr/Sr* for Mesoproterozoic felsic gneisses.	93	132. Spidergrams for early Palaeozoic granites from the eastern Amery Ice Shelf and Mawson Escarpment.	114
105. Spidergrams for Mesoproterozoic orthopyroxene and biotite-bearing felsic gneisses.	93	133. Chondrite-normalised REE plots for early Palaeozoic granites from the eastern Amery Ice Shelf.	114
106. Chondrite-normalised REE plots for Mesoproterozoic orthopyroxene-bearing felsic gneisses.	93	134. Interlayered felsic gneiss, amphibolite and calc-silicate gneiss cut by small stocks and veins of Cambrian granite; southwestern Mount Borland.	114
107. Normative Q–Ab–Or and Ab–Or–An diagrams for Mesoproterozoic garnet-bearing felsic gneisses.	95	135. Interlayered felsic gneiss, metapelitic schist, quartzite and amphibolite cut by a dense network of Cambrian granite and pegmatite dykes; northwestern tip of Mount McCauley.	115
108. Spidergrams for Mesoproterozoic garnet-bearing felsic gneisses.	96	136. Pegmatite vein intruded along a ductile shear zone (D_7); Carter Peaks.	116
109. Alkalies– SiO_2 plot for amphibolites and mafic granulites from the Beaver-Lambert Terrane.	96	137. Vertical quartz veins; Mount Butterworth.	116
110. AFM diagram for amphibolites and mafic granulites from the Beaver-Lambert Terrane.	98	138. Spidergrams for early Palaeozoic granite from Jetty Peninsula and granite dykes.	117
111. Ce–Y plot for amphibolites and mafic granulites from the Beaver-Lambert Terrane.	98	139. Phanerozoic alkaline mafic rocks.	118
112. Plot of normative Q against modal percentage of hornblende for mafic granulites.	99	140. Geological sketch map of part of Kamenistaja Platform, Jetty Peninsula.	122
113. Geological sketch map of serpentinite body; southwestern McLeod Massif.	99	141. AFM diagrams for alkaline mafic rocks.	123
114. Outcrops of orthopyroxene granite; southeastern Crohn Massif.	100	142. Alkalies– SiO_2 plot for alkaline mafic rocks.	124
115. Gradational contact between orthopyroxene granitoid and semi-pelitic gneiss; White Massif.	101	143. mg^* variation diagrams for alkaline mafic rocks.	124
116. Coarse-grained orthopyroxene granite; Crohn Massif.	101	144. Logarithmic plots of various incompatible elements against Zr for alkaline mafic rocks.	126
117. Normative Q–Ab–Or and Ab–Or–An diagrams for Neoproterozoic granitic rocks of the Beaver-Lambert Terrane.	102	145. Spidergrams for Jetty Peninsula mafic dykes.	127
118. Plot of ASI against SiO_2 for Neoproterozoic granitic rocks.	102	146. Spidergrams for Radok Lake mafic dykes.	128
119. SiO_2 variation diagrams for Neoproterozoic granitic rocks.	104	147. Basanite dyke; Mount Kirkby.	128
120. Spidergrams for Neoproterozoic orthopyroxene granitoids.	105	148. Spidergrams for basaltic dykes from the NPCM.	129
121. Chondrite-normalised REE plots for Neoproterozoic orthopyroxene granitoids.	105	149. Upper Northern (Severnoe) alkaline ultramafic stock; Jetty Peninsula.	130
		150. Geological map of the Amery Peaks–Beaver Lake–Jetty Peninsula area (Amery Oasis).	131
		151. Geological sketch maps of Mesozoic alkaline ultramafic stocks; Jetty Peninsula.	132
		152. $\text{MgO–Al}_2\text{O}_3\text{–CaO}$ diagram for Mesozoic alkaline ultramafic rocks.	133
		153. Spidergrams for Mount Bayliss lamproites, NPCM lamprophyres and Manning Massif lavas.	134

154. Mantle peridotite nodules in the Upper Northern (Severnoe) alkaline ultramafic stock.	135	182. High-grade overprinting of low to medium-grade assemblages in Menzies Series metapelites.	166
155. Thin kimberlite dyke; southeastern Fisher Massif.	138	183. Retrograde assemblages in Menzies Series metapelites.	167
156. Magmatic layering in kimberlite dyke; southeastern Fisher Massif.	138	184. Rocks from the Beaver-Lambert Terrane used for P–T estimates.	170
157. Kimberlite dyke; Fisher Massif.	138	185. P–T diagrams showing estimated peak and retrograde metamorphic conditions in the Beaver-Lambert Terrane.	171
158. Stratigraphy of Amery Group sedimentary rocks.	140	186. Petrogenetic T–a _{CO2} grid for the system CaO–Al ₂ O ₃ –SiO ₂ –CO ₂ –H ₂ O.	171
159. Radok Conglomerate and Bainmedart Coal Measures cut by thin trachydolerite dyke; east of Radok Lake.	141	187. Reaction textures in calc-silicate rocks.	172
160. Coal seam in Bainmedart Coal Measures; east of Radok Lake.	143	188. Replacement of cordierite by andalusite, quartz, chlorite, carbonate, and muscovite; Mount Meredith.	173
161. Stratigraphy of the Pagodroma Group on southeastern Fisher Massif.	144	189. ϵ_{Nd} evolution diagram for the Fisher Complex.	183
162. Major recumbent fold in felsic gneiss and amphibolite; southern Blake Nunataks.	148	190. Reconstruction of part of Gondwana, showing major Precambrian metamorphic terranes and Neoproterozoic to Mesozoic fold belts.	192
163. Tight, near-recumbent folds in felsic gneiss, metasediments and amphibolite cut by Cambrian pegmatite veins; western side of Mount Twigg.	149		
164. Deformation of metadolerite dykes cutting Archaean felsic orthogneiss.	150		
165. Major thrust zone; southeastern Mount Maguire.	150		
166. Tightly folded felsic gneiss, metasediments and amphibolite cut by locally discordant amphibolite bodies and Cambrian pegmatite veins; western side of Mount Twigg.	151		
167. Minor folds in banded ironstone; Mount Ruker.	152		
168. Interpretive geological map of the Fisher Terrane and adjacent parts of the Beaver-Lambert Terrane, based on magnetic and gravimetric data.	153		
169. Early structural relationships in Beaver-Lambert Terrane gneiss lithologies.	155		
170. Entrained mafic xenoliths in felsic orthogneiss; Mount Kirkby.	156		
171. Tightly folded (F ₄) felsic to mafic gneiss with layers of calc-silicate granulite; Corry Massif.	156		
172. Structural relationships involving younger intrusive lithologies of the Beaver-Lambert Terrane.	157		
173. Dominant structural trends (S ₃ /S ₆) in the Porthos and Aramis Ranges.	158		
174. Major F ₆ antiform; eastern face of Mount Gardner.	158		
175. Schematic block diagram showing regional F ₆ folds defined by upright S ₆ high-strain zones and flat-lying zones in which S ₃ and F ₄ structures are preserved.	159		
176. Major recumbent fold in migmatitic felsic gneiss, amphibolite and paragneiss; southeastern Mount Johns.	159		
177. Pseudotachylite veins in orthopyroxene granitoid.	160		
178. Evidence for a possible early high-grade event in the Ruker Terrane.	161		
179. Metamorphic map of the SPCM.	162		
180. Lower amphibolite-facies assemblages in Menzies Series metapelites.	164		
181. Garnet amphibolite; Mount Cresswell.	165		

Note: In some cases a figure is not located where it is first mentioned in the text, but instead near the main reference to it.

MAP

Geology of the Prince Charles Mountains (1:1 000 000 scale map)—see inside back cover sleeve.

ACKNOWLEDGMENTS

The authors gratefully acknowledge the considerable efforts of members of Australian National Antarctic Research Expeditions (ANARE) and VNIIOkeangeologia (former NIIGA)/PMGRE field parties that ensured the success of field programs over many years. Logistic support was provided by the Antarctic Division, Hobart, Tasmania, and the Soviet/Russian Antarctic Expedition, St Petersburg, Russia.

The authors thank David Ellis, Garrik Grikurov, German Leitchenkov and Steve Boger for invaluable discussions. Financial support for participation of the Russian authors in preparation of this bulletin was provided by the Russian Federal Research Program 'World Ocean'. EVM greatly appreciates private financial aid from his father Vitaly Mikhalsky, and also from Hans-Ulrich Wetzel and Tom

and Maggie Elliot who provided help and inspiration. JWS thanks David Ellis and Richard Arculus whose provision of facilities in the Geology Department, Australian National University enabled him to contribute to this bulletin. Bruce Cruikshank, Julie Haldane, Bill Pappas, John Pyke, Tibor Slezak and Elizabeth Webber of AGSO – Geoscience Australia (known hereafter as Geoscience Australia) are thanked for chemical analyses, and Boris Beliatsky (Institute of Geology and Geochronology of the Precambrian) and Shen-Su Sun (Geoscience Australia) for isotopic analyses. Thanks are also due to Alexander Andronikov (VNIIOkeangeologia/University of Michigan) for providing geochemical data for Mesozoic alkaline ultramafic rocks.

ABSTRACT

The Prince Charles Mountains (PCM) constitute by far the best-exposed cross section through the East Antarctic Shield, extending for over 500 kilometres along the drainage basin of the Lambert Glacier–Amery Ice Shelf system. They consist of three distinct geological terranes: the Archaean to ?Mesoproterozoic Ruker Terrane in the south and the Mesoproterozoic to early Neoproterozoic Fisher and Beaver-Lambert Terranes in the north.

The Ruker Terrane comprises an Archaean (c.3200–3000 Ma) granitic gneiss basement (Mawson orthogneiss and granite plutons) which appears to be overlain by a variety of metasedimentary and metavolcanic rocks of three distinct groups. The Archaean–?Palaeoproterozoic Menzies Series includes prominent thick white to greenish quartzite units, associated with pelitic and calcareous metasediments and amphibolite. It typically contains lower amphibolite-facies assemblages of relatively high-pressure Barrovian type (staurolite + kyanite \pm garnet). The Ruker Series is probably of similar age, and consists of relatively low-grade mafic to felsic metavolcanic rocks (including tuffaceous rocks) and associated metadolerite sills, metapelitic schist, slate, phyllite and banded ironstone. The presumably Proterozoic Sodruzhestvo Series is also of greenschist facies, but of more calcareous composition (metapelitic and calcareous schist, phyllite and slate, with minor marble, quartzite and metaconglomerate). Its metamorphism appears to be prograde, and original sedimentary features are locally preserved. The granitic basement rocks and Menzies and Ruker Series are all cut by mostly metamorphosed and commonly deformed ?Palaeo- to Mesoproterozoic dolerite dykes. The Sodruzhestvo Series is not, however, and is therefore thought to be of Mesoproterozoic (or Neoproterozoic?) depositional age, although this is poorly constrained, and a Palaeoproterozoic age cannot be discounted. The age of regional metamorphism of the Ruker Terrane is uncertain, but it is tentatively assigned to the same late Mesoproterozoic to early Neoproterozoic (c.1000 Ma) metamorphism that resulted in formation of the Beaver-Lambert Terrane. However, there is evidence for a relatively high-grade (up to granulite-facies) Archaean event, and possibly others at c.2500 and 1900 Ma. Widespread retrogression, and possibly prograde metamorphism of the Sodruzhestvo Series, occurred during a Pan-African or Ross age (c.500 Ma) event in which locally abundant granitic rocks were emplaced.

The Beaver-Lambert Terrane consists mainly of high-grade (upper amphibolite to granulite-facies) metamorphic rocks formed in the late Mesoproterozoic to early Neoproterozoic (c.1000–950 Ma). Paragneisses (comprising most of the Athos Series), commonly containing cordierite, sillimanite and garnet, were derived from pelitic, psammo-pelitic and, less commonly, calcareous sedimentary protoliths of largely Mesoproterozoic depositional age. Orthogneisses (comprising most of the Porthos Series) commonly contain orthopyroxene, and were mostly derived from felsic igneous (tonalitic to granitic) rocks. Syn- to late-

metamorphic orthopyroxene granitoids ('charnockites') are widespread. Mainly amphibolite-facies rocks (felsic biotite–hornblende orthogneiss and minor meta-sedimentary rocks) of the Astronomov Series occur in the central part of the Beaver-Lambert Terrane, and may be either retrogressed granulite-facies rocks or lower grade equivalents. The northern part of the Southern PCM is also underlain by upper amphibolite-facies (locally transitional to granulite-facies) rocks (Lambert Series), invaded by abundant early Palaeozoic pegmatite and granite veins and small stocks. Concordant amphibolite and mafic granulite layers may be deformed relics of intrusive rocks, but mafic dykes are generally rare, except in a few small areas.

The Fisher Terrane occupies part of the central PCM, apparently within the Beaver-Lambert Terrane, but comprises rocks which are of much lower metamorphic grade (epidote- to garnet-amphibolite facies) than those in the Beaver-Lambert Terrane. Metavolcanic and intrusive rocks are particularly abundant—metasediments being relatively minor—and there is a large proportion of mafic to intermediate composition (basalt to andesite, and gabbroic rocks). The highly deformed volcanic and intrusive rocks are cut by a variety of pre- to post-tectonic granites and mafic dykes. The geochemistry of the metavolcanic rocks, as well as associated granitoids, suggests formation in an active continental margin with an associated island arc.

The detailed relationships between the Fisher and Beaver-Lambert Terranes are uncertain. They may have been formed from ?Palaeo- to Mesoproterozoic protoliths as both have isotopic evidence for c.1000 Ma metamorphism—although only in the Beaver-Lambert Terrane does this appear to have been the dominant regional event. Both terranes appear to have formed in the same accretionary terrane. The Fisher Terrane possibly represents a higher crustal level part of the Beaver-Lambert Terrane, although the presence of a major suture zone between two lithospheric blocks is quite possible. An active continental margin probably existed until some time before 1000 Ma, when closure of the oceanic basin culminated in continental collision between the Ruker Terrane and the Indian plate. Partial melting of overthickened crust associated with emplacement of mantle-derived magma at the base of the crust produced widespread orthopyroxene granitoids ('charnockites'). The Beaver-Lambert Terrane forms part of a global-scale Grenvillean orogenic belt which appears to have been related to assembly of the Rodinia supercontinent, which was completed by about 1050 Ma. There is some isotopic evidence for a felsic magmatic event of unknown extent and significance at c.800–750 Ma that may have been related to the breakup of Rodinia.

The c.500 Ma Pan-African event may have been related, if less directly, to assembly of Gondwana. No evidence for a suture zone or juvenile volcanics of this age has yet been found in the PCM, however. Continental collision in nearby parts of the East Antarctic Shield (Lützow-Holm

Bay and Denman Glacier areas) makes it likely that a zone of compressional deformation also existed at that time along the Indo-Antarctic suture, but heating caused by mafic underplating is likely to have been a major factor. The Pan-African event was presumably responsible for the final exhumation of the Beaver-Lambert Terrane towards the surface. This must have been achieved in at least part of the area by the Permian when Amery Group sediments (sandstone, shale, conglomerate and coal measures) were deposited. Uplift was accompanied by extensive faulting

and emplacement of a variety of alkaline mafic dykes that were probably associated with the initial formation of the Lambert Graben. Eventual breakup of the Gondwana supercontinent occurred during the Jurassic and Cretaceous, with India rifting off Antarctica during the Early Cretaceous. During this time alkaline ultramafic bodies were emplaced in the PCM. Further geological activity in the area included extrusion of Eocene tephritic phonolite lavas, and formation of the Neogene Pagodroma Group tillites and younger glacial deposits.

INTRODUCTION

The Prince Charles Mountains (PCM) are situated between latitudes 70–75° S and longitudes 60–70° E, to the south of the Australian National Antarctic Research Expeditions (ANARE) station at Mawson (Fig. 1). The PCM constitute the best cross-section through the East Antarctic Shield, extending about 600 kilometres inland. Virtually all other outcrops are within 250 kilometres of the coast.

The PCM are exposed in a major 600 x 300 kilometres trough in the East Antarctic ice sheet, resulting from drainage through the Lambert Glacier–Amery Ice Shelf system (Fig. 2; Trail 1964a). The Lambert Glacier (Fig. 3), the largest in the world, and its major tributary glaciers (Fisher, Geysen, Collins and Mellor) control the topography of the area. It is located on a major crustal

structure: the Lambert Graben (Crawford 1974; Wellman & Tingey 1976; Fedorov et al. 1982b). Outcrops consist of isolated peaks and nunataks near the edge of the trough (Fig. 4), and flat-topped, commonly steep-sided massifs near the major glaciers, particularly in the Southern Prince Charles Mountains (SPCM) (Figs 5, 6). The massifs mostly range up to 500 square kilometres in area and stand up to 1000 metres above the surrounding ice, but the Mawson Escarpment (Fig. 7) is even larger (130 km long and up to 25 km across). These larger ice-free areas are generally covered with *felsenmeeren* of broken rock debris, mostly of local origin. Hence, dominant bedrock trends can be mapped by air-photo interpretation (Fig. 8). Bedrock locally protrudes through this debris. The best exposures

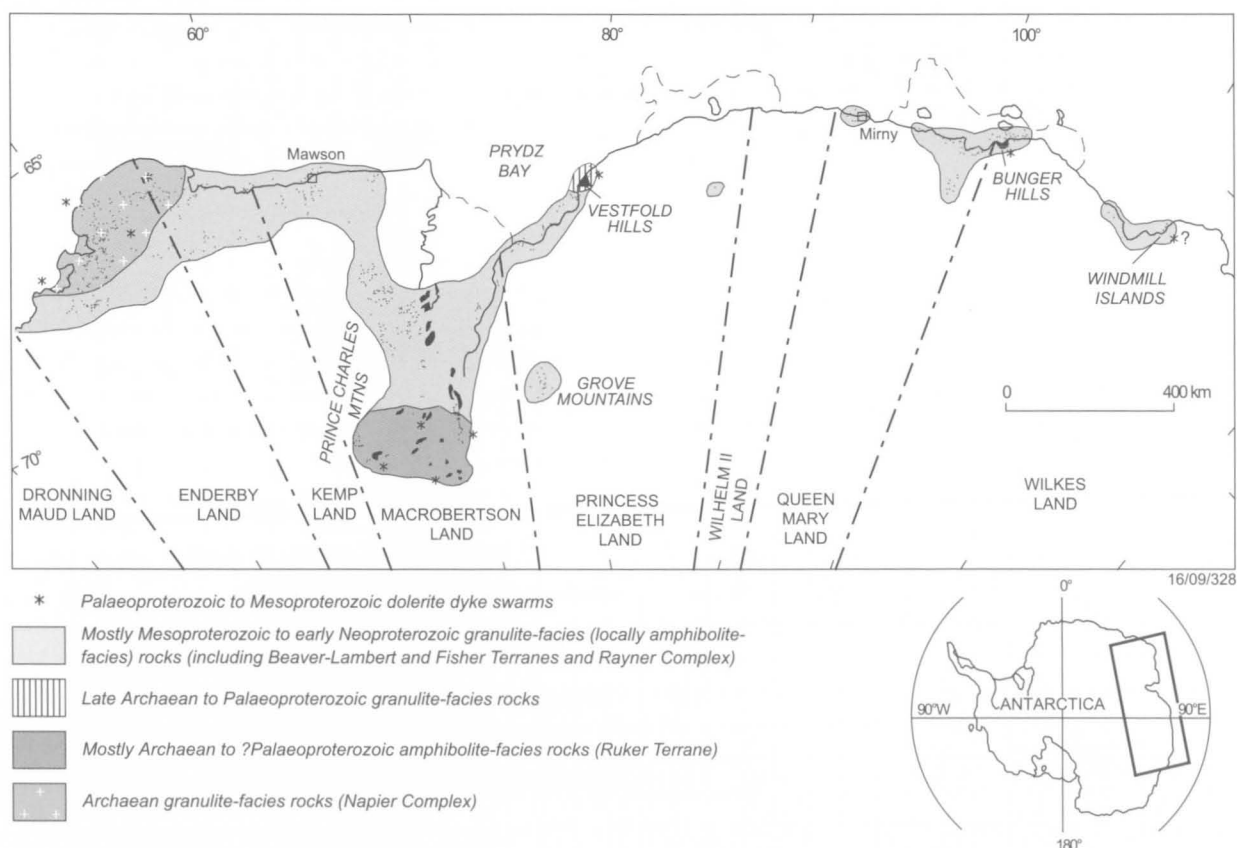


FIGURE 1

Part of East Antarctica, showing major metamorphic complexes and outcrops (black). Mesoproterozoic to early Neoproterozoic metamorphic rocks in the northern part of the Southern Prince Charles Mountains (Beaver-Lambert Terrane) are mainly amphibolite facies; metamorphic rocks of similar age in Enderby and Kemp Lands are termed Rayner Complex. The age of high-grade rocks in the Grove Mountains is uncertain, but they appear to have undergone high-grade metamorphism at about 500 Ma. Palaeoproterozoic to Mesoproterozoic dolerite dyke swarms are present in all the Archaean complexes, as well as in the Bunge Hills area and possibly the Windmill Islands.

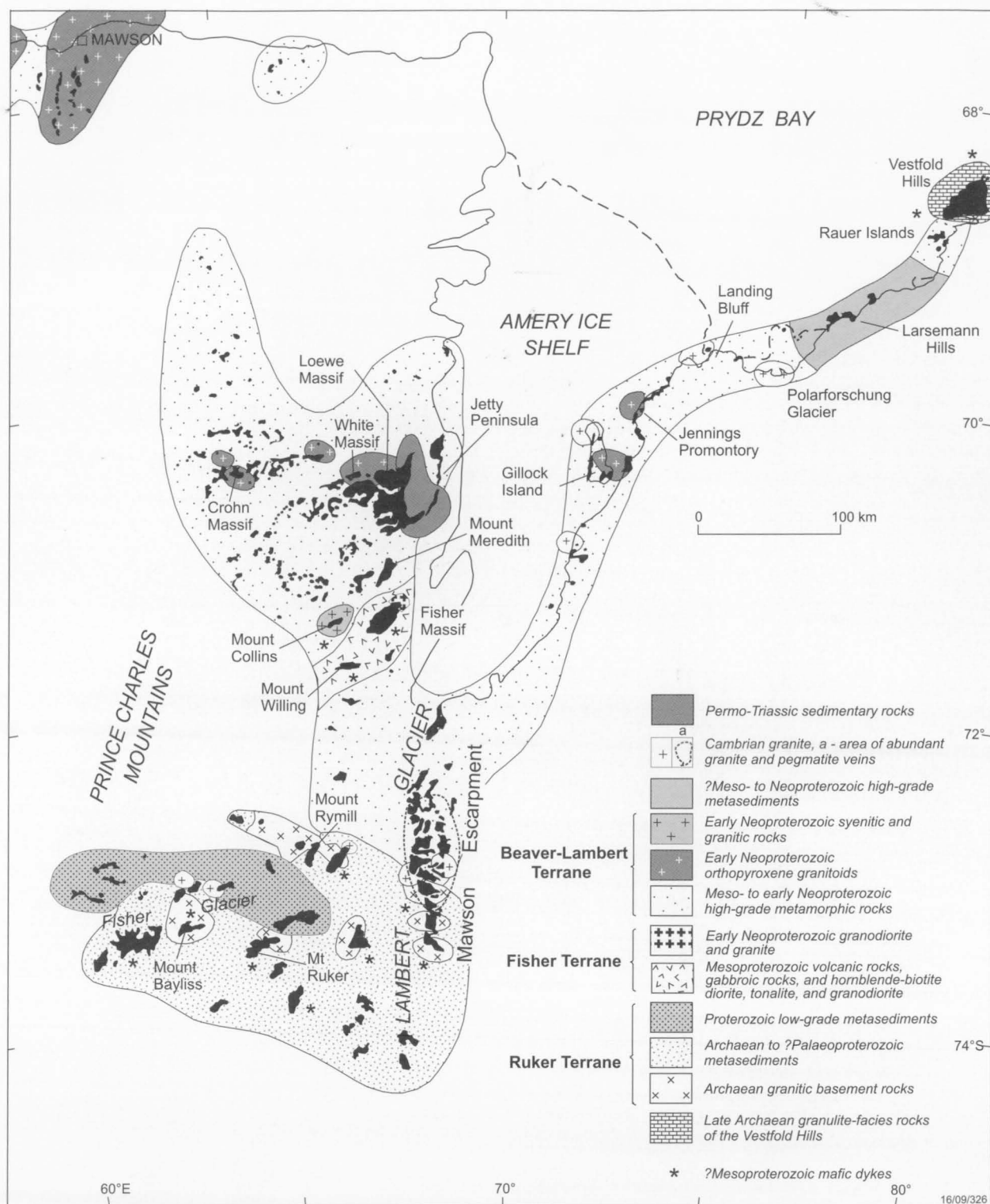


FIGURE 2

Generalised geological map of the Prince Charles Mountains–Amery Ice Shelf area, showing terranes and main granitoid intrusions. Solid black depicts outcrop; geological boundaries away from outcrops are diagrammatic only. Metasediments of probable Meso- to Neoproterozoic age on the Prydz Bay Coast are granulite facies, whereas Proterozoic metasediments in the Fisher Glacier area (Sodruzhestvo Series) are greenschist facies.



FIGURE 3
Lambert Glacier, about 40 km across in this area, looking north. Northern Mawson Escarpment at right, with Clemence Massif behind and Fisher Massif in the far distance (top left), about 150 km away.



FIGURE 4
Part of the Athos Range, looking east from Mount Bechervaise. Hunt Nunataks, Mount Dovers and Mount Peter are in the middle distance. These outcrops consist mainly of paragneiss and garnet-bearing granitic leucogneiss.



FIGURE 5

Beaver Lake, looking northeast from near Radok Lake, with Else Platform and Jetty Peninsula in the distance. Pagodroma Gorge and Glossopteris Gully (lower right) are cut into Permo-Triassic Amery Group sedimentary rocks.



FIGURE 6

Northeastern face of Mount Stinear, looking south towards the similar flat-topped massifs of Cumpston Massif (left) and Mount Rubin. The cliffs are about 900 m high and consist of interfolded Menzies Series metasediments, with a prominent white quartzite unit near Edwards Pillar, and Archaean granitic rocks.



FIGURE 7

Southern Mawson Escarpment, looking south, with Lambert Glacier at right. The cliffs are about 800 m high and comprise interfolded Archaean granitic rocks and Menzies Series metasediments. Note the major isoclinal fold at bottom left.

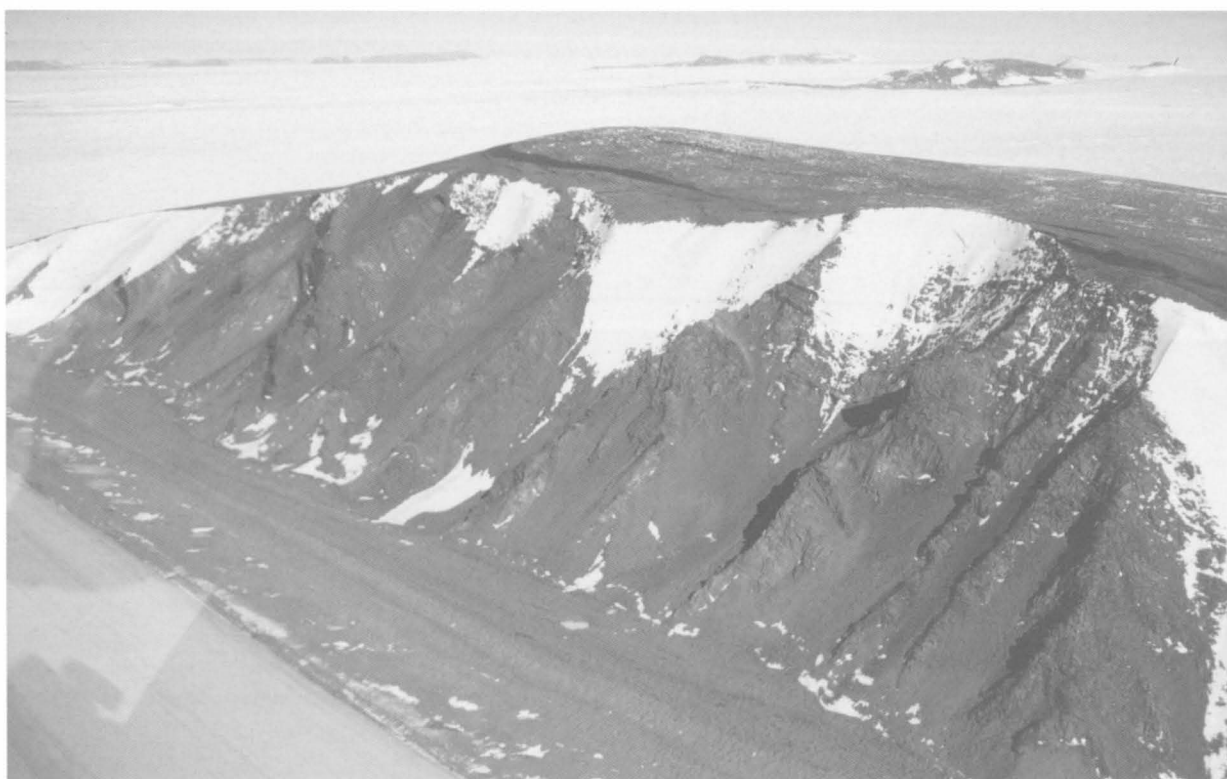


FIGURE 8

Eastern part of Mount Ruker, looking southeast towards Mounts Bird and Newton. In the foreground are 350 m high cliffs of late Archaean biotite granite cut by metadolerite dykes. Note the continuation of bedrock trends exposed in cliff faces (mafic dykes) into summit areas covered by frost-heaved rock debris (*felsenmeer*).



FIGURE 9

Moat or 'wind scour' near Mount Cresswell, site of the ANARE summer field camp from 1972 to 1974.



FIGURE 10

Mount Menzies (about 3300 m), the highest peak in the PCM, looking east from Mount Mather. The moraine in the foreground consists mainly of Archaean quartzite of the Menzies Series.

are in the cliff faces, many of which have adjacent deep moats or 'wind-scours' (Fig. 9), probably formed by a combination of wind erosion and ablation due to radiative heating from nearby rocks. The general concordance of summit levels in both the NPCM and SPCM suggests that they may represent old erosion surfaces (Crohn 1959; Trail 1963a; Wellman & Tingey 1981). A major exception is Mount Menzies, the highest peak in the area at about 3300 metres (Fig. 10). Apart from the Mawson Escarpment, most major bedrock exposures are on the western side of the Lambert Glacier—although there is also a number of smaller outcrops along the eastern side of the Amery Ice Shelf.

The PCM were first sighted in 1947 from United States Navy aircraft during Operation Highjump, which carried out the first surveys of many parts of the Antarctic continent (Bertrand 1967; Rose 1980). They were named when a ground party from Mawson reached Stinear Nunataks in 1954. Further visits, by land and air, were made between 1955 and 1957. The results of geological observations during these early trips were presented by Stinear (1956) and Crohn (1959), who recorded the presence of a range of high-grade metamorphic rocks of both sedimentary and igneous origin, as well as orthopyroxene granitoids (charnockites), rare mafic dykes, and an overlying Permian sedimentary sequence (the Amery Group).

An overland route to the SPCM was pioneered in 1957–58 by a seismic party (Fowler 1971). Australian National Antarctic Research Expedition (ANARE) aircraft manned by the Royal Australian Air Force (RAAF) Antarctic

Flight were based at Mawson from 1956 to 1961, and flew aerial photography and reconnaissance missions over a wide area, including the PCM. Landings in the SPCM in 1957 and 1958 included visits by McLeod (1959) to Clemence Massif and Wilson Bluff. Other geological investigations in the SPCM during the late 1950s and early 1960s were reported by Ruker (1963), McLeod (1964), and Trail (1963a,b, 1964a,b). These authors showed that the rocks are generally of much lower metamorphic grade (greenschist to amphibolite facies) than those of the Northern Prince Charles Mountains (NPCM), and include thick metasedimentary sequences with conspicuous quartzite units and abundant metamorphosed mafic dykes.

The results of these early studies were incorporated in geological maps compiled by Trail & McLeod (1969) and Craddock (1972). Systematic regional geological mapping by BMR (Bureau of Mineral Resources, now Geoscience Australia) geologists seconded to ANARE did not begin until 1969, continuing until 1974, after which summer field operations moved to Enderby Land. Most significant outcrops in the PCM were visited during this helicopter-supported mapping program, the first three years of which concentrated on the NPCM and operated from a field camp near Moore Pyramid.

Four 1:250 000 scale geological maps of the NPCM were subsequently published, and accounts of the geology were given by Mond (1972) and Tingey (1972, 1974, 1981). Mapping of the SPCM in 1972–74 was carried out from a field camp at Mount Cresswell. Eight 1:250 000 maps of the SPCM were published, together with a summary map of the whole area at 1:500 000 scale (Tingey 1982b). Geological descriptions of the various outcrops were given by Tingey & England (1973), England & Langworthy (1975), and Tingey et al. (1981), and a summary of the geology of the PCM was published by Tingey (1982a). The mapping program included the first substantial Rb–Sr isotopic dating study of PCM rocks, carried out by P.A. Arriens of the Australian National University, Canberra (Arriens 1975). One of the most interesting and unexpected results of this study was the recognition that granitic basement rocks and overlying metasediments in the SPCM are of Archaean age, whereas granulite-facies rocks of the NPCM are Meso- to Neoproterozoic (c.1000 Ma). This was at variance with earlier ideas that the higher-grade rocks were likely to be older (e.g., Soloviev 1972; Ravich & Kamenev 1975; Ravich & Grikurov 1976).

Soviet Antarctic Expedition (SAE) geologists also made important contributions towards understanding the geological evolution of the PCM. They first visited the SPCM in 1965, and noted the occurrence of jaspilites (banded ironstones) at Mount Ruker (Soloviev 1972). Further geological work in the area was carried out by the SAE in 1971–72, 1972–73 and 1973–74, with field camps at Mounts Maguire, Ruker, Rubin, Stinear, Rymill, Dummett and McCauley (see Frontispiece), and included airborne investigations. Deep-seismic soundings and airborne magnetic and gravimetric surveys (with line spacing of 20 km) revealed the main crustal features—the Lambert Glacier–Amery Ice Shelf rift zone being one of the most important discoveries.

The results of this field work were published by Soloviev (1972), Grikurov & Soloviev (1974), Fedorov et al. (1982a, b), Kamenev (1982), Kurinin & Grikurov

(1982), Lopatin & Semenov (1982), Ravich (1982), Ravich & Fedorov (1982), Ravich et al. (1982), and Kadmina et al. (1983), among many others. Widespread granulite-facies rocks in the NPCM were believed to be of Archaean age. Metasedimentary sequences overlying Archaean granitic basement rocks in the SPCM (Soloviev 1971) were subdivided into the greenschist to amphibolite-facies Ruker and Menzies Series, thought to be Palaeo- to Mesoproterozoic, and the greenschist-facies Sodruzhestvo Series, assigned to the Neoproterozoic or early Palaeozoic. Only the first two series are cut by metadolerite dykes. Highly migmatitic rocks (garnet–biotite tonalitic gneiss, migmatite and ‘shadow’ granite or anatexite, minor amphibolite and quartzite) of the central part of the PCM were assigned to the Lambert Series. A comprehensive account of the geology of MacRobertson Land, which included much detailed petrological work, was published by Ravich et al. (1978; English translation 1984). The data and interpretations were used in the compilation of geological (Ravich & Grikurov 1976), metamorphic facies (Kamenev & Ravich 1979), and tectonic (Grikurov 1980) maps of Antarctica.

From the mid-1980s, ANARE geological studies have been mostly confined to various parts of the NPCM, and tended to be more problem-orientated, with the involvement of many specialists from Australian universities. Many papers have been published on the structural and metamorphic histories of particular areas, and one of the authors (JWS) has amassed a large amount of whole-rock geochemical data for both the NPCM and SPCM. Moreover, many more isotopic ages are available, both from the NPCM and adjacent parts of the East Antarctic Shield, including ion-microprobe (SHRIMP) U–Pb zircon data. Because this technique enables parts of single zircon grains to be dated, it is particularly applicable to rocks in complex polymetamorphic terranes like the PCM. Such rocks commonly contain zircons of several different ages, so there is a danger that conventional zircon dating can produce geologically meaningless ‘mixed’ ages (Harley & Black 1997).

A field base (Soyuz) on Jetty Peninsula served as the logistic centre for Soviet geological investigations between 1982 and 1991, after which Progress Station in the Larsemann Hills was used. The results of helicopter-supported regional mapping at scales of 1:200 000 and 1:500 000 were summarised by Ivanov & Kamenev (1990) and Kamenev et al. (1993). Other work included detailed petrogenetic, geochemical and isotopic studies of metavolcanic rocks, layered gabbros and alkaline mafic and ultramafic rocks; structural investigations in the SPCM; and stratigraphic studies of coal-bearing strata of the Beaver Lake area. Extensive airborne magnetic and radio-echo sounding surveys were carried out, with line spacing at two or five kilometres.

Several tectonic provinces were distinguished by Kamenev et al. (1990, 1993): the Beaver Belt, Lambert Province, Fisher Belt and Ruker Terrane. The Beaver Belt of the NPCM consists of earliest Neoproterozoic granulite-facies metamorphics (Beaver Complex), which were distinguished as a part of the Proterozoic Wegener–Mawson polycyclic mobile belt (Kamenev 1991, 1993). Five cycles of tectonic activity—at about 2900, 2400, 1700, 1000 and 550 Ma—were distinguished in this

belt. The Lambert Province occupies much of the central PCM, and was distinguished by its upper amphibolite-facies mineral assemblages, and abundance of banded gneiss and schist, calcareous rocks, and Cambrian leucogranite and pegmatite veins. The metamorphic rocks were collectively named the Lambert Complex by Kamenev et al. (1990), and at least partly overlap with the Lambert Series of Ravich et al. (1978). They were considered to be a tectonic mixture of retrogressed Beaver Belt granulite and progressively metamorphosed Ruker Terrane supracrustal rocks and granitoids (Kamenev et al. 1993). However, there are no distinctive compositional features, and the rocks have given similar isotopic ages to the Beaver Belt. The greenstone Fisher Belt, located within the Lambert Province, was thought to have originated during a major Neoproterozoic tectonic cycle that produced most of the granulite and amphibolite-facies rocks in the NPCM. The Ruker Terrane of the SPCM was considered to represent a granite–greenstone terrane, made up of several small greenstone belts, granitic rocks and proto-cratonic fragments. It consists of granitic rocks (termed Mawson granitoids), and metasedimentary and ultramafic to felsic metavolcanic rocks of the Menzies and Sodruzhestvo supracrustals—all considered Archaean in age (Kamenev & Krasnikov 1991) and collectively named the Ruker Complex by Kamenev et al. (1990). A summary of the geology of the PCM–Prydz Bay region was published as a 1:1 000 000 geological map by Thost et al. (1998).

The large amount of data now available, including new isotopic ages, allows a more detailed geological history of the PCM to be established, and more meaningful regional comparisons and correlations than have hitherto been possible. A new and detailed synthesis of the geology of the PCM is now warranted, even though there are still many outstanding problems to be solved, particularly in the SPCM where modern geochronological data are still very sparse. Unfortunately, for logistic reasons, access to this southern area has been severely restricted for more than 20 years; field activities were conducted only in 1987–88 and 1998–99 (Mawson Escarpment) and 1989–90 (Mounts Ruker and Rubin).

The main goal of this bulletin is to summarise all available field and laboratory data and to outline the major geological features of the PCM. However, because many geologists from two independent organisations took part in the field investigations, quite different interpretations of the same outcrop were sometimes made. Combined with the lack of detailed geological information in some areas, particularly in parts of the SPCM, it has not always been possible to produce unambiguous geological models. Where this is the case, a number of alternative interpretations are given. Clearly more work, including detailed field and laboratory studies, needs to be done before a comprehensive geological history of the area can be produced. Hopefully this bulletin provides a stimulus for such work.

The tectonic subdivision of Kamenev et al. (1990, 1993) and Kamenev (1993) is used, with some modifications, in this bulletin. Thus, the geology is described in terms of three different terranes: Ruker, Fisher, and Beaver-Lambert. The Lambert Province is considered to be part of the Beaver-Lambert Terrane, and the Fisher Belt to

represent a distinct terrane (Fig. 2). Supracrustal rocks of the Ruker Terrane comprise three series: Menzies, Ruker and Sodruzhestvo. The highly deformed granulite-facies rocks of the Beaver-Lambert Terrane in the NPCM are not so easily amenable to stratigraphic definitions (though several attempts had been made), so their description is based on lithology rather than stratigraphy.

Igneous rock names follow the classification of Le Maitre (1989), as recommended by the International Union of Geological Sciences. Following this scheme, trondhjemite is used for the leucocratic variety of tonalite, which is equivalent to the plagiogranite of Russian geologists. Mineral abbreviations are given in Table 1.

TABLE 1. Mineral abbreviations used in this bulletin.

Ab,	albite	Ky,	kyanite
Ac,	actinolite	Ms,	muscovite
Ad,	andalusite	Ol,	olivine
An,	anorthite	Opx,	orthopyroxene
Bt,	biotite	Or,	orthoclase
Cal,	calcite	Pl,	plagioclase
Car,	carbonate mineral	Px,	pyroxene
Cd,	cordierite	Qz,	quartz
Chl,	chlorite	Scp,	scapolite
Cpx,	clinopyroxene	Si,	sillimanite
Ctd,	chloritoid	Sp,	spinel
Gt,	garnet	St,	staurolite
Hb,	hornblende	Wo,	wollastonite
Kf,	K-feldspar	Zo,	zoisite

Most whole-rock analyses were carried out in Geoscience Australia’s geochemical laboratory. Major and most trace elements were determined by X-ray fluorescence spectrometry (XRF), using the methods of Norrish & Hutton (1969) and Norrish & Chappell (1977). Li, Be, Ni, Cu and Zn were analysed by atomic absorption spectrophotometry. FeO was determined by titration with standard potassium dichromate solution, and Fe₂O₃ by difference from XRF total Fe. Combined water (H₂O⁺), moisture (H₂O⁻), and total carbon (carbonate and carbon, quoted as CO₂) were measured gravimetrically. Further details of methods, precision and accuracy may be obtained from the Geoscience Australia geochemical laboratory on request. Some additional major-element analyses were obtained by wet chemistry at VNIIOkeangeologia or Arkhangelskgeologia (Russia). Trace elements were determined either by XRF in the Institute of Precambrian Geology and Geochronology (IPGG) or, for a restricted range of trace elements that showed good agreement with other methods, by XRF at Sevzapgeologia (Russia). Rare-earth elements (REE) were determined by instrumental neutron activation analysis (INAA) at St Petersburg State University. Isotopic studies were conducted at IPGG by isotope dilution using an 8-collector Finnigan-MAT mass spectrometer, technical details being given by Beliaty et al. (1994).

RUKER TERRANE

The Ruker Terrane occupies the southern part of the PCM, most outcrops being concentrated on isolated uplifted mountain blocks up to 30 kilometres long which strike mainly east–west or northeast–southwest. The highest point is about 3300 metres (Mount Menzies), and elevations above the ice level commonly reach 1000 metres (Mawson Escarpment, Mount Stinear) and 1600 metres at Mount Menzies. The Ruker Terrane extends at least as far north as Mounts Rymill and Stinear, and probably Mount Cresswell and Binders Nunataks on the western side of the Lambert Glacier, and the central Mawson Escarpment on its eastern side. It is likely that at least the southern half of the Mawson Escarpment represents tectonically modified Archaean to Palaeoproterozoic Ruker Terrane rocks, as an age of 2708 ± 90 Ma (recalculated from Tingey 1991a) was obtained from near the centre of the escarpment. Rb–Sr isotopic data (Table 24) also suggest that the northern part of the Mawson Escarpment may be partly underlain by highly reworked equivalents of the Ruker Terrane sequences, although it is presently impossible to map out such older crustal relics and this area is therefore included in the Beaver–Lambert Terrane. Nevertheless, there may have been significant dextral displacement of up to 50–80 kilometres along the Lambert Glacier rift zone (Ivanov & Kamenev 1990).

The Archaean to Proterozoic rocks of the Ruker Terrane in the SPCM (Fig. 2) comprise a variety of metasedimentary and metavolcanic rocks (Menzies and Sodruzhestvo supracrustals of Kamenev et al. 1990) which apparently overlie a presumed granitic orthogneiss basement. All the lithologies were collectively named the Ruker Complex by Kamenev et al. (1990). The rocks have been metamorphosed under greenschist to amphibolite-facies conditions (Tingey 1982a, 1991a; Lopatin & Semenov 1982; Grew 1982), with rare granulite-facies relics preserved at Mount Newton and possibly the southern Mawson Escarpment. There are relatively few modern geochronological data, but Rb–Sr isochron ages of granitic orthogneisses are about 2700–2800 Ma (Tingey 1991a), and U–Pb zircon ages are significantly older at 3000–3200 Ma (Kovach & Belitsky 1991, and unpublished data; Boger et al. 2001).

The evidence for basement–cover relationships is unclear. Archaean granitic rocks at Mount Ruker are faulted against greenschist-facies quartzite, slate, phyllite, calc-silicate schist, metavolcanic rocks and banded ironstone (Ruker Series) of probable late Archaean to Palaeoproterozoic age. However, the metasediments contain Archaean detrital zircons, presumably derived from a granitic basement. Basement–cover relationships were also suggested at Blake Nunataks, Mount Stinear and the southern Mawson Escarpment by Tingey et al. (1981),

although the contacts are generally either unexposed or tectonically modified (sheared or faulted). The suggestion that orthogneiss near the southern tip of the Mawson Escarpment contains small intrafolial isoclinal folds, that are not present in nearby metasediments (Tingey et al. 1981), was not confirmed by subsequent more detailed mapping. However, the orthogneiss is characterised by migmatitic structures suggesting a somewhat higher metamorphic grade (upper amphibolite facies) than that which pertained in the metasediments. Similarly, metasediments at Blake Nunataks appear to be less deformed and of lower grade than associated orthogneiss. Nevertheless, it is possible that some interlayered metasedimentary rocks may represent an older sedimentary sequence than the Menzies Series—that is, the present Menzies Series may be a composite unit. Because no direct indications for basement–cover relationships (e.g., an unconformity) have been found yet, Kamenev et al. (1990) suggested that all the lithologies are of broadly the same Archaean–Palaeoproterozoic age.

The presumed granitic basement rocks and many of the metasedimentary rocks are cut by metadolerite dykes, most of which appear to be geochemically equivalent to Mesoproterozoic dykes in the Vestfold Hills and Enderby Land (Sheraton et al. 1987a; Lanyon et al. 1993). However, granite at Mount Ruker and various lithologies in the southern Mawson Escarpment (and possibly elsewhere) are cut by high-Mg mafic to ultramafic dykes which are geochemically similar to Palaeoproterozoic dykes in the Vestfold Hills (c.2240; Lanyon et al. 1993). Locally abundant early Palaeozoic granitic rocks and rare lamproite dykes are described in separate sections.

ARCHAEAN GRANITIC ROCKS

Archaean felsic orthogneiss crops out in the SPCM at Cumpston Massif, Machin Nunatak, Mounts Bloomfield, Rymill and Stinear, the southern Mawson Escarpment, and a small nunatak at the northeastern tip of Mount Scherger. Similar orthogneiss at southern Blake Nunataks, Keyser Ridge, and Mounts Bird, Borland, Newton and Twigg tends to be more closely interlayered with metasedimentary rocks, but is probably of similar age. Most gneiss appears to have been metamorphosed under middle to upper amphibolite-facies conditions, as migmatitic structures are common, but greenschist or lower amphibolite-facies retrogression is widespread. Relict granulite-facies assemblages appear to be present in orthogneiss in the southern Mawson Escarpment. Larger, variably deformed granite plutons crop out at Mounts Ruker, Rymill, Stinear and Bayliss.

Felsic orthogneiss (Mawson Orthogneiss)

Archaean felsic orthogneiss is widespread in the Ruker Terrane and occurs as tectonic blocks or slabs up to two to four kilometres thick, but commonly much thinner. Folded veins and lenses of leucocratic pegmatite are locally abundant and typically have a prominent mineral lineation. Rb–Sr isochron ages for felsic orthogneiss from the southern Mawson Escarpment are 2762 ± 222 Ma (initial $^{87}\text{Sr}/^{86}\text{Sr}$ ratio, $\text{Sr}_i = 0.7050 \pm 0.0008$) and 2708 ± 90 Ma (Sr_i 0.7210 ± 0.0091 , probably a reset age) (Table 24). A poorly defined four-point whole-rock reference line at 3000 ± 400 (Sr_i 0.7060 ± 0.0010) Ma (E. Kamenev & B. Beliatsky, unpublished data) also supports a late Archaean age for these rocks. Hornblende–biotite granite gneiss from the same area has given U–Pb zircon ages of 3070 ± 44 and 2981 ± 27 Ma (Table 22), and Sm–Nd mineral and whole-rock isochron ages of 3124 ± 130 and 3176 ± 140 Ma (Table 23), respectively (V.P. Kovach & B.V. Beliatsky, unpublished data). Ion-microprobe U–Pb zircon ages of about 3370 and 3160 Ma were considered by Boger et al. (2001) to reflect inheritance and crystallisation, respectively. Tonalitic orthogneiss has given Sm–Nd mineral–whole-rock isochron ages of 2942 ± 100 and 1880 ± 68 Ma, the latter presumably reflecting a younger metamorphic event. Thermal ionisation mass spectrometry (TIMS) model Pb–Pb zircon ages of 2985 ± 10 and 3035 ± 10 were obtained for felsic orthogneisses from the southern Mawson Escarpment (N.N. Krasnikov & B.V. Beliatsky, unpublished data).

The felsic orthogneiss commonly has a marked compositional layering (Figs 11, 12) and a wide range of composition, from tonalite and trondhjemite (plagiogranite) to granite (s.s.). Both biotite–quartz–feldspar gneiss and hornblende–biotite–quartz–feldspar gneiss are common, and the latter contains relatively abundant allanite and titanite. Much felsic orthogneiss shows the effects of low-grade alteration (sericitisation of feldspar, chloritisation of biotite, etc.). Felsic gneiss at southern Blake Nunataks, Keyser Ridge, and Mounts Newton and Twigg is predominantly biotite-bearing; hornblende is less common, and garnet is present at a few localities (e.g., Mount Newton). Garnet-bearing felsic gneiss occurs at Binders Nunatak and Mount Cresswell, although it is uncertain whether these outcrops are part of the Ruker Terrane. It is intimately interlayered with metasedimentary rocks and has a more variable composition, commonly being rich in quartz (40–60%), suggesting a sedimentary origin.

In some areas, such as the southern Mawson Escarpment, Cumpston Massif and Mount Stinear, the felsic orthogneiss contains locally abundant amphibolite layers of variable thickness (20–30 cm to 2–3 m). It may thus partly represent a metamorphosed bimodal volcanic sequence (Kamenev et al. 1990). At other localities the felsic gneiss contains rare concordant layers of mafic rocks that may represent highly deformed dykes. As well, layers or tectonic lenses of biotite–hornblende–quartz–plagioclase schist, mica amphibolite and ultramafic rocks are present, suggesting that the sequence may represent a tectonic melange of plutonic rock types. The massive



FIGURE 11

Archaean felsic orthogneiss and locally discordant amphibolite dykes, cut by Cambrian biotite granite and pegmatite veins; a small outcrop at the northeastern tip of Mount Scherger. The cliff is about 100 m high.

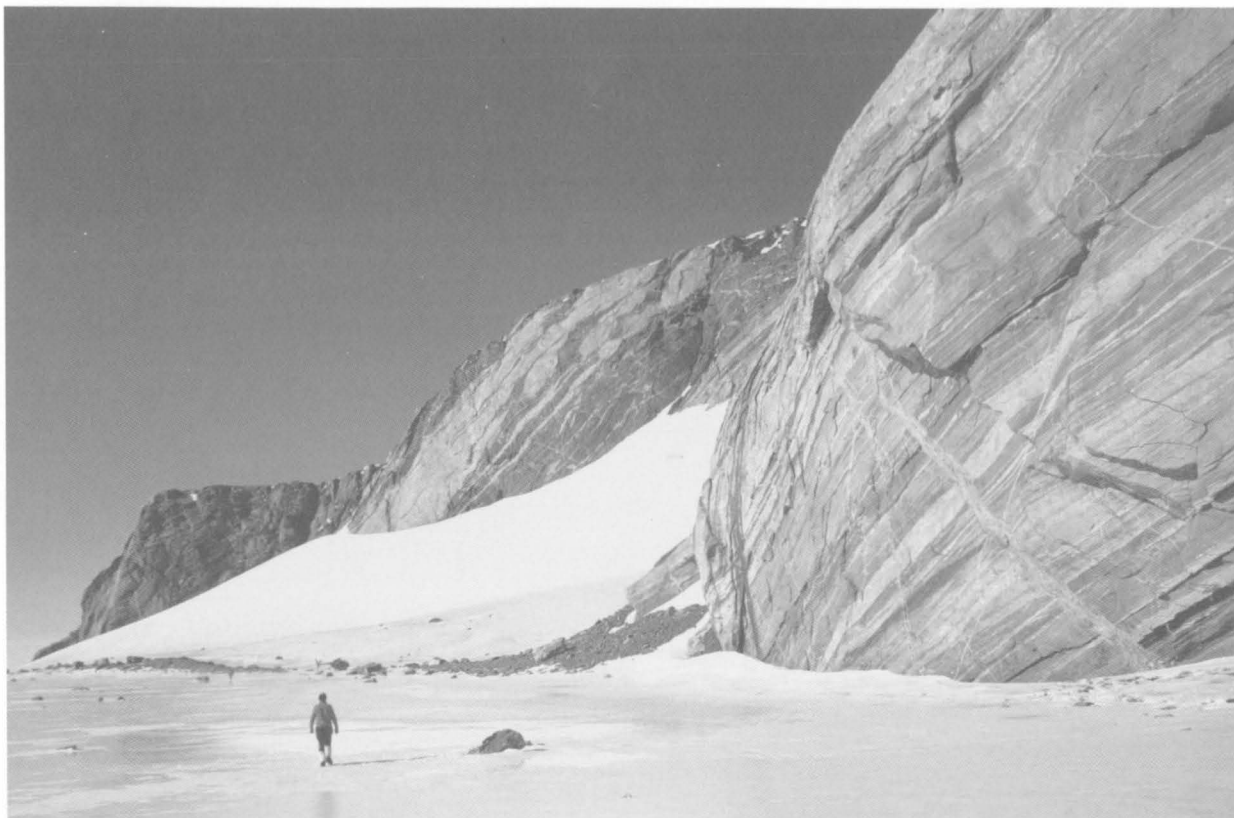


FIGURE 12

Migmatitic biotite–quartz–feldspar gneiss with minor interlayered sillimanite±garnet metapelite and amphibolite, cut by biotite–muscovite±garnet±tourmaline-bearing pegmatites of probable Cambrian age; northwestern Mount Twigg. Note the figure for scale.

biotite–hornblende granite gneiss unit, described below, almost certainly represents highly deformed plutonic rocks. It is noteworthy that at Mount Monolitnaya (southern Mawson Escarpment) hornblende trondhjemitic orthogneiss locally contains dark-coloured orthopyroxene-bearing zones and lenses. This may represent a relict high-grade assemblage, a primary magmatic assemblage, or possibly incipient charnockitisation (V.M. Mikhailov & E.N. Kamenev, unpublished data).

Much of the felsic orthogneiss in the Ruker Terrane is of granitic (s.s.) composition, but tonalitic and trondhjemitic gneiss (or plagiogneiss) are also quite common in some areas, particularly the southern Mawson Escarpment (Fig. 13). Tonalitic to trondhjemitic orthogneisses, from the southern Mawson Escarpment, Cumpston Massif, Blake Nunataks, and possibly elsewhere (e.g., Mount Stinear, where grey tonalitic gneiss was found), commonly have the Y-depleted, Sr-undepleted compositions typical of Archaean tonalite–trondhjemite–granodiorite (TTG) suites (Tarney et al. 1987; Martin 1993). Indeed, most of the more sodic orthogneisses appear to have these characteristics, although a sample of potassic (i.e., granitic) orthogneiss from Mount Twigg is also Y-depleted (Fig. 13). Such *Y-depleted orthogneisses* are thought to represent new sialic crust formed by hydrous partial melting of a garnet and/or amphibole-bearing mafic source—either a mafic underplate or subducted oceanic crust (Tarney et al. 1987; Windley 1998). Spidergrams are

quite different to those of most of the other, mainly granitic (s.s.) orthogneisses, having positive or only small negative Sr anomalies, and negative rather than positive Y anomalies (Fig. 14). REE patterns of Y-depleted tonalitic orthogneisses from the southern Mawson Escarpment are strongly fractionated, with $(La/Yb)_n$ ratios of 21–23 and $(Ce/Y)_n$ 7.0–9.7; Eu anomalies are near-zero or positive (Fig. 15).

Other orthogneisses are predominantly granitic, but grade into trondhjemitic compositions (Fig. 13). They commonly have higher LILE (large ion-lithophile elements: K, Rb, Ba, etc.), HFSE (high field-strength elements, particularly Zr, Nb and Y), and possibly LREE (light rare-earth elements), and lower Sr than the Y-depleted group (Fig. 14). Such *Y-undepleted orthogneiss* samples from the southern Mawson Escarpment have a wide range of REE contents and abundance patterns, but generally lower $(La/Yb)_n$ (4.4 to 5.7 or 12.3 to 18.7) and $(Ce/Y)_n$ (2.3–7.6) than Y-depleted orthogneisses (Fig. 15). Eu anomalies range from negative to positive, suggesting that the granitic orthogneisses form a genetically heterogeneous group. Derivation of the parent magmas from a range of crustal source materials under a range of conditions is likely, and the primary magmatic compositions may well have been modified by plagioclase fractionation and/or cumulus processes.

A distinctive variety of Y-undepleted orthogneiss is the brown-weathering *massive biotite–hornblende granite gneiss* which crops out at Mounts Bloomfield, Rymill

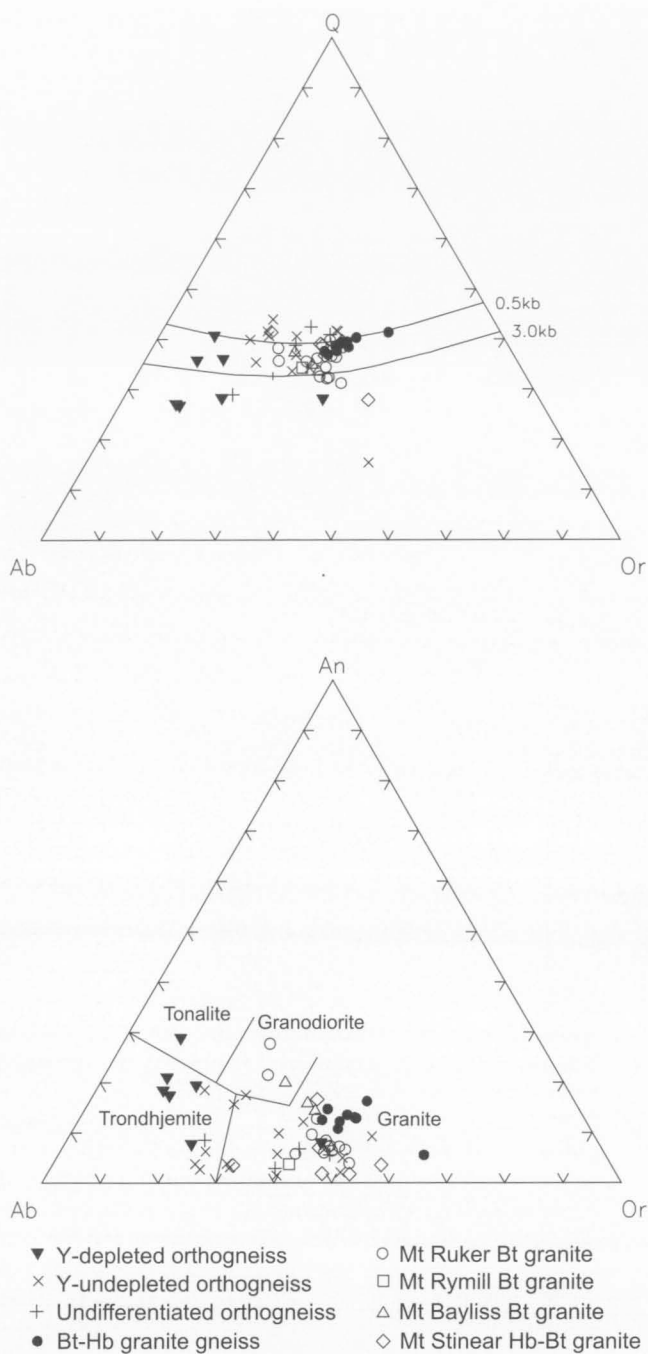


FIGURE 13

Normative Q–Ab–Or and Ab–Or–An diagrams for Archaean granitic rocks of the Ruker Terrane. The former plot shows the quartz–feldspar field boundaries at 0.5 and 3 kb P_{H_2O} and positions of quaternary isobaric minima (after Tuttle & Bowen 1958), and the latter plot shows the granitoid fields of Barker (1979). Y-depleted and Y-undepleted felsic orthogneiss classification after Sheraton & Black (1983); undifferentiated orthogneisses do not have trace-element data.

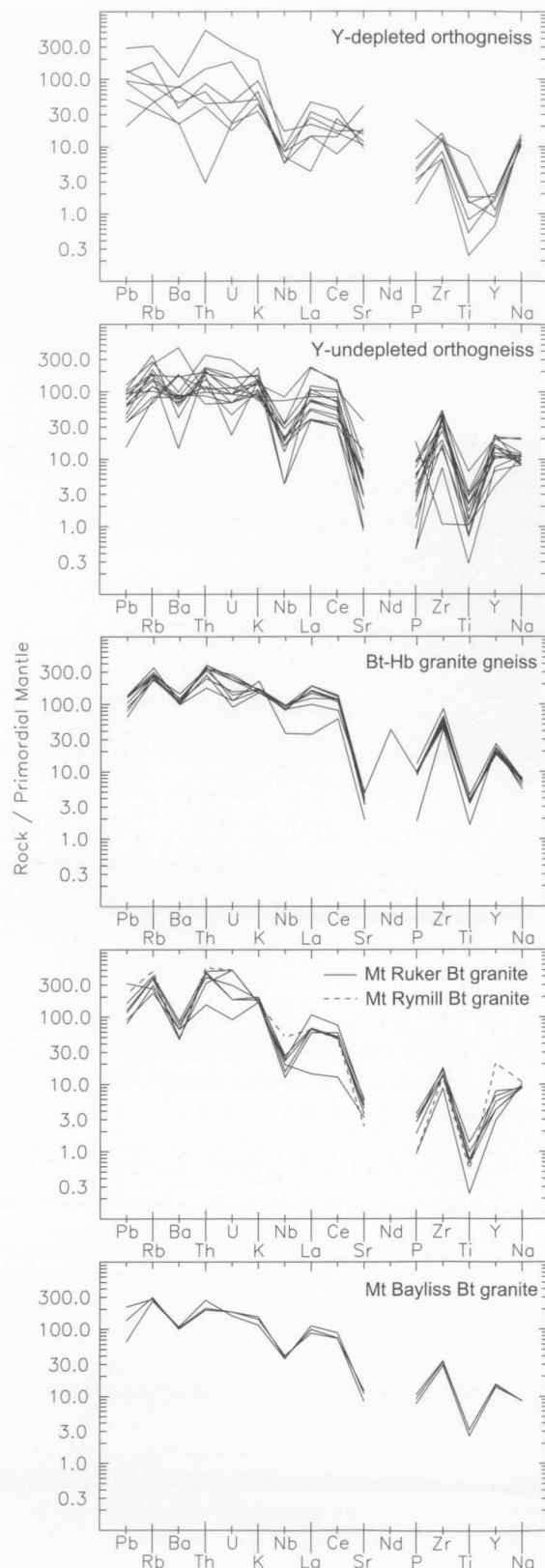


FIGURE 14

Primordial mantle-normalised incompatible element abundance diagrams (spidergrams) for Archaean granitic rocks. Note that most samples do not have Nd data. Normalising values after Sun & McDonough (1989).

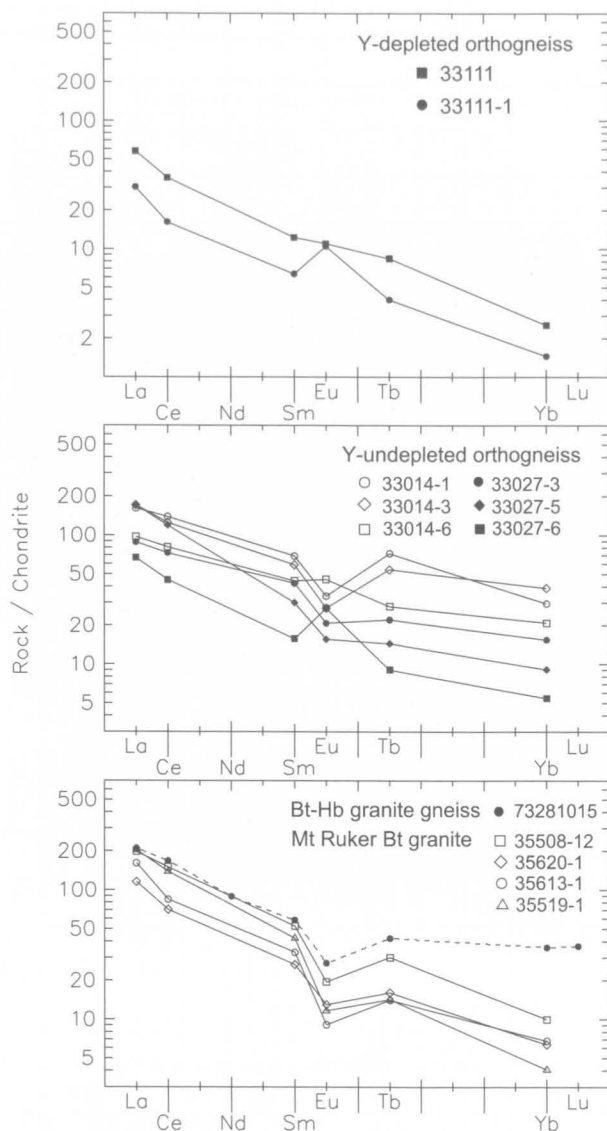


FIGURE 15

Chondrite-normalised (Nakamura 1974; Evensen et al. 1978) rare-earth element abundance plots for Archaean granitic rocks. Orthogneisses are from the southern Mawson Escarpment and Bt-Hb granite gneiss from Mount Bloomfield.

(north), Stinear, Cumpston Massif and the southern Mawson Escarpment. Although this gneiss is largely recrystallised (granoblastic-polygonal or interlobate) and generally strongly foliated, its massive homogeneous appearance and local preservation of zoned plagioclase phenocrysts indicate an intrusive origin (Fig. 16A, B). Dark green potassian hastingsite or ferro-tschermakite (atomic $100\text{Mg}/(\text{Mg} + \text{Fe}^{2+})$, $mg = 22-25$; 2–7 volume %), dark brown biotite ($mg = 22-25$; 2–6%), zoned oligoclase (15–30%), quartz (30%), and microcline (30–40%) are major constituents, with minor titanite, metamict allanite, magnetite, ilmenite, pyrite, epidote, apatite and zircon. Massive biotite-hornblende orthogneiss at southwest Cumpston Massif is relatively sodic (albite granite), and contains small amounts of secondary muscovite, chlorite and carbonate, as well as metasedimentary enclaves.

The very restricted range of major and trace element

compositions (Table 2; Figs 13, 14) of this massive granite gneiss from geographically widespread parts of the Ruker Terrane, provides good evidence that it represents a single intrusive suite. A sample of hornblende-bearing gneiss from Mount McCauley, apparently a basement relic tectonically interlayered with Menzies Series metasediments, has a virtually identical composition and almost certainly belongs to the same suite. All analysed samples of the suite are metaluminous (Di normative), with ASI (alumina-saturation index: molecular $\text{Al}_2\text{O}_3/(\text{CaO} + 3.33\text{P}_2\text{O}_5 + \text{Na}_2\text{O} + \text{K}_2\text{O})$ values less than one, suggesting that they were derived by partial melting of igneous precursors (i.e., they are equivalent to I-type granitoids on the classification of Chappell & White 1974). The granite gneiss is characterised by unusually high HFSE and LREE, but relatively low Al_2O_3 , Sr, and mg (22.3–29.6) (Table 2). Spidergrams are quite fractionated, with marked depletion of Sr, P and Ti, relative to La, Ce, Nd, Zr and Y (Fig. 14); REE patterns are also moderately fractionated ($(\text{La}/\text{Yb})_n = 5.83$, $(\text{Ce}/\text{Y})_n = 2.7-7.1$), with a negative Eu anomaly (Fig. 15).

As pointed out by Sheraton & Black (1988), such high HFSE and LREE contents suggest affinities with A-type (commonly anorogenic) granitoids, although $10^4\text{Ga}/\text{Al}$ (2.5–2.8) is lower and CaO is higher than for typical A-types (Collins et al. 1982; Whalen et al. 1987). Most of the compositional features of A-type granitoids, particularly high HFSE and REE contents, can be explained by high-temperature melting of virtually anhydrous granulite-facies felsic crustal rocks, as such elements are more soluble in high-temperature melts (e.g., Watson & Harrison 1983). Solubilities are generally higher in F-rich melts (Keppler 1993) and F is commonly enriched in A-type granitoids (Whalen et al. 1987), but neither the Ruker Terrane granite gneisses (average of 5 samples is 500 ppm) nor their biotite and amphibole have particularly high F. An alternative origin proposed for A-type granitoids is by extreme fractionation of mantle-derived mafic magma through AFC (assimilation-fractional crystallisation: DePaolo 1981) processes (Javoy & Weis 1987; Turner et al. 1992). Indeed, most A-types may represent mixtures of mantle and crust-derived components, with either being predominant in particular cases (Eby 1990; Kerr & Fryer 1993). In the case of the Ruker Terrane granite gneiss, relatively small Nb anomalies (Fig. 14) are difficult to explain entirely in terms of intracrustal melting, because most felsic crustal rocks (both igneous and sedimentary) have marked negative anomalies which are ultimately a consequence of subduction-related magmatism (Saunders et al. 1991; Tarney & Jones 1994). Thus a predominantly mafic source, possibly with a Nb-rich OIB (ocean island basalt) type mantle component (Sun & McDonough 1989), is perhaps more likely (Sheraton et al. 1996). Whatever their origin and tectonic setting, their A-type chemical affinities and concentration in the within-plate granitoid (WPG) field on the Rb vs Y+Nb diagram of Pearce et al. (1984) are consistent with them being significantly younger than both the crust into which they were emplaced and any early metamorphic event.

Like the massive biotite-hornblende granite gneiss unit, many of the granitic orthogneisses (mostly also hornblende-bearing) described earlier have broadly similar 'A-type' chemical characteristics, and some may be

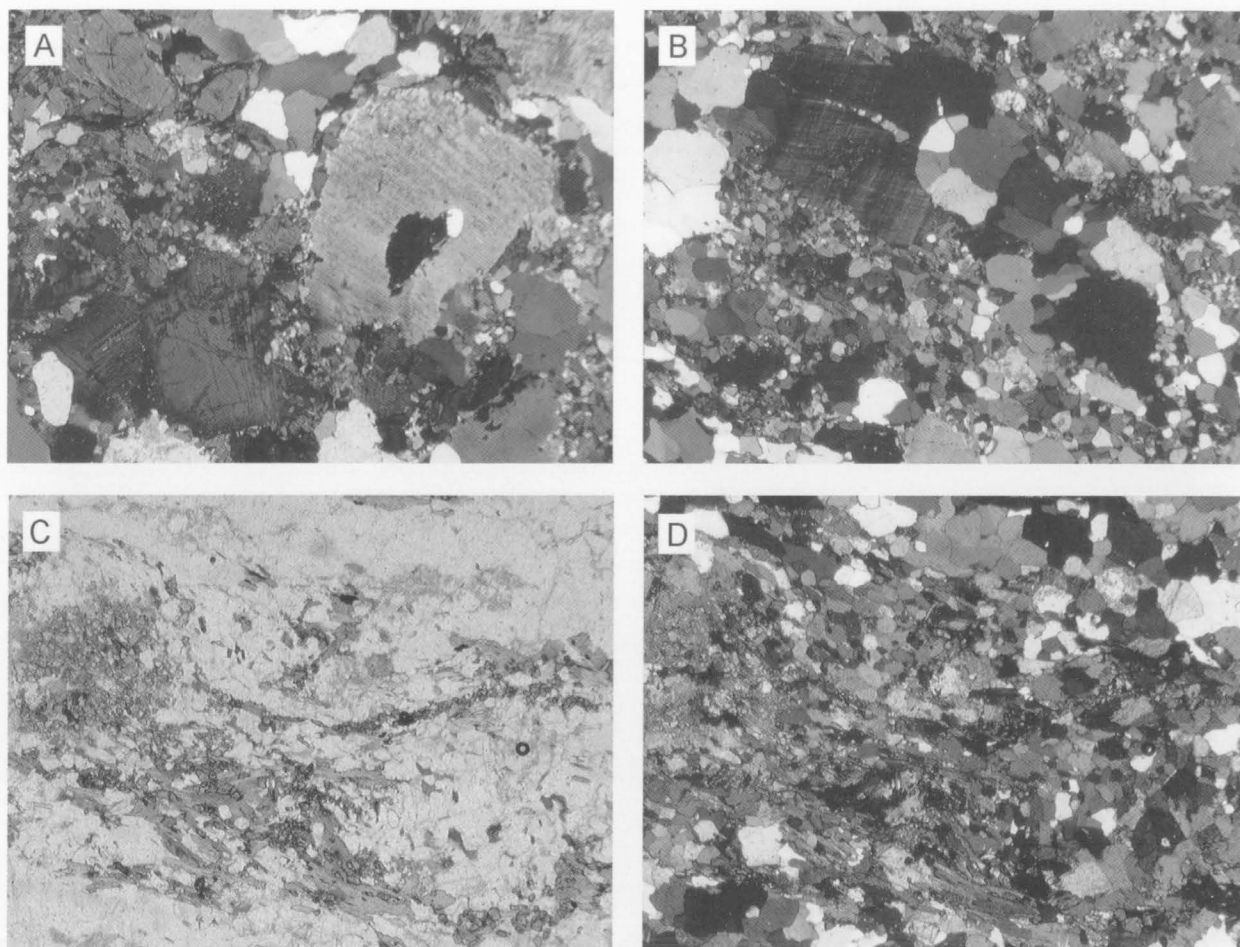


FIGURE 16

Archaean granitic rocks. (A) Partly recrystallised biotite–hornblende granite gneiss showing relict igneous hypidiomorphic to allotriomorphic granular texture; Mount Stinear. Gneiss comprises very dark green hornblende, dark brown biotite, microcline, oligoclase, quartz, and minor titanite, allanite, and epidote. Sample 73281383. (B) Strongly foliated, recrystallised biotite–hornblende granite gneiss; Mount Stinear. Sample 72280758. (C, D) Augen granite gneiss containing dark brown biotite, quartz, microcline, sericitised albite–oligoclase, epidote, and titanite; Mount Bayliss. Sample 73281543. Cross-polarised light in A, B and D; width of field: 4 mm.

genetically related. Thus Zr, Y and, in some rocks, LREE contents tend to be high, and Sr is low (Table 2). However, they tend to be more siliceous, with higher 10^4Ga/Al (2.5–3.5) and lower *mg*; spidergrams mostly show much more pronounced negative Nb anomalies, but are otherwise similar (Fig. 14). The generally high Na_2O and low CaO of most Y-undepleted granitic to trondhjemitic orthogneisses produce a relatively sodic trend on an Ab–Or–An diagram (Fig. 13), which contrasts with the more calcic trend of Mesoproterozoic felsic orthogneisses of the Beaver–Lambert Terrane (Fig. 102). Biotite–quartz–feldspar orthogneisses from Blake Nunataks, Keyser Ridge and Mount Twigg plot on the same trend, consistent with them also being Archaean. However, they lack the high HFSE and LREE of the hornblende-bearing orthogneisses, and most have higher Sr, suggesting derivation from a compositionally distinct source.

The relative abundance of granitic (s.s.) orthogneisses, particularly those with A-type geochemical characteristics, in the Ruker Terrane is not typical of Archaean TTG gneiss terranes. General comparisons with Archaean granite–greenstone terranes (Kamenev 1991, 1993) must

therefore be somewhat tenuous, especially as typical ‘greenstones’ are relatively uncommon. It is, however, possible that tonalitic rocks are more abundant at deeper crustal levels, which may be more like the granulite-facies terranes of the Vestfold Hills and Napier Complex in composition (Sheraton & Collerson 1984; Sheraton et al. 1980, 1987b). Isotopic age data (V.P. Kovach & B.V. Beliatky, unpublished data) are consistent with this interpretation, with the tonalitic orthogneiss tending to have older depleted-mantle ($T_{\text{DM}}^{\text{Nd}}$) model ages (c.3440–3800 Ma, using parameters given in Table 23) than spatially associated biotite–hornblende granite gneiss (mostly 3340–3510 Ma).

Granitic plutons

Larger bodies of granite crop out at Mounts Ruker (Fig. 8), Rymill (south), Stinear (centre) and Bayliss. They are generally less strongly deformed than the felsic orthogneiss, but may grade locally into granite gneiss. The Mount Ruker granite is the least deformed, being affected mainly by brittle to semibrittle (rather than ductile)

TABLE 2. Chemical analyses and CIPW norms of representative Archaean granitic rocks from the Ruker Terrane

Sample no.	33111	73281917	73281933	73282120	74282541	73281048A	73281421	73281551	73281541	73281314
Locality	Mawson	Mount	Cumpston	Mawson	Mawson	Mount	Mawson	Mount	Mount	Mount
	Eascarpment	Twigg	Massif	Eascarpment	Eascarpment	McCauley	Eascarpment	Ruker	Bayliss	Rymill
Lithology	Hb-Bt-Qz- Pl gneiss (Low-Y)	Bt-Qz-Kf- Pl gneiss	Bt-Hb-Qz- Pl-Kf gneiss	Bt-Hb-Qz- Pl-Kf gneiss	Hb-Bt-Qz- Kf-Pl gneiss	Hb-Bt granite gneiss	Hb-Bt granite gneiss	Bt granite	Bt granite gneiss	Bt granite
SiO ₂	70.69	73.70	77.60	74.90	70.10	71.00	71.80	73.70	69.70	75.70
TiO ₂	0.37	0.22	0.28	0.35	0.45	0.78	0.73	0.21	0.68	0.11
Al ₂ O ₃	15.63	14.61	11.21	11.23	13.15	12.34	11.93	13.43	13.33	13.37
Fe ₂ O ₃	0.16	0.31	0.69	1.58	1.60	1.41	1.34	0.71	1.31	0.35
FeO	2.20	1.15	2.05	2.30	4.45	3.70	2.95	1.25	3.00	1.15
MnO	0.04	0.03	0.06	0.05	0.09	0.07	0.07	0.02	0.07	0.03
MgO	0.88	0.44	0.08	0.26	0.79	0.72	0.57	0.33	1.07	0.24
CaO	2.88	1.43	0.70	1.18	2.09	2.29	2.07	1.30	2.43	0.51
Na ₂ O	5.10	4.20	4.45	3.75	4.20	2.40	2.95	3.60	3.35	4.20
K ₂ O	1.18	3.98	2.98	3.58	2.57	4.62	4.44	4.43	3.93	4.42
P ₂ O ₅	0.04	0.09	0.06	0.11	0.13	0.22	0.21	0.06	0.23	0.02
H ₂ O ⁺	0.12	0.18	0.20	0.42	0.60	0.46	0.40	0.50	0.76	0.22
Rest	0.10	0.14	0.29	0.19	0.44	0.32	0.31	0.18	0.25	0.15
Total	99.39	100.48	100.65	99.90	100.66	100.33	99.77	99.72	100.11	100.47
O=F,S,Cl	0.00	0.00	0.02	0.00	0.12	0.02	0.00	0.02	0.00	0.00
Total	99.39	100.48	100.63	99.90	100.54	100.31	99.77	99.70	100.11	100.47
Q	27.60	29.87	37.84	36.08	27.71	32.11	32.07	32.06	27.64	32.19
C	0.82	1.01	-	-	-	-	-	0.49	-	0.80
Or	6.97	23.52	17.61	21.16	15.19	27.30	26.24	26.18	23.22	26.12
Ab	43.15	35.54	37.65	31.73	35.54	20.31	24.96	30.46	28.35	35.54
An	14.03	6.51	1.81	3.24	9.44	9.25	6.20	6.06	9.73	2.40
Di	-	-	1.12	1.64	0.07	0.57	2.30	-	0.69	-
Hy	5.56	2.64	2.45	2.24	8.20	5.97	3.48	2.22	5.75	2.29
Mt	0.23	0.45	1.00	2.29	2.32	2.04	1.94	1.03	1.90	0.51
Il	0.70	0.42	0.53	0.66	0.85	1.48	1.39	0.40	1.29	0.21
Ap	0.09	0.21	0.14	0.26	0.31	0.52	0.50	0.14	0.54	0.05
F	-	-	480	-	2750	560	<200	380	-	-
V	-	12	2	12	<1	27	18	7	50	2
Cr	8	11	<3	4	5	12	8	4	27	3
Ni	27	5	2	4	2	6	4	20	19	3
Cu	-	3	3	6	11	9	16	134	18	<2
Zn	-	28	54	64	85	71	69	21	68	40
Ga	-	17	18	19	19	16	17	18	18	23
Rb	31	118	47	75	96	220	174	166	188	304
Sr	350	278	39	59	138	68	70	92	256	49
Y	8	18	49	73	46	89	102	19	69	93
Zr	170	159	464	432	210	535	745	157	378	141
Nb	6	11	11	20	15	61	68	16	29	36
Ba	150	415	1242	589	613	720	837	321	696	312
La	19	37	27	51	27	112	109	46	62	46
Ce	31	70	55	106	60	213	207	88	134	86
Pb	18	20	3	12	16	27	25	63	27	44
Th	3.6	16	6	9	8	35	31	44	18	50
U	0.4	0.5	1.5	2.0	1.5	5.0	6.0	11.0	4.0	11.0
K/Rb	316	280	526	396	222	174	212	222	174	121
(Ce/Y) _n	9.7	9.7	2.8	3.6	3.3	6.0	5.1	11.6	4.9	2.3
Th/U	9.5	32	4.0	4.5	5.3	7.0	5.2	4.0	4.5	4.6
Nb/Nb*	0.24	0.16	0.21	0.28	0.32	0.53	0.61	0.20	0.35	0.45
mg	41.6	40.5	6.5	16.8	24.0	25.8	25.6	32.0	38.9	27.1

mg = atomic 100Mg/(Mg + Fe²⁺); (Ce/Y)_n is primordial mantle normalised;

Nb/Nb* = Nb/(0.5(K+La)), all element concentrations primordial mantle normalised.

deformation. It is spatially associated with greenschist-facies metamorphic rocks.

Medium- to coarse-grained, grey to pink granite at **Mount Ruker** comprises aggregates of dark brown biotite (1–8%), quartz (20–35%), saussuritised oligoclase (15–40%), sericitised microcline (30–55%), and minor hornblende, allanite, titanite, apatite, zircon and opaque minerals; secondary chlorite, muscovite, epidote and carbonate are also commonly present. The western part of the granite body contains more plagioclase and has a monzodioritic composition—such compositional variation probably reflecting within-pluton magmatic differentiation. A soft greenish variety at the eastern end of Mount Ruker consists largely of quartz, sericite and clay minerals (possibly kaolinite), and may be the result of late-stage hydrothermal alteration.

The Mount Ruker granite has a massive porphyritic to weakly foliated structure and a highly schistose texture, with the schistosity having a different orientation to that in the adjacent Ruker Series metamorphic rocks. Cataclastic structures, mylonites, shear zones and quartz-rich zones are abundant. The cataclastic structures appear to be parallel to the axial planes of folds in the metamorphic rocks, suggesting that the granite has undergone two deformational events. The granite contains quartz-rich lenses of uncertain origin, and numerous metamorphosed or partly altered mafic and high-Mg ultramafic dykes that do not cross-cut the contact with the metamorphic rocks. Similar mafic dykes are present in the metamorphic rocks, so post-dyke faulting must account for the present relationships of the granite and supracrustal sequence. This does not preclude basement/cover relationships, which would be supported if, as appears to be the case, the granite contains structures that are not present in the metamorphic rocks. Moreover, certain high-Mg dykes of probable Palaeoproterozoic age intrude the granite, but appear to be absent from the metamorphic country rocks, although mafic sills in the latter have some geochemical similarities (see below).

Pink to red, even-grained granite at **Mount Rymill** is somewhat recrystallised, but not strongly deformed. It contains biotite, quartz, microcline, albite and minor titanite.

More strongly deformed and altered granite augen gneiss at **Mount Bayliss** contains hornblende (up to 1%), dark brown, partly chloritised biotite (5–6%), quartz (25–30%), microcline (~30%), sericitised albite–oligoclase (30–40%), and minor titanite, allanite, epidote, zircon and opaque minerals (Fig. 16C, D). A single sample of leucogranite of uncertain relationships from Mount Bayliss contains conspicuous fluorite.

Gneissose or rarely massive pinkish-grey fine- to medium-grained granite at **Mount Stinear** consists of quartz (20–35%), plagioclase An_{25-32} (10–40%), K-feldspar (20–50%), hornblende (up to 7%), biotite (5–8%), and magnetite (up to 1%). Secondary epidote, carbonate and chlorite are common. The granite is younger than the host tonalitic orthogneiss. This is confirmed by a thick contact reworking zone in the orthogneiss, and by abundant orthogneiss and other xenoliths within the granite (Ravich et al. 1978).

Granite gneiss at Mount Bayliss has given an imprecise Rb–Sr isochron age of 2750 ± 402 Ma (Sr_i 0.7076 \pm 0.0153),

whereas granites at Mounts Ruker and Rymill have given much younger ages of 1412 ± 157 (Sr_i 0.8902 \pm 0.0162) and 1169 ± 237 (Sr_i 1.1139 \pm 0.0621), respectively (Table 24; Tingey 1991a). Such exceptionally high initial ratios are very difficult to explain even by melting of very old protoliths, and are almost certainly a consequence of isotopic resetting. All these granites are cut by metadolerite dykes, most of which are correlated on geochemical grounds with the Mesoproterozoic dolerite dykes in the Vestfold Hills (Sheraton et al. 1987a; Lanyon et al. 1993). Average T_{UR}^{Sr} model ages of all three granites are late Archaean (2660–2870 Ma).

An Archaean age (3005 ± 57 Ma) for the Mount Ruker granite (35306-1) was confirmed by U–Pb zircon dating (V.P. Kovach & B.V. Beliatky, unpublished data), and the data also indicate prominent U loss during an early Palaeozoic (Ross or Pan-African age, 515 ± 20 Ma) event (Table 22). T_{DM}^{Nd} Sm–Nd model ages of 3270–3420 Ma (N.N. Krasnikov & B.V. Beliatky, unpublished data) are consistent with an earlier Archaean age for the source of the Mount Ruker granite. Additional studies of a highly sheared granite (35317-1) and spatially associated metasedimentary and metavolcanic rocks showed that major thermal events must have occurred between 3175 and 2500 Ma (or possibly somewhat later, as the latter value may be misleading in view of the highly discordant character of the data points), with strong overprinting at about 500 Ma (Fig. 26). This agrees with previous suggestions based on Rb–Sr data (Ravich et al. 1978). Zircons from the deformed granite are metamict, slightly rounded, lack typical crystal shapes, and are pink to light magenta. They are morphologically akin to metamorphic zircons, like those in the associated metasedimentary rocks, rather than the typical euhedral, white to partly transparent zircons in the undeformed granite. Both zircon types occur within the same granite pluton, so the metamorphic zircons may well have formed during extensive shearing at about 2850 Ma (Fig. 26)—although subsequent U loss at about 500 Ma has obscured the isotopic signature of this event. Some zircon fractions suggest the presence of an older inherited component that may be about 3200 Ma old, comparable with the T_{DM}^{Nd} model ages.

A younger episode of granitoid emplacement apparently occurred in the southern Mawson Escarpment at about 2500 Ma (low-alumina trondhjemitic gneiss, TIMS Pb–Pb zircon age: V.P. Kovach & B.V. Beliatky, unpublished data). The Mount Stinear granite has not been dated and could conceivably represent a younger, post-Archaean phase of igneous activity—but this seems unlikely.

Granites at Mounts Ruker, Rymill and Stinear are generally of near minimum-melt composition, whereas that at Mount Bayliss is slightly less siliceous (Table 2; Fig. 13). None of these granites is as enriched in HFSE and REE as the massive biotite–hornblende granite gneiss. The Mounts Bayliss and Rymill granites, however, have moderately high HFSE (particularly Y and Nb) and thus, like the granite gneiss, have ‘within-plate’ chemical characteristics (Pearce et al. 1984). Spidergrams (Fig. 14) show large negative Nb, Sr, P and Ti anomalies, typical of I-type granitoids produced by partial melting of felsic crustal rocks with residual plagioclase but not garnet

(Tarney et al. 1987). Granites from Mount Ruker have quite strongly fractionated REE patterns with negative Eu anomalies, consistent with melting of felsic crustal rocks, plagioclase fractionation, or both (Fig. 15). The granite plutons are more fractionated than most felsic orthogneisses from the Ruker Terrane, suggesting they are genetically unrelated to the latter and may have been derived by partial melting of such rocks.

ARCHAEAN–PALAEOPROTEROZOIC PEGMATITE

As already indicated, granitic pegmatites are associated with the felsic orthogneiss. Others that cut Menzies Series metasediments and are therefore not strictly part of the presumed granitic basement are probably younger. For example, a Rb–Sr muscovite age of 2580 Ma for pegmatite at Mount Stinear suggests that the quartzite-rich metasediments are Archaean. A granite pegmatite that cuts biotite–hornblende granite gneiss (c.3000 Ma), plagiogneiss (c.2500 Ma), and a boudinaged high-Mg mafic dyke (c.2375 Ma) in the southern Mawson Escarpment was dated at 2300–2000 Ma (all TIMS Pb–Pb zircon ages: V.P. Kovach & B.V. Beliaty, unpublished data). Another pegmatite in the same area has an ion-microprobe U–Pb zircon age of about 2645 Ma with

inherited cores of about 3150 Ma (Boger et al. 2001). Deformed pegmatites at Keyser Ridge have given Rb–Sr muscovite ages of about 1708 and 1995 Ma, and a model muscovite age of about 2100 Ma has been obtained on a similar pegmatite at Mount Newton (Tingey 1991a).

ARCHAEAN–?PALAEOPROTEROZOIC MAINLY METASEDIMENTARY ROCKS (MENZIES SERIES)

The presumed Archaean granitic basement appears to be overlain by a variety of metasedimentary and minor meta-igneous rocks (Menzies Series of Ravich et al. 1978). Prominent thick units (up to 200 m) of white to greenish quartzite associated with pelitic and calcareous rocks, as well as amphibolite units (Fig. 17), are widespread—particularly at Mounts Mather, Menzies, Rymill, Stinear and Borland, Cumpston Massif, Seavers Nunatak and the southern Mawson Escarpment. Both metasediments and granitic basement are cut by mostly metamorphosed and commonly deformed ?Palaeo- to Mesoproterozoic mafic dykes. The Archaean age assigned to these metasediments is based on a single Rb–Sr muscovite age of 2580 Ma for a probably deformed pegmatite that cuts quartzite at Mount Stinear (Tingey 1991a).

Metasedimentary sequences without the thick quartzite beds were also assigned to the Menzies supracrustals by Kamenev et al. (1993). They crop out at a number of other places in the southern part of the SPCM (e.g., Blake Nunataks, Mounts Bird, Newton and Twigg, Keyser Ridge and Wilson Bluff). Like the quartzite-rich sequences, they are cut by metamorphosed and more or less deformed mafic dykes at many localities, and may, in part, be correlated with these late Archaean metasediments. However, the absence of the distinctive white to green quartzite units suggest that at least some of these rocks could be somewhat younger, possibly Palaeoproterozoic.

Exposed contacts between basement and presumed cover are generally faulted (e.g., at Mounts Ruker and Stinear) or tectonically modified (e.g., the southern Mawson Escarpment), so their original nature is difficult to demonstrate. Conglomerate layers in quartzite at Mount Stinear contain clasts of quartzite, mafic rocks and granitic rocks. In some places, such as northern Cumpston Massif, the basement gneiss is tectonically interleaved with metasedimentary rocks. This may reflect extreme deformation of both basement and cover, or may represent an older sequence of sedimentary rocks. Clearly, the granitic rocks of the basement must have been emplaced into older crustal rocks of some sort, although plagiogneiss like that at Mount Stinear and the southern Mawson Escarpment might be the best candidate. Metasedimentary enclaves in granite gneiss at southwestern Cumpston Massif may be either downfaulted blocks of the cover, or xenoliths or roof pendants of older country rocks.

Most of the metasediments contain lower amphibolite-facies assemblages which may have been formed during the late Mesoproterozoic–early Neoproterozoic (c.1000 Ma) metamorphism, but there is some evidence for an earlier higher grade event (or events). Thus, garnet+staurolite forms rims around a possible altered cordierite porphyroblast in metapelite at Mount Stinear,

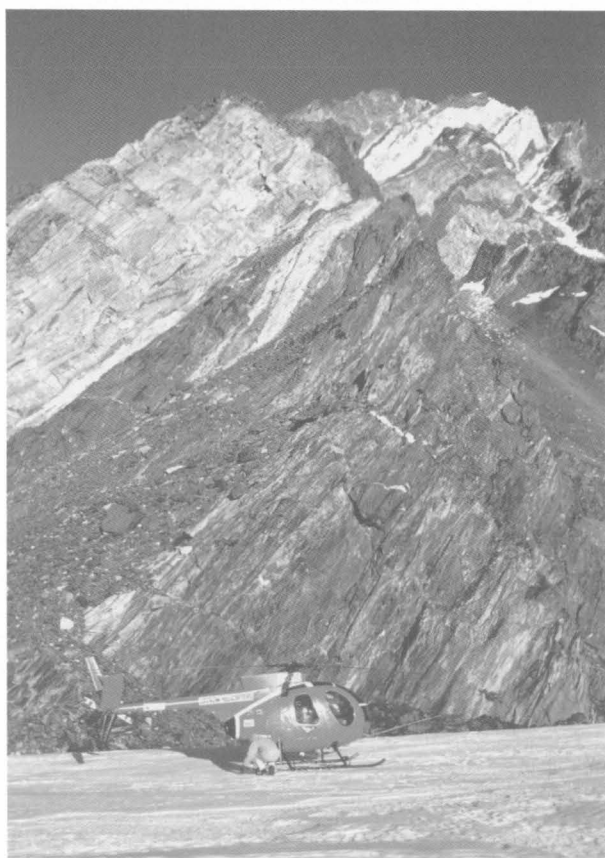


FIGURE 17

Staurolite–garnet schist and massive white quartzite of the Menzies Series; southwestern Mount Stinear. Although not obvious from the photograph, the schist at this locality shows extensive malachite staining.

and growth of euhedral garnet around an earlier generation of altered and broken garnet has occurred. Similarly, two generations of garnet are present in metasediments of the southern Mawson Escarpment (England & Langworthy 1975). Metasedimentary rocks of similar metamorphic grade at Mounts McCauley and Scherger, which were included in a younger metasedimentary sequence (the Sodruzhestvo Series) by Tingey (1982a, 1991a), show petrographic evidence for a kyanite–staurolite-grade event, and are assigned here to the Menzies Series. They are more strongly deformed than Sodruzhestvo Series greenschist-facies metasediments at Mount Rubin and, as pointed out above, appear to be spatially associated with Archaean granitic basement rocks.

Concordant amphibolite bodies are commonly interlayered with the metasedimentary rocks. Most are no more than a few metres thick, and are believed to represent highly deformed and sometimes folded mafic dykes or sills. Their chemical composition is therefore discussed in the relevant section. A mafic granulite layer at Mount Newton is the only known occurrence of mafic granulite which clearly pre-dates the c.1000 Ma(?) metamorphism and may be of Archaean age.

The Menzies Series in the southern part of **Mount Stinear** is 2500 metres thick and forms four highly heterogeneous metasedimentary members (Ravich et al. 1978) consisting (from bottom to top) predominantly of: (1) mica–quartz schist and quartzite (500 m); (2) biotite–hornblende–quartz±garnet schist, quartzite, metaconglomerate and staurolite–mica–quartz schist (1300 m); (3) metaconglomerate (400 m); and (4) kyanite–staurolite–garnet–mica schist and ferruginous quartzite, alternating with magnetite–hematite quartzite containing garnet–quartz–magnetite laminae (300 m). Conglomerate clasts are composed of quartzite (85–90%), mica–quartz schist (5–7%), and metabasite (5–7%), and are

highly deformed with axial ratios between 1:3 and 1:8. Numerous amphibolite layers (?sills) and metabasite dykes were found.

The 1700 metre-thick metasedimentary sequence at **Mount McCauley** (Fig. 18) comprises three members composed of: (1) biotite–hornblende–quartz–feldspar gneiss or schist and quartzite; (2) kyanite–garnet–mica–quartzite; and (3) pelitic (high-Al) mica–quartz schist. Much of the lower member (1) is compositionally similar to the Mawson Orthogneiss, but no disconformity was found. Local development of cordierite–sillimanite-bearing assemblages may be due to contact metamorphism associated with emplacement of abundant Cambrian granite and pegmatite dykes. A number of amphibolite bodies, at least some of which may be metamorphosed mafic sills, cut the metasediments in a few places. A 10 metre-thick phlogopite–tremolite marble and a 45 metre-thick olivine–tremolite (ultramafic) rock occur within the middle member.

At **Mount Rymill** (Fig. 19) the Menzies Series is represented by chlorite–mica–quartz schist (locally staurolite and kyanite-bearing), quartzite, biotite–hornblende–plagioclase schist and quartz–biotite schist, which together are more than 700 metres thick. Metamorphosed mafic sills (amphibolite), up to 100 metres thick, intrude the metasediments.

Similar amphibolite-facies metasediments, predominantly of pelitic composition, are tectonically interlayered with quartzo-feldspathic gneiss at Keyser Ridge and Mounts Bird and Newton. They are cut by metadolerite dykes and both dykes and country rocks have been locally strongly retrogressed under greenschist-facies conditions. Rb–Sr muscovite ages of 1708 and 1995 Ma have been obtained on an older generation of foliated pegmatite at Keyser Ridge (Tingey 1991a). Amphibolite-facies metasediments are also associated with felsic gneiss

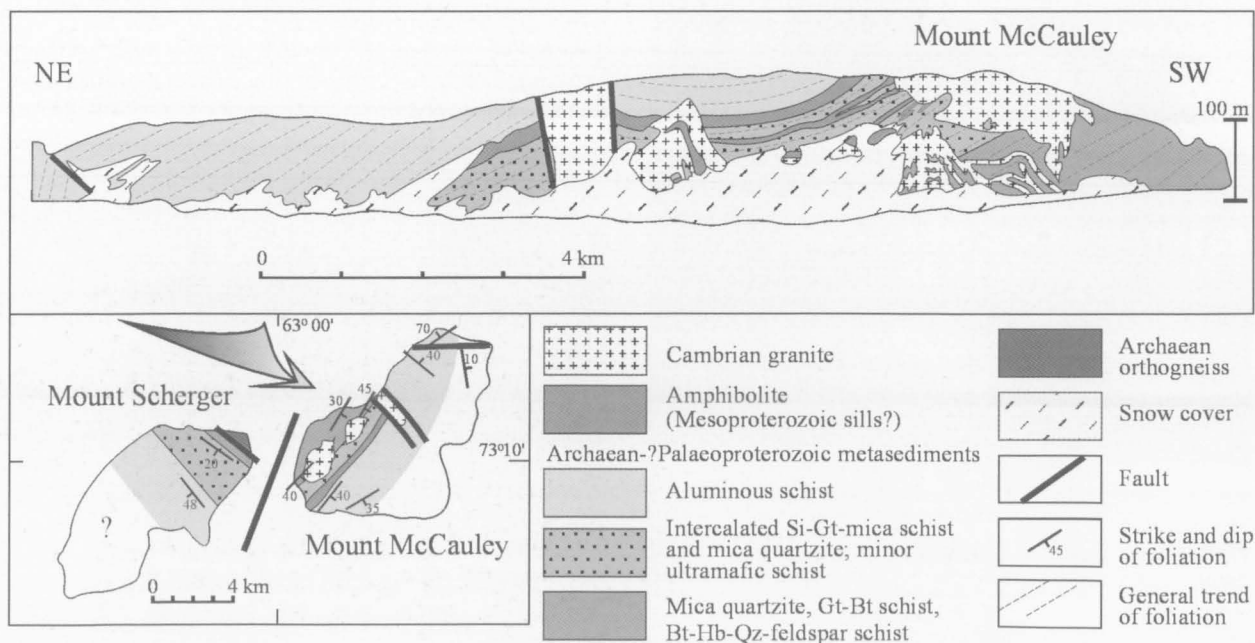


FIGURE 18

Schematic geological cross-section of Mount McCauley (modified from Ravich et al. 1978).

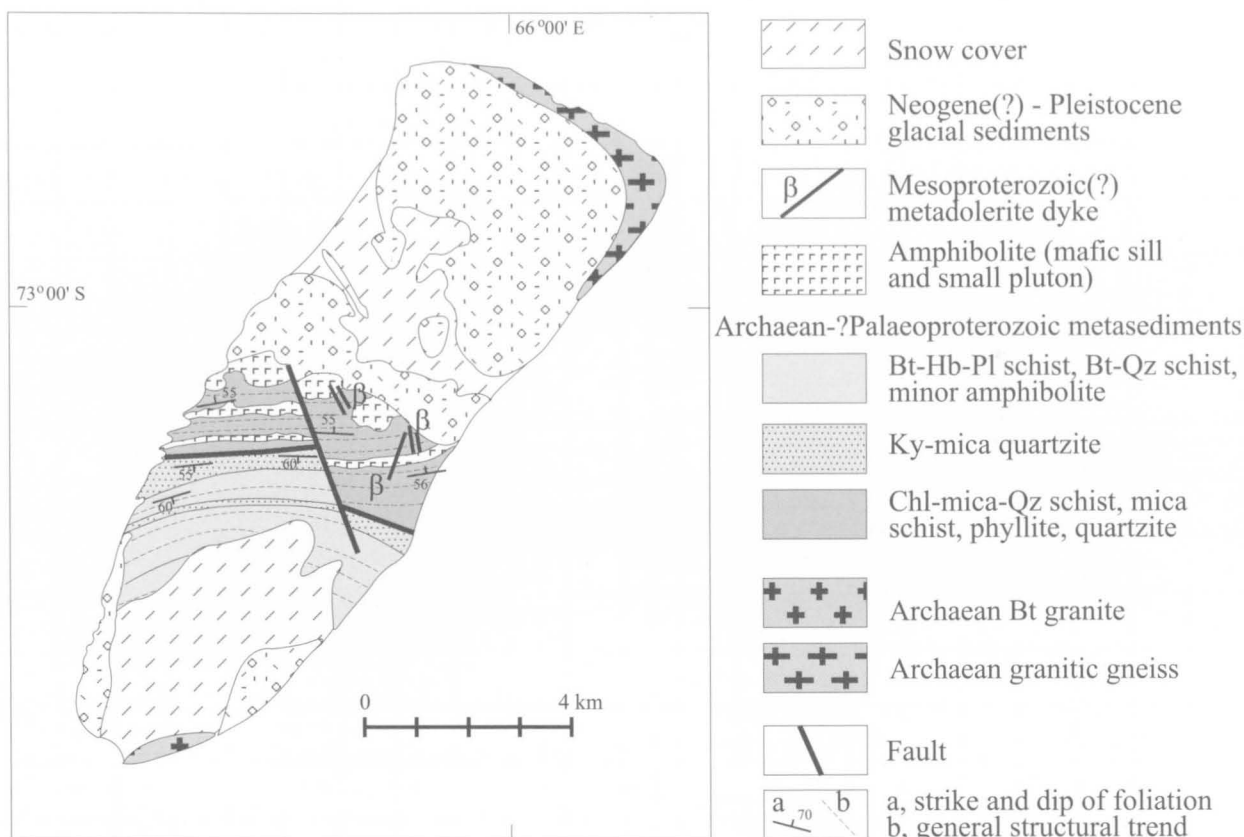


FIGURE 19

Geological sketch of Mount Rymill (after M.M. Polyakov & V.V. Samsonov, unpublished).

at Mount Borland and the isolated Komsomol'skiy Peak (150 km south of Keyser Ridge). More extensive metasediments, including quartzite, calcareous quartzite and pelitic schist, crop out at Blake Nunataks, Mount Twigg and Wilson Bluff. The presence at Mount Twigg of slightly discordant amphibolite layers is consistent with these rocks being the more strongly deformed equivalents of the Archaean granitic basement and cover rocks interpreted elsewhere in the SPCM. Metasediments interlayered with felsic gneiss at Mount Cresswell and Binders Nunataks are of uncertain age, but the presence of relict kyanite at the latter locality, and of secondary sillimanite \pm cordierite at both, suggests correlations with the Ruker Terrane rather than the Beaver-Lambert Terrane.

Somewhat lower grade pelitic and calcareous metasediments at northern Blake Nunataks and Mount Maguire may possibly overlie the more strongly deformed gneiss and quartzite exposed at the former locality. They may be part of a younger sedimentary sequence, as suggested by Tingey (1982b). Metasediments at southern Mount Maguire are interlayered with amphibolite of probable mafic igneous origin, whereas mafic rocks appear to be absent from the sequence at northern Mount Maguire. Hence, it is possible that the latter may be the somewhat higher grade equivalents of the Sodruzhestvo Series. However, the evidence is far from conclusive, and so all the Mount Maguire and Blake Nunataks metasediments have been tentatively correlated with the Menzies Series.



FIGURE 20

Probable Menzies Series metasediments; northern Mount Maguire. Darker beds are kyanite-staurolite-garnet-mica-quartz schist, and lighter beds are quartzite and mica quartzite. The stratigraphic position of these rocks is uncertain, and they were mapped as possible Sodruzhestvo Series by Tingey (1982b). Note the figures for scale.

Four members were distinguished at northern **Mount Maguire** (Ravich et al. 1978), namely, from bottom to top: (1) mica-quartz schist and quartzite, locally staurolite and kyanite-bearing; (2) staurolite-garnet schist; (3) epidote-mica-quartz schist, containing a 20 metre-thick gypsum-carbonate bed; and (4) quartz-albite schist, together about 2000 metres thick (Fig. 20). The mica-quartz schist sequence is overthrust by an interlayered garnet-hornblende-mica schist and mica-quartz schist unit some 250 metres thick, containing boudinaged amphibolite bodies (metabasite ?sills). The thrust plane gently dips to south (Fig. 165). The main metasedimentary sequence at northern Mount Maguire has many similarities (lithology, metamorphic grade, and the absence of granite) with Menzies Series metasediments at Mount Stinear. It differs in its more homogeneous semipelitic to arkosic protolith composition and apparent absence of conglomerate, as well as its metamorphosed mafic sills and dykes.

Metasediments (mica-quartz and epidote-mica-quartz schist containing metaconglomerate lenses) at northern Goodspeed Nunataks resemble some of the Mount Maguire rocks, and the presence of kyanite and staurolite suggests that they may represent a local variant of the Menzies Series. Alternatively, they could be a higher grade equivalent of the Sodruzhestvo Series, as mapped by Tingey (1982b).

Two lithologically distinct suites were distinguished in the **southern Mawson Escarpment**: one metasedimentary, and the other apparently meta-igneous (Kamenev et al. 1990). Both suites are strongly folded and sheared, and occur as tectonic slabs and nappes, so their thickness and relative abundance are difficult to assess. The metasedimentary suite consists mostly of quartzite and aluminous schist. Typical lithologies are: pure quartzite; garnet-biotite, hornblende-biotite, garnet-cummingtonite, magnetite-biotite-garnet, biotite-sillimanite, and tourmaline-muscovite-kyanite quartzite; sillimanite-garnet-biotite-plagioclase-quartz rock; and muscovite-garnet-biotite, staurolite-muscovite-biotite, garnet-kyanite-muscovite-biotite, garnet-hornblende, and garnet-staurolite schist. Minor marble, metaconglomerate and metagreywacke occur locally. All these rock types are interlayered and typically have a reddish or rusty colour.

The meta-igneous suite consists of various lithologies, with mafic and ultramafic schists being most prominent. The exposed thickness is between 200 and 800 metres. The most common rocks are mafic hornblende-plagioclase schist (various amounts of biotite, garnet, epidote, quartz and muscovite), lenses and well-rounded blocks of ultramafic amphibolite (actinolite or tremolite), quartz-plagioclase rock, quartzite and epidote-rich rock. The different lithologies are intercalated, and the suite has a pronounced layering. Kamenev et al. (1990) suggested that this suite represents a tectonic melange of metamorphosed igneous (presumably volcanic) rocks of ultramafic to intermediate and possibly felsic composition, and correlated it with ophiolite complexes. Alternatively, some possible cumulus geochemical features suggest an intrusive origin. Compositions are similar to certain metamorphosed mafic intrusive rocks in the Ruker Terrane, so derivation from a layered crustal intrusion cannot be

discounted. Until the nature and origin of its protoliths are better understood, this suite is tentatively included in the Menzies Series, whilst recognising that it may well represent a distinct rock unit.

The major sedimentary lithologies comprising the Menzies Series are: (1) pelitic metasediments (mica and garnet-mica schist and gneiss, commonly containing staurolite and/or kyanite); (2) quartzite; (3) calcareous metasediments; and (4) conglomerate. Mafic and ultramafic rocks comprise a minor, and possibly the lowermost, part of the composite Menzies Series section. The latter rocks are of uncertain origin and may either have been derived from plutonic protoliths, as suggested by geochemical data, or from volcanic protoliths, as favoured by one of the authors (ENK) on the basis of field observations.

Pelitic metasediments

Pelitic and psammo-pelitic schist and gneiss are interlayered with quartzite at all the localities mentioned above. Such rocks make up about 60 to 80 per cent of the Menzies Series (Ravich et al. 1978), occurring as interlayered beds from 30 centimetres to a few metres thick, or rarely as units 20 to 30 metres thick. Quartz (20–55%), biotite (5–40%), muscovite (up to 25%), chlorite (up to 10%), garnet (up to 25%, rarely 40%), staurolite (up to 23%), kyanite (up to 8%, rarely 20%), sillimanite (up to 15%), cordierite (up to 3%), and plagioclase (An₄₀₋₅₅, up to 20%) are common major constituents (Fig. 180A, B), although much of the chlorite is of retrograde origin (Fig. 180E), and secondary plagioclase (An₂₅₋₃₄) occurs at Mount Stinear. Accessory minerals comprise opaque minerals, rutile, zircon, titanite, epidote and tourmaline. Typical assemblages are:

quartz + biotite + muscovite ± chlorite,
quartz + biotite + muscovite + chlorite + garnet ± plagioclase,
quartz + biotite + muscovite + garnet ± plagioclase,
quartz + biotite + muscovite + chlorite + garnet ± staurolite ± plagioclase, and
quartz + biotite + muscovite + garnet + staurolite + kyanite ± plagioclase.

Metapelitic rocks at Cumpston Massif and Mount Stinear contain K-feldspar:

quartz + biotite + chlorite + staurolite + kyanite + plagioclase + K-feldspar,
quartz + biotite + garnet + plagioclase + K-feldspar, and
quartz + biotite + muscovite + garnet + plagioclase + K-feldspar.

Cordierite appears to have co-existed with kyanite (but not staurolite) in metapelite at Cumpston Massif (Fig. 180C, D).

Cummingtonite and anthophyllite are present in metapelite at Mount Stinear and the southern Mawson Escarpment, commonly forming late randomly orientated porphyroblasts.

The assemblage

quartz + biotite + garnet + cummingtonite ± plagioclase ± K-feldspar occurs at Mount Stinear, and
quartz + biotite + anthophyllite + cordierite + plagioclase ± garnet, and

TABLE 3. Chemical analyses of representative quartzites and metapelites of the Menzies Series

Sample no.	72280713F	72280750A	73281513	72280774	73281118	73281274	73281347
Locality	Mount Menzies	Mount Stinear	Mount Mather	Mount Stinear	Seavers Nunatak	Keyser Ridge	Mount McCauley
Lithology	Ky quartzite	Ms quartzite	Ms-St-Ky quartzite	Chl-Gt-St- Bt-Qz metapelite	Gt-Pl-Chl-Ms- Bt-St-Ky-Qz metapelite	Chl-Bt-Cld- Ms-Gt-St-Qz metapelite	Ky-St-Bt-Pl- Qz(-Si-Cd) metapelite
SiO ₂	94.20	89.10	92.20	58.40	67.80	53.40	59.10
TiO ₂	0.17	0.30	0.24	0.79	0.75	0.85	0.98
Al ₂ O ₃	4.62	7.68	6.58	18.43	17.77	26.47	24.91
Fe ₂ O ₃	<0.05	<0.05	<0.05	5.19	1.62	5.77	0.92
FeO	0.16	0.20	0.04	8.30	3.85	6.50	4.40
MnO	<0.01	<0.01	<0.01	0.11	0.12	0.09	0.06
MgO	<0.10	<0.10	<0.10	3.87	2.44	1.18	3.82
CaO	<0.01	<0.01	<0.01	0.29	0.60	0.27	0.30
Na ₂ O	0.05	0.30	0.05	0.17	0.70	0.37	0.80
K ₂ O	0.10	1.92	<0.01	2.70	2.46	2.18	2.24
P ₂ O ₅	0.01	0.01	0.03	0.16	0.11	0.11	0.11
H ₂ O ⁺	0.18	1.00	0.24	1.45	1.60	2.48	1.70
Rest	0.07	0.10	0.09	0.26	0.25	0.19	0.29
Total	99.56	100.61	99.47	100.12	100.07	99.86	99.63
V	11	41	12	192	143	155	217
Cr	203	167	155	682	424	189	648
Ni	25	7	1	232	153	60	185
Cu	10	<2	7	7	101	4	49
Zn	8	<2	4	64	119	71	107
Ga	6	10	8	21	23	35	33
Rb	5	52	1	114	105	134	92
Sr	9	59	4	22	153	57	156
Y	9	14	13	33	44	25	32
Zr	137	171	337	148	192	174	158
Nb	5	8	7	10	14	18	13
Sn	1	1	-	2	-	-	-
Ba	34	205	14	369	347	428	422
La	22	19	23	38	58	-	23
Ce	40	41	45	58	61	86	49
Pb	17	9	1	3	7	10	9
Th	10	8	11	7	9	35	8
U	2.0	1.0	2.5	2.0	2.0	4.0	3.0
K/Rb	166	307	-	197	194	135	202
(Ce/Y) _n	11.1	7.3	8.7	4.4	3.5	8.6	3.8
Th/U	5.0	8.0	4.4	3.5	4.5	8.8	2.7
Nb/Nb*	0.40	0.23	-	0.19	0.23	-	0.32
mg	-	-	-	45.4	53.0	24.4	60.7

mg = atomic 100Mg/(Mg + Fe²⁺).

quartz + biotite + muscovite + chlorite + cummingtonite + cordierite + plagioclase

in the southern Mawson Escarpment. Rare cordierite and sillimanite (fibrolite) in metapelite at these places, as well as the central Mawson Escarpment, may have been formed by metamorphism of kyanite + staurolite-bearing assemblages associated with emplacement of granitic intrusive rocks. However, the association quartz + biotite + muscovite + sillimanite + plagioclase + K-feldspar at Mount Borland appears to be a primary assemblage.

Metapelite at Mount Twigg contains:

quartz + biotite + muscovite + chlorite,

quartz + biotite + muscovite + sillimanite + plagioclase, and

quartz + biotite + muscovite + garnet + plagioclase + K-feldspar.

Sillimanite forms aggregates of fibrolite, and some secondary chlorite and carbonate are also present. Quartz + biotite + sillimanite + plagioclase + microcline occurs at Komsomol'skiy Peak. Metasediments at Binders Nunataks contain quartz + biotite + muscovite + garnet + plagioclase + K-feldspar + sillimanite, although sillimanite commonly partly replaces biotite, and some rocks contain relict kyanite.

Metapelite at Mount Newton contains the upper amphibolite-facies assemblage

quartz + biotite + garnet + sillimanite ± plagioclase ± K-feldspar (Fig. 178A). Some rocks also contain altered ?cordierite (chlorite + sericite). Biotite-orthopyroxene-garnet-hornblende-labradorite granulite may also be of sedimentary origin.

At Mount Newton (Fig. 183C, D) and more particularly at Mount Bird, metapelite contains retrograde chlorite and chloritoid-bearing assemblages:

quartz + muscovite + chlorite + chloritoid (± relict sillimanite and garnet), and

quartz + biotite + muscovite + chlorite + plagioclase ± K-feldspar.

Retrograde quartz + muscovite + chlorite + chloritoid metapelites are also common near the summit of Mount Menzies; some contain relict kyanite or staurolite.

Somewhat lower-grade metapelite at Keyser Ridge contains:

quartz + biotite + muscovite + garnet ± plagioclase, and

quartz + cummingtonite + garnet.

Moraine, of possible local derivation, near the summit of Keyser Ridge contains the assemblages (all in apparent equilibrium):

quartz + biotite + muscovite + chloritoid + staurolite + garnet,

quartz + biotite + muscovite + chloritoid + staurolite + ?kyanite, and

quartz + biotite + muscovite + staurolite + garnet + ?kyanite.

Minor chlorite has partly replaced staurolite, but here there is no evidence for the chloritoid being a retrograde phase (Fig. 180E). These rocks could therefore post-date the earlier high-grade metamorphism seen at Mounts Bird and Newton.

Typical assemblages at northern Blake Nunataks are:

quartz + biotite + muscovite + garnet ± plagioclase ± K-feldspar ± chlorite, and

quartz + biotite + muscovite + garnet + staurolite + kyanite.

The assemblage quartz + biotite + hornblende + garnet ± cummingtonite occurs at northern Mount Maguire.

Assemblages in metapelite at Mounts McCauley and Scherger include:

quartz + biotite + muscovite ± plagioclase ± K-feldspar, quartz + biotite + garnet + plagioclase ± cummingtonite, and

quartz + biotite + muscovite + kyanite + staurolite + plagioclase.

Contact metamorphosed metapelite at these localities contains:

quartz + biotite + muscovite + sillimanite + plagioclase, and

quartz + biotite + muscovite + sillimanite + cordierite + plagioclase.

Relict kyanite and staurolite may also be present. Sillimanite occurs as felted masses of fibrolite which replace biotite, muscovite, kyanite or staurolite (Fig. 182).

Andalusite was found at Mounts Stinear, Maguire, and Rymill as subhedral to euhedral crystals (3–4 mm across), partly replaced by chlorite, white mica and K-feldspar (Ravich et al. 1978; Grew 1982; V.S. Semenov,

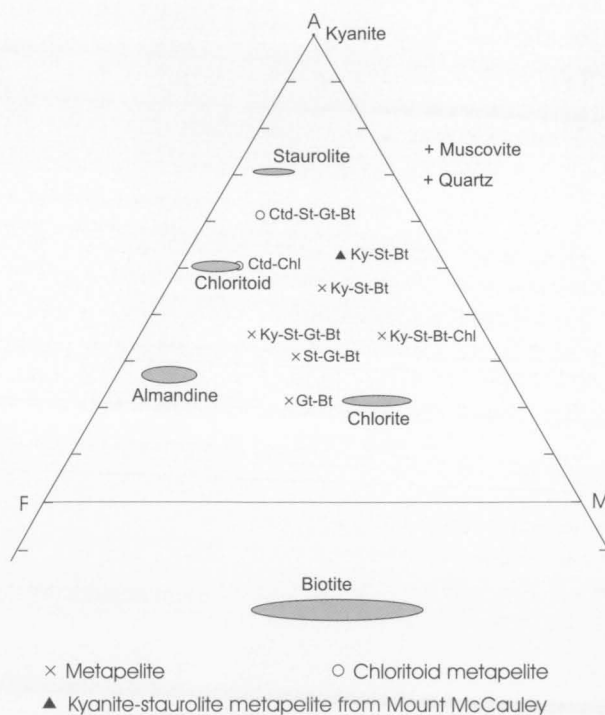


FIGURE 21

AFM diagram (after Winkler 1974) for late Archaean-Palaeoproterozoic Menzies Series metapelites, including retrograde chloritoid-bearing rocks from Mount Bird and Keyser Ridge, and kyanite-staurolite metapelite from Mount McCauley. $A = (Al_2O_3 - 3K_2O)/(Al_2O_3 - 3K_2O + MgO + FeO)$; $F = FeO/(MgO + FeO)$; $M = MgO/(MgO + FeO)$ (all as molecular proportions).

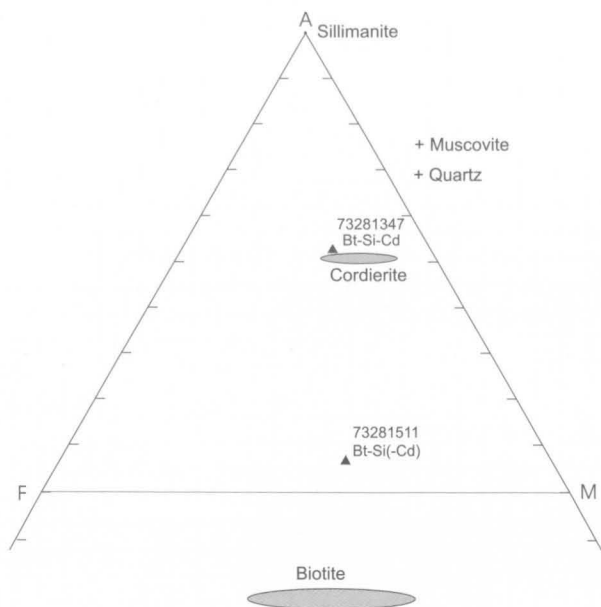


FIGURE 22
AFM diagram for contact metamorphosed metapelites from Mount McCauley. Sample 73281347 contains relict kyanite and staurolite and is also plotted on Figure 21.

unpublished data). Kyanite was found post-dating andalusite at Mounts Stinear and Maguire.

As in most pelitic sediments, CaO and Na_2O are relatively low but Al_2O_3 is high (Table 3). k (atomic $\text{K}/(\text{K}+\text{Na})$) values are mostly greater than 0.60, and mg mostly between 45 and 70. Metapelites with kyanite + staurolite + garnet + biotite-bearing assemblages are plotted on an AFM diagram (Fig. 21, after Winkler 1974). Retrograde chloritoid-bearing rocks have particularly low CaO and mg (20–25), but high Al_2O_3 (Table 3, Fig. 21)—features which appear to be necessary for the formation of chloritoid (Winkler 1974, p.205). Compositions of two contact metamorphosed pelites from Mount McCauley are plotted on Figure 22.

Sheraton (1980) showed that late Archaean to Palaeoproterozoic (in terms of probable depositional age) metapelites of the Ruker Terrane have, like most Archaean metapelites of Enderby Land, higher Cr and Ni contents than Mesoproterozoic metapelites of the NPCM–Mawson Coast area (Table 14). As noted below, late Archaean quartzites also have relatively high Cr. This may reflect differences in the amounts of mafic and ultramafic rocks in the respective source regions. On the rather limited data available, there are no other obvious differences in chemical composition between late Archaean–Palaeoproterozoic amphibolite-facies metapelites of the Ruker Terrane and the later Proterozoic granulite-facies metapelites of the Beaver–Lambert Terrane.

Psammitic metasediments

Massive quartzite layers crop out at Cumpston Massif, Mounts Borland, Mather, Menzies, Rymill and Stinear, the

southern Mawson Escarpment and Seavers Nunataks. They are commonly white, but some are pale to dark green, with greenish muscovite (?fuchsite). Apart from quartz, small amounts (<10% in total) of biotite, muscovite and chlorite (commonly retrograde) are present in many rocks. Kyanite is common in quartzite at Mounts Mather and Menzies, and at Mount Stinear it contains cummingtonite. Minor garnet, sodic plagioclase, K-feldspar, staurolite and actinolite occur at some localities; accessory minerals include rutile, opaque minerals, zircon, tourmaline, epidote and titanite. Retrogressed quartzite at Mount Menzies contains the assemblage quartz + muscovite + chlorite + chloritoid; relict kyanite is partly replaced by chloritoid, and pyrophyllite is present in one sample.

Thinner, commonly more impure beds of quartzite are interlayered with schist of various compositions in much of the Menzies Series. That at Blake Nunataks and Wilson Bluff has a marked brown-weathering appearance. Quartz + biotite + actinolite is the most common assemblage at Wilson Bluff, and diopside, epidote and muscovite may also be present. The occurrence of calc-silicate minerals suggests a more calcareous protolith than that of the massive white to green quartzite. Biotite, muscovite, garnet, albite and microcline occur in quartzite at Mounts Borland and Twigg. Impure quartzite in the southern Mawson Escarpment includes garnet–biotite, hornblende–biotite, garnet–cummingtonite, magnetite–biotite–garnet, biotite–sillimanite, and tourmaline–muscovite–kyanite quartzite. Quartzite also crops out at Binders Nunataks (minor albite and tourmaline) and Mount Cresswell (minor muscovite and tourmaline).

Major element contents (other than SiO_2) of the massive green to white quartzite units reflect the abundances of minor phases. Most trace elements are present at low concentrations, although Cr, Zr and Ba each reach several

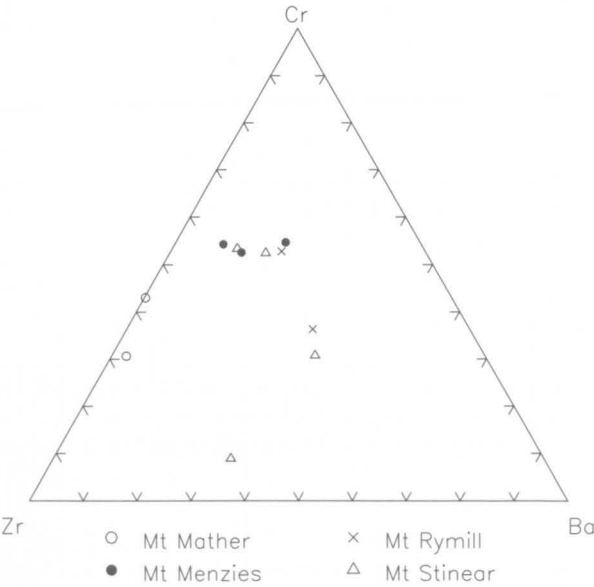


FIGURE 23
Cr–Zr–Ba plot for late Archaean Menzies Series quartzites.

hundred parts per million (Table 3). Ba and Zr are somewhat lower than average sandstone values, but Cr is relatively high (Table 4).

Table 4. Comparison of quartzite and average sandstone

	1	2	3
Cr	138	60	27
Zr	121	220	188
Ba	57	60	316

1. Average of 11 quartzites from the SPCM.
2. Average of 262 sandstones (Katchenkov 1967).
3. Average sandstone (Shiraki 1975; Erlank et al. 1978; and Puchelt 1972, respectively).

Cr contents are positively correlated with Al_2O_3 (i.e., total minor mineral content), but there is little correlation with K_2O (i.e., muscovite content). Neither is there any obvious correlation between Cr and green colouration. Zr contents probably reflect the distribution of zircon, and Ba that of muscovite. Macpherson (1958) and Danchin (1967) have shown that Archaean sediments tend to be more enriched in Cr than younger ones, possibly because of a higher proportion of mafic and ultramafic rocks in their source regions.

Six of eleven analysed quartzites, including all those from Mount Menzies, plot in a restricted field on a Cr–Zr–Ba diagram (Fig. 23), but the remaining samples show considerable scatter. Those from Mount Stinear are quite variable in composition, and those from Mount Mather have low Ba. These results suggest that the quartzite from Mount Menzies had a common source with at least some of that from Mounts Rymill and Stinear. However, there are also marked regional variations in composition. Clearly, much more extensive sampling would be necessary to investigate such regional variations and to adequately assess the use of chemical composition as a means of correlation.

Calcareous metasediments

Calcareous schist appears to be most abundant in the area between the Fisher and upper Lambert Glaciers, but also occurs in significant amounts at Mounts Menzies, McCauley and Stinear, and the southern Mawson Escarpment. The assemblages

quartz + biotite + actinolite + garnet,
quartz + garnet + epidote + carbonate, and
quartz + biotite + epidote + carbonate

occur at Mount Menzies, and

quartz + hornblende + epidote + plagioclase ± garnet,
quartz + hornblende + epidote + plagioclase ± diopside ± scapolite, and

quartz + biotite + chlorite + muscovite + epidote + carbonate

at Mount Stinear. Quartz + hornblende + epidote + plagioclase + titanite ± diopside ± biotite occurs as enclaves in granitic gneiss at Cumpston Massif. Quartz + biotite + hornblende + epidote + K-feldspar + carbonate + titanite schist, and marble, with minor quartz, biotite, epidote and magnetite, were found at Mount Bayliss by Trail (1963a). Titanite and opaque minerals are common

accessories in many of these rocks, and rutile, apatite and allanite have also been noted.

Quartz + actinolite + diopside + epidote + muscovite + titanite ± biotite is a typical assemblage at Mounts Borland and Twigg. Quartz + biotite + chlorite + hornblende/actinolite + carbonate ± plagioclase ± K-feldspar, and quartz + biotite + muscovite + chlorite + garnet + hornblende/actinolite + epidote are present in calcareous schist at northern Blake Nunataks and Mount Maguire. The assemblage quartz + hornblende + diopside + epidote occurs at Mount Cresswell. Prominent marble layers crop out at northern Blake Nunataks. Quartz, diopside, actinolite, biotite, plagioclase and scapolite occur in calc-silicate rocks from moraine at Komsomol'skiy Peak.

Calcareous quartzite and calc-silicate gneiss at Wilson Bluff contain the assemblages

quartz + diopside + plagioclase + titanite ± actinolite, and
quartz + actinolite + diopside + epidote + muscovite + titanite ± biotite.

Diopside is partly replaced by pale green actinolite in some rocks, and plagioclase is locally altered to clinozoisite, calcite and sericite.

Diopside is also a common constituent of calc-silicate schist at Mount McCauley:

quartz + actinolite/hornblende + diopside + epidote + microcline + titanite ± carbonate, and

quartz + actinolite/hornblende + diopside + epidote + garnet + plagioclase + carbonate + titanite. Amphibole includes both pale green actinolite and green hornblende.

Minor retrograde calc-silicate rocks at Mount Newton contain quartz + biotite + hornblende + epidote + plagioclase + carbonate + titanite. Quartz + biotite + epidote + carbonate, and quartz + diopside + albite + titanite (+ secondary hornblende) occur at Keyser Ridge.

A prominent white impure marble–calcareous schist at the southern end of the Mawson Escarpment is of uncertain age—either late Archaean or part of a younger sedimentary sequence. It may be younger than the early high-grade event exhibited by nearby felsic orthogneiss that contains isoclinal intrafolial folds and migmatitic structures not found in the nearby calcareous rocks. However, associated pelitic and calcareous schists are similar to ?late Archaean Menzies Series metasediments elsewhere in the Ruker Terrane, and are cut by metadolerite dykes. The marble is up to 200 metres thick, and consists of dolomite with large (several cm) randomly orientated euhedral crystals of colourless tremolite. The associated metasediments include grey impure marble layers, with prominent curved rosettes of dark grey tremolite, as well as quartz, ?phlogopite, and scattered grains of pyrite; rusty-weathering, crumbly impure marble contains rosettes of pale green tremolite, up to 15 centimetres across, commonly surrounded by epidote-rich zones. Calcareous schist consists of quartz, actinolite or tremolite, epidote, biotite, chlorite, carbonate, and minor titanite and opaque minerals. One of the authors (ENK) suggested that the thick marble bed could represent a metamorphosed ultramafic body.

Some amphibolite layers may be of sedimentary origin (para-amphibolite), although the majority were clearly derived from mafic igneous rocks (see below). Those with significant amounts of diopside and unusually calcic



FIGURE 24

Contact of Menzies Series metaconglomerate with mica-staurolite-quartz schist; Mount Stinear. The hammer is 0.7 m long.

plagioclase (e.g., bytownite) are likely to be metamorphosed Ca-rich sediments, and are commonly associated with calcareous schist. Similarly, some garnet amphibolite may be of sedimentary origin as it commonly has abundant modal quartz (up to 10%) and is compositionally layered. More massive layers with less than five per cent garnet are probably ortho-amphibolite.

Metaconglomerate

Metaconglomerate occurs at Mount Stinear and in the southern Mawson Escarpment. Most clasts in metaconglomerate at Mount Stinear are between one and 10 centimetres across, but many exceed 0.5 metres and a few reach 1.5 metres. Quartzite and plagioclase-quartz rock account for 95 to 98 per cent of the clasts, but other lithologies include mafic hornblende schist and garnet-mica schist. The clasts are strongly deformed and elongated (Fig. 24), and are sometimes very difficult to distinguish from the matrix which consists of mica, garnet-mica, or garnet-biotite-hornblende schist (20–50 volume % of the rock). Metaconglomerate in the southern Mawson Escarpment forms lenses up to 15 metres thick with an internal layering, and contains up to 30 volume per cent of quartzite and amphibolite pebbles. The pebbles are highly deformed and enclosed in a schistose biotite-garnet-muscovite-quartz matrix.

Mafic and ultramafic schists of the southern Mawson Escarpment

The presumably meta-igneous suite of the southern Mawson Escarpment consists mainly of a variety of high-Mg mafic to ultramafic schists. The most common rock is mafic hornblende-plagioclase schist (amphibolite), with various amounts of biotite, garnet, quartz, muscovite and epidote. Blocks of ultramafic rocks, some 10 centimetres to 10 metres across, are concentrated in relatively narrow zones (up to 20 m thick) enclosed in mafic schist. They include ultramafic amphibolite, talc-anthophyllite or talc-tremolite schist, and calcite-chlorite-talc schist. The rocks consist of amphibole (actinolite, tremolite or

anthophyllite), magnetite, rare relict pyroxene and olivine, and secondary talc, serpentine, epidote, phlogopite, carbonate, chlorite and titanite. They are commonly schistose—although massive varieties also occur—and medium to coarse grained. Textures are nemato- to lepidogranoblastic, or rarely fibroblastic.

The extreme degrees of alteration of these rocks makes estimates of their primary compositions highly uncertain, but SiO_2 contents (mostly 47–57%) are more comparable with those of mafic than ultramafic rocks (Fig. 27). However, CIPW norms of nine samples include between 75 and 83 per cent pyroxene (Di + Hy), suggesting derivation from pyroxenite protoliths (orthopyroxenite or, most cases, websterite). Low TiO_2 , Al_2O_3 , Na_2O , and K_2O , high MgO, Cr and Ni, relatively high SiO_2 , and variable FeO and CaO (Table 5, Fig. 29) are all consistent with this possibility. Two other analysed rocks are strongly Ol-normative, suggesting metamorphism of peridotitic (or possibly olivine gabbroic) protoliths. Many samples have relatively high Fe, as well as Mg—a feature of many Archaean mafic to ultramafic (picritic) rocks, and attributed by Francis et al. (1999) to a more Fe-rich Archaean mantle source. The Mawson Escarpment rocks differ from high-Mg mafic to ultramafic metavolcanics at Mount Ruker in their lower TiO_2 , Al_2O_3 , and alkalis, and higher CaO—although their source characteristics, as quantified by ratios of many incompatible elements, seem to be generally similar and enriched in LILE (Fig. 30). They have higher than chondritic CaO/TiO_2 (15–40), $\text{CaO}/\text{Al}_2\text{O}_3$ (0.7–4.8), and Zr/Y (up to 7.4), lower Ti/Zr (37–83), highly variable $\text{Al}_2\text{O}_3/\text{TiO}_2$ (3–58), and plot in the peridotitic komatiite field on an Al-(Fe+Ti)-Mg plot (Fig. 33). Most of these features can be attributed to cumulus processes involving pyroxene that can produce large changes in Ca/Ti, Ca/Al, and Al/Ti ratios. It is therefore possible that most, if not all, the Mawson Escarpment rocks may be of intrusive rather than volcanic origin. A sequence of mafic to ultramafic schists in the middle part of the southern Mawson Escarpment is cut by metamorphosed high-Mg mafic dykes. Zircon from a similar dyke from the southernmost Mawson Escarpment yielded a TIMS Pb-Pb model age of about 2375 Ma (Mikhalsky et al. 1992), suggesting that the schist may be of Archaean age.

LATE ARCHAEOAN-PALAEOPROTEROZOIC(?) METAVOLCANIC AND METASEDIMENTARY ROCKS (RUKER SERIES)

This unit corresponds to the Ruker Series of Ravich et al. (1978) and to the lower part of the Sodruzhestvo Series of Kamenev et al. (1990). It is typically composed of low to medium-grade (biotite subfacies of the greenschist facies) metavolcanic and metasedimentary rocks that crop out at Mount Ruker, and possibly Mounts Seddon, Rymill and Stinear. Age relationships with Archaean granite at Mount Ruker are equivocal, but there is some indirect evidence that the supracrustal rocks form a cover sequence (see above). One of the authors (LVF) suggested the presence of a fossil weathering zone overlying granite at Mount Ruker. Metasediments at Mount Ruker are noteworthy for the occurrence of banded ironstone (jaspilite). Ironstone also occurs in higher-grade (epidote-

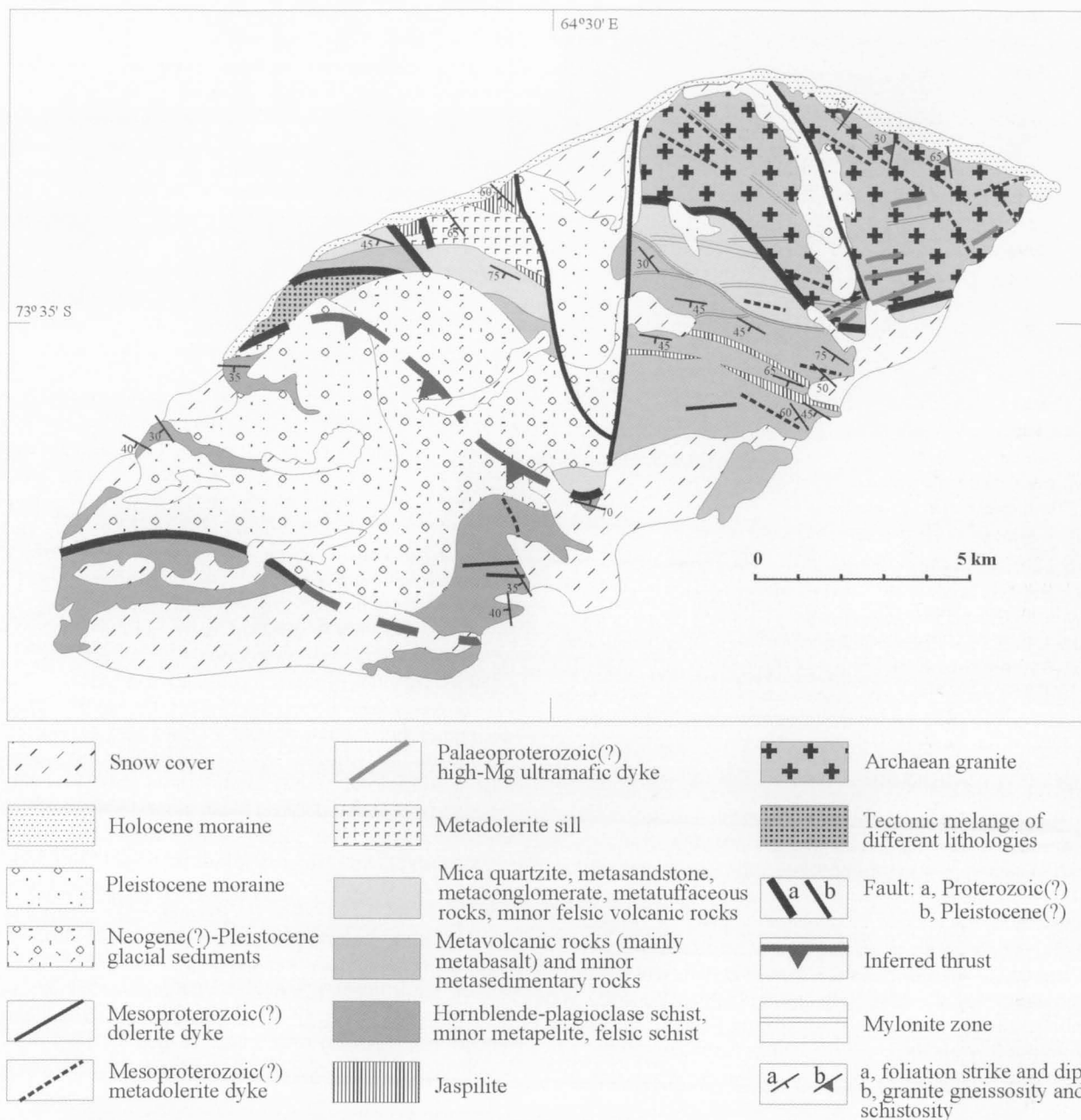


FIGURE 25

Geological sketch map of Mount Ruker.

amphibolite to almandine-amphibolite facies) Menzies Series metamorphics at Mount Stinear, where ferruginous quartzite, with alternating magnetite–hematite–quartz and garnet–quartz–magnetite laminae, is interlayered with kyanite–staurolite–garnet schist (Ravich et al. 1978). Jaspilite occurs as clasts in moraine on the western side of Beaver Lake. Mafic to ultramafic schists in the southern Mawson Escarpment are of somewhat higher grade than, and show significant geochemical differences to, mafic metavolcanic rocks at Mount Ruker (see below), so these sequences cannot be directly correlated.

At **Mount Ruker** (Fig. 25), two compositionally diverse medium-grade sequences were distinguished: a presumed lower volcanic sequence and a presumed upper volcanic–sedimentary sequence. All these rocks occur as

tectonic slabs, concordant with the foliation, which suggests a dominant role of tectonic stacking and overthrusting. In the southern part of Mount Ruker, higher-grade (epidote-amphibolite facies) metamorphic rocks probably overthrust the lower grade volcanic–sedimentary sequence. These rocks are mainly biotite–epidote–hornblende schist (up to 80%) and mica–chlorite–epidote-bearing siliceous or calcareous schist (20%).

The volcanic sequence is composed mainly of dark green or greyish-green mafic to felsic chlorite-actinolite-mica schist, black slate, phyllite of a wide range of composition, and banded ironstone. Metabasalt (some with globular structures) and chlorite–actinolite schist derived from mafic volcanic rocks constitute about 40

percent of the outcrops, metamorphosed intermediate to felsic volcanic rocks 20 per cent, metadolerite sills 25 per cent, and banded ironstone 15 per cent. Quartz-rich schist (metamorphosed sandstone) and mica quartzite beds are also present. Banded ironstone forms highly deformed lenses, beds from 0.2 to 4 metres thick, and bodies up to 400 metres thick within the lower part of the exposed sequence; intermediate to felsic volcanics are confined to the upper part. In spite of their highly varied lithological composition, the strata have a more or less homogeneous field appearance and comprise just a few compositionally distinct members some hundred metres thick. The mafic rocks are commonly of fine-grained lepidogranoblastic texture, but coarse-grained relict ophitic or doleritic textures are present locally. The sequence contains thick metadolerite bodies (probably sills, see below) that have transitional rather than sharp contacts with mafic schist, suggesting a close genetic relationship between volcanic and intrusive rocks.

The volcanic–sedimentary sequence is composed of magnetite–mica–quartz slate (metapelite), chlorite–mica–quartz slate and quartzite (metamorphosed tuffite, tuffogenic sandstone, and sandstone), (chlorite)–calcite–mica–plagioclase–quartz slate (felsic metavolcanic rock), metaconglomerate, and tuffaceous breccia. Quartz, sericite, calcite, biotite, albite and chlorite are the major constituents. The rocks are mostly grey to brown, or rarely black, with a fine- to medium-grained lepidogranoblastic texture. A relict psammitic texture may commonly be discerned. Pelitic magnetite–mica–quartz schist accounts for 65 per cent, tuffaceous rocks for 15 per cent, mica quartzite for 12 per cent, and metadolerite for eight per cent of the exposed sequence. Psammite predominates in the lower third of the sequence, and pelitic and/or siliceous (?chert) metasediments in the overlying part. Conglomerate forms layers up to 20 centimetres thick or beds 10 to 20 metres thick. The conglomerate clasts consist of coarse-grained quartz or fine-grained quartzite. A rhythmic intercalation of the various lithologies was reported by Ravich et al. (1978).

U–Pb dating of zircons from two metamorphic rocks (albite–chlorite–mica–quartz slate and quartzite, of presumed volcano–sedimentary and sedimentary origin, respectively) from Mount Ruker was carried out. The zircons are mostly rounded, anhedral, pink to light magenta grains, or slightly recrystallised grain fragments, similar to those in the deformed granite at northern Mount Ruker (see above). Hence, granitic basement was probably a major source for the sedimentary rocks in this succession, although the rounded shape of most zircon grains suggests that they have been affected by the same major metamorphic event as the deformed granite. The zircon fractions show considerable scatter (Fig. 26), suggesting derivation of detrital zircon from different sources, and possibly also multistage U loss during different Proterozoic and/or Cambrian events. Nevertheless, all zircon fractions seem to have crystallised between 3200 and 2500 Ma ago (or possibly even later, as the zircon fractions are highly discordant, and the c.2500 Ma intercept may represent a maximum estimate of the time of metamorphism). T_{DM}^{Nd} model ages of these and similar rocks are mostly 2800 to 2700 Ma, with one sample giving 3150 Ma, thus supporting their derivation from late Archaean source regions. The similarity of zircon ages and

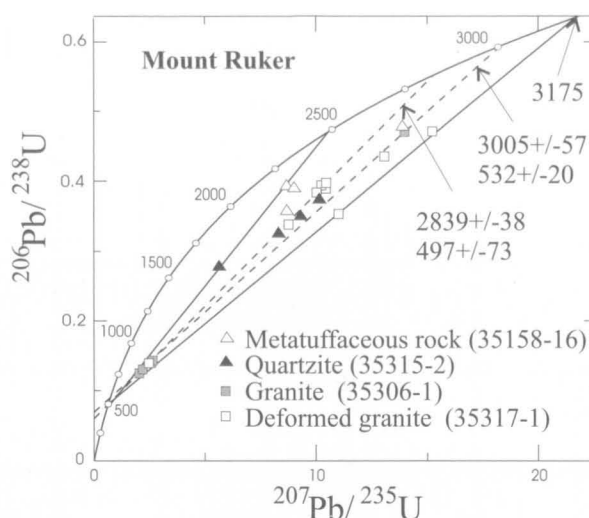


FIGURE 26

U–Pb concordia diagram for zircons from biotite granite and metasedimentary rocks from Mount Ruker.

T_{DM}^{Nd} model ages for the granitic rocks suggests that juvenile continental crust formed between about 3300 and 3000 Ma. However, the highly deformed partly tuffaceous metasediments at Mount Ruker must be younger than about 2800 to 2700 Ma to account for their T_{DM}^{Nd} model ages. The similar zircon morphologies in the metasediments and deformed granite suggest that both were affected by the same late Archaean(?) deformation (implying that the sedimentary protoliths are older than this). In view of the intensity of the c.500 Ma event (many of the zircon fractions plot close to the c.500 Ma lower intercept, and all the others are highly discordant), which could also account for the similar zircon morphologies, additional studies are needed to confirm an Archaean age for the Ruker Series rocks.

Metavolcanic rocks

Metavolcanic rocks at Mount Ruker are represented by green chlorite–actinolite–mica schist of various compositions, and altered mafic to felsic volcanic rocks. Chlorite, carbonate (siderite or dolomite), quartz, sericite, biotite, plagioclase, actinolite and hornblende are the major constituents, although these phases occur in widely varying amounts. Chlorite, biotite, hornblende or actinolite may separately account for as much as 30 to 60 volume per cent of the rock. Magnetite, tourmaline, fuchsite, zoisite, serpentinite, chloritoid, titanite, pyrite and garnet are minor phases. The colour index is mostly between 40 and 80, but rare ultramafic varieties range from 90 to 100. All lithological types form thin intercalated beds or layers up to a few metres thick, consistent with a volcanic origin. Relict globular structures, two to 10 millimetres across, consist of calcite and quartz. Microfelsite, thought to represent recrystallised volcanic glass, occurs in a few rocks and comprises up to 25 volume per cent. Some felsic rocks contain relict plagioclase megacrysts, which probably represent deformed phenocrysts—also supporting a volcanic origin.

The metavolcanic rocks show extremely wide variations

TABLE 5. Chemical analyses and CIPW norms of representative metavolcanic rocks of the Ruker Series and ultramafic schists from the southern Mawson Escarpment

Sample no.	35512-10-9	35307-1	35314-2	35155-12	35625-1	35622-3	35316-3	33503-3	33040-7	33104-10
Locality	Mount Ruker	Mount Ruker	Mount Ruker	Mount Ruker	Mount Ruker	Mount Ruker	Mount Ruker	S. Mawson Escarpment	S. Mawson Escarpment	S. Mawson Escarpment
Lithology	Car-Chl-Ac ultramafic schist	Mafic schist	Pl-Car-Chl-Bt-Qz mafic schist	Bt-Car-Qz mafic schist	Chl-Qz-Zo-Hb mafic schist	Car-Ms-Bt-Pl-Qz felsic schist	Car-Ms-Bt-Qz felsic schist	Ultramafic schist	Talc-tremolite schist	Bt-Ac schist
Composition	Ultramafic	Basalt	Basalt	Basaltic andesite	Andesite	Dacite	Rhyolite	Ultramafic	Ultramafic	Ultramafic
SiO ₂	32.00	48.50	50.00	53.05	58.95	69.80	72.40	42.05	48.00	52.75
TiO ₂	0.23	1.88	0.97	0.68	0.61	0.54	0.37	1.96	0.30	0.23
Al ₂ O ₃	4.70	14.15	12.80	13.05	11.74	12.08	11.60	6.30	2.50	4.45
Fe ₂ O ₃	0.94	4.49	4.86	2.59	1.90	1.91	1.57	*15.70	*12.72	*9.56
FeO	8.50	9.50	6.25	7.75	7.10	3.97	1.75	-	-	-
MnO	0.12	0.20	0.13	0.22	0.11	0.05	0.04	0.16	0.16	0.13
MgO	21.93	6.31	4.37	7.39	7.00	0.74	1.89	17.53	18.72	18.45
CaO	2.65	7.85	7.07	8.00	6.41	1.37	1.47	8.66	12.01	10.28
Na ₂ O	0.04	1.80	2.78	3.68	1.30	1.45	2.12	0.33	0.23	0.44
K ₂ O	0.71	1.74	1.74	1.04	1.44	5.07	2.48	1.10	0.05	1.05
P ₂ O ₅	0.05	0.17	0.08	0.09	0.10	0.13	0.14	0.15	0.03	0.03
LOI	28.14	3.74	8.98	2.88	2.74	1.97	4.23	5.88	4.91	2.65
Rest	0.78	0.16	0.17	0.18	0.21	0.00	0.16	0.46	0.78	0.38
Total	100.79	100.49	100.20	100.60	99.61	99.08	100.22	100.28	100.41	100.40
Q	-	0.79	3.20	-	18.66	34.97	43.21	-	-	0.71
C	-	-	-	-	-	2.03	3.09	-	-	-
Or	4.20	10.28	10.28	6.15	8.51	29.96	14.65	6.50	0.30	6.20
Ab	0.34	15.23	23.52	31.14	11.00	12.27	17.94	2.79	1.95	3.72
An	10.55	25.39	17.31	16.02	21.95	5.95	6.38	12.46	5.64	7.07
Di	1.81	10.31	14.38	18.91	7.51	-	-	23.74	43.08	34.87
Hy	15.89	27.11	17.45	17.36	25.44	9.14	8.65	14.56	32.36	41.34
Ol	36.05	-	-	3.92	-	-	-	24.92	6.69	-
Mt	2.26	3.27	2.57	2.44	2.13	1.37	0.76	3.42	2.77	2.08
Il	0.44	3.57	1.84	1.29	1.16	1.03	0.70	3.72	0.57	0.44
Ap	0.12	0.40	0.19	0.21	0.24	0.31	0.33	0.36	0.07	0.07
Sc	-	-	-	-	-	-	-	24	40	12
V	101	387	229	257	214	-	53	240	160	46
Cr	4195	164	107	352	409	-	169	2300	3300	1000
Co	82	51	37	48	42	-	5	110	92	50
Ni	918	63	65	102	114	-	48	420	2000	1700
Rb	37	44	58	17	86	-	107	-	-	-
Sr	100	171	93	173	123	-	135	-	-	-
Y	6	33	27	18	17	-	26	22	15	5
Zr	26	106	115	65	118	-	156	140	23	37
Nb	1	8	4	4	11	-	13	-	-	-
Ba	63	156	625	295	463	-	561	-	-	-
Pb	4	7	11	10	14	-	48	-	-	-
Th	1	<1	10	<1	12	-	19	-	-	-
mg*	83.9	49.4	47.8	62.0	63.9	22.5	57.1	73.4	78.4	82.7

mg* = atomic 100Mg/(Mg + 0.85Fe(total)); LOI = loss on ignition; * total Fe as Fe₂O₃.

in chemical composition, from ultramafic to felsic (Table 5, Figs 27–29). Hydrous, often secondary, mineral phases are common, so that loss on ignition (LOI) values are high, particularly for the mafic (typically 3–10%) and ultramafic (up to 28%) rocks. Such highly altered rocks have clearly undergone significant compositional changes, including SiO_2 , during metamorphism. Their primary compositions therefore are uncertain. The relatively mobile alkalis (Na_2O and K_2O) show particularly large variations, with some samples having less than 0.2 per cent Na_2O —much lower than any likely magmatic value. Conversely, two rocks contain more than nine per cent K_2O . A few samples with very low Na_2O and K_2O have either undergone extreme alteration, or could possibly be of sedimentary origin or have a significant sedimentary component. SiO_2 contents of the mafic to intermediate rocks are mainly between 44 and 58 per cent, so most samples are classified as basalt, basaltic andesite, or andesite on an alkalis– SiO_2 plot (Fig. 27), with basalt being the most abundant. Two ultramafic rocks (not shown) have very low SiO_2 (25 and 32%). Most samples are subalkaline, and the higher alkali contents of others may well be metamorphic effects. Felsic metavolcanics have a distinct range of SiO_2 content (68–76%), with dacitic to rhyolitic compositions. The presence of this compositional gap, and the fact that both mafic and felsic rocks have similar mg values suggest that they are not genetically related. Moreover, the two groups were not found interlayered, except tectonically, which is consistent with them representing distinct volcanic suites.

On most major and trace element plots, the mafic to

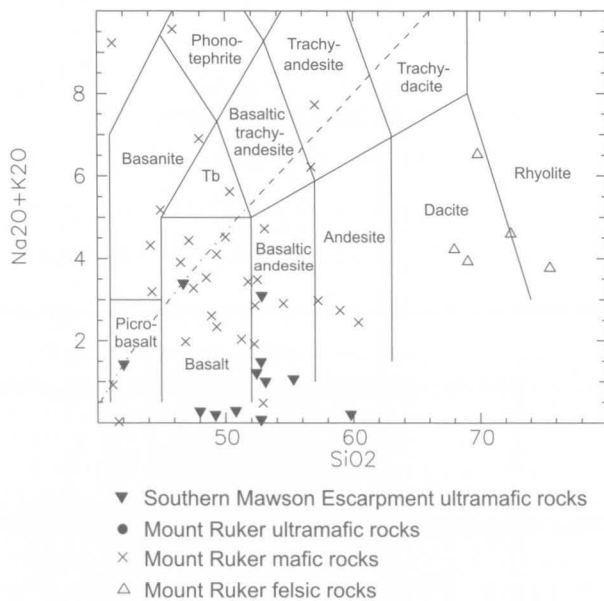


FIGURE 27

Alkalis– SiO_2 plot for metavolcanic rocks of the Ruker Series and ultramafic schists from the southern Mawson Escarpment. Two low- SiO_2 ultramafic rocks from the Ruker Series are not plotted here, but appear on Figures 28–30 and 33. The fields correspond to the volcanic rock classification of Le Bas et al. (1986), and the dashed line divides the alkaline (upper) and subalkaline fields of Irvine & Baragar (1971). Tb, trachybasalt.

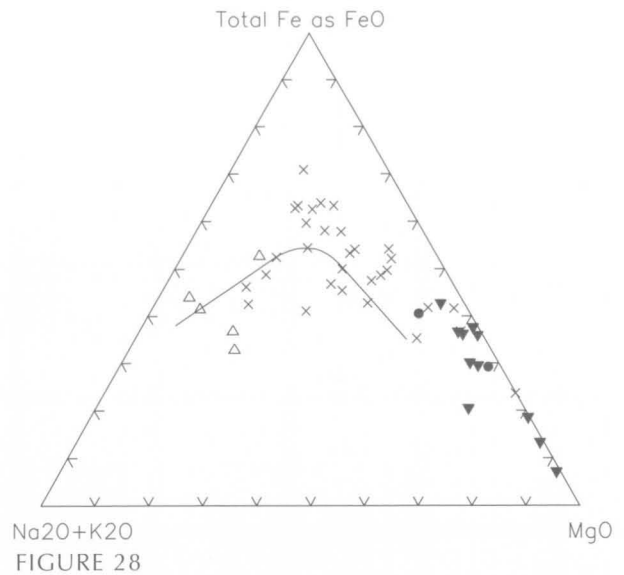


FIGURE 28

A($\text{Na}_2\text{O}+\text{K}_2\text{O}$) – F(total FeO) – M(MgO) diagram for metavolcanic rocks of the Ruker Series and ultramafic schists from the southern Mawson Escarpment. A line divides the tholeiitic (upper) and calc-alkaline fields of Irvine & Baragar (1971). Symbols as in Figure 27.

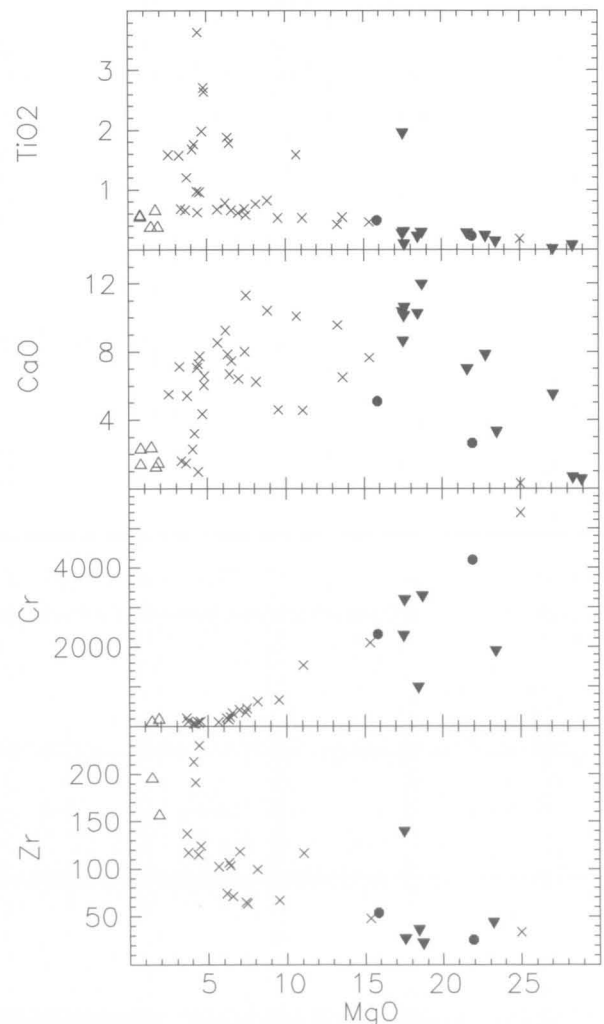


FIGURE 29

MgO variation diagrams for metavolcanic rocks of the Ruker Series and ultramafic schists from the southern Mawson Escarpment. Symbols as in Figure 27.

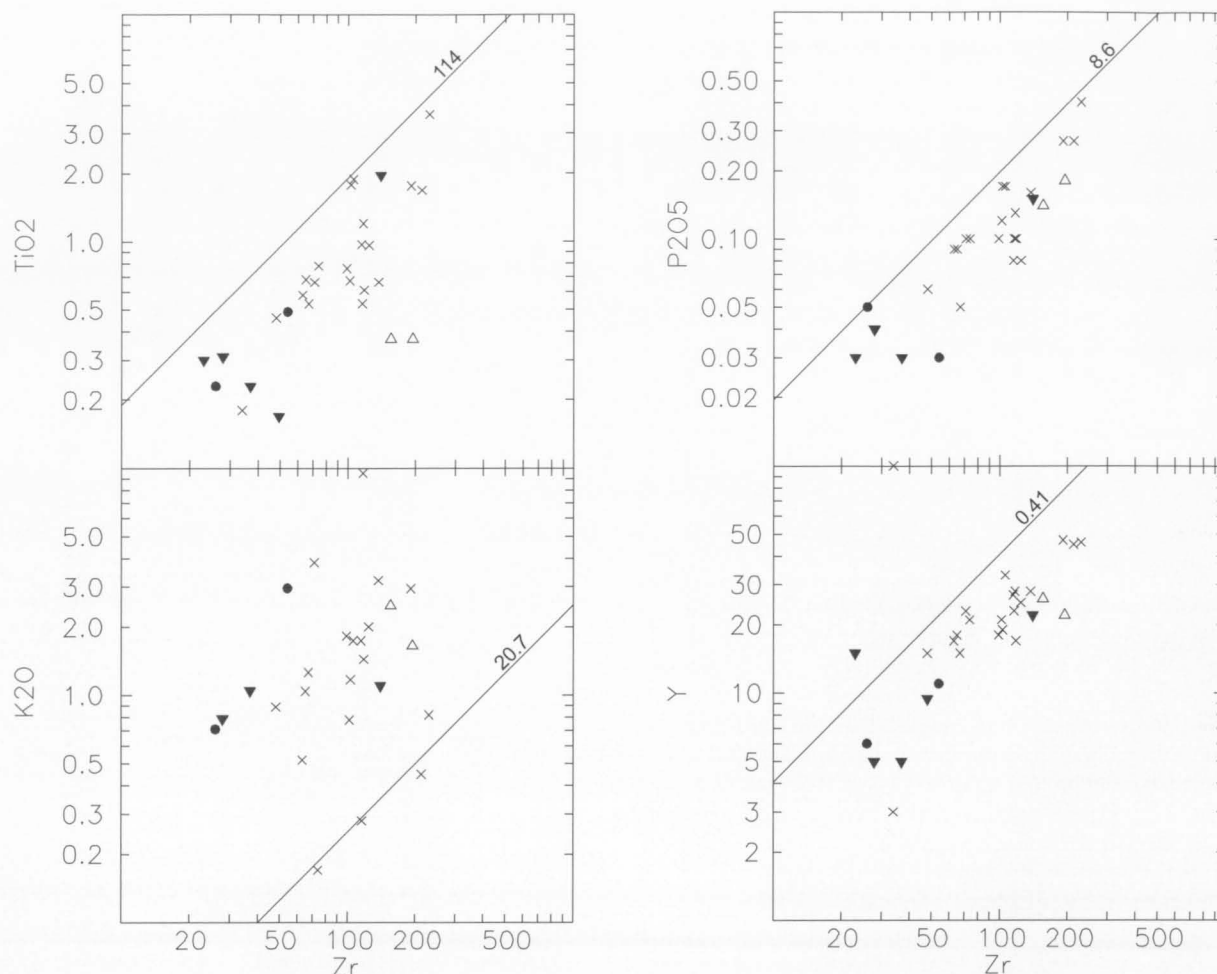


FIGURE 30

Logarithmic plots of various incompatible elements against Zr for metavolcanic rocks of the Ruker Series and ultramafic schists from the southern Mawson Escarpment. The lines of unit slope have constant element/Zr ratios; estimated primordial mantle ratios (after Sun & McDonough 1989) are indicated. Symbols as in Figure 27.

intermediate metavolcanic rocks form more or less coherent trends suggesting a broadly co-genetic origin. Strong positive correlations of MgO with Ni and Cr are consistent with olivine control, through fractional crystallisation and/or partial melting processes, and clinopyroxene (\pm plagioclase) fractionation was probably important below about seven per cent MgO (Fig. 29). Magnetite may also have fractionated, buffering TiO_2 in some rocks. Most mafic to intermediate metavolcanics have similar ratios of many minor and trace elements, supporting a co-genetic, or at least closely related, origin. For example, Ti/Zr , P/Zr and Y/Zr are all significantly lower than chondritic ratios (Fig. 30), suggesting derivation of the parent magma(s) from a Zr-rich, possibly depleted, mantle source, whereas Nb/Zr is close to chondritic. In contrast, consistently higher than chondritic Ba/Zr and K/Zr , albeit with much scatter, suggests melting of LILE-enriched lithospheric mantle and/or involvement of a LILE-rich (possibly subduction-derived) fluid. Such near-constant element ratios over large ranges of element abundances could reflect either separation of minerals that did not cause significant fractionation of these elements, or various degrees of partial melting. Either way, the elements in question behaved near-incompatibly. TiO_2 , in particular, shows a rather irregular variation trend (Fig.

29), implying that a range of parent melts of somewhat different composition was involved.

Spidergrams show a general coherence for relatively compatible elements (Nb to Y), but more scatter for the most incompatible elements (Pb to K) and Na (Fig. 31). This shows that the former elements were probably more or less immobile during metamorphism and that any petrogenetic conclusions based on abundances of these elements should have some validity. In contrast, LILE show wide variations consistent with alteration. Few LREE data are available, but two rocks apparently have only small Sr anomalies and a third has a large negative anomaly, suggesting at least some plagioclase fractionation. Bearing in mind likely K mobility, most rocks appear to display marked negative Nb anomalies consistent with the involvement of LILE-enriched, possibly subduction-modified mantle source regions. Although Phanerozoic plate tectonic models do not necessarily apply to Archaean tectonics, such an assumption may not be unreasonable (Windley 1998). Mafic metavolcanics show smooth REE patterns (Fig. 32) with only small Eu anomalies and slight LREE enrichment reflected by $(\text{La/Yb})_n$ between 2.3 and 4.6—values typical of calc-alkaline basalts of destructive plate margins (Wilson 1989). Such REE patterns suggest partial melting of an enriched

mantle source, and high heavy REE abundances (Yb_n values ~ 10) imply that the source was garnet-free.

Some rocks, including the two low- SiO_2 ultramafics, have high MgO (10–25%), Cr (1530–5390 ppm), and Ni (385–1445 ppm), as well as relatively low TiO_2 , Na_2O , P_2O_5 , HFSE and, to some extent, CaO (Table 5). The very low Na_2O may be partly a metamorphic feature, however. In terms of the Al–(Fe+Ti)–Mg plot of Jensen (1976), the more magnesian metavolcanic rocks plot mainly in the basaltic komatiite field, whereas most samples plot in the tholeiite field (Fig. 33), consistent with an AFM plot (Fig. 28). However, the high-Mg rocks have certain major and trace element ratios that are rather different to typical chondritic or komatiitic values (Nesbitt & Sun 1980). Zr/Y (3–5) is higher, and Ti/Zr (30–57), CaO/TiO_2 (6–20), and CaO/Al_2O_3 (0.4–0.8) are lower, although Al_2O_3/TiO_2 (18–22) is similar. Thus, these rocks may be more akin to boninitic than typical komatiitic rocks, and derived from previously depleted rather than fertile mantle. Alternatively, low CaO/TiO_2 and CaO/Al_2O_3 , as well as high Zr/Y , could be due to clinopyroxene fractionation or even alteration. Whatever the origin of these high-Mg volcanics, it appears to have been rather different to that of typical greenstone belt rocks, but further analytical work is necessary to more fully elucidate their petrogenesis.

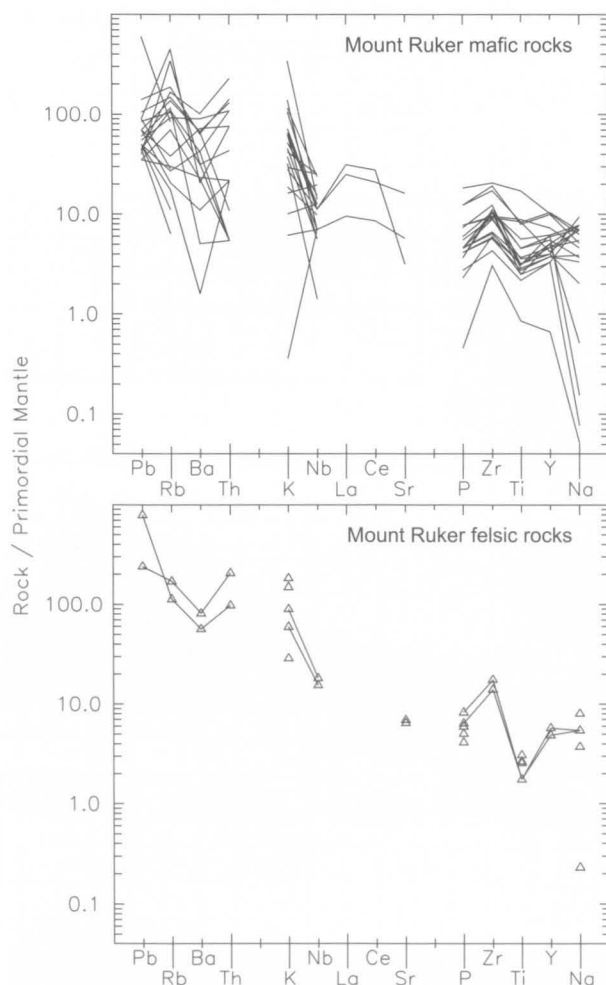


FIGURE 31
Spidergrams for metavolcanic rocks of the Ruker Series.

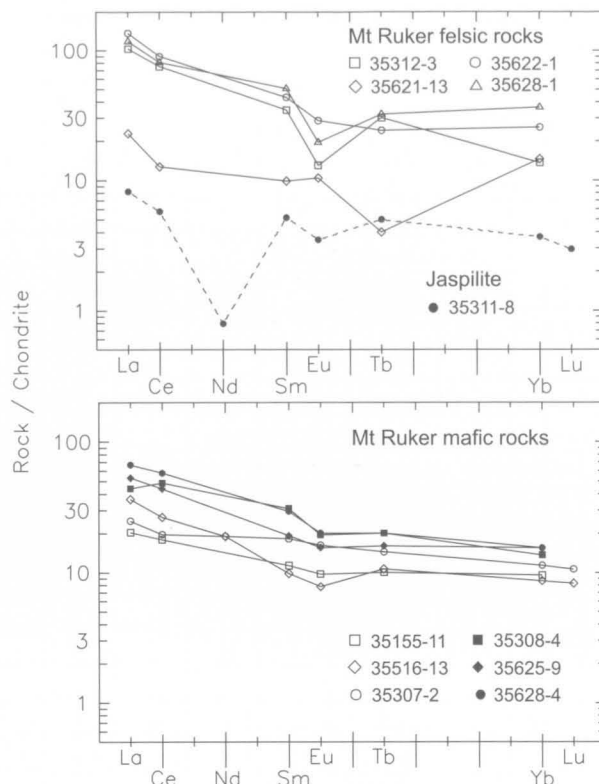


FIGURE 32
Chondrite-normalised rare-earth element abundance plots for metavolcanic rocks of the Ruker Series.

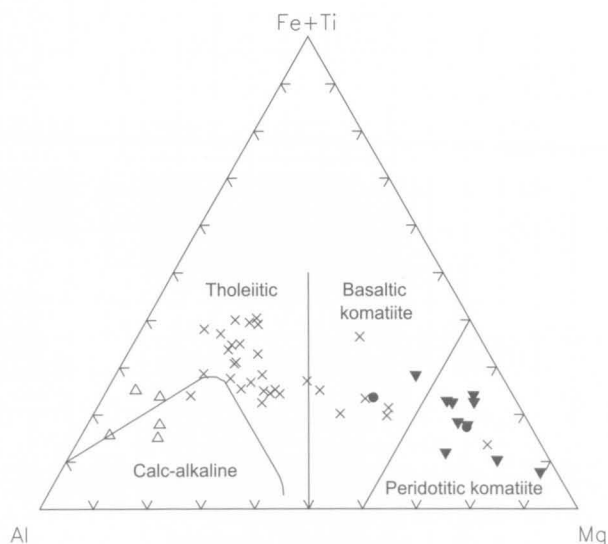


FIGURE 33
Atomic Al – (Fe+Ti) – Mg plot for metavolcanic rocks of the Ruker Series and ultramafic schists from the southern Mawson Escarpment. The fields correspond to the sub-alkaline igneous rock classification of Jensen (1976). Symbols as in Figure 27.

Felsic metavolcanic rocks have somewhat different more irregular spidergram patterns, with marked Ti and P depletions (Fig. 31) consistent with either extensive fractional crystallisation or partial melting of crustal rocks. Although only a few trace-element analyses are available, their close similarity suggests that the effects of alteration are small. In contrast to the mafic volcanics, some felsic rocks show marked negative Eu anomalies, suggesting plagioclase fractionation. Three of the four samples analysed are more strongly REE-enriched with $(La/Yb)_n$ of 3.5 to 8.0 (Fig. 32). Compared with Archaean granitic rocks of the Ruker Terrane, the felsic volcanics have less fractionated REE patterns and generally higher HREE concentrations, implying a somewhat different (?crustal) source. However, the relatively young T_{DM}^{Nd} model ages (c.2800–2700 Ma) obtained for tuffaceous rocks at Mount Ruker, compared to 3270–3420 Ma for the Mount Ruker granite, suggest the involvement of either a younger crustal component or juvenile mantle material in the petrogenesis of these rocks.

Pelitic metasediments

Greenschist-facies metasediments at Mount Ruker include black slate, phyllite, metagreywacke and quartz–chlorite–muscovite schist. The rocks commonly contain quartz, biotite, muscovite and carbonate; plagioclase and actinolite may also be present.

Psammitic metasediments

Recognisable detrital grains in quartzite are

predominantly quartz, with rare magnetite and carbonate. Quartz grains range from well rounded to angular, which suggests derivation of at least some rocks from a proximal felsic crystalline source. They are mostly monocrystalline, 0.1 to 1.0 millimetres across, and are marginally recrystallised to form an interlobate texture. The fine-grained carbonate–epidote–mica–quartz matrix accounts for up to 40 volume per cent of the rock. Microfelsite is a minor matrix constituent, and forms small isolated pods and lenses in some rocks. The matrix of some rocks may possibly represent highly deformed and metamorphosed feldspar or lithic fragments, and some beds consist of meta-arkose or greywacke. However, such rocks constitute only a minor part of the sequence. Quartz-rich metasandstone strongly predominates, providing evidence for a continental, rather than an orogenic or magmatic arc, source area (Dickinson et al. 1983).

Calcareous metasediments

Calcareous schist at Mount Ruker typically contains quartz, carbonate, muscovite, biotite and chlorite, with lesser amounts of plagioclase, opaque minerals and tourmaline. Minor ?talc–carbonate rocks are also present. At least some of the carbonate, which commonly occurs as large grains up to one centimetre across, is dolomite. Such rocks grade compositionally into some metavolcanic and metapelitic rocks, from which they differ in their much higher carbonate content.

Banded ironstone

Banded ironstone (jaspilite) occurs as part of the



FIGURE 34

Banded ironstone (jaspilite) on headlands dipping southwards beneath a sequence of greyish-green slate and metagreywacke; northwestern side of Mount Ruker.

TABLE 6. Chemical analyses of representative metasedimentary rocks of the Ruker Series.

Sample no. Lithology	35157-1 Meta- tuffite	35627-13 Meta- tuffite	35622-1 Meta- sandstone	35619-3 Impure quartzite	35634-8 Quartzite	35627-16 Quartzite	73281717 Banded ironstone	73281999 Banded ironstone
SiO ₂	52.80	53.95	71.45	74.55	86.60	96.55	29.80	32.60
TiO ₂	0.74	0.43	0.67	0.60	0.21	0.06	<0.01	0.08
Al ₂ O ₃	12.70	8.70	10.15	9.90	5.45	1.20	0.28	2.12
Fe ₂ O ₃	4.14	8.71	1.79	1.41	0.57	0.88	*65.60	*60.10
FeO	7.75	15.49	3.97	4.19	1.65	0.51	-	-
MnO	0.12	0.12	0.07	0.04	0.03	0.02	0.09	0.09
MgO	6.10	3.18	1.77	0.81	0.77	0.05	2.08	1.49
CaO	3.98	1.51	2.15	0.60	1.34	0.12	0.26	0.10
Na ₂ O	0.78	0.03	1.70	1.86	0.54	0.01	<0.05	<0.05
K ₂ O	1.35	1.11	2.13	3.29	1.07	0.23	0.36	0.78
P ₂ O ₅	0.12	0.20	0.20	0.21	0.20	0.01	<0.01	0.05
LOI	9.10	5.61	2.74	1.36	1.03	0.12	-	-
Rest	0.20	0.08	0.14	0.19	0.10	0.15	0.00	0.03
Total	99.88	99.12	98.93	99.01	99.56	99.81	98.47	97.44
V	189	109	-	2	45	18	-	-
Cr	397	131	32	25	131	158	-	-
Co	45	36	9	13	3	-	-	-
Ni	107	21	12	11	16	16	-	-
Cu	-	-	-	-	-	-	4	239
Zn	-	-	-	-	-	-	11	22
Rb	40	22	104	152	53	7	-	-
Sr	248	30	23	17	76	7	-	-
Y	30	14	67	86	10	7	-	-
Zr	128	78	350	521	195	47	-	-
Nb	10	8	21	27	4	1	-	-
Ba	276	132	413	691	240	990	-	-
La	-	-	45	-	-	-	-	-
Ce	-	-	78	-	-	-	-	-
Pb	15	16	6	14	14	20	<1	10
Th	19	8	23	12	8	-	-	-
mg	58.4	26.8	44.3	25.6	45.4	14.9	-	-

mg = atomic 100Mg/(Mg + Fe²⁺); * total Fe as Fe₂O₃.

predominantly volcanic sequence at Mount Ruker (Fig. 34). The main jaspilite body has an apparent thickness of about 400 metres, but thinner beds are interlayered with chlorite–carbonate–schist, calcareous quartzite, metasandstone, metasilstone and metabasic rocks above and below the main body (Ravich et al. 1978). The sequence is tightly folded on a microscopic to mesoscopic scale (England & Langworthy 1975; Fig. 167). Aeromagnetic data suggest that jaspilites extend along a total strike length of about 120 kilometres under the ice to the Mount Mather area (Soloviev 1972; Ravich et al. 1978, 1982). The Mount Ruker jaspilite resembles the miogeosynclinal Lake Superior type of iron formation (Gross 1970), although the presence of abundant volcanic

rocks suggests comparison with the eugeosynclinal Algoma type of environment.

The jaspilite consists of microfolded alternating quartz-rich and magnetite-rich layers, ranging from one millimetre to several centimetres in thickness. Magnetite + hematite contents range from 25 to 50 percent, with magnetite being more abundant. Carbonate (siderite, ankerite, dolomite and calcite: commonly 5–10%) and dark blue strongly pleochroic riebeckite (up to 20%) are commonly present. Microcline, albite, biotite, pyrite and garnet (?spessartine) are of more restricted occurrence, and some rocks contain small amounts (up to 2%) of stilpnomelane, bright green ?minnesotaite and apatite. Grew (1982) has also reported the occurrence of

TABLE 7. Chemical analyses and C.I.P.W. norms of representative amphibolites, metadolerite sills, and dolerite and metadolerite dykes from the Ruker Terane.

Sample no.	35621-2	35512-21-5	73281252	73281300E	73281921	72280856	73281929	91286350	91286354	73281077	91286352	91286355	73281927
Locality	Mount Ruker	Mount Ruker	Mount Menzies	Blake Nunataks	Mount Twigg	Mount Ruker	Cumpston Massif	Mawson Escarpment	Mawson Escarpment	Mount Rymill	Mawson Escarpment	Mawson Escarpment	Cumpston Massif
Lithology	Metadolerite sill	Metadolerite sill	Amphibolite	Bt amphibolite	Amphibolite	Dolerite dyke	Meta- dolerite dyke	Meta- dolerite dyke	Meta- dolerite dyke	High-Mg metadolerite dyke	High-Mg metadolerite dyke	High-Mg metadolerite dyke	High-K metadolerite dyke
SiO ₂	49.80	52.50	54.70	47.70	49.60	49.00	49.90	49.67	49.12	47.30	51.24	45.09	51.30
TiO ₂	0.57	0.69	0.11	3.67	3.03	1.94	1.02	2.05	1.50	0.35	0.55	2.71	2.37
Al ₂ O ₃	18.40	14.70	15.59	13.55	12.13	13.30	14.79	13.18	13.64	15.12	12.52	9.59	11.20
Fe ₂ O ₃	1.78	5.47	0.98	2.37	2.62	1.58	1.99	1.85	2.91	1.15	1.19	2.68	3.13
FeO	6.60	5.65	5.75	12.30	13.40	12.20	8.95	12.24	11.03	8.10	9.04	12.78	9.35
MnO	0.11	0.14	0.15	0.19	0.23	0.22	0.20	0.20	0.22	0.15	0.16	0.17	0.20
MgO	5.83	6.42	7.46	6.45	5.48	5.86	8.03	6.09	5.93	14.39	10.95	12.80	4.66
CaO	9.75	7.95	11.32	9.74	9.70	10.83	12.33	10.39	10.48	10.30	8.97	6.67	9.03
Na ₂ O	3.22	2.08	1.90	2.35	2.05	2.30	1.65	2.28	1.74	1.15	1.82	1.46	1.55
K ₂ O	0.42	0.80	0.29	0.54	0.62	0.36	0.38	0.42	1.06	0.16	0.66	2.25	5.21
P ₂ O ₅	0.06	0.10	0.03	0.44	0.29	0.19	0.13	0.19	0.18	0.05	0.09	0.37	0.41
H ₂ O ⁺	-	-	1.40	0.56	0.74	1.40	0.76	-	-	2.15	-	-	0.80
CO ₂	-	-	-	-	-	-	-	-	-	-	-	-	0.55
LOI	3.49	3.54	-	-	-	-	-	1.36	2.16	-	2.78	3.39	-
Rest	0.15	0.14	0.11	0.22	0.21	0.17	0.14	0.32	0.27	0.23	0.32	0.48	0.26
Total	100.18	100.18	99.79	100.08	100.10	99.35	100.27	100.24	100.24	100.60	100.29	100.44	100.02
O=F,S,Cl	0.00	0.00	0.00	0.00	0.00	0.00	0.00	0.04	0.02	0.00	0.02	0.02	0.00
Total	100.18	100.18	99.79	100.08	100.10	99.35	100.27	100.20	100.22	100.60	100.27	100.42	100.02
Q	-	6.82	7.84	0.43	4.26	1.25	0.62	1.94	1.56	-	0.91	-	-
Or	2.48	4.73	1.71	3.19	3.66	2.13	2.25	2.48	6.26	0.95	3.90	13.30	30.79
Ab	27.25	17.60	16.08	19.89	17.35	19.46	13.96	19.29	14.72	9.73	15.40	12.35	13.12
An	34.51	28.41	33.15	24.83	22.06	24.90	31.83	24.49	26.28	35.62	24.04	12.97	8.22
Di	11.04	8.55	18.48	17.01	20.17	22.92	23.30	21.43	20.41	12.16	16.09	14.37	28.21
Hy	12.55	25.91	19.13	22.47	21.40	19.77	22.55	21.26	21.94	21.77	33.13	11.52	4.64
Ol	5.43	-	-	-	-	-	-	-	-	15.00	-	22.32	4.93
Mt	1.98	2.56	1.60	3.49	3.81	3.29	2.60	3.36	3.30	2.21	2.44	3.67	2.94

Il	1.08	1.31	0.21	6.97	5.75	3.68	1.94	3.89	2.85	0.66	1.04	5.15	4.50
Ap	0.14	0.24	0.07	1.04	0.69	0.45	0.31	0.45	0.43	0.12	0.21	0.88	0.97
S	-	-	-	-	-	-	-	800	400	-	400	500	-
Sc	-	-	-	-	-	-	-	39	38	-	39	26	-
V	198	242	115	365	438	342	294	376	426	122	203	287	242
Cr	460	232	205	166	115	97	172	208	151	741	990	780	99
Ni	116	88	164	102	77	68	116	112	108	554	215	544	65
Cu	-	-	2	51	189	239	69	281	185	30	40	76	<2
Zn	-	-	55	137	152	114	90	182	142	72	86	163	182
Ga	-	-	14	20	24	21	15	23	20	11	12	21	21
Rb	13	29	8	13	14	8	4	10	13	7	22	92	140
Sr	204	155	126	484	226	182	151	198	221	76	117	150	183
Y	11	18	18	26	37	29	19	35	26	9	17	29	79
Zr	33	84	31	162	181	111	56	149	117	29	66	225	271
Nb	4	6	1	11	9	6	3	11	15	1	<2	19	18
Ba	-	135	42	117	77	81	41	102	174	15	172	741	660
La	1.8	-	7	9	10	6	3	14	15	2	13	28	31
Ce	4.3	-	19	21	35	18	11	32	35	6	24	53	67
Nd	-	-	-	-	-	-	-	22	16	-	12	28	-
Pb	6	14	2	6	3	2	3	3	4	1	<2	4	16
Th	-	9	1	2	2	1	<1	<2	<2	<1	3	3	8
U	-	-	0.5	5.0	6.0	1.0	<0.5	0.5	<0.5	<0.5	1.0	<0.5	3.5
K/Rb	268	229	301	345	368	374	789	349	677	190	249	203	309
(Ce/Y) _n	1.0	-	2.6	2.0	2.4	1.6	1.5	2.3	3.4	1.7	3.5	4.6	2.1
Ba/Zr	-	1.61	1.35	0.72	0.43	0.73	0.73	0.68	1.49	0.52	2.61	3.29	2.44
Ce/Zr	0.13	-	0.61	0.13	0.19	0.16	0.20	0.21	0.30	0.21	0.36	0.24	0.25
Nb/Zr	0.12	0.07	0.03	0.07	0.05	0.05	0.05	0.07	0.13	0.03	-	0.08	0.07
Nb/Nb*	0.64	-	0.10	0.96	0.69	0.78	0.47	0.88	0.71	0.33	-	0.44	0.22
Sr/Sr*	-	-	-	-	-	-	-	0.56	0.68	-	0.51	0.29	-
mg*	59.8	56.0	70.2	48.4	42.2	47.4	61.1	47.9	47.7	76.8	69.4	63.9	44.5

mg* = atomic 100Mg/(Mg + 0.85Fe(total)); Sr/Sr* = Sr/(0.5(Ce+Nd)), all element concentrations primordial mantle normalised.

yellow-green aegirine. There appears to be a complete gradation between jaspilite and black slate.

Total Fe content of jaspilites ranges from 25 to 55 per cent, with an average of 35 per cent (Table 6). Cu, Pb and Zn contents appear to be low, except for sample 73281999 which contains about 10 per cent pyrite and has 239 ppm Cu. For comparison, three samples of ferruginous quartzite from Mount Stinear average only 22 per cent Fe. In view of the relatively low grade and remote location of these deposits, economic development is extremely unlikely in the foreseeable future (Tingey 1990). A single REE analysis of Mount Ruker jaspilite shows very low REE abundances and, apart from extreme Nd depletion, a smooth normalised pattern broadly similar to those of the mafic metavolcanic rocks (Fig. 32). This suggests that a volcanic component was involved in jaspilite formation, which was co-genetic with the metabasaltic rocks.

LATE ARCHAEOAN-MESOPROTEROZOIC MAFIC INTRUSIVE ROCKS

Amphibolite

Concordant amphibolite bodies, as well as lower grade mafic layers, are widespread in late Archaeoan to Palaeoproterozoic rocks of the Ruker Terrane. They are commonly interlayered with metasedimentary rocks, and mostly up to a few metres thick, but range up to 100 metres or so in places (e.g., Mounts Bayliss, Ruker and Seddon). Such rocks occur in both the Mawson Orthogneiss and Menzies Series, but their compositional similarities suggest that they represent highly deformed mafic dykes and sills. Contact alteration zones may sometimes be distinguished (especially at Mount Rymill), although these are usually obliterated by subsequent deformation.

The typical assemblage is amphibole (pale green to brownish-green hornblende, actinolite, or rarely riebeckite: 10–70, but mostly 40–60%), plagioclase (commonly oligoclase or andesine-labradorite: 15–50%), quartz (generally <10%, but up to 25% in amphibolite-facies rocks), opaque minerals (up to 6%), and biotite (mostly <5%, but up to 15% in amphibolite-facies rocks). Titanite and apatite are common minor constituents, and epidote/clinozoisite and chlorite (up to 15–20%) are present in some rocks. Garnet (up to 10%) amphibolite and clinopyroxene amphibolite occur at Mount Twigg, garnet amphibolite at Mounts Cresswell (Fig. 181) and McCauley, and cumingtonite is present in amphibolite at Mount Newton. Amphibolite at many places (e.g., Mounts Bayliss, Menzies and Stinear, and Cumpston Massif) contains pale green acicular or prismatic hornblende or actinolite. In contrast, dark green to brownish-green hornblende and granoblastic-polygonal textures are more typical of slightly higher-grade amphibolites at Mounts Bird, Borland, Newton and Twigg, southern Blake Nunataks and Keyser Ridge. Some amphibolite is strongly foliated, particularly where significant amounts of aligned biotite are present. A 200 metre-thick subconcordant amphibolite body exposed on the eastern cliffs of Mount Seddon (Ruker 1963) has not been studied in detail.

Most concordant amphibolite bodies are petrographically similar to the more strongly recrystallised Palaeo- or Mesoproterozoic metadolerite dykes in the Ruker Terrane, described below. They are probably of similar mafic intrusive origin (sills or deformed dykes), although intrusive contacts and igneous textures are rarely preserved. Stages in the progressive deformation of mafic dykes to concordant amphibolite bodies are well displayed in cliffs at Cumpston Massif. Although many concordant amphibolite bodies are probably the deformed and metamorphosed equivalents of these dolerite dykes, some are clearly older. For example, concordant amphibolite and mafic granulite layers pre-date dolerite dyke emplacement at Mount Newton. This is the only known locality where mafic granulite which pre-dates the Mesoproterozoic(?) M_2 metamorphism is exposed. Possibly of Archaeoan age, it consists of plagioclase (45%), greenish-brown hornblende (30%), clinopyroxene (15%), orthopyroxene (5%), quartz (5%), and minor biotite. At Keyser Ridge, some amphibolite layers contain pale green acicular amphibole and others have dark greenish-brown equidimensional hornblende, suggesting the presence of two distinct generations of mafic body. Both concordant and discordant amphibolite bodies crop out at several localities (e.g., Mounts Bird, Menzies, and Rymill). Some of the former may represent sills, as at Mount Menzies. Although most amphibolite bodies are probably metamorphosed intrusive rocks (dolerite or gabbro), others could be of volcanic origin like the mafic metavolcanic rocks of the Ruker Series. As noted above, some compositionally layered amphibolites may be of Ca-rich sedimentary origin.

Most of the analysed amphibolite layers are of tholeiitic composition (Figs 35, 36) and have very similar trace element characteristics (incompatible-element ratios) to the mostly amphibolitised dolerite (metadolerite) dykes in the Ruker Terrane (Table 7; Fig. 37), as well as to group II dolerites of Enderby Land and the Vestfold Block (Sheraton 1984; Sheraton et al. 1987a). This feature is consistent with at least some being the strongly deformed

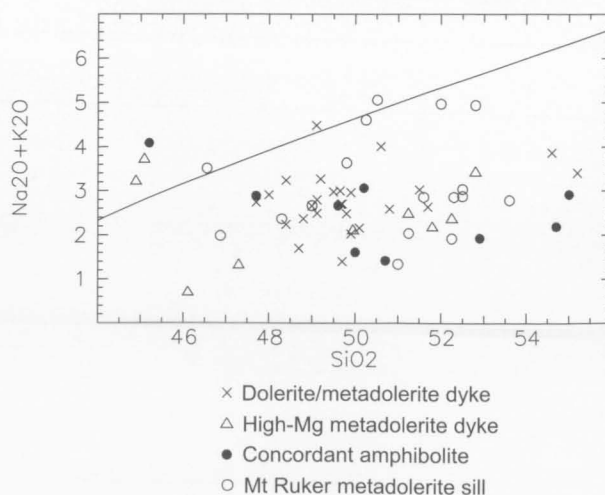


FIGURE 35

Alkalies-SiO₂ plot for concordant amphibolites, metadolerite dykes and metadolerite sills of the Ruker Terrane. A line divides the alkaline (upper) and subalkaline fields of Irvine & Baragar (1971).

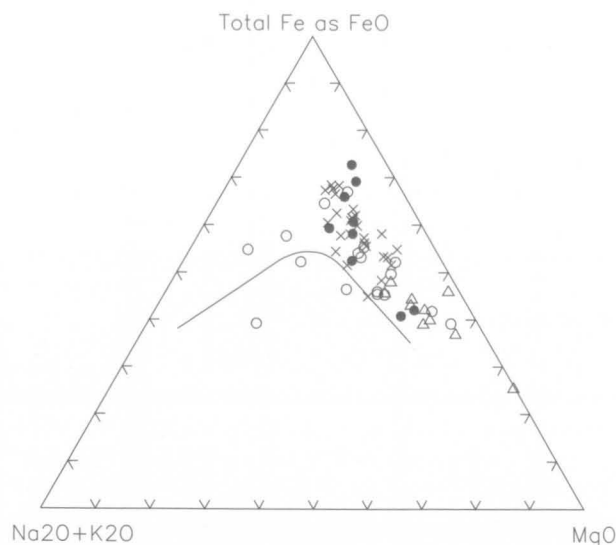


FIGURE 36

AFM diagram for amphibolites, metadolerite dykes, and metadolerite sills. A line divides the tholeiitic (upper) and calc-alkaline fields of Irvine & Baragar (1971). Symbols as in Figure 35.

and metamorphosed equivalents of these dolerite dyke suites. There is more scatter for some minor elements on variation diagrams compared to the metadolerite dykes, but no evidence for significant metamorphic depletion of any except certain LILE (K, Rb, Ba, etc.). Thus, some amphibolites have apparently lost Rb (relative to K) and possibly Ba, as well as Th, whereas a few with significant amounts of biotite (4–7%) are enriched in K, Rb, Ba and Pb (Sheraton 1984).

Two relatively magnesian ($mg^* = \text{atomic } 100\text{Mg}/(\text{Mg} + 0.85 \times \text{total Fe}) = 70\text{--}71$) amphibolites from Mount Menzies have strongly Q-normative basaltic andesite compositions with relatively low TiO_2 , FeO and Ti/Zr, and high LILE/Zr, LREE/Zr and Ce/Y (Table 7). An even more siliceous amphibolite from Mount Mather has similar compositional characteristics. Assuming these are not metamorphic features, these rocks cannot be genetically related to most of the metadolerite dykes, but may well be related to certain high-Mg dykes (see below). Alternatively, they may represent a distinct phase of intrusive (or extrusive) activity, possibly related to the Mount Ruker metadolerite sills or mafic metavolcanic rocks. They may even have been derived from volcanogenic sediments.

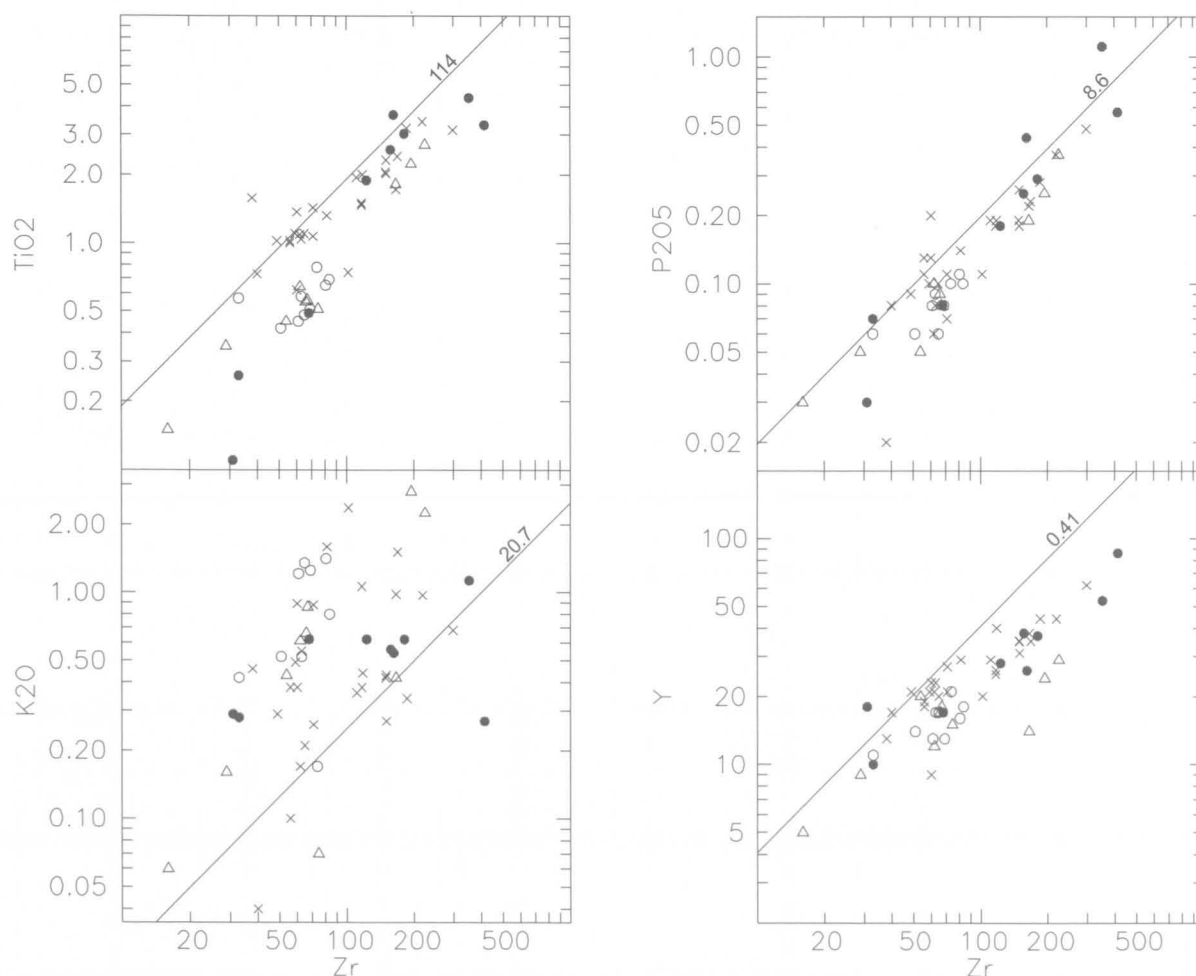


FIGURE 37

Logarithmic plots of various incompatible elements against Zr for amphibolites, metadolerite dykes and metadolerite sills. Lines of estimated primordial mantle ratios (after Sun & McDonough 1989) are indicated. Symbols as in Figure 35.

Metadolerite sills of Mount Ruker

A metamorphosed 30–40 metre-thick metadolerite sill at Mount Ruker has given K–Ar ages between 1040 and 830 Ma (A.Ya. Krylov & M.G. Ravich, unpublished data), but these probably reflect metamorphic—perhaps merely thermal—rather than magmatic event(s). One sample contains altered plagioclase (50%), amphibole (30%), ilmenite + leucosene (5%), and chlorite (2%). Another metadolerite sample from the same area comprises actinolite (70%), chlorite (10%), zoisite (10%), quartz (5%), plagioclase (3%), and minor microcline, sericite, titanite and apatite.

Metadolerite samples from Mount Ruker show significant compositional differences to most Ruker Terrane amphibolites and dolerite dykes. They have slightly lower CaO and tend to be more siliceous (Fig. 35), but also more magnesian (Fig. 36). Incompatible-element ratios are also distinctive: higher LILE/Zr and lower Ti/Zr, but similar P/Zr and Y/Zr (Fig. 37); spidergrams have positive Zr anomalies (Fig. 38) and REE patterns are mostly moderately enriched, with small negative Eu anomalies—although one less enriched sample has a positive anomaly (Fig. 39). These features are closely comparable with those of the mafic metavolcanic rocks from Mount Ruker (see above), although the presence of a small positive Eu anomaly and large positive Sr anomaly in one sample suggests, assuming they are not due to metamorphism, significant plagioclase accumulation. Such

compositional similarities are consistent with a co-genetic origin for mafic intrusive and extrusive rocks at Mount Ruker, which supports the field observations of gradational contacts between the two rock types. They also suggest that some mafic intrusives may be of late Archaean or Palaeoproterozoic age. High-Mg mafic dykes, which have quite similar compositions to the Mount Ruker mafic rocks, are probably also Palaeoproterozoic (see below).

Mafic dykes

Mafic dykes of at least three distinct groups were recognised. Two generations of mafic dyke are present at Mounts Ruker, Rymill and Stinear, and at least three in the southern Mawson Escarpment. However, there are generally few obvious petrographic differences between these, apart from a distinctive suite of mafic to ultramafic dykes in the southern Mawson Escarpment and Mount Ruker. The earliest are highly deformed (tightly folded in the southern Mawson Escarpment, or boudinaged and faulted at Mount Ruker) *high-Mg mafic to ultramafic dykes* composed mainly of melanocratic amphibolite or schist. Slightly deformed metamorphosed mafic (*metadolerite*) dykes cut the high-Mg suite in the southern Mawson Escarpment. Fresh or slightly altered *dolerite* dykes are relatively rare, and are best exposed in the southern Mawson Escarpment. They may either be less altered and deformed examples of the metadolerite dykes, or represent a significantly younger, possibly post-metamorphic magmatic suite.

Metamorphosed dolerite dykes (including both relict subophitic and granoblastic varieties) are common in much of the Ruker Terrane, where they intrude Archaean to ?Palaeoproterozoic metamorphic rocks. They are notably absent from the Meso- to early Neoproterozoic high-grade Beaver-Lambert Terrane to the north, which contains only rare compositionally distinct (mostly alkaline) dykes. Metadolerite dykes which crop out in the Fisher Terrane are also geochemically distinct from those in the Ruker Terrane (see below). In contrast, close geochemical similarities with dated (Palaeo- to Mesoproterozoic) dolerite dykes in both of the other Archaean cratons in this part of East Antarctica (Vestfold Hills and Napier Complex of Enderby Land) suggest that most Ruker Terrane dykes may be of similar age. Such a correlation is consistent with the fact that dolerite dykes in all three areas are regionally extensive, and may thus be genetically related. All other mafic dykes in this part of East Antarctica, although locally abundant, are geographically of very restricted occurrence. They are mostly of Palaeozoic age and differ markedly in their alkaline compositions.

Locally (e.g., at Mount Ruker and the southern Mawson Escarpment: Fig. 40) the dykes form networks with complex cross-cutting relationships, but elsewhere (e.g., Cumpston Massif) they tend to be subconcordant (Fig. 41). In the southern Mawson Escarpment, such dykes are mostly thin (1–2 m, rarely up to 10 m), and either trend east–west and dip gently north, or trend northeast–southwest and are steeply dipping. Younger dolerite dykes are typically steeply dipping and trend north–south or northwest–southeast. In some places shearing, probably associated with recumbent folding

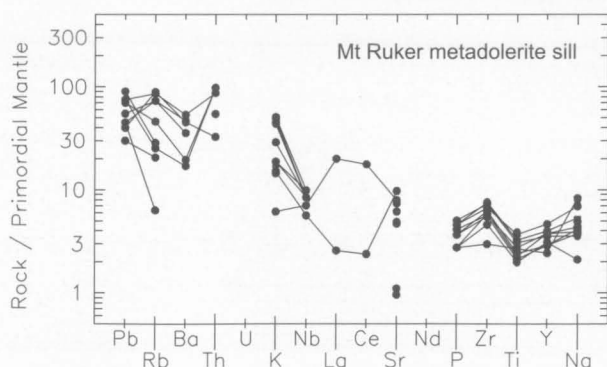


FIGURE 38
Spidergrams for metadolerite sills from Mount Ruker.

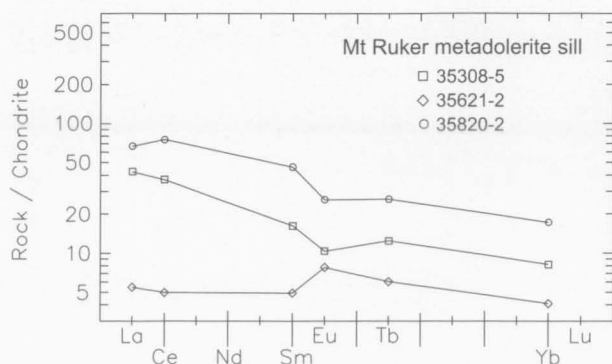


FIGURE 39
Chondrite-normalised rare-earth element abundance plots for metadolerite sills from Mount Ruker.



FIGURE 40

Several generations of metadolerite dykes cutting Archaean granitic rocks and subordinate metasediments; southern Mawson Escarpment. The cliff is about 800 m high.

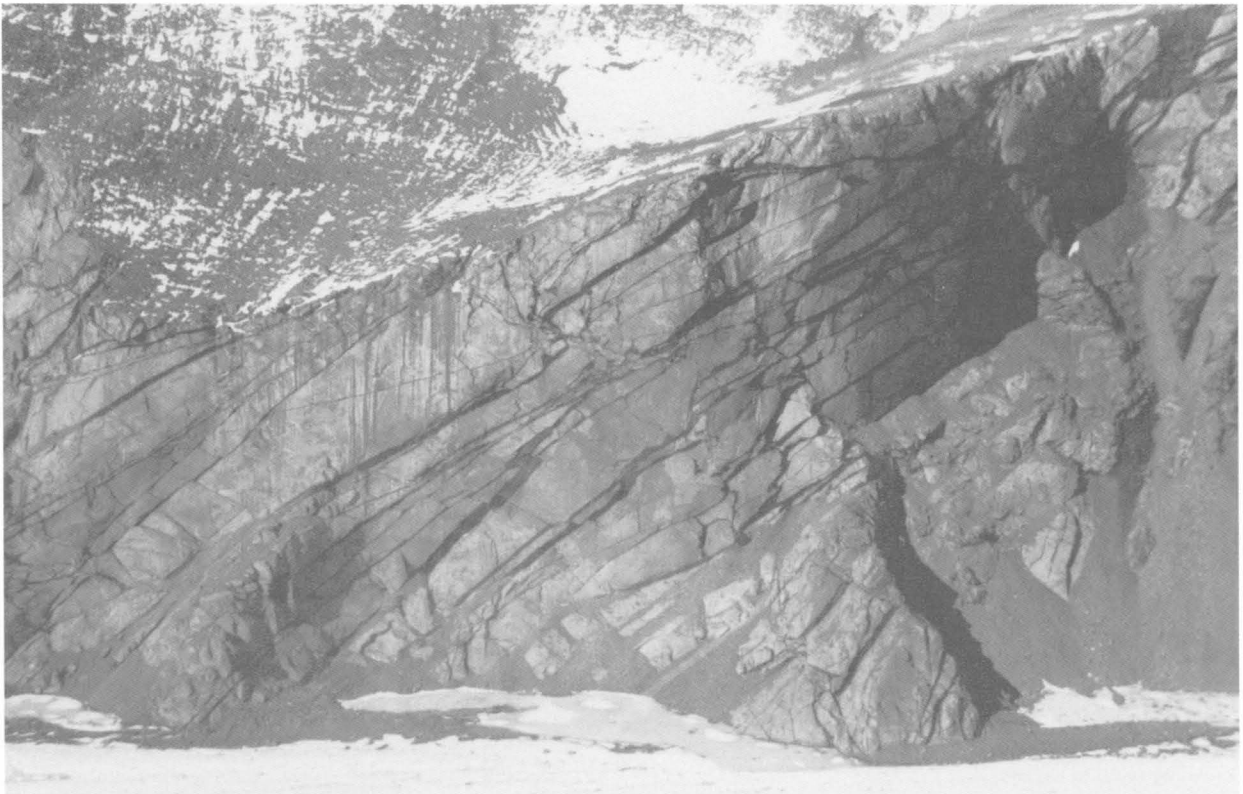


FIGURE 41

Metadolerite dykes cutting Archaean felsic orthogneiss; western side of Cumpston Massif. The dykes are largely concordant with the gneissic foliation, but discordant offshoots are common (e.g., near centre of photograph). The cliff is about 500 m high.

during c.1000 Ma(?) metamorphism, has caused the dykes to be streaked out into subconcordant amphibolite lenses and layers (Fig. 11). The presumed intrusive igneous origin of many concordant amphibolite layers is not directly apparent (see previous section).

Only a few fairly fresh dolerites have been found at Mounts Newton and Ruker, but they are more abundant in the southern Mawson Escarpment. Those at Mount Newton show patchy low-grade retrogression, and are partly boudinaged (England & Langworthy 1975). They have gabbroic to subophitic textures, and contain clinopyroxene (40–45%), labradorite (50–60%), opaque minerals (2–3%), and minor quartz, hornblende and biotite (Fig. 42A). Pyroxene may be partly replaced by pale green actinolitic amphibole and, in a Mount Ruker dyke, chlorite. Secondary garnet occurs in slightly altered dolerite dykes in the southern Mawson Escarpment. Compositions of coexisting garnet and clinopyroxene indicate equilibration temperatures about 400 to 430°C, calculated from Fe–Mg cation exchange reactions (Ellis & Green 1979).

Most metadolerite dykes are completely amphibolitised and more or less thoroughly recrystallised. Those from Mounts Ruker and Rymill and the southern Mawson Escarpment commonly have relict igneous textures, whereas dykes at Machin Nunatak and the small nunatak at the northeastern tip of Mount Scherger are granoblastic and folded. The lowest grade of alteration observed in the dolerites is replacement of clinopyroxene by pale green actinolite (Fig. 42B). More extensive recrystallisation results in the formation of sieve-like aggregates of dark green hornblende with quartz inclusions (Fig. 42C–E) and, ultimately, under upper amphibolite-facies conditions, granoblastic–polygonal amphibolites with dark greenish-brown hornblende are formed (Fig. 42F). Amphibolitised dolerites (metadolerites) contain amphibole (40–70%), andesine–labradorite (25–55%), quartz (up to 10%), titanite (up to 4%), and minor biotite, epidote and opaque minerals. Ilmenite is partly or entirely replaced by titanite. Scapolite is present in one dyke, and a dyke from Mount Scherger contains four per cent biotite. The higher modal quartz and lower modal plagioclase compared to fresh dolerites results from the reaction:

pyroxene + plagioclase \rightarrow hornblende + quartz.

Ultramafic dykes crop out at Mount Ruker and the southern Mawson Escarpment, pre-dating metadolerite dykes at the latter locality. They consist of hornblende (55–95%), biotite (2–30%), opaque minerals (up to 15%), and minor plagioclase. Ultramafic dykes at Mount Ruker have only been found in Archaean granite, suggesting that they are the oldest dyke suite and that they may pre-date the Ruker Series. They are up to 20 metres thick, and strike mostly east-northeast. These dykes include ultramafic amphibolite and talc–carbonate or serpentine–talc–actinolite schist. Hornblende or actinolite (up to 100%), talc (up to 50%), and chlorite (5–45%) are the principal minerals, with minor carbonate, biotite, serpentine and sericite. The rocks are schistose, with a foliation parallel to the dyke margins. No primary textures are preserved.

In terms of chemical composition, most mafic dykes are typical continental olivine or quartz tholeiites (Table 7, Figs 43, 44). The analysed fresh dolerites and most of the amphibolitised (metadolerite) dykes are virtually identical

in composition to the most abundant suite of tholeiites (group II) of Enderby Land (Amundsen Dykes) and the Vestfold Hills (Figs 45, 46), but differ in trace element characteristics from other tholeiite suites in those areas (Sheraton & Black 1981; Collerson & Sheraton 1986a; Sheraton et al. 1987a). For example, Sr contents and Ce/Y (Fig. 47) and Nb/Zr ratios are much lower than those of group I tholeiites of the Vestfold Hills, and Y/Zr is higher. Spidergrams of the metadolerite dykes show considerable scatter, especially for the more mobile LILE, and most (but not all) have marked negative Nb anomalies (Fig. 48). Those of the fresh dykes are generally similar, but tend to be relatively flat and without significant Nb anomalies. REE patterns of the metadolerites are also more fractionated ((La/Yb)_n mostly 4.4–7.4) than that of a fresh dyke ((La/Yb)_n 1.8; Fig. 49). Negative Nb anomalies are typical of group II tholeiites (Sheraton & Black 1981; Collerson & Sheraton 1986a), so it is possible that the fresh dolerites, although otherwise very similar to the metadolerites, may not be part of the same cogenetic suite. Alternatively, they may merely represent melts of the least LILE-enriched part of a heterogeneous mantle source, as was proposed by Sheraton & Black (1981) for group II dolerites in Enderby Land. A third possibility is that their slightly lower LILE contents are merely a function of their lack of alteration. Compared to estimated primordial mantle (Sun & McDonough 1989), the source of most Ruker Terrane dolerite dykes appears to have been variably enriched in LILE (Fig. 46), but to much smaller extents than the Mount Ruker metadolerite sills and mafic volcanic rocks (Figs 30, 31, 37, 38, 46, 48). Such enrichment in group II dolerites from Enderby Land and the Vestfold Hills was attributed by Sheraton & Black (1981) and Collerson & Sheraton (1986a) to metasomatism of the subcontinental lithosphere with a possibly subduction-derived LILE-rich fluid or melt.

Highly-deformed mafic to ultramafic dykes from the southern Mawson Escarpment and Mount Ruker have high MgO (10–25%), Cr (700–2400 ppm), and Ni (200–1500 ppm). At least two compositionally distinct types of high-Mg dyke appear to be present: (1) strongly Ol-normative melanocratic rocks with high TiO₂, P₂O₅, Nb, Y, Zr, LREE and LILE, and (2) more siliceous, slightly Q-normative tholeiites with higher CaO, but lower contents of most incompatible elements (Figs 43, 45). Spidergrams for the former group show much larger negative Sr anomalies (Fig. 48). This group also has much higher Zr/Y (typically 8–12), and lower Al₂O₃/TiO₂ (3–4) and CaO/TiO₂ (2–5), which suggests relatively low percentage melting at high pressures, with residual garnet.

In spite of these differences, close similarities in many incompatible element ratios imply that all the high-Mg dykes were derived by melting of a generally similar, strongly LILE and LREE-enriched mantle source. Compared to most of the dolerite and metadolerite dykes, as well as to estimated primordial mantle, they have low Ti/Zr and Y/Zr, and high Ce/Y, LILE/Zr and LREE/Zr (Figs 46, 47). The more melanocratic group resembles, in some respects, two atypical high-Mg olivine tholeiites from the Vestfold Hills (Fig. 45; Collerson & Sheraton 1986a), but their much lower SiO₂ contents are unlike any high-Mg dykes described from either there or Enderby Land. The second group compares closely with high-Mg

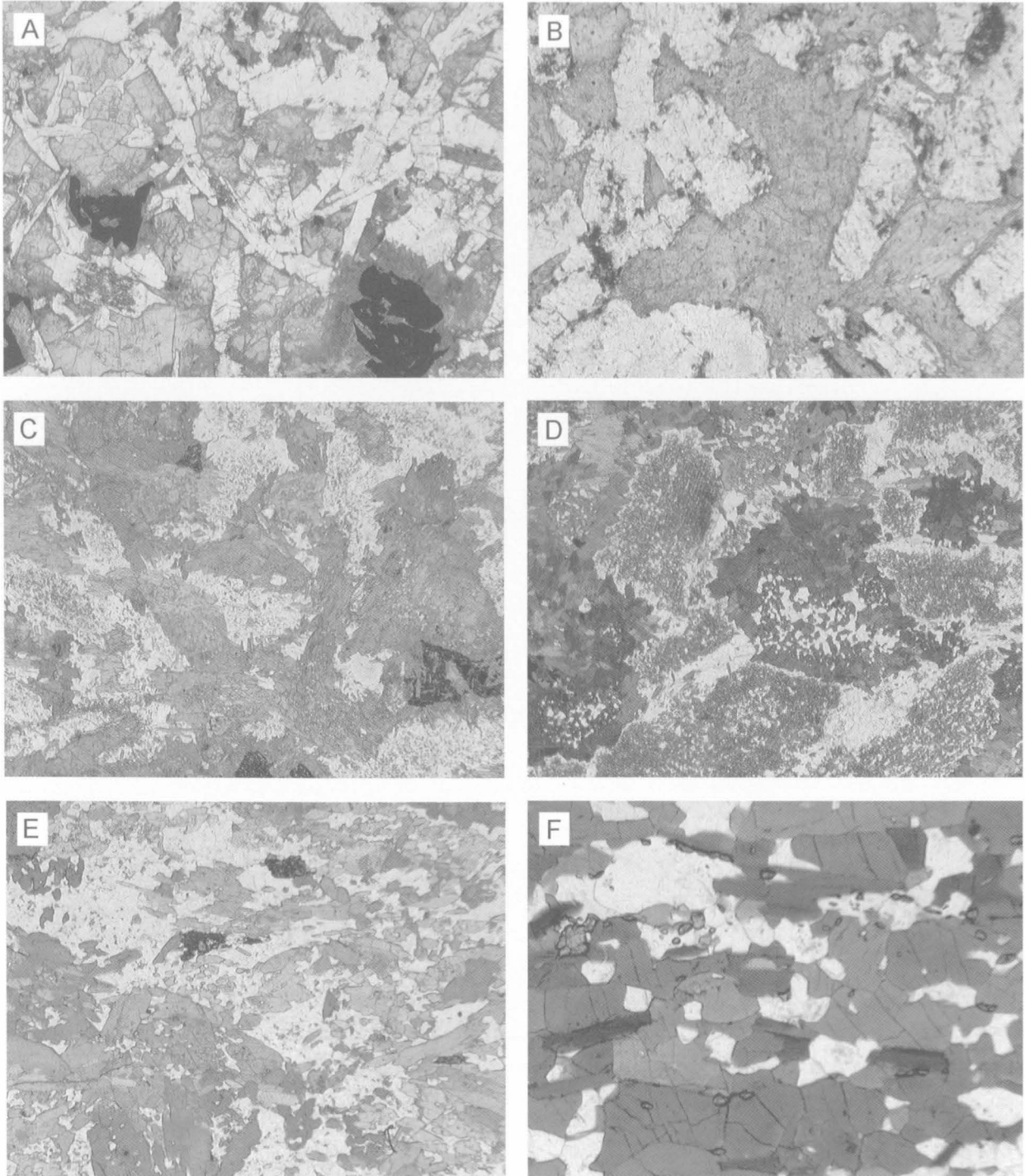


FIGURE 42

Stages in the metamorphism of dolerite dykes. (A) Slightly altered dolerite with subophitic to intergranular texture; Mount Ruker. Clinopyroxene is partly replaced by pale green actinolite, with minor biotite and chlorite. Sample 72280856. (B) Altered dolerite with relict subophitic texture; Mount Ruker. Clinopyroxene is almost entirely replaced by actinolite and opaque grains have thin rims of titanite. Sample 73281620B. (C) Altered dolerite with relict subophitic texture; Mount Rymill. Pale green amphibole and minor biotite form moderately well crystallised aggregates with sieve-like centres. Opaque grains (mainly ilmenite) are largely replaced by skeletal granular aggregates of titanite. Sample 73281313. (D) Largely recrystallised metadolerite containing aggregates of well-crystallised dark green hornblende with centres full of small quartz grains; southern Mawson Escarpment. Igneous plagioclase grains are crowded with epidote inclusions. Sample 73282106. (E) Recrystallised metadolerite comprising green hornblende, granular plagioclase, and minor quartz and titanite; Cumpston Massif. Sample 73281929. (F) Granuloblastic metadolerite containing olive-green hornblende, zoned plagioclase, aligned reddish-brown biotite, and minor quartz and titanite; Mount Scherger. Sample 73281098. Width of field: 4 mm.

Palaeoproterozoic dykes from the Vestfold Block and Enderby Land. Such dykes (siliceous high-magnesian basalts) appear to be more akin to Archaean komatiites than modern boninites (Sun et al. 1989). It is noteworthy that all these high-Mg dykes, like the metadolerite sills and mafic volcanic rocks at Mount Ruker and the mafic to ultramafic schists in the southern Mawson Escarpment, appear to have been derived from generally similar LILE-rich mantle source regions (Figs 27, 28, 30–32, 35–9). This is in marked contrast to the much less enriched source(s) of the younger (probably Mesoproterozoic) metadolerites.

Two metadolerites from the southern Mawson Escarpment have certain trace-element ratios which are quite different from either group II tholeiites (higher Ce/Y, Ce/Zr, and particularly Nb/Zr: Figs 46, 47) or high-Mg dykes (higher Ti/Zr and lower LILE/Zr) of the Vestfold Hills and Enderby Land, and thus cannot be correlated

with any of the mafic dyke suites in these areas. However, a dyke which intrudes Archaean granite gneiss at Mount Rymill (73281077) is similar, apart from very low LILE contents, to high-Mg olivine tholeiites from these areas (Table 7). This dyke may possibly have been depleted in LILE during metamorphism, although its K/Rb ratio (186) is similar to unaltered high-Mg dykes (Sheraton & Black 1981).

Although there is no evidence for significant systematic depletion or enrichment of LILE from most metadolerites, they show considerable scatter on variation diagrams (Figs 45, 46), indicating at least some LILE mobility during metamorphism (Sheraton 1984). Strong deformation can certainly result in major chemical changes, and some sheared dykes contain significant amounts of biotite. One sheared, amphibolitised dolerite at Cumpston Massif (73281927)—which contains hornblende, microcline, and minor plagioclase, quartz, biotite, carbonate and titanite—is highly enriched in K, Rb, Ba, Pb, and possibly Th, U, La and Ce, but depleted in Na and Cu (Table 7; Fig. 48). Apart from LILE, most incompatible element ratios are similar to those of the group II dolerites, and this dyke

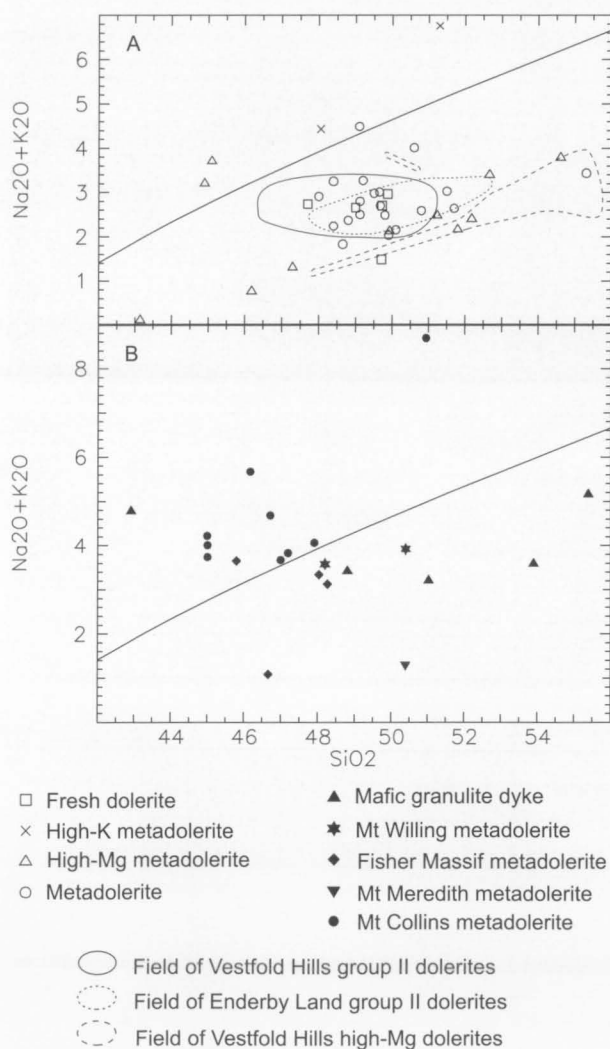


FIGURE 43

Alkalies-SiO₂ plots for mafic dykes of the (A) Ruker Terrane, and (B) Fisher and Beaver-Lambert Terranes. Fields of Mesoproterozoic group II dolerites from Enderby Land and the Vestfold Hills, and Palaeoproterozoic high-Mg dykes from the Vestfold Hills (after Sheraton & Black 1981 and Collerson & Sheraton 1986a) are shown.

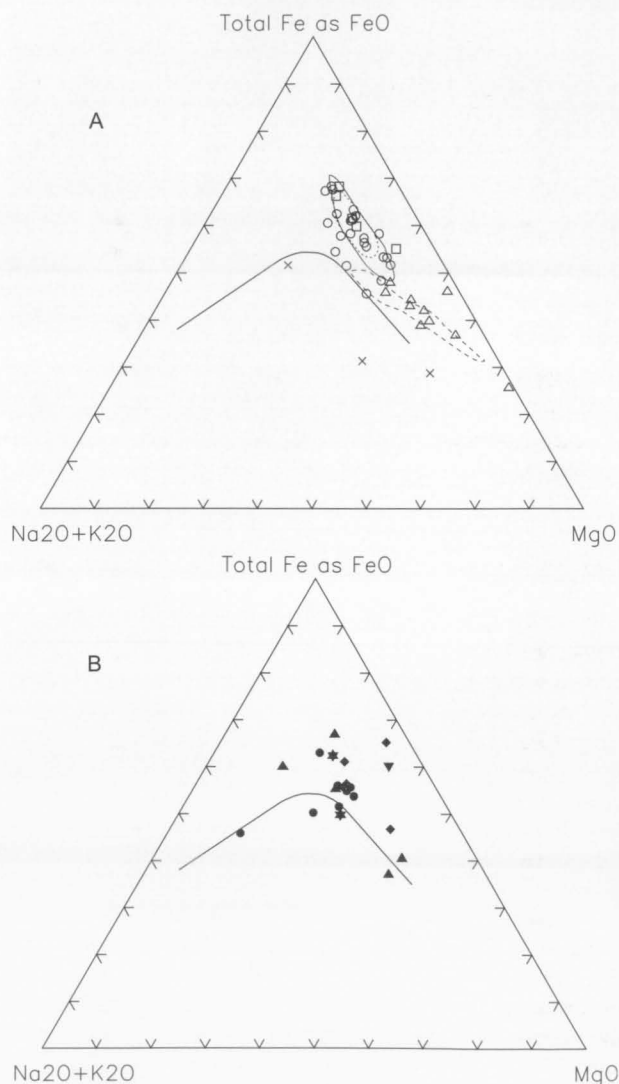


FIGURE 44

AFM diagram for mafic dykes. Symbols and fields as in Figure 43.

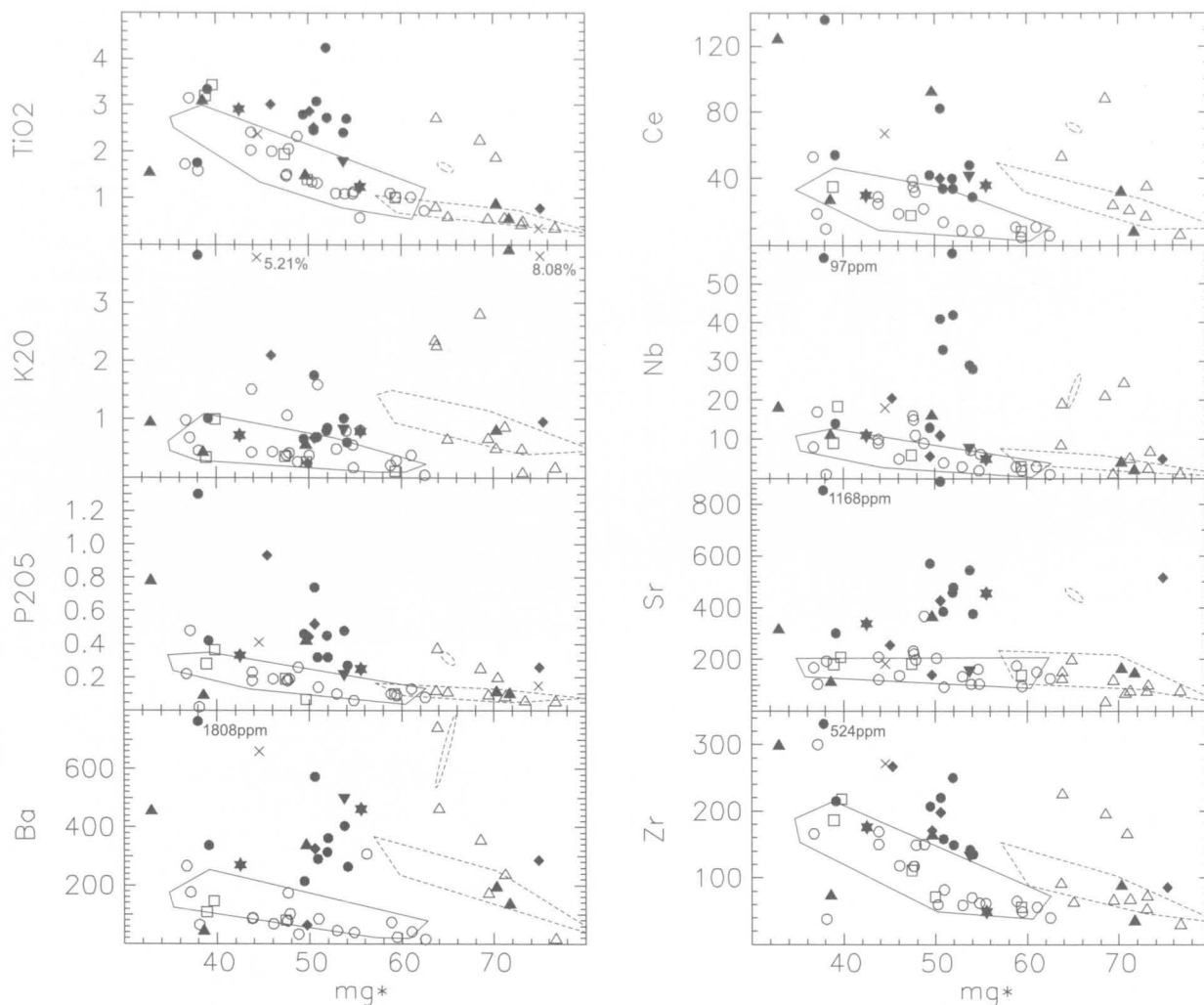


FIGURE 45

mg^* (atomic $100Mg/(Mg + 0.85 \times \text{total Fe})$) variation diagrams for mafic dykes. Symbols and fields as in Figure 43, except that field of Enderby Land group II dolerites has been omitted for clarity. Note that two Vestfold Hills high-Mg dykes (shown as separate fields in most plots) have much higher contents of most incompatible elements than other high-Mg dykes.

may be a metasomatised equivalent, as suggested by Sheraton (1984). Its Hy-normative composition and low Sr and Ce/Y would be more consistent with this than with it being an originally high-K (e.g., syenitic) intrusion. It certainly has a very different composition to the Mount Collins syenites (see below). An alkaline mafic origin cannot be entirely discounted, as rare high-K amphibolite dykes are also known elsewhere in the SPCM (e.g., Mount Ruker and the southern Mawson Escarpment). However, Ravich et al. (1978) also suggested a metasomatic origin for these rocks, and an example from the southern Mawson Escarpment has low TiO_2 , Na_2O and Sr.

No reliable isotopic age data are available for the Ruker Terrane mafic dykes and dating of dolerite dykes in Enderby Land and the Vestfold Hills has revealed complex histories of mafic dyke emplacement. A group II dyke in the Vestfold Hills has given a U-Pb zircon ion-microprobe age of 1380 ± 7 Ma (group 3 of Lanyon et al. 1993), comparable to the much less precise Rb-Sr whole-rock isochron age of 1374 ± 125 Ma determined by Collerson & Sheraton (1986a). Other Vestfold Hills dolerite suites were dated by Lanyon et al. (1993) at 1754 ± 16 Ma (their group

2) and 1241 ± 5 Ma (their group 4). Although it is not possible to unequivocally correlate these with dyke suites which gave Rb-Sr isochron ages of 1791 ± 62 Ma (Vestfold Hills: group I of Collerson & Sheraton 1986a) and 1190 ± 200 Ma (Enderby Land: group I of Sheraton & Black 1981), the latter, at least, are geochemically distinct from group II. Hence, the balance of the geochemical evidence is that most of the Ruker Terrane metadolerites probably belong to the 1380 ± 7 Ma group II suite, although the possibility that some dykes are either older (c.1750 Ma) or younger (c.1240 Ma) cannot be discounted. The youngest dyke emplacement event could be represented by the fresh dolerite dykes at Mount Ruker, the southern Mawson Escarpment, and possibly elsewhere—although the available geochemical data do not confirm this as the few analysed fresh dolerites are geochemically very similar to the metadolerites (and group II dolerites), but distinct from the c.1200 Ma Enderby Land group I dykes, at least.

Two high-Mg dykes in the Vestfold Hills gave U-Pb zircon ages of 2241 ± 4 and 2238 ± 7 Ma (Lanyon et al. 1993). This is somewhat younger than Rb-Sr isochron ages of 2424 ± 72 Ma from the Vestfold Hills (Collerson & Sheraton

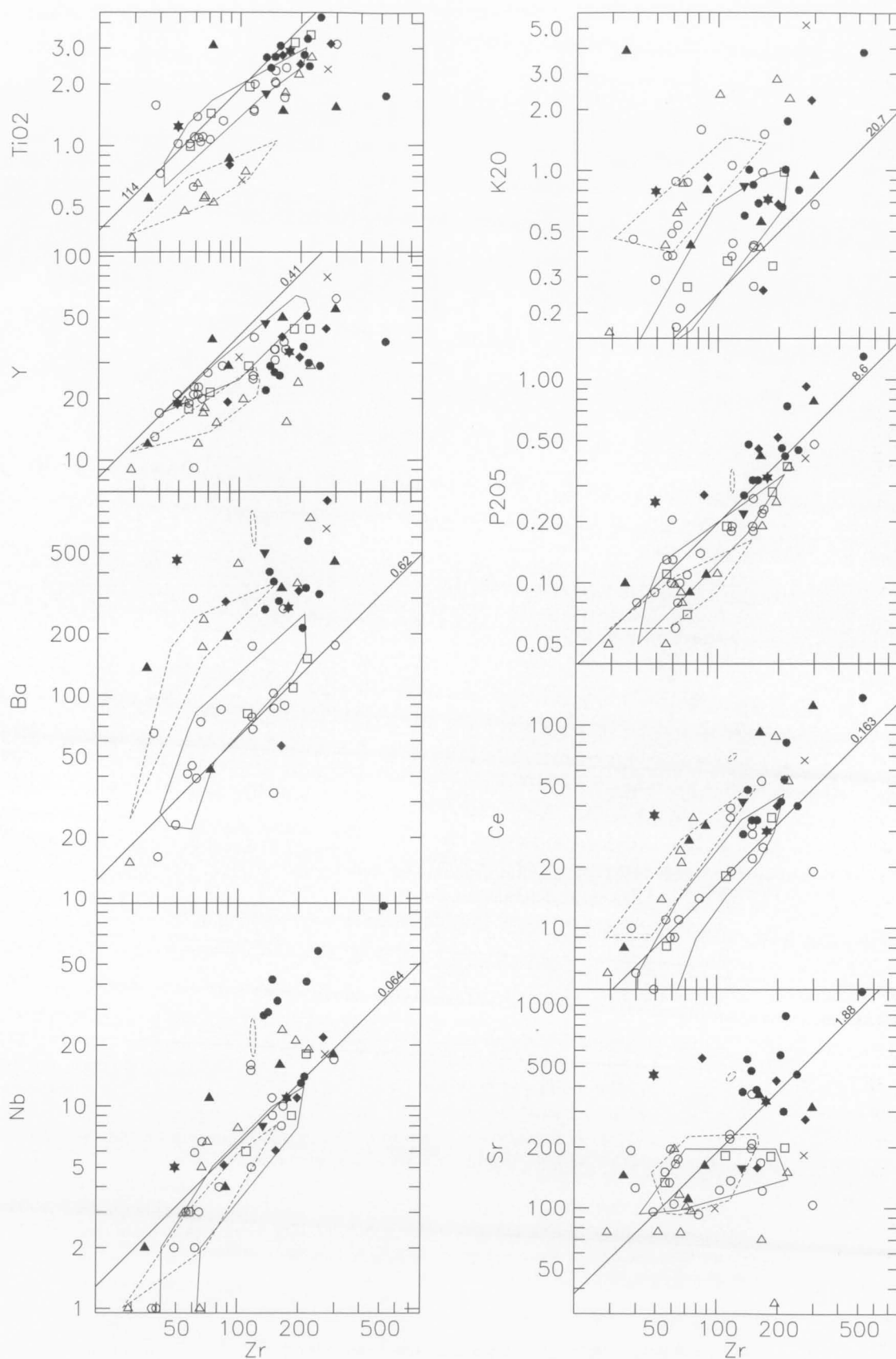


FIGURE 46

Logarithmic plots of various incompatible elements against Zr for mafic dykes. Lines of estimated primordial mantle ratios (after Sun & McDonough 1989) are indicated. Such lines of unit slope are also those for which the bulk mineral–melt distribution coefficient (K_d) is zero. The K_d value can be estimated from the expression $K_d = 1 - \text{slope}$ (Allègre et al. 1977); for some elements it is much greater than zero (e.g., ~ 0.7 for Sr in Vestfold Hills group II dykes, in which it reflects plagioclase fractionation). Symbols and fields as in Figure 43.

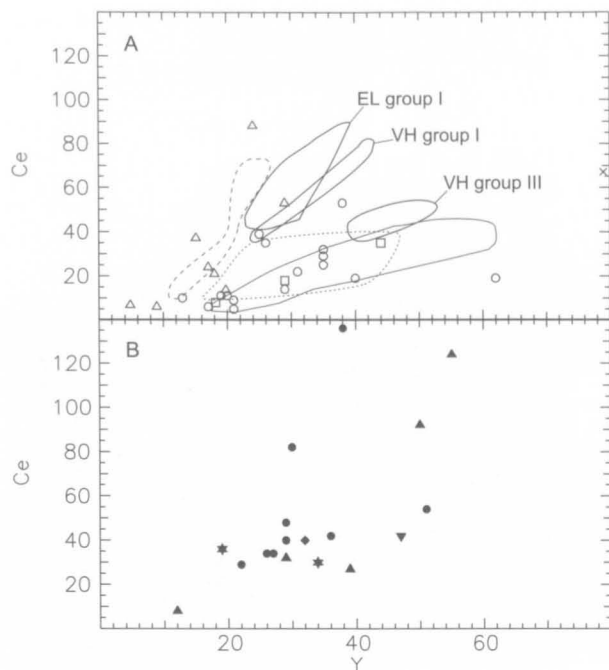


FIGURE 47

Ce–Y plots for mafic dykes. Symbols and fields as in Figure 43, with the addition of fields of group I dolerites from Enderby Land and groups I and III dolerites from the Vestfold Hills.

1986a) and 2350 ± 48 Ma from Enderby Land (Sheraton & Black 1981). A high-Mg dyke from the southern Mawson Escarpment has given a TIMS zircon Pb–Pb model age of about 2400 Ma (Mikhalsky et al. 1992), consistent with high-Mg dykes from all these areas being roughly co-eval and originating from similar source region(s). It is noteworthy that metadolerite sills and mafic metavolcanic rocks at Mount Ruker were apparently both derived from very similar enriched mantle source regions to those of the high-Mg dykes, so it is possible that all these rocks were formed during a single magmatic event. High-Mg dykes appear to be confined to Archaean granitic basement rocks at Mount Ruker, none having been found in the nearby Ruker Series metavolcanics. However, both the Mount Ruker metadolerite sills and mafic volcanic rocks are generally more evolved (lower MgO) than the high-Mg dykes, and even the latter show significant compositional variations which preclude them from being a single comagmatic suite. Hence, these dykes more likely reflect one or more Archaean and/or Palaeoproterozoic magmatic events that may pre-date the more voluminous mafic magmatism at Mount Ruker. Only isotopic dating of these various suites can potentially resolve this problem. Whatever the exact ages of the different mafic dyke suites in the Ruker Terrane, they are still very useful stratigraphic markers.

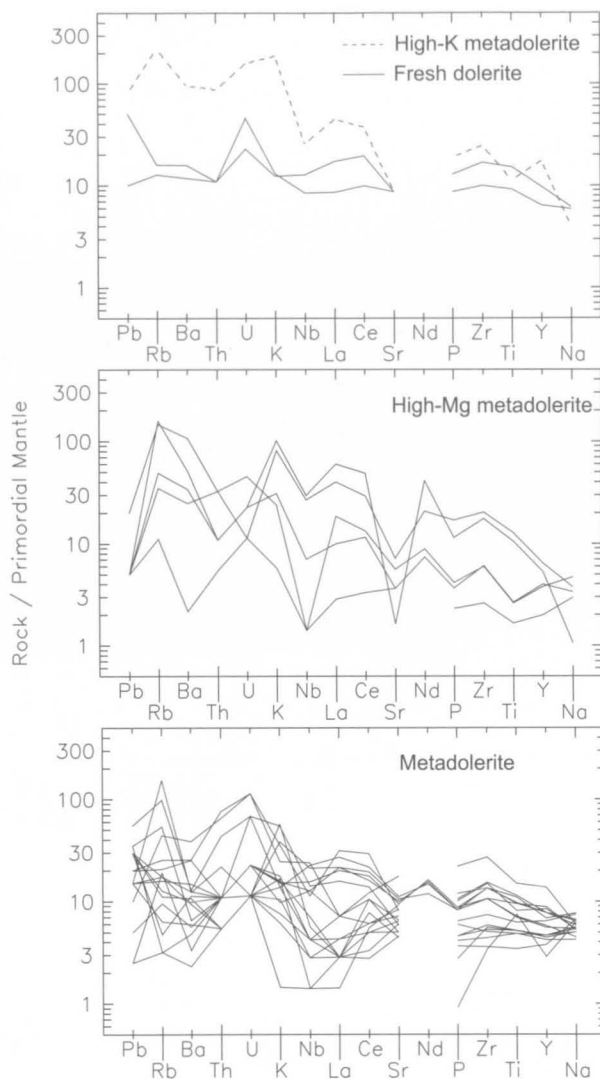


FIGURE 48

Spidergrams for mafic dykes of the Ruker Terrane.

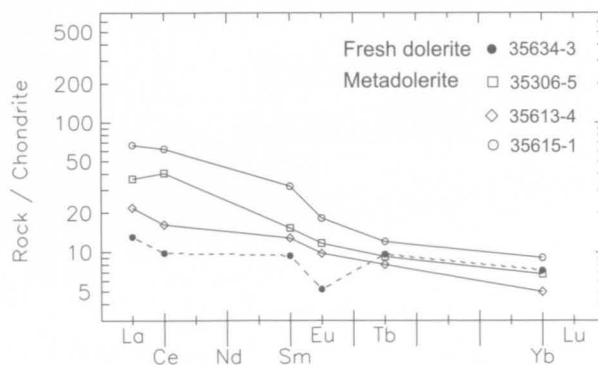


FIGURE 49

Chondrite-normalised rare-earth element abundance plots for mafic dykes of the Ruker Terrane.



FIGURE 50

Greenschist-facies metasediments (Sodruzhestvo Series), showing tight concentric folds; northern side of Mount Rubin. The cliff is about 700 m high.



FIGURE 51

Cross-bedding in psammitic schist of the Sodruzhestvo Series; Goodspeed Nunataks.

PROTEROZOIC METASEDIMENTARY ROCKS (SODRUZHESTVO SERIES)

Relatively low-grade (predominantly greenschist-facies) metasediments (the presumed upper part of the Sodruzhestvo supracrustals of Kamenev et al. 1990 and Kamenev 1993) crop out at Mounts Rubin (Fig. 50), Dummett and Seddon, Goodspeed Nunataks, and possibly southeastern Cumpston Massif. Metasedimentary rocks at northern Mount Maguire, included in the Sodruzhestvo Series by Tingey (1982a, 1991a) and Thost et al. (1998), are of somewhat higher grade. They are therefore included in the Menzies Series in this bulletin, although their stratigraphic position is presently far from clear. Slightly higher grade (lower amphibolite-facies) metasedimentary rocks at Mounts McCauley and Scherger, which were included in this group by Tingey (1982a, 1991a), show petrographic evidence for two metamorphism events, including a kyanite–staurolite-grade event. They are therefore also assigned to the Menzies Series. Thus, in this bulletin the Sodruzhestvo Series essentially comprises lower grade metasedimentary rocks without metamorphosed mafic dykes or even concordant amphibolite, as opposed to the higher grade Menzies Series. Both features have been used to distinguish these series in the field, although local variations in the metamorphic grade of both have led to some uncertainties and hence different interpretations on Australian and Russian maps (e.g., at northern Goodspeed Nunataks and Mount Maguire).

Compared to the Archaean–Palaeoproterozoic Menzies Series, the Sodruzhestvo Series appears to be of predominantly more calcareous composition. The metamorphism appears to be prograde, and there is little (if any) evidence for an earlier high-grade event. Original sedimentary features, such as ripple marks, mud cracks and cross-bedding, are preserved in some places (e.g., Goodspeed Nunataks and Mount Rubin; Fig. 51). These metasediments are not cut by metadolerite (amphibolite) dykes, which in some areas are present in higher grade

metamorphic rocks at nearby outcrops; also mafic rocks are conspicuously absent, which is thought to be a key stratigraphic feature (Tingey 1982a, 1991a). The metasediments are intruded by small bodies of Cambrian granite and pegmatite at outcrops on the northern side of the Fisher Glacier (Fig. 134), and a few rocks at Mount Dummett and Goodspeed Nunataks contain sillimanite or cordierite of probable contact metamorphic origin. Such a Cambrian tectonothermal event may also have been responsible for the widespread, but patchy, retrogression seen in many of the rocks affected by the c.1000 Ma(?) event (e.g., at Mount Menzies).

There has been much debate over the age of the Sodruzhestvo Series and its relationships with the Ruker Series. Low-grade metasediments at Mount Ruker were originally classified as Sodruzhestvo supracrustals by Soloviev (1972), but Ravich et al. (1978) distinguished them as a separate group. However, Ravich & Fedorov (1982) and Kamenev et al. (1990, 1993) suggested a close correlation on compositional and structural grounds, with no major age difference. Tingey (1982a, 1991a) considered of critical importance the fact that the Ruker Series rocks are cut by metadolerite dykes and are therefore likely to be older. The presence of jaspilite clasts in conglomerate at Mount Rubin (Halpern & Grikurov 1975) indicate that the rocks there are younger (although not necessarily much younger) than those at Mount Ruker. On these grounds the Sodruzhestvo Series should be younger than the mafic dykes (probably c.1380 Ma), but older than the granitic rocks (c.500 Ma). Il'tchenko (1972) described Riphean (Meso- to Neoproterozoic) acritarchs from Mounts Rubin and Seddon (*Protoleiosphaeridium infriatum* Andr., *Rifenite mirabilis* Naum., *Orygmato-sphaeridium rubiginosum* Andr., *Contextus laevisus* Andr., and *Prolaminarites gurosus* Il't.), so that a late Mesoproterozoic depositional age may be most likely. However, a broadly similar acritarch assemblage was also recovered from metasedimentary rocks at Mount Ruker (Il'tchenko 1972), which makes the significance of these data uncertain.

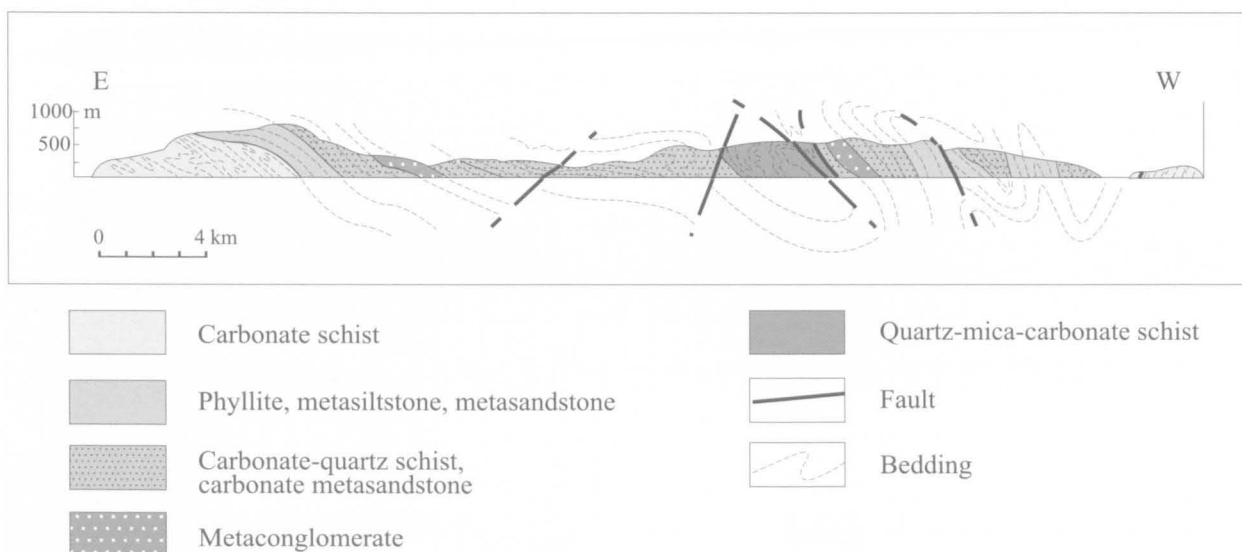


FIGURE 52

Schematic geological cross-section along the northern slope of Mount Rubin (after Grikurov & Soloviev 1974).

The prograde metamorphism of at least some of these rocks may be equivalent to the lower amphibolite-facies (kyanite-staurolite-grade) event seen in much of the Ruker Terrane, which, if it is of late Mesoproterozoic to early Neoproterozoic (c.1000 Ma) age, also produced the high-grade Beaver-Lambert Terrane to the north. However, there is an indication that the metamorphism could be significantly younger, although the evidence is far from conclusive. Halpern & Grikurov (1975) cited a poorly-defined Rb-Sr isochron age of about 495 Ma (recalculated to 512 Ma using the most recent decay constant in Table 24), with Sr_i 0.738, for phyllite at Mount Rubin, and an age of about 800 Ma (recalculated to 830 Ma, Sr_i 0.730) for granitic clasts from directly overlying conglomerate at the same locality. The average T_{UR}^{Sr} model age of 670 Ma for the former suggests that the original sediments may post-date the c.1000 Ma metamorphism, but it is possible that preferential absorption of Rb onto the original clay minerals in such rocks could have resulted in anomalously young model ages. The 830 Ma age of the granitic clasts is of uncertain significance and may reflect partial resetting of an originally heterogeneous group of granitoids: two tonalitic samples have very low Rb/Sr and two granite gneisses have high Rb/Sr. Nevertheless, an isochron age obtained by combining the two granite gneisses with three phyllites is 505 ± 40 Ma (Sr_i 0.7444 ± 0.0032 ; Table 24). Taken at face value, the young Rb-Sr T_{UR} ages of the phyllites (670, 846 Ma; Table 24) would indicate a relatively young age for the Sodruzhestvo Series. However, none of the evidence is fully convincing, and a much older (even Palaeoproterozoic) age cannot be completely ruled out.

The type cross-section was measured at **Mount Rubin** (Fig. 52), where metasediments form at least seven compositionally distinct members about 3500 metres thick. The predominant lithologies from bottom to top are: (1) porphyroblastic sericite-carbonate-quartz schist; (2) chlorite-sericite-quartz phyllite; (3) calcareous quartz and mica-quartz metasandstone; (4) quartzite and metaconglomerate; (5) calcareous quartz metasandstone; (6) carbonate metasiltstone; and (7) quartzite and metasiltstone. Individual layers, mostly between 0.1 and two metres thick, are characterised by a wide range of

colour. In some localities different lithological types are interbedded and have a flysch-like appearance. Mica-carbonate-quartz schist (?metamorphosed marl) and calcareous metasandstone are the most common rock types, constituting more than 80 per cent of the strata. Thin marble and ferriferous sandstone beds or lenses (with up to 15% opaque phases) occur sporadically. Porphyritic and globular textures in some rocks suggest that they may represent metamorphosed volcanic flows. A few lenses of leucocratic biotite-microcline-quartz schist with relict felsitic or microgranitic textures are thought to represent felsic volcanic rocks. Tuff, tuffite and tuffaceous sandstone are thought to be minor constituents of the sequence. At both Mounts Rubin and Dummett (Fig. 53), the strata are highly folded and sheared. Representative chemical analyses of Sodruzhestvo Series metasediments are given in Table 8.

TABLE 8. Chemical analyses of representative Sodruzhestvo Series metasedimentary rocks from Mount Rubin.

Sample no.	35644-3	35523-3	35646-1	35523-1	35649-2
Lithology	Mafic tuffite	Tuffite	Felsic tuffite	Meta- greywacke	Quartzite
SiO ₂	54.85	60.72	73.25	67.55	86.2
TiO ₂	0.62	0.74	0.49	0.82	0.26
Al ₂ O ₃	14.42	15.22	9.29	13.15	5.7
Fe ₂ O ₃	5.71	*6.93	0.37	4.47	0.65
FeO	1.09	-	0.52	1.23	0.51
MnO	0.1	0.04	0.07	0.04	0.02
MgO	3.7	3.44	0.79	2.88	0.62
CaO	5.17	2.39	3.91	0.87	0.98
Na ₂ O	0.9	2.13	2.62	2.54	1.9
K ₂ O	3.93	3.33	1.95	2.87	0.96
P ₂ O ₅	0.18	0.15	0.11	0.16	0.07
LOI	9.11	4.58	3.75	3.01	1.45
Total	99.78	99.67	97.12	99.59	99.32
mg	85.8	-	73.0	80.7	68.4

mg = atomic 100Mg/(Mg + Fe²⁺); * total Fe as Fe₂O₃.

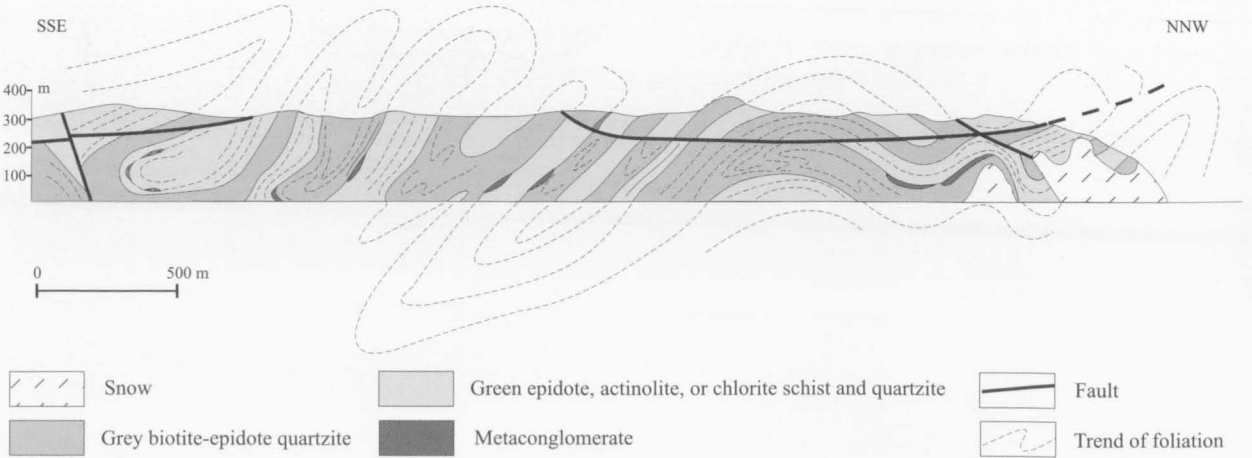


FIGURE 53
Schematic geological cross-section of Mount Dummett (after O.A. Tarutin & V.S. Semenov).

Pelitic metasediments

Mineral assemblages in slaty and phyllitic metapelite at Mounts Rubin and Seddon are similar to those in the more schistose rocks at Mount Dummett and Goodspeed Nunataks. There are gradations into the more calcareous compositions described below, with increases in the proportions of carbonate and calc-silicate minerals. Typical assemblages are:

quartz + biotite + muscovite + carbonate \pm epidote,
quartz + biotite + muscovite + microcline, and
quartz + biotite + muscovite + chlorite \pm plagioclase \pm K-feldspar \pm epidote.

Some of the chlorite is of retrograde origin, and opaque minerals, apatite, zircon, titanite and tourmaline are common accessory phases. Soloviev (1971) noted the generally minor role of K-feldspar in the metasediments, and suggested that non-migmatitic, lower amphibolite-facies rocks were the major source.

Pelitic schist at Goodspeed Nunataks commonly contains large (up to 5 mm) randomly orientated poikilitic grains of biotite and, in some places, microcline. Quartz + biotite + muscovite + secondary chlorite + cordierite occurs in one probably contact metamorphosed rock. A sample from northern Goodspeed Nunataks contains the assemblage quartz + biotite + muscovite + albite + kyanite, suggesting either a slightly higher metamorphic grade there or the presence of Menzies Series rocks in this area.

Psammitic metasediments

Quartzite is much less abundant than in the Menzies Series, but impure quartzite is interlayered with calcareous and pelitic rocks at most of the localities mentioned above. Detrital grains are rounded and mostly composed of quartz (80–95%), feldspar, and rarely phyllite, and are enclosed in a sericite–biotite–opaque–carbonate matrix. Conglomerate with quartzite pebbles is present at Mount Dummett and Goodspeed Nunataks (Fig. 54). Quartz (40–70%), biotite (up to 10%), sericite (7–30%), carbonate (8–30%), and chlorite are generally present. Plagioclase, epidote and opaque minerals are less abundant, but widespread, constituents. Quartz + biotite + muscovite + microcline \pm plagioclase \pm carbonate occurs at Goodspeed Nunataks, and quartz + muscovite + plagioclase + microcline + carbonate \pm biotite \pm chlorite \pm tourmaline in calcareous quartzite at Mount Rubin.

Calcareous metasediments

Calcareous schist at Mounts Rubin and Seddon commonly contain prominent crystals of carbonate (siderite, calcite, or dolomite; Ravich et al. 1978), several millimetres across, suggesting derivation from carbonate-rich sediments. Alternatively, the presence of carbonate porphyroblasts may be due to a reaction of the sedimentary protoliths with a CO₂-rich fluid, and may not necessarily imply derivation from originally Ca-rich sediments. Typical assemblages are similar to those in more aluminous rocks:

quartz + biotite + muscovite + chlorite + epidote + carbonate,
quartz + biotite + muscovite + chlorite + plagioclase + K-feldspar + carbonate, and
quartz + biotite + muscovite + chlorite + actinolite + epidote + carbonate.

K-feldspar (microcline) and titanite are more widespread at Mount Dummett and northern Goodspeed Nunataks:

quartz + biotite + actinolite/hornblende + epidote + microcline + titanite \pm chlorite \pm plagioclase \pm carbonate,
quartz + biotite + muscovite + epidote \pm microcline \pm carbonate \pm titanite, and
biotite + actinolite + diopside + epidote + microcline \pm plagioclase \pm carbonate \pm titanite.

Amphibole is blue-green hornblende or actinolite. Accessory minerals include opaque minerals, rutile and tourmaline.

Marble layers occur at a few places, such as Mounts Rubin, Dummett (with minor tremolite) and Goodspeed Nunataks (minor quartz, biotite, muscovite, epidote and titanite).

Metaconglomerate

At Mount Rubin, metaconglomerate is interlayered with mica-feldspar–carbonate schist and is concentrated in the upper part of the exposed sequence. Most conglomerate layers are up to two metres thick and contain abundant well-rounded clasts. A single 30 metre-thick breccia bed contains less than 20 percent angular to rounded, unsorted clasts up to 30 centimetres across. Clasts include various crystalline rock types (deformed granite and tonalite, quartzite, mica–epidote and mica–carbonate–quartz schist, limestone and marble, sericite phyllite, and opaque–biotite–albite schist). The opaque–biotite–albite schist has a relict ophitic texture and may represent a metamorphosed mafic dyke. Metaconglomerate at Mount Dummett and Goodspeed Nunataks (Fig. 54) contains mainly quartzite pebbles, together with jaspilite at Mount Dummett. It is noteworthy that conglomerate occurs only as intraformational beds, and no basal conglomerate was found.



FIGURE 54
Sodruzhestvo Series metaconglomerate; Goodspeed Nunataks.

FISHER TERRANE

The Fisher Terrane occupies the relatively poorly exposed area in the southern part of the NPCM, with the main outcrops at Fisher Massif, Mount Willing and Nilsson Rocks (Fig. 2). It comprises rocks which are quite different to those in adjacent parts of the Beaver-Lambert Terrane, being of much lower metamorphic grade and including abundant mafic to felsic metavolcanic and intrusive rocks. The proportions of mafic and intermediate igneous rocks (basalt to andesite, and gabbroic rocks) are much greater than elsewhere in the PCM, where felsic orthogneiss and metasediments predominate. The highly deformed volcanic and intrusive rocks, and subordinate metasediments, were mostly metamorphosed under epidote-amphibolite to garnet-amphibolite-facies conditions, and are cut by a variety of post-tectonic granites and mafic dykes. It is possible that amphibolite and felsic orthogneiss at Shaw Massif (and perhaps elsewhere) may be higher-grade (upper amphibolite-facies) equivalents of some Fisher Terrane rocks. However, they more closely resemble metamorphic rocks in the Clemence Massif–northern Mawson Escarpment–Mount Johns area, and so are described here in the Beaver-Lambert Terrane chapter. No similar rocks are known east of the Lambert Glacier. The geochemistry of Fisher Massif metavolcanic rocks, as well as associated granitoids, suggests formation in an active continental margin with an associated island arc (Mikhalsky et al. 1996). The rocks are therefore considered to belong to a distinct terrane. Nevertheless, as these rocks crop out in a relatively narrow zone (not exceeding 50 km across), it is possible that they represent a suture zone between two major lithospheric blocks. However, there is presently little evidence (except for slightly different metamorphic grade, see next chapter) to suggest that the rock associations to the north and south of the Fisher Terrane belong to distinct terranes.

The Fisher Terrane occupies an area near the boundary between the two major tectonic provinces distinguished in the PCM (Tingey 1982a, 1991a; Kamenev 1993): the mainly Archaean to Palaeoproterozoic Ruker Terrane in the south, and the Mesoproterozoic to early Neoproterozoic mobile belt (Beaver-Lambert Terrane) in the north, although it appears to be within the latter. Its tectonic position is not well understood, and several different interpretations have been proposed. Thus, earlier researchers tentatively considered that the Fisher Terrane rocks represent an Archaean block within the Beaver-Lambert Terrane (Tingey 1991a), a Proterozoic granite–greenstone belt (Kamenev 1993), or were formed in a Mesoproterozoic active continental margin during development of the mobile belt (Mikhalsky et al. 1996; Sheraton et al. 1996). The occurrence of a Mesoproterozoic layered gabbro intrusion at Mount Willing led Mikhalsky et al. (1992, 1993) to propose a rift-related origin for the rocks of this area.

U–Pb zircon dating of intermediate and felsic metavolcanic rocks from Fisher Massif indicates emplacement about 1300 Ma ago (Table 22; Beliatsky et al. 1994; Kinny et al. 1997). Ion-microprobe U–Pb zircon ages of granitic rocks (1293 ± 28 Ma for granodiorite and 1020 ± 48 Ma for granite; Kinny et al. 1997) also suggest late Mesoproterozoic emplacement, and a Rb–Sr whole-rock isochron age of 870 ± 150 Ma for granodiorite was reported by Krasnikov & Fedorov (1992). A plagiogranite gave a somewhat older conventional zircon age of about 1500–1450 Ma (one discordant point forced through 500 Ma), which may reflect the earliest crust-forming event in the area (Mikhalsky 1993). An inherited c.1900 Ma zircon xenocryst in a dacite was reported by Kinny et al. (1997), and a model $^{207}\text{Pb}/^{206}\text{Pb}$ age of 2560 Ma for a rhyodacite was given by Beliatsky et al. (1994). Tonalite gneiss and younger granite at Mount Willing have given zircon U–Pb ages of 1177 ± 16 and 1194 ± 1 Ma, respectively, although tonalite emplacement probably occurred near the time of the older age estimate (c.1194 Ma). A quartz diorite (migmatite) vein yielded a U–Pb age of 1113 ± 3 Ma (2-point zircon upper intercept). Rb–Sr and Sm–Nd mineral–whole-rock isochron ages of 636 ± 13 and 1009 ± 5 Ma, respectively, for amphibolite lenses in the tonalite gneiss apparently date younger metamorphic events (Mikhalsky et al. 1999; A.A. Laiba, unpublished data). Emplacement of layered gabbro at Mount Willing was dated at about 1300–1200 Ma (Sm–Nd whole-rock data, Mikhailov et al. 1991; Mikhalsky et al. 1992), with 1292 ± 67 (Sm–Nd pyroxene data, A.A. Laiba, unpublished data) considered to be the best estimate, followed by metamorphism at 1023 ± 33 Ma (Sm–Nd mineral data: Mikhalsky et al. 1993), 1118 ± 31 , and a thermal event at 810 Ma (both U–Pb zircon data: Laiba & Mikhalsky 1999).

Fisher Massif is an isolated, northeast–southwest orientated, highland block some eight to 12 kilometres wide and 32 kilometres long. It is made up of metavolcanic and minor tuffaceous rocks, clastic metasediments, marble and ironstone, intruded by various plutonic bodies (gabbro, diorite, tonalite, granodiorite and granite; Fig. 55). The volcanic rocks were metamorphosed under lower amphibolite-facies conditions, and retrograde greenschist-facies assemblages were developed. Rare dykes of metadolerite, dolerite, dacite, basaltic trachyandesite or trachydolerite, and unmetamorphosed ultramafic rocks (kimberlite) are present.

Mount Willing is an uplifted block, about four by 14 kilometres, composed of four main rock types (Fig. 56), generally similar to those exposed at Fisher Massif, but of somewhat higher metamorphic grade: (1) a mafic to felsic meta-igneous sequence which is probably mainly of high-level intrusive (subvolcanic) or volcanic origin; (2) partly metamorphosed gabbroic intrusions, retaining pristine

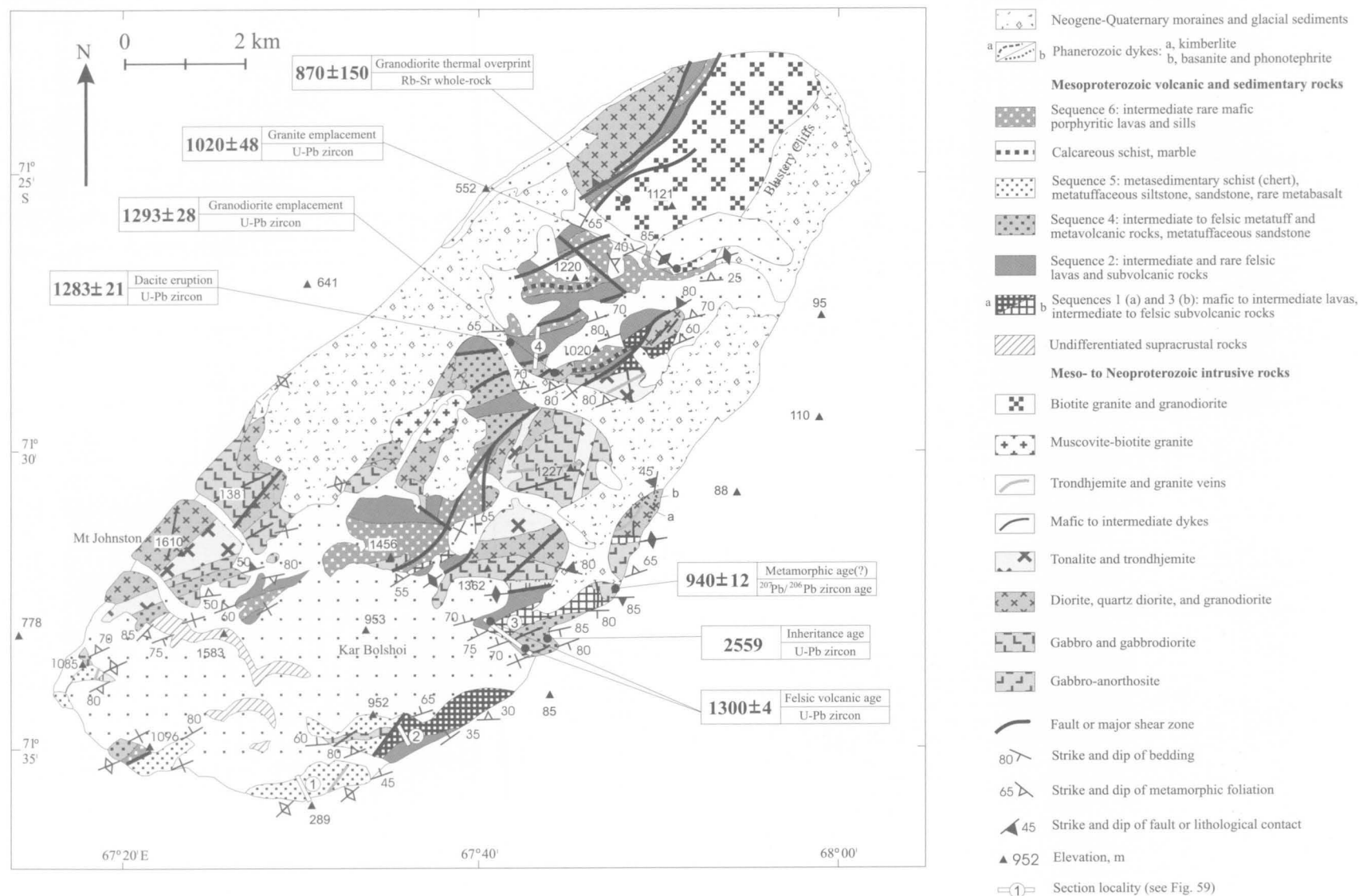


FIGURE 55

Geological map of Fisher Massif (modified from Kamenev et al. 1993), showing locations of measured sections shown in Figure 59. Sources of age data: Krasnikov & Fedorov (1992), Beliatsky et al. (1994), Kinny et al. (1997), and A.A. Laiba (unpublished data).

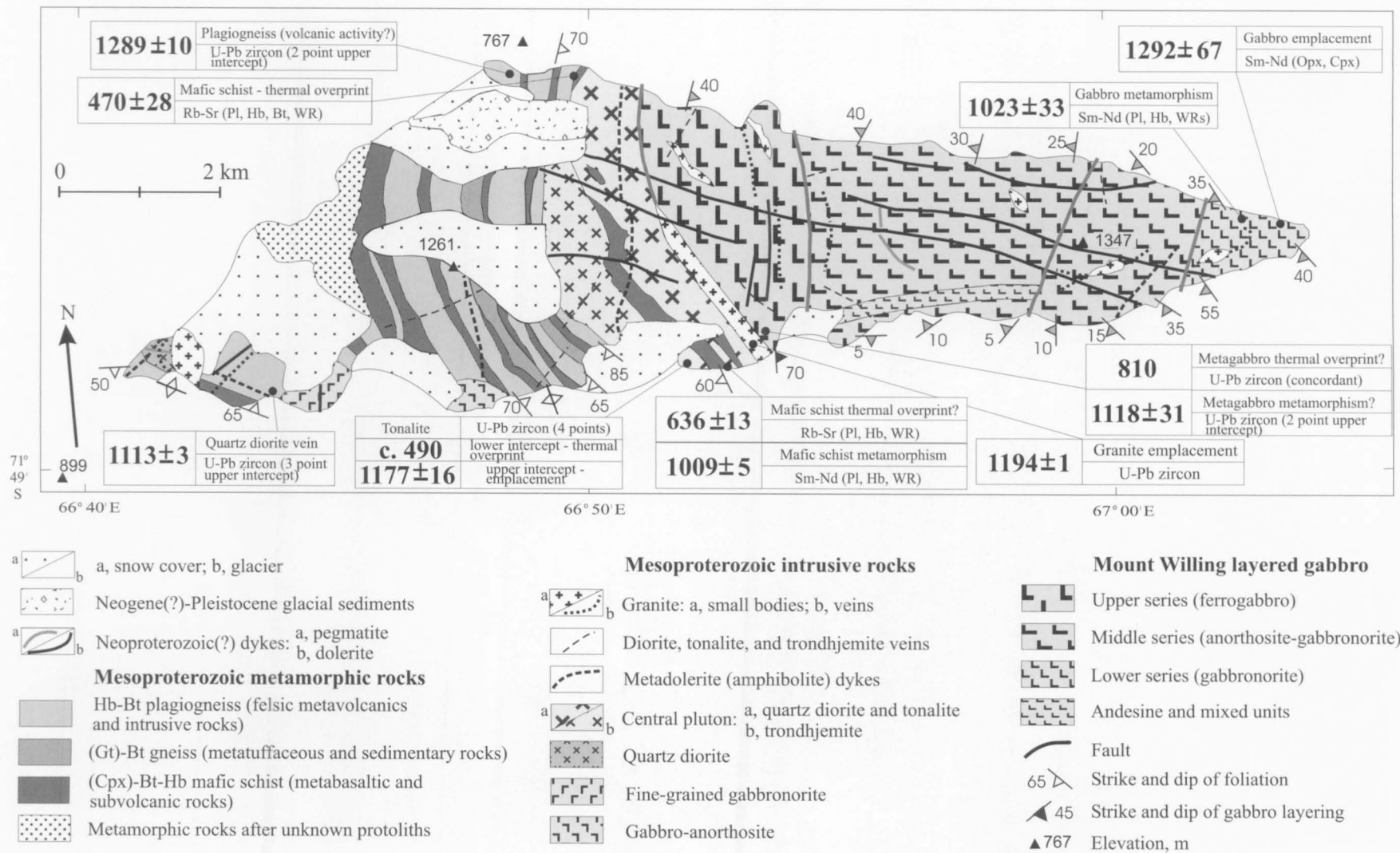


FIGURE 56

Geological map of Mount Willing. Sources of age data: Laiba & Mikhalsky (1999), Mikhalsky et al. (1999), and A.A. Laiba (unpublished data).

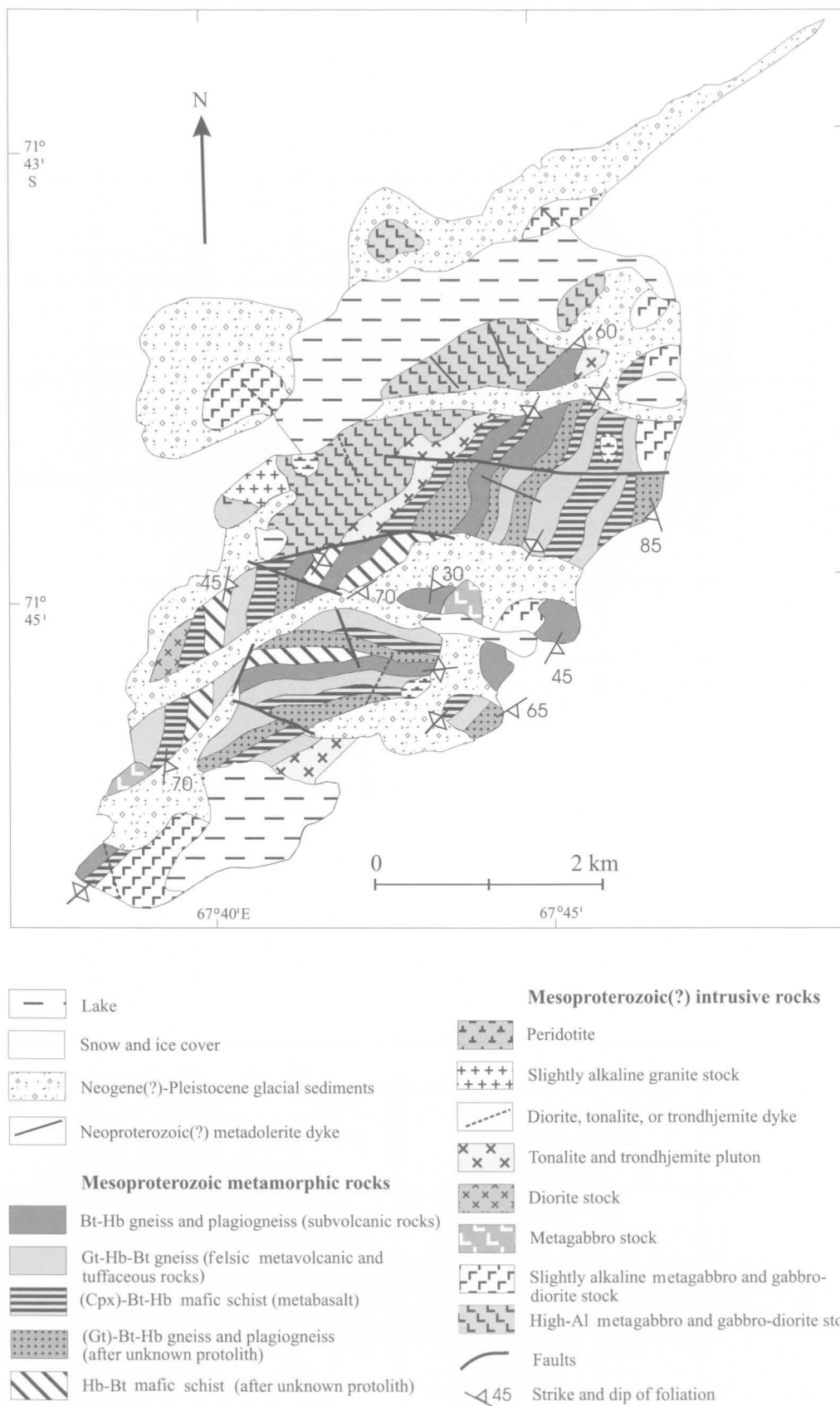


FIGURE 57
Geological map of Nilsson Rocks.

igneous mineral phases and textures in some parts, and including the Mount Willing layered intrusion; (3) deformed felsic intrusive bodies; and (4) abundant post-metamorphic dykes and veins of various compositions. The flat-lying Nilsson Rocks also consist of mafic to felsic metamorphic rocks, gabbro, granite and minor peridotite (Fig. 57). Most rocks are higher-grade (upper amphibolite facies, although some orthopyroxene-bearing metamorphic rocks crop out at Mount Willing) and could in part represent the basement on which the lower-grade metavolcanic rocks of Fisher Massif were deposited—but most authors consider this to be unlikely.

The close association of generally co-eval metavolcanic and plutonic rocks of broadly similar age and chemical composition, which originated in a similar tectonic environment (a convergent plate margin including volcanic and/or continental arcs), at Mount Willing, Fisher Massif and Nilsson Rocks allowed Mikhalsky et al. (1999) to describe them as a distinct Mesoproterozoic Fisher Complex. The lower grade metavolcanic rocks at Fisher Massif apparently represent higher crustal levels. The occurrences of high-Ti mafic volcanic rocks at Mount Willing and mildly alkaline gabbro at Nilsson Rocks suggest that subcontinental lithospheric mantle sources underlie this portion of the terrane.

MESOPROTEROZOIC METAVOLCANIC AND SUBVOLCANIC ROCKS

Fisher Massif

Metavolcanic rocks are best exposed in a 400 metre-high escarpment that forms the southeastern and southern slopes of Fisher Massif (Fig. 58). They mostly dip steeply to the north-northwest or northwest at 50–80°, but more gently (25–50°) in some places. Lava flows and tuffaceous beds are commonly 10 to 20 metres thick and rarely up to 200 metres. Preliminary U–Pb zircon data show that intermediate and felsic metavolcanic rocks at Fisher Massif

were emplaced about 1300 Ma ago (Beliatsky et al. 1994), consistent with an ion-microprobe U–Pb zircon age of 1283 ± 21 Ma for a metadacite (Kinny et al. 1997). Calculated initial $^{143}\text{Nd}/^{144}\text{Nd}$ (for $T = 1300$ Ma) ratios for three metavolcanic rocks range from 0.51104 to 0.51109, with $\epsilon^{1300}_{\text{Nd}}$ from +1.6 to +2.5 (Mikhalsky et al. 1996). Corresponding $T_{\text{DM}}^{\text{Nd}}$ model ages (1870–2250 Ma) are of uncertain reliability because of high $^{147}\text{Sm}/^{144}\text{Nd}$.

Field studies have revealed at least four successive sequences of different lithology, and two others that cannot be directly correlated with any of these (Fig. 59). Thin upper flow zones locally exhibit chilled textures suggesting that in some places the bedding is overturned. Further evidence of overturning is that the markedly tuffaceous sequence 4 is not intruded by felsic subvolcanic bodies. These are characteristic of sequences 1 to 3 and were presumably intruded prior to, or contemporaneously with, the emplacement of sequence 4 rocks. Moreover, chemical data are more consistent with sequence 1 being the oldest (see below). In the following description, it is therefore assumed that the succession is locally overturned. Overall, the volcanic sequences (excluding the mainly felsic subvolcanic bodies) at Fisher Massif comprise basalt (37 volume %), basaltic andesite (14%), andesite (20%), dacite (14%) and rhyodacite (15%); metasedimentary rocks account for 12 to 15 percent of the outcrops.

The presumed oldest *sequence 1* is at least 1000 metres thick and crops out in the southern part of Kar Bolshoi (Fig. 55). It is composed of fine-grained aphyric or rarely porphyritic basalt (classified as geochemical group B1, see below), intruded by numerous, mainly felsic subvolcanic bodies (predominantly sills, although dykes, small laccoliths of complex shape, and probable necks are also present). Porphyritic basalt forms thin layers and beds (0.2–3.0 m) and contains up to 25 percent of plagioclase megacrysts which are probably of cumulus origin. Subvolcanic bodies, which vary greatly in size (0.5–100 m), form nearly half of the sequence. They consist of dacite and rhyodacite, with minor andesite, and contain

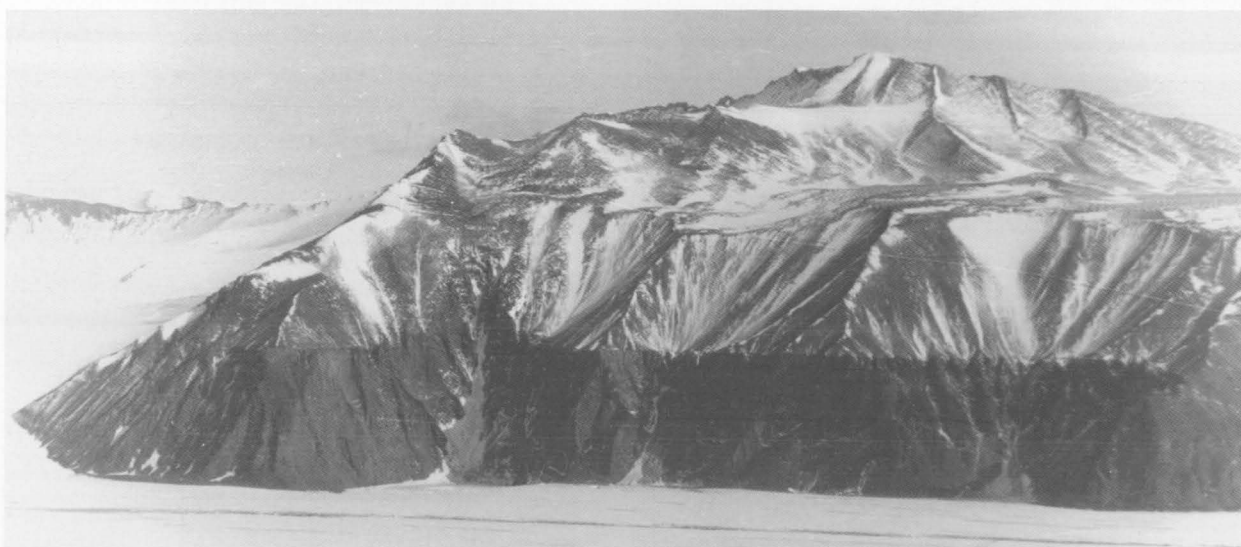


FIGURE 58

Central part of the southeastern slope of Fisher Massif, showing outcrops of metavolcanic rocks. The sharp horizontal line marks the lower limit of an erosion surface covered by thick glacial sediments.

numerous basaltic xenoliths. Porphyritic textures are common and there are abundant quartz megacrysts.

The 650 metre-thick *sequence 2*, exposed in the northeastern flank of Kar Bolshoi, consists of basalt (3%), basaltic andesite (40%), andesite (27%) and dacite (30%), intruded by numerous intermediate to felsic subvolcanic bodies which form a total of 200 metres of section. Lithological and textural features enable sequence 2 to be subdivided into three units (I–III; Fig. 59). Unit I comprises aphyric basalt, basaltic andesite, andesite and dacite. Unit II consists of intercalated beds of basaltic andesite and andesite. Unit III is composed mostly of dacite and rhyodacite, with the latter predominating higher in the section. The intermediate to felsic volcanic

rocks are termed geochemical group A1. Felsic subvolcanic rhyodacite bodies intrude all three units.

Sequence 3 (600 m thick) is composed mainly of massive or slightly schistose, locally diffusely layered, aphyric or rarely plagioclase-phyric basalt (geochemical groups B1 and B2, which form separate flows), with minor melanocratic amphibolite, basaltic andesite and felsic subvolcanic rocks. Concordant bodies, six to 27 metres thick, of mafic rock with coarse-grained, relict ophitic or gabbroic textures in the lower part of the section are probably sills.

Sequence 4 (1100 m) is strikingly different from sequences 1 to 3. It is composed of tuffaceous (62%) and volcanic (23%) rocks, and schistose metasediments (15%). Volcanic rocks comprise basaltic andesite (27%), andesite (25%), dacite (24%), and rhyodacite (24%). Three lithological units (IV–VI) are distinguished (Fig. 59). Unit IV consists of fine- or coarse-grained lapilli-bearing tuffaceous rocks of andesitic to dacitic composition, intercalated with one to 50 metre-thick beds of fine-grained micaceous quartz-feldspar schist formed from tuffite and/or silty sandstone. Unit V is made up of tuffaceous rocks of andesite to basaltic andesite composition. Unit VI comprises thin intercalated beds of dacite, rhyodacite and fine-grained banded tuff. As a whole, sequence 4 does not show a consistent trend towards more felsic rocks, but rather a number of andesite–dacite cycles. Most rocks have relatively high K_2O , and are classified as geochemical group A2. As already pointed out, the felsic subvolcanic bodies which are common in sequences 1 to 3 are absent from sequence 4.

Sequence 5 is exposed in the southern part of Fisher Massif. It is composed of mica–quartz schist and quartzite representing metamorphosed siltstone, silty sandstone, minor gravelstone, tuffaceous rocks and marble, with an overall thickness of 600 metres. A few thin beds (up to 1.5 m) of mildly alkaline basalt (geochemical group B3) and basaltic tuff occur within this sequence.

Sequence 6 occupies the central and northern parts of Fisher Massif (Fig. 55). It is about 1000 metres thick and

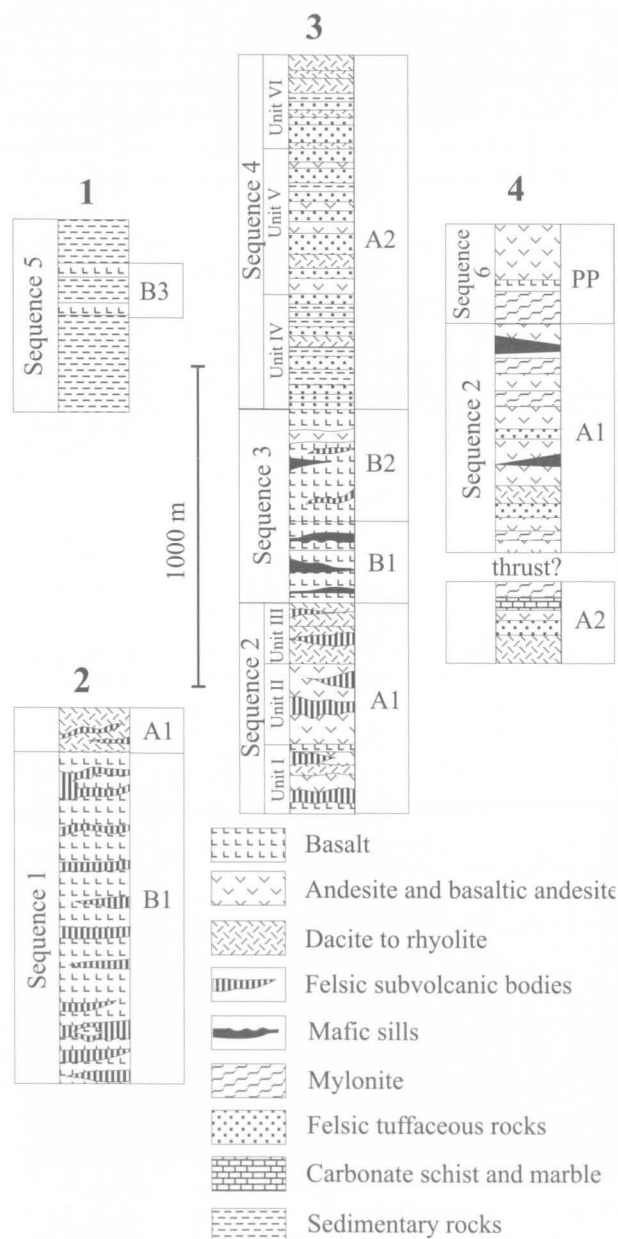


FIGURE 59

Schematic measured sections at Fisher Massif, showing the metavolcanic sequences and their geochemical groupings (see Fig. 55 for locations and text for details). Note that the sections are depicted in their inferred original orientations, with sequence 1 being the oldest.



FIGURE 60

Tight folds in marble bed; northeastern Fisher Massif. The hammer points to a mafic epidote-actinolite schist lens enclosed in marble. Similar smaller lenses occur within some thin marble layers or along folded planes.



FIGURE 61
Minor folds in marble-schist bed; northeastern Fisher Massif.



FIGURE 62
Slightly layered marble inclusion (2 x 4 m) in metabasalt; northeastern Fisher Massif.

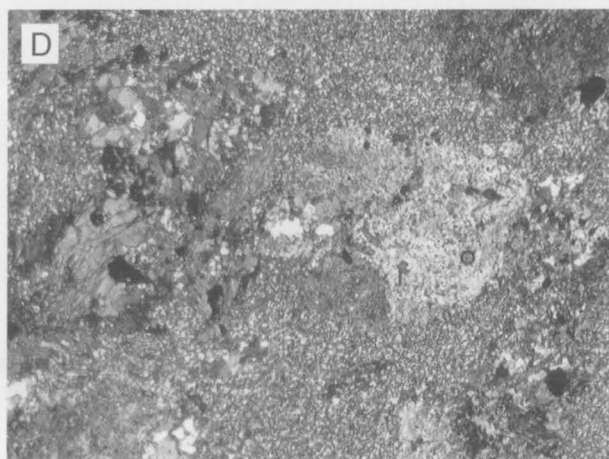
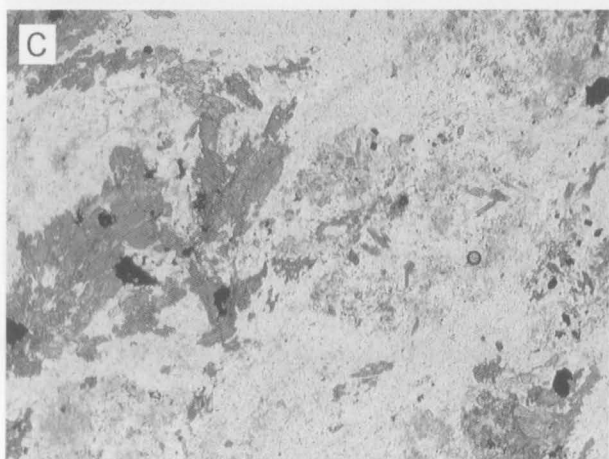
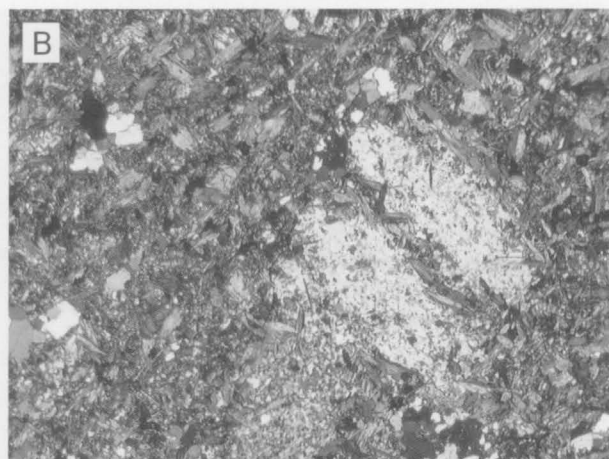
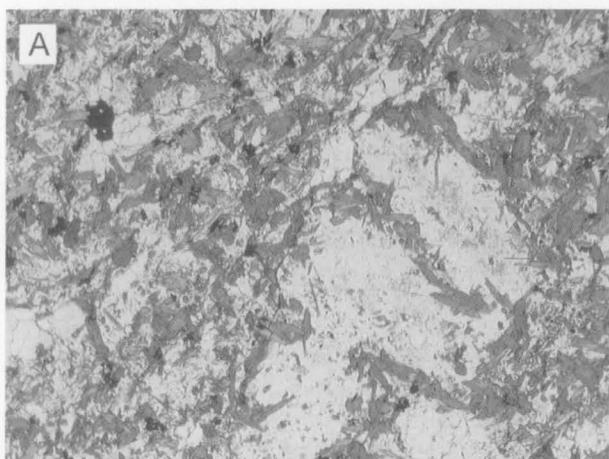


FIGURE 63
Metavolcanic rocks from Fisher Massif. (A, B) Meta-basaltic andesite with recrystallised quartz aggregates (amygdales?) (left) and rare recrystallised plagioclase microphenocrysts (centre right). Other constituents are bluish-green hornblende and minor biotite, opaque minerals and epidote. Sample 71280242. (C, D) Strongly recrystallised metadacite with aggregates of pale green amphibole and minor biotite, epidote and carbonate in a very fine-grained quartz-plagioclase matrix. A few recrystallised plagioclase and quartz microphenocrysts are visible. Sample 91286417. Cross-polarised light in B and D; width of field: 4 mm.

consists mainly of andesite, basaltic andesite and plagioclase porphyry (geochemical group PP), with large plagioclase phenocrysts forming 15 to 40 percent of the rocks. Globular structures, filled with quartz–epidote aggregates and up to 30 centimetres across, are typical of these rocks, which are highly mylonitised. The sequence contains a few conformable 10 to 20 metre-thick layers of marble, carbonate schist and banded ironstone, described below. Carbonate rocks are intensely deformed (Figs 60, 61) and recrystallised, and probably mark thrust zones. In a few places the plagioclase porphyries contain large andesite and marble blocks (Fig. 62), suggesting that they are at least partly of intrusive origin.

As no regional faults or thrusts have been found within the 1500 metre-thick sequences 2 to 4, they are considered to represent an actual succession of volcanic flows making up a thick tectonic slab or nappe. The total thickness of the metavolcanic and associated rocks is thus more than 2600 metres, or 3300 metres if the subvolcanic bodies intruded into sequences 1 to 3 are included.

Metamorphosed basalt and basaltic andesite are dark greenish-grey, fine-grained rocks with a characteristic pervasive schistosity, although massive varieties also occur. Most rocks are aphyric or contain rare recrystallised plagioclase phenocrysts up to one centimetre long (Fig. 63A, B), but abundant plagioclase megacrysts (10–40%) occur in some cumulus rocks. Relict intersertal, microlitic and locally ophitic textures are distinguishable in the groundmass. The rocks consist mainly of plagioclase and hornblende, with minor biotite, quartz, epidote, chlorite, opaque minerals, titanite, carbonate, sericite and garnet. Colour index ranges widely between 40 and 90, with the most mafic varieties being coarse-grained amphibolite.

Meta-andesites are grey, fine-grained schistose to diffusely layered or homogeneous rocks, with colour index between 20 and 35. They are commonly

porphyritic, and lepidoblastic, nematogranoblastic and cataclastic textures predominate. Sparse zoned plagioclase megacrysts (up to 2 mm) are enclosed in a relict felsitic or prismatic matrix, and a few rocks contain deformed K-feldspar megacrysts. Mafic minerals comprise amphibole (bluish-green hornblende, secondary actinolite, and rare cummingtonite: up to 35%), biotite (up to 25%), epidote (up to 10%), and opaque minerals (2–7%), and small amounts of chlorite, garnet, carbonate and sericite may also be present. Andesites of sequence 4 are typically biotite rich, whereas most of those in other sequences are amphibole rich.

Dacite and rhyodacite are light-coloured, sparsely porphyritic rocks. Metamorphic porphyroblastic, lepidoblastic and blastocataclastic textures are common (Fig. 63C, D). Relict phenocrysts comprise quartz, K-feldspar and plagioclase. The felsitic groundmass (quartz and feldspar) contains various amounts of bluish hornblende, pale green actinolite, epidote, colourless cummingtonite and biotite. Common minor phases are sericite, opaque minerals, garnet, chlorite, calcite, titanite, apatite and zircon. Colour index ranges from 10 to 25.

Variously coloured fine- to coarse-grained tuffaceous rocks commonly exhibit thin compositional layering and contain finer grained felsic inclusions up to one centimetre across, interpreted as lapilli. The matrix consists of fine-grained aggregates of quartz and feldspar. Some beds also contain up to 20 percent of large bombs (up to 50 cm across) of dacitic or rhyodacitic composition. The colour index ranges from 15 to 40, with biotite, bluish hornblende, actinolite, epidote and opaque minerals being common mafic phases.

Subvolcanic rocks are mainly of intermediate to felsic composition and are relatively coarse grained. They contain abundant zoned plagioclase and, in some rocks, quartz phenocrysts, quartz globules (?amygdales), and various amounts of prismatic amphibole, biotite, chlorite, carbonate, sericite, opaque minerals and apatite.

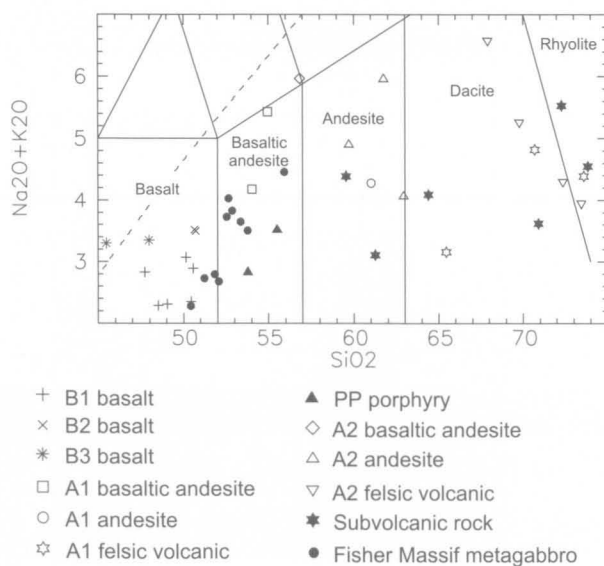


FIGURE 64

Alkalies–SiO₂ plot for volcanic and subvolcanic rocks and metagabbros from Fisher Massif. Fields correspond to the volcanic rock classification of Le Bas et al. (1986), and dashed line divides the alkaline (upper) and subalkaline fields of Irvine & Baragar (1971).

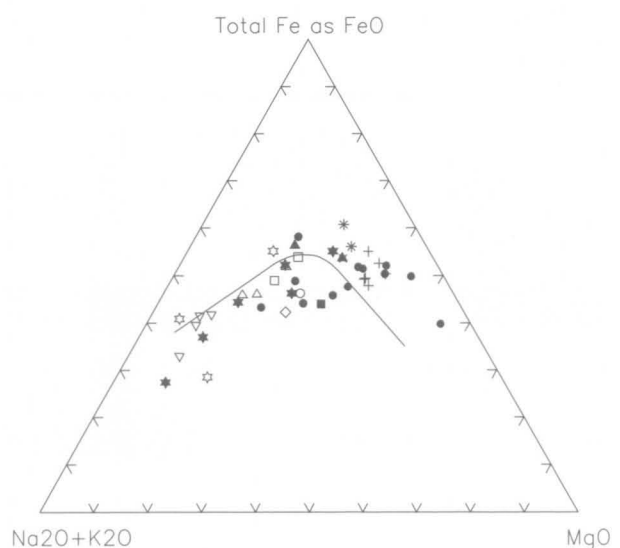


FIGURE 65

AFM diagram for volcanic and subvolcanic rocks and metagabbros from Fisher Massif. Symbols as in Figure 64.

TABLE 9. Chemical analyses and C.I.P.W. norms of representative metavolcanic and subvolcanic rocks from the Fisher Terrane.

Sample no.	93286663	93286675	31182-2	93286661	93286668	93286670	93286677	93286678	93286665	93286666	93286680
Field no.	36712-17	36811-19	31182-2	34521-12	36812-6	36812-20	36719-16	36719-17	36712-29	36713-2	36719-26
Locality	Southeast	Southeast	Southwest	North	Southeast	Southeast	Southeast	Southeast	Southeast	Southeast	Southeast
	Fisher	Fisher	Fisher	Fisher	Fisher	Fisher	Fisher	Fisher	Fisher	Fisher	Fisher
	Massif	Massif	Massif	Massif	Massif	Massif	Massif	Massif	Massif	Massif	Massif
Lithology	Porphyritic metabasalt	Metabasalt	Metabasalt	Porphyritic meta-basaltic andesite	Meta-basaltic andesite	Meta-andesite	Meta-basaltic andesite	Meta-andesite	Metadacite	Meta-rhyodacite	Meta-rhyodacite
Group	B1	B2	B3	PP	A1	A1	A2	A2	A1	A1	A2
SiO ₂	50.57	50.64	47.97	55.50	54.03	61.01	56.83	61.74	65.44	73.59	69.77
TiO ₂	0.93	1.54	2.14	0.97	1.17	0.74	0.66	0.59	0.48	0.24	0.48
Al ₂ O ₃	15.50	15.18	16.68	17.54	14.55	14.21	15.42	15.22	14.83	13.59	13.32
Fe ₂ O ₃	1.89	2.55	*12.29	3.11	3.72	2.24	2.58	3.04	2.98	1.98	1.75
FeO	7.58	8.99	—	5.36	5.66	4.95	5.30	4.76	3.34	1.57	3.09
MnO	0.14	0.17	0.20	0.13	0.12	0.13	0.10	0.09	0.07	0.02	0.12
MgO	7.22	6.25	5.86	2.80	3.54	3.82	4.44	2.84	1.74	0.46	1.24
CaO	11.68	8.52	9.82	8.97	8.33	5.97	6.18	3.57	6.35	3.32	2.75
Na ₂ O	2.77	3.27	2.26	2.68	3.35	2.99	3.58	3.41	3.00	4.33	3.30
K ₂ O	0.12	0.25	1.13	0.84	0.83	1.29	2.39	2.55	0.16	0.06	1.96
P ₂ O ₅	0.11	0.20	0.50	0.30	0.22	0.18	0.26	0.16	0.14	0.05	0.13
LOI	1.47	2.42	0.60	1.77	3.99	2.36	2.26	2.03	1.17	0.78	2.08
Rest	0.15	0.16	0.00	0.26	0.67	0.33	0.32	0.34	0.41	0.08	0.25
Total	100.13	100.14	99.45	100.23	100.18	100.22	100.32	100.34	100.11	100.07	100.24
O=F,S,Cl	0.00	0.01	0.00	0.01	0.25	0.06	0.00	0.00	0.16	0.01	0.00
Total	100.13	100.13	99.45	100.22	99.93	100.16	100.32	100.34	99.95	100.06	100.24
Q	—	1.34	—	13.44	10.13	19.35	6.85	18.25	31.08	40.11	34.03
C	—	—	—	—	—	—	—	0.74	—	0.49	1.08
Or	0.71	1.48	6.68	4.96	4.90	7.62	14.12	15.07	0.95	0.35	11.58
Ab	23.44	27.67	19.12	22.68	28.35	25.30	30.29	28.85	25.39	36.64	27.92
An	29.50	26.00	32.03	33.35	22.21	21.54	18.95	16.67	26.53	16.14	12.79
Di	22.58	12.28	11.05	7.56	14.41	5.63	8.15	—	3.32	—	—
Hy	16.09	21.70	19.10	9.16	7.39	13.01	13.77	12.49	5.72	2.03	6.74
Ol	1.41	—	1.94	—	—	—	—	—	—	—	—
Mt	2.74	3.70	2.68	4.51	5.39	3.25	3.74	4.41	4.32	2.87	2.54
Il	1.77	2.92	4.06	1.84	2.22	1.41	1.25	1.12	0.91	0.46	0.91
Ap	0.26	0.47	1.18	0.71	0.52	0.43	0.62	0.38	0.33	0.12	0.31
Li	4	6	—	10	12	23	18	21	5	2	13
Be	—	1	—	—	—	—	1	3	—	1	3
S	40	200	—	250	4950	1120	50	80	3120	110	90
Sc	46	40	—	34	35	24	24	21	28	14	15
V	248	259	—	392	317	168	318	190	81	13	57
Cr	240	45	—	25	24	125	113	73	8	2	10
Co	—	—	—	—	—	—	—	—	—	—	—
Ni	79	56	—	10	14	47	43	32	3	<1	3
Cu	17	8	—	102	118	56	129	118	33	3	12
Zn	67	129	—	85	66	78	72	73	22	8	96
Ga	16	18	—	20	17	16	18	18	15	13	15
Rb	1	5	—	16	26	35	48	61	2	<1	47
Sr	170	177	—	744	294	455	699	726	368	257	391
Y	25	35	—	16	28	25	19	18	20	19	26
Zr	75	118	—	75	97	120	115	90	56	93	107
Nb	4	12	—	4	4	9	5	3	3	4	3
Ba	61	97	—	242	252	458	733	1187	89	68	1082
La	3	5	—	13	9	20	26	12	7	5	25
Ce	12	21	—	31	25	45	52	36	27	14	57
Nd	7	15	—	16	11	22	25	14	12	<2	27
Pb	<2	5	—	7	4	7	11	11	<2	<2	12
Th	<2	5	—	<2	2	6	8	8	3	<2	8
U	<0.5	2.5	—	<0.5	<0.5	<0.5	1.0	0.5	0.5	1.0	<0.5
K/Rb	996	415	—	436	265	306	413	347	664	—	346
(Ce/Y) _n	1.2	1.5	—	4.8	2.2	4.5	6.8	5.0	3.4	1.8	5.5
Ba/Zr	0.81	0.82	—	3.23	2.60	3.82	6.37	13.2	1.59	0.73	10.1
Ce/Zr	0.16	0.18	—	0.41	0.26	0.38	0.45	0.40	0.48	0.15	0.53
Nb/Zr	0.05	0.10	—	0.05	0.04	0.08	0.04	0.03	0.05	0.04	0.03
Nb/Nb*	1.31	2.09	—	0.23	0.26	0.34	0.11	0.08	0.54	1.21	0.08
Sr/Sr*	1.38	0.75	—	2.46	1.28	1.06	1.42	2.30	1.48	—	0.73
mg	62.9	55.3	52.6	48.2	52.7	57.9	59.9	51.5	48.1	34.3	41.7

mg = atomic 100Mg/(Mg + Fe²⁺), except for samples without FeO, when 100Mg/(Mg + 0.85Fe(total)) was used.

Sample no.	93286682	93286686	93286688	93286687	39135-18	39135-26	39120-1	39140-2	40046	40090	40071
Field no.	36726-17	36712-25	36809-27	36809-20	39135-18	39135-26	39120-1	39140-2	40046	40090	40071
Locality	Southeast Fisher Massif	Southeast Fisher Massif	Southeast Fisher Massif	Southeast Fisher Massif	Mount Willing	Mount Willing	Mount Willing	Mount Willing	Rocks	Nilsson Rocks	Nilsson Rocks
Lithology	Meta- rhyodacite	Meta- rhyolite	Metadacite	Meta- andesite	Metabasalt (schist)	Metabasalt (schist)	Metabasaltic andesite (schist)	Metadacite (gneiss)	Metabasalt (schist)	Meta- andesite (gneiss)	Metadacite (gneiss)
Group	A2	Sub- volcanic	Sub- volcanic	Subv- volcanic	HTP	LTP			LTP		
SiO ₂	73.44	73.83	64.39	59.55	45.85	46.91	55.74	65.61	48.45	59.19	63.32
TiO ₂	0.41	0.28	0.57	0.83	2.45	1.34	0.69	0.50	1.22	0.90	0.70
Al ₂ O ₃	12.70	12.97	14.36	15.35	14.78	12.67	15.62	15.03	13.20	14.31	16.09
Fe ₂ O ₃	1.27	1.38	1.39	3.10	*15.28	*15.24	*9.13	*4.92	*10.45	*7.72	*5.65
FeO	1.91	2.05	5.06	5.36	—	—	—	—	—	—	—
MnO	0.08	0.07	0.10	0.13	0.21	0.23	0.18	0.08	0.22	0.20	0.13
MgO	0.72	1.06	3.24	3.06	7.06	7.78	5.56	2.63	10.19	6.11	2.43
CaO	3.47	2.52	5.21	6.09	9.99	11.93	7.02	4.52	12.24	4.90	4.95
Na ₂ O	2.35	4.01	3.90	3.57	2.46	1.74	4.21	5.21	1.52	3.86	3.75
K ₂ O	1.60	0.54	0.19	0.82	0.70	0.71	0.99	1.25	1.04	1.68	1.99
P ₂ O ₅	0.06	0.07	0.11	0.32	0.43	0.15	0.19	0.10	0.11	0.27	0.27
LOI	1.94	1.16	1.46	1.70	0.40	0.90	0.60	0.40	0.60	0.70	0.40
Rest	0.26	0.15	0.15	0.29	0.18	0.14	0.31	0.16	0.22	0.28	0.29
Total	100.21	100.09	100.13	100.17	99.79	99.74	100.24	100.41	99.46	100.12	99.97
O=F,S,Cl	0.02	0.04	0.01	0.05	0.00	0.00	0.00	0.00	0.00	0.00	0.00
Total	100.19	100.05	100.12	100.12	99.79	99.74	100.24	100.41	99.46	100.12	99.97
Q	44.43	40.61	22.80	17.15	—	—	2.48	16.33	—	8.73	17.89
C	0.94	1.37	—	—	—	—	—	—	—	—	—
Or	9.45	3.19	1.12	4.85	4.14	4.20	5.85	7.39	6.15	9.93	11.76
Ab	19.89	33.93	33.00	30.21	20.82	14.72	35.62	44.09	12.86	32.66	31.73
An	16.82	12.04	21.12	23.44	27.22	24.66	20.80	13.93	26.12	16.76	21.19
Di	—	—	3.31	3.85	16.11	27.67	10.49	6.45	27.37	4.70	1.33
Hy	3.72	4.93	13.81	11.88	7.14	10.25	19.56	9.00	11.23	21.67	11.72
Ol	—	—	—	—	13.52	9.69	—	—	9.15	—	—
Mt	1.84	2.00	2.02	4.49	3.33	3.32	1.99	1.07	2.27	1.68	1.23
Il	0.78	0.53	1.08	1.58	4.65	2.54	1.31	0.95	2.32	1.71	1.33
Ap	0.14	0.17	0.26	0.76	1.02	0.36	0.45	0.24	0.26	0.64	0.64
Li	11	5	8	14	—	—	—	—	—	—	—
Be	3	3	1	2	—	—	—	—	—	—	—
S	420	770	250	1060	—	—	—	—	—	—	—
Sc	12	14	27	25	—	—	—	—	—	—	—
V	20	28	135	152	212	292	175	75	267	187	62
Cr	6	5	80	27	103	123	228	83	525	355	54
Co	—	—	—	—	43	51	30	11	40	25	7
Ni	3	2	22	14	57	68	883	44	125	95	29
Cu	21	23	59	78	—	—	—	—	—	—	—
Zn	57	16	59	88	—	—	—	—	—	—	—
Ga	14	11	16	19	—	—	—	—	—	—	—
Rb	41	10	5	19	15	7	27	43	14	55	55
Sr	385	128	199	421	361	215	482	355	315	711	1125
Y	33	19	23	25	43	29	17	16	19	22	29
Zr	164	93	122	98	194	74	72	186	59	109	165
Nb	5	3	6	5	13	<5	6	8	4	6	12
Ba	915	154	136	426	298	212	514	511	243	701	852
La	32	5	11	20	16	—	—	—	—	—	—
Ce	72	16	29	40	35	—	—	—	—	—	—
Nd	33	4	11	23	22	—	—	—	—	—	—
Pb	13	2	<2	6	11	15	10	10	20	25	21
Th	9	2	2	<2	6	<5	<5	10	<1	<1	7
U	1.0	<0.5	<0.5	<0.5	—	—	—	—	—	—	—
K/Rb	324	448	315	358	395	893	304	241	617	254	300
(Ce/Y) _n	5.5	2.1	3.2	4.0	2.0	—	—	—	—	—	—
Ba/Zr	5.58	1.66	1.11	4.35	1.54	2.86	7.14	2.75	4.12	6.43	5.16
Ce/Zr	0.44	0.17	0.24	0.41	0.18	—	—	—	—	—	—
Nb/Zr	0.03	0.03	0.05	0.05	0.06	—	0.08	0.04	0.07	0.06	0.07
Nb/Nb*	0.14	0.32	0.75	0.24	0.73	—	—	—	—	—	—
Sr/Sr*	0.57	1.04	0.79	1.03	0.97	—	—	—	—	—	—
mg	40.2	48.0	53.3	50.4	51.8	54.3	58.6	55.4	69.4	64.8	50.0

Fisher Massif metavolcanic rocks show a wide compositional range (47–74% SiO₂), with no significant compositional gaps (Table 9). Virtually all samples plot within the sub-alkaline field on Figure 64, but show a wide range of alkali contents, even within individual rock groups. Such wide variations, together with extremely low alkali contents in some samples, suggest redistribution during late-magmatic or subsequent (metamorphic) events. Nevertheless, in spite of the wide variations due to alteration, there are consistent and statistically significant compositional differences between different rock groups. It is therefore likely that the consistently low K₂O in the subvolcanic rocks is essentially a primary feature.

Most of the volcanic sequences distinguished in the field have distinctive chemical compositions, although there is some overlap (Mikhalsky et al. 1996). Basalts of sequence 1 and the lower part of sequence 3 are slightly Ol-normative tholeiites (Fig. 64) with relatively high *mg** (54–66) and are termed *B1 basalts*. They plot in the tholeiite field on an AFM diagram (Fig. 65). Because of the very limited compositional variations and scatter of the data, partly due to alteration, the nature of possible fractionating phases for group B1 basalts is difficult to determine. However, marked decreases of Ni and Cr with *mg** decreasing from 62 to 56, and wide variations of MgO and Al₂O₃ with relatively small changes in SiO₂ suggest some degrees of olivine and/or pyroxene fractionation. The lack of Sr depletion does not allow for much plagioclase fractionation; indeed, minor plagioclase accumulation could account for the negative correlation between MgO and CaO, and small positive Sr anomalies (Fig. 66).

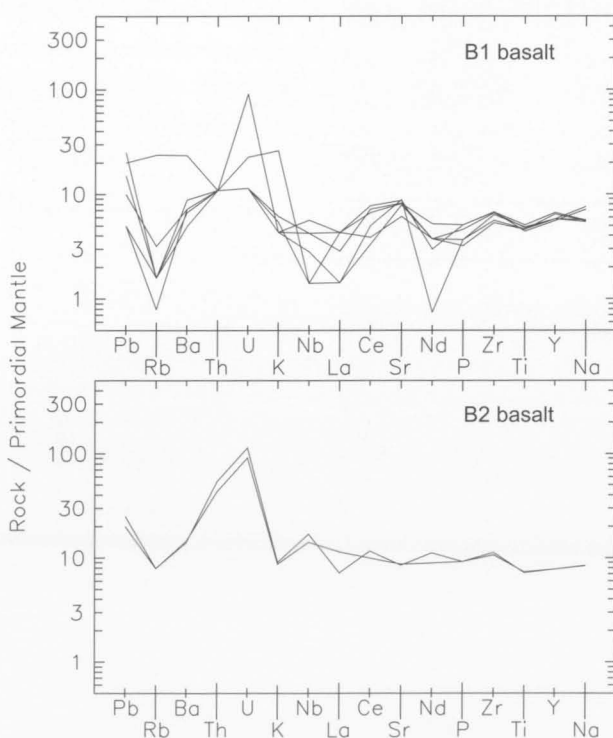


FIGURE 66
Spidergrams for groups B1 and B2 basalts from Fisher Massif.

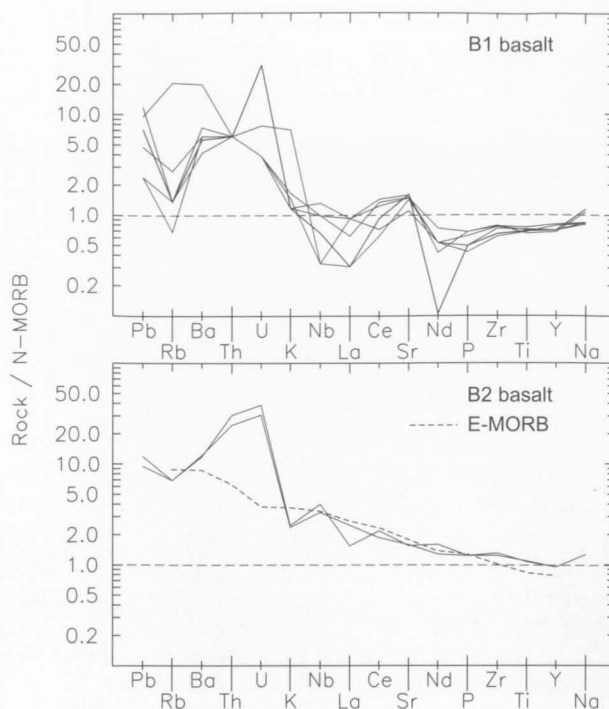


FIGURE 67
N-MORB-normalised spidergrams for groups B1 and B2 basalts from Fisher Massif, with E-MORB shown for comparison. Normalising values from Sun & McDonough (1989).

Most samples have moderately smooth, flat spidergram patterns (Fig. 66), including many elements (Ba, K and Sr) commonly mobilised by hydrous fluids, suggesting that, at least for less mobile elements, there were no major chemical changes during subsequent metamorphic events. However, significant depletions in Rb and, in some rocks, LREE are probably at least partly secondary features. The lack of significant LREE enrichment or Nb depletion, along with low La/Nb ratios (<1), preclude any major role for crustal contamination (Thompson et al. 1984). The much higher K, Rb and Ba of one sample is probably due to alteration. Much of the scatter for Th, U, Nb and LREE can be attributed to the analytical uncertainties inherent in measuring such low concentrations by XRF.

Group B1 basalts have some similarities to N-MORB (Fig. 67), but are slightly depleted in Nd, P, Zr, Ti and Y, and markedly enriched in LILE. They differ from E-MORB in having lower K, Rb, LREE and HFSE. These features are consistent with derivation from a depleted mantle source, with low LREE, HFSE, La/Ce, Ce/Y and Nb/Zr, broadly similar to N-MORB, but with an additional LILE-rich component. This component is necessary to explain the consistently high Ba/La ratios of the B1 rocks (17–20), which are more comparable with those of island-arc basalts (Arculus & Powell 1986). They may well reflect metasomatic enrichment of the mantle wedge by fluids or partial melts derived from subducted oceanic sediments (Hole et al. 1984). Group B1 may therefore represent a low-K volcanic-arc tholeiite suite, typical of subduction-related equivalents of MORB, such as back-arc basin basalts (Wilson 1989).

B2 basalts in the upper part of sequence 3 are slightly Q-normative tholeiites. They differ from B1 basalts in having higher LILE, LREE, and HFSE (particularly Th and U), but lower MgO, CaO, Cr, Ni and mg^* values (46–54) (Fig. 66). B2 basalts are similar to E-MORB (or even ocean island basalt), albeit with slightly different HFSE and LREE abundances and marked, probably secondary, Th and U enrichment (Fig. 67). Significant differences in some incompatible element ratios (e.g., higher Nb/Zr and Nb/Y) compared to B1 basalts cannot be due to fractionation, even though the B2 basalts are slightly more evolved. Much of the relative enrichment could be due to lower percentage melting, but a compositionally distinct, undepleted ($(Ce/Y)_N > 1$), slightly more LILE and LREE-enriched source is nevertheless required.

B3 basalts occur only in the predominantly sedimentary sequence 5. Although they border on alkaline compositions on an alkalis– SiO_2 plot (Fig. 64) the basalts are strongly Hy-normative (Table 9). They have markedly higher K_2O , TiO_2 (>2%), and P_2O_5 (0.5%), and lower Ti/P than B1 and B2 basalts, suggesting derivation from a distinct source, but may also have been formed by somewhat lower degrees of mantle melting.

Plagioclase porphyries (*group PP*) are basaltic andesites (Fig. 64) with characteristically high Al_2O_3 contents (16.5–19.0%; Fig. 68). They are more strongly evolved (Q-normative) than the basaltic rocks, and have a wide range of mg (39 to 55). The variations in alkali content are too large to be due to fractionation or different degrees of partial melting and probably reflect secondary alteration.

Compared to the B1 and B2 basalts, PP rocks are enriched in most LILE, depleted in Ti and Y, and have prominent negative Nb and positive Sr anomalies (Fig. 69). Many incompatible element ratios are quite different to those of group B1 basalts (e.g., higher K/Zr, La/Nb, Nb/Y and Ce/Y, and lower Y/Zr), and PP rocks appear to have much closer affinities with groups A1 and A2 volcanic rocks and, more particularly, the metagabbros (see below). A strong negative correlation of Sr with Zr, along with the positive Sr anomalies, shows that Sr was far from incompatible and suggests that plagioclase accumulation was an important process.

Basaltic andesites, andesites and subordinate dacites of sequence 2, defined as *group A1*, have wide ranges of SiO_2 (54–74%), K_2O (0.06–1.29%), and mg (34–58). A1 andesitic rocks tend to be enriched in most LILE and LREE, but have similar HFSE contents to B1 and B2 basalts (Figs 64, 68). Spidergrams show marked negative Nb anomalies and are generally similar to those of the PP group, except for higher HFSE (particularly Y) and much smaller Sr anomalies (Fig. 69). These andesitic rocks form a rather heterogeneous group. For example, the basaltic andesites include high-Al (16–18% Al_2O_3) and low-Al (14–15%) varieties (Fig. 68). Low-Al rocks show an initial positive correlation of Al_2O_3 with SiO_2 , which could be due to crystal fractionation dominated by ferromagnesian phases (olivine + clinopyroxene). At later stages, fractionation involving major plagioclase is supported by decreasing Al_2O_3 and negative Zr–Sr and Zr–Ba correlations. The high-Al rocks cannot have formed from low-Al magma by

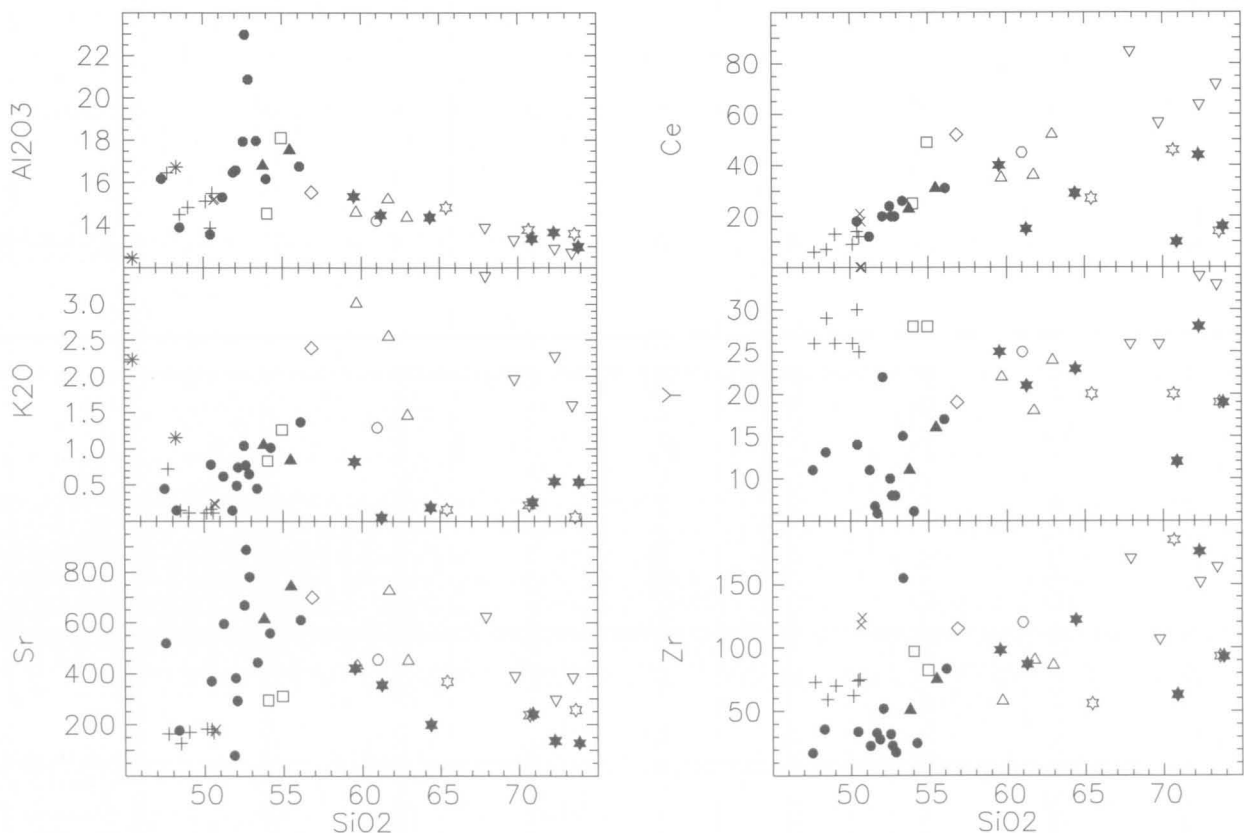


FIGURE 68

SiO_2 variation diagrams for volcanic and subvolcanic rocks and metagabbros from Fisher Massif. Symbols as in Figure 64.

plagioclase accumulation. Plagioclase phenocrysts are lacking and one sample has a negative Sr anomaly, as well as a large positive P anomaly (Fig. 69). In contrast, two low-Al samples have small positive Sr anomalies and the more siliceous of these (andesite 36812-20) has relatively high Cr, Ni and *mg*. All these features indicate the presence of several distinct magma types (assuming no major alteration effects), which implies distinct parent magmas and probably different source compositions. Most of the dacitic rocks have very low LILE, especially K and Rb, which indicate that they cannot be genetically related to the andesitic rocks. Their similar Sr contents to the latter and lack of negative Sr anomalies (Fig. 69) are also inconsistent with an origin by plagioclase-dominated fractionation of an andesitic magma.

Sequence 4 rocks (classified as *group A2*) also have a wide range of composition, from basaltic andesite to rhyolite (55–73% SiO₂), but they tend to be more felsic and to have higher LILE contents than those of group A1 (Figs 64, 68). The andesitic rocks have particularly high K₂O (1.46–3.01%), being of high-K type on the

classification of Le Maitre (1989), whereas the more felsic rocks are mostly of medium-K type. A2 andesitic rocks have similar spidergram patterns to those of group A1, but tend to be even more LILE-enriched and to have higher Ni and Cr and lower Nb, Ti, Y and Nb/Zr (Fig. 69), precluding a close genetic relationship. The dacites and rhyolites have very irregular patterns with negative Nb, Sr, P and Ti anomalies (Fig. 70), typical of fractionated felsic igneous rocks in general (Tarney et al. 1987). They differ from group A1 felsic rocks in having higher LREE, Y, Sr and, in particular, K, Rb, Ba, Th and Pb, as well as lower Na.

Petrographic and chemical data are consistent with much of the compositional variation of group A2 being due to low-pressure fractionation involving major plagioclase (and possibly K-feldspar in the more felsic rocks) in addition to mafic phases. Spidergrams (Figs 69, 70) appear to be generally consistent with the felsic group A2 rocks having formed by fractionation, possibly through AFC (assimilation–fractional crystallisation; DePaolo 1981) processes, of an intermediate (andesitic) magma (large negative P and Ti anomalies, and smaller negative Sr

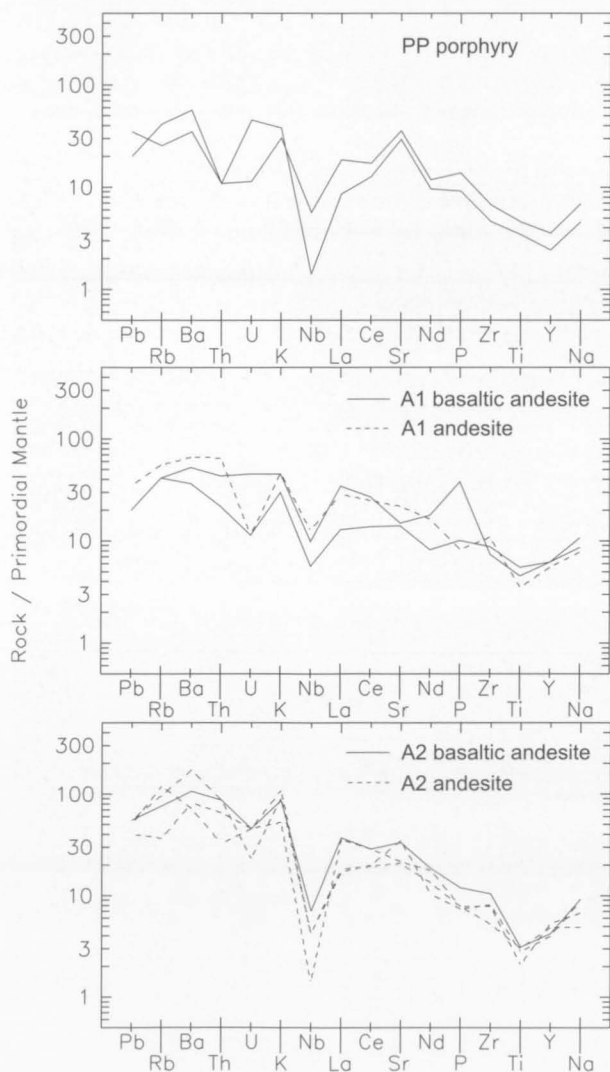


FIGURE 69

Spidergrams for andesitic volcanic rocks of groups PP, A1 and A2 from Fisher Massif.

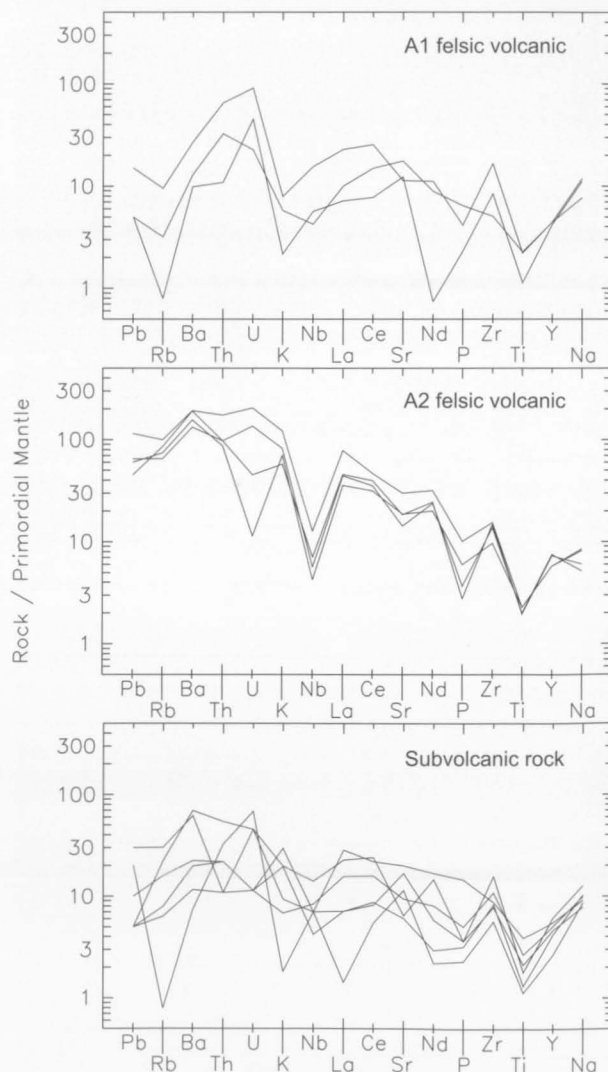


FIGURE 70

Spidergrams for felsic volcanic rocks of groups A1 and A2, and subvolcanic rocks from Fisher Massif.

anomalies in rhyolites). However, direct fractionation of an A2 andesitic magma is unlikely because, in contrast to the felsic rocks, they are of high-K type. Alternatively, formation of the felsic volcanics by partial melting of felsic to intermediate lower crustal rocks is possible, although the relatively small negative Sr anomalies are more difficult to explain by such a process. In either case, a significant continental crustal component is likely, and is supported by zircon U–Pb data for felsic metavolcanic rocks, including a single 1900 Ma zircon xenocryst in a dacite (Kinny et al. 1997) and a model $^{207}\text{Pb}/^{206}\text{Pb}$ age of 2560 Ma for an A2 tuffaceous rhyodacite (Beliatsky et al. 1994).

Thin subvolcanic bodies of andesite, dacite and rhyodacite cutting sequences 1 to 3 mostly have compositions similar to the more felsic rocks of group A1, with low LILE and LREE (Figs 64, 68, 70). Such consistent compositional features suggest that they are largely primary, although the particularly low K and Rb of one andesite may well be due to alteration.

Groups A1 and A2 show calc-alkaline affinities on an AFM diagram, whereas the cumulus PP rocks tend to plot in the tholeiite field (Fig. 65). Andesitic rocks of all these groups have many island-arc characteristics: large negative Nb anomalies, generally small positive Sr anomalies, high LILE/LREE, and low Ti and Y (Fig. 69)—all of which suggest magma generation from broadly similar source regions in a subduction environment. Nevertheless, group A2 high-K andesites are more LILE-enriched and have distinctive incompatible element ratios (e.g., lower Ti/Zr) which imply a somewhat different source region to that of group A1. Assuming that they are not entirely due to fractionation, lower Ti and Y contents (Figs 68, 69) suggest derivation from a more depleted (?refractory) mantle source that subsequently underwent enrichment in LILE and LREE, probably from slab-derived fluids. Felsic rocks of both groups A1 and A2, as well as the subvolcanic intrusives, have the low Rb, Y and Nb contents characteristic of volcanic-arc, rather than collisional, within-plate, or ocean ridge, granitoids on the classification of Pearce et al. (1984). Similarly, most Fisher Massif granitoids have volcanic-arc type compositions (Sheraton et al. 1996; see also below).

As discussed by Mikhalsky et al. (1996), the lithological and chemical compositions of the Fisher Massif metavolcanic rocks show that several different source components were involved in a complex history of magma generation. Assuming that the succession exposed in the Kar Bolshoi area is overturned, then group B1 tholeiitic basalts would be the oldest. These rocks are likely to have originated from a subduction-modified depleted mantle source region, possibly in an island arc or back-arc basin. Rocks of the mostly andesitic group A1 are of island-arc calc-alkaline character and were derived from a distinct mantle source, with a more significant additional (either partly or wholly subduction-derived) crustal component. They originated before the earlier mantle-melting event ceased, and rocks of both basaltic and andesitic composition are commonly intercalated. At a later stage, somewhat more evolved melts (B2 basalts) of a relatively Nb-rich P-MORB or OIB-like mantle source appeared, perhaps generated in a back-arc marginal basin environment. Intermediate to felsic medium to high-K volcanic rocks of group A2 post-date the main basaltic

successions, probably reflecting a more evolved stage of arc activity with greater crustal involvement in an Andean-type continental margin. Relatively alkaline B3 basalts appear to post-date the high-K group A2 rocks. High-Al plagioclase porphyries (PP) appear to terminate the volcanic activity, and were derived from a mantle (+ crustal) source broadly similar to those of the groups A1 and A2 andesitic rocks. Such a progression from predominantly tholeiitic to calc-alkaline (and possibly mildly alkaline) volcanics is typical of the evolution of magmatic arcs (Wilson 1989; Yanagi & Yamashita 1994).

Mount Willing

Metamorphic rocks crop out on the western part of Mount Willing, striking northwest or north to northeast on the northern slope, and east–west near the western extremity (Fig. 56). They are mostly steeply dipping, but locally dip at 20–50°. The strike variations imply broad open folds, with amplitudes of 100 to 200 metres and east–west axes. The metamorphic rocks consist of two rock series: one *mafic* and the other *composite mafic-felsic*. The mafic series consists mainly of mafic schist and minor felsic plagiogneiss (tonalitic orthogneiss). The composite series, which crops out in the central part of Mount Willing, is predominantly felsic plagiogneiss, with subordinate mafic schist and paragneiss. Plagiogneiss

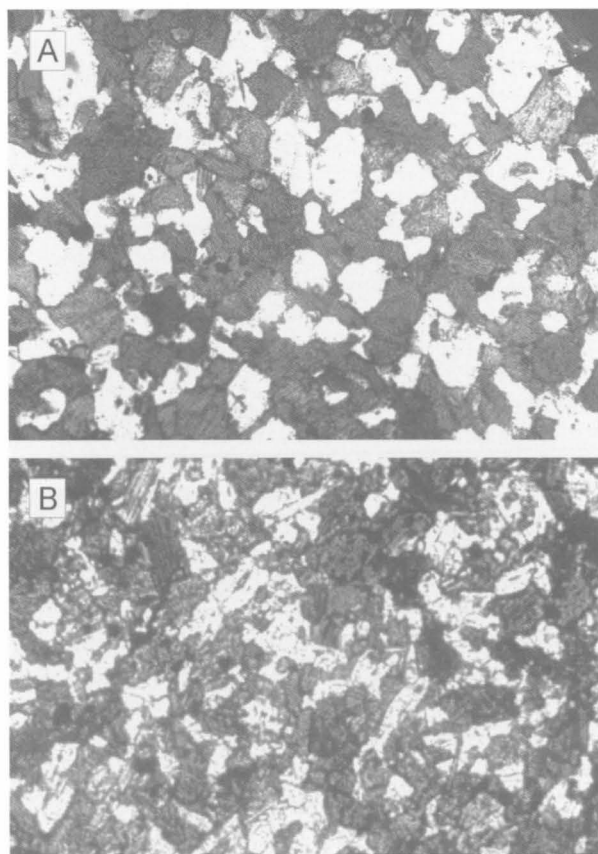


FIGURE 71

Mafic rocks from Mount Willing.

(A) Plagioclase–hornblende schist with relict microgabbroic texture. Sample 39132-3.

(B) Plagioclase–hornblende schist with relict subophitic texture. Sample 39143-1. Width of field: 4 mm.

forms thick (50–500 m) units that contain thin layers of mafic schist (possibly deformed dykes) and paragneiss. It probably represents mainly concordant subvolcanic bodies, but some units may be of volcanic or more deep-seated intrusive origin. Mafic schist forms members five to 150 metres (and rarely 750 metres) thick, intercalated with plagiogneiss. It is fine to very fine grained and homogeneous, with relict ophitic or gabbroic textures, and so could represent either intrusive bodies (sills) or thick, well-crystallised lava flows (i.e., be either subvolcanic or volcanic). Biotite paragneiss is exposed in a few localities as minor units some 10 to 100 metres thick.

Thus, the metamorphic sequence at Mount Willing comprises three lithologies: (1) biotite–amphibole and rare orthopyroxene–biotite *mafic schist*; (2) amphibole–biotite, rarely garnet-bearing, *felsic plagiogneiss*; and (3) layered biotite *paragneiss* (described in the next section). Almost all rocks have been metamorphosed under almost amphibolite-facies conditions, although orthopyroxene occurs locally. Small concordant veins of quartz diorite to granite composition occur in a few places in spatial association with plagiogneiss. These veins probably resulted from localised melting during tonalite emplacement rather than during regional metamorphism, though the latter may not be discounted.

Mafic schists are fine-grained melanocratic rocks (colour index 25–70, but mostly 35–55); relict primary igneous minerals and textures (microgabbroic or ophitic) are locally preserved (Fig. 71). The rocks consist of partly zoned plagioclase (An_{35-45} , rarely An_{54-64} or An_{20-50} ; 30–65%), amphibole (usually 15–65%, but absent from a few samples), biotite (up to 18%), opaque minerals (0.5–5%), and quartz (up to 7%). Rare orthopyroxene (mg 38–39 to 63–65; 5–30%) forms short prismatic grains or irregular anhedral grains, 0.2 to 1.0 millimetres across. It shows marginal hydration, reflected by anthophyllite rims. Orthopyroxene has a wide compositional range (Al_2O_3 1–3%, CaO 0.2–0.8%, MnO 0.4–1.2%, and Cr_2O_3 0–0.4%). One sample (39135-24) has a composition similar to those in granulite-facies mafic granulites and tonalitic gneisses from the Beaver-Lambert Terrane (Ravich & Kamenev 1975; Ravich et al. 1978), but most Mount Willing orthopyroxenes have lower Al_2O_3 contents similar to those in the Mount Willing layered gabbro. So although high-grade (up to granulite-facies) metamorphic rocks may occur locally, this event must have been of very restricted extent as igneous textures would hardly survive a regional granulite-facies event. It is possible that such rocks may be older basement relicts, but they more likely represent metamorphosed plutonic bodies. Green, or rarely bluish-green, amphibole (mostly tschermakitic hornblende or magnesio-hornblende) forms fine-grained prismatic or irregular grains and aggregates. Buff-brown biotite (mg 55–57, rarely 34 or 68) forms fine disseminated flakes partly replacing hornblende. Opaque minerals are mostly ilmenite, with minor magnetite and sulphides. Secondary minerals include chlorite, sericite and carbonate, replacing hornblende and plagioclase.

Felsic plagiogneiss is predominantly of quartz dioritic, tonalitic, or trondhjemitic composition. Colour index ranges from 18 to 30 (quartz diorite) or 10 to 16 (tonalite and trondjemite). Quartz diorite gneiss contains plagioclase (50–60%), quartz (13–20%), biotite (4–25%),

amphibole (1–23%), garnet (up to 2%) and opaque minerals (up to 3%); apatite, titanite and zircon are accessory phases. Tonalite and trondhjemitic gneiss contains more quartz (25–35%) and less amphibole (up to 5%). Plagioclase is An_{28-31} or rarely An_{37-40} . Amphibole comprises green to bluish-green hornblende (magnesio-hornblende, tschermakitic hornblende, or ferro-hornblende) that forms large poikiloblasts and aggregates of fine prismatic or acicular grains. Small biotite (mg 45–56) flakes are widespread in all lithologies. Pale pink garnet forms rounded fractured grains in a few rocks. It has low MgO (1.8–4.6%), and high FeO (28–34%) and MnO (1.3–7%), typical of amphibolite-facies garnets reported by Ravich & Kamenev (1975) and Ravich et al. (1978) from elsewhere in the PCM. Retrograde chlorite, epidote, sericite and carbonate (forming up to 3–5% of the rock) are associated with brittle deformation structures.

Mafic schists have mg^* values ranging from 43 to 68, with most between 50 and 60. Basaltic rocks are most common, but basaltic andesite and rare andesite are also present (Fig. 72). Most basalts are strongly Ol-normative (6–17%) and have tholeiitic compositions (Fig. 73), with up to 21 percent normative Hy; others are transitional to slightly alkaline (two are slightly Ne-normative). They are predominantly low-Al and medium-K (on the classification of Gill 1981). One rock with very high Al_2O_3 (23.6%) may be a plagioclase-rich cumulate, although its low Sr (133 ppm) may be more consistent with a calc-silicate origin. A distinctive feature of the Mount Willing mafic schists is the presence of rocks relatively enriched in TiO_2 (2.2–2.7%) and P_2O_5 (0.24–0.91%). These samples also have higher total FeO (13–15%), LREE (e.g., Ce 33–102 ppm), Y (40–84 ppm), Zr (119–600 ppm), and Nb (7–30 ppm), but slightly lower SiO_2 (Table 9; Fig. 74). Such high-Ti, high-P (HTP) schists crop out in the western part of Mount Willing (the *mafic series*), whereas low-Ti, low-P (LTP) basalts and basaltic andesites occur in the central part of Mount Willing (within the *composite mafic-felsic series*).

Mafic schists from Mount Willing have broadly similar compositions to mafic metavolcanic rocks from Fisher Massif, with both tholeiitic and calc-alkaline rock series

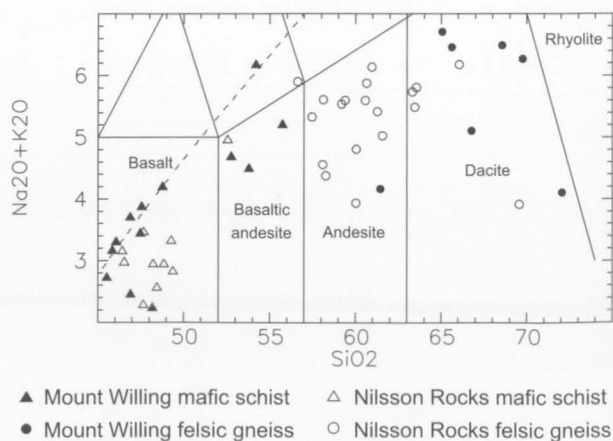


FIGURE 72

Alkalies– SiO_2 plot for metavolcanic rocks from Mount Willing and Nilsson Rocks. Fields correspond to the volcanic rock classification of Le Bas et al. (1986), and dashed line divides the alkaline (upper) and subalkaline fields of Irvine & Baragar (1971).

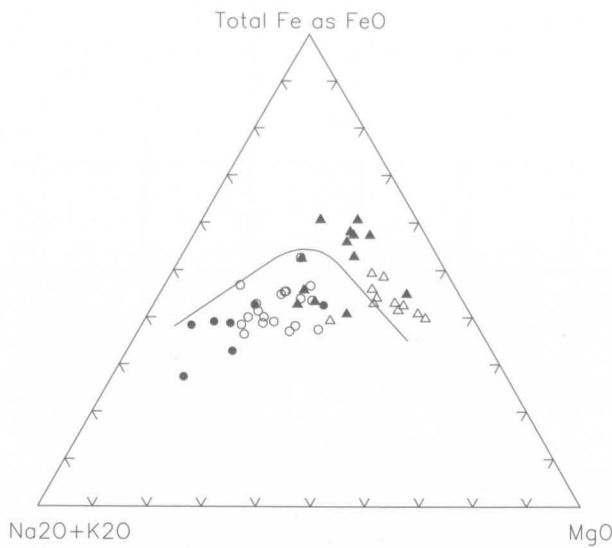


FIGURE 73
AFM diagram for metavolcanic rocks from Mount Willing and Nilsson Rocks. Symbols as in Figure 72.

being distinguished by Mikhalsky et al. (1999). However, there are significant differences (Table 9, Figs 65–68, 72–75). HTP basalts appear to be rare at Fisher Massif, but may be represented by the relatively alkaline group B3 basalts (see above). Basaltic rocks from both areas have similar ratios of many incompatible element ratios, notably the HFSE (e.g., Ti/Zr, P/Zr, Nb/Zr and Y/Zr), and these are close to estimated primordial mantle values (Sun & McDonough 1989). However, mafic rocks from Mount Willing, especially the LTP group, have variable but

generally much higher K/Zr and Ba/Zr—although it is uncertain to what extent this reflects alteration processes. Most minor and trace elements, including HFSE, show rather poor correlations with SiO₂ (Fig. 74) or *mg**; the relatively low HFSE of more evolved (low-*mg**) rocks are probably due to fractionation processes. Spidergrams of most HTP rocks are not dissimilar to B2 basalts from Fisher Massif, with only small Nb and Sr anomalies, although they show somewhat greater enrichment in most incompatible elements (Pb–Zr: Figs 66, 75). One rock (39135-17) has anomalously high contents of many incompatible elements, a small positive Nb anomaly, and apparently a negative Sr anomaly. LTP basalts appear to have more irregular spidergrams with more marked negative Nb anomalies, lower LREE and HFSE, and similar LILE. They are generally more evolved, and clearly cannot be directly genetically related to the HTP suite. A sample with a large positive Sr anomaly is probably a plagioclase cumulate, and others may also have cumulus features. This would suggest that at least some mafic schists are of intrusive origin.

The Mount Willing mafic rocks appear to have been derived from mantle source regions that differed mainly in their degrees of LILE enrichment. Assuming that LILE variability is not solely a consequence of alteration, the LTP basalts seem to have been derived from the more enriched source, consistent with their larger negative Nb anomalies. Whether this enrichment reflects melting of a distinct mantle source region or a more enriched part of a heterogeneous mantle source, or whether it was due to introduction of a subduction-derived LILE-rich fluid during magma generation is uncertain. Much of the variation in the abundances of many other minor and trace elements, such as REE and HFSE, probably reflects differences in the

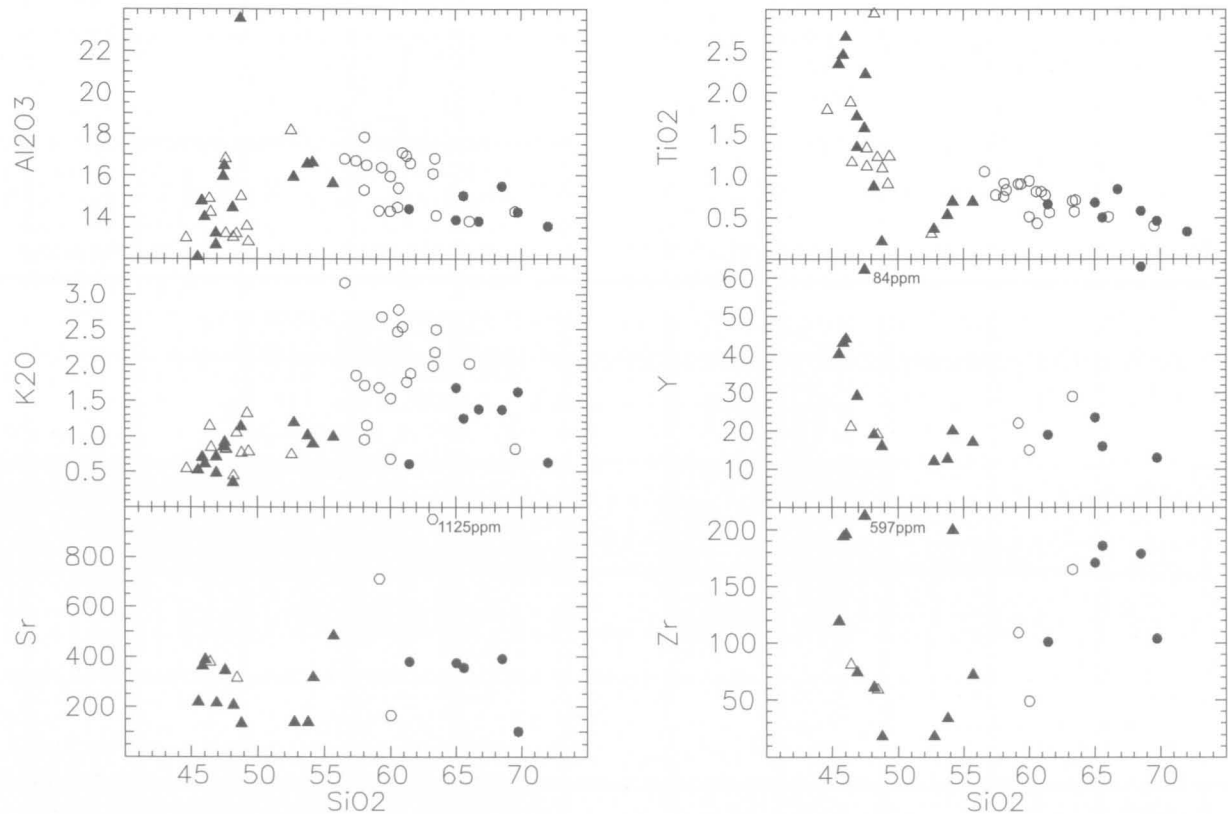


FIGURE 74
SiO₂ variation diagrams for metavolcanic rocks from Mount Willing and Nilsson Rocks. Symbols as in Figure 72.

degrees and/or conditions of melting, together with any superimposed crystal fractionation. Thus, the HTP group was probably derived by somewhat lower degrees of melting than the LTP group. Few REE data are available, but a single HTP basalt has a chondrite-normalised $(La/Yb)_n$ ratio of 3.0 compared to 2.7 and 1.1 for two LTP basalts (Fig. 76). The small difference could easily reflect a smaller percentage melting of a slightly enriched source for the former. T_{DM}^{Nd} model ages for two mafic schists are 1370 and 1580 Ma, broadly similar to values between 1520 and 1830 Ma for felsic rocks. However, if the Mount Willing rocks were derived from a less-depleted mantle source, their crustal formation ages would be younger (e.g., 1200–1600 Ma, assuming ϵ_{Nd} (1300 Ma) of +2.5–3.5 for the source, as used for Fisher Massif metavolcanic rocks by Mikhalsky et al. 1996).

The plagiogneisses are of quartz dioritic to tonalitic and trondhjemitic composition. They have both petrographic and compositional features (e.g., ASI <1.1) typical of granitoids derived by melting of igneous, rather than sedimentary, precursors (I-type of Chappell & White 1974). Low Sr_i ratios (0.704–0.706) are consistent with this

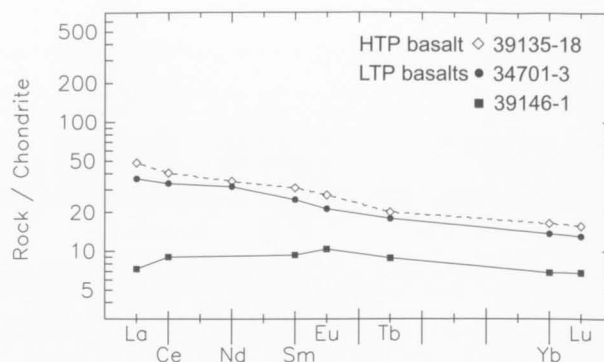


FIGURE 76

Chondrite-normalised rare-earth element abundance plots for metabasaltic rocks from Mount Willing.

(Mikhalsky et al. 1999). Calc-alkaline affinities on an AFM diagram (Fig. 73), high Sr and low Y contents (Fig. 74), and spidergrams with marked negative and (probably) positive Sr anomalies (Fig. 75) are all typical of volcanic-arc granitoids (Pearce et al. 1984; Sheraton et al. 1996). Low-Y, high-Sr compositions suggest a generally similar origin to Archaean TTG suites, namely hydrous partial melting of a garnet and/or amphibole-bearing mafic source. For Mesoproterozoic rocks, at least, this suggests involvement of subducted oceanic crust (Tarney et al. 1987). The plagiogneisses are similar in these respects to granitic intrusive rocks that crop out at Mount Willing and other parts of the Fisher Terrane. These are described below.

Nilsson Rocks

Metavolcanic (or subvolcanic) rocks are also abundant at Nilsson Rocks (Fig. 57). They occur as intercalated beds and units of mafic schist and plagiogneiss, 10 to 200 metres thick, with a total apparent thickness of about 1000 to 1500 metres. The rocks are highly deformed and metamorphosed, but relict primary igneous textures and globular structures suggestive of a volcanic origin are locally preserved. Unlike at Fisher Massif and Mount Willing, mafic schist is subordinate (25–30%) to felsic plagiogneiss (70–75%). The sequence exhibits large open and small isoclinal folds. The plagiogneiss is intermediate to felsic in composition (Table 9), and appears to be compositionally similar to sequence 4 at Fisher Massif. The gneiss consists of plagioclase (An_{30-40} : 55–70%), quartz (10–30%), biotite (13–25%), hornblende or cummingtonite (up to 15%), opaque minerals (2–3%), garnet (up to 15%), K-feldspar (2–15%), and minor diopside. Mafic schist (colour index 45–70) comprises plagioclase (An_{50-60} : 30–55%), hornblende or cummingtonite (40–60%), biotite (up to 10%), opaque minerals (up to 12%), titanite (up to 5%), diopside (up to 45%), and epidote (up to 50%).

The presumed metavolcanic sequence at Nilsson Rocks has many compositional features in common with those at Fisher Massif and Mount Willing. Basaltic rocks include both HTP and LTP varieties, but the latter appears to dominate (Fig. 74). However, the mafic rocks are more primitive with mg^* mostly between 62 and 74, and basaltic andesites are less common (Figs 72, 73). Plagiogneisses tend to be more potassic and less siliceous than those from Mount Willing, and range from quartz diorite (or andesite)

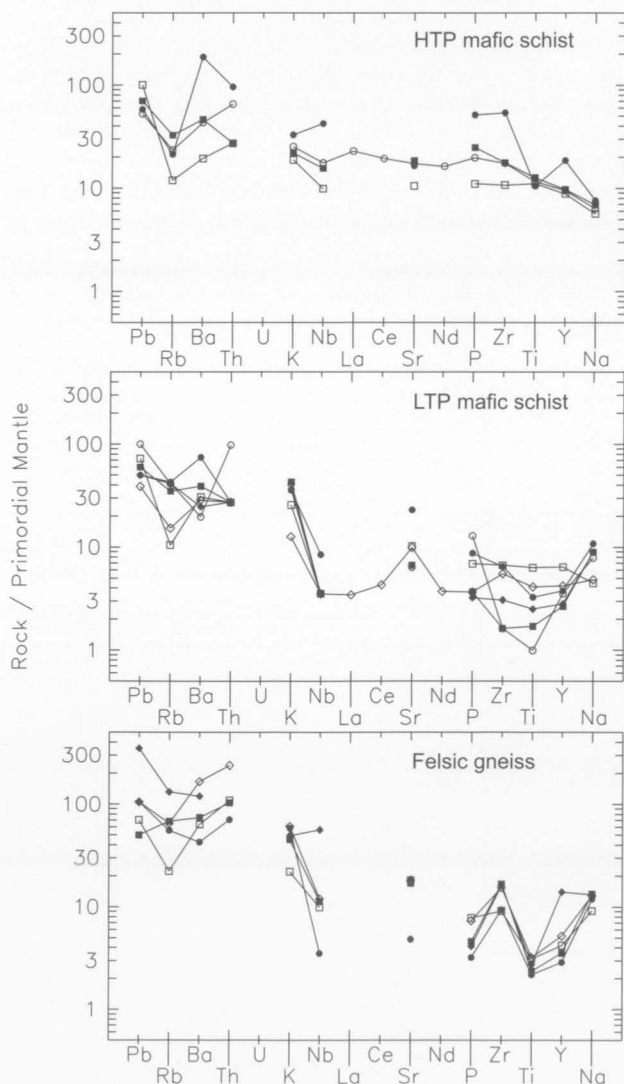


FIGURE 75

Spidergrams for metavolcanic rocks from Mount Willing.

to tonalite and granodiorite. Only a few trace-element data are available, but these suggest similar low-Y, high-Sr characteristics to the Mount Willing plagiogneisses.

The presence of metamorphic rocks with a wide range of bulk chemical composition—from basalt, through basaltic andesite and andesite, to dacite—in all three major outcrops of the Fisher Terrane is consistent with generation in a volcanic arc setting. Basaltic rocks have MORB and island-arc, rather than within-plate, characteristics on the $10\text{MnO-TiO}_2-10\text{P}_2\text{O}_5$ diagram of Mullen (1983). Relatively high K_2O and calc-alkaline affinities of the intermediate to felsic rocks suggest an origin in a mature arc environment, probably involving enriched subcontinental lithospheric mantle sources. Mikhalsky et al. (1996) suggested that a continental block (possibly the Ruker Terrane) may have been involved in the tectonic processes in the Fisher Terrane. The more widespread occurrence of felsic rocks compared to typical island arcs is consistent with major continental crustal involvement in a continental arc, possibly post-dating island-arc tholeiite formation. Moreover, felsic plagiogneisses have low HFSE contents characteristic of volcanic-arc, rather than collisional, within-plate, or ocean ridge granitoids on the classification of Pearce et al. (1984). The common association of mafic to felsic metavolcanic rocks with plutonic rocks of similar composition (see below) implies that they represent a single litho-tectonic unit (the Fisher Complex).

MESOPROTEROZOIC METASEDIMENTARY ROCKS

As already mentioned, some of the mostly metavolcanic sequences at Fisher Massif contain significant amounts of metasedimentary rocks. The 600 metre-thick sequence 5, which crops out in southern Fisher Massif, consists predominantly of metamorphosed immature tuffaceous sandstone, silty sandstone, tuffite, quartzite, tuffaceous metasandstone and siltstone. Beds of fine-grained light-coloured micaceous (mostly muscovite-bearing) plagioclase-quartz schist contain small amounts of epidote, garnet, apatite and tourmaline. Greenschist-facies pelitic schist contains

quartz + biotite + muscovite, and

quartz + biotite + muscovite + garnet + carbonate.

Marble in the same area contains minor ?phlogopite and plagioclase.

Sequence 6 in northern Fisher Massif contains a few conformable 10 to 20 metre-thick layers of marble, calcareous schist and fine-banded ironstone (Table 10). Carbonate-rich rocks are composed of calcite, amphibole, epidote, quartz, sericite, chlorite and opaque minerals. They are intensely deformed (Figs 60, 61) and recrystallised, and probably mark thrust zones. Banded ironstone is composed of thin (mm scale) intercalated layers of magnetite/hematite-quartz, with garnet and cummingtonite being minor constituents (Krylov & Krutikova 1994). Axial planes of open to tight folds dip steeply northwest, conformable with the bedding and foliation in the host metavolcanic rocks.

Part of sequence 4 (unit IV) contains one to 50 metre-thick beds of fine-grained micaceous quartz-feldspar schist, formed by metamorphism of tuffites and/or silty sandstones.

Thinly layered biotite paragneisses are exposed at a few

localities on Mount Willing. They form minor units some 10 to 100 metres thick, intercalated with plagiogneiss and mafic schist. They are fine-grained, moderately to thinly layered leucocratic rocks; relict psammitic textures are preserved locally. Colour index ranges from three to 16. The rocks typically consist of plagioclase (An_{10-25} ; 40–50%), quartz (30–45%), K-feldspar (microcline: up to 7%), biotite (3–15%), amphibole (up to 1%) and opaque minerals (up to 1%, rarely 5%).

TABLE 10. Chemical analyses of representative metasedimentary rocks from Fisher Massif.

Sample no. Lithology	31180 Bt-Ms-Qz schist (meta- sandstone)	31190-9 Bt-Ms phyllite- (meta siltstone)	31181-2 Mica quartzite	31418 Marble	31418a Carbonate schist
SiO_2	63.40	73.90	91.10	9.15	18.97
TiO_2	0.60	0.40	—	0.22	0.35
Al_2O_3	18.90	13.30	2.30	2.32	4.28
Fe_2O_3	*7.2	*4.2	*1.2	1.25	1.90
FeO	—	—	—	0.35	1.69
MnO	—	—	—	0.08	0.16
MgO	1.30	0.60	0.30	1.00	1.80
CaO	0.10	0.30	1.80	47.44	38.73
Na_2O	0.40	0.40	0.10	0.50	1.00
K_2O	5.80	4.00	0.60	0.38	0.38
P_2O_5	0.34	—	—	—	—
CO_2	—	—	—	37.64	31.00
LOI	1.00	0.55	0.35	—	—
Total	99.04	97.65	97.75	100.33	100.26

* Total Fe as Fe_2O_3 .

MESOPROTEROZOIC METAGABBRO

Gabbroic rocks crop out at Fisher Massif, Mount Willing and Nilsson Rocks. A layered gabbroic intrusion at Mount Willing has a Sm–Nd whole-rock isochron age of 1233 ± 160 Ma and a more precise mineral (orthopyroxene–clinopyroxene) age of 1292 ± 67 Ma. There is evidence for isotopic resetting of minerals at 1023 ± 33 Ma (Mikhalsky et al. 1992). Zircon growth occurred at 1118 ± 31 (two-point upper intercept; ?metamorphism) and 810 Ma (concordant zircon; ?thermal overprint) (Laiba & Mikhalsky 1999). Thus, the Mount Willing layered gabbro was probably emplaced at about 1300–1250 Ma, metamorphosed at 1020–1000, and overprinted at 810 Ma. Another metamorphic event, dated at 1113 ± 3 Ma, is recorded by zircons in quartz diorite veins in the metamorphic host rocks.

Mount Willing

A layered gabbro body occupies the eastern half of Mount Willing (Fig. 56). The exposed part of the pluton is 3.5 by 7.5 kilometres, and magnetic data show it to be of isometric shape and 10 to 12 kilometres across. It forms a

cup-shaped body with a measured thickness of 3100 metres, and dips at 30–70° inwards in the marginal zones (Fig. 77); the layering is near-horizontal in the centre (Laiba & Mikhalsky 1995, 1999). Contacts are poorly exposed and may be tectonic. A 60 metre-thick granite dyke occurs along at least part of the contact (Fig. 78). Veins and dykes of tonalite to granite, pegmatite, and metadolerite dykes of two generations (older amphibolites and metadolerites, and younger altered dolerites) cut both gabbroic and metamorphic country rocks. A much smaller gabbro body (the Western stock) crops out in the southwestern part of Mount Willing. It is composed of fine-grained ophitic gabbronorite and gabbro-anorthosite, and may be an apophysis from the main gabbro pluton. It may represent a more rapidly chilled magma batch with a chemical composition approximating that of the parent melt.

The Mount Willing layered intrusion comprises three major series dominated by different rock types: (1) *lower* gabbronorite; (2) *middle* anorthosite-gabbronorite; and (3) *upper* ferrogabbro (Fig. 81). These series occur as three different blocks separated by steeply dipping normal faults, the rocks dipping at various angles within those blocks (Fig. 56).

The *lower series* (1280 m) consists of partly metamorphosed gabbronorite to melanocratic gabbronorite, with minor layers of olivine gabbro, leucogabbro and ferrogabbro. Hornblende is a common primary magmatic mineral. Two compositionally distinct zones were distinguished: zone I (the lower 620 m) and zone II (the upper 660 m). Zone I rocks are more commonly Ol-normative and more melanocratic. The uppermost horizons of both members are leucocratic and relatively enriched in opaque minerals, which suggests that they represent two different crystallisation cycles.

The *middle series* (1020 m) is the most heterogeneous. It contains a wide range of rock types in layers 0.3 to 20 metres thick, giving it a pronounced layered structure. It comprises (from bottom to top) zone III, andesine unit, mixed unit, and zone IV. Zone III is made up of intercalated olivine-bearing and olivine-free gabbronorite, norite and anorthosite, which form four crystallisation cycles. The lowermost layers are more melanocratic, and the uppermost layers are opaque mineral-enriched (ilmenite and magnetite). Cycle thickness decreases

upward from 130 to 10 metres, and rocks grade upward to more leucocratic compositions. The andesine unit (110 m) consists of ferrogabbro containing relatively sodic plagioclase (andesine) and Fe-rich orthopyroxene. The mixed unit (80 m) is composed of ultramafic to mafic hornblende (normative troctolite), leucocratic norite and ferrogabbro containing accessory apatite. This unit is compositionally heterogeneous, comprising various lithologies that also occur elsewhere in the pluton. It appears to record emplacement of a new magma batch, but also seems to reflect the effects of such processes as magma mixing, temperature gradients and fluid activity. It may be equivalent to the economically important 'reefs' (such as the critical zone of the Bushveld intrusion) that occur at similar stratigraphic positions in other layered plutons, but its highly metamorphosed nature makes interpretation difficult. Zone IV (490 m) comprises gabbro and leucogabbro containing abundant ilmenite and magnetite.

The *upper series* (800 m) is made up predominantly of ferrogabbro, with minor norite and olivine norite. These rocks differ from the rest of the pluton in their higher ilmenite, magnetite and apatite contents, and some contain quartz. Individual layers range in thickness from some 10 metres in the lower part of the series to about a metre in the upper part. The colour index decreases upward from 50 to 40. The series is subdivided into the lower, more homogeneous, ilmenite-dominant zone V (650 m), and the upper layered, magnetite-dominant zone VI (150 m).

The most common rock type in the intrusion is gabbro (colour index 35–55), consisting of cumulus orthopyroxene and plagioclase (together 30–70%), and intercumulus clinopyroxene, plagioclase, orthopyroxene and opaque phases. Intercumulus amphibole (greenish-brown hornblende) sporadically occurs throughout the section, but is more typical of the upper series. Clinopyroxene commonly contains minor lamellae of subcalcic augite-ferroaugite to intermediate pigeonite ($\text{Ca}_{10-30}\text{Mg}_{10-65}\text{Fe}_{30-75}$), or rarely orthopyroxene. Cumulus orthopyroxene also contains augite lamellae. Leucocratic varieties (colour index 20–35) contain up to five percent of opaque phases. Olivine is a rare cumulus phase (3–10%,



FIGURE 77
Layered metagabbro intrusion; northern side of Mount Willing (photo by V.M. Mikhailov).

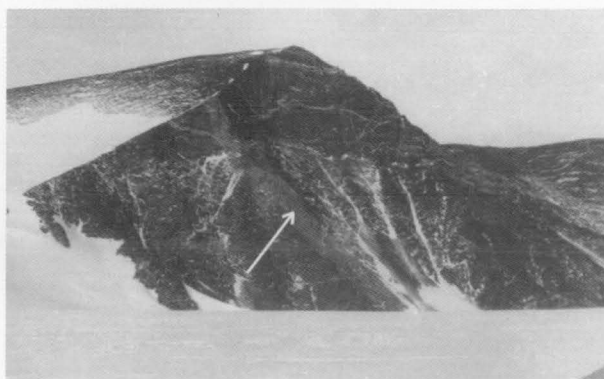


FIGURE 78
Tonalite (left) and gabbro (right) separated by a granite body (arrowed) dated at 1194 ± 1 Ma; southern side of Mount Willing. The gabbro is cut by a number of subhorizontal granitoid veins (towards top of cliff).

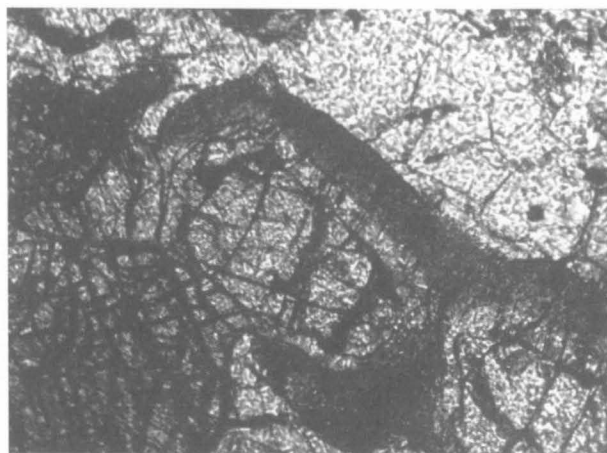


FIGURE 79

Olivine gabbronorite, showing olivine grain (centre) surrounded by an inner rim of cummingtonite and a darker outer rim of green amphibole (tschermakite to magnesio-hastingsite) adjacent to plagioclase; Mount Willing. Olivine is in contact with orthopyroxene at lower left. Sample 39113-14; width of field: 2.5 mm.

rarely up to 20%). Ferrogabbro contains eight to 15 percent opaque minerals: magnetite and/or ilmenite, which mostly crystallised separately. Apatite (1–3%) is characteristic of the upper series, where it is usually associated with amphibole and sometimes quartz (up to 3%). Zircon is a rare accessory. Calculated cation-exchange temperatures are in the ranges 700–1100° (Boyd 1973) and 840–1260°C (Wells 1977). Plagioclase–hornblende geothermometers (Perchuck 1970; Plyusnina 1982) indicate intercumulus crystallisation temperatures as high as 800–850°C for lower series rocks, but lower (610–730°C) for the middle and upper sequences.

Some olivine is mantled by orthopyroxene and shows resorption features; *mg* values of olivine and orthopyroxene do not show any correlation. In contrast, a

few lower series rocks contain texturally equilibrated olivine and orthopyroxene with consistent *mg*. Olivine-bearing rocks commonly show reaction relationships between olivine and plagioclase. Adjacent to plagioclase, olivine is mantled by two rims: (1) an inner rim of an acicular aggregate of colourless Fe–Mg amphibole (cummingtonite or anthophyllite) containing rare relict orthopyroxene; and (2) an outer rim of green amphibole (low-Ti magnesio-hastingsite) and rare spinel (Fig. 79). Non-equilibrium relationships of olivine and plagioclase indicate crystallisation at pressures above six to eight kilobars (Green & Hibberson 1970). Disequilibrium relationships between olivine and orthopyroxene would suggest much lower crystallisation pressures, so a xenocrystic origin for the olivine is more likely. Olivine (Fo_{70}) which crystallised from a more primitive melt with *mg* 55 (calculated from the empirical olivine/liquid $D_{(\text{Fe}/\text{Mg})}$ value of 0.3: Roeder & Emslie 1970) may have been entrained in a more evolved melt with *mg* 40–45, as indicated by the orthopyroxene composition (En_{72}). Crystallisation at pressures above six kilobars would imply that the volcanic pile into which the gabbro pluton was emplaced was buried to mid-crustal levels, so that the overlying strata may have reached a thickness of up to 15 or 20 kilometres.

The occurrence of quartz-bearing rocks in the upper series suggests that the 'orthopyroxene divide' was crossed by at least the residual intercumulus melt, which would imply relatively low-pressure conditions. However high H_2O partial pressure, as well as low confining pressure, could also account for the melt evolution from Ol-normative to Q-normative compositions. The presence of primary magmatic hornblende, even in the lower parts of the pluton, is consistent with both high H_2O activity and the observed olivine–plagioclase reaction. Separate crystallisation of ilmenite and magnetite and the lack of sulphides suggest high oxygen fugacity. Hence high-pressure crystallisation conditions, coupled with high H_2O

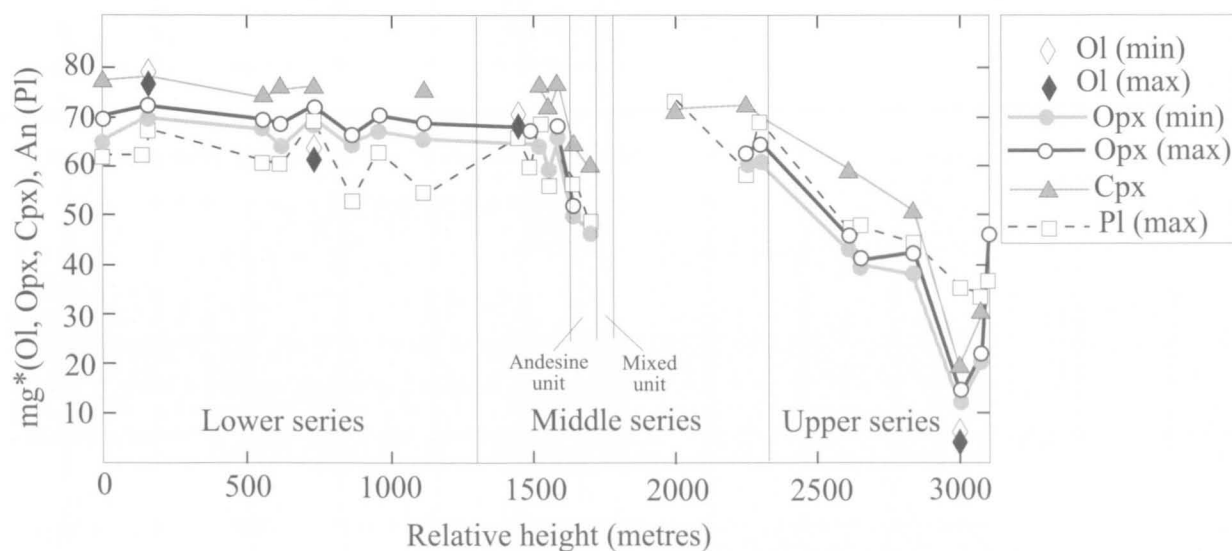


FIGURE 80

Mineral compositional variations with stratigraphic height in the Mount Willing layered gabbro intrusion. Two distinct megacycles are present, with mineral compositions becoming more evolved in their upper sections—although the uppermost part of the intrusion (zone VI) is much less fractionated and may represent a chilled contact zone.

partial pressure, could account for the observed petrographic features.

Mineral compositions reveal the presence of two megacycles in the Mount Willing layered intrusion (Fig. 80). The first (lower) megacycle comprises the lower series and part of the middle series (zone III). These rocks contain relatively Mg-rich olivine (Fe_{76-79}), orthopyroxene (mg 65–70), and clinopyroxene (mg 58–80: salite $Ca_{45-49}Mg_{40-45}Fe_{10-14}$ to augite $Ca_{41-45}Mg_{42-45}Fe_{10-14}$), and Ca-rich plagioclase (An_{52-69} or An_{70-74} in all except the andesine unit). The second (upper) megacycle includes zone IV and the upper series, and is made up of more Fe-rich olivine (down to Fe_{4-5}), orthopyroxene (mg 61–65 to 14–46), and clinopyroxene (mg 71–73 to 36–48: augite $Ca_{41}Mg_{31}Fe_{26}$ to $Ca_{38-43}Mg_{11-19}Fe_{38-52}$), and Ca-poor plagioclase (An_{52-56} to An_{34-50}), all values decreasing upwards.

A sharp increase in mineral mg values above the mixed unit probably reflects emplacement of a new primitive magma batch. Smaller compositional variations within the pluton may also be due to introduction of new, but less voluminous magma batches, combined with fractional crystallisation and cumulus processes. However, mineral compositions may also reflect the influence of other processes. For example, the magma may have become H_2O -saturated, which would cause changes in O_2 fugacity and induce rapid crystallisation of Fe–Ti oxides. One sensitive indicator of primary melt composition is $\epsilon_{Nd}(T)$ (DePaolo & Wasserburg 1976), which is higher than for most other layered plutons. $\epsilon_{Nd}(1300)$ ranges from 1.8 to 3.5 for rocks from both the lower and upper sequences, with only one sample having a lower value of 0.25 (Mikhailov et al. 1991; Laiba & Mikhalsky 1999). Thus, the Mount Willing gabbro appears to have crystallised from isotopically similar magma batches. Relatively high ϵ_{Nd} militates against a significant role for crustal contamination, but does not preclude minor involvement of relatively young (Mesoproterozoic) juvenile crust similar to that described from Fisher Massif ($\epsilon_{Nd}(1300)$ 2.5–3.5).

Metamorphic (garnet-amphibolite facies) alteration is reflected in the presence of dark green amphibole (magnesio-hornblende to tschermakitic hornblende), brown biotite and rare garnet. The degree of alteration ranges from insignificant to complete, and transitional zones between fresh gabbro and metagabbro (amphibolite) are very thin (a few cm). Such zones are conformable with the magmatic layering. Metagabbro and fresh gabbro are intercalated, and up to 50 percent of the rocks are altered to some degree. Calculated plagioclase–hornblende equilibration temperatures are 520–600°C (Plyusnina 1982; Perchuck et al. 1985), similar to those (530–560°C) of the host metamorphic rocks in the western part of Mount Willing (Mikhalsky et al. 1999). Later greenschist-facies retrogression is reflected by development of minor chlorite, actinolite, titanite, sericite, quartz, magnetite and calcite. These phases generally make up less than five volume percent of the rock, but predominate in thin shear zones, which are conformable with the magmatic layering and metamorphic foliation.

The upper parts of both megacycles are strongly enriched in TiO_2 , P_2O_5 , Nb, Y and Zr, which have clearly behaved incompatibly (Table 11, Figs 81, 82). The uppermost part of zone V shows the most extreme enrichment in these elements, whereas the overlying zone

VI appears to be less evolved. This suggests that zone VI is actually the top of the intrusion. Examples of similar 'reversed' crystallisation sequences occur in the roof zones of some other layered plutons (Sharkov 1983). FeO, Na_2O , K_2O and Ba show rather less well defined, but still significant, upward increases in each megacycle, whereas CaO, MgO, Cr, Ni and mg^* show corresponding decreases. SiO_2 , Al_2O_3 and Sr show more irregular trends. LREE appear to be higher in the upper than the lower series, but there are insufficient data to define stratigraphic trends.

The layered gabbroic rocks have a wide compositional range, and show an overall tholeiitic Fe-enrichment trend on an AFM diagram (Fig. 83). A number of samples with high $Na_2O + K_2O$, but moderately high mg^* , are plagioclase-rich cumulates (leucogabbros). mg^* variation diagrams suggest two distinct compositional trends: a dominant Fe-enrichment trend to ferrogabbro and ferrogabbro-norite, and a plagioclase-cumulus trend (Fig. 84). The latter is characterised by marked increases in SiO_2 , Al_2O_3 , Na_2O , Sr, and probably LILE (but not CaO), whereas the former shows the greatest enrichment in TiO_2 , P_2O_5 and HFSE. Spidergrams are of limited value in cumulate sequences, but they show as much, or more, variation in less incompatible HFSE as in LILE (Fig. 85). Most rocks have marked negative Zr anomalies, although these might reflect apatite and Ti oxide accumulation as much as Zr depletion. High Sr is consistent with plagioclase accumulation.

Comparison of compositionally similar and spatially associated fresh and metamorphosed rocks shows that metagabbros tend to have higher K_2O and Rb (Fig. 84), whereas Cr, Co, Sr, Y, Zr, Nb, Ba, Pb and Th do not show any systematic differences, and were presumably more or less immobile. Two ultramafic hornblendites also have high K_2O and Rb that may be attributed to alteration. They are Cr and Sr-rich, which suggests that orthopyroxene, rather than olivine, was the main primary phase.

The composition of the parent magma may be estimated from either the bulk pluton weighted average composition, assuming crystallisation from compositionally similar magma batches, or the composition of the most magnesian of the fine-grained ophitic rocks (sample 39141-5) in the smaller Western intrusion (Table 11). The two estimates are quite similar, except for MgO and P_2O_5 , but both have relatively low mg^* (62.6 and 67.2, respectively) and high TiO_2 , which preclude their being *primitive* melts and suggest a prolonged mantle or crustal evolution. The Western intrusion sample is the less evolved of the two, and is strongly Ol-normative. Most major and trace elements, as well as ϵ_{Nd} values, are comparable to mature volcanic-arc associations in the Kurilo-Kamchatka area (Sharkov 1983) and elsewhere (Bogatikov et al. 1987).

Earlier comparisons of the Mount Willing intrusion with the Stillwater Complex (Mikhailov et al. 1991) are not well supported by data included in this bulletin, although the assumed primary melt compositions share some common features (Laiba & Mikhalsky 1999). In contrast to the Stillwater Complex, ultramafic horizons are virtually absent, even from the mixed unit that appears to be the genetic equivalent of the 'critical' zones known from many layered plutons elsewhere. Only a few thin hornblendite layers may represent metamorphosed pyroxenite. Other contrasting features are the much poorer layering in the Mount Willing

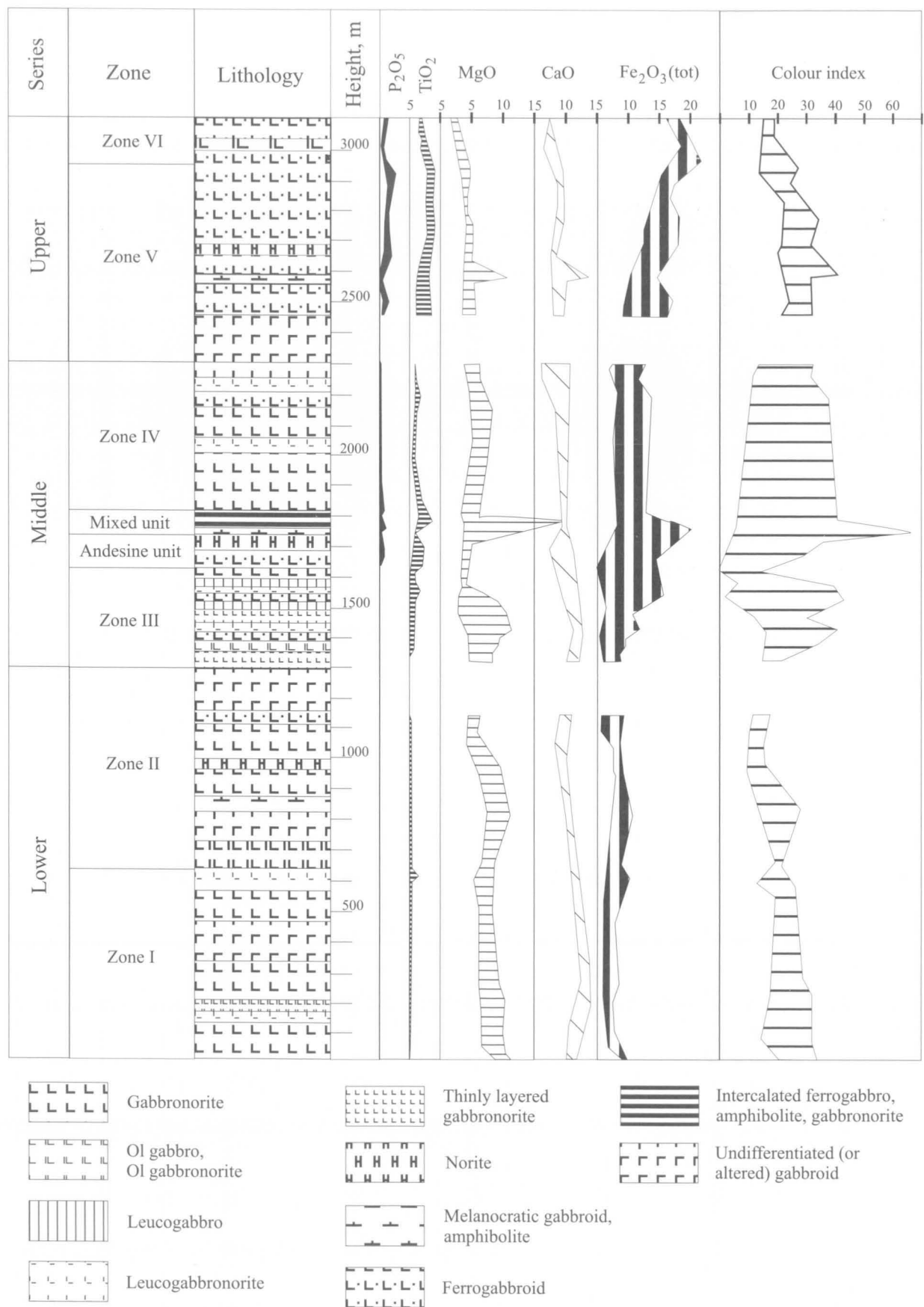


TABLE 11. Chemical analyses and C.I.P.W. norms of representative gabbroic rocks from the Fisher Terrane.

Sample no. Locality	39113-1 Mount Willing	39113-14 Mount Willing	39116-4 Mount Willing	39116-12 Mount Willing	39138-7 Mount Willing	39134-11 Mount Willing	39134-8 Mount Willing	Mount Willing	39141-5 Mount Willing	34512-7 Western Fisher Massif	34511-12 Southwest Fisher Massif	34520-16 Central Fisher Massif	40080 Nilsson Rocks	40113 Nilsson Rocks	40206-10 Nilsson Rocks	40076 Nilsson Rocks	40056 Nilsson Rocks
Lithology	Gabbro- norite	Olivine gabbro	Metagabbro	Leuco- gabbro	Metagabbro	Gabbro- norite	Ferronorite	Average of 132 samples	Metagabbro-Metagabbro dolerite	Metaleuco- gabbro	Metagabbro	Metagabbro	Metagabbro	Bt meta- gabbro	Bt meta- gabbro	Ultramafic rock	
Strat. height	555	730	1460	1485	1770	2840	2960										
SiO ₂	46.50	47.81	48.53	50.69	46.96	45.71	45.77	49.68	47.56	47.43	52.87	52.07	50.75	52.72	48.76	52.92	43.93
TiO ₂	2.06	0.49	0.19	0.23	3.17	3.05	1.49	0.91	0.98	0.68	0.45	0.72	0.90	0.20	0.84	1.06	0.55
Al ₂ O ₃	14.42	17.62	19.65	22.96	13.75	14.96	14.84	17.56	17.22	16.20	20.87	16.58	20.49	18.19	17.56	16.97	8.24
Fe ₂ O ₃	*14.88	1.29	*7.65	*4.5	*16.97	2.88	7.16	*9.40	*11.03	3.47	1.73	2.71	*8.23	*7.94	*8.98	*8.59	*10.58
FeO	—	7.74	—	—	—	12.60	14.40	—	—	8.00	4.29	6.92	—	—	—	—	—
MnO	0.20	0.13	0.10	0.07	0.33	0.28	0.46	0.18	0.18	0.21	0.09	0.15	0.10	0.13	0.19	0.13	0.15
MgO	7.06	8.92	9.34	2.82	3.77	3.60	2.85	6.75	9.70	8.35	3.57	6.03	4.59	6.50	6.09	5.97	25.86
CaO	9.77	12.53	11.63	12.64	9.93	9.97	6.35	9.43	10.16	11.51	10.32	9.54	10.15	8.70	10.98	7.77	4.08
Na ₂ O	2.65	2.29	2.00	4.88	2.45	3.30	3.62	2.71	2.21	1.43	3.18	2.19	3.54	4.36	2.92	2.93	0.10
K ₂ O	0.90	0.13	0.32	0.25	0.66	0.34	0.10	0.42	0.38	0.44	0.65	0.49	0.43	0.55	2.06	2.59	0.01
P ₂ O ₅	0.46	—	0.02	0.02	1.77	1.72	0.46	0.23	0.14	0.09	0.17	0.10	0.23	0.02	0.44	0.41	0.11
LOI	0.70	0.40	0.80	0.70	0.10	—	0.30	—	—	2.11	1.80	2.48	0.70	0.80	1.00	0.50	6.30
Rest	0.11	0.13	0.12	0.12	0.11	0.12	0.11	—	0.13	0.19	0.23	0.19	0.15	0.10	0.21	0.30	0.37
Total	99.71	99.48	100.35	99.88	99.97	98.53	97.91	97.27	99.70	100.11	100.22	100.17	100.27	100.22	100.03	100.14	100.28
Q	—	—	—	—	3.32	—	—	0.07	—	—	3.42	5.41	—	—	—	—	—
C	—	—	—	—	—	—	—	—	—	—	—	—	—	—	—	—	0.91
Or	5.32	0.77	1.89	1.48	3.90	2.01	0.59	2.48	2.25	2.60	3.84	2.90	2.54	3.25	12.17	15.31	0.06
Ab	22.42	19.38	16.92	26.89	20.73	27.92	30.63	22.93	18.70	12.10	26.91	18.53	29.95	36.89	18.49	24.79	0.85
An	24.79	37.41	43.69	40.00	24.57	25.00	23.95	34.51	35.94	36.48	40.75	33.96	38.75	28.44	28.72	25.50	19.52
Ne	—	—	—	—	7.80	—	—	—	—	—	—	—	—	—	3.37	—	—
Di	17.05	20.08	11.18	18.53	11.08	11.18	3.93	8.79	10.99	16.40	7.69	10.45	8.30	11.89	18.70	8.45	—
Hy	5.00	1.53	11.30	—	20.91	14.09	16.52	23.39	11.61	20.54	12.83	22.27	11.15	4.08	—	18.37	44.18
Ol	14.83	16.70	11.73	2.52	—	4.72	12.58	—	14.55	5.32	—	—	3.98	11.93	12.04	1.35	23.51
Mt	3.24	2.15	1.67	0.98	3.69	3.67	5.04	2.04	2.40	2.69	1.41	2.26	1.79	1.73	1.96	1.87	2.30
Il	3.91	0.93	0.36	0.44	6.02	5.79	2.83	1.73	1.86	1.29	0.85	1.37	1.71	0.38	1.60	2.01	1.04
Ap	1.09	—	0.05	0.05	4.19	4.07	1.09	0.54	0.33	0.21	0.40	0.24	0.54	0.05	1.04	0.97	0.26

Sc	—	—	—	—	—	—	—	—	—	—	28	37	—	—	—	—	—
V	152	215	79	44	54	112	—	—	174	349	189	263	172	188	223	152	115
Cr	129	220	126	77	—	65	10	—	166	276	103	95	146	219	58	243	1311
Co	45	60	43	15	41	37	55	—	43	52	—	—	33	31	34	112	—
Ni	47	92	109	31	8	—	—	—	143	55	30	37	17	32	31	97	1000
Cu	—	—	—	—	—	—	—	—	—	—	143	108	—	—	—	—	—
Zn	—	—	—	—	—	—	—	—	—	—	54	82	—	—	—	—	—
Ga	—	—	—	—	—	—	—	—	—	—	22	18	—	—	—	—	—
Rb	—	8	14	9	11	5	10	—	8	15	19	16	5	6.5	42	57	—
Sr	386	375	440	646	370	490	448	—	317	512	781	293	659	211	968	712	58
Y	8	7	6	9	37	45	20	—	22	11	8	22	19	8.6	16	23	12
Zr	6	5	—	—	30	45	151	—	82	15	18	52	100	21	38	122	44
Nb	—	—	—	—	9	10	10	—	—	3	<2	4	4	0.7	9	14	1
Ba	107	—	126	177	302	174	180	—	—	122	321	200	11	<100	246	979	<100
La	—	—	—	—	—	—	—	—	—	—	8	9	—	—	—	—	—
Ce	—	—	—	—	—	—	—	—	—	—	20	20	—	—	—	—	—
Nd	—	—	—	—	—	—	—	—	—	—	5	8	—	—	—	—	—
Pb	—	14	—	—	23	—	13	—	14	8	11	<2	11	12	25	18	8
Th	—	—	—	—	—	—	—	—	—	—	3	<2	<1	<1	11	<1	<1
U	—	—	—	—	—	—	—	—	—	—	1	<0.5	—	—	—	—	—
<hr/>																	
K/Rb	—	135	190	231	498	564	83	—	394	244	284	254	714	702	407	377	—
Ba/Zr	17.8	—	—	—	10.1	3.87	1.19	—	—	8.1	17.8	3.85	0.11	—	6.47	8.02	—
Nb/Zr	—	—	—	—	0.30	0.22	0.07	—	—	0.20	—	0.08	0.04	0.03	0.24	0.11	0.02
Sr/Sr*	—	—	—	—	—	—	—	—	—	—	5.07	1.65	—	—	—	—	—
mg*	52.5	67.8	74.0	59.3	34.1	33.2	22.3	62.6	67.2	61.2	56.1	57.5	56.5	65.6	61.2	61.8	85.1

mg* = atomic 100Mg/(Mg + 0.85Fe(total)); * total Fe as Fe₂O₃.

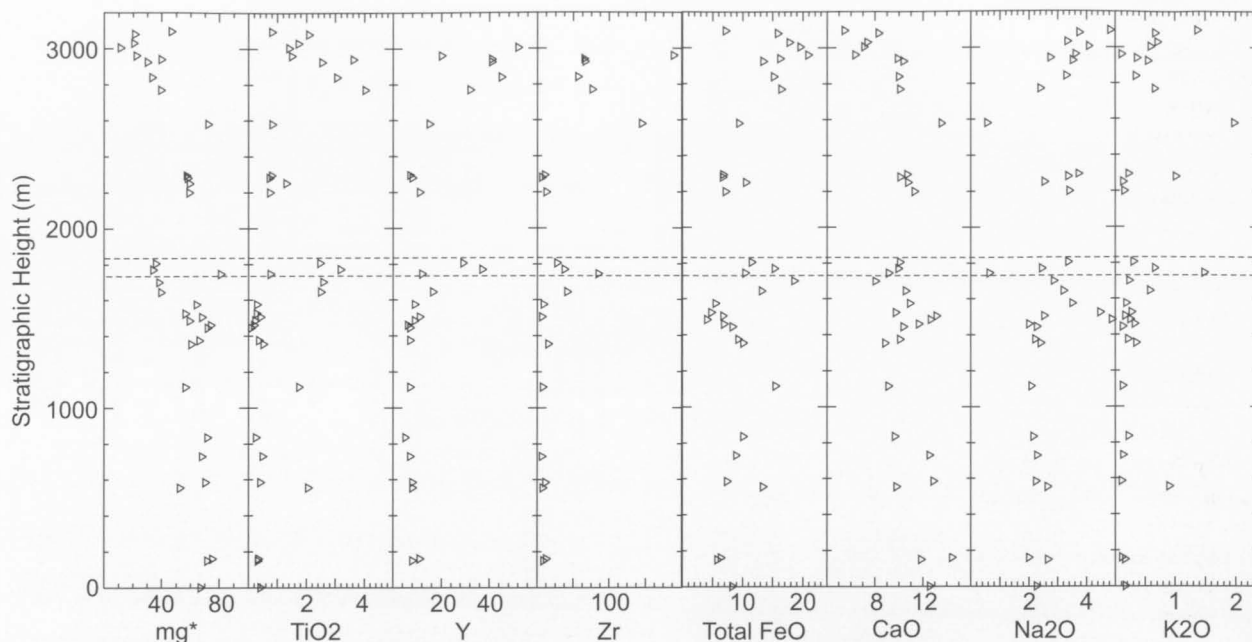


FIGURE 82

Plots of major and trace elements against stratigraphic height for the Mount Willing layered gabbro intrusion. The dashed lines indicate the position of the mixed unit.

intrusion, the restricted amount of anorthosite, the lack of chromite, the extreme rarity of monomineralic cumulates, and the common appearance of plagioclase in the cotectic association. Subsequent deformation and tonalite to granite intrusion are not typical features of most Stillwater-type intrusions. Thus it is likely that Mount Willing gabbros crystallised from a compositionally rather different primary

melt under quite different thermodynamic conditions, and probably in a different tectonic environment. High and possibly widely varying water activity might have been the most important factor that influenced liquidus temperatures and mineral phase relationships.

Fisher Massif

Metagabbro and metagabbro-diorite (transitional from gabbro to diorite) form four small plutons (2–4 km across) and a number of even smaller stocks and sills. Intrusive contacts are exposed, and xenoliths of the metamorphic host rock are locally abundant within the gabbro. In a few places the gabbro plutons show magmatic layering (Fig. 86), with individual layers between two to three and 20–30 metres thick. As well as metagabbro (with colour index 40–80) and metagabbro-diorite (colour index 20–40), ultramafic hornblendite, serpentinite (?metaperidotite), gabbro-anorthosite and anorthosite are of sporadic occurrence. In some cases the colour index increases upwards, suggesting either an overturned body or crystallisation in the border facies of the pluton. Intrusive relationships between different gabbro and/or gabbro-diorite bodies can be seen in a few places, indicating multiple emplacement. Apart from extensive metamorphic recrystallisation, the Fisher Massif gabbro plutons are mostly highly sheared—although relict primary magmatic textures, but never primary mafic minerals (except hornblende), are commonly preserved.

Metagabbroic rocks consist of pale to dark green hornblende (20–40% in metagabbro-diorite, 40–80% in metagabbro), zoned plagioclase (An_{30-70} ; 25–65%), biotite (5–10%), quartz (up to 8%), and minor epidote, actinolite, apatite, titanite, tourmaline, allanite, garnet, sericite, chlorite, calcite and opaque minerals. Much of the hornblende is secondary, but some is well crystallised and may be primary. Relict gabbroic textures are commonly

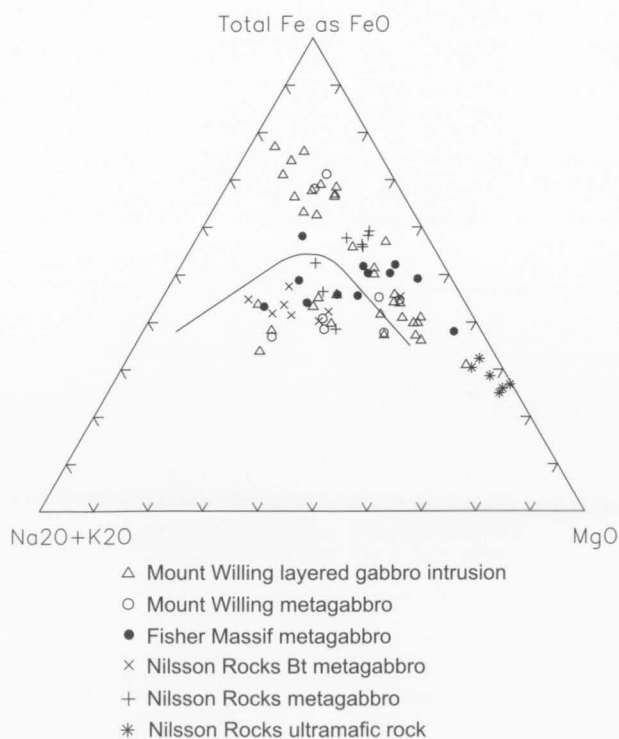


FIGURE 83

AFM diagram for gabbroic rocks of the Fisher Terrane.

present. Metagabbro-anorthosite consists of large plagioclase (An_{85-90} ; 70–75%) grains, with interstitial hornblende and minor biotite and epidote.

Analysed metagabbros and metagabbro-diorites from Fisher Massif are mostly Q-normative quartz gabbros or diorites (Table 11, Fig. 64). They have a wide compositional range (mg^* 40–76; Figs 83, 84), implying significant fractionation and/or cumulus processes. They have broadly similar compositions to metagabbros from Mount Willing and Nilsson Rocks, and many of the gabbroic rocks of the Mount Willing layered intrusion (Figs 83, 84), but these are mostly silica-undersaturated (Ol-normative). Moreover, equivalents of the highly evolved (mg^* 10–40), but mostly Ol-normative, ferrogabbros and ferrogabbro-norites from the Mount Willing intrusion are lacking. Gabbroic rocks from Fisher Massif appear to be closely related to the basaltic andesites from the same area, particularly the plagioclase porphyries (group PP: Figs 65, 68). Like the porphyries, they commonly have high Al_2O_3 and Sr, and spidergrams that show marked Nb, Ti and Y depletion and large positive Sr anomalies (Fig. 85), consistent with various amounts of plagioclase accumulation. Such chemical similarities strongly suggest a genetic relationship.

Metagabbros from the western and eastern parts of Fisher Massif have small, but consistent, differences in major and trace element compositions. Thus, metagabbros from western Fisher Massif are enriched in K_2O , Al_2O_3 , Rb, Sr, Zr and Ba, and depleted in MgO. It is noteworthy that spatially associated diorites and plagiogranites show similar differences, those from the west having higher K_2O

(i.e., K–Na series) than those from the east (Na series) (see below). Therefore it is suggested that two compositionally distinct plutonic associations (series) crop out at Fisher Massif. Such systematic regional variations are difficult to explain in terms of alteration processes, even though the biggest differences are in LILE contents. Moreover, a plagiogranite with high K and other LILE intrudes low-K rocks at eastern Fisher Massif. This suggests that primary melt composition was the most important factor, and that the K–Na series post-dates the Na series.

Nilsson Rocks

Metagabbro and quartz metagabbro-diorite form a two-by four-kilometre pluton at Nilsson Rocks (Fig. 57). Smaller (up to 300x750 m) stocks consist of biotite metagabbro, a rock type absent from other localities of the Fisher Terrane. This suggests the occurrence of a third, K-rich, plutonic rock series in the Fisher Terrane, in addition to the Na and K–Na series described above. No magmatic layering was found, but a metamorphic foliation is well developed. A distinctive feature of the Nilsson Rocks metagabbroic rocks is the occurrence of pre- or syn-deformational ultramafic layers and lenses, conformable with the metamorphic foliation. Small (6x10 to 20x75 m) stock-like bodies of massive ultramafic hornblende or chlorite-amphibole metaperidotite containing relict olivine (Table 11) apparently post-date the gabbro.

Metagabbro consists of plagioclase (An_{55-65} ; 40–50%) and hornblende (30–40%), with minor biotite (up to 5%) and metamorphic garnet, diopside and quartz (up to 20%); apatite, monazite, cummingtonite, epidote, chlorite,

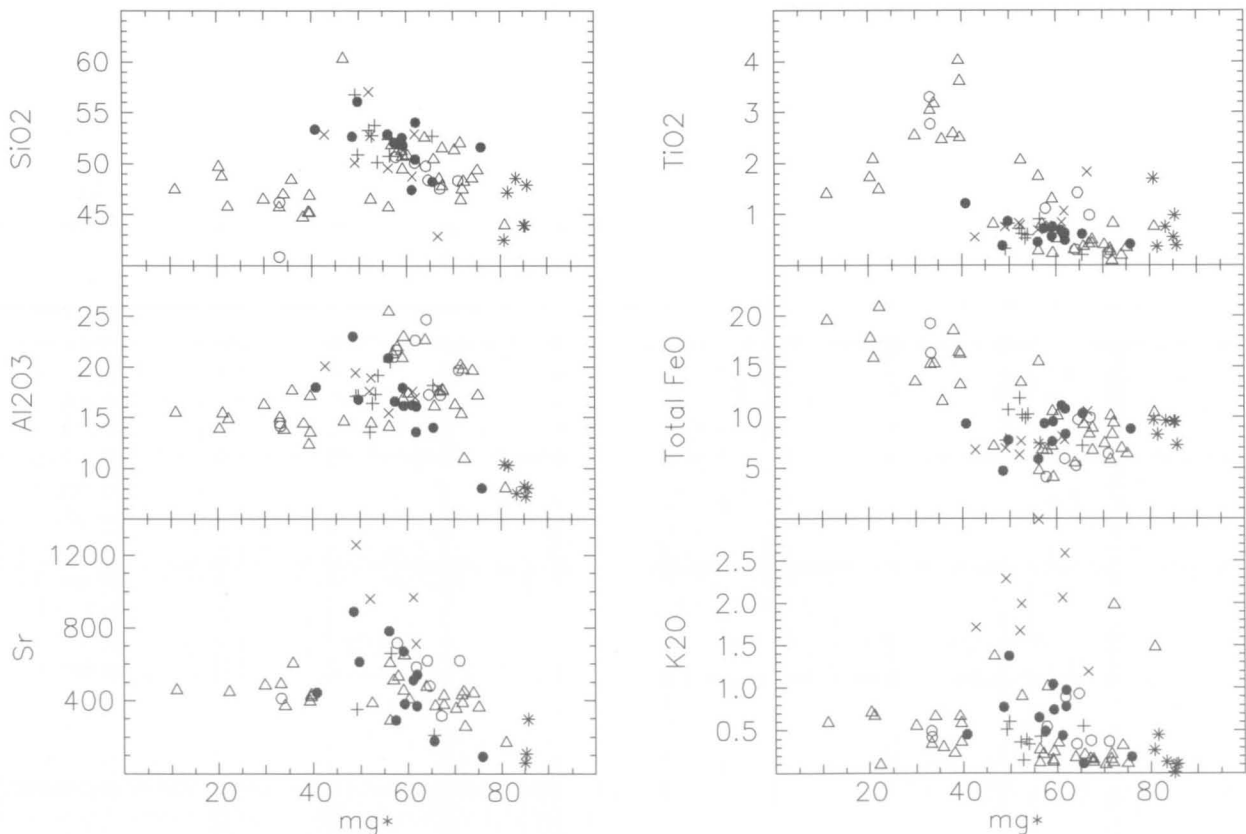


FIGURE 84
 mg^* variation diagrams for gabbroic rocks of the Fisher Terrane. Symbols as in Figure 83.

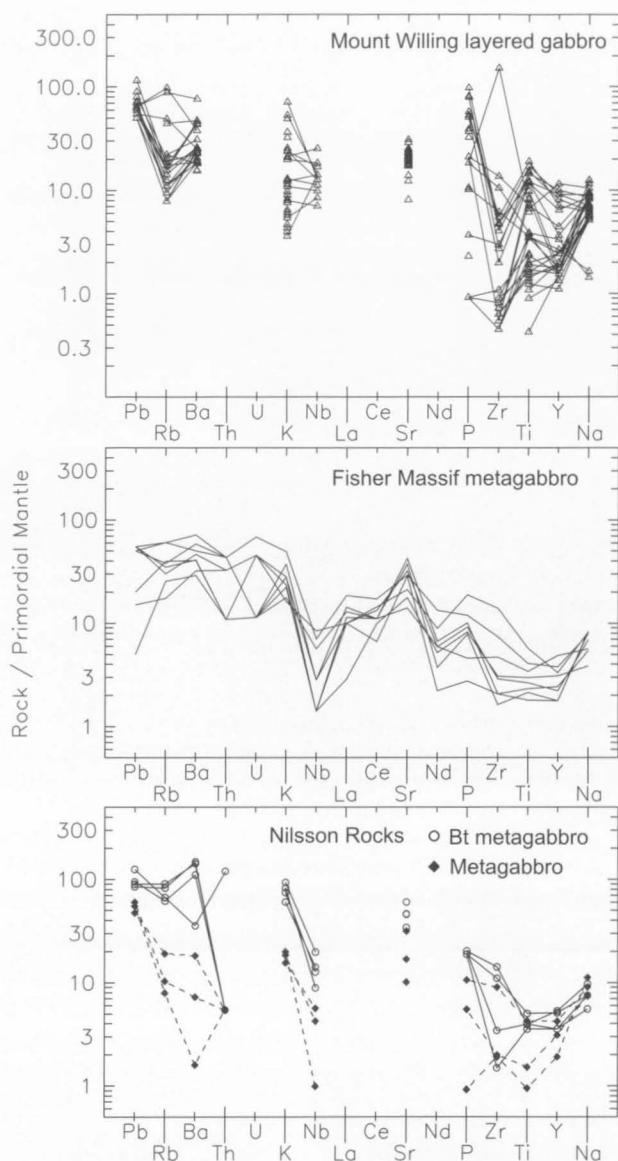


FIGURE 85
Spidergrams for gabbroic rocks from Mount Willing and Fisher Massif.



FIGURE 86
Steeply dipping contact between melagabbro and leucogabbro; northern side of Mount Johnston, southwestern Fisher Massif.

actinolite, calcite and sericite are minor constituents. Primary quartz occurs in more leucocratic metagabbro-diorites. Thin, fine-grained, concordant plagioclase-quartz veinlets, which account for three to 30 volume percent of the rock, probably represent partial melts. Biotite metagabbro is finer-grained, and contains 10–25 percent biotite, plagioclase phenocrysts in some places, and rare K-feldspar.

Most Nilsson Rocks metagabbros are compositionally similar to gabbros and metagabbros from Mount Willing, although, as at Fisher Massif, highly evolved ferrogabbros are lacking (Figs 83, 84). Metamorphosed ultramafic rocks have high *mg** (77–83), Cr and Ni, and low Al_2O_3 , CaO (mostly) and Na_2O . CIPW norms suggest that most of these were derived from olivine melagabbro protoliths. Biotite-bearing metagabbros not only have markedly higher LILE (K, Rb, Sr, Ba and Pb) than biotite-free metagabbros, but also higher P, Nb and possibly Ti (Table 11, Figs 83–85). This suggests derivation from different parent magmas and probably mantle sources, rather than being due entirely to LILE enrichment during metamorphism.

MESOPROTEROZOIC–NEOPROTEROZOIC GRANITOIDS

Variably deformed and partly metamorphosed granitoid intrusions are widespread throughout the Fisher Terrane. Diorite, quartz diorite, tonalite, trondjemite, granodiorite and granite are common rock types. (Note that trondjemite is synonymous with both leucotonalite and plagiogranite, the latter term being used by Russian geologists.) These rocks form plutons (mostly 1x4 km, but up to 4x8 km), small stocks, and dykes or highly elongated bodies at Fisher Massif, Mount Willing (Fig. 87) and Nilsson Rocks. Diorite and tonalite are spatially associated with gabbro to gabbro-diorite plutons, and may form a late-stage magmatic phase of a gabbro-diorite-tonalite association. Tonalite gneiss and younger granite at Mount Willing have given zircon U–Pb ages of 1176 ± 16 and 1194 ± 1 Ma, respectively (Table 22; Mikhalsky et al. 1999; A.A. Laiba, unpublished data), so the tonalite was probably emplaced at c.1190–1195 Ma. Four zircon fractions from the tonalite define a highly imprecise c.490 Ma lower intercept age, but somewhat better constrained are Rb–Sr and Sm–Nd mineral (hornblende–plagioclase)–whole-rock isochron ages for mafic schist of 636 ± 13 and 1009 ± 5 Ma, respectively (Mikhalsky et al. 1999). A biotite granodiorite (transitional to tonalite) from Fisher Massif was dated at 1293 ± 28 Ma (ion-microprobe U–Pb zircon age: Kinny et al. 1997), which is more comparable to the age of gabbroic rocks from the Fisher Terrane. In contrast, granite and granodiorite bodies are younger and in some places clearly intrude diorite to tonalite plutons. Biotite granite at northern Fisher Massif (Blustery Cliffs) has given an ion-microprobe U–Pb zircon age of 1020 ± 48 Ma (Kinny et al. 1997).

A variety of intermediate to felsic intrusive rocks crops out at **Fisher Massif**, particularly in the southwestern, central and northeastern parts, where they intrude mafic to felsic metavolcanic rocks and minor metasediments (Fig. 55). Contacts with the country rocks are commonly mylonitised, but clearly intrusive in some places.



FIGURE 87

Layered gabbro intruded by tonalite (plagiogranite) bodies; western Mount Willing (photo by V.V. Samsonov). The slope is about 100 m high.

Predominantly mafic xenoliths are locally abundant in the granitic rocks (Fig. 88), although intermediate and felsic xenoliths are also present. Most of the granitic rocks are of I-type, although a small body of S-type two-mica granite crops out near the centre of Fisher Massif (Mikhalsky 1993).

Hornblende–biotite diorite and tonalite, and biotite±hornblende granodiorite form small plutons, cut by metadolerite dykes, in central Fisher Massif. *Diorite and quartz diorite* consist of biotite (15–20%), hornblende (5–10%), plagioclase (An_{30-35} ; 60–70%), and quartz (up to 20%); opaque minerals, apatite, titanite, zircon and tourmaline are accessories. *Tonalite and trondhjemite* contain dark brown biotite (*mg* 35 in one sample; up to 20%), dark green hornblende (up to 10%), quartz (20–30%), microcline, zoned oligoclase–andesine, and minor ilmenite, magnetite, titanite, allanite, apatite and zircon. Widespread metamorphic effects include sericitisation and saussuritisation of plagioclase, partial replacement of biotite by chlorite, kink banding of biotite, and development of secondary carbonate, muscovite and epidote. Despite extensive recrystallisation, the original medium-grained igneous hypidiomorphic to allotriomorphic inequigranular texture is commonly preserved. Zoned plagioclase phenocrysts occur locally. Poikiloblastic hornblende crystals are probably of metamorphic origin and may replace pyroxene, although no fresh pyroxene has been found.

Biotite granite in central and northeastern Fisher Massif differs from the tonalite in the absence of hornblende and presence of 20 to 30 percent microcline. Like the tonalite, it is extensively altered, but does not appear to be cut by metadolerite dykes. Relatively Mg-rich biotite (*mg* ~50) indicates that the granite is unrelated to the tonalite, consistent with its much younger ion-microprobe U–Pb zircon age (1020 ± 48 Ma; Kinny et al. 1997). Xenoliths of fine- to medium-grained hornblende–biotite quartz diorite to tonalite are extensively recrystallised in some of the granitoids, including the biotite granite, but contain sericitised plagioclase phenocrysts up to five millimetres long. They mostly appear to represent intrusive rocks, but it is possible that some may be genetically related to the intermediate volcanic rocks.



FIGURE 88

Abundant metabasaltic xenoliths in granite near the contact zone; southern Blustery Cliffs, Fisher Massif.

A tonalite pluton crops out in the central part of **Mount Willing**. The rocks comprise plagioclase (An_{25-40} ; 40–55%), quartz (20–35%), biotite (5–15%), hornblende (up to 15%), and rare K-feldspar (up to 5%). The rock is generally gneissose, and grades into tonalite gneiss in the western part of the body. A 60 metre-thick granite dyke dated at 1194 ± 1 Ma (U–Pb zircon: A.A. Laiba, unpublished data) occurs between layered gabbro and tonalite in the central part of Mount Willing. It consists of microcline (30–60%), plagioclase (An_{15-25} , 20–40%), quartz (25–30%), biotite (1–5%), and accessory magnetite and sillimanite. Smaller pods and dykes of hornblende–biotite tonalite and granodiorite, and biotite granite are present in metagabbro. The layered gabbro is cut by at least two generations of tonalite–trondhjemite vein (Fig. 89). Granitoids at Mount Willing are petrographically similar to those at Fisher Massif, and are probably of similar age. They are somewhat less altered than the Fisher Massif rocks, but pale green hornblende forms poikiloblastic crystals suggesting replacement of pyroxene; some of the biotite also appears to be secondary. One tonalite sample (73281802) contains orthopyroxene, as well as biotite. Migmatitic hornblende–biotite tonalite and trondhjemite also crop out at **Nilsson Rocks**.

Biotite–hornblende tonalite at Fisher Massif forms a compositionally rather heterogeneous suite of I-type granitoids, with both low- SiO_2 (64.3) and more abundant high- SiO_2 (71.9–75.4) varieties (Table 12; Figs 90–92). One of the former (91286493) has high *mg* (59.6) and particularly low K_2O , Ba and K/Rb (103). It is very similar in composition to a hornblende tonalite xenolith (71280239), although the latter has even lower K_2O and Rb. Both are metaluminous (Di-normative: Fig. 93).



FIGURE 89

Layered gabbro intruded by two generations of tonalite (plagiogranite) vein; eastern Mount Willing (photo by V.M. Mikhailov). The older generation is folded (centre of photo).

Slightly peraluminous high-SiO₂ leucotonalites (trondhjemites) have much lower *mg* (28.1–39.4), but higher LILE, Sr and K/Rb (376–420). HFSE show large variations, with the most siliceous rock (91286492) being strongly depleted in P₂O₅, Nb, Y and LREE. Such compositional differences cannot all be due to fractionation or alteration processes, and indicate that several distinct magmas were involved. Spidergrams of both tonalite groups have negative Nb, P and Ti anomalies, positive or small negative Sr anomalies, and various degrees of Y depletion (Fig. 94). The REE pattern of one sample is moderately fractionated ((La/Yb)_n 5.30, (Ce/Y)_n 4.1), with only a small negative Eu anomaly (Fig. 95). A single analysed biotite granodiorite (73281647) has particularly high Sr (630 ppm), together with relatively high P₂O₅, LILE (K, Rb, Pb), Th and U (Fig. 92). It cannot, therefore, be genetically related to the tonalites. It has a slightly more fractionated REE pattern ((La/Yb)_n 6.07, (Ce/Y)_n 5.2) than the tonalite, with no significant Eu anomaly (Fig. 95).

Quartz diorites from central Fisher Massif have higher LILE and Sr than most tonalites, and are closer to granodiorite in composition (Figs 90–93). However, they have lower Al₂O₃ and Sr, and higher LREE than the biotite granodiorite sample. Their spidergrams lack the marked positive Sr anomaly of the latter (Fig. 94), precluding a direct genetic relationship. Hornblende–biotite quartz diorite xenoliths in the granitoids have broadly similar compositions to the intrusive quartz diorites, but are less siliceous and have higher LREE and HFSE, particularly Y. Spidergrams show smaller Nb anomalies, but pronounced negative Sr anomalies (Fig. 94). Lower *mg* (50.2–55.7) and higher contents of most incompatible elements, especially LILE, also preclude a close relationship to the low-SiO₂ tonalites. Like the tonalites, these intermediate intrusives form a rather heterogeneous group derived from a range of parent magmas.

The tonalites are compositionally similar to many of the subvolcanic rocks that intrude the metavolcanic sequences 1 to 3 (see above)—although the latter are compositionally more diverse and tend to have even lower K and Rb (Figs 90–93). They also resemble the felsic metavolcanic rocks of

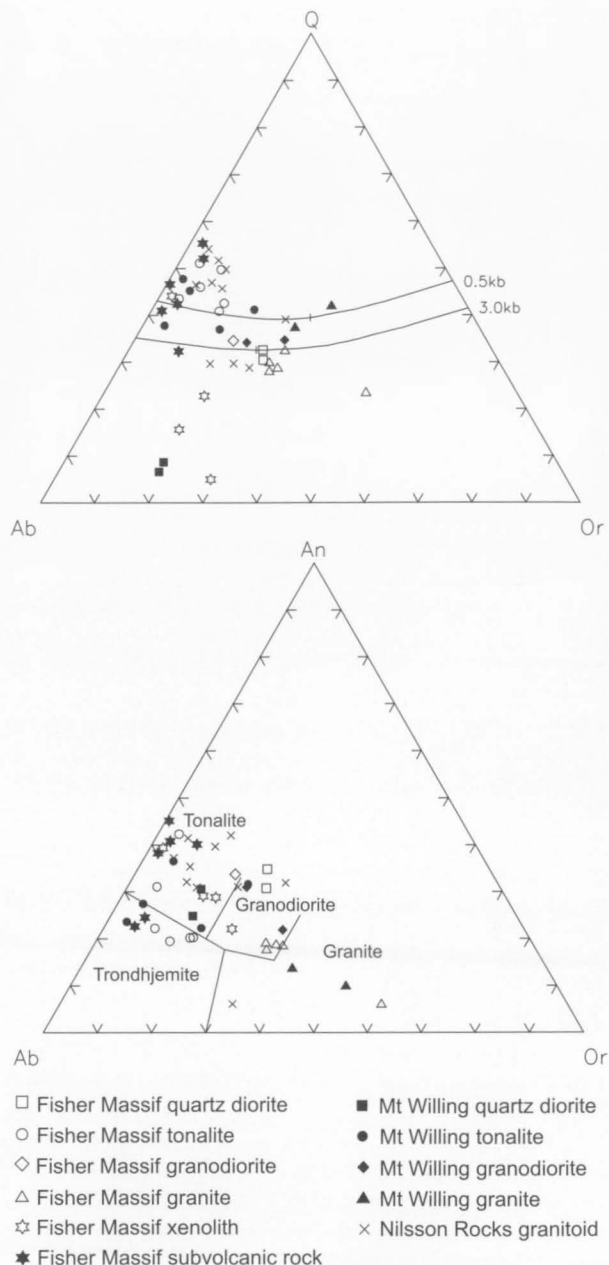


FIGURE 90

Normative Q–Ab–Or and Ab–Or–An diagrams for granitic and subvolcanic rocks of the Fisher Terrane.

group A1, suggesting a similar origin. The quartz diorites (including xenoliths in the more felsic intrusives) differ from the less siliceous subvolcanic rocks in their much higher LILE contents. They have many similar compositional features to the andesitic metavolcanic rocks, although the quartz diorite xenoliths have much higher HFSE, particularly Nb. At least some of the quartz diorites may well have been formed by fractionation of a mantle-derived gabbroic magma, but the high HFSE contents of the xenoliths preclude them being derived from a parent magma of similar composition to the metagabbros (even allowing for the cumulus nature of the latter). Nevertheless, it is noteworthy that tonalite and diorite from western Fisher Massif have higher K₂O than those from the east, a feature also observed for spatially associated gabbroic rocks. This suggests some sort of genetic

relationship, and the presence of two compositionally distinct gabbro–diorite–tonalite associations.

In contrast to the intermediate and tonalitic intrusives, most biotite granites have a very restricted range of composition (Figs 90–93), with generally similar HFSE and LREE contents to the tonalites, but higher K_2O , Rb, Ba, Th and U; Sr (331–407 ppm) and mg (45.3–58.1) are relatively high for granites (s.s.). Spidergrams (Fig. 94)

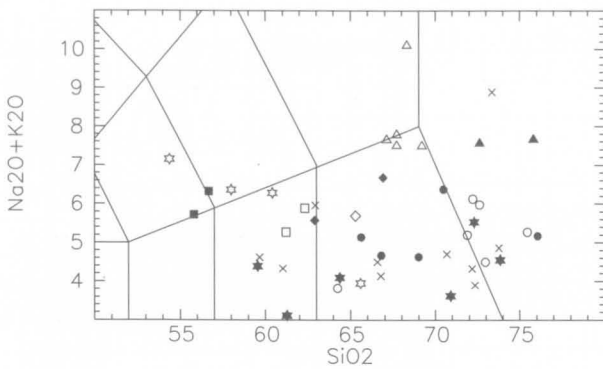
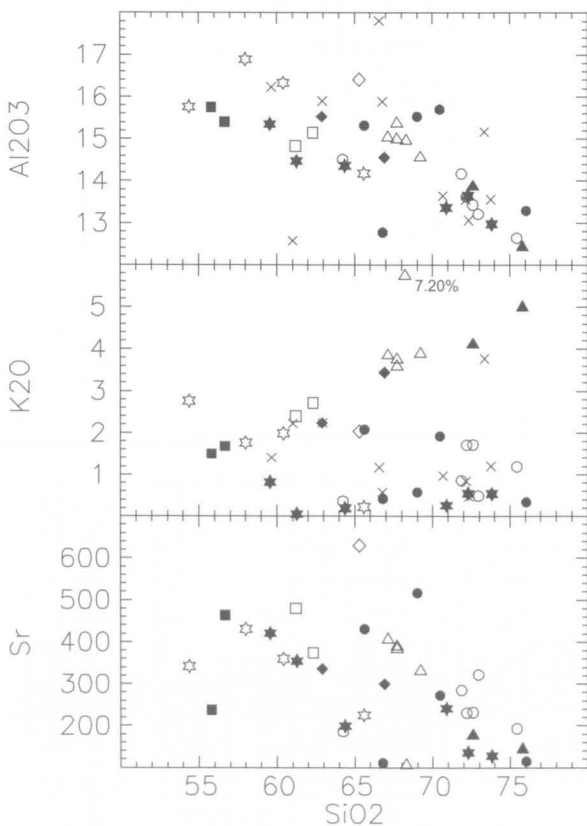


FIGURE 91

Alkalies– SiO_2 plot for granitic and subvolcanic rocks of the Fisher Terrane. Symbols as in Figure 90. The volcanic rock classification fields of Le Bas et al. (1986) are included to aid comparison with Figure 64.



are not unlike those of the tonalites, except for the much greater enrichment in LILE, and do not show significant Sr depletion, precluding major plagioclase fractionation. $(Ce/Y)_n$ is 5.0–5.7 and K/Rb 180–237. One, presumably unrelated, granite (71280028) is much more fractionated (mg 12.0), but with a similar SiO_2 content (68.3%) and high K/Rb (650); it has very high Zr and LREE. It has a strongly fractionated spidergram, with large Nb, Sr, P and Ti depletions (Fig. 94); REE are strongly fractionated $((La/Yb)_n$ 25.2, $(Ce/Y)_n$ 60) (Fig. 95), but $(La/Ce)_n$ is unusually low (0.54, confirmed by XRF data), suggesting LREE (mainly Ce?) mobility during alteration. There is no obvious chemical correlation of the Fisher Massif granites with any of the felsic metavolcanic rocks, although this would not be expected in view of their different ages. Even the relatively high-K felsic rocks of group A2 have significantly lower K_2O and Rb than the granites.

Relatively SiO_2 -poor quartz diorites from Mount Willing are compositionally similar to certain xenoliths from Fisher Massif, rather than clearly intrusive quartz diorites from the latter area (Figs 90–94). Tonalites from Mount Willing are also similar to those from Fisher Massif, with a similar range of SiO_2 content. The orthopyroxene–biotite tonalite differs mainly in its higher Al_2O_3 and Sr and lower Rb (Figs 90–93); its spidergram is characterised by marked Y depletion (Fig. 96), like two of the Fisher Massif tonalites. Small granodiorite bodies from Mount Willing differ from the Fisher Massif granodiorite in having higher

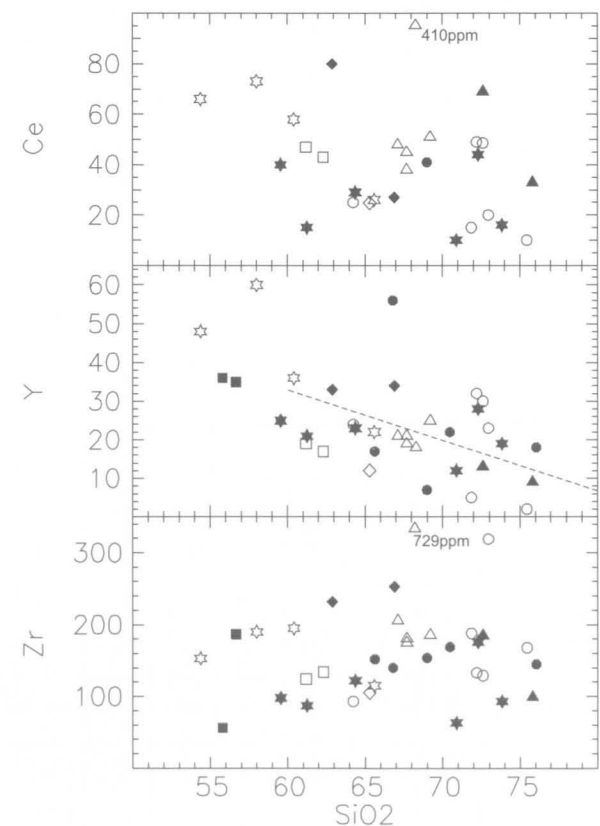


FIGURE 92

SiO_2 variation diagrams for granitic and subvolcanic rocks from Fisher Massif and Mount Willing. The dashed line on the Y plot indicates the approximate boundary between fields of Y-depleted and Y-undepleted felsic orthogneisses of the Archaean Napier Complex, Enderby Land (after Sheraton & Black 1983). Symbols as in Figure 90.

TABLE 12. Chemical analyses and C.I.P.W. norms of representative granitic intrusive rocks from the Fisher Terrane.

Sample no.	71280029B	93286650	91286491	91286493	73281647	71280028	91286490	73281802	65280257	65280256
Locality	Southeast Fisher Massif	Southwest Fisher Massif	Fisher Massif	Fisher Massif	Southwest Fisher Massif	Southeast Fisher Massif	Fisher Massif	Mount Willing	Mount Willing	Mount Willing
Lithology	Bt quartz diorite xenolith	Quartz diorite	Hb tonalite	Hb tonalite	Bt granodiorite	Bt granite	Bt granite	Opx-Bt tonalite	Hb-Bt granodiorite	Bt granite
SiO ₂	58.00	61.20	72.20	64.25	65.30	68.30	67.70	69.00	62.90	72.60
TiO ₂	0.94	0.68	0.32	0.52	0.40	0.37	0.49	0.50	0.97	0.37
Al ₂ O ₃	16.89	14.83	13.62	14.51	16.41	14.96	14.99	15.53	15.53	13.87
Fe ₂ O ₃	2.22	1.90	1.33	1.37	1.93	2.45	1.86	1.77	2.46	1.16
FeO	4.21	4.21	1.60	4.32	2.30	1.31	1.30	1.80	4.18	0.98
MnO	0.17	0.09	0.07	0.09	0.09	0.03	0.07	0.09	0.14	0.05
MgO	2.77	2.75	0.56	3.57	1.68	0.10	1.01	1.01	2.10	0.45
CaO	4.79	5.81	2.53	5.75	4.61	0.89	2.82	4.50	4.14	1.77
Na ₂ O	4.60	2.87	4.42	3.46	3.65	2.90	3.91	4.05	3.33	3.45
K ₂ O	1.76	2.40	1.71	0.36	2.04	7.20	3.59	0.58	2.24	4.11
P ₂ O ₅	0.40	0.23	0.08	0.08	0.16	0.02	0.16	0.10	0.30	0.05
H ₂ O ⁺	—	—	—	—	1.05	0.62	—	0.36	0.98	0.65
CO ₂	—	—	—	—	—	0.11	—	—	0.07	<0.05
LOI	3.32	3.01	1.25	1.58	—	—	1.93	—	—	—
Rest	0.23	0.26	0.15	0.12	0.21	0.29	0.28	0.19	0.26	0.26
Total	100.30	100.24	99.84	99.98	99.83	99.55	100.11	99.48	99.60	99.77
O=F,S,Cl	0.01	0.00	0.00	0.00	0.00	0.00	0.00	0.00	0.00	0.00
Total	100.29	100.24	99.84	99.98	99.83	99.55	100.11	99.48	99.60	99.77
Q	9.32	18.53	33.26	23.63	23.36	21.88	24.09	31.82	21.85	32.33
C	—	—	0.09	—	0.20	0.83	—	0.30	0.82	0.65
Or	10.40	14.18	10.10	2.13	12.05	42.55	21.21	3.43	13.24	24.29
Ab	38.92	24.29	37.40	29.28	30.89	24.54	33.09	34.27	28.18	29.19
An	20.24	20.49	12.03	23.00	21.82	4.28	12.75	21.67	18.58	8.45
Di	0.74	5.60	—	4.09	—	—	0.15	—	—	—
Hy	11.19	9.30	2.83	12.99	6.32	0.25	2.61	3.70	9.53	1.44
Mt	3.22	2.75	1.93	1.99	2.80	3.25	2.70	2.57	3.57	1.68
Il	1.78	1.29	0.61	0.99	0.76	0.70	0.93	0.95	1.84	0.70
Ap	0.95	0.54	0.19	0.19	0.38	0.05	0.38	0.24	0.71	0.12
Li	46	14	7	20	—	—	17	—	—	—
Be	4	—	3	3	—	1	3	—	3	2
S	120	90	30	40	—	—	60	—	—	—
Sc	19	20	12	24	10	13	9	—	17	4
V	145	171	15	139	85	<1	48	26	108	23
Cr	25	81	3	102	17	<3	5	5	36	<3
Ni	15	25	3	26	9	4	5	4	15	<2
Cu	21	70	2	6	36	4	2	6	22	10
Zn	99	63	49	48	57	45	30	45	80	29
Ga	19	17	15	13	16	19	15	16	20	15
Rb	124	98	35	29	83	92	126	8	60	77
Sr	431	480	231	186	630	106	390	517	336	177
Y	60	19	32	24	12	18	19	7	33	13
Zr	190	124	133	93	105	729	181	154	232	185
Nb	19	8	8	4	4	4	8	3	11	6
Sn	2	<2	<2	9	<2	<2	2	—	2	<2
Ba	346	759	612	50	641	693	1372	723	1025	1560
La	29	19	22	12	11	84	17	24	43	42
Ce	73	47	49	25	25	410	38	41	80	69
Nd	45	19	21	15	13	74	22	—	38	26
Pb	7	19	2	7	13	25	9	12	21	29
Th	15	9	5	<2	5	33	6	2	6	10
U	4.5	1.0	<0.5	<0.5	1.9	2.4	2.0	0.5	2.0	1.0
K/Rb	118	203	406	103	204	650	237	602	310	443
(Ce/Y) _n	3.0	6.2	3.8	2.6	5.2	56.9	5.0	14.6	6.1	13.3
Th/U	3.3	9.0	—	—	2.7	14	3.0	4.0	3.0	10
Nb/Nb*	0.51	0.20	0.24	0.37	0.13	0.03	0.15	0.15	0.22	0.08
Sr/Sr*	0.56	1.15	0.52	0.71	2.62	0.04	1.00	0.00	0.44	0.30
mg	54.0	53.8	38.4	59.6	56.6	12.0	58.1	50.0	47.2	45.0

mg = atomic 100Mg/(Mg + Fe²⁺).

HFSE, especially Y, but lower Sr and Sr/Sr*. Dyke sample 71280230 has anomalously low LREE (Fig. 96), although it is possible that the exceptionally low La may be an analytical error. Biotite granites are more siliceous than those from Fisher Massif, but could represent a more evolved variety, derived by fractionation of plagioclase, apatite, Fe–Ti oxide, and a mafic phase such as hornblende that would account for their relative depletions in Sr, P, Ti and Y (Fig. 96). More extensive fractionation of a granodioritic parent magma is also possible, and it is noteworthy that both granites and granodiorites from Mount Willing plot on near-linear trends on many SiO₂ variation diagrams (Figs 91, 92). However, the much lower Y, but similarly peraluminous compositions (Fig. 93), of the granites indicate that they cannot actually be comagmatic. Nevertheless, the granites are likely to have been derived by fractionation of an intermediate to felsic parent magma, rather than a gabbroic magma as suggested by Tingey (1972).

Metamorphosed granitoids from Nilsson Rocks are mostly of quartz dioritic or tonalitic composition, generally similar to those at Fisher Massif and Mount Willing (Figs 90–93). In terms of K₂O contents, rocks from all three areas can be subdivided into two groups: (1) low-K tonalites and trondhjemites, including subvolcanic rocks from Fisher Massif; and (2) high-K quartz diorites (including most of the Fisher Massif xenoliths), granodiorites and granites. Apart from LILE, there appear to be few other major compositional differences between these two groups. Of the felsic metavolcanic rocks described earlier, group A1 rocks from Fisher Massif are low-K and Group A2 are medium- to high-K. Those from Nilsson Rocks (plagiogneisses) are medium- to high-K, whereas those from Mount Willing have low- to medium-K compositions.

In spite of these compositional variations (and the different ages), spidergrams of virtually all the granitic rocks from Fisher Massif and Mount Willing, including the xenoliths, emphasise some significant common features—notably moderate Nb anomalies, positive or small negative

Sr anomalies, and significant Y depletion in many samples. Such characteristics can be explained by partial melting of a plagioclase-poor mafic source, although the moderate degrees of Y depletion in most rocks (except for two high-SiO₂ tonalites) are probably not consistent with major residual garnet (Tarney et al. 1987). However, quite variable degrees of Y depletion suggest magma generation over a wide range of pressures and therefore depths, as was postulated for the Peninsula Ranges Batholith of southwestern North America (Silver & Chappell 1988). This is reflected in the good inverse correlation between Y and Sr/Sr* (Fig. 97). Only three fractionated granites, likely to have been depleted in Sr by extensive plagioclase fractionation, plot significantly off the trend. Only one of these has the very large negative Sr anomaly (and P and Ti anomalies) more typical of granitoids derived by melting of felsic crustal rocks.

One possible origin for the granitoids is melting of subducted hydrated oceanic crust (amphibolite), perhaps with an additional crustal component (Sheraton & Black 1983). Involvement of a subduction-derived LILE-rich fluid could explain the wide variations in K₂O contents of the various intrusive and extrusive rocks. Alternatively, melting of a hydrated mafic to intermediate underplate is possible, but would probably require relatively high degrees of melting to account for the lack of major Sr anomalies (cf. Champion & Sheraton 1997). However, this constraint would be reduced if a residual LREE-rich phase was present. Some of the granitoids, such as the granodiorites, may have been derived by partial melting of gabbroic rocks similar to those exposed in the area, probably under relatively high P_{H₂O} conditions, although rocks of the very low LILE contents of the tonalitic are difficult to explain by such a process. For similar reasons, generation of tonalitic melts by fractionation of a gabbroic magma is unlikely. On the other hand, at least some of the intermediate rocks (diorite and quartz diorite) may well have originated by various degrees of fractionation of mantle-derived gabbroic magma. The systematic variation in the K₂O contents of mafic to intermediate intrusives at Fisher Massif referred to above would be explicable on this basis. Relatively high $\epsilon^{1300}\text{Nd}$ values (+2.4 to +3.0) of three Fisher Massif granodiorites are inconsistent with melting of much older felsic crust, and are only slightly higher than those of metavolcanic rocks (+1.6 to +2.5), the difference only slightly exceeding the analytical uncertainty ($\pm 0.5 \epsilon$). $T^{\text{Nd}}_{\text{DM}}$ model ages are 1640 to 1700 Ma (Table 23; Mikhalsky et al. 1996).

In terms of the Rb versus Y+Nb classification of Pearce et al. (1984), all the Fisher Massif granitoids have volcanic-arc characteristics (Sheraton et al. 1996), as do the felsic metavolcanic and subvolcanic rocks. As suggested above, they were probably formed during the later stages of magmatic arc activity in an Andean-type continental margin.

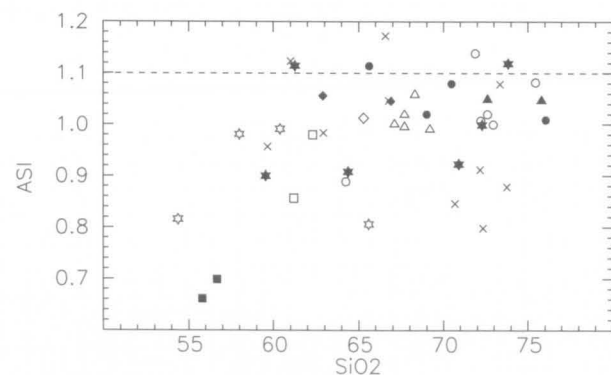


FIGURE 93

Plot of molecular $\text{Al}_2\text{O}_3/(\text{Na}_2\text{O}+\text{K}_2\text{O}+\text{CaO})$ (alumina saturation index, ASI) against SiO₂ for granitic and subvolcanic rocks of the Fisher Terrane. The dashed line indicates ASI = 1.1, the value taken by Chappell & White (1974) as commonly separating I-type (igneous-derived) from S-type (sediment-derived) granitoids; note that CaO is that present in silicate minerals only, a correction being made for that present in apatite. Symbols as in Figure 90.

MESOPROTEROZOIC–NEOPROTEROZOIC MAFIC DYKES

Metadolerite dykes cut metagabbro and granitic rocks at Fisher Massif, Mount Willing and Nilsson Rocks. Two mafic dyke generations crop out at Mount Willing: older amphibolite dykes of highly variable strike, and younger west-northwest-trending altered dolerite dykes. One of the latter dykes (71280229) has a relict igneous texture,

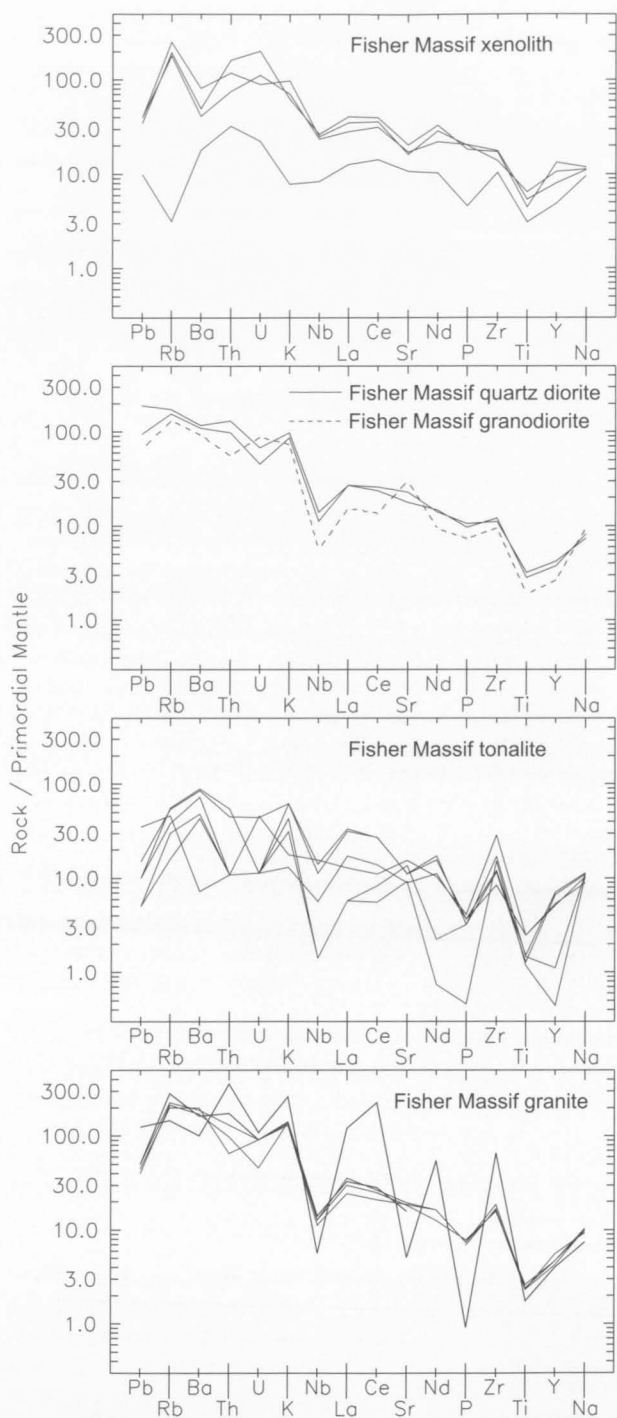
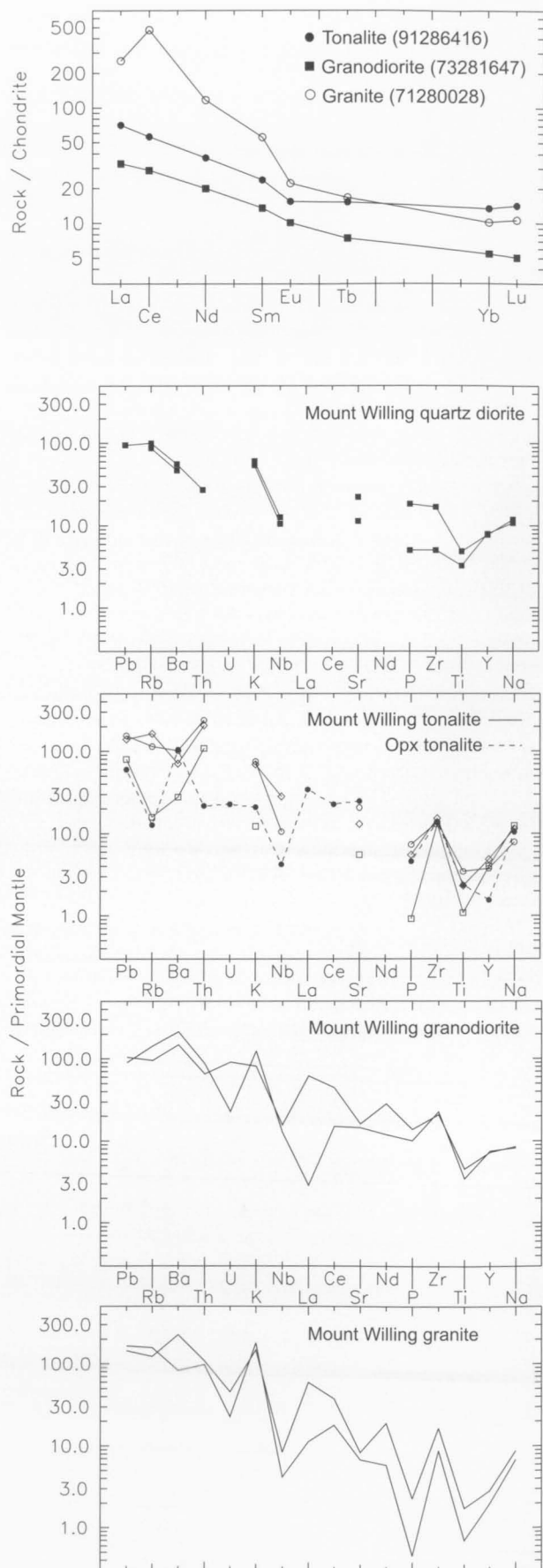


FIGURE 94
(above): Spidergrams for granitic rocks (including xenoliths) from Fisher Massif.

FIGURE 95
(top right): Chondrite-normalised rare-earth element abundance plots for granitic rocks from Fisher Massif.

FIGURE 96
(right): Spidergrams for granitic rocks from Mount Willing.



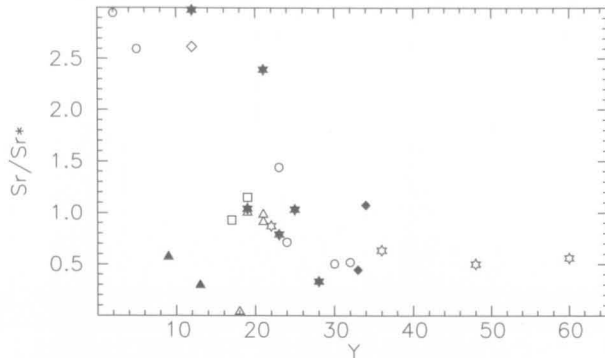


FIGURE 97

Plot of Y against Sr/Sr^* for granitic and subvolcanic rocks from Fisher Massif and Mount Willing. Sr/Sr^* is the primordial mantle-normalised Sr abundance divided by the interpolated value obtained by averaging the normalised Ce and Nd abundances (i.e., a measure of the Sr anomaly on the spidergram). Symbols as in Figure 90.

and is petrographically similar to metadolerites of the Ruker Terrane; an almost identical sample from Fisher Massif (73281646) may also be from a dyke, but the field relations are unclear. Another dyke sample (65280258) from Mount Willing differs in the presence of relict clinopyroxene (~10%) and both secondary green clin amphibole and colourless ortho-amphibole. The texture is more granoblastic than the other dykes, but strongly zoned plagioclase phenocrysts are present, suggesting crystallisation relatively deep in the crust. Metadolerite dykes at Fisher Massif, some of which are deformed, intrude 1293 ± 28 Ma granodiorite, but apparently not 1020 ± 48 Ma granite (Kinny et al. 1997). However, most dykes at Mount Willing seem to have escaped major metamorphic recrystallisation (c.1000 Ma), and thus may be Neoproterozoic (or even early Palaeozoic) in age.

All the analysed dolerite dykes are of slightly Ol or Q-

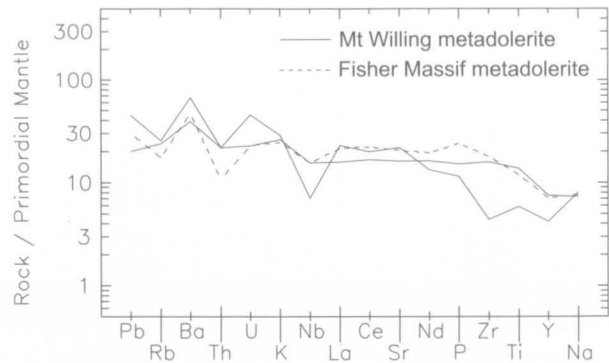


FIGURE 98

Spidergrams for metadolerite dykes from Fisher Massif and Mount Willing.

normative tholeiitic composition (Table 13; Figs 43, 44). One of the dykes from Mount Willing (71280229) has a very similar composition to Fisher Massif sample 73281646, suggesting a correlation. However, 65280258 from Mount Willing has quite different incompatible element contents and ratios—for example, much higher LILE/Zr, Ce/Zr, P/Zr, La/Nb and Ce/Y (Figs 45–47, 98).

Metadolerite dykes from Fisher Massif also form a compositionally rather heterogeneous group and may well be of more than one age. One deformed dyke has unusually low LILE (Na_2O 0.79%, K_2O 0.25%, Rb 4 ppm, Ba 57 ppm), but this may well be a metamorphic effect. Nevertheless, this sample apart, higher Sr contents and systematic differences in incompatible element ratios (such as Ba/Zr, P/Zr and Y/Zr) mean that none of the Fisher Massif or Mount Willing dykes can be correlated with the Ruker Terrane metadolerites, or with any of the dolerite suites of the Vestfold Block or Enderby Land. This is consistent with them being significantly younger. They appear to have been derived from a generally more enriched lithospheric mantle source than those of most Ruker Terrane metadolerites, with the source of Mount Willing dyke 65280258 being particularly enriched.

TABLE 13. Chemical analyses and C.I.P.W. norms of representative metadolerite and mafic granulite dykes from the Fisher and Beaver-Lambert terranes and ultramafic intrusives from McLeod Massif.

Sample no.	36711-13	36726-7	73281646	65280258	91286404	91286438	91286345	91286347	71280362	32P4/1	32P2/1	32602	32512
Locality	Fisher	Fisher	SW Fisher	Mount	White	Loewe	Mount	Mount	E Mount	McLeod	McLeod	McLeod	McLeod
Lithology	Massif Metadolerite dyke (deformed)	Massif Metadolerite dyke	Massif Metadolerite ?dyke	Willing Metadolerite dyke	Massif Bt-Px-Hb- Pl granulite dyke	Massif Qz-Opx-Pl granulite dyke	Collins Metadolerite dyke	Collins Metadolerite dyke	Meredith Metadolerite dyke	Massif Serpentinite ?pluton	Massif Serpentinite ?pluton	Massif Meta- lherzolite dyke	Massif Meta- lherzolite dyke
SiO ₂	48.27	48.05	45.80	50.40	42.91	55.39	47.91	45.00	50.40	37.25	38.30	42.85	44.60
TiO ₂	2.98	0.78	2.51	1.24	0.55	1.54	3.34	2.72	1.80	0.56	0.73	0.76	0.68
Al ₂ O ₃	14.97	12.01	16.28	17.06	16.59	15.78	12.86	14.77	15.51	10.10	8.45	8.80	4.22
Fe ₂ O ₃	5.60	3.41	5.13	2.67	1.46	4.07	4.31	2.46	1.35	2.13	2.11	4.00	3.80
FeO	8.66	7.10	8.27	7.20	8.68	8.38	10.70	10.99	11.33	4.12	6.64	10.84	10.14
MnO	0.16	0.18	0.21	0.18	0.14	0.21	0.22	0.18	0.19	0.07	0.08	0.25	0.17
MgO	5.45	14.54	6.29	5.73	12.11	2.82	4.47	6.82	6.96	31.60	30.20	23.44	20.50
CaO	7.98	8.64	9.08	8.91	9.87	4.93	8.30	10.06	9.25	4.92	2.66	5.69	6.18
Na ₂ O	1.13	2.37	2.97	3.13	0.88	4.22	3.05	3.16	0.46	0.06	0.09	0.43	0.70
K ₂ O	2.06	0.96	0.68	0.79	3.90	0.94	1.01	0.85	0.84	0.06	0.06	0.24	0.61
P ₂ O ₅	0.93	0.27	0.52	0.25	0.10	0.78	0.42	0.32	0.22	0.12	0.21	0.24	0.32
H ₂ O ⁺	—	—	1.97	1.59	—	—	—	—	2.17	—	—	—	—
CO ₂	—	—	<0.05	0.18	—	—	—	—	<0.05	—	—	—	—
LOI	1.97	1.66	—	—	1.89	0.91	3.16	2.55	—	9.00	10.13	1.79	7.75
Rest	0.23	0.26	0.21	0.20	0.21	0.23	0.50	0.37	0.21	0.00	0.00	0.00	0.00
Total	100.39	100.23	99.92	99.53	99.29	100.20	100.25	100.25	100.69	99.99	99.66	99.33	99.67
O=F,S,Cl	0.00	0.00	0.00	0.00	0.00	0.00	0.12	0.06	0.00	0.00	0.00	0.00	0.00
Total	100.39	100.23	99.92	99.53	99.29	100.20	100.13	100.19	100.69	99.99	99.66	99.33	99.67
Q	5.27	—	—	—	—	7.86	0.25	—	9.45	—	—	—	—
C	—	—	—	—	—	0.72	—	—	—	1.28	3.90	—	—
Or	12.17	5.67	4.02	4.67	1.26	5.55	5.97	5.02	4.96	0.35	0.35	1.42	3.60
Ab	9.56	20.05	25.13	26.49	—	35.71	25.81	20.01	3.89	0.51	0.76	3.64	5.92
An	29.69	19.30	29.08	30.17	29.80	19.36	18.42	23.61	37.77	23.62	11.82	21.37	6.57
Lc	—	—	—	—	17.08	—	—	—	—	—	—	—	—
Ne	—	—	—	—	4.03	—	—	3.64	—	—	—	—	—
Di	3.17	17.52	10.37	10.20	14.94	—	16.75	19.93	5.50	—	—	4.24	17.66
Hy	26.86	4.62	4.84	19.25	—	22.01	18.36	—	29.83	3.90	25.53	23.18	31.19
Ol	—	26.38	14.90	1.43	26.39	—	—	15.98	—	58.41	43.15	38.04	21.50

Mt	3.31	2.46	3.11	2.32	2.42	2.91	3.52	3.19	3.03	1.46	2.06	3.49	3.28
Il	5.66	1.48	4.77	2.35	1.04	2.92	6.34	5.17	3.42	1.06	1.39	1.44	1.29
Ap	2.20	0.64	1.23	0.59	0.24	1.85	0.99	0.76	0.52	0.28	0.50	0.57	0.76
S	–	–	–	–	100	100	2500	1200	–	–	–	–	–
Sc	–	–	30	27	24	25	43	32	35	–	–	–	–
V	211	183	289	229	153	31	467	233	239	–	–	–	–
Cr	28	523	55	50	117	2	109	196	182	–	–	–	–
Ni	37	258	47	41	298	7	23	117	35	–	–	–	–
Cu	–	–	35	70	2	8	31	65	10	–	–	–	–
Zn	–	–	98	72	100	166	154	142	114	–	–	–	–
Ga	–	–	22	20	13	25	24	22	21	–	–	–	–
Rb	77	19	11	16	455	19	24	24	62	–	–	–	–
Sr	250	521	427	456	145	314	301	478	158	–	–	–	–
Y	41	19	32	19	12	55	51	27	47	–	–	–	–
Zr	271	84	198	49	35	298	215	149	134	–	–	–	–
Nb	20	5	11	5	2	18	14	42	8	–	–	–	–
Ba	911	284	326	462	136	454	337	362	502	–	–	–	–
La	–	–	15	16	9	59	24	18	20	–	–	–	–
Ce	–	–	40	36	8	124	54	34	42	–	–	–	–
Nd	–	–	26	18	6	58	39	21	26	–	–	–	–
Pb	10	16	6	9	8	18	8	<2	6	–	–	–	–
Th	–	4	1	2	<2	8	2	2	4	–	–	–	–
U	–	–	0.5	1.0	<0.5	2.0	<0.5	<0.5	1.0	–	–	–	–
K/Rb	222	419	513	410	71	411	349	294	112	–	–	–	–
(Ce/Y) _n	–	–	3.1	4.7	1.7	5.6	2.7	3.2	2.2	–	–	–	–
Ba/Zr	3.36	3.38	1.65	9.43	3.89	1.52	1.57	2.43	3.75	–	–	–	–
Ce/Zr	–	–	0.20	0.73	0.23	0.42	0.25	0.23	0.31	–	–	–	–
Nb/Zr	0.07	0.06	0.06	0.10	0.06	0.06	0.07	0.28	0.06	–	–	–	–
Nb/Nb*	–	–	0.67	0.27	0.04	0.43	0.56	2.10	0.38	–	–	–	–
Sr/Sr*	–	–	0.99	1.31	1.57	0.27	0.49	1.33	0.36	–	–	–	–
mg*	45.5	75.0	50.6	55.6	71.8	32.9	39.1	52.0	53.8	91.7	88.1	77.3	76.0

mg* = atomic 100Mg/(Mg + 0.85Fe(total)).

BEAVER-LAMBERT TERRANE

High-grade metamorphic rocks of both the NPCM and northern part of the SPCM are included in the Beaver-Lambert Terrane (Fig. 2), as isotopic dating indicates virtually identical early Neoproterozoic metamorphic ages (c.1000–900 Ma). The slightly lower grade rocks of the Shaw Massif–Mount Johns area (central PCM) were included in a separate Lambert Province by Kamenev et al. (1990, 1993) on the basis of metamorphic grade, as well as the abundance of ‘banded gneiss and schist’, calcareous rocks, migmatites and early Palaeozoic granites and pegmatites. It was suggested that the Lambert Province rocks (Lambert Complex) were derived from both prograde metamorphosed Ruker Terrane rocks and retrogressed granulite-facies NPCM (Beaver Belt) rocks, with a number of new crustal additions (Kamenev et al. 1990, 1993). However, the available model Rb–Sr (T_{UR}) and Sm–Nd (T_{DM}) ages puts this interpretation in doubt. In the absence of definitive geological and isotopic data, the authors of this bulletin consider the NPCM and northern part of the SPCM (excluding the Fisher Terrane) to be a single unit or terrane showing a slight decrease in metamorphic grade from north to south. For the same reason the original Lambert *Series* of Ravich et al. (1978) is used, excluding the Archaean rocks of the Ruker Terrane assigned to the Lambert *Series* by them, rather than Lambert *Province*. Thus, in this bulletin the Lambert *Series* includes the mostly upper amphibolite-facies rocks of the Shaw Massif–Mount Isabelle–Mount Johns area, together with Clemence Massif and the northern and central Mawson Escarpment.

Gneisses of both igneous and sedimentary origin are widespread in the Beaver-Lambert Terrane. Ravich et al. (1978) described and mapped two distinctive metamorphic rock associations in the Prydz Bay–Amery Ice Shelf area: the Reinbolt *Series* (orthopyroxene-bearing tonalitic to granitic orthogneiss, migmatite, garnet–biotite ‘shadow’ granite or anatexite, garnet and biotite plagiogneiss, and minor calc-silicate rocks) and the Larsemann *Series* (high-Al paragneiss and schist, migmatite, granite gneiss, and minor orthopyroxene-bearing tonalitic to granitic orthogneiss, mafic schist, quartzite, and calc-silicate rocks). Mikhailov & Sergeyev (1997) distinguished three metamorphic rock associations in the NPCM: the Porthos Orthogneiss (predominately orthopyroxene-bearing tonalitic to granitic orthogneiss, granite gneiss, and minor mafic schist), the Athos Paragneiss (predominantly garnet and biotite–garnet gneiss, granite gneiss, high-Al pelitic gneiss, orthopyroxene-bearing felsic gneiss, and minor calc-silicate rocks), and the Astronomov Paragneiss (predominantly garnet and biotite–garnet gneiss, granite gneiss, biotite and biotite–hornblende gneiss, mafic schist, and minor high-Al paragneiss and calc-silicate rocks), which appears to include a major orthogneiss component.

In this bulletin essentially the same three units are used (termed *series*) to classify the high-grade metamorphic rocks of the Beaver-Lambert Terrane. Because such highly deformed units include a variety of different rock types, the terrane is described here in terms of lithology rather than stratigraphy. No detailed lithological comparisons and correlations between these *series* and the classification of Ravich et al. (1978) were made, but the Porthos *Series* seems to be broadly similar in composition to the Reinbolt *Series*. However, the Athos *Series* cannot be directly correlated with the Larsemann *Series*, as metasedimentary rocks in the Larsemann Hills area, at least, have since been shown to have been affected by c.500 Ma high-grade metamorphism (Zhao et al. 1992; Carson et al. 1996; Kinny 1998). Most of the slightly lower grade rocks of the Lambert *Series* may well be compositionally and geochronologically equivalent to the Athos and Porthos *Series*, albeit with some reworked Ruker Terrane rocks in the Mawson Escarpment. In addition, plutonic orthopyroxene granitoids (‘charnockites’) occur in many parts of the NPCM. Concordant amphibolite and mafic granulite layers and lenses crop out in some places and may be deformed relics of intrusive rocks. Mafic dykes are generally rare, except in a few small areas, and most such dykes appear to be of Phanerozoic age.

MESOPROTEROZOIC METASEDIMENTARY ROCKS

Metasediments of a range of composition are the major constituents of the Athos *Series*, which is interlayered with felsic orthogneiss (the main component of the Porthos *Series*) in the NPCM. Most are of granulite-facies (Fig. 99), whereas comparable rocks in the central PCM (Lambert *Series*) are predominantly of upper amphibolite facies, although transitional amphibolite–granulite-facies conditions were reached in the northern Mawson Escarpment and Mount Isabelle. All these metasedimentary rocks are of much higher metamorphic grade than typical Ruker Terrane metasediments. Their depositional ages are not well constrained. The only available T_{DM}^{Nd} model ages are 2220, 2030 and 1600 Ma (Zhao et al. 1997; S-S Sun, unpublished data), but these would be maximum values for the source terranes. The depositional ages are most likely to be Mesoproterozoic, although the possibility of some Palaeoproterozoic sedimentary protoliths cannot be ruled out. Felsic biotite gneisses of probable sedimentary origin from Mount Meredith contains detrital zircon populations of about 2800–2500 and 2100–1800 Ma, perhaps derived from the Ruker Terrane rocks, but no isotopic evidence for Meso-

to Neoproterozoic metamorphism was found (Kinny et al. 1997).

Rocks of distinctive sedimentary composition (aluminous or calcareous) appear to be generally less abundant in the Lambert Series than quartzo-feldspathic gneiss, although some of the latter is probably of sedimentary origin (see below). Calc-silicate gneiss crops out at Ely Nunatak, Mount Johns and Shaw Massif, and is relatively abundant in the northern half of the Mawson Escarpment. Both pelitic and calcareous rocks are widespread in the NPCM.

Pelitic metasediments

In the NPCM, aluminous metasedimentary rocks are most common in the paragneiss sequences (Athos Series) of the Athos Range, Stinear Nunataks, and the small isolated outcrops around Single Island on the northwestern side of the Amery Ice Shelf. They are commonly interlayered with garnet-biotite-bearing felsic gneiss, much of which is probably also of sedimentary origin as described below. Metapelitic rocks are typically medium- to coarse-grained, well-layered to migmatitic gneisses, with large (up to 3 cm) garnet porphyroblasts and cordierite in a quartzo-feldspathic matrix (Fig. 169D; Fitzsimons & Thost 1992; Thost & Hensen 1992).

The most common assemblages are:

quartz + biotite + garnet + cordierite + plagioclase + K-feldspar, and

quartz + biotite + garnet + cordierite + sillimanite + plagioclase + K-feldspar.

Rare garnet-orthopyroxene-cordierite-biotite-bearing units are interlayered with garnet-sillimanite-bearing metapelite at Jetty Peninsula (Hand et al. 1994a). These assemblages thus differ from those of the Lambert Series mainly in the greater abundance of cordierite. Garnet is commonly pyrope-rich almandine (typically *mg* 20–45, decreasing towards the rim) and contains inclusions of sillimanite, cordierite, spinel, biotite, quartz, ilmenite and rutile (Fig. 184B; Nichols & Berry 1991; Thost & Hensen 1992; Hand et al. 1994b; Scrimgeour & Hand 1997). Grossular (2.3–3.7%) and spessartine (1.0–2.7%) contents of garnet are low, but show slight rimward increases. Cordierite (*mg* 55–82) is locally altered and commonly contains rounded quartz inclusions. Reddish-brown biotite inclusions in garnet range from *mg* 66–79, whereas matrix biotite, commonly retrograde, tends to be more Fe-rich (*mg* 50–77) and may have a marked preferred orientation. Orthopyroxene, which is extensively replaced by biotite, has *mg* about 65 and shows a rimward decrease in Al_2O_3 from about 4.5 percent to 3.5 percent (Hand et al. 1994b). Sillimanite occurs as five to 10 millimetre long prismatic crystals in the matrix, and mostly constitutes less than five percent of the rock, although in individual layers it can reach 90 percent. K-feldspar is generally orthoclase perthite and plagioclase is sodic andesine (An_{33-37}). Accessory minerals comprise ilmenite, zircon and, less commonly, monazite and rutile. Hercynite-rich spinel (with up to 20 mol. % gahnite) is present in some metapelitic rocks, and appears to be part of the peak assemblage (with garnet, sillimanite, cordierite and/or

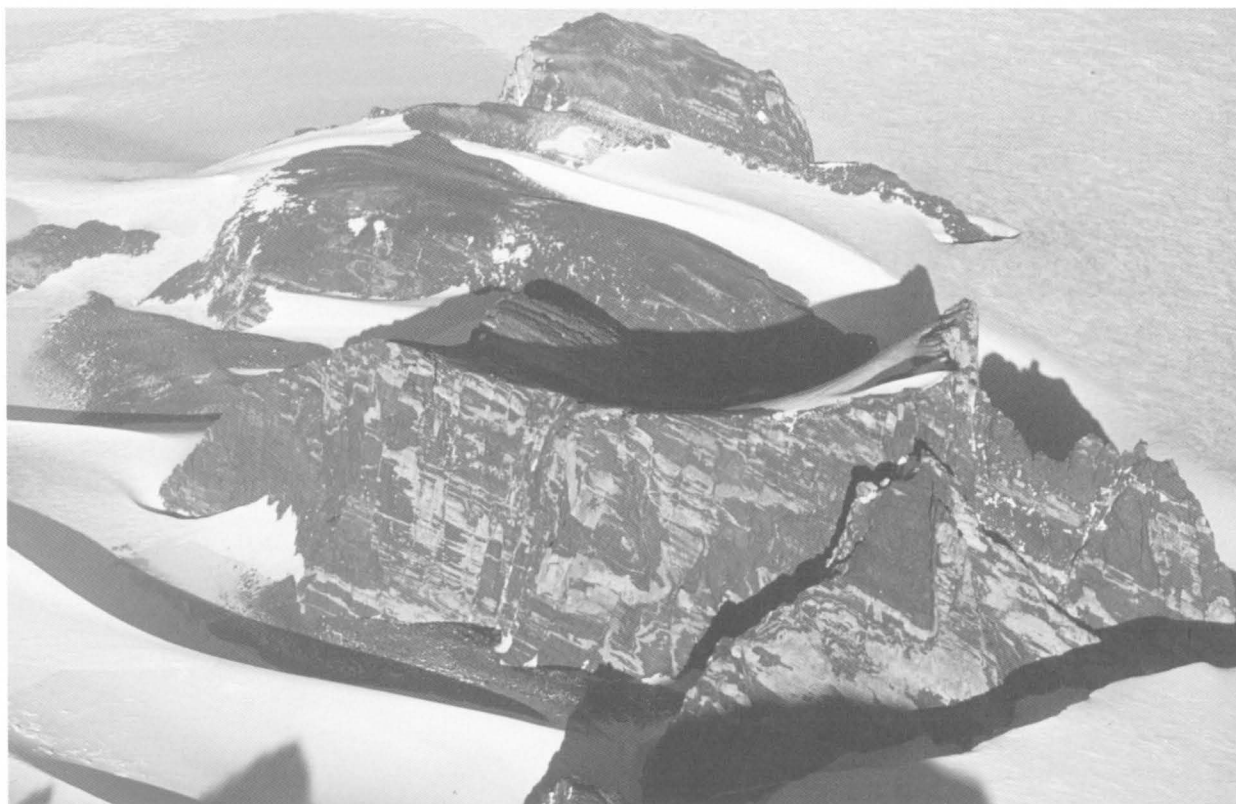


FIGURE 99

Granulite-facies metasediments and garnet-bearing granitic leucogneiss; Zebra Peak, Stinear Nunataks. The cliff is about 200 m high.

ilmenite) at Depot Peak (Stüwe & Hand 1992), Fox Ridge and Trost Rocks (Scrimgeour & Hand 1997). Spinel inclusions in garnet or sillimanite tend to be more magnesian (*mg* 36–49) and richer in Zn (10–21 mol %) and Cr (3–10 mol %) than symplectitic grains (*mg* 28–45, Zn 4–12%, Cr 0–2%; Hand et al. 1994b). Corundum occurs in metapelite at Trost Rocks and Fox Ridge (Scrimgeour & Hand 1997). Some rocks contain secondary chlorite and muscovite. Cordierite, anthophyllite, garnet, plagioclase and biotite occur in pelitic lenses in felsic gneiss at southern Mount Meredith (Fig. 188). Secondary muscovite is also present, and cordierite is partly replaced by andalusite, quartz, chlorite and carbonate.

A variety of reaction coronas is present in metapelite from Jetty Peninsula (Hand et al. 1994b). Garnet + sillimanite ± biotite-bearing rocks contain symplectites of cordierite ± spinel ± ilmenite, whereas garnet in orthopyroxene-bearing rocks is commonly rimmed by orthopyroxene–cordierite–plagioclase symplectites. Cooling from peak metamorphic conditions is suggested by garnet + biotite ± sillimanite overprinting some peak assemblages. The formation of cordierite + garnet + biotite + ilmenite, cordierite + garnet + sillimanite + ilmenite, and cordierite + orthopyroxene assemblages may have resulted from a subsequent increase in temperature. Similar reaction textures have been reported from Trost Rocks and Fox Ridge by Scrimgeour & Hand (1997). The significance of these reactions is discussed in more detail in the section on metamorphism.

Similar assemblages to those in the NPCM are present in metapelite of the Mawson Coast area, although spinel is a more common minor phase, and co-exists with quartz at one locality (Kidson Island). Sapphirine and corundum occur in a few places, but not in contact with quartz.

The most common assemblage in metapelite of the Lambert Series is quartz + biotite + garnet + sillimanite + plagioclase ± K-feldspar, which crops out at Mount Johns and Shaw Massif. A metasediment from Mount Johns (73281373) contains garnet + K-feldspar partly replacing biotite. Retrograde metamorphism is common at Shaw Massif, where it appears to be associated with large-scale folding; garnet and biotite are altered to chlorite, and feldspar is saussuritised and sericitised. Accessory minerals comprise opaque minerals, zircon, apatite, rutile and tourmaline.

Metapelite in the northern half of the Mawson Escarpment is petrographically similar:

quartz + biotite + garnet + sillimanite + cordierite + K-feldspar, and

quartz + biotite + garnet + sillimanite + plagioclase + K-feldspar.

However, quartz + biotite + anthophyllite + orthopyroxene + cordierite + bytownite occurs in the extreme north of the Escarpment, in association with mafic two-pyroxene granulite. Retrograde metapelite contains secondary chlorite and muscovite, and cordierite and feldspar are much altered. Contact metamorphism, probably due to the emplacement of Cambrian granite, produced similar assemblages (quartz + biotite + garnet + sillimanite + cordierite + plagioclase) in originally staurolite (and possibly kyanite) bearing metapelite in the central Mawson Escarpment. The original presence of the

association kyanite + staurolite suggests, however, that these are relict Ruker Terrane rocks.

As noted earlier, Mesoproterozoic (in terms of their likely depositional age) metapelites of the Beaver-Lambert Terrane are little different in chemical composition from late Archaean to Palaeoproterozoic metapelites of the Ruker Terrane, apart from having lower Cr and Ni contents. Granulite-facies metapelites of the Beaver-Lambert Terrane (and Mawson Coast) do not have higher K/Rb ratios than lower grade metapelites (Sheraton 1980); in fact, their K/Rb ratios are mostly lower than the estimated crustal average (230: Taylor, 1966). However, Th/U ratios are somewhat higher (Table 14), consistent with some depletion of U relative to Th during high-grade metamorphism — the average value of 11 compares with an estimated crustal average of 3.8 (Taylor & McLennan 1985). The compositions of biotite + garnet + cordierite + plagioclase + K-feldspar + quartz ± sillimanite metapelites are plotted on an A'FM diagram (after Winkler 1974) in Figure 100.

Psammitic metasediments

Quartzite is relatively uncommon, but crops out at Mounts Beck and Thomas (minor biotite and garnet) and the Taylor Platform area (plagioclase quartzite) in the NPCM.

Well layered to migmatitic *biotite–garnet–quartz–feldspar gneiss* (semi-pelitic gneiss of Fitzsimons & Thost 1992) is particularly common in association with metapelitic rocks in the Athos Range. It is also widespread elsewhere in the NPCM, notably in the Mount Bewsher–Mount Gleeson area and on Jetty Peninsula. A strong foliation, defined by oriented biotite grains, is parallel to a compositional layering consisting of

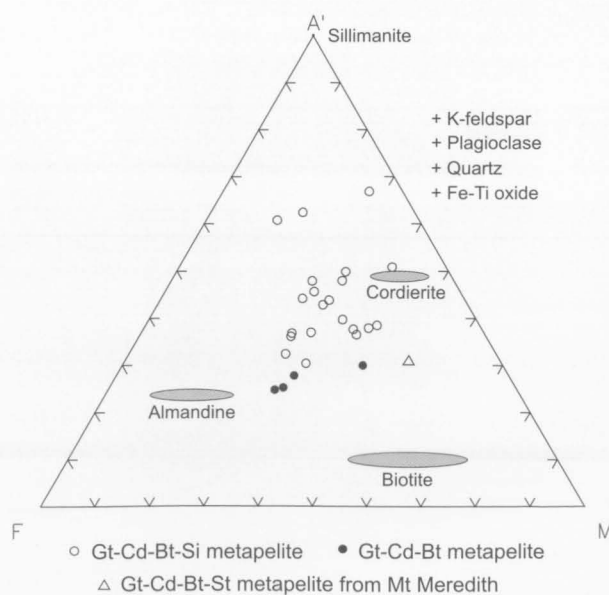


FIGURE 100

Modified A'FM diagram (based on Winkler 1974) for Mesoproterozoic high-grade metapelites of the Beaver-Lambert Terrane. A' = Al_2O_3 – ($\text{K}_2\text{O} + \text{Na}_2\text{O} + \text{CaO}$); F = total Fe as FeO; M = MgO (all as molecular proportions).

TABLE 14. Chemical analyses of representative metapelites from the Beaver-Lambert Terrane.

Sample no.	69280226	70280277	73281767	73281781	91286442
Locality	Fox Ridge	Mount Fox	Mount Bechervaise	Moore Pyramid	Mount Meredith
Lithology	Sp-Gt-Cd-Kf-Pl-Qz-Si metapelite	Bt-Si-Cd-Pl-Gt-Qz-Kf metapelite	Si-Bt-Cd-Gt-Qz-Kf metapelite	Bt-Cd-Gt-Pl-Kf-Qz metapelite	Bt-St-Gt-Pl-Cd-Qz(-Chl-Ad) metapelite
SiO ₂	64.14	61.34	49.90	65.40	39.37
TiO ₂	1.34	0.85	1.20	1.44	0.94
Al ₂ O ₃	19.43	19.27	22.43	14.11	20.50
Fe ₂ O ₃	1.98	2.90	0.97	0.72	9.54
FeO	5.40	5.14	12.71	8.19	12.65
MnO	0.16	0.16	0.43	0.12	0.21
MgO	1.53	2.64	4.89	2.76	10.78
CaO	0.54	1.40	0.28	1.90	0.76
Na ₂ O	0.59	1.48	0.74	1.66	0.68
K ₂ O	3.00	3.83	4.38	2.24	1.79
P ₂ O ₅	0.08	0.06	0.10	0.07	0.04
H ₂ O ⁺	-	-	0.89	0.97	-
CO ₂	-	-	0.07	0.11	-
LOI	1.04	0.59	-	-	3.00
Rest	0.35	0.42	0.36	0.28	0.22
Total	99.58	100.08	99.35	99.97	100.48
O=F,S,Cl	0.01	0.03	0.00	0.00	0.00
Total	99.57	100.05	99.35	99.97	100.48
Li	31	56	-	-	32
Be	8	7	5	3	4
S	260	630	-	-	<100
Sc	10	17	31	18	19
V	188	132	300	271	218
Cr	150	139	176	156	99
Ni	35	42	118	52	68
Cu	15	12	172	31	4
Zn	227	106	134	100	119
Ga	33	26	35	19	29
Rb	115	225	224	100	92
Sr	49	212	92	164	18
Y	32	56	57	37	30
Zr	277	338	218	259	321
Nb	28	16	20	16	13
Ba	668	1199	1019	648	534
La	117	56	77	80	14
Ce	252	110	146	152	32
Nd	110	38	58	63	11
Pb	86	46	29	19	6
Th	83	39	42	48	19
U	2.5	3.0	4.5	3.0	3.0
K/Rb	217	141	162	186	162
(Ce/Y) _n	19.7	4.9	6.4	10.3	2.7
Th/U	33	13	9.3	16	6.3
Nb/Nb*	0.29	0.21	0.21	0.23	0.43
Sr/Sr*	0.02	0.23	0.07	0.12	0.07
mg	33.6	47.8	40.7	37.5	60.3

mg = atomic 100Mg/(Mg + Fe²⁺).

garnet–biotite-rich and quartzo-feldspathic layers. Migmatitic structures include small, locally discordant felsic segregations with garnet–biotite-rich selvages, and discordant leucogneiss sheets and lenses containing garnet–biotite schlieren (Fitzsimons & Thost 1992). Garnet-bearing felsic gneiss usually contains less reddish-brown biotite (<6%) than that in the Lambert Series, K-feldspar is commonly orthoclase perthite (although microcline occurs locally), and orthopyroxene is present. In the Nemesis Glacier area, garnet and orthopyroxene preserve polygonal grain boundaries where in contact; at Crohn Massif they tend to be confined to separate layers in the quartz–feldspar–biotite matrix (Fitzsimons & Thost 1992). Orthopyroxene in a garnet–orthopyroxene–biotite gneiss from the latter area is much more magnesian (*mg* 58–61) than coexisting garnet (*mg* 36–37; Thost & Hensen 1992). Much garnetiferous gneiss is relatively rich in quartz (up to 50%) or perthite (up to 55%), and some has relatively abundant garnet, all of which suggest a sedimentary (arkose or greywacke) origin. However, because it is not always possible to unequivocally distinguish between garnet-bearing felsic gneisses derived from sedimentary and those derived from igneous protoliths, the geochemistry of all such gneisses is described in the felsic orthogneiss section.

Garnet–biotite–quartz–feldspar gneiss is also a major component of the Lambert Series in the SPCM. Most is fine to medium grained, and textures are commonly granoblastic inequigranular interlobate, with biotite commonly having a marked preferred orientation. Major constituents are dark brown or reddish-brown biotite (up to 15%), garnet (up to 20%), quartz (20–60%), orthoclase or microcline (up to 60%), and oligoclase–andesine (10–60%), with accessory opaque minerals, apatite, zircon, and rare allanite, titanite and chevkinite or perrierite. Retrograde effects are common in some areas, with alteration of garnet and biotite to chlorite and saussuritisation and sericitisation of feldspar; secondary muscovite and carbonate may also be present. As in the NPCM, the high abundance of quartz (40–60%) and variable composition of much of this garnet-bearing gneiss are consistent with a sedimentary origin (i.e., paragneiss); some contains little or no K-feldspar, whereas some is K-feldspar-rich. Small amounts of sillimanite may be present, and there are gradations into more aluminous metasediments.

Calcareous metasediments

Discontinuous layers and pods of calc-silicate rocks and marble are commonly interlayered with both felsic gneiss and metapelitic rocks in the NPCM, although they are volumetrically minor. They are generally fine to medium grained, with granoblastic inequigranular textures, and commonly contain wollastonite (Fig. 184A; Fitzsimons & Harley 1992; Fitzsimons & Thost 1992; Thost & Hensen 1992; Hand et al. 1994a). The following assemblages are typical:

quartz + diopside + wollastonite + scapolite + plagioclase ± carbonate ± titanite,
 quartz + diopside + wollastonite + scapolite + carbonate + titanite,
 quartz + diopside + wollastonite + carbonate ± garnet ± titanite,

quartz + hornblende + diopside + plagioclase ± biotite ± orthopyroxene ± titanite,
 quartz + diopside + scapolite + plagioclase ± biotite,
 quartz + garnet + diopside + scapolite + plagioclase + carbonate,
 forsterite + diopside + carbonate ± phlogopite ± spinel, and
 diopside + plagioclase + spinel.

Dark green or greenish-brown hornblende is present in some rocks, but is much less abundant than in calc-silicate rocks of the Lambert Series. K-feldspar and orthopyroxene occur locally and minor opaque minerals and apatite may be present.

Fitzsimons & Thost (1992) identified two types of calc-silicate body in the NPCM: complex bodies of interlayered marble and calc-silicate rock (e.g., at Amery Peaks, Corry Massif and Mount Wishart) and more homogeneous, but mineralogically zoned, calc-silicate boudins. The complex bodies are commonly between three and 10 metres across. They consist of interlayered forsterite ± diopside marble and calc-silicate that comprise various combinations of clinopyroxene, meionite-rich scapolite, wollastonite, calcite, plagioclase, quartz, biotite, or phlogopite, and minor titanite and apatite. Individual layers are typically one to 15 centimetres thick and have well-defined boundaries. Those near marble units are dominated by wollastonite–diopside–scapolite–calcite and scapolite–quartz, whereas more distant layers are dominated by plagioclase and quartz. Zoned calc-silicate boudins are mostly less than two metres across and have cores characterised by diopside, wollastonite, scapolite and rare grossularite, and rims dominated by diopside, quartz and plagioclase.

The original granoblastic polygonal texture in scapolite–wollastonite assemblages in both types of calc-silicate body is overprinted by a variety of reaction textures. These include grossularite rims between scapolite and calcite (Figs 184A, 187A), grossularite–quartz rims between scapolite or plagioclase and wollastonite (Fig. 187B), calcite–quartz intergrowths in wollastonite (Fig. 187C), and calcite–plagioclase symplectites in scapolite (Fig. 187D). Such reaction textures are interpreted to have formed during a period of near-isobaric cooling (Fitzsimons & Harley 1992; Fitzsimons & Thost 1992; Thost & Hensen 1992; Hand et al. 1994a). Epidote group minerals and tremolite-bearing veins post-date these textures. Pegmatites containing abundant calc-silicate minerals form discordant veins at Mounts Gavaghan and Tarr and Corry Massif.

Calc-silicate rocks which crop out at Ely Nunatak, Mount Johns and Shaw Massif in the SPCM (Lambert Series) typically have the assemblage quartz + diopside ± biotite (or phlogopite) ± hornblende ± plagioclase ± scapolite. K-feldspar, carbonate and epidote may also be present, and titanite, opaque minerals and apatite are accessory phases. Hornblende is commonly dark green, but in some rocks is partly of retrograde origin. Plagioclase is mostly of calcic composition (labradorite or bytownite).

Calc-silicate gneiss, with subordinate marble, is relatively abundant in the central and northern Mawson Escarpment. Throughout the area the following occur:

quartz + hornblende + diopside + plagioclase + carbonate + titanite,
 quartz + hornblende + diopside + plagioclase + K-feldspar + scapolite + carbonate + titanite,
 quartz + garnet + diopside + plagioclase + titanite,
 hornblende + diopside + scapolite ± carbonate ± titanite,
 garnet + hornblende + scapolite + carbonate, and
 garnet + diopside + plagioclase + scapolite + carbonate + titanite, but
 biotite + hornblende + diopside + plagioclase + clinozoisite + carbonate

is confined to the central Mawson Escarpment. Retrograde calc-silicate rocks in parts of the northern Escarpment contain much secondary chlorite, amphibole, muscovite and carbonate replacing diopside, garnet and plagioclase. Marble layers crop out at a number of places and contain up to about 20 percent of forsterite (partly replaced by serpentine), diopside, biotite or phlogopite, garnet, hornblende, or scapolite. One marble layer contains small, well-crystallised flakes of graphite, and titanite crystals up to one centimetre across.

MESOPROTEROZOIC FELSIC ORTHOGNEISS

Mesoproterozoic felsic orthogneiss crops out in the northern part of the SPCM (Bosse and Ely Nunataks, Clemence and Shaw Massifs, the northern Mawson Escarpment, and Mounts Isabelle and Johns), as well as throughout the NPCM and eastern side of the Amery Ice Shelf. Biotite+orthopyroxene-bearing orthogneiss comprises most of the Porthos (and Reinbolt) Series, whereas biotite±hornblende-bearing orthogneiss forms a significant component of the Astronomov Series. Orthogneiss in the SPCM (Lambert Series) is almost entirely of amphibolite facies (biotite-bearing)—although transitional granulite-facies conditions were reached at Mount Isabelle; most of that in the NPCM is of granulite facies. Garnet occurs in some granitic orthogneiss, but much garnet-bearing felsic gneiss is probably of sedimentary origin, as noted above.

Rb–Sr isochron ages of various precisions range from 769 ± 36 to 1042 ± 347 Ma, with most between about 870 and 970 Ma (Table 24). However, zircon U–Pb ion-microprobe ages of 990–940 Ma on syn- to late-metamorphic felsic intrusive rocks (Table 22; Kinny et al. 1997) show that most of the Rb–Sr ages are underestimates, and presumably reflect partial or complete resetting during later metamorphic event(s). Only one T_{DM}^{Nd} model age is available (1770 Ma for orthopyroxene-bearing granitic orthogneiss from Mount Gardner: S-S Sun, unpublished data), suggesting a Mesoproterozoic, rather than Palaeoproterozoic emplacement age. In support of this, T_{DM}^{Nd} model ages of 1520 and 1700 Ma (ion-microprobe zircon ages) felsic orthogneisses in the Bunge Hills are 2150 and 2340 Ma, respectively (Sheraton et al. 1990)—some 650 Ma older than their emplacement ages.

Felsic orthogneiss in the NPCM (Porthos Series) is typified by the occurrence of orthopyroxene, indicating metamorphism under granulite-facies conditions. *Biotite–orthopyroxene–quartz–feldspar gneiss* is widespread, particularly in the Aramis and Porthos

Ranges, as well as on the eastern side of the Amery Ice Shelf (e.g., in the McKaskle and Reinbolt Hills). It tends to be relatively homogeneous and contains layers and boudins of mafic and ultramafic granulite, but locally occurs interlayered with garnet-bearing gneiss and metapelite. It is generally fine to medium grained, and the fabric ranges from massive to strongly foliated or lineated—the foliation being defined by lenticular quartz aggregates, elongated aggregates of orthopyroxene grains, and a preferred orientation of mafic minerals. Reddish-brown biotite (typically up to 4%), orthopyroxene (commonly 1–8%), quartz (20–35%), orthoclase perthite (up to 50%), and plagioclase (commonly andesine antiperthite: 20–65%) are major components, with accessory opaque minerals (including ilmenite and magnetite), apatite and zircon. Small amounts of hornblende and clinopyroxene are present locally and fayalite occurs in gneiss at Corry Massif. Titanite and allanite are generally absent. Biotite occurs as aligned grains and randomly oriented secondary grains around orthopyroxene or hornblende. Orthopyroxene is commonly partly replaced by a yellowish-brown iddingsite-like material. Quartz occurs both as large recrystallised xenoblastic grains and small rounded grains in feldspar. Plagioclase and perthite commonly show deformed twin lamellae. Most orthopyroxene-bearing gneisses have compositions consistent with metamorphism of felsic igneous rocks ranging from tonalite to granite (s.s.).

A relatively homogeneous variety of the *biotite–garnet–quartz–feldspar gneiss* is also quite common, and probably mostly of intrusive igneous origin. It is generally leucocratic (garnet leucogneiss) and of similar granitic (s.s.) composition to the clearly intrusive late-metamorphic garnet granitoids described in a later section, although it locally contains schlieren or xenoliths of metapelite rocks (Hand et al. 1994a). That near Radok Lake is medium to coarse grained, with abundant perthite and quartz, minor plagioclase, and less than five percent garnet. Myrmekite is common. The texture ranges from pegmatitic to strongly foliated and recrystallised, suggesting that it represents a pre- or syntectonic pegmatite (McKelvey & Stephenson 1990). Large prismatic feldspar grains (megacrysts or phenocrysts) are locally abundant. Small subconcordant to discordant bodies of leucocratic garnet–biotite granite gneiss crop out at Pickering Nunatak, Fox Ridge and Thomson Massif. At the last locality the gneiss contains only minor plagioclase, but the feldspar approaches mesoperthite in composition, suggesting relatively dry, high-temperature conditions.

A distinctive group of felsic *biotite and biotite–hornblende-bearing gneisses* that crops out on Taylor Platform, southern McLeod Massif, and northern Mount Lanyon, and outcrops to the north and west of the latter, was assigned to the Astronomov Series (Fig. 150). Other constituents of this unit are garnet and biotite–garnet gneiss, minor metapelite, granite gneiss and mafic schist. Orthopyroxene-bearing rocks are uncommon. These somewhat lower grade gneisses have not been studied in detail and their relationships with the other rock units in the NPCM are presently unknown. They may have been derived from a distinct suite of sedimentary–volcanic protoliths (Mikhailov & Sergeyev

1997) or a currently unrecognised plutonic suite. Alternatively, they may represent highly retrogressed equivalents of Athos and Porthos Series rocks, or a regional variation in metamorphic grade, as suggested by Tingey (1972).

Felsic orthogneiss in the Lambert Series of the SPCM is virtually all of amphibolite facies (mostly *biotite-quartz-feldspar gneiss*). It differs from Archaean orthogneiss of the Ruker Terrane because it is generally more strongly layered and contains significant amounts of garnet, but only rare hornblende, allanite and titanite. Hornblende is confined to some garnet-free gneiss, as at Clemence Massif and Mount Johns. Hornblende-orthopyroxene-biotite-orthoclase-quartz-plagioclase gneiss crops out at Mount Izabelle. Massive biotite granitic orthogneisses at Dalton Hills and Barkell Platform, both on the northern Mawson Escarpment, are probably deformed intrusive bodies. Many smaller conformable leucocratic layers are probably also deformed granitoids, but there appears to be few large plutons like those in the NPCM or Ruker Terrane granitic basement.

Chemical data (Table 15, Figs 101, 102) for biotite-orthopyroxene-quartz-feldspar gneisses from the NPCM-Amery Ice Shelf area are consistent with a felsic igneous origin, with most rocks being metaluminous or only slightly peraluminous (i.e., I-type, with $ASI < 1.1$). Composition ranges from tonalite, through granodiorite, to granite. Although there are relatively few analyses, biotite-quartz-feldspar gneisses from the Lambert Series appear to be mainly granite (s.s.). Orthogneiss from Mount Izabelle has a granodioritic composition. It is generally unclear whether these gneisses represent metamorphosed intrusive or extrusive rocks. More massive orthogneiss may well be intrusive, whereas at least some of that interlayered with metasedimentary rocks could be of volcanic origin.

Many orthopyroxene-bearing gneisses (mostly tonalitic or granodioritic) belong to the Y (and HREE) depleted suite of Sheraton & Black (1983) (Fig. 103). These tend to have high Sr, and spidergrams show little or no Sr depletion; many even have significant positive Sr anomalies (Figs 104, 105). REE patterns are mostly

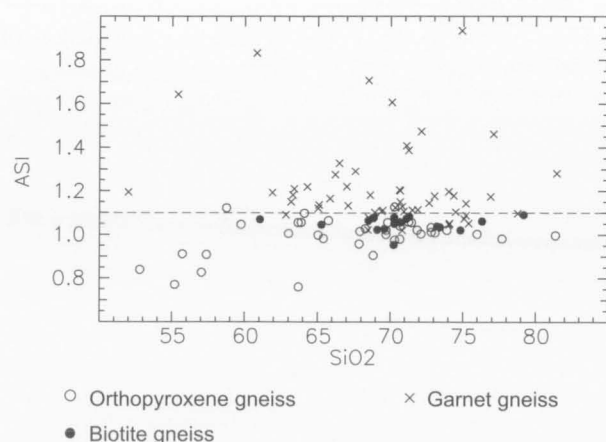


FIGURE 101

Plot of ASI against SiO_2 for Mesoproterozoic felsic gneisses of the Beaver-Lambert Terrane.

strongly fractionated ($(La/Yb)_n$ 6.2–118, $(Ce/Y)_n$ mostly 4–30), and major Eu anomalies are lacking (Fig. 106). Similar gneisses from other granulite terranes, such as the Napier Complex of Enderby Land, commonly have positive Eu anomalies (Sheraton et al. 1985). Such *Y-depleted, Sr-undepleted gneisses* are thought to represent new (i.e., primary) continental crust derived by partial melting of a hornblende±garnet-bearing, but feldspar-poor, mafic source (such as subducted hydrated oceanic crust or a mafic underplate; Tarney et al. 1987).

In contrast, some orthopyroxene-bearing gneisses (predominantly of granitic (s.s.) composition), as well as most orthopyroxene-free biotite gneisses, are not depleted in Y (or presumably HREE) (Fig. 103). They tend to have low Sr and less fractionated REE patterns ($(Ce/Y)_n$ mostly 3–8); spidergrams, particularly for the more fractionated siliceous granites, have moderate to large negative Sr anomalies (Figs 104, 105), consistent with residual

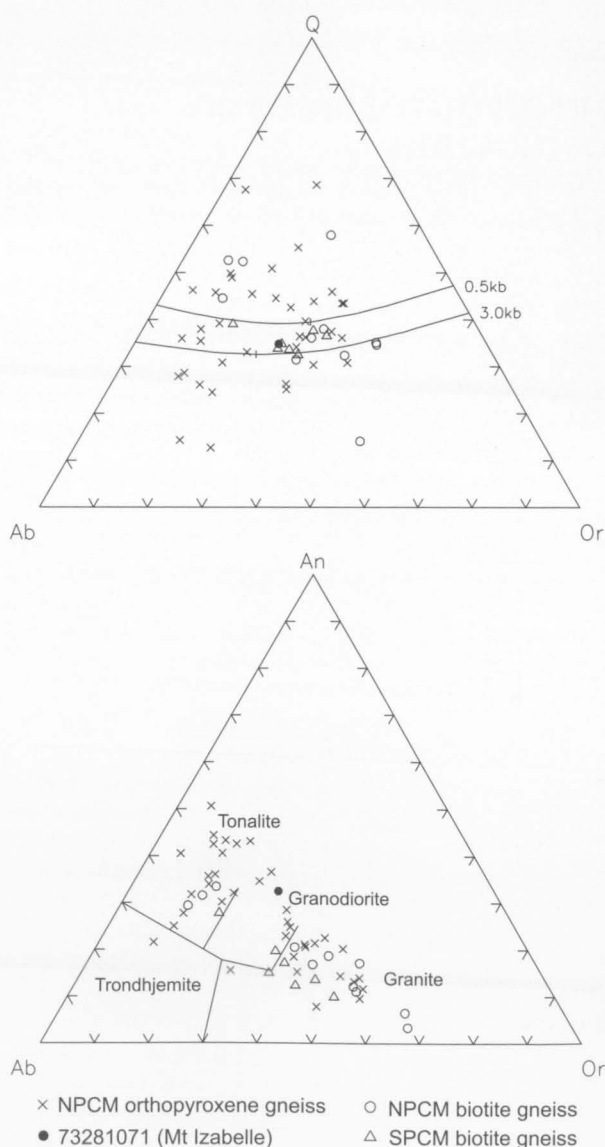


FIGURE 102

Normative Q-Ab-Or and Ab-Or-An diagrams for Mesoproterozoic orthopyroxene and biotite-bearing felsic gneisses.

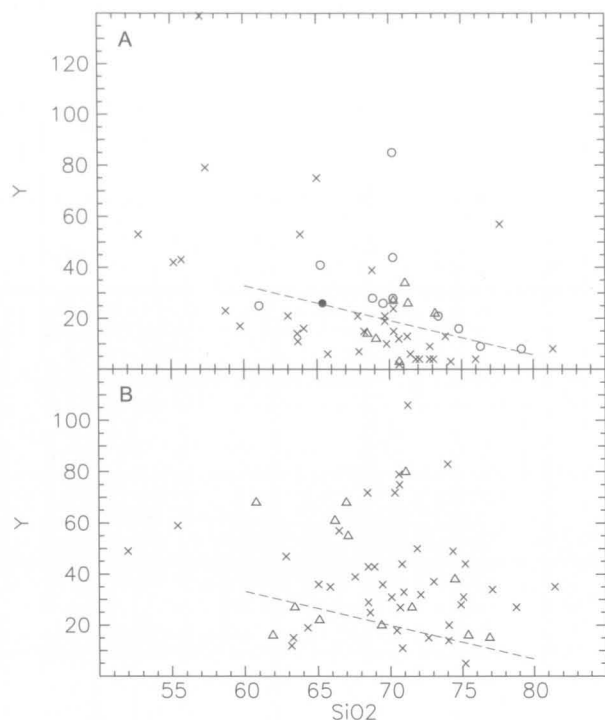


FIGURE 103

Y-SiO₂ plots for (A) orthopyroxene and biotite-bearing and (B) garnet-bearing Mesoproterozoic felsic gneisses. A dashed line indicates the approximate boundary between Y-depleted and Y-undepleted felsic orthogneisses (Sheraton & Black 1983). Symbols as in Figures 102 and 107.

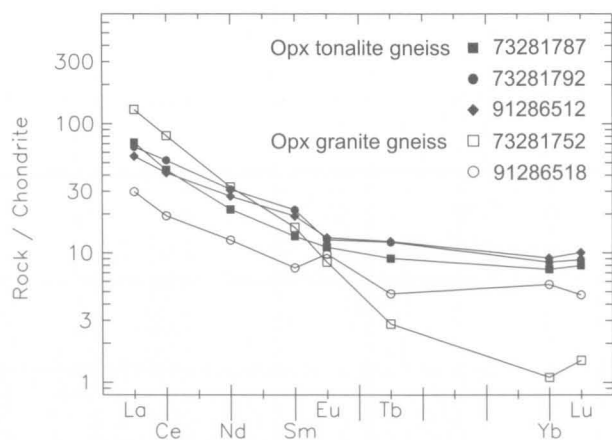


FIGURE 106

Chondrite-normalised rare-earth element abundance plots for Mesoproterozoic orthopyroxene-bearing felsic gneisses. Most belong to the Y-depleted suite of Sheraton & Black (1983), only sample 91286518 being Y-undepleted.

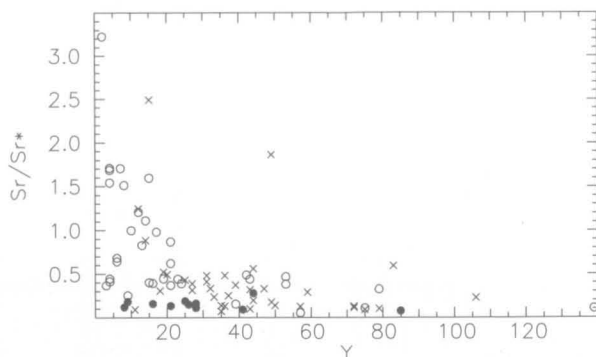


FIGURE 104

Plot of Y against Sr/Sr* for Mesoproterozoic felsic gneisses. Symbols as in Figure 101.

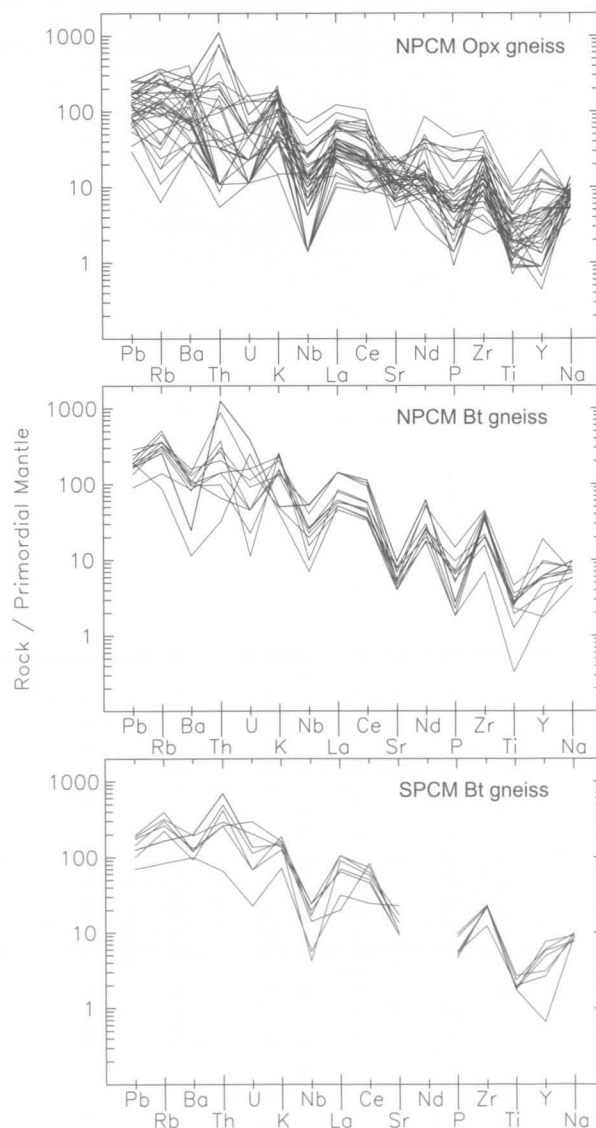


FIGURE 105

Spidergrams for Mesoproterozoic orthopyroxene and biotite-bearing felsic gneisses.

TABLE 15. Chemical analyses and CIPW norms of representative felsic gneisses from the Beaver-Lambert Terrane. Rock classification based on Barker (1979) and the Y-depleted and undepleted orthogneiss grouping of Sheraton & Black (1983).

Sample no.	73281071	70280091	73281752	73281792	73281557	70280493	91286412	73281142	70280265	73281768	91286516
Locality	Izabelle	Mount Bewsher	N Mount Gardner	Mount Wishart	N Mawson Escarpment	Moore Pyramid	Mount Meredith	Shaw Massif	Mount Albion	NW Mount Bechervaise	Mount McCarthy
Lithology	Hb-Opx-Bt-Kf-Qz-Pl gneiss	Opx-Bt-Kf-Qz-Pl gneiss	Opx-Qz-Kf-Pl gneiss	Opx-Kf-Qz-Pl gneiss	Bt-Qz-Kf-Pl gneiss	Bt-Chl-Pl-Qz-Kf gneiss	Bt-Qz-Kf-Pl gneiss	Gt-Bt-Qz-Kf-Pl gneiss	Bt-Gt-Opx-Qz-Pl-Kf gneiss	Bt-Gt-Kf-Pl-Qz gneiss	Gt-Qz-Opx-Pl-Kf gneiss
Classif.	Undepleted granodiorite	Depleted tonalite	Depleted granodiorite	Undepleted tonalite	Depleted granodiorite	Undepleted granite	Undepleted tonalite	Undepleted granodiorite	Undepleted granite	Qz-rich paragneiss	Kf-rich paragneiss
SiO ₂	65.40	67.91	72.80	69.70	68.50	74.83	70.27	69.40	68.46	77.10	62.83
TiO ₂	0.61	0.39	0.20	0.39	0.57	0.41	0.53	0.46	0.63	0.73	0.59
Al ₂ O ₃	15.72	17.32	14.28	13.01	14.70	12.43	13.86	14.92	14.21	10.20	13.03
Fe ₂ O ₃	1.44	0.42	0.68	0.58	0.87	0.21	2.07	0.52	0.99	0.90	1.97
FeO	3.75	1.59	0.95	4.90	3.40	0.82	2.19	2.60	4.17	3.75	5.78
MnO	0.10	0.02	0.03	0.49	0.04	0.02	0.06	0.06	0.07	0.12	0.20
MgO	1.55	0.90	0.61	1.92	1.10	0.26	0.98	1.20	0.47	1.39	5.27
CaO	4.45	3.78	2.09	3.85	2.71	0.64	3.64	2.51	2.91	1.53	1.02
Na ₂ O	3.00	5.37	3.40	3.10	3.40	2.27	3.09	3.65	2.92	1.70	1.54
K ₂ O	2.98	1.48	4.30	1.13	3.49	7.07	1.36	2.92	4.15	1.54	7.06
P ₂ O ₅	0.11	0.11	0.10	0.14	0.21	0.16	0.14	0.11	0.29	0.11	0.04
H ₂ O ⁺	0.36	-	0.36	0.46	0.58	-	-	0.64	-	0.28	-
LOI	-	0.61	-	-	-	0.70	0.93	-	0.52	-	0.63
Rest	0.23	0.16	0.24	0.16	0.19	0.23	0.19	0.19	0.35	0.20	0.27
Total	99.70	100.06	100.04	99.83	99.76	100.05	99.31	99.18	100.14	99.55	100.23
O=F,S,Cl	0.00	0.00	0.00	0.00	0.00	0.00	0.00	0.00	0.01	0.00	0.00
Total	99.70	100.06	100.04	99.83	99.76	100.05	99.31	99.18	100.13	99.55	100.23
Q	22.95	20.99	31.05	32.63	26.39	32.95	37.52	28.46	26.78	53.93	13.11
C	-	0.27	0.47	0.02	0.90	0.26	1.02	1.45	0.32	3.22	1.10
Or	17.61	8.75	25.41	6.68	20.62	41.78	8.04	17.26	24.52	9.10	41.72
Ab	25.39	45.44	28.77	26.23	28.77	19.21	26.15	30.89	24.71	14.38	13.03
An	20.63	18.03	9.72	18.19	12.07	2.13	17.14	11.73	12.54	6.87	4.80
Di	0.61	-	-	-	-	-	-	-	-	-	-
Hy	8.42	4.21	2.43	13.55	7.39	1.34	3.99	6.68	7.10	8.61	21.51
Mt	2.09	0.61	0.99	0.84	1.26	0.30	3.00	0.75	1.44	1.30	2.86
Il	1.16	0.74	0.38	0.74	1.08	0.78	1.01	0.87	1.20	1.39	1.12
Ap	0.26	0.26	0.24	0.33	0.50	0.38	0.33	0.26	0.69	0.26	0.09
Li	-	19	-	-	-	9	17	-	29	-	11
Be	-	6	-	-	-	2	4	-	3	-	6
S	-	30	-	-	-	10	100	-	160	-	50
Sc	-	6	3	18	-	1	15	-	12	-	19
V	62	37	19	52	32	3	51	43	15	79	3
Cr	45	11	9	90	18	<1	15	41	14	117	2
Ni	8	7	4	39	9	1	12	16	6	41	13
Cu	<2	2	5	32	11	1	13	<2	16	6	4
Zn	91	38	17	74	54	24	49	62	84	59	161
Rb	96	68	113	36	141	287	88	119	146	92	244
Sr	334	480	250	184	193	84	162	244	159	144	80
Y	26	7	4	19	14	16	44	20	72	34	47
Zr	171	170	120	85	253	467	219	179	471	273	366
Nb	6	7	1	5	14	11	14	12	26	10	7
Sn	-	<2	-	-	-	<2	5	-	<2	-	4
Ba	959	282	1329	548	642	780	590	713	1303	569	1157
La	22	16	42	22	49	32	36	26	78	39	17
Ce	49	30	70	45	91	60	65	54	150	74	26
Nd	-	14	21	20	-	24	27	-	66	-	12
Pb	18	27	35	23	20	37	18	24	44	23	23
Th	6	<2	21	4	38	6	13	17	40	29	5
U	1.0	<0.5	1.2	1.2	1.5	1.0	3.5	1.5	1.0	3.0	1.5
K/Rb	258	181	316	261	205	204	128	204	236	139	240
(Ce/Y) _n	4.7	10.7	43.7	6.0	16.3	9.4	3.7	6.8	5.2	5.4	1.4
Th/U	6.0	-	17	3.1	25	6.0	3.7	11	40	9.7	3.3
Nb/Nb*	0.12	0.26	0.01	0.20	0.20	0.10	0.39	0.24	0.28	0.25	0.07
Sr/Sr*	-	1.71	0.44	0.45	-	0.16	0.28	-	0.12	-	0.33
mg	42.4	50.2	53.4	41.1	36.6	36.1	44.4	45.1	16.7	39.8	61.9

mg = atomic 100Mg/(Mg + Fe²⁺).

plagioclase and/or plagioclase fractionation. Such *Sr-depleted, Y-undepleted gneisses* are considered to represent partial melts of predominantly felsic crustal rocks with little or no residual garnet. Many gneisses from the eastern Amery Ice Shelf area belong to this suite, although some relatively SiO_2 -poor (quartz dioritic) rocks may represent fractionated mantle-derived magmas.

Biotite–garnet–quartz–feldspar gneisses differ in being markedly peraluminous (ASI mostly 1.05–1.8; Fig. 101) and having generally higher K_2O , Rb, Th, U, Zr, Nb, Y, LREE, Cr and Ni, and slightly lower CaO, Na_2O and Sr (Table 15). Many of the more strongly peraluminous garnet-bearing gneisses have very high normative Q or, less commonly, Or, indicating direct metamorphism of sedimentary protoliths. They belong to the paragneiss group described in the previous section. However, many garnet leucogneisses have near-minimum melt (i.e., granitic, s.s.) compositions (Fig. 107), consistent with (but not necessarily proving) an intrusive igneous origin. In contrast to most orthopyroxene-bearing felsic orthogneisses, these are of S-type (derived by melting of

sedimentary source rocks: Chappell & White 1974). Most analysed garnet gneisses (both orthogneisses and paragneisses) have relatively high Y (Figs 103, 104) but low Sr and moderately fractionated $(\text{Ce}/\text{Y})_n$ (mostly 2–10), typical of felsic igneous rocks formed by intracrustal melting and of clastic sedimentary rocks derived therefrom (Tarney et al. 1987). Spidergrams show marked negative Nb, Sr, P and Ti anomalies (Fig. 108).

Unlike many other granulite terranes that appear to have undergone depletion in LILE (K, Rb), Th and U during metamorphism (Tarney et al. 1972), K/Rb ratios are not particularly high (mostly 100–350), implying little loss of Rb relative to K (Sheraton & Black 1983). This may partly reflect the comparative rarity in the PCM of biotite or K-feldspar-free rocks (e.g., anhydrous tonalitic gneisses), which are the most susceptible to metamorphic depletion because they do not contain a phase capable of retaining much Rb (Tarney & Windley 1977). On the other hand, Th/U ratios are much higher (up to about 100) than the estimated crustal average (~3.8; Taylor & McLennan 1985). This is consistent with metamorphic depletion of U, relative to Th, possibly during dehydration.

As a group, the Mesoproterozoic felsic gneisses of the Beaver-Lambert Terrane tend to be less siliceous than Archaean Ruker Terrane orthogneisses to the south, and have generally higher CaO and MgO. Consequently, they show a more An-rich trend on an Ab–Or–An diagram (cf. Figs 13 & 102). Moreover, the garnet-bearing gneisses are slightly to strongly peraluminous, and commonly have high normative Q. None of these features is consistent with direct re-metamorphism of Archaean rocks (Sheraton & Black 1983).

MESOPROTEROZOIC MAFIC TO ULTRAMAFIC ROCKS

Amphibolite

Concordant amphibolite bodies are commonly interlayered with felsic gneiss and metasediments in much of the Lambert Series in the SPCM (e.g., Mounts Johns and Izabelle, Shaw Massif, and the northern Mawson Escarpment). Compared to many of those in late Archaean to Palaeoproterozoic metamorphics of the Ruker Terrane, they tend to be of relatively high grade, with dark greenish-brown hornblende and granoblastic polygonal textures. Relict gabbroic textures are locally preserved, as at Shaw Massif. Apart from hornblende and plagioclase (commonly andesine–labradorite), lesser amounts of quartz, biotite, titanite, opaque minerals and apatite are commonly present. Clinopyroxene amphibolite occurs at Shaw Massif and the northern Mawson Escarpment.

Amphibolite gneiss (biotite–quartz–plagioclase–hornblende \pm orthopyroxene \pm K-feldspar) is interlayered with metasedimentary gneiss at a few places in the NPCM (Fitzsimons & Thost 1992). It has a well-developed layering defined by hornblende-rich and hornblende-poor layers. Biotite and opaque minerals commonly occur around hornblende grains that are aligned parallel to the layering.

Like the amphibolite bodies in the Ruker Terrane, many of those in the Beaver-Lambert Terrane may be deformed

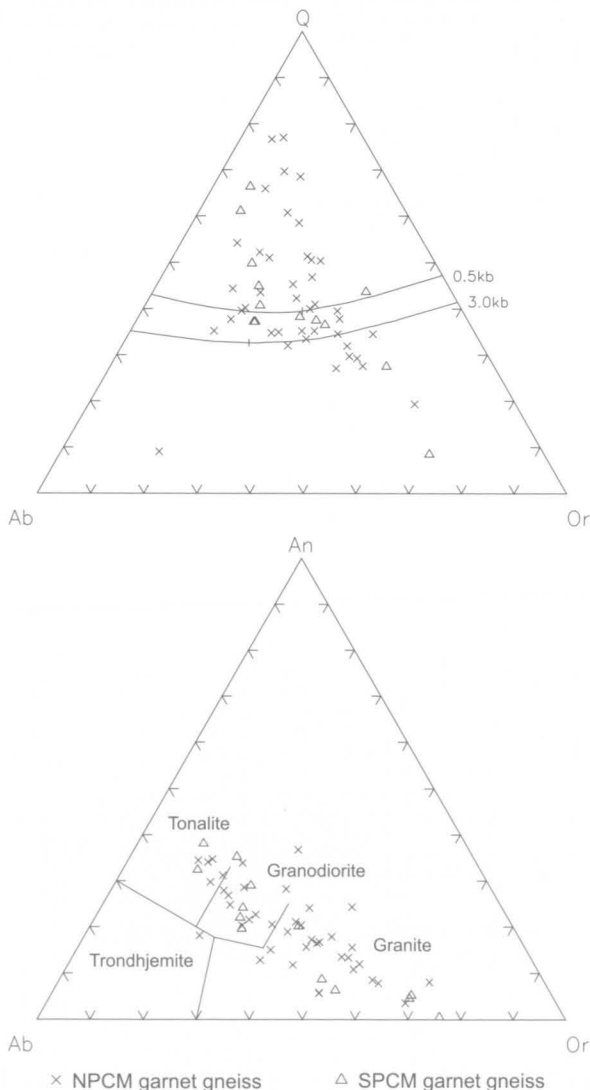


FIGURE 107

Normative Q–Ab–Or and Ab–Or–An diagrams for Mesoproterozoic garnet-bearing felsic gneisses.

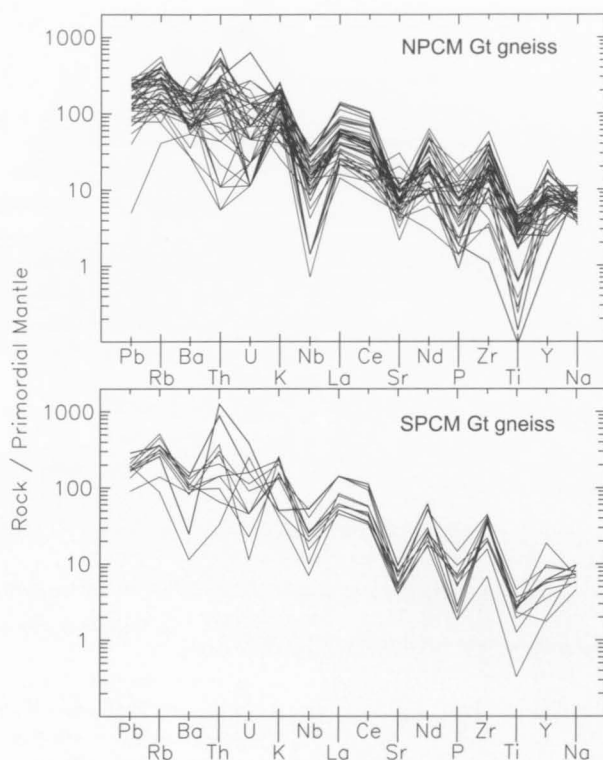


FIGURE 108
Spidergrams for Mesoproterozoic garnet-bearing felsic gneisses.

and metamorphosed tholeiitic dolerite dykes or small gabbro plutons, but discordant contacts are rare. Chemical data (Table 16; Figs 109–111) are mostly consistent with this possibility, although there are wide variations in LILE contents. For example, some biotite-rich amphibolites appear to have been enriched in LILE during metamorphism (Sheraton 1984). However, for most samples, ratios of less mobile elements (Ce/Zr, P/Zr, Nb/Zr, Ti/Zr, Y/Zr and Ce/Y) are broadly similar to those of the Ruker Terrane metadolerite dykes. Although this implies derivation from a broadly similar mantle source region, the data show considerable scatter and do not necessarily indicate a co-eval origin. A diopside-bearing amphibolite from Shaw Massif (73281303) has high normative Di and An and very low TiO_2 , Na_2O , P_2O_5 , Cu, Rb, Y, Zr, Nb, La and Ce. These features suggest a calcareous sedimentary origin.

Mafic granulite

Mafic granulite occurs throughout much of the NPCM and in the northern Mawson Escarpment in the SPCM. It commonly forms pods, boudins and discontinuous layers within felsic gneiss—the boudins probably representing originally continuous mafic layers. Some layers are tens of metres thick, and larger bodies were mapped in a few localities. In some places the mafic granulite preserves early structures (e.g., S_1 foliation, L_1 lineation, and F_2 folds) not seen in the host gneiss (Fitzsimons & Thost 1992). S_1 , which is truncated by the foliation (S_3) in the host gneiss, is defined by partial segregation of plagioclase from mafic minerals, alternation of

hornblende-rich and pyroxene-rich layers, and a preferred orientation of hornblende. An early orthopyroxene–clinopyroxene assemblage in mafic granulite at Else Platform is overprinted by a foliation defined by hornblende, plagioclase, ilmenite and magnetite (Hand et al. 1994a). Leucosomes within the granulite contain plagioclase + orthopyroxene \pm clinopyroxene \pm hornblende \pm quartz.

Typical mafic granulite is medium grained (1–4 mm) with a granoblastic polygonal texture. It contains clinopyroxene (commonly 10–25%), orthopyroxene (5–20%), andesine–labradorite (40–60%), biotite (mostly less than 2%), and minor opaque minerals (including ilmenite) and apatite. Brown hornblende is a common additional phase, particularly on the northern Mawson Escarpment where some rocks contain up to 50 percent. Quartz (up to 10%) may also be present, but generally not in association with primary hornblende. Biotite is commonly of late crystallisation and may define a foliation. Retrograde biotite and pale green amphibole may rim pyroxene grains. Garnet coronas separate pyroxene from plagioclase in some rocks (Fig. 184C, D), and there are very fine-grained overgrowths of pyroxene + plagioclase on the secondary hornblende rims of pyroxene in a granulite near Radok Lake (McKelvey & Stephenson 1990). Mafic granulite from Mount McCarthy contains orthopyroxene (mg 55–57), clinopyroxene (mg 68), zoned plagioclase (An_{53-66}), and secondary garnet (mg 29–33; Thost and Hensen 1992).

Some mafic granulite is rich in orthopyroxene, with little or no clinopyroxene, as at Crohn Massif, Mount Kirkby and the Radok Lake area. At the last locality, metanorite lenses in garnet–biotite gneiss consist of orthopyroxene (>50%), plagioclase (~20%), clinopyroxene (0–30%), and minor phlogopite, pale green hornblende, quartz, and retrograde colourless amphibole and talc (McKelvey & Stephenson 1990). The least deformed parts contain coarse-grained (5–10 cm) poikilitic orthopyroxene crystals enclosing the other phases, as well as coarse intergrowths of orthopyroxene, clinopyroxene and plagioclase.

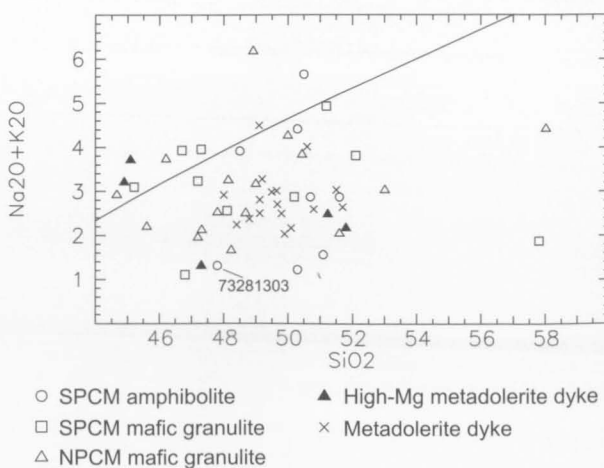


FIGURE 109
Alkalies– SiO_2 plot for concordant amphibolite and mafic granulite bodies of the Beaver-Lambert Terrane, compared with metadolerite dykes of the Ruker Terrane. Sample 73281303 is probably of calcareous sedimentary origin (calc-silicate granulite).

TABLE 16. Chemical analyses and CIPW norms of representative amphibolites and mafic granulites from the Beaver-Lambert Terrane.

Sample no.	73281303	73281264	73281867	73281667	73282141	73281763	73281875	91286436
Locality	Shaw	Mount	N Mawson	N Mawson	N Mawson	SE Crohn	Mount	White
Lithology	Massif Cpx amphibolite	McCauley Bt amphibolite	Escarpment Cpx amphibolite	Escarpment Cpx-Opx-Hb- Pl granulite	Escarpment Hb-Bt-Opx- Pl granulite	Massif Hb-Cpx-Opx- Pl granulite	Gardner Hb-Cpx-Opx- Pl granulite	Massif Cpx-Opx-Pl- Hb granulite
SiO ₂	47.80	48.50	50.70	47.20	51.20	51.60	47.80	44.66
TiO ₂	0.23	1.81	0.93	2.09	1.66	0.26	0.55	1.15
Al ₂ O ₃	15.49	13.68	13.57	14.35	16.62	8.77	16.27	13.45
Fe ₂ O ₃	2.21	3.01	3.55	3.02	2.79	3.16	5.59	2.71
FeO	6.95	12.10	10.60	12.40	10.50	10.50	6.40	12.87
MnO	0.18	0.22	0.24	0.23	0.16	0.29	0.20	0.21
MgO	10.44	5.45	6.92	7.13	3.71	12.72	8.40	8.40
CaO	14.72	9.48	10.35	9.39	5.94	9.11	11.13	11.76
Na ₂ O	0.96	2.40	2.30	2.55	3.05	1.70	2.25	2.41
K ₂ O	0.35	1.51	0.57	0.68	1.88	0.34	0.27	0.51
P ₂ O ₅	0.03	0.21	0.09	0.19	0.40	0.15	0.17	0.08
H ₂ O ⁺	0.92	1.05	0.66	0.58	1.20	0.52	0.22	-
LOI	-	-	-	-	-	-	-	1.48
Rest	0.08	0.20	0.14	0.19	0.21	0.27	0.16	0.20
Total	100.36	99.62	100.62	100.00	99.32	99.39	99.41	99.89
Q	-	-	0.03	-	1.98	-	-	-
Or	2.07	8.92	3.37	4.02	11.11	2.01	1.60	3.01
Ab	8.12	20.31	19.46	21.58	25.81	14.38	19.04	12.65
An	36.92	22.09	25.02	25.70	26.11	15.29	33.50	24.38
Ne	-	-	-	-	-	-	-	4.20
Di	29.05	19.70	21.35	16.27	0.63	23.54	16.89	27.64
Hy	9.54	12.85	25.14	10.59	24.97	39.03	10.03	-
Ol	10.91	6.93	-	12.94	-	0.12	13.41	20.25
Mt	2.16	3.58	3.33	3.65	3.14	3.22	2.76	3.70
Il	0.44	3.44	1.77	3.97	3.15	0.49	1.04	2.18
Ap	0.07	0.50	0.21	0.45	0.95	0.36	0.40	0.19
S	-	-	-	-	-	-	-	100
Sc	-	-	-	-	-	-	-	61
V	204	322	264	368	205	246	286	734
Cr	79	147	233	230	132	968	33	18
Ni	81	78	114	125	63	182	68	106
Cu	<2	283	96	134	79	49	50	32
Zn	82	143	81	137	209	113	86	116
Ga	12	18	18	24	24	11	14	16
Rb	4	69	7	3	92	2	4	4
Sr	105	114	61	152	237	167	338	130
Y	6	32	22	32	18	8	17	25
Zr	4	70	55	104	249	25	17	31
Nb	<1	5	3	8	18	2	1	4
Ba	40	198	30	37	174	143	311	46
La	<2	4	7	5	31	15	6	<2
Ce	5	15	18	27	64	36	20	5
Nd	-	-	-	-	-	-	-	7
Pb	5	9	1	5	17	6	9	3
Th	<1	<1	1	<1	1	<1	1	<2
U	<0.5	1.0	2.5	<0.5	1.5	<0.5	0.5	0.5
K/Rb	726	182	676	1880	170	1410	560	1060
(Ce/Y) _n	2.1	1.2	2.1	2.1	8.9	11	2.9	0.5
Ba/Zr	10.0	2.83	0.55	0.36	0.70	5.72	18.3	1.48
Ce/Zr	1.25	0.21	0.33	0.26	0.26	1.44	1.18	0.16
Nb/Zr	-	0.07	0.05	0.08	0.07	0.08	0.06	0.13
Nb/Nb*	-	0.23	0.28	0.71	0.45	0.17	0.15	-
mg*	71.0	43.6	51.3	49.7	37.4	66.7	60.6	53.5

mg* = atomic 100Mg/(Mg + 0.85Fe(total)).

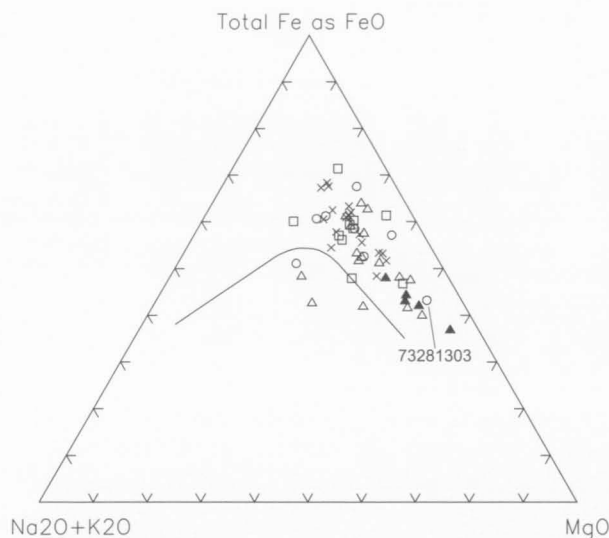


FIGURE 110
AFM diagram for amphibolites and mafic granulites of the Beaver-Lambert Terrane, compared with metadolerite dykes of the Ruker Terrane. Symbols as in Figure 109.

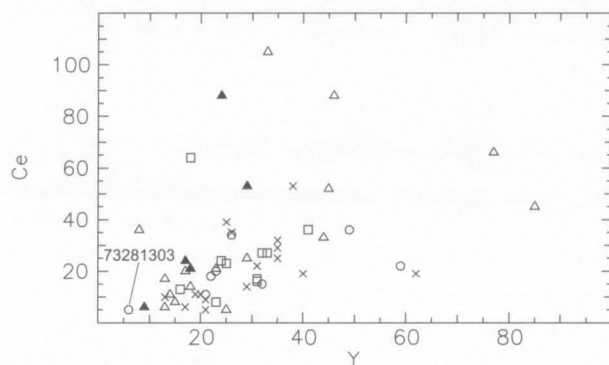


FIGURE 111
Ce-Y plot for amphibolites and mafic granulites of the Beaver-Lambert Terrane, compared with metadolerite dykes of the Ruker Terrane. Symbols as in Figure 109.

The general instability of hornblende + quartz is well seen in mafic granulite of the northern Mawson Escarpment and is consistent with the prograde reaction: hornblende + quartz \rightarrow plagioclase + clinopyroxene + orthopyroxene.

Thus, hornblende reacts with quartz until one or the other is consumed, so that some granulite has a compositional layering defined by alternating pyroxene + plagioclase + quartz and hornblende + pyroxene + plagioclase assemblages. Irregular veins of relatively coarse-grained hornblende-free granulite within hornblende-rich granulite may reflect original quartz veins that have reacted away during prograde metamorphism. Some granulite contains large (up to 1 cm) poikiloblastic pyroxene grains or intergrowths of orthopyroxene \pm plagioclase, which suggest a prograde reaction like that above. The assemblage biotite + hornblende + orthopyroxene + andesine (\pm minor cummingtonite and garnet) also occurs in mafic rocks at the central Mawson

Escarpment (near Harbour Headland), but no two-pyroxene granulite has been found there.

Chemical data are consistent with the observation that hornblende is only stable in quartz-free granulite. Hornblende-rich (25–50%) granulites are SiO_2 -undersaturated (i.e., strongly Ol-normative), whereas those with little or no hornblende (<6%) are Q-normative or only slightly Ol-normative (Fig. 112). The relatively high K_2O contents of the hornblende-rich granulites may either be a primary feature or reflect the higher distribution coefficient for K in hornblende compared to pyroxene or plagioclase.

Most of the analysed mafic granulites are of tholeiitic composition, but there is even more compositional variation than for the metadolerite dykes and amphibolites (Table 16; Figs 109, 110). Like the amphibolites, many samples have broadly similar Ce/Y (Fig. 111) and other incompatible element ratios to those of the Ruker Terrane metadolerite dykes and group II tholeiites of Enderby Land and the Vestfold Block (Table 7), consistent with derivation from a similar source. Again the comparison is only a general one, and does not prove that the granulites were derived by metamorphism of dykes of similar age. Indeed, some mafic granulites from the NPCM, in particular, have relatively high Ce/Zr, P/Zr, Nb/Zr, Ti/Zr and/or Y/Zr, suggesting derivation of these, at least, from compositionally distinct mafic igneous protoliths. There is evidence for metamorphic depletion of Rb, Th, and possibly, in some rocks, K and Ba (Sheraton 1984). Many granulites, including most of those from the northern Mawson Escarpment, therefore have very high K/Rb ratios (400–2200).

Ultramafic granulite and serpentinite

Boudins of coarse-grained pyroxenite and ultramafic amphibolite (hornblendite), commonly with minor plagioclase, biotite, and rarely with spinel, are enclosed in felsic gneiss. Like the mafic bodies, they may contain a foliation oblique to that of the host (Fitzsimons & Thost 1992). Some early fabrics may be relict igneous features. An ultramafic body at Crohn Massif comprises orthopyroxene crystals up to 15 centimetres long, randomly aligned within a foliation of possible cumulus origin. Boudins at Jetty Peninsula consist of coarse-grained (>7 cm) orthopyroxene with accessory magnetite and plagioclase (Hand et al. 1994a). Orthopyroxene is commonly mantled by retrograde biotite + quartz, and replaced by clinopyroxene, biotite, amphibole and quartz along recrystallised grain boundaries, but secondary garnet is absent. Ultramafic granulite at Mount Creighton and Corry Massif forms agmatitic structures—lensoid bodies consisting of blocks of granulite in a pegmatite matrix, foliated only at their margins (Munsgaard et al. 1992).

A relatively thick serpentinite body, possibly an intrusion or a tectonic slab (i.e., a protrusion), crops out in the southern part of **McLeod Massif** (immediately west of Radok Lake) (Fig. 113). The contacts are poorly exposed and mostly of tectonic origin. The serpentinite forms a concordant or slightly discordant body more than 700 metres long and up to 200 metres thick. The country rocks are felsic amphibole-biotite gneiss and mafic pyroxene-amphibole schist. They contain pods and veins of two pyroxenes or phlogopite-hornblende in a one to five metre contact zone, and phlogopite-magnetite lenses

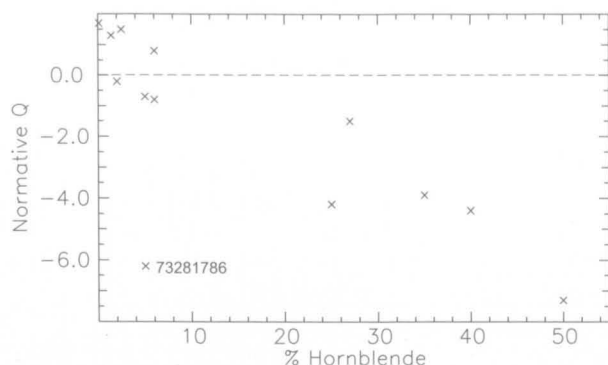


FIGURE 112

Plot of normative Q against modal percentage of hornblende for mafic granulites. Negative values represent silica deficiencies corresponding to the amounts of normative Ol. Sample 73281786 contains about eight modal percent biotite.

along the actual contact. Serpentine is a black fine-grained rock of fibrous structure, composed of colourless or pale yellow (in thin section) serpentine (50–100%), and minor dark green spinel (up to 7%), chromite (up to 5%), magnetite, sulphide, muscovite, and rare small carbonate pods. Relict olivine (up to 50 volume %), orthopyroxene and clinopyroxene are of sporadic occurrence.

The serpentinite has high MgO (30–35%), NiO (up to 0.4%), Cr_2O_3 (up to 0.3%), and unusually high Al_2O_3 (3–12%; Table 13). CIPW norms therefore show high Ol (43–66%) and An (8–25%), but mostly low (or zero) pyroxene (Di and Hy). The excess Al_2O_3 is reflected in normative corundum in three out of four samples; only that with relatively low Al_2O_3 is Di-normative. The original

composition of the body has almost certainly been considerably modified by serpentinisation so that it is impossible to determine the exact nature of the protolith. The highly variable normative mineral compositions may well be at least partly due to alteration, but may also reflect the effects of cumulus processes involving plagioclase (although no secondary minerals replacing plagioclase were found). Alternatively, the rocks may have been derived from high- Al_2O_3 (amphibole-bearing?) ultramafic protoliths. Compositionally rather similar spinel-bearing metaperidotite dykes also have relatively high Al_2O_3 (see below), which tends to support an origin from high- Al_2O_3 ultramafic melts.

The serpentinite body contains pods and elongated lenses that locally form chains and relatively short veins (0.5–2 m thick) composed of prehnite, phlogopite, late-stage chlorite and anthophyllite. Monazite, apatite and thorite are accessory phases. The origin of these rocks is uncertain, and they may be metasomatised gabbroic rocks, plagioclase-rich cumulates, or even xenoliths. Two monazite fractions from this rock gave an upper intercept age of 1165 ± 13 Ma, but it is unclear whether this reflects the time of high-grade metamorphism or low-grade reworking. Either way, the high-grade metamorphism of this rock would appear to have occurred at least 1160 Ma ago. This is difficult to reconcile with the c.1000–950 Ma granulite-facies metamorphic ages obtained from elsewhere in the Beaver-Lambert Terrane, but is broadly similar to ages for felsic magmatic and metamorphic events in the Fisher Terrane (Table 22). Inheritance from the country rocks (if, for example, the prehnite-rich rocks are metamorphosed xenoliths) cannot be entirely ruled out, but seems unlikely. The monazite age may thus be evidence for an earlier high-grade event in the Beaver-Lambert Terrane, although its exact significance remains unclear.



FIGURE 113

Geological sketch map of serpentinite body; southwestern McLeod Massif (see Fig. 150 for location).

NEOPROTEROZOIC FELSIC IGNEOUS ROCKS

Orthopyroxene granitoids

Orthopyroxene-bearing granitoids ('charnockite', s.l., of many authors) are widespread in the NPCM-Amery Ice Shelf area (Fig. 2): at northern Corry Massif, southern Crohn Massif (Fig. 114), Mount Gavaghan, Gillock Island, Jennings Promontory, Mount McCarthy, Thomas Nunataks, and the Loewe Massif-White Massif-northern Amery Peaks area. The last body crops out over an area of at least 300 square kilometres, but the other intrusions appear to be considerably smaller. Contacts with country rocks are typically subconcordant to gradational and commonly deformed (e.g., Mount Gavaghan, White Massif: Fig. 115), but elsewhere they are clearly discordant (e.g., Crohn and Loewe Massifs). Blocks and large schlieren of gneissic country rocks occur locally. Emplacement of orthopyroxene granitoid plutons occurred after the metamorphic peak, between D_4 and D_5 , and their fabric ranges from weak (in areas of low D_6 strain, e.g., Crohn Massif) to strong (in areas of high D_6 strain, e.g., Mount McCarthy: Fitzsimons & Thost 1992). They have a distinctive dark greenish-brown colour in outcrop, making mapping of the different compositional varieties difficult, and many contain K-feldspar megacrysts. Quartz monzonite at Loewe Massif has given an ion-microprobe U-Pb zircon age of 980 ± 21 Ma (Kinny et al. 1997).

The **Loewe Massif-White Massif** batholith is compositionally varied, with a large-scale compositional

layering. It is cut by mafic granulite dykes and contains lenses of mafic granulite that probably also represent deformed dykes. The most melanocratic rocks comprise quartz monzonite or quartz monzodiorite, containing reddish-brown biotite (mg 63–66; up to 4%), greenish-brown potassian ferroan pargasitic hornblende (mg 49–53; 2–4%), orthopyroxene ($\text{Ca}_2\text{Mg}_{42}\text{Fe}_{56}$; 4–6%), quartz, andesine antiperthite (An_{34-42}), orthoclase perthite, and minor clinopyroxene, ilmenite, magnetite, apatite and zircon. Granite (s.s., grading into granodiorite) is more abundant, and contains biotite (mg 50–52; up to 1%), orthopyroxene ($\text{Ca}_{0.5}\text{Mg}_{40}\text{Fe}_{59}$; 1–4%), and more sodic plagioclase (oligoclase–sodic andesine), but little or no hornblende or clinopyroxene. Textures are medium to coarse grained, subhedral to anhedral inequigranular, and many rocks are porphyritic (perthite). Myrmekitic intergrowths are common. The granitoids are locally foliated and partly recrystallised to granoblastic interlobate textures. Orthopyroxene is commonly partly replaced by biotite or iddingsite. Fabrics in the high-strain zones are defined by quartz ribbons, aligned K-feldspar grains, and fine-grained, elongated aggregates of mafic minerals. Biotite and amphibole in this batholith are relatively F-rich (1.67–3.44% and 0.84–1.82%, respectively), although this may reflect crystallisation at low $\text{P}_{\text{H}_2\text{O}}$ (resulting in smaller modal abundances of hydrous phases) rather than from unusually F-rich magmas.

Orthopyroxene granite (s.s.) at **Mount Gavaghan** and **Crohn Massif** is petrographically similar to the Loewe-White Massif granite, although that at Crohn Massif (Fig. 116) contains about two percent of hornblende and only minor orthopyroxene. Porphyritic orthopyroxene granite at Mount Gavaghan is cut by shear zones and



FIGURE 114
Outcrops of orthopyroxene granite; southeastern Crohn Massif.

extensively recrystallised. Strongly deformed hornblende–biotite granite (augen gneiss) at **Thomas Nunataks** appears to be the deformed equivalent of a similar granite. Much of **Mount McCarthy** is made up of porphyritic orthopyroxene–garnet granite. This contains xenoblastic garnet grains two to three millimetres across in a much recrystallised matrix of K-feldspar, plagioclase, quartz, orthopyroxene and minor biotite. Garnet ranges from *mg* 24 in the cores to *mg* 22 at rims near orthopyroxene, which is more magnesian (*mg* 50) than matrix orthopyroxene (*mg* 45; Thost and Hensen 1992).

Biotite–orthopyroxene granite (grading into granodiorite and quartz monzodiorite) at **Gillock Island** (Gillock Charnockite of Tingey 1981, and part of the Reinbolt Charnockite of Nichols & Berry 1991) contains minor garnet, but lacks significant hornblende. It is locally quite strongly deformed (augen gneiss), with much granulation of quartz, feldspar and orthopyroxene ($\text{Ca}_1\text{Mg}_{39}\text{Fe}_{60}$). It was considered syn- D_2 by Nichols & Berry (1991). Biotite–hornblende–orthopyroxene granite and granodiorite in the **Jennings Promontory** area (Jennings Charnockite of Tingey 1981) are essentially undeformed (post- D_3 according to Nichols & Berry 1991), but contain anhedral K-feldspar phenocrysts up to eight centimetres long—the alignment of which produces a foliation. They are relatively evolved in terms of mineral *mg* values (orthopyroxene, $\text{Ca}_3\text{Mg}_{34}\text{Fe}_{73}$; biotite, *mg* 28–30; potassian ferro-pargasitic hornblende, *mg* 25–28), although not SiO_2 content. The granite is cut by veins of garnet–biotite and hornblende–biotite pegmatite and a hornblende–orthopyroxene granite dyke.

Most orthopyroxene granitoid samples define a relatively potassic (Ab-poor) trend on an Ab–Or–An diagram (Fig. 117), although, apart from two granites from Jennings Promontory, not as extreme as that of the Mawson Charnockite (Sheraton 1982). All the analysed rocks are of I-type, and marginally metaluminous or peraluminous ($\text{ASI} < 1.1$; Fig. 118). Orthopyroxene granitoids include *low-SiO₂* (58.9–62.1%) and *high-SiO₂* (66.2–74.0%) varieties. The low SiO_2 group includes quartz monzonite from the Loewe Massif–White Massif batholith, as well as relatively melanocratic granite of Gillock Island and Jennings Promontory. The high SiO_2 group consists of orthopyroxene granite (and minor granodiorite) from Loewe and White Massifs, together with a sample of orthopyroxene–hornblende–biotite granite from Crohn Massif.

Most of the low- SiO_2 rocks (<61%) are relatively enriched in Al_2O_3 , HFSE, LREE and Sr, whereas high- SiO_2 granites are more depleted in these elements (Table 17; Fig. 119). Spidergrams of the former group show smaller negative Nb, P and Ti anomalies and little or no Y depletion (Fig. 120); REE patterns are quite strongly fractionated ($(\text{La/Yb})_n$ 18.0–26.8, $(\text{Ce/Y})_n$ 7.6–15.3), with small negative Eu anomalies (Fig. 121). High- SiO_2 granites have larger Nb, P and Ti anomalies, but Sr anomalies are similar or even smaller (one Loewe Massif granite has a positive anomaly) and most samples are Y-depleted (on the orthogneiss classification of Sheraton & Black 1983); REE patterns are more varied, that is moderately to very strongly fractionated ($(\text{La/Yb})_n$ 12.6, $(\text{Ce/Y})_n$ 3.0–45.6). The co-eval Mawson Charnockite also has a wide compositional range and broadly similar chemical

features, apart from lower Na_2O , Ba and Sr, higher MgO , and a particularly wide range of K_2O (Figs 119, 120).

Very similar spidergrams and REE patterns (apart from minor differences in P and Y contents and larger differences in the relatively mobile Th and U) of the low- SiO_2 granitoids suggest a common origin. Nevertheless, a variety of parent magmas is implied by the large variations in many incompatible element contents (particularly LREE) for only a small range of SiO_2 (Fig. 119). For example, granites from Jennings Promontory have particularly low *mg* (24–25), Cr and Ni, and high Zr, whereas quartz monzonites from Loewe Massif have relatively high Ce, Y and Sr. 1170 Ma quartz monzogabbro in the Bunger Hills forms a geochemically coherent suite

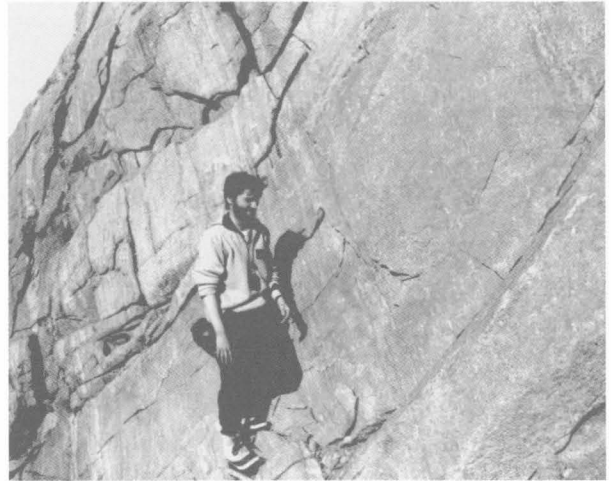


FIGURE 115

Gradational contact between massive orthopyroxene granitoid (right) and layered garnet–biotite semi-pelitic gneiss; White Massif.



FIGURE 116

Coarse-grained orthopyroxene granite, containing K-feldspar phenocrysts in a hornblende–orthopyroxene–quartz–plagioclase matrix; Crohn Massif.

with associated gabbro and quartz gabbro, and is therefore considered to have been derived by fractionation of mafic magma (Sheraton et al. 1992). A similar origin from mantle-derived magma is possible for the NPCM low-SiO₂ granitoids, although the parent magmas may have tended towards an intermediate (e.g., monzodioritic) rather than mafic composition (cf. Stern & Hanson 1991). However, marked negative Sr anomalies suggest significant plagioclase fractionation. Partial melting of mafic to intermediate granulite-facies crustal rocks (Young & Ellis 1991; Kilpatrick & Ellis 1992; Zhao et al. 1997) would require a very large, and possibly unrealistic, heat input, particularly as relatively 'dry'

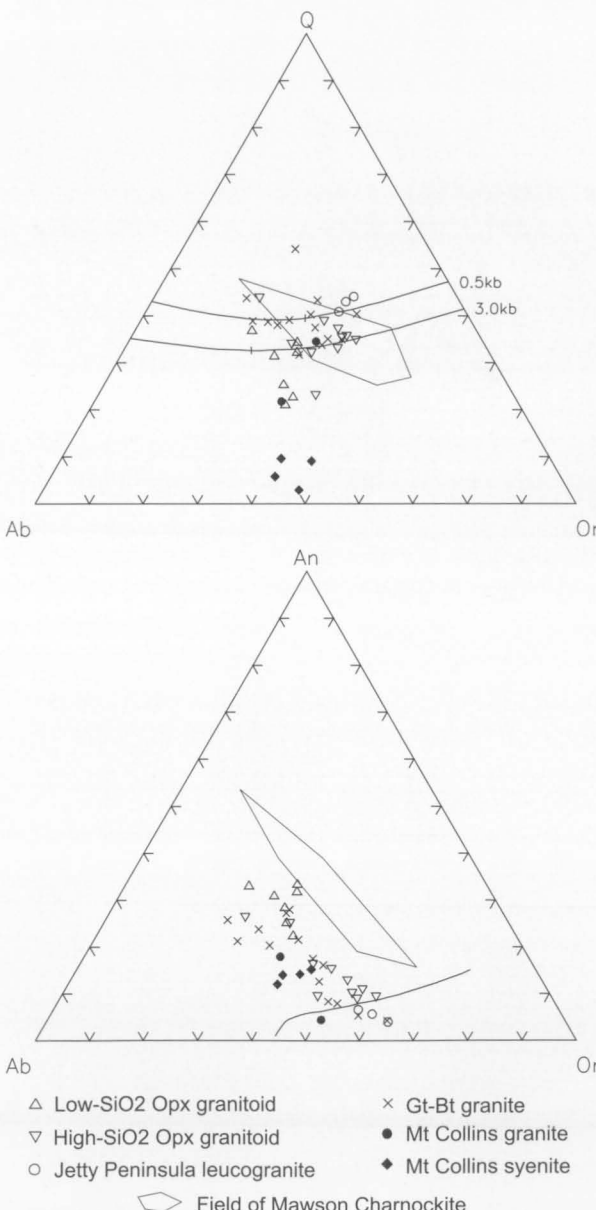


FIGURE 117
Normative Q–Ab–Or and Ab–Or–An diagrams for Neoproterozoic granitic rocks of the Beaver-Lambert Terrane. The latter shows the plagioclase–alkali feldspar field boundary at 1000 bars P_{H_2O} , projected onto the Ab–Or–An face of the tetrahedron (after James & Hamilton 1969). The field of Mawson Charnockite (from Sheraton 1982) is indicated.

melting is implied. Moreover, experimental data (Beard et al. 1994) show that water-undersaturated melting of a dioritic source produces siliceous (>72% SiO₂) melts even for degrees of melting as high as 50 percent.

It is unlikely that both the low-SiO₂ and high-SiO₂ granitoids represent a single fractionation sequence, because Sr and Eu anomalies of the latter group are no larger (and in some cases are smaller), precluding plagioclase-dominated fractionation. The large decrease in Y over the complete range of SiO₂ (Fig. 119) could only be explained by major clinopyroxene (or hornblende) fractionation, but this is inconsistent with the relatively small change in ASI (Fig. 118). Moreover, the lack of correlation of either *mg* or K/Rb with SiO₂ is inconsistent with fractionation being the sole cause of the compositional variations. The much larger degrees of Nb and Y depletion of the high-SiO₂ group are also difficult to explain entirely by fractionation. For example, Nb/La is largely unaffected by crystal fractionation processes, at least for mafic to intermediate rocks (Sheraton et al. 1992; Thirlwall et al. 1994), but could be markedly reduced if major crustal assimilation (through AFC processes) occurred.

It is thus likely that most or all of the high-SiO₂ orthopyroxene granites represent a distinct magma or magmas, produced by high-degree, high-temperature melting of dry intermediate to felsic lower crustal rocks, or at least have a large crustal component. A high-grade source could explain their higher Th/U (average of 18.4 for 10 samples, compared to 8.0 for 7 low-SiO₂ granitoids). The low Y and high Ce/Y of most samples (particularly those with >70% SiO₂), which contrast with the Y-undepleted character of the low-SiO₂ rocks, suggest high-pressure melting with residual garnet, and possibly relatively small amounts of plagioclase to account for the moderate Sr anomalies. Much of the compositional variation, particularly for Y, could be due to partial melting control, with variations in the amount of residual garnet, as was postulated for the Archaean Lewisian orthogneisses of Northwest Scotland by Weaver & Tarney (1980). Similar features of the low-Ti subgroup of the Mawson Charnockite were taken by Young & Ellis (1991) to imply melting of thickened crust in an Andean or Himalayan-type plate margin.

Although Y-depleted, these granites differ markedly in composition from the relatively LILE-poor Archaean tonalite-trondhjemite-granodiorite (TTG) suite, thought to have been formed by hydrous partial melting of a plagiog-

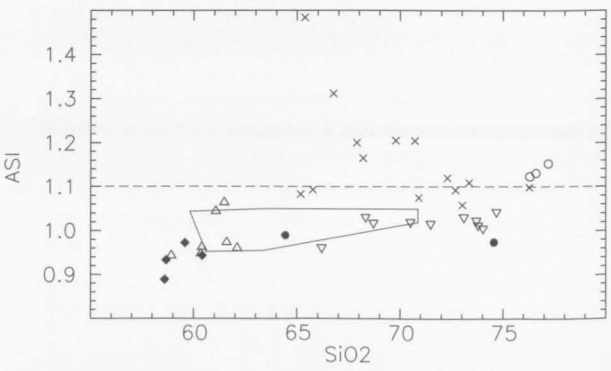


FIGURE 118
Plot of ASI against SiO₂ for Neoproterozoic granitic rocks. Symbols and field as in Figure 117.

TABLE 17. Chemical analyses and C.I.P.W. norms of representative Neoproterozoic granitic intrusive rocks from the Beaver-Lambert Terrane.

Sample no. Locality	69280109 E Gillock Island granite	91286507 Loewe Massif Hb-Bt-Opx quartz monzonite	71280003 S Crohn Massif Opx-Hb-Bt granite	71280109 W Amery Peaks Opx granite	91286406 White Massif Opx granodiorite	91286402 Mount McCarthy Opx-Gt granite	91286421 Mount Collins Cpx-Opx quartz syenite	91286420 Mount Collins Hb-Bt granite	71280224 Wall Peak Bt-Gt granite gneiss	91286405 White Massif Gt-Bt granite	675 Jetty Peninsula Bt-Gt leucogranite gneiss
SiO ₂	61.48	60.35	66.20	74.68	71.48	67.53	58.66	74.55	72.29	67.89	76.60
TiO ₂	1.23	1.54	0.72	0.09	0.21	0.85	0.81	0.21	0.31	0.59	0.14
Al ₂ O ₃	15.50	14.63	14.70	13.56	13.96	14.38	17.80	12.45	14.30	15.61	12.45
Fe ₂ O ₃	1.73	2.27	1.76	0.33	0.78	1.37	2.28	0.86	0.22	1.01	0.31
FeO	5.92	5.32	2.79	0.44	2.07	4.56	4.07	1.31	1.88	3.30	0.93
MnO	0.11	0.12	0.06	0.01	0.04	0.09	0.16	0.05	0.04	0.07	0.03
MgO	2.35	2.27	1.34	0.30	1.01	1.52	0.64	0.12	0.56	1.28	0.15
CaO	4.18	4.51	3.84	1.36	3.17	2.75	3.40	0.79	1.65	2.45	0.68
Na ₂ O	2.85	3.11	2.99	2.69	3.28	2.51	4.31	3.36	2.94	3.17	2.29
K ₂ O	2.90	3.95	3.66	5.70	2.49	3.37	5.89	5.44	4.73	3.23	5.61
P ₂ O ₅	0.36	0.90	0.24	0.03	0.05	0.12	0.24	0.03	0.08	0.07	0.03
H ₂ O ⁺	-	-	0.85	-	-	-	-	-	-	-	0.38
CO ₂	-	-	0.26	-	-	-	-	-	-	-	-
LOI	0.84	0.83	-	0.58	0.59	0.54	1.25	0.51	0.37	0.37	-
Rest	0.39	0.54	0.33	0.24	0.19	0.36	0.53	0.18	0.23	0.20	0.11
Total	99.84	100.34	99.74	100.01	99.32	99.95	100.04	99.86	99.60	99.24	99.75
O=F,S,Cl	0.01	0.01	0.00	0.01	0.00	0.00	0.01	0.00	0.00	0.00	0.00
Total	99.83	100.33	99.74	100.00	99.32	99.95	100.03	99.86	99.60	99.24	99.75
Q	18.90	14.58	24.42	33.76	33.40	29.48	2.17	31.94	31.65	28.14	39.63
C	0.93	-	-	0.56	0.23	1.89	-	-	1.54	2.61	1.45
Or	17.14	23.34	21.63	33.68	14.71	19.91	34.81	32.15	27.95	19.09	33.15
Ab	24.12	26.32	25.30	22.76	27.75	21.24	36.47	28.43	24.88	26.82	19.38
An	18.39	14.29	15.88	6.55	15.40	12.86	11.83	2.82	7.66	11.70	3.18
Di	-	1.82	1.31	-	-	-	2.97	0.78	-	-	-
Hy	13.46	10.32	5.28	1.15	5.40	9.78	4.62	1.33	4.23	7.56	1.65
Mt	2.51	3.29	2.55	0.48	1.13	1.99	3.31	1.25	0.32	1.46	0.45
Il	2.34	2.92	1.37	0.17	0.40	1.61	1.54	0.40	0.59	1.12	0.27
Ap	0.85	2.13	0.57	0.07	0.12	0.28	0.57	0.07	0.19	0.17	0.07
Li	30	20	-	8	19	17	6	4	23	17	14
Be	2	5	2	1	2	1	2	3	3	1	-
S	110	200	-	160	<100	20	250	20	60	<100	<200
Sc	21.0	19.6	10.0	2.0	9.1	16.5	21.2	2.0	4.0	11.0	4.0
V	137	106	70	5	38	102	9	<2	22	59	7
Cr	65	41	9	3	33	54	3	1	6	30	1
Ni	27	13	4	4	6	27	6	3	2	15	2
Cu	27	15	12	8	4	27	10	1	1	2	2
Zn	102	105	50	10	42	60	69	59	32	66	10
Ga	21	20	18	12	14	18	22	21	16	21	14
Rb	134	131	107	185	81	84	83	98	278	122	240
Sr	242	574	323	132	177	202	411	57	147	141	58
Y	32	69	29	8	9	63	19	53	18	30	34
Zr	363	447	288	95	85	264	916	377	169	211	63
Nb	23	43	11	<2	4	12	11	30	15	10	3
Cs	0.8	0.5	-	7.0	0.1	0.2	0.2	-	8.0	-	-
Ba	1536	2039	1619	1148	1004	1678	2441	278	860	689	359
La	82.4	146.0	69.0	55.0	17.2	75.4	31.4	107.0	48.0	45.0	26.0
Ce	160.0	322.2	128.0	96.0	31.7	150.6	64.1	216.0	90.0	88.0	38.0
Nd	65.2	144.0	51.0	32.0	12.7	57.2	32.2	86.0	30.0	37.0	11.0
Pb	28	45	23	68	34	37	18	22	60	47	53
Th	26.1	5.6	10.0	51.0	7.3	33.0	2.2	16.0	76.0	30.0	10.0
U	1.4	1.3	1.0	1.0	1.4	1.1	1.1	<0.5	6.5	2.0	1.5
K/Rb	180	250	284	256	255	333	589	461	141	220	194
(Ce/Y) _n	12.5	11.7	11.0	30	8.8	6.0	8.4	10.2	12.5	7.3	2.8
Th/U	18.5	4.2	10	51	5.3	31	2.0	-	11.7	15	6.7
Nb/Nb*	0.29	0.34	0.13	-	0.10	0.15	0.12	0.24	0.18	0.16	0.04
Sr/Sr*	0.17	0.19	0.29	0.16	0.63	0.15	0.66	0.03	0.20	0.18	0.19
mg	41.4	43.2	46.1	54.9	46.5	37.3	21.9	14.0	34.7	40.9	22.3

mg = atomic 100Mg/(Mg + Fe²⁺).

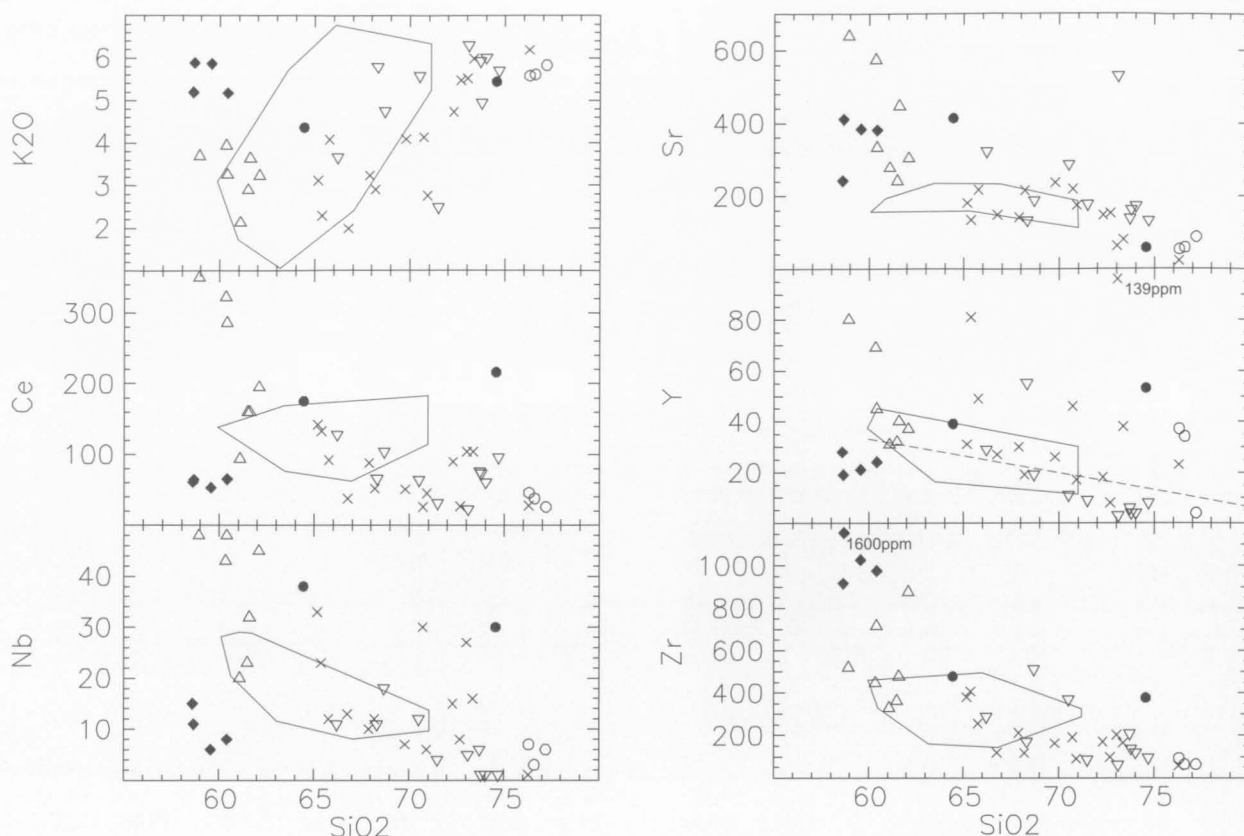


FIGURE 119

SiO₂ variation diagrams for Neoproterozoic granitic rocks. Symbols and field as in Figure 117. A dashed line on Y–SiO₂ plot indicates the approximate boundary between Y-depleted and Y-undepleted felsic orthogneisses (Sheraton & Black 1983).

clase-poor mafic source (e.g., garnet amphibolite or eclogite) (Tarney et al. 1979; Rapp et al. 1991). Their distinctive trend towards the Or apex, rather than the H₂O-saturated granite minimum, on an Ab–Or–An diagram can be explained by the experimental data of Ebadi & Johannes (1991) and Beard et al. (1994), which show that low P_{H₂O} melting of felsic crustal rocks produces liquids with high Or/Ab. Incorporation of calcic plagioclase (i.e., the An component) into the melt would enhance this effect (James & Hamilton 1969). Hence, there seems to be no reason to invoke a ‘residual’ granulite source, as postulated by Sheraton (1982) for the Mawson Charnockite. Kilpatrick & Ellis (1992) pointed out that the very high temperatures (~1000°C) required to produce ‘C-type’ magmas can be attained in granulite terranes, although a major heat input, such as emplacement of mantle-derived magma near the base of the crust, would clearly be necessary (Zhao & Ellis 1994).

It seems improbable that the generally similar trend shown by both low-SiO₂ and high-SiO₂ granitoids on the Ab–Or–An diagram (Fig. 117) is entirely fortuitous. It may have resulted because dry An-rich intermediate liquids (i.e., low-SiO₂ type) would also tend to fractionate towards an Or-rich minimum melt composition. This would imply a source for the high-SiO₂ group compositionally similar (but, for reasons given above, not identical) to the low-SiO₂ granitoids. An alternative, and perhaps more likely, model is that the two groups merely represent parts of a continuum from a largely mantle-derived mafic-intermediate end member to a predominantly crust-

derived felsic one. Relatively evolved initial ⁸⁷Sr/⁸⁶Sr (0.7063 to 0.7100) and ε_{Nd} (-2.9 to -5.9) values imply significant crustal components in both low-SiO₂ and high-SiO₂ granitoids (Zhao et al. 1997). However, the available isotopic data do not provide unambiguous support for a higher crustal component in the more siliceous granitoids, which, although having higher ⁸⁷Sr/⁸⁶Sr (0.7091 to 0.7100), also have higher ε_{Nd} (-2.9 to -4.9). Similarly, all subgroups (including low-SiO₂ types) of the Mawson Charnockite have evolved isotopic compositions (Young & Ellis 1991; Young et al. 1997). Whether these data reflect significant direct crustal inputs in the low-SiO₂ magmas, derivation from an isotopically evolved mantle source, or a combination of these is presently unclear.

Syenitic and granitic rocks of Mount Collins

Dark brown monzonite, quartz monzonite, and quartz syenite at Mount Collins are commonly K-feldspar-phyric and locally have a marked foliation. The least altered samples are medium to coarse-grained and have a hypidiomorphic inequigranular texture. They contain pale green clinopyroxene (Ca₄₄Mg_{18–24}Fe_{32–38}; 4–6%), showing exsolution textures, primary dark brownish-green potassian hastingsitic hornblende (mg 18–33; up to 1%), quartz (1–6%), oligoclase (An_{25–28}; 25–35%), slightly perthitic microcline (55–65%), ilmenite + magnetite (1%), and minor orthopyroxene (Ca₄Mg_{24–34}Fe_{62–72}), apatite, allanite and zircon. In other partly recrystallised and locally somewhat foliated rocks, clinopyroxene is

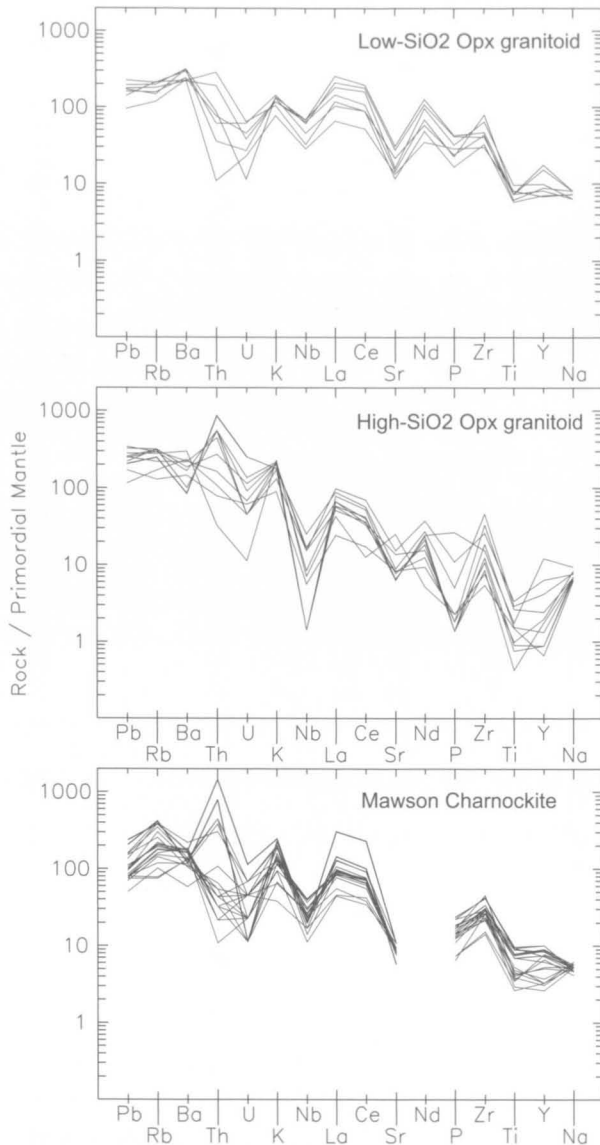


FIGURE 120
Spidergrams for Neoproterozoic orthopyroxene
granitoids.

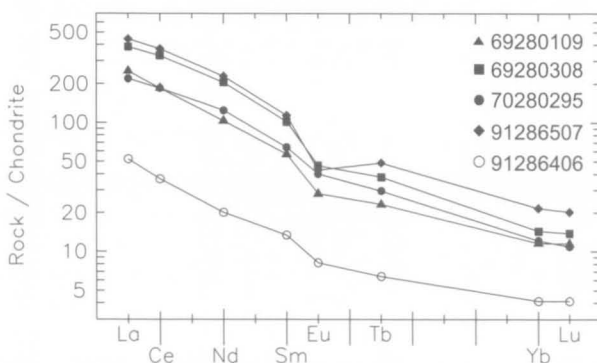


FIGURE 121
Chondrite-normalised rare-earth element abundance
plots for Neoproterozoic orthopyroxene granitoids.
Most belong to the low-SiO₂ group, only sample
91286406 having high SiO₂.

extensively altered to amphibole and biotite, and some pseudomorphs of colourless clino-amphibole, biotite, and/or iddingsite may represent altered orthopyroxene. One quartz monzonite contains about six percent of dark green hornblende that forms sieve-like aggregates with quartz, presumably replacing pyroxene. Allanite is a significant accessory mineral in many of these rocks and all contain abundant zircon.

The syenitic rocks appear to grade into pink granitic rocks, although the actual contacts are not exposed. Both rock types are cut by abundant metadolerite dykes. The more felsic of the pink rocks are granite (s.s.), whereas rocks with slightly less quartz (15–20%) are quartz monzonite or quartz syenite. Dark green potassian hastingsitic hornblende (*mg* 9–10; up to 4%) and dark brown biotite (*mg* 7–10; 1–6%) are the major mafic minerals, clinopyroxene being rare. In most rocks, slightly to strongly perthitic microcline is commonly much more abundant than plagioclase (albite–oligoclase in the most leucocratic varieties), so they can be more precisely termed syenogranites. Some granites are porphyritic and there is a slight foliation locally, but most are much less altered than the syenitic rocks. Allanite is a conspicuous accessory mineral.

Both the syenitic and granitic rocks have indistinguishable ion-microprobe U–Pb zircon ages of 984 ± 12 and $984 \pm 7/976 \pm 25$ Ma, respectively (Kinny et al. 1997). However, other syenitic rocks were recently dated at c. 1250–1220 Ma, and a cross-cutting monzodiorite dyke at c. 1120 Ma (preliminary U–Pb zircon data: A. Laiba and B. Belitsky, unpublished), suggesting that some of these plutonic rocks are Mesoproterozoic, although the significance of these new data is presently unclear; they may indicate a correlation with the Fisher Terrane. Although more or less co-eval, neither the syenitic nor granitic rocks at Mount Collins have close geochemical affinities with the orthopyroxene quartz monzonite at Loewe Massif, and thus represent a distinct magmatic suite.

The syenitic intrusives are highly evolved metaluminous rocks with high Al₂O₃, Na₂O, K₂O, Ba and Zr, but low *mg* (7.6–27.0), MgO, CaO, Cr, Ni, and V (Table 17; Figs 117–119). REE and most HFSE (Nb, P, Ti and Y) are not enriched, and $10^4\text{Ga}/\text{Al}$ (2.3–2.6) is not particularly high. Spidergrams show little variation, and have small negative Sr and moderate Nb anomalies, but very large positive Zr anomalies (Fig. 122); REE patterns are moderately fractionated ($(\text{La}/\text{Yb})_n$ 4.58–8.00, $(\text{Ce}/\text{Y})_n$ 5.7–6.8) with large positive Eu anomalies (Fig. 123).

These spidergrams are quite different from those of the Cambrian syenites of the Yamato Mountains (Dronning Maud Land) which, apart from negative Nb and Ti anomalies, are relatively smooth (Zhao et al. 1995a). They also differ from the highly fractionated Cambrian syenites of David Island (Queen Mary Land) that have much more irregular patterns with large negative Nb, Sr, P and Ti anomalies (Sheraton et al. 1992). The Yamato syenites were considered by Zhao et al. (1995a) to have formed from an alkali basalt parent magma by AFC processes, with subsequent low-pressure crystal fractionation. Fractionation of mafic magma, probably combined with some degree of crustal assimilation, has also been proposed for many other syenitic complexes (see various

papers in Fitton & Upton 1987). A similar origin, albeit with some distinct features, could account for many of the compositional characteristics of the Mount Collins rocks. Relatively unevolved Sr and Nd isotopic compositions ($^{87}\text{Sr}/^{86}\text{Sr}$ 0.70434 to 0.70442, ϵ_{Nd} -0.19 to -0.73; Zhao et al. 1997) are consistent with a largely mantle derivation, although inherited zircon in some (Mikhalsky et al. 1992, 1996) indicates an additional crustal component. However, it is difficult to produce the observed Zr enrichment without also enriching LREE (the lower LREE contents are a major difference from the David Island syenites). Thus, either fractionation of an REE-bearing phase (probably allanite, but not zircon) or accumulation of zircon (but not an REE-bearing phase) is indicated. The former seems an inadequate explanation, in isolation, even for F-rich melts in which zircon is much more soluble than REE phosphates, such as monazite (Keppler 1993), but may have produced an initial degree of Zr enrichment. Accumulation of feldspar (plagioclase and/or K-feldspar), in addition to zircon, could account for the large positive Eu anomalies and Al_2O_3 and Ba enrichment. The lack of corresponding positive Sr anomalies in the presumed cumulates requires an evolved parent liquid with negative Sr anomalies. This is consistent with the low mg, Cr and Ni of these rocks.

This fractionation model is generally similar to that proposed for the low- SiO_2 orthopyroxene granitoids, so it is possible that the major difference is that syenitic liquids require a more SiO_2 -undersaturated alkaline, rather than a tholeiitic, parent magma. High-pressure magma generation or, less likely, initial fractionation involving garnet could account for the relatively low Y of these

rocks. More extreme fractionation, without producing excessive SiO_2 -oversaturation, is necessary for the Mount Collins (and David Island) syenites to account for their low mg. Apart from low La/Zr, the Mount Collins rocks have some other enigmatic features. Their high K/Rb (550–920) and K/Cs (190–380) might suggest a significant granulite-facies crustal component, but their low Th/U (1.4–1.9) is difficult to explain on this basis. Alternatively, fractionation of a low K/Rb phase, such as phlogopite or biotite, at some stage in their petrogenesis is possible—but there is no petrographic evidence for this.

Hornblende–biotite granitoids at Mount Collins are just metaluminous and have high HFSE, REE and, for the more siliceous granite sample, high Ga/Al, suggesting A-type affinities (Table 17; Figs 117–119). They cannot be related to the syenitic rocks by fractionation processes, because the less-evolved sample (a quartz monzonite) has higher SiO_2 , MgO, Sr, V, Cr and Ni; Nb, Y and LREE are relatively enriched, whereas Zr is much lower. Spidergrams are markedly irregular, with moderate to large negative Nb, Sr, P and Ti anomalies (Fig. 122), typical of partial melts of intermediate to felsic crustal rocks with residual plagioclase, but not garnet. The more siliceous sample has the more fractionated pattern, consistent with fractionation of plagioclase, apatite and a Fe–Ti oxide, as well as a ferromagnesian phase. Similar, relatively high Nb/La for both granite samples supports a comagmatic origin, as do the age data of Kinny et al. (1997). Thus the pink granite, although co-eval with at least some of the syenitic rocks, does not appear to be genetically related.

Garnet granitoids

As well as the layered garnet-bearing orthogneisses described earlier, more clearly intrusive syn to late-metamorphic garnet–biotite granitoids are widespread in the NPCM. They commonly form relatively small (tens of metres) subconcordant sheets and lenses, but reach thicknesses of several hundred metres in a few places, such as Jetty Peninsula (Manton et al. 1992; Hand et al. 1994a) and Depot Peak (Stüwe & Hand 1992). They are generally foliated (leucogneiss), but most clearly post-date the pervasive regional foliation (S_3) and contain schlieren and larger enclaves of metasedimentary country rocks (Fitzsimons & Thost 1992). They are thus mainly of late-

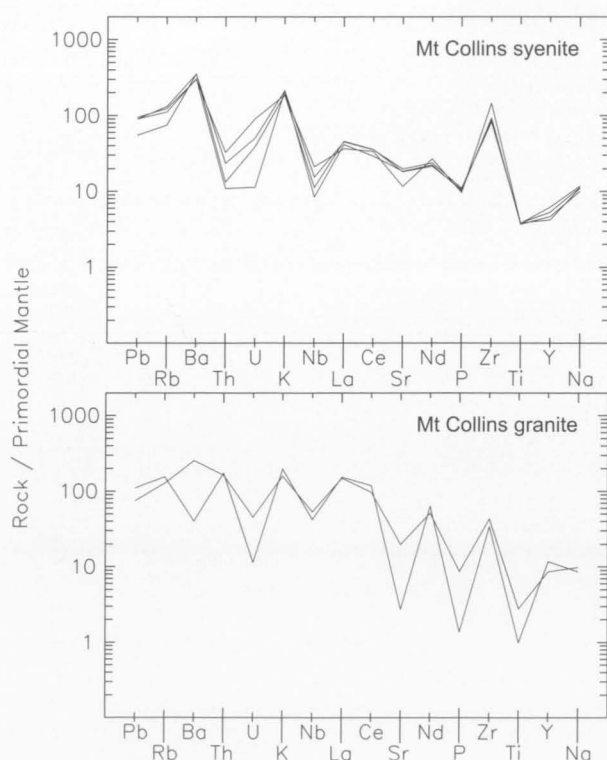


FIGURE 122

Spidergrams for Neoproterozoic syenitic and granitic rocks from Mount Collins.

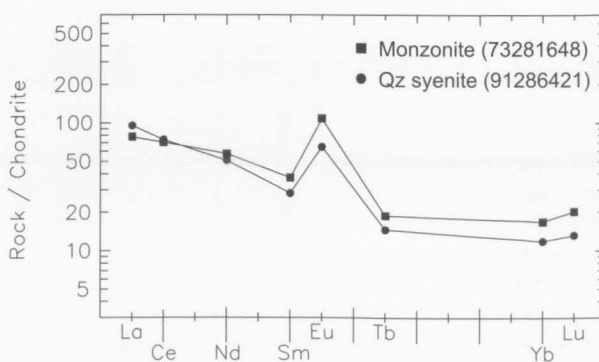


FIGURE 123

Chondrite-normalised rare-earth element abundance plots for Neoproterozoic syenitic rocks from Mount Collins.

metamorphic age (i.e., pre- D_6), although several generations are present. For example, a leucogneiss layer at Mount Kirkby is isoclinally folded (F_4), whereas most garnet leucogneiss bodies cross-cut such folds. Two generations of leucogneiss crop out at Mounts Gaston and Bunt, those at the latter locality being post- F_5 . Two generations of gneissic garnet leucogranite also occur at Mount McCarthy and were apparently formed by partial melting of metasedimentary country rocks during emplacement of nearby orthopyroxene–garnet granite, consistent with the ion-microprobe U–Pb zircon age of one body of 990 ± 30 Ma (Kinny et al. 1997). Locally pegmatitic biotite–garnet leucogranite gneiss with K-feldspar megacrysts at White Massif probably has a similar origin. A syn- D_4 garnet–biotite granite sheet near Radock Lake has given a U–Pb zircon age of 990 ± 18 Ma (Boger et al. 2000).

Several generations of deformed, but at least locally discordant, garnet-bearing granitoids have been recognised on **Else Platform** at the northern end of Jetty Peninsula (Hand et al. 1994a). The oldest is K-feldspar megacrystic garnet granite (Fig. 124), which makes up 20 percent of the exposed rocks and is interpreted as being of syn- D_1 age (possibly equivalent to D_3 of Fitzsimons & Thost 1992). Gneissic biotite–garnet leucogranite dykes and layers are particularly common and locally intrude megacrystic granite. They range from a few metres thick to several hundred metres across and are discordant to S_1 . Locally they contain an intense S_2 foliation (equivalent to $S_3(2)$ and S_6 , respectively, of Fitzsimons & Thost 1992), defined by elongated aggregates of xenoblastic garnet and quartz. One such layer, just south of Else Platform, has given a U–Pb zircon age of 940 ± 20 Ma (Manton et al. 1992). It is a medium to coarse-grained (1–10 mm) rock containing quartz, micropertitic microcline, plagioclase, minor biotite, sporadic garnet, secondary chlorite, muscovite and epidote, and accessory apatite, zircon, opaque minerals and monazite. A large area of homogeneous garnet granite on Else Platform, which occupies the core of a major F_2 fold (F_6 of Fitzsimons & Thost 1992), also has a variably developed S_2 ($=S_6$) foliation, but is not cut by the leucogranite dykes.

Most garnet granitoids have granitic (s.s.) compositions, but some are granodioritic. They are generally medium to coarse grained, and myrmekitic intergrowths are common. They typically contain foxy red biotite (up to 5%), garnet (up to 5%), quartz, K-feldspar (micropertite and microcline), oligoclase–andesine, and minor opaque minerals, apatite, zircon and, less commonly, monazite. Garnet porphyroblasts in some granitoids have inclusions of quartz, biotite and opaque minerals. Small amounts of secondary chlorite, muscovite and epidote reflect low-grade alteration (chloritisation of biotite, sericitisation of plagioclase). Biotite commonly has a preferred orientation and locally there is much recrystallisation, with elongated aggregates of xenoblastic garnet and quartz in a granoblastic matrix of quartz and feldspar. Quartz in less-deformed rocks shows sub-grain development and deformation lamellae; most feldspar grains have bent twin lamellae.

Unlike most other granitoids in the NPCM, the majority of garnet–biotite granites and granodiorites have $ASI > 1.1$ (Fig. 118) and are thus of S-type. They probably represent relatively localised partial melts of predominantly

metasedimentary country rocks formed during high-grade metamorphism and therefore comprise a rather heterogeneous group (Table 17; Fig. 119), with mg from 28.9 to 54.7. Spidergrams are mostly highly irregular (fractionated) with marked negative Nb, Sr, P and Ti anomalies, consistent with melting of felsic crustal protoliths (Fig. 125). Many are relatively enriched in Y and have only moderately fractionated REE ($(Ce/Y)_n$ 3–8), which suggest either that garnet was not a major residual phase (which would be surprising) or that much of the garnet is xenocrystic and did not equilibrate with the melt. Th/U ranges up to high values of about 40, similar to those of the granulite-facies country rocks.

Foliated biotite–garnet leucogranite at Jetty Peninsula is particularly strongly fractionated (SiO_2 76.3–77.2, mg 17.5–29.1), with low Sr, Zr, Nb and LREE contents. Two samples have low $(Ce/Y)_n$ (2.8, 3.1), whereas a third, garnet-free, but otherwise compositionally very similar sample has much higher $(Ce/Y)_n$ (16.3) and lower Y (4 ppm; Figs 119, 125)—a feature attributed by Manton et al. (1992) to separation of garnet (and possibly monazite) depleting the melt in Y.

Minor intrusions

Granite and pegmatite dykes and veins are common at many places in the NPCM, such as Armonini Nunatak, Mount Gleeson and Mount Meredith, as well as at New Year and Pickering Nunataks. Some of these, such as hornblende–orthopyroxene granite dykes at Jennings Promontory, are clearly associated with the c.980 Ma orthopyroxene granitoid intrusives, and others may well be associated with the various generations of garnet granitoid described above. It is possible that some of the pegmatites in the Ruker Terrane may be of similar early Neoproterozoic age, particularly those that contain

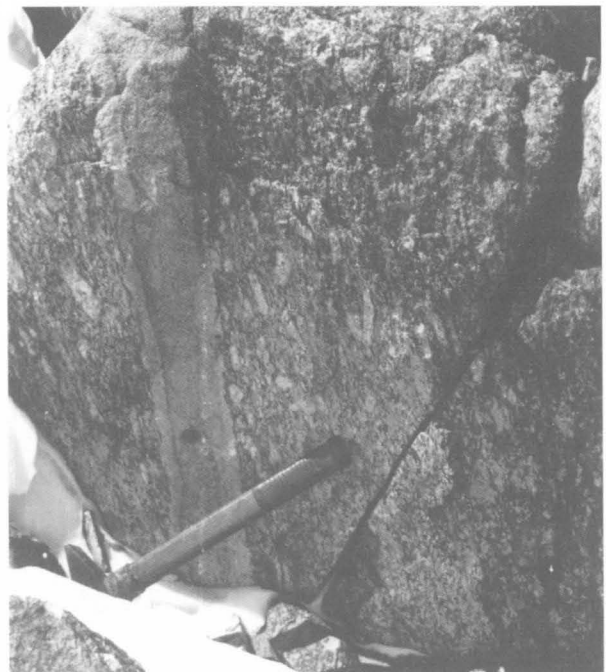


FIGURE 124

K-feldspar megacrystic garnet–biotite granite gneiss cut by aplite vein; Else Platform.

minerals characteristic of the Mesoproterozoic to early Neoproterozoic(?) metamorphism, such as kyanite. However, there is presently no isotopic evidence to prove this, and many felsic dykes are of early Palaeozoic (Ross or Pan-African) age (see below).

NEOPROTEROZOIC MAFIC IGNEOUS ROCKS

Mafic granulite dykes

Fine- to medium-grained hornblende–orthopyroxene–clinopyroxene–plagioclase granulite dykes, with small amounts of quartz, biotite, apatite and opaque minerals, are commonly 0.5 to two metres wide. They are commonly discordant to the foliation in the metamorphic rocks, but may be boudinaged and weakly foliated (Fig. 126). In high-strain zones, in which S_6 is strongly developed, they have an intense fabric and cross-cutting relationships may no longer be apparent. At least two generations of metamorphosed dyke occur in the Porthos Range, as at Mount Tarr, where a highly deformed granulite dyke is cut by a narrower dyke (Fitzsimons & Thost 1992).

Mafic granulite dykes post-date 980 ± 21 Ma orthopyroxene granitoids at Loewe and White Massifs, Mount Gavaghan and northern Webster Peaks, although a dyke at Manning Massif (91286409) is cut by the younger of several generations of orthopyroxene-bearing pegmatite. A deformed dyke at White Massif (91286404) is rich in biotite and hornblende and has a foliation parallel

to that in the host granite. Dykes at Loewe Massif are relatively quartz and orthopyroxene-rich (quartz norite or diorite). Many of these dykes were probably emplaced very soon after the granitic batholiths—that is, they are syn-plutonic.

The granulite dykes are chemically quite varied (Table 13; Figs 43–47), but none can be correlated with any of the other mafic dykes in the Beaver-Lambert Terrane. The White Massif dyke is Ne and strongly Ol-normative, with low SiO_2 and very high K_2O (3.90%). However, the latter may well be a metamorphic feature, as the spidergram has large K and Rb spikes (Fig. 127). Apart from high K_2O and Rb, this dyke, together with the olivine tholeiite from Manning Massif, has some compositional similarities (e.g., high MgO, LILE/Zr and Ce/Zr, and low Ti/Zr) with the ?Palaeoproterozoic high-Mg dykes of the Ruker Terrane and elsewhere (Figs 45, 46). This suggests an origin by partial melting under similar conditions of a broadly similar mantle source, but the granulite dykes clearly cannot be correlated with the much older high-Mg suite. Three dykes from Loewe Massif are all quartz tholeiites with high normative Hy. They are quite evolved (mg^* 33–50), with negative Sr anomalies (Fig. 127), and all have relatively high Y. Two of these dykes are characterised by high Ba/Zr, Ce/Zr, P/Zr and Ce/Y, and low Ti/Zr (Figs 46, 47). However, the third dyke has much higher K/Zr, Nb/Zr and Ti/Zr and lower Sr, Ba/Zr, P/Zr, La/Nb and Ce/Y, and is probably genetically unrelated.

Ultramafic dykes

Spinel-bearing metamorphosed peridotite forms slightly deformed dykes and small plutons (up to 50 m across) at Jetty Peninsula and McLeod Massif. They may be related to the ?Mesoproterozoic serpentinite body described above, but are much less altered. They comprise various proportions of olivine, orthopyroxene and clinopyroxene, with green or rarely brown spinel (3–12%), opaque minerals (magnetite and chromite, 1–4%), and secondary pargasitic amphibole and phlogopite. The texture is polygonal granoblastic. The dykes trend northwest and are clearly discordant to the foliation in the host rocks. The presence of brown spinel suggests that some of the dykes were emplaced under granulite-facies conditions. All the analysed dykes are strongly Ol and Hy-normative, with highly variable Di and Pl (An+Ab), reflecting variable Al_2O_3 contents (3.7–8.8%; Table 13). It is not possible to quantify the chemical effects of alteration, but, if taken at face value, the normative compositions suggest derivation from protoliths ranging from harzburgite to lherzolite and olivine websterite. Compared to the serpentinite body, the dykes have lower normative Ol and higher Hy and, in some cases, Di.

Metadolerite dykes

Metadolerite dykes at **Mount Collins** appear to be younger than those at nearby Fisher Massif, as they intrude 984 ± 7 Ma granitic rocks (Kinny et al. 1997). Two such dykes (71280247, 396) have essentially igneous (intergranular) textures, but contain abundant well-crystallised brown hornblende (~35%), as well as clinopyroxene and altered ?orthopyroxene (5–10%), zoned plagioclase (50–55%), opaque minerals (3–4%),

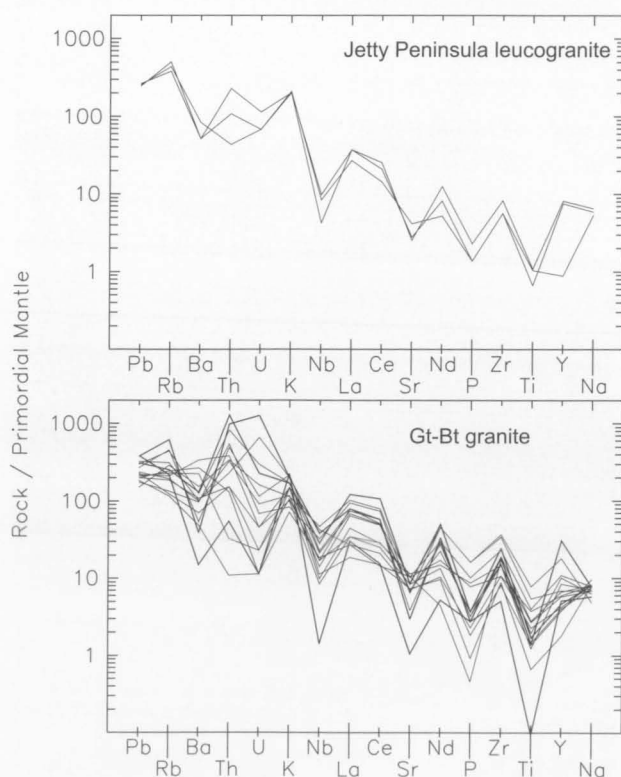


FIGURE 125 Spidergrams for Neoproterozoic garnet-biotite granitoids and Jetty Peninsula leucogranites.

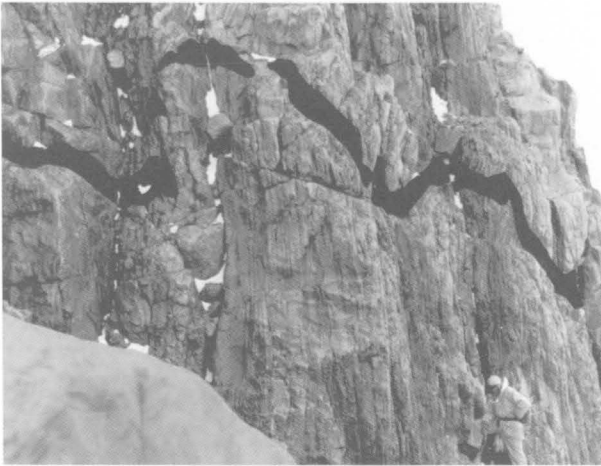


FIGURE 126

Mafic granulite dyke (emphasised in black) with parasitic F_6 folds in a D_6 low-strain zone; Mount Kirkby. The dyke is discordant to the steeply dipping foliation (S_3), which is adjacent to a D_6 high-strain zone.

biotite (2%), and minor apatite (Fig. 128A, B). The well-crystallised hornblende in association with igneous plagioclase suggests crystallisation under relatively high P_{H_2O} conditions. Texturally (although not compositionally), these dykes are somewhat similar to metatholeiites (two-pyroxene + plagioclase \pm hornblende granulites) in Enderby Land considered by Sheraton & Black (1981) to have been emplaced at considerable depths in the crust. A coarser grained dyke at Mount Collins (71280394) contains greenish-brown hornblende (both primary and secondary: 25%), relict pyroxene (predominantly orthopyroxene: 15%), plagioclase (55%), and minor biotite, quartz, opaque minerals, carbonate and cummingtonite.

An intergranular to microgabbroic textured dyke of uncertain age that cuts metamorphic rocks at **Mount Meredith** (71280362) contains quartz (4%), pale orange-brown biotite (4%), well-crystallised colourless cummingtonite (~40%), anorthite (50%), and minor pale green hornblende, opaque minerals, apatite and zircon (Fig. 128C, D). The extremely calcic plagioclase (~ An_{95}) is noteworthy.

Most of the metadolerites from Mount Collins clearly belong to a single distinctive suite, as they have very similar incompatible element abundances and ratios. They are transitional to alkaline olivine dolerites (Figs 43, 44), characterised by low Y/Zr and high Sr, LILE/Zr and, in particular, Nb and Nb/Zr (Figs 45, 46). They differ from the Ruker Terrane metadolerites in being strongly Ol-normative and having higher contents of most incompatible elements, except Pb and Y. They also differ from the Mount Meredith and Mount Willing-Fisher Massif dykes in many of these respects. Much higher Nb/Zr is reflected in positive Nb anomalies on the spidergrams (Fig. 127), suggesting derivation from a distinct ocean-island basalt-type source. Two of the Mount Collins dykes (91286348, 9) show strong enrichment in most incompatible elements, with particularly high Sr, LILE/Zr, Ce/Zr and Ce/Y. However, two dykes (91286345, 6) do not share the Nb enrichment typical of the other dykes (Table 13; Figs 45, 46, 127). It is apparent

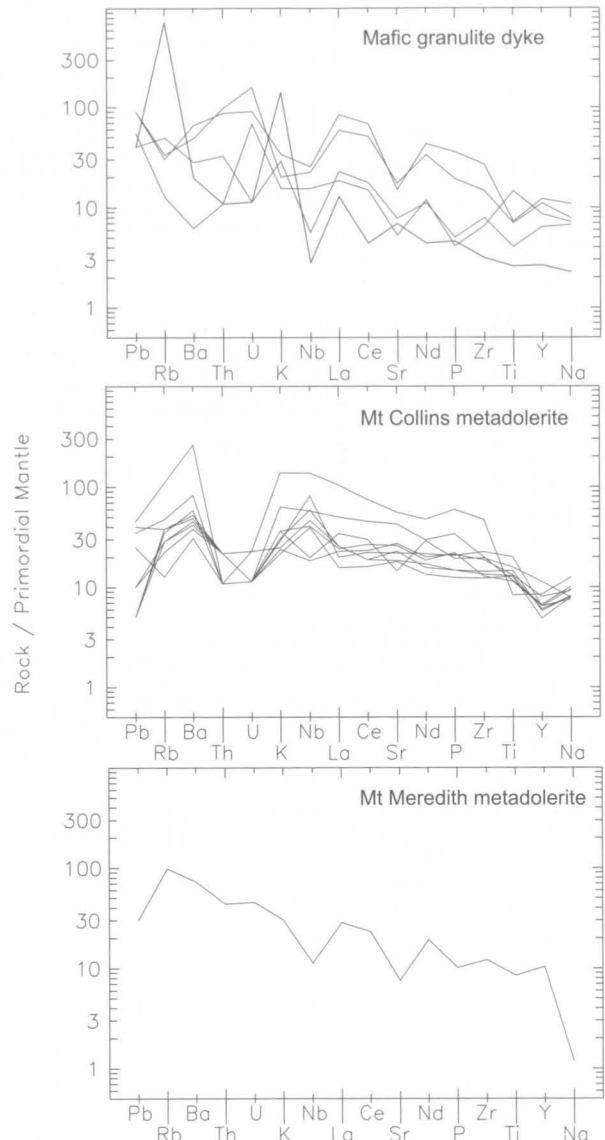


FIGURE 127

Spidergrams for mafic dykes of the Beaver-Lambert Terrane.

that even related dykes from a small area can show considerable compositional variations.

In contrast to those from Mount Collins, the Mount Meredith metadolerite dyke is strongly Q and Hy-normative (Table 13), reflecting its extremely low Na_2O content (0.46%) which is presumably a metamorphic feature. Of all the mafic dykes of probable Proterozoic age in the Beaver-Lambert Terrane, this dyke has the closest chemical similarity to the Ruker Terrane metadolerites, but it is more enriched in LILE (especially Rb and Ba) and has higher LILE/Zr and Ce/Zr (Fig. 46). Although it is possible that most of these differences could be due to the effects of high-grade metamorphism, which commonly affects mainly LILE and Th (Sheraton 1984), it is much more likely that this dyke is unrelated and was emplaced during the waning stages of the Neoproterozoic event. As indicated above, textures of the post-980 Ma Mount Collins metadolerites would also be consistent with this interpretation. Similar relationships have been noted for Palaeoproterozoic tholeiites emplaced at considerable crustal depths during the waning stages of granulite-facies

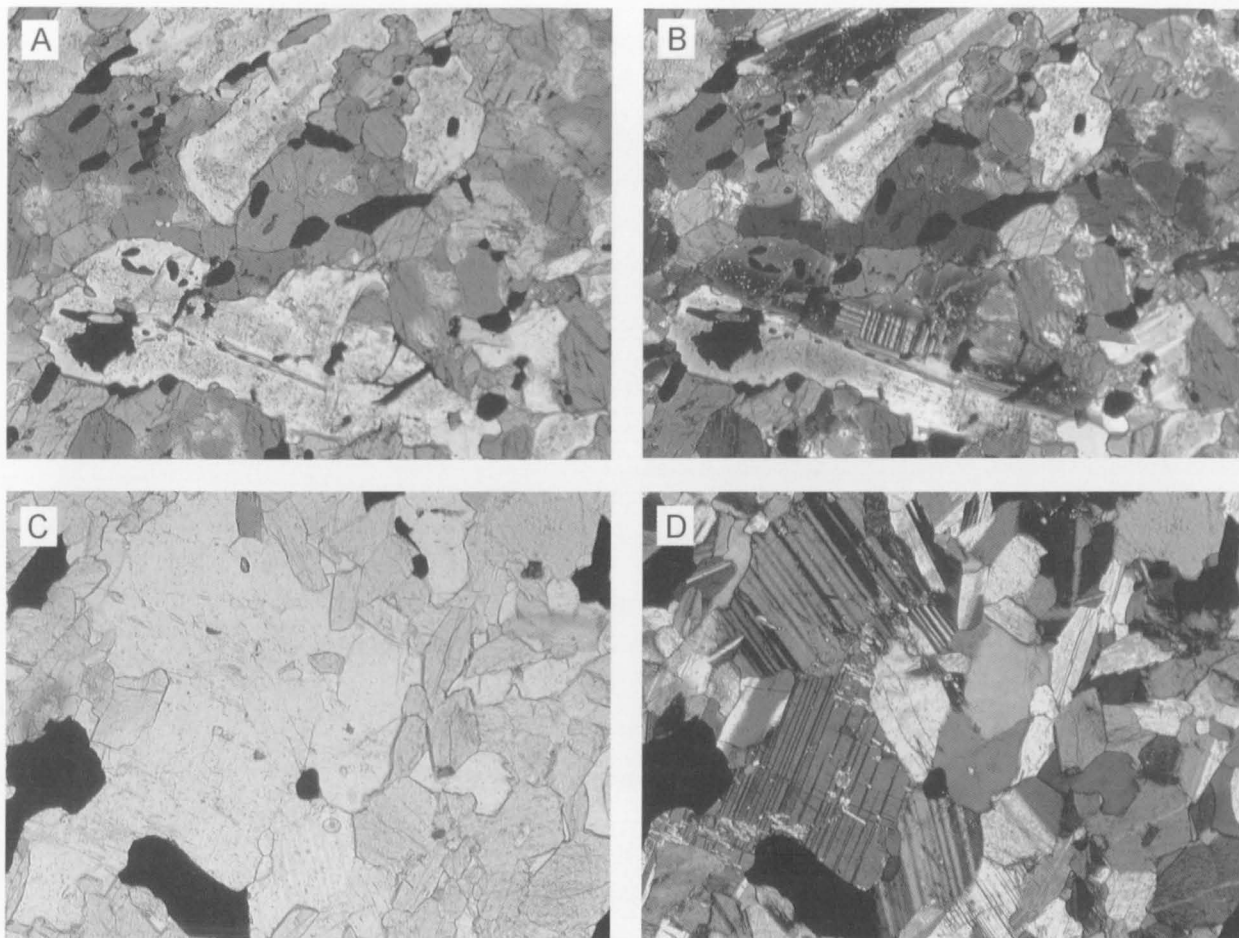


FIGURE 128

Metadolerite dykes. (A, B) Metadolerite with intergranular texture containing dark greenish-brown hornblende, zoned igneous plagioclase, and minor altered pyroxene, biotite and opaque minerals; Mount Collins. Sample 71280247. (C, D) Metadolerite comprising colourless cummingtonite, anorthite and minor quartz and pale orange-brown biotite; Mount Meredith. The texture is intergranular, tending to granuloblastic, and the dyke may have crystallised relatively deep in the crust during the waning stages of high-grade metamorphism. Sample 71280362. Cross-polarised light in B and D; width of field: 1.2 mm.

PHANEROZOIC IGNEOUS ROCKS

EARLY PALAEOZOIC GRANITOIDS

Hornblende–biotite granite of the eastern Amery Ice Shelf

A large (at least 15 km across) pluton of hornblende–biotite granite (Landing Bluff Adamellite of Tingey 1981) crops out around **Landing Bluff** at the eastern corner of the Amery Ice Shelf (Fig. 2). It has given a Rb–Sr whole-rock isochron age of 493 ± 17 Ma (Tingey 1991a) and a U–Pb zircon age of about 500 Ma (Sheraton & Black 1988). The granite is a massive medium- to coarse-grained pinkish-grey rock with conspicuous poikilitic K-feldspar phenocrysts up to six centimetres long. It contains xenoliths of hornblende–biotite granodiorite and hornblende+biotite-rich segregations, and is cut by white even-grained biotite granite (aplite) and pegmatite dykes. Major constituents are dark greenish-brown potassian ferro-pargasite or ferro-pargasitic hornblende (*mg* 17–18; up to 5%), dark brown biotite (*mg* 25–27; 3–10%), quartz (25–35%), oligoclase–andesine (An_{34-45} ; 20–35%), and microcline perthite (30–50%). Biotite and amphibole have moderate F contents (1.3–1.6% and ~0.7%, respectively). A distinctive, relatively abundant accessory mineral suite comprises magnetite, ilmenite, apatite, zircon, fluorite, metamict allanite, and metamict chevkinite or perrierite ($(CaCeTh)_4(FeMg)_2(TiFe)_3Si_4O_{22}$), as well as traces of pyrite and chalcopyrite. The texture is hypidiomorphic to allotriomorphic granular. A sample from Collins Nunatak, eight kilometres south of Landing Bluff, has even more Fe-rich mafic minerals (potassian ferro-pargasite, *mg* 5–6; biotite, *mg* 7).

Biotite–hornblende granite in the **Polarforschung Glacier** area (Polarforschung Granite of Tingey 1981), about 50 kilometres east of Landing Bluff, is probably of similar age. It differs in being relatively leucocratic and in containing minor fayalite (Fe_{3-4}), together with potassian ferro-pargasitic hornblende (*mg* 17–24) and biotite (*mg* 13–23). Similar porphyritic biotite and hornblende–biotite granite also crops out at **Corry Rocks** near the northern end of Gillock Island. One sample contains about one percent of euhedral largely metamict allanite crystals up to five millimetres long. More even-grained biotite granite, which occurs as veins and concordant sheets at **New Year Nunatak**, contains accessory allanite and may be genetically related. The intrusive suite thus extends for at least 150 kilometres (and possibly 200 km if the New Year Nunatak granites are included) along the Prydz Bay Coast and eastern side of the Amery Ice Shelf.

These K-rich (Fig. 129), slightly peraluminous (Fig. 130) granites have a fairly wide range of composition

(65.7–76.9% SiO_2), but their generally similar chemical characteristics suggest that they form a closely related, although not comagmatic, group. They have low *mg* (~6–30.6) and Na_2O , and are enriched in LILE, HFSE (especially Zr) and, in particular, LREE (Table 18; Fig. 131); $10^4 Ga/Al$ (2.6–3.4) and Zn/Fe are relatively high. However, there are consistent compositional differences between individual intrusions. For example, the Landing

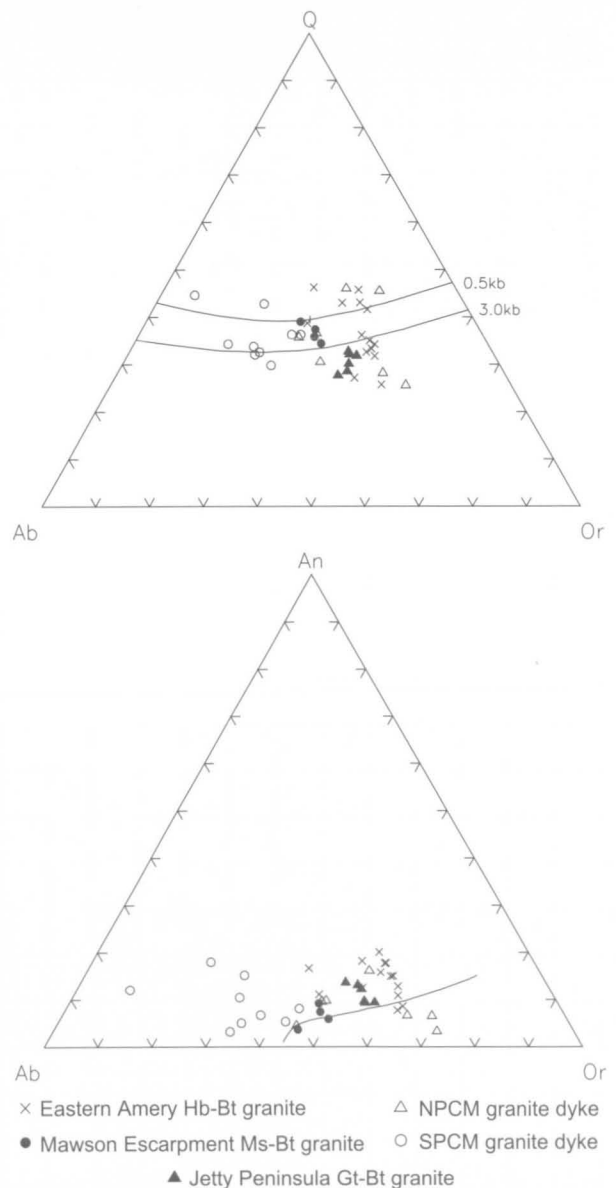


FIGURE 129

Normative Q–Ab–Or and Ab–Or–An diagrams for early Palaeozoic granitic rocks.

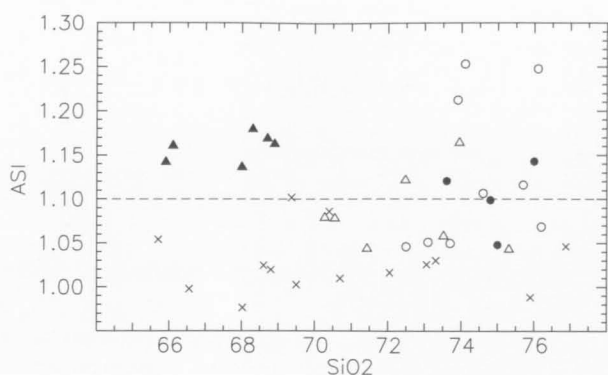


FIGURE 130
Plot of ASI against SiO_2 for early Palaeozoic granitic rocks. Symbols as in Figure 129.

Bluff body has higher F (2000–2700 ppm) and *mg* and lower Ga/Al than the more evolved granite in the Polarforschung Glacier area. Spidergrams are highly irregular, and very similar, except for one granite from New Year Nunatak which has relatively low P_2O_5 , Zr and Y, and may be unrelated (Fig. 132). REE are strongly fractionated ($(\text{La}/\text{Yb})_n$ 32.1–49.5, $(\text{Ce}/\text{Y})_n$ 15.2–41.0), with moderate to large negative Eu anomalies, although sample 69280171 from Collins Nunatak has less fractionated REE ($(\text{La}/\text{Yb})_n$ 13.4; Fig. 133). Such chemical features are typical of A-type granitoids, derived by melting of near-anhydrous granulite-facies lower crustal rocks (Sheraton & Black 1988). High Th/U (12–93 by XRF, 19–47 for five

samples by INAA) is consistent with such a source. However, F contents are extremely variable, suggesting either secondary redistribution or that high-F source rocks are not essential for formation of A-type magmas (cf. Collins et al. 1982; Whalen et al. 1987).

Muscovite–biotite granite stocks

Numerous small stocks of grey, relatively even-grained muscovite–biotite granite crop out in the **central Mawson Escarpment**. These rocks form a dense network of veins, with the largest exceeding 100 metres across, and collectively form more than 60 percent of the outcrop area. Similar stocks of muscovite granite, one to two kilometres across, also occur elsewhere in the SPCM—for example, at **Mount Stinear**. They appear to be the largest Cambrian (or latest Neoproterozoic) intrusives in the PCM. The central Mawson Escarpment granite has given a Rb–Sr whole-rock isochron age of 551 ± 74 Ma (Tingey 1991a). It contains rafts and xenoliths of metasediments up to 100 metres thick, and is cut by white leucogranite and associated pegmatite bodies with biotite, muscovite and garnet. The granite comprises muscovite (up to 2%), reddish-brown biotite (1–5%), quartz (30–35%), zoned oligoclase–albite (20–30%), microcline (35–45%), and minor opaque minerals, apatite, zircon, monazite and secondary chlorite.

The Mawson Escarpment granites have near-minimum melt compositions (Fig. 129). They are significantly peraluminous (ASI 1.05–1.14) (Fig. 130), although not to

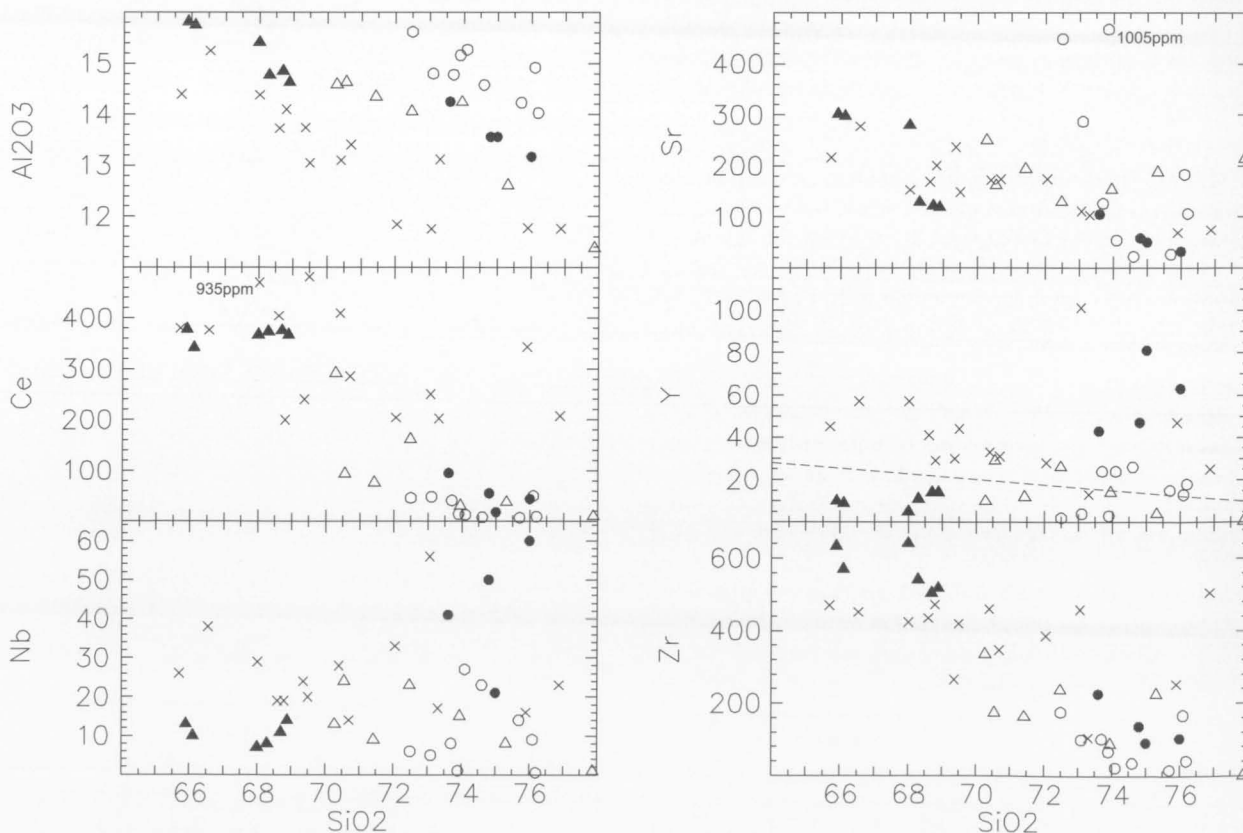


FIGURE 131
 SiO_2 variation diagrams for early Palaeozoic granitic rocks. Symbols as in Figure 129. A dashed line on Y– SiO_2 plot indicates the approximate boundary between Y-depleted and Y-undepleted felsic orthogneisses (Sheraton & Black 1983).

TABLE 18. Chemical analyses and CIPW norms of representative early Palaeozoic granitic intrusive rocks.

Sample no.	81285376	81285399	69280171	73282122	618E	669A	71280307	71280325	72280846	73281337
Locality	Landing Bluff	Meknattane Nunataks	Collins Nunatak	C Mawson Escarpment	Jetty Peninsula	Jetty Peninsula	Armonini Nunatak	Mount Gleeson	Mount Dummett	Mount McCauley
Lithology	Hb-Bt granite	Ol-Hb-Bt granite	Porphyritic Hb-Bt granite	Ms-Bt granite	Porphyritic Bt granite	Bt granite	Porphyritic Bt granite dyke	Bt granite dyke	Bt-Ms granite vein	Bt-Ms granite vein
SiO ₂	68.60	75.90	73.06	74.80	68.30	65.90	70.55	70.28	75.70	74.10
TiO ₂	0.85	0.25	0.40	0.14	0.78	0.93	0.31	0.37	0.02	0.06
Al ₂ O ₃	13.73	11.77	11.75	13.56	14.77	15.82	14.64	14.59	14.23	15.27
Fe ₂ O ₃	0.77	1.21	0.80	0.14	0.56	0.48	0.63	0.56	0.03	0.28
FeO	3.39	1.41	3.12	1.45	2.70	3.07	1.76	1.30	0.25	0.85
MnO	0.05	0.02	0.05	0.05	0.02	0.02	0.05	0.02	0.01	0.02
MgO	0.53	<0.10	0.23	0.12	0.76	0.88	0.61	0.53	0.09	0.13
CaO	2.29	1.14	1.52	0.98	1.47	2.11	1.58	1.15	0.67	0.79
Na ₂ O	2.08	2.00	2.23	3.25	2.58	2.86	3.33	2.35	4.90	3.80
K ₂ O	6.04	6.14	4.89	4.93	5.71	5.44	5.30	7.39	3.63	4.38
P ₂ O ₅	0.30	0.04	0.11	0.05	0.24	0.24	0.21	0.18	0.19	0.10
H ₂ O ⁺	0.70	0.51	-	0.44	0.92	0.90	-	-	0.40	0.74
LOI	-	-	0.80	-	-	-	0.88	0.81	-	-
Rest	0.56	0.22	0.33	0.15	0.43	0.61	0.24	0.41	0.05	0.07
Total	99.89	100.61	99.29	100.06	99.33	99.31	100.09	99.94	100.17	100.59
O=F,S,Cl	0.08	0.00	0.00	0.00	0.01	0.01	0.01	0.00	0.00	0.00
Total	99.81	100.61	99.29	100.06	99.32	99.30	100.08	99.94	100.17	100.59
Q	26.59	37.97	36.04	33.79	26.36	21.59	26.15	24.97	32.08	33.05
C	0.33	-	0.29	1.22	2.25	1.97	1.06	1.07	1.48	3.08
Or	35.69	36.28	28.90	29.13	33.74	32.15	31.32	43.67	21.45	25.88
Ab	17.60	16.92	18.87	27.50	21.83	24.20	28.18	19.89	41.46	32.15
An	9.40	5.00	6.82	4.54	5.72	8.90	6.47	4.53	2.08	3.27
Di	-	0.35	-	-	-	-	-	-	-	-
Hy	5.60	1.03	5.07	2.71	5.14	5.93	3.81	2.67	0.64	1.59
Mt	1.12	1.75	1.16	0.20	0.81	0.70	0.91	0.81	0.04	0.41
Il	1.61	0.47	0.76	0.27	1.48	1.77	0.59	0.70	0.04	0.11
Ap	0.71	0.09	0.26	0.12	0.57	0.57	0.50	0.43	0.45	0.24
Li	16	7	25	-	25	37	30	12	-	-
Be	4	2	6	-	-	-	5	3	-	-
F	2000	80	-	-	-	-	-	-	-	-
S	-	-	50	-	300	300	140	60	-	-
Sc	7.9	3.3	15.4	-	3.0	6.0	5.0	3.0	-	-
V	32	4	4	4	30	50	15	11	<1	<1
Cr	10	<3	9	<3	3	5	4	1	<3	<3
Ni	5	<2	<1	3	3	3	3	3	<2	<2
Cu	7	9	14	<2	5	5	2	1	4	<2
Zn	87	52	90	42	135	136	44	35	27	44
Ga	20	18	21	22	23	26	17	17	21	30
Rb	278	239	218	402	315	316	287	295	216	245
Sr	169	69	111	58	129	302	162	251	26	54
Y	41	47	101	47	11	10	29	10	15	24
Zr	436	253	458	137	542	634	174	336	16	22
Nb	19	16	56	50	8	13	24	13	14	27
Sn	<1	<1	4	12	-	-	4	<2	1	9
Cs	-	-	0.9	-	-	-	7.0	17.0	-	-
Ba	901	268	881	318	1079	2542	776	1614	32	63
La	208	171	144	27	195	249	51	156	<2	4
Ce	404	343	250	55	373	378	94	291	7	13
Nd	159	142	115	-	140	109	32	102	-	-
Pb	50	33	37	53	117	87	56	74	71	65
Th	115	93	29	45	206	53	56	146	3	4
U	3.1	2.0	1.5	13.0	5.5	3.5	8.0	3.5	3.0	5.5
K/Rb	180	213	186	102	150	143	153	208	140	148
(Ce/Y) _n	24.6	18.2	6.2	2.9	85	95	8.1	73	1.2	1.4
Th/U	37	47	19	3.5	37	15	7.0	42	1.0	0.7
Nb/Nb*	0.10	0.10	0.41	0.65	0.05	0.07	0.26	0.07	-	0.46
Sr/Sr*	0.05	0.02	0.05	-	0.04	0.10	0.21	0.10	-	-
mg	21.8	<11	11.6	12.9	33.4	33.8	38.2	42.1	39.1	21.4

mg = atomic 100Mg/(Mg +Fe²⁺).

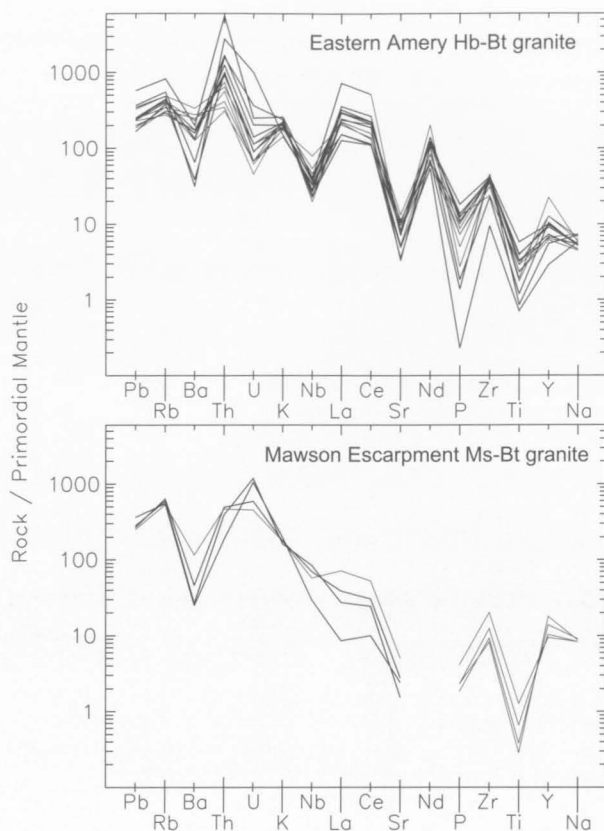


FIGURE 132
Spidergrams for early Palaeozoic granites from the eastern Amery Ice Shelf and Mawson Escarpment.

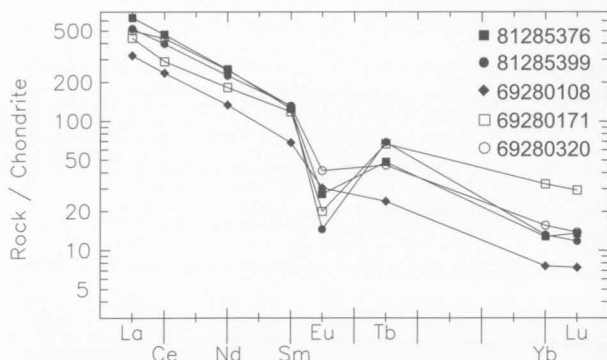


FIGURE 133
Chondrite-normalised rare-earth element abundance plots for early Palaeozoic granites from the eastern Amery Ice Shelf.

the extent that they can definitely be classified as S-type. However, the presence of muscovite, monazite and associated garnet-bearing granite bodies is consistent with a major sedimentary component in their source. High Nb, Y and $10^4\text{Ga}/\text{Al}$ (2.8–3.6) and low mg (5.6–23.9) suggest A-type affinities, although LREE are low (Table 18; Fig. 131). REE are unfractionated to moderately fractionated ($(\text{Ce}/\text{Y})_n$ 0.6–5.5, average 2.3). They differ from the eastern Amery A-type granites in having much higher U and Sn, lower Th/U, and highly fractionated spidergrams without significant Nb anomalies (Fig. 132), suggesting an unusually Nb-rich source. The widespread Archaean biotite–hornblende granite gneiss of the SPCM also has

unusually high Nb and Y, and, in theory, would be a suitable source. However, the young average $T_{\text{UR}}^{\text{Sr}}$ model age (1067 Ma) and relatively peraluminous compositions of the Mawson Escarpment granites are not consistent with this.

Minor intrusions

Smaller, but probably related, post-metamorphic (i.e., essentially undeformed; post- D_6 in the Beaver-Lambert Terrane) granite dykes, veins and other small bodies occur at many places in the PCM, and are commonly associated with granitic pegmatites.

Fine- to medium-grained leucogranite bodies, as well as pegmatites, intrude Archaean to ?Mesoproterozoic metamorphic rocks of the Ruker Terrane in the SPCM (Figs 134, 135), notably near the Fisher Glacier at Mounts Dummett, Mather, McCauley and Scherger. They commonly contain both muscovite (up to 8%) and biotite (up to 5%), as well as quartz (30–40%), microcline (15–40%), sericitised albite–oligoclase (25–50%), and minor opaque minerals, apatite, zircon and monazite; small amounts of beryl, garnet and tourmaline may be present. Pegmatites also contain topaz, chalcophyrite, magnetite, Nb–Ta minerals and fluorite (Ivanov & Kamenev 1990). Greisenisation and albitisation are common autometamorphic processes. The compositional diversity of these granites appears to reflect the country rock compositions, suggesting a local derivation.



FIGURE 134
Interlayered biotite–quartz–feldspar gneiss, leucogneiss, amphibolite and minor calc-silicate gneiss cut by small stocks and veins of Cambrian granite; southwestern Mount Borland.

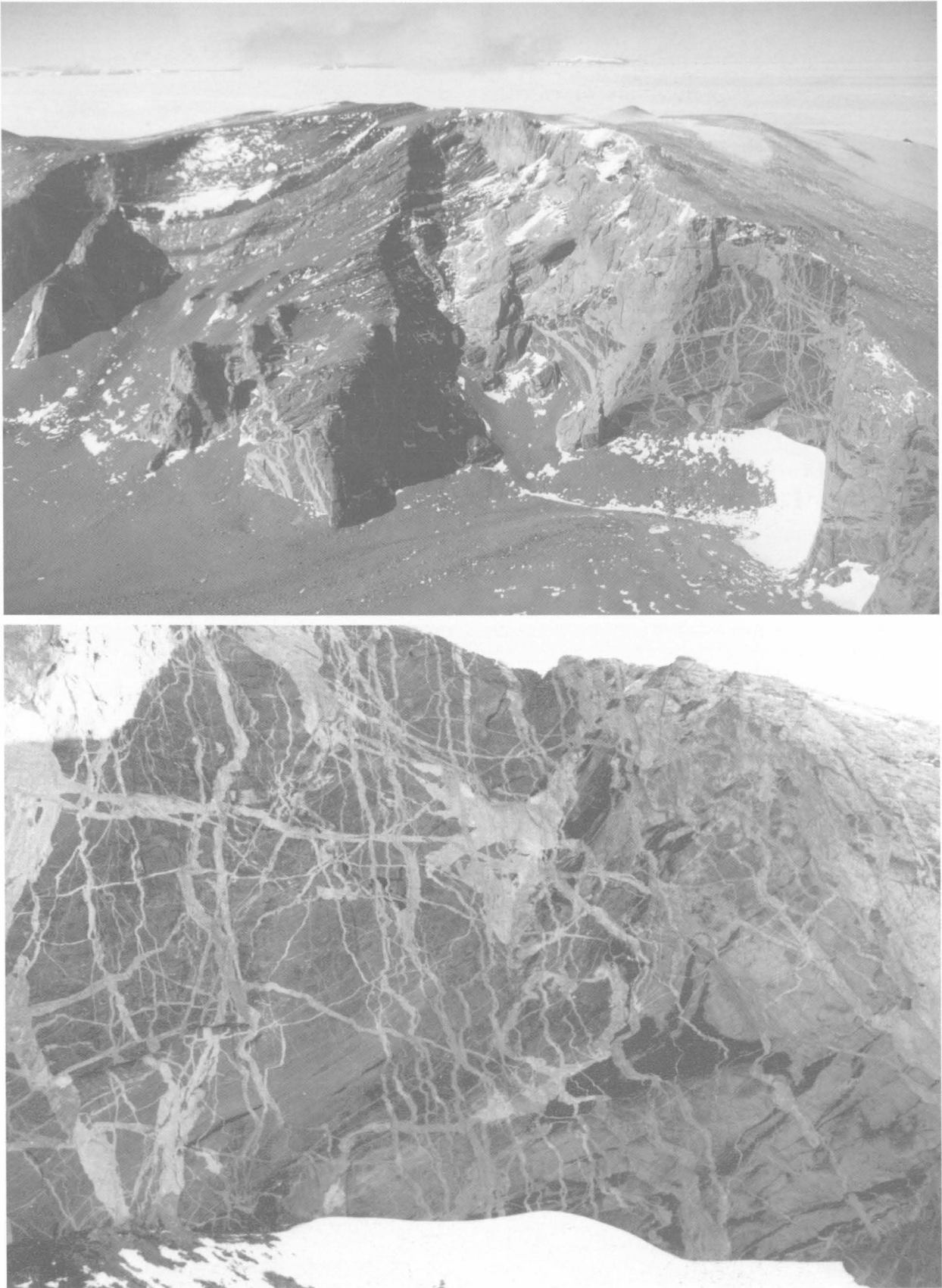


FIGURE 135

Interlayered felsic hornblende–biotite gneiss, metapelitic schist, mica quartzite and amphibolite cut by a dense network of Cambrian granite and pegmatite dykes, shown in detail in lower photograph; northwestern tip of Mount McCauley. The cliffs are about 500 m high.



FIGURE 136

Pegmatite vein intruded along a ductile shear zone (D7); Carter Peaks. Note the ice axe for scale.

Dykes and veins in the Beaver-Lambert Terrane are typically biotite granite and garnet-biotite granite, locally with secondary muscovite and chlorite. However, some of those in the Nemesis Glacier area, which appear to cut D_6 structures, contain orthopyroxene (Fitzsimons & Thost 1992). They form both planar dykes and more irregular bodies up to three metres wide, and are generally unfoliated. Porphyritic and non-porphyritic garnet-biotite granite bodies crop out at Else Platform, on Jetty Peninsula (Manton et al. 1992); the former variety contains finely perthitic, simply twinned K-feldspar phenocrysts. Both varieties are cut by pegmatitic segregations with biotite and garnet, and have a steeply dipping, indistinct foliation that may result from flow, although Hand et al. (1994a) suggested that apparently equivalent migmatitic granite dykes were emplaced along active shear zones. Apatite, zircon and monazite are ubiquitous accessories.

Coarse-grained quartz-K-feldspar-plagioclase \pm biotite \pm muscovite \pm magnetite pegmatites in the NPCM are typically less than one metre wide. They truncate all regional fabrics and are generally planar, although some are more irregular (Fitzsimons & Thost 1992). They range from sub-horizontal to near-vertical, and intrude locally along ductile shear zones (Fig. 136). Mylonite zones are commonly sub-parallel to pegmatite bodies, and occasionally occur within them. Pegmatites on Jetty Peninsula contain a diverse suite of accessory minerals, including tourmaline, zircon, monazite, arsenopyrite, molybdenite, beryl and chrysoberyl; pegmatite at Carter Peaks contains sillimanite, tourmaline and dumortierite (Fitzsimons & Thost 1992; Manton et al. 1992). Manton et al. (1992) also reported cummingtonite aggregates, probably after orthopyroxene, in pegmatites on Jetty Peninsula. Following Sandiford (1985), they also suggested that the occurrence of Be, B and Nb-bearing minerals in NPCM pegmatites implies melting of underlying rocks that had not been affected by granulite-facies metamorphism. Near-vertical north-striking quartz veins crop out at Mounts Butterworth (Fig. 137) and Creighton, as well as Else Platform (Hand et al. 1994a; Shulyatin 1995). Those at Mount Creighton cut late pegmatites and mylonite zones. They may be related to late epidote-rich veins of similar orientation at Mount Butterworth, which are associated with greenschist-facies metamorphism in adjacent gneiss (Fitzsimons & Thost 1992).

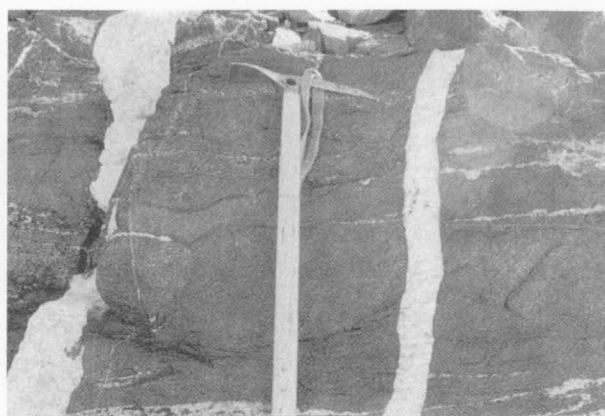


FIGURE 137

Vertical quartz veins; Mount Butterworth.

Muscovite and biotite Rb-Sr ages, mainly from the SPCM, are mostly between 470 and 530 Ma (Tingey 1991a), suggesting emplacement during the early Palaeozoic Ross orogeny. Dykes and veins of garnet-biotite granite at Jetty Peninsula have given poorly-defined zircon U-Pb ages of about 565 and 524 Ma, whereas Rb-Sr isochron ages are somewhat younger (480 ± 13 , 483 ± 12 Ma), possibly due to resetting associated with pegmatite emplacement (Manton et al. 1992). It is noteworthy that U-Pb dating of zircon and monazite from some granites and pegmatites in the Mesoproterozoic Rayner Complex of western Enderby Land, which have also given early Palaeozoic Rb-Sr isochron and mineral ages, indicate much older (~ 770 Ma) emplacement ages (Black et al. 1987). Hence, it is possible that some 'late' granites in the PCM are Neoproterozoic rather than early Palaeozoic.

Late dykes and veins in the NPCM are predominantly K-rich, siliceous granites, and most are only slightly peraluminous (Table 18; Figs 129, 130). They do not show extreme fractionation, as the majority are not particularly depleted in Ba and Sr and have moderate *mg* (31.4–45.5). LILE and HFSE vary considerably (Fig. 131), and some dykes are quite depleted; many have high Th (average 49 ppm) and U (average 5.3 ppm), but Th/U is also high (average 9.4). Spidergrams show negative Nb, Sr, P and Ti anomalies and variable Y depletion (Fig. 138); $(Ce/Y)_n$ ratios are highly variable (1–73).

Garnet-biotite granite dykes and veins at Jetty Peninsula are relatively low in SiO_2 (65.9–68.9%; Fig. 131) and have high Th (53–206 ppm), U (3–9 ppm), Zr (506–642 ppm), LREE (Ce 342–378 ppm), and $10^4 Ga/Al$ (2.8–3.1). The more evolved porphyritic variety differs from the non-porphyritic in containing more Th and U and less Ba and Sr (Fig. 138). They are markedly peraluminous (ASI 1.14–1.18; Fig. 130), suggesting a largely metasedimentary source (consistent with the presence of garnet and monazite). However, very high Zr, LREE and Ga/Al suggest A-type affinities (Manton et al. 1992), in common with many other late to post-orogenic granitoids in this part of East Antarctica (Sheraton & Black 1988; Sheraton et al. 1996).

Muscovite-biotite granite dykes in the SPCM are compositionally quite distinct from those of the NPCM, being much more sodic (Table 18; Fig. 129). Al_2O_3 contents are relatively high (Fig. 131) and many are

markedly peraluminous (ASI 1.05–1.21; Fig. 130). As in the NPCM dykes, LILE and HFSE show considerable variation, but LREE are generally lower (Fig. 131); $(\text{Ce}/\text{Y})_n$ ranges from 1 to 58, with some samples having unfractionated REE. U (average 3.2 ppm) and particularly Th (average 11.2 ppm) are lower than in the NPCM dykes, so that Th/U (average 3.5) is significantly lower, similar to that of estimated average crust (~3.8; Taylor & McLennan, 1985) and consistent with melting of lower-grade (mainly amphibolite-facies) metamorphic rocks. Spidergrams are very irregular, and show extremely variable degrees of Sr and Y depletion (Fig. 138). The reasons for the distinctive compositions of these dykes are unclear, but they may

partly reflect the relatively sodic compositions of many Archaean country rocks. Melting under higher $\text{P}_{\text{H}_2\text{O}}$ conditions would also produce liquids with lower Or/Ab (Ebadi & Johannes 1991).

PALAEOZOIC MAFIC DYKES

In contrast to the Ruker Terrane, mafic dykes are rare in the Mesoproterozoic to early Neoproterozoic Beaver-Lambert Terrane, although significant numbers crop out in the Jetty Peninsula area. The dykes described in this section form a petrologically and chemically heterogeneous group, although the majority have alkaline affinities. They commonly show extensive deuteric alteration, but are unmetamorphosed and hence post-date the c.1000 Ma tectonothermal event; those dated have yielded a range of Palaeozoic ages (Table 25; Sheraton 1983).

Lamproite dykes

A three to four metre-thick, east-west-trending lamproite dyke crops out at **Mount Rubin**, in the SPCM. It is a massive fine-grained, dark greenish-grey rock with abundant small rounded grains of K-feldspar and a few large (0.3–1.0 cm) felsic ocelli. The rock consists of K-feldspar (40 %), alkali amphibole (25–30%), phlogopite (20–25%), and opaque minerals (up to 5%). Accessory apatite, zircon and titanite make up about two to three volume percent. Phenocrysts comprise olivine and alkali amphibole. Secondary minerals (sericite, chlorite and carbonate) constitute up to five percent of the rock.

K-feldspar occurs as rounded, pseudohexagonal, or more rarely elongated grains, 0.1–0.8 millimetres across. It is characterised by an inhomogeneous, sieve-like texture, and was probably formed by replacement of leucite at a late-magmatic stage. Opaque mineral inclusions are abundant within some inner zones. The unit cell parameters of the feldspar ($a = 8.595 \pm 0.003 \text{ \AA}$, $b = 13.033 \pm 0.002 \text{ \AA}$, $c = 7.207 \pm 0.003 \text{ \AA}$, $\beta = 116.05 \pm 0.03^\circ$) indicate sanidine. The sanidine has very low $^{87}\text{Sr}/^{86}\text{Sr}$ (0.702) and Rb/Sr (0.002), which are presumably features of the mantle source (Mikhalsky et al. 1994b). It is partly replaced by microcline that probably formed at the subsolidus stage. Small flakes and aggregates, 0.1–0.3 millimetres across, of randomly oriented high-Ti phlogopite (TiO_2 9–10%, *mg* 73–75) partly fills interstices between the sanidine grains. The phlogopite is compositionally similar to that in the West Kimberley wolgidites (Mitchell 1985). Fibrous aggregates of brownish-green (with a bluish tinge) amphibole make up the remainder of the groundmass. The amphibole comprises low-Ti potassic varieties of ferrichterite and magnesian arfvedsonite, similar to lamproitic amphiboles (Mitchell 1985), but is much lower in TiO_2 (1–2%) and has higher total FeO (20–27%) and Na_2O (4.6–5.7%). The grains are zoned, with cores enriched in MgO (*mg* 52–55) and Na_2O , and rims enriched in FeO (*mg* 28–39) and TiO_2 and depleted in Na_2O (Mikhalsky et al. 1994b).

The ocelli are made up of coarse-grained aggregates of carbonate, opaque minerals, barite, chlorite, nepheline, alkali feldspar and plagioclase in various proportions. Their outer zones, up to 0.5 millimetre thick, are distinguished by a brown colouration caused by the development of fine-grained unidentified minerals. The

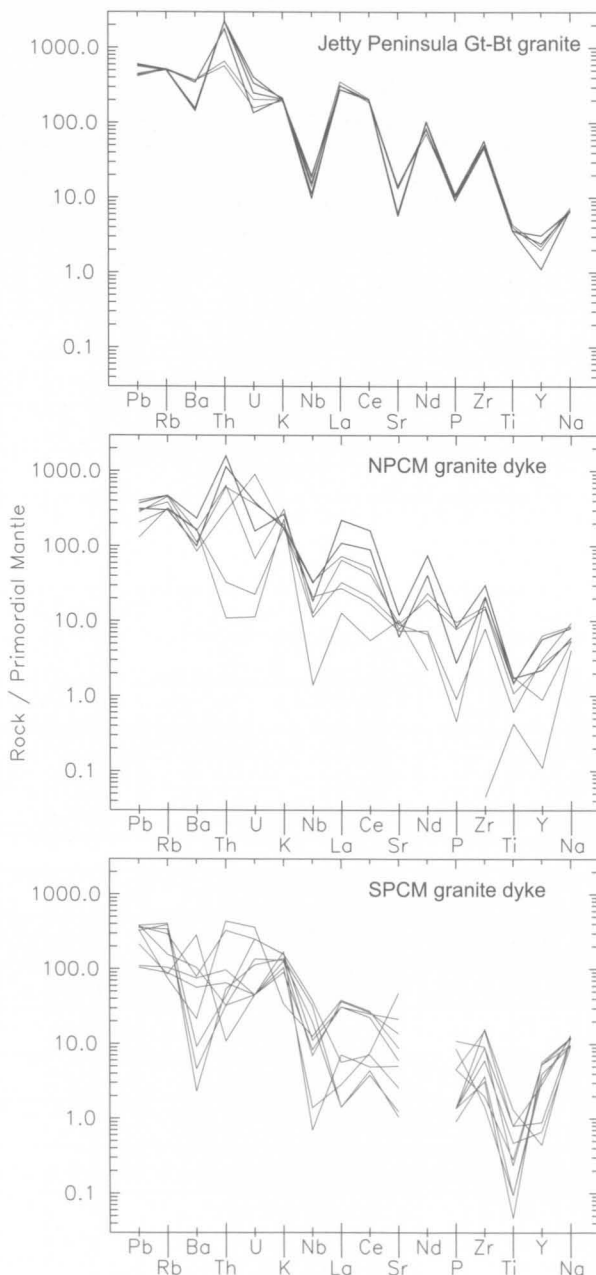


FIGURE 138

Spidergrams for early Palaeozoic granite from Jetty Peninsula and granite dykes from the NPCM (in the Beaver-Lambert Terrane) and SPCM (mostly in the Ruker Terrane).

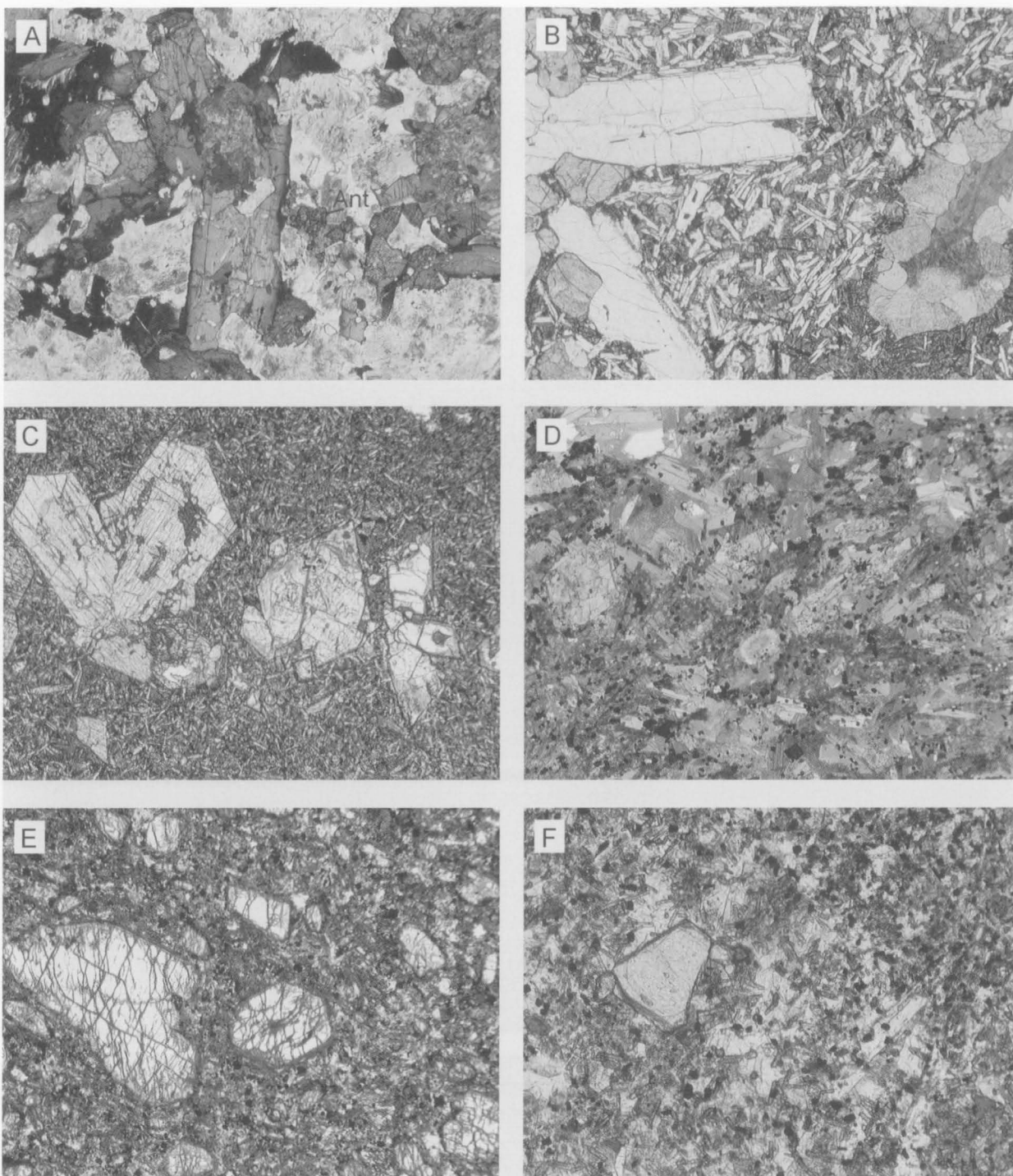


FIGURE 139

Phanerozoic alkaline mafic rocks. (A) Lamproite dyke containing microcline, amphibole (pink to yellow K-richichterite and pink or yellow to dark blue or green K-arfvedsonite), and minor phlogopite, apatite and anatase (Ant: 2.5%); Mount Bayliss. Sample 73281545; width of field: 4 mm. (B) Basaltic andesite dyke comprising phenocrysts of andesine-labradorite and clinopyroxene (with cores of orthopyroxene) in a well-crystallised groundmass of clinopyroxene, plagioclase, Fe-Ti oxides and carbonate (in ocelli, right); Taylor Platform. Sample 71280126; width of field: 4 mm. (C) Basanite dyke with partly altered olivine (right) and zoned augite-salite (left) phenocrysts in a partly altered groundmass of clinopyroxene, plagioclase, alkali feldspar, reddish-brown amphibole, and minor ilmenite; Mount Kirkby. Sample 71280007; width of field: 4 mm. (D) Polzenite sill comprising olivine (partly altered to serpentine, talc and carbonate), phlogopite, melilite (largely replaced by cebollite and juanite), and nepheline, with smaller amounts of clinopyroxene, ilmenite, magnetite, pyrite, perovskite, apatite and carbonate; Radok Lake. Sample 69280153; width of field: 4 mm. (E) Lamprophyre dyke with partly altered olivine phenocrysts in an altered fine-grained groundmass of phlogopite, pale brown amphibole, carbonate and opaque minerals; Mount Meredith. Sample 91286414; width of field: 4 mm. (F) Tephritic phonolite lava containing olivine microphenocrysts, clinopyroxene, alkali feldspar, reddish-brown biotite, and Fe-Ti oxides; Fox Ridge. Sample 71280140; width of field: 1.2 mm.

ocelli are generally rounded, with complex reticulated outlines. Small angular fragments of the same composition were also found, suggesting that the ocelli represent reworked country rock fragments. However, the low $^{87}\text{Sr}/^{86}\text{Sr}$ ratio of plagioclase (0.7048) does not support this suggestion (Mikhalsky et al. 1994b). Sheraton & England (1980) argued for the formation of similar ocelli through silicate liquid immiscibility.

The compositions of minerals from the Mount Rubin lamproite indicate crystallisation from an evolved melt at low pressure and temperature (Mitchell 1985), but the petrographic features suggest that crystallisation did not occur entirely after magma emplacement. Strong zoning of amphibole is consistent with a high degree of melt fractionation. Crystallisation of arfvedsonitic amphibole may be the result of relatively low temperatures (below 725°C) and oxygen fugacities during fractionation of the melt (Ernst 1962).

The compositions of bulk-rock and mineral separates (microcline and phlogopite) define a Rb–Sr isochron corresponding to an age of 461 ± 23 Ma (Sr_i 0.716). This date may reflect igneous crystallisation or autometamorphic (deuteric) alteration, which was accompanied by the formation of the microcline, but either way, probably approximates the emplacement age. $T_{\text{DM}}^{\text{Nd}}$ model ages for two samples are 1270 and 1330 Ma, which may be interpreted as the time of mantle enrichment processes corresponding to the major crust formation event in the Fisher (and possibly the Beaver-Lambert) Terrane.

A five metre-thick lamproite (alkali melasyenite of Sheraton & England 1980) dyke at **Mount Bayliss** contains microcline (50%), amphibole (pink to yellow K-richterite and pink or yellow to dark blue or green K-arfvedsonite, 40%), phlogopite (3%), apatite (3%), pale blue anatase (2.5%), and minor magnetite, zircon and calcite (Fig. 139A). K-richterite has given Silurian K–Ar ages of 413 and 414 ± 10 Ma, and K-arfvedsonite 430 ± 12 Ma (Sheraton & England 1980). A sample collected from nearby moraine (R11370) is petrographically similar but much finer grained, apparently representing a chilled margin or shallower level intrusion. It contains more phlogopite (13%), less amphibole (17%), and minor ilmenite. As in the Mount Rubin dyke, rounded to subhexagonal aggregates of turbid K-feldspar, 0.05 to 0.4 millimetres across, may represent altered leucite. Larger (up to 6 mm) coarser grained ocelli, containing quartz, K-feldspar, calcite, zircon, anatase and minor K-arfvedsonite, suggest liquid immiscibility.

The Mounts Bayliss and Rubin lamproites are peralkaline rocks, with very high $\text{K}_2\text{O}/\text{Na}_2\text{O}$ (4.5–5.1). Nevertheless, they are silica-oversaturated (Q and Hy-normative) in spite of being Ac, Ns and Ks-normative. The Mount Rubin dyke has much higher mg^* (79.9) than those from Mount Rubin (58.0–61.9). All samples show extreme enrichment in LILE (K, Rb, Ba, Sr and Pb), LREE, HFSE (Ti, Zr and Nb) and P, but have relatively low Al_2O_3 and CaO (Table 19; Figs 141, 142). This is reflected in the spidergrams. They show broadly similar degrees of enrichment from Pb to Zr (especially Rb, K and Zr), moderate enrichment in Ti, and little or no enrichment in Y and Na (Fig. 153). The two Mount Bayliss samples are compositionally very similar, except that the coarser

grained dyke has much lower Ba. The Mount Rubin dyke, with a very similar trace-element composition, has an intermediate Ba content.

The Mounts Bayliss and Rubin dykes belong to the rare ultrapotassic mafic rock suite that includes the leucite lamproites of the West Kimberley area of Western Australia (Prider 1960), the volcanic rocks of the Leucite Hills, Wyoming (Carmichael 1967), and the olivine leucites of Gaussberg, Antarctica (Sheraton & Cundari 1980). Such extreme compositions are thought to reflect small degrees of melting of highly enriched (metasomatised), phlogopite-bearing mantle source regions, with much of the LILE and probably some of the LREE having ultimately been derived by dehydration and/or partial melting of subducted sediments (Rogers et al. 1987; Nelson & McCulloch 1989).

A highly enriched mantle source for the Mount Rubin dyke is evidenced by its very low ϵ_{Nd} ($T = 460$ Ma) of -15 (Mikhalsky et al. 1994b). The high Zr contents of dykes from both SPCM occurrences are comparable to typical lamproites (Mitchell 1985). However, some other incompatible elements (Ba, Sr and Sm) are relatively low, so Rb/Sr and Rb/Ba are high. The SPCM dykes also have low K/Ti and only small negative Nb and P anomalies. Some of these features are similar to the Western Australian lamproites (Bergman 1987), but the much lower Ba and Rb are more typical of lamproites from southeastern Spain (Nixon et al. 1984). The negative Sr and Ba anomalies, as well as relatively low Ni and Cr of the SPCM dykes, are consistent with the mineralogical evidence of extensive melt evolution during ascent through the crust. In view of the variety and complexity of the processes that were probably involved in the petrogenesis of lamproites (including small degrees of melting with a variety of major and accessory residual phases, fluid activity, source metasomatism, etc.), it is not surprising that there should be such a range of trace-element abundances. Perhaps more surprising are the geochemical similarities.

A compositionally similar dyke crops out at northern Webster Peaks in the NPCM (Munksgaard et al. 1992). The Webster Peaks dyke differs in being silica undersaturated (Ol, Lc and Ne-normative), and having higher Ba and Rb, and lower Ti, Na, P, Sr and Zr (Munksgaard et al. 1992). The only other reported occurrence of chemically similar rocks in this part of East Antarctica is a few dykes at Priestley Peak and elsewhere in Enderby Land (Sheraton & England 1980). Phlogopite–arfvedsonite lamproite at Priestley Peak has given an Ordovician Rb–Sr isochron age of 482 ± 3 Ma (Black & James 1983).

Mafic dykes of the Jetty Peninsula area

Mafic dykes form a relatively dense swarm on Jetty Peninsula and Else Platform (Fig. 140) where they cut Mesoproterozoic metamorphic rocks, but are not known to intrude Permian sedimentary rocks (Mikhalsky & Sheraton 1993). The predominant strike is north ($355\text{--}010^\circ$), and the swarm may thus mark a north–south fracture zone related to the Lambert Glacier rift graben. Fracturing and dyke emplacement are believed to represent an initial stage of rifting in the Carboniferous.

The dykes have thin chilled margins, dip to the west at $40\text{--}50^\circ$, and are commonly 0.5 to 1.5 metres thick—although a few attain five to eight metres. They have

TABLE 19. Chemical analyses and CIPW norms of representative Phanerozoic mafic igneous rocks.

Sample no.	73281545	R11370	35647-3	91286344	91286324	91286340	91286332	91286338	91286334	91286335	2013
Field no.	73281545	R11370	35647-3	34-10-10	30-4/6.2	30-11/3	30-6-1	30-19/4	30-1-4	30-42-4	2013
Locality	Mount Bayliss	Mount Bayliss	Mount Rubin	Jetty Peninsula	Jetty Peninsula	Jetty Peninsula	Jetty Peninsula	Jetty Peninsula	Jetty Peninsula	Jetty Peninsula	Jetty Peninsula
Lithology	Lamproite dyke	Lamproite (moraine)	Lamproite dyke	Ophitic dolerite dyke 1a	Intergranular dolerite dyke 1b	Porphyritic dolerite dyke 1c	Camptonite (basanite) dyke 1d	Trachydol. (phonoteph.) dyke 2b	Trachydol. (tephriphon.) dyke 2c	Trachydol. (trachybas.) dyke 2b	Qz diorite porphyry dyke 3
Group Age	Silurian	Silurian	?Ordovician	Carbonif.	Carbonif.	Carbonif.	Carbonif.	Carbonif.	Carbonif.	Carbonif.	
SiO ₂	52.90	50.30	50.40	45.66	46.76	44.53	45.65	50.65	53.29	49.87	62.60
TiO ₂	4.45	5.43	5.38	2.02	2.22	2.11	2.26	1.62	1.21	2.20	1.18
Al ₂ O ₃	8.92	8.90	7.35	14.62	16.12	13.02	14.94	17.29	17.55	14.83	14.40
Fe ₂ O ₃	2.64	2.72	*4.44	3.85	2.50	3.25	2.21	1.82	2.14	1.86	2.53
FeO	5.30	6.00	-	8.61	8.42	7.48	8.17	7.98	7.20	7.11	5.15
MnO	0.11	0.11	0.09	0.15	0.15	0.15	0.14	0.14	0.18	0.13	0.10
MgO	5.95	5.56	7.57	7.35	7.47	10.25	7.47	2.09	1.36	5.91	1.49
CaO	4.00	5.06	5.41	9.84	7.19	8.91	8.95	4.56	3.75	6.69	1.60
Na ₂ O	2.05	1.75	1.86	2.59	3.57	2.47	3.11	4.54	4.95	3.48	3.16
K ₂ O	9.35	8.90	8.44	1.11	1.03	1.41	2.92	3.58	5.10	2.83	3.72
P ₂ O ₅	1.75	1.85	1.36	0.37	0.53	0.52	0.63	1.04	0.71	0.85	0.54
H ₂ O ⁺	0.89	1.06	-	-	-	-	-	-	-	-	-
CO ₂	0.25	1.45	-	-	-	-	-	-	-	-	-
LOI	-	-	3.81	3.66	3.88	5.79	3.43	4.59	2.51	4.15	2.71
Rest	0.99	1.05	0.53	0.44	0.47	0.52	0.54	0.54	0.44	0.56	0.30
Total	99.55	100.14	96.65	100.27	100.31	100.41	100.42	100.44	100.39	100.47	99.48
O=F,S,Cl	0.14	0.17	0.00	0.08	0.07	0.06	0.05	0.05	0.02	0.05	0.00
Total	99.41	99.97	96.65	100.19	100.24	100.35	100.37	100.39	100.37	100.42	99.48
Q	4.35	2.01	5.64	-	-	-	-	-	-	-	21.85
C	-	-	-	-	-	-	-	0.15	-	-	3.56
Or	48.70	48.59	40.13	6.56	6.09	8.33	17.26	21.16	30.14	16.72	21.98
Ab	-	-	-	21.76	30.21	18.91	11.73	37.50	32.55	29.45	26.74
An	-	-	-	24.99	24.92	20.27	18.18	15.83	10.61	16.49	4.41
Ne	-	-	-	0.08	-	1.08	7.90	0.49	5.06	-	-
Ac	3.70	4.07	1.93	-	-	-	-	-	-	-	-
Ns	3.06	2.37	3.15	-	-	-	-	-	-	-	-
Ks	1.82	1.11	2.70	-	-	-	-	-	-	-	-
Di	6.74	10.42	9.86	17.56	5.94	16.58	17.98	-	2.89	9.08	-
Hy	16.40	13.26	14.28	-	2.52	-	-	-	-	5.90	12.51
Ol	-	-	-	17.41	18.17	21.02	15.12	12.35	9.99	9.76	-
Mt	-	-	-	2.92	2.58	2.51	2.46	2.32	2.21	2.12	1.79
Il	8.45	10.31	7.33	3.84	4.22	4.01	4.29	3.08	2.30	4.18	2.24
Ap	4.15	4.38	3.22	0.88	1.26	1.23	1.49	2.46	1.68	2.01	1.28
F	2800	3300	-	-	-	-	-	-	-	-	-
S	360	400	-	1700	1500	1200	1100	1000	500	1000	-
Sc	-	-	-	27	25	27	24	11	10	19	9
V	94	133	97	228	193	195	189	30	8	114	39
Cr	215	180	339	189	286	398	416	20	80	685	18
Ni	131	128	153	141	144	329	158	20	14	109	36
Cu	43	34	-	95	77	80	64	35	19	31	-
Zn	140	116	-	130	91	110	103	112	104	112	-
Ga	20	22	-	20	20	17	21	21	22	22	-
Rb	210	149	142	45	51	48	80	62	104	56	-
Sr	1779	1259	972	491	513	606	778	997	642	817	570
Y	32	37	36	22	24	24	24	34	38	22	23
Zr	1582	1242	1185	143	183	197	237	295	363	319	275
Nb	145	102	138	32	51	58	73	114	126	83	-
Ba	412	1320	1043	455	727	923	1065	1632	1359	1055	1600
La	162	156	-	27	33	36	49	79	85	55	-
Ce	276	270	-	50	75	72	92	148	154	111	-
Nd	-	-	-	23	37	33	40	59	59	47	-
Pb	28	19	52	3	5	4	5	13	15	8	-
Th	14	19	41	<2	4	4	5	11	15	5	-
U	2.0	2.0	-	<0.5	0.5	<0.5	0.5	<0.5	2.0	2.0	-
K/Rb	370	496	493	205	168	244	303	479	407	420	-
(Ce/Y) _n	21.6	18.2	-	5.7	7.8	7.5	9.6	10.9	10.1	12.6	-
Ba/Zr _n	0.26	1.06	0.88	3.18	3.97	4.69	4.49	5.53	3.74	3.31	5.82
Ce/Zr	0.17	0.22	-	0.35	0.41	0.37	0.39	0.50	0.42	0.35	-
Nb/Zr	0.09	0.08	0.12	0.22	0.28	0.29	0.31	0.39	0.35	0.26	-
Nb/Nb*	0.72	0.53	-	1.15	1.70	1.60	1.17	1.33	1.16	1.29	-
Sr/Sr*	-	-	-	1.05	0.71	0.90	0.93	0.76	0.48	0.81	-
mg*	61.9	58.0	79.9	56.1	59.5	67.4	60.7	31.3	23.8	58.5	29.6

mg* = atomic 100Mg/(Mg + 0.85Fe(total)); * total Fe as Fe₂O₃.

Sample no.	70280296	71280126	69280217	91286452	36810-19b	D40	D35	D49	73281594
Field no.	70280296	71280126	69280217	91286452	36810-19b	D40	D35	D49	73281594
Locality	N Amery Peaks	Taylor Platform	New Year Nunatak	Hunt Nunataks	Fisher Massif	Radok Lake	Radok Lake	Radok Lake	SW Manning Massif
Lithology	Basalt dyke	Basaltic andesite dyke	Trachybasalt dyke	Basanite dyke	Alk. dolerite (basanite) dyke	Basanite dyke	Basanite dyke	Basaltic trachyand. dyke	Tephritic phonolite lava
Group Age		Permo-Trias.				Pl-phyric	Cpx-phyric ?Permian	Aphyric ?Permian	Eocene
SiO ₂	45.70	53.10	48.30	45.00	47.97	47.15	46.52	52.04	51.10
TiO ₂	2.29	1.64	2.45	2.19	1.81	2.72	1.97	1.60	1.17
Al ₂ O ₃	13.75	15.15	13.87	14.71	15.20	16.68	13.42	12.92	16.86
Fe ₂ O ₃	3.20	2.04	2.60	2.58	2.65	3.83	1.79	1.19	2.70
FeO	7.55	6.70	6.68	6.95	6.24	7.23	6.42	7.02	3.25
MnO	0.36	0.12	0.13	0.13	0.12	0.18	0.13	0.13	0.09
MgO	7.80	4.57	6.65	8.10	5.08	3.72	6.89	6.48	4.00
CaO	7.60	7.43	8.26	9.05	7.51	6.55	7.87	5.42	4.11
Na ₂ O	1.69	3.50	2.99	2.84	2.91	3.31	1.92	3.02	5.75
K ₂ O	1.63	1.62	2.67	2.83	3.64	3.59	5.74	3.19	5.59
P ₂ O ₅	0.45	0.43	0.83	0.48	0.59	0.65	0.96	0.53	1.42
H ₂ O ⁺	4.94	0.51	3.04	-	-	3.02	2.13	1.71	2.79
CO ₂	2.45	3.22	0.60	-	-	1.24	3.86	4.33	<0.05
LOI	-	-	-	4.24	6.26	-	-	-	-
Rest	0.30	0.27	0.38	0.55	0.00	0.60	0.72	0.52	0.75
Total	99.71	100.30	99.45	99.65	99.95	100.47	100.34	100.10	99.58
O=F,S,Cl	0.00	0.00	0.00	0.05	0.00	0.08	0.05	0.05	0.06
Total	99.71	100.30	99.45	99.60	99.95	100.39	100.29	100.05	99.52
Q	-	3.48	-	-	-	-	-	0.71	-
C	-	-	-	-	-	-	-	-	-
Or	9.63	9.57	15.78	16.72	21.51	21.27	34.04	18.97	33.03
Ab	14.30	29.62	25.30	10.50	21.23	22.65	4.32	25.72	22.13
An	25.12	20.84	16.54	19.03	17.66	20.06	11.11	12.26	3.68
Ne	-	-	-	7.33	1.84	2.95	6.51	-	14.37
Ac	-	-	-	-	-	-	-	-	-
Ns	-	-	-	-	-	-	-	-	-
Ks	-	-	-	-	-	-	-	-	-
Di	7.85	10.87	15.43	18.39	12.90	6.86	17.65	9.10	6.06
Hy	26.36	15.68	1.37	-	-	-	-	20.91	-
Ol	0.68	-	12.13	15.26	11.55	12.51	12.42	-	9.70
Mt	2.52	2.06	2.18	2.24	2.08	2.58	1.95	1.96	1.37
Il	4.35	3.11	4.65	4.16	3.44	5.17	3.76	3.06	2.22
Ap	1.07	1.02	1.97	1.14	1.40	1.54	2.27	1.28	3.36
F	-	-	-	-	-	-	-	-	1150
S	-	-	-	1000	-	1500	900	900	140
Sc	20	-	13	24	-	13	15	13	-
V	199	113	138	182	-	162	107	95	48
Cr	238	116	91	138	-	13	124	207	68
Ni	175	86	84	148	-	17	100	138	66
Cu	56	20	32	44	-	27	30	28	30
Zn	102	119	92	103	-	100	96	144	90
Ga	15	20	17	20	-	19	18	20	23
Rb	32	44	33	122	-	86	184	95	130
Sr	460	535	740	604	-	1004	1390	635	1208
Y	21	20	20	25	-	24	19	19	26
Zr	172	158	240	197	-	219	240	290	1118
Nb	41	27	62	72	-	68	84	49	162
Ba	671	907	1378	1819	-	1822	2547	1557	1420
La	36	31	55	37	-	51	95	65	156
Ce	61	59	89	66	-	90	148	104	243
Nd	32	-	46	30	-	44	65	46	-
Pb	4	5	2	5	-	10	9	25	36
Th	4	4	6	7	-	6	11	9	36
U	1.0	1.0	1.5	1.0	-	2.0	3.0	<1.0	4.0
K/Rb	423	306	672	193	-	347	259	279	357
(Ce/Y)n	7.3	7.4	11.1	6.6	-	9.4	19.5	13.7	23.4
Ba/Zr	3.90	5.74	5.74	9.23	-	8.32	10.6	5.37	1.27
Ce/Zr	0.35	0.37	0.37	0.34	-	0.41	0.62	0.36	0.22
Nb/Zr	0.24	0.17	0.26	0.37	-	0.31	0.35	0.17	0.14
Nb/Nb*	1.05	0.74	1.00	1.31	-	0.92	0.66	0.64	1.07
Sr/Sr*	0.77	-	0.85	0.99	-	1.17	1.02	0.66	0.00
mg*	61.1	52.9	60.7	64.7	55.3	42.2	64.3	62.7	59.6

D35, D40, and D49 from Stephenson & Cook (1992), recalculated to original totals for consistency with other analyses.

sharp, straight contacts that commonly exhibit cataclastic structures and quartz veinlets. Three dyke emplacement events were recognised in the field.

The oldest dykes (group 1) comprise transitional (rarely tholeiitic) to alkaline dolerite and camptonite. Camptonite dykes contain rare, small lherzolite nodules of deep-seated origin. Group 2 dykes are rare and consist of trachydolerite (or monzodiorite on the plutonic rock classification of Le Maitre 1989). The youngest dykes (group 3) are represented by a few compositionally distinct diorite porphyries. Groups 1 and 2 dykes from this

area have given K–Ar ages of 310 Ma (Hofmann 1991) and 321 ± 10 Ma (Mikhalsky & Sheraton 1993). The very high MSWD value (47) for the latter age suggests some K and Ar mobility. Diorite porphyries have given K–Ar ages of 239 ± 12 and 245 ± 11 Ma (Hofmann 1991).

The three dyke groups differ from each other in mineralogy, texture and chemical composition, with much smaller variations within each group. Group 1 and 2 dykes can be subdivided further on the basis of textural and/or mineralogical criteria, which correlate with geochemical variations. Most rocks are nearly fresh, but some are

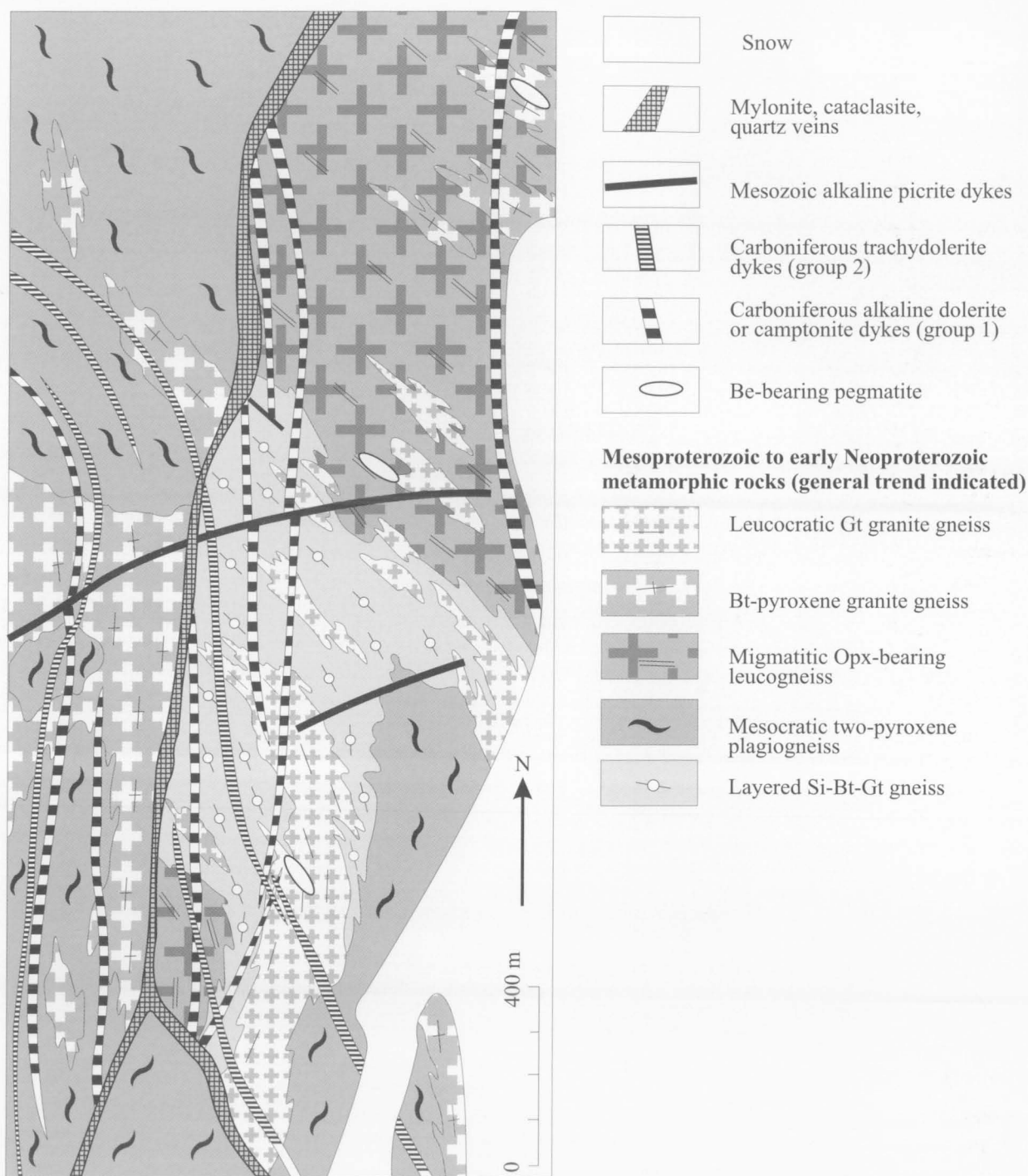


FIGURE 140

Geological sketch map of part of Kamenistaja Platform, Jetty Peninsula (Fig. 150), showing mafic and ultramafic dykes. The dykes are not to scale.

strongly altered with uraltic amphibole, albite, fine-grained biotite, and serpentine reflecting deuteric (autometamorphic) alteration. Other secondary minerals, including chlorite, carbonate, leucoxene, saussurite, opacite and epidote, probably reflect younger tectonic events and hydrothermal activity.

Group 1 dolerites are fine- to medium-grained dark greenish-grey or grey rocks with massive or ocellar structure. The texture varies considerably, whereas the

gross mineralogical composition remains more or less constant. Three textural varieties may be distinguished: ophitic (subgroup 1a), intergranular (subgroup 1b), and porphyritic (subgroup 1c) dolerites. Small spherical ocelli are more common in porphyritic rocks and are composed of carbonate or epidote. Accessory minerals include apatite, titanite and Fe-Ti oxides. *Ophitic dolerites* consist of relatively large plagioclase laths (An_{50-60} ; 35–40%), anhedral ophitic grains of augite ($Ca_{44}Mg_{41}Fe_{15}$; 40–45%) and some interstitial alkali feldspar ($Na_{54}K_{27}Ca_{19}$), late magmatic plagioclase (10–20%), chlorite (altered glass, 5%), and opaque minerals (up to 5%). *Intergranular dolerites* consist of fine-grained interstitial subhedral salite ($Ca_{45}Mg_{45}Fe_{10}$ to $Ca_{47}Mg_{37}Fe_{16}$; 40–50%) between small plagioclase laths (An_{45-50} ; 40–45%), primary biotite (*mg* 51–55), and chloritised glass (5–15%). The rocks also contain sparse prismatic altered ferromagnesian grains, now composed of talc and minor chlorite, that are probably pseudomorphs after olivine. *Porphyritic dolerites* contain numerous (10–20%) small zoned phenocrysts (or primocrysts) of clinopyroxene (with salite or augite $Ca_{44-46}Mg_{41-46}Fe_{10-13}$ cores and Ti-augite $Ca_{50}Mg_{37}Fe_{13}$ rims) and olivine (Fe_{80-85}). Some irregular and tabular olivine grains may represent fragments of a restite phase. The groundmass consists of plagioclase (An_{24-60}), albite, K-feldspar, euhedral salite ($Ca_{48}Mg_{37}Fe_{15}$), and biotite (*mg* 38–49).

Group 1 camptonites (subgroup 1d) are fine-grained black rocks with characteristic porphyritic textures and ocellar structure. Hypidiomorphic granular or poikilitic textures are typical of the groundmass. The rocks contain clinopyroxene and olivine phenocrysts (15–40%); clinopyroxene phenocrysts are zoned from cores of enodiopside ($Ca_{42}Mg_{50}Fe_8$) to Ti-augite rims ($Ca_{50}Mg_{37}Fe_{13}$). Olivine phenocrysts (Fe_{79-81}) are strongly resorbed. The groundmass consists of euhedral kaersutite grains (20–30%), up to 1.5 millimetres in length, and small grains of Ti-augite ($Ca_{51}Mg_{35}Fe_{14}$; 10–15%) enclosed in relatively large plagioclase crystals (An_{50-55} ; 20–30%). Minor primary biotite (*mg* 49) and alkali feldspar (up to 10 %) are present. The rocks contain carbonate ocelli (up to 5 mm) and smaller leucocratic globules that consist mainly of alkali feldspar and minor amphibole. The lack of boundary nucleation and the similarity in chemical composition of amphiboles from both rock groundmass and globules suggest that the leucocratic ocelli represent droplets of an immiscible liquid phase.

Group 2 trachydolerites are fine-grained, light greenish-grey rocks with rare carbonate ocelli, and phenocrysts of augite ($Ca_{37}Mg_{47}Fe_{16}$) and/or plagioclase (An_{45-50}). Textures are porphyritic, hypidiomorphic granular, or subophitic. The groundmass consists of plagioclase (An_{35-40} cores, An_{5-15} rims), alkali feldspar (anorthoclase) and ferromagnesian minerals. Albite seems to be of late igneous, rather than of metasomatic origin. Feldspars comprise 70–85 percent of the rocks, their relative proportions varying widely. Three varieties can be distinguished according to their ferromagnesian mineral assemblages: pyroxene–biotite (subgroup 2a), biotite (subgroup 2b), and amphibole-bearing trachydolerites (subgroup 2c). The ferromagnesian minerals include anhedral salite ($Ca_{48}Mg_{31}Fe_{21}$; 0–10%), subhedral biotite (*mg* 24; 5–25%), and ferropargasite (0–20%). Low *mg*

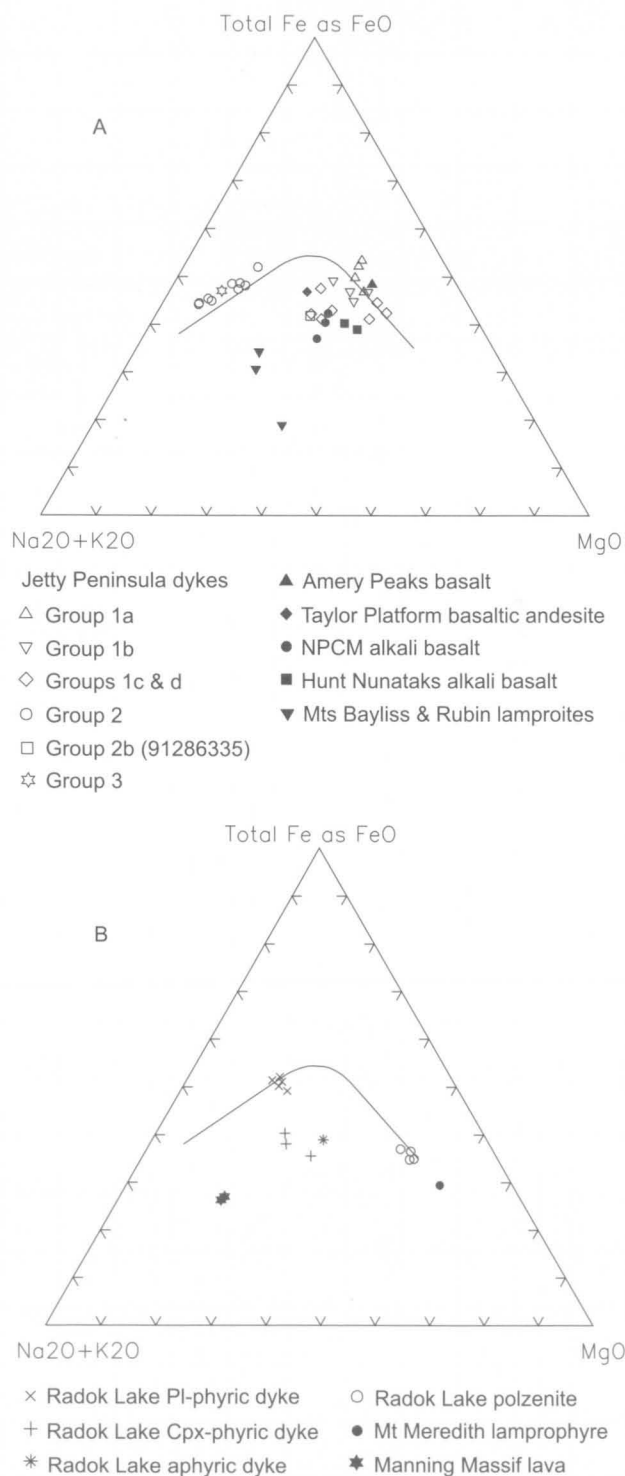


FIGURE 141

AFM diagrams for (A) Palaeozoic and (B) Permian–Eocene alkaline mafic rocks.

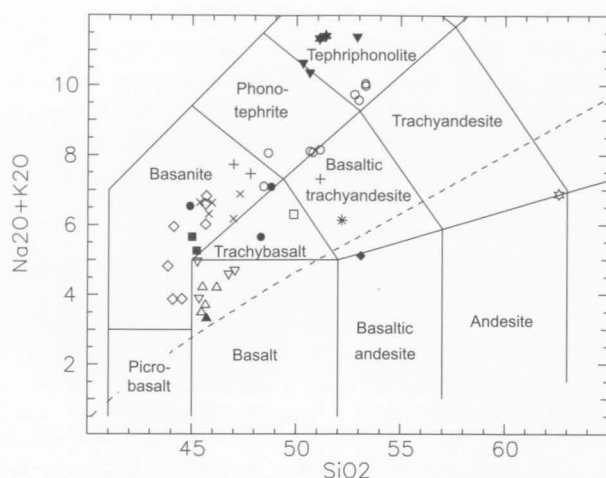


FIGURE 142

Alkalies-SiO₂ plot for alkaline mafic rocks. Symbols as in Figure 141A and B (Radok Lake dykes and Manning Massif lava only). Fields correspond to the volcanic rock classification of Le Bas et al. (1986).

suggests that most biotite is of secondary origin. Amphibole-bearing rocks contain euhedral amphibole crystals up to one millimetre across and abundant alkali feldspar (up to 60%). Accessories include magnetite and Ti-magnetite (1–5%), apatite and titanite.

Group 3 diorite porphyries are medium-grained, light grey rocks with porphyritic textures. Large plagioclase phenocrysts are strongly altered to sericite and form up to 20 percent of the rock. The groundmass consists of plagioclase laths (An_{30–35}; 50–60%), anhedral biotite (10–20%), hornblende (5%), K-feldspar (5%), and quartz (2–3%). Secondary albite (10–15%) is also present. More evolved dykes contain up to 20 percent quartz.

All groups 1 and 2 dykes are alkaline in terms of the total alkalies vs SiO₂ plot of Irvine & Baragar (1971) (Fig. 142). Subgroups 1a and 1b are silica-saturated (Hynormative) to slightly silica-undersaturated (Nenormative), and can be classified as tholeiitic to transitional dolerites (Ringwood 1975; Table 19; Fig. 141). Groups 1c and 1d have up to 11 per cent of normative Ne and are of basanitic composition on the classification of Le Bas et al. (1986) (Fig. 142). Relatively low *mg** (55–62 for

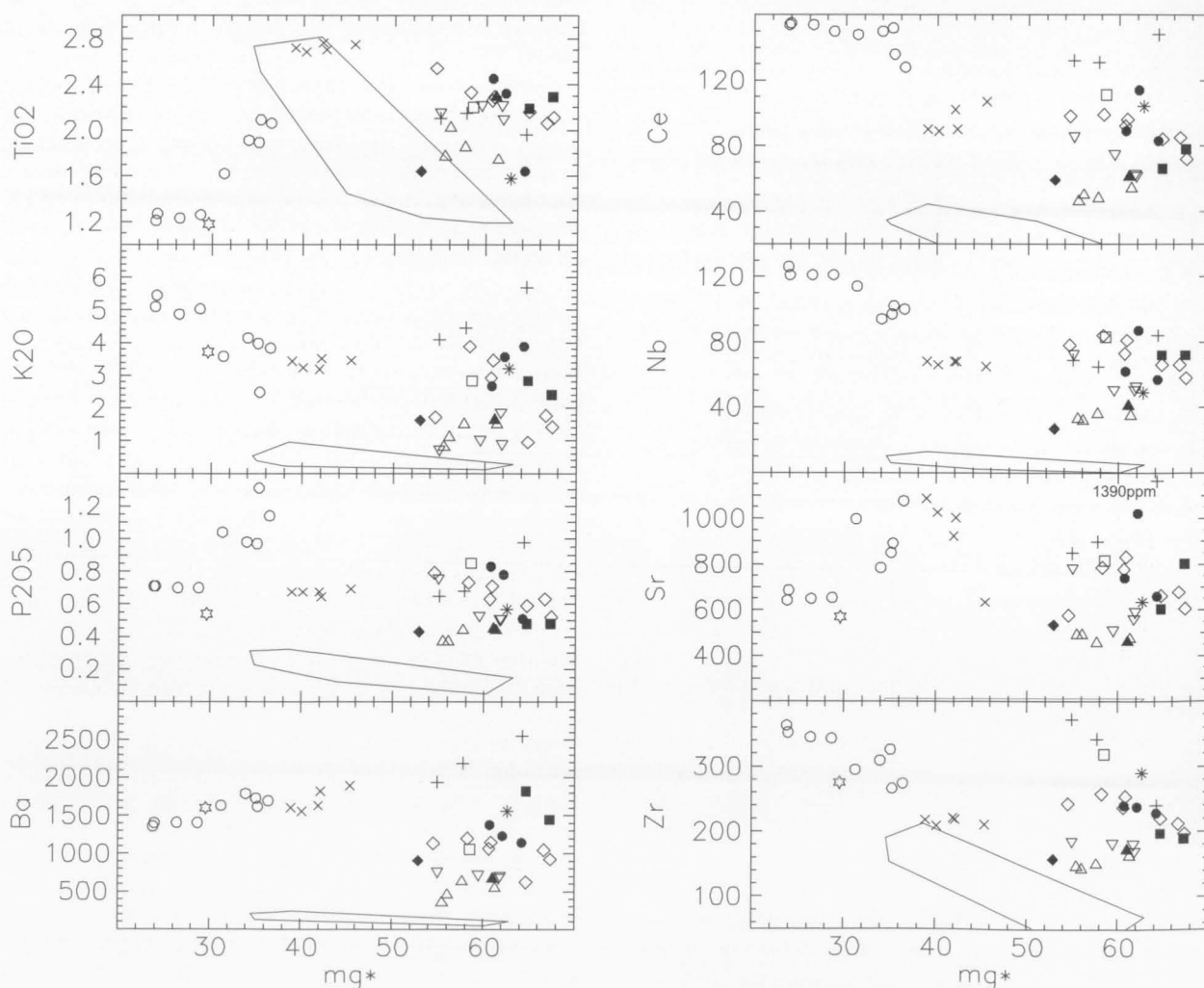


FIGURE 143

*mg** variation diagrams for alkaline mafic rocks. Symbols as in Figure 141A and B (Radok Lake dykes only). The field of group II dolerites from the Vestfold Hills is shown for comparison.

subgroups 1a & b and 53–67 for subgroups 1c & d), Ni (100–330 ppm), and Cr (170–400 ppm) suggest that the melts were not primitive.

Although there are few clear correlations between mg^* and major and trace element abundances for the group 1 rocks as a whole, some subgroups (particularly 1d) show reasonable correlations for many elements (Fig. 143). Mass balance calculations are consistent with much of the compositional range of subgroups 1c and 1d being due to fractionation of amphibole (kaersutite) + olivine + clinopyroxene (Mikhalsky & Sheraton 1993). The lack of correlation between mg^* and Sr/Sr* ratio and near-constant Sr/Zr ratio (~ 3.4 ; Fig. 144) preclude significant plagioclase fractionation (except for two of the most evolved samples).

Subgroups 1c and 1d are compositionally virtually identical, and the Jetty Peninsula dyke suite thus appears to represent a mineralogical transition between mildly alkaline dolerite and lamprophyre. Both subgroups are more enriched in many LILE, LREE and HFSE, but have similar SiO_2 contents and mg^* values to subgroups 1a and 1b (Fig. 143). Subgroup 1b is also generally more enriched than subgroup 1a suggesting different degrees of partial melting were probably important in determining the different incompatible element abundances. Subgroups 1c and 1d represent the lowest degrees of melting and have lamprophyric affinities. Most group 1 rocks exhibit near-constant ratios on many incompatible element/Zr plots, although subgroups 1c and 1d have slightly higher LILE/Zr (Fig. 144). Many other incompatible element ratios (K/Nb, K/Ba, P/Ce, Rb/Sr, K/Rb) also show relatively little variation, suggesting that the different subgroups originated from very similar, strongly enriched mantle source regions. This is consistent with the very similar spidergram patterns for all subgroups (Fig. 145). However, Ti/Zr and Y/Zr ratios of subgroups 1c and 1d are consistently lower than subgroups 1a and 1b. Ce/Y is higher, implying that Y and Ti were more compatible for these lower degree melts and suggesting pyroxene, garnet and/or Fe–Ti oxide control (during partial melting, fractionation, or both). Subgroups 1a & b also appear to have been more depleted in Th and U, possibly via a late fluid phase, than subgroups 1c and 1d.

Some of the petrographic and compositional differences between the subgroups may also reflect different fluid activities during initial melting and/or melt evolution during ascent of magma through the crust. More rapid ascent of volatile-rich camptonite magma probably prevented ferromagnesian phenocrysts from resorption, whereas slower ascent of volatile-poor magma led to their common resorption. The presence of ocelli in camptonites indicates liquid immiscibility that may have been facilitated by high fluid activity. Some enrichment of the source region (e.g., in LILE), possibly due to a metasomatising volatile flux penetrating the lithosphere (Bailey 1987), may have occurred during magma generation. Isotopic data suggest that mantle enrichment was much earlier, however (see below). Nevertheless, the textural and mineralogical features of the lamprophyres may be largely explained by interaction between a mildly alkaline melt and a volatile flux during magma ascent towards the surface.

Preliminary Sm–Nd data for groups 1 and 2 rocks show considerable scatter, with ϵ_{Nd} (calculated at 321 Ma) ranging between -0.18 and -3.05 , and decreasing with increasing Ba, Th, Nb, La, Ce, Sr and Zr (Mikhalsky & Sheraton 1993). These features may reflect either source heterogeneity or different degrees of crustal involvement. However, as the near-constant incompatible element ratios are not consistent with significant crustal contamination through AFC processes, the evolved Nd isotopic compositions more likely indicate magma generation from a somewhat heterogeneous, long-term enriched mantle source.

Group 2 trachydolerites have a relatively wide range of composition (Figs 141, 142), with some being Ne-normative (up to 5%) and others slightly Hy-normative. Most are of phonolitic tephrite or tephritic phonolite composition (Le Bas et al. 1986), or monzodiorite on the plutonic rock classification of Le Maitre (1989). They are more evolved than group 1, with lower mg^* (22–36), Ni and Cr. Many elements show reasonably good correlations with mg^* — K_2O , Ce, Nb, Y, and Zr increase and TiO_2 , P_2O_5 , Ba and Sr decrease with decreasing mg^* (Fig. 143). In spite of this, mass balance calculations (Mikhalsky & Sheraton 1993) show that more-evolved varieties (subgroup 2b) could only be derived from less-evolved (subgroup 2a) melts by fractional crystallisation of olivine + clinopyroxene + amphibole + plagioclase, which is inconsistent with the observed phenocryst assemblages. However, major plagioclase control is confirmed by negative correlations of Sr and Sr/Sr* with mg^* . Subgroup 2c compositions cannot be related to more primitive rocks by any feasible fractional crystallisation process. Hence, dykes of the various subgroups (2a–c) probably crystallised from distinct parent magmas. On the other hand, most group 2 dykes could have been derived by fractionation of olivine, clinopyroxene, amphibole, plagioclase, apatite and Ti-magnetite from a parent melt similar to that of group 1. Nevertheless, melting of a slightly more enriched source is likely. One trachydolerite (91286335), assigned to group 2b on petrographic criteria, is compositionally similar in most respects to subgroups 1c and 1d dykes, although with somewhat higher SiO_2 and Zr (Figs 141–145).

Many incompatible element ratios of subgroups 2a and 2b (K/Nb, K/Ba, P/Ce, Rb/Sr, Nb/Zr, Y/Zr) are generally similar to those of group 1, whereas K/Rb, Ce/Y, Ba/Zr and Ce/Zr ratios are consistently higher and Ti/Zr lower (Fig. 144). Subgroup 2c dykes show even more divergent ratios with, for example, low Ba/Zr, P/Zr and Sr/Zr. Many of these differences could have been caused by more extensive plagioclase, clinopyroxene, apatite and Ti-magnetite fractionation. Variations in Ce/Y probably reflect variations in the amount of residual clinopyroxene and/or garnet. Some degree of source heterogeneity may be required to explain, for example, the high Ba/Zr and P/Zr of subgroup 2a, the latter suggesting variable apatite in the source region. Spidergram patterns for individual samples are broadly similar to each other and to group 1 rocks, particularly subgroups 1c and 1d (Fig. 145), suggesting a generally similar enriched mantle source. Depletions in Ti and Sr probably reflect Ti-magnetite and plagioclase fractionation, respectively. Subgroup 2c rocks are the most enriched in the more incompatible elements (Rb–Nb), but are relatively depleted in Sr, P and Ti, consistent with them

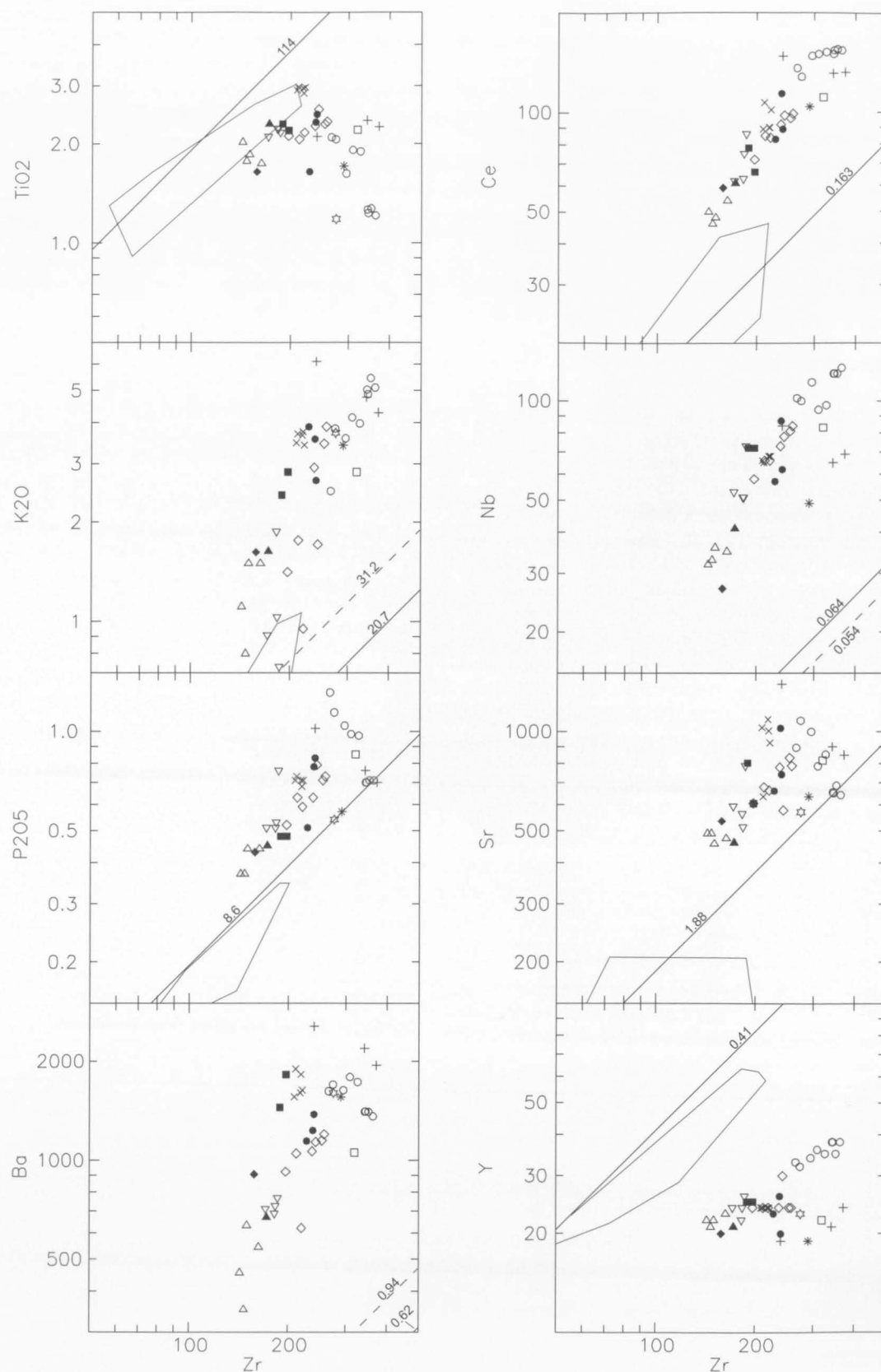


FIGURE 144

Logarithmic plots of various incompatible elements against Zr for alkaline mafic rocks. Symbols as in Figure 141A and B (Radok Lake dykes only). Lines of estimated primordial mantle ratios (after Sun & McDonough 1989) and the field of group II dolerites from the Vestfold Hills are shown. Note that most or all of the Vestfold Hills dolerites fall outside the plotting areas for K₂O, Ba and Nb, so the average values of K/Zr, Ba/Zr and Nb/Zr are shown as dashed lines.

having undergone the most extensive fractional crystallisation. Group 2 appears to have been somewhat depleted in U, but less so in Th (Fig. 145).

Group 2 rocks have a similar range of Sm–Nd compositions to group 1 rocks. ϵ_{Nd} is somewhat lower (–2.26 to –4.63), decreasing with increasing LREE, Th, Zr, Nd and Rb, and decreasing Sr and Ba. Such a relatively small range of ϵ_{Nd} is unlikely to reflect significant crustal

contamination, but minor contamination cannot be discounted.

To summarise, groups 1 and 2 dykes were apparently derived from very similar enriched mantle source regions, although systematic variations in bulk composition and incompatible element abundances imply significant differences in degrees of melting, as well as some source heterogeneity. For relatively low degrees of melting, some of the ‘incompatible’ trace elements considered in the above discussion might not have been truly incompatible, and some of the minor differences in incompatible element ratios between the different subgroups may reflect this. Collectively, groups 1 and 2 dykes form a genetically related, but not comagmatic, suite. Their source region was apparently much more strongly enriched in incompatible elements than typical Mesoproterozoic tholeiite dykes (group II) in the Vestfold Hills (Collerson & Sheraton 1986a), having relatively high Ba/Zr, K/Zr, Nb/Zr, Ce/Zr, P/Zr and Nb/Y. (Figs 143, 144).

Although minor crustal contamination is possible, very low La/Nb ratios (0.6–0.7 for group 1 rocks and 0.7–0.85 for group 2) make significant contamination unlikely (Thompson et al. 1984). Low La/Nb and relatively high Th/Yb and Ta/Yb ratios suggest a within-plate tectonic environment (Pearce 1982). Such compositional features could be explained in terms of magma derivation from a Nb-rich OIB (ocean-island basalt)-like source, or involvement of a Nb-rich eclogitic component.

If crustal assimilation was not important, the range of ϵ_{Nd} for groups 1 and 2 dykes must reflect varying degrees of mantle LREE enrichment. $T^{\text{Nd}}_{\text{DM}}$ model ages are mostly 1050–1200 Ma, although these are likely to represent upper limits for the time of mantle enrichment event(s). They are, in fact, only slightly older than the age of high-grade metamorphism in the NPCM, consistent with co-eval crust-forming and mantle-enrichment events in the late Mesoproterozoic. A mantle-enrichment event also seems to have been roughly co-eval with felsic crust formation in the Bunge Hills, where 500 Ma alkaline mafic dykes were derived from long-term enriched mantle (T_{DM} ages are 2080–2290 Ma; Sheraton et al. 1990). Jurassic Karoo picritic basalts of Zimbabwe were apparently formed by melting of lithospheric mantle that underwent Sm–Nd fractionation about 1050 Ma ago, a time of crust formation in adjacent parts of Gondwana (Ellam & Cox 1989).

Group 3 rocks (diorite and quartz diorite porphyries) are the most evolved of the dykes (mg^* 11–30). Their relatively high Ni contents and high normative Q and Hy indicate that they cannot be related to groups 1 or 2 through crystal fractionation processes. They were clearly derived from a distinct (possibly even crustal) source region. Different Ba/Y, P/Zr, Ti/Zr and Zr/Y ratios are consistent with this suggestion (Figs 143, 144). Group 3 dykes appear to have calc-alkaline affinities and probably represent the evolved products of distinct parent melts formed either by melting in the lower crust due to heating by mantle-derived magma, or by fractionation of such magma.

Mafic dykes of the Radok Lake area

Alkaline basaltic dykes intrude both high-grade metamorphic rocks and Permo–Triassic Amery Group sedimentary rocks near Radok Lake, southwest of Beaver

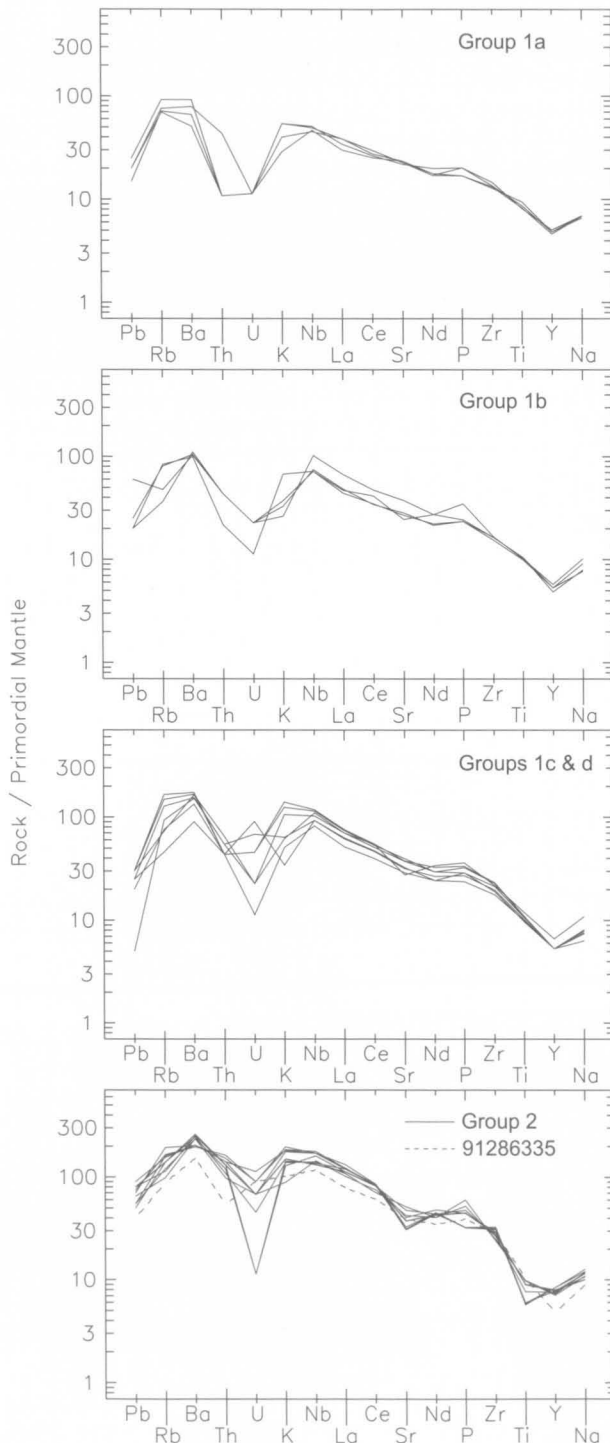


FIGURE 145
Spidergrams for Jetty Peninsula mafic dykes.

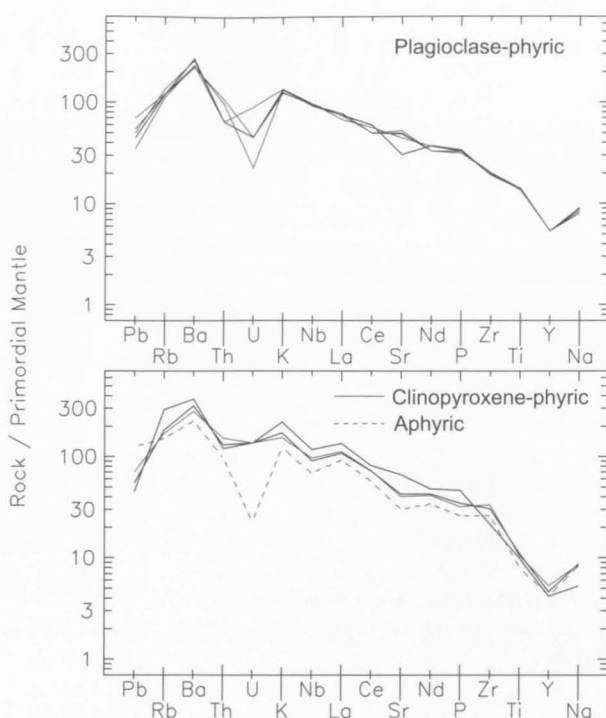


FIGURE 146
Spidergrams for Radok Lake mafic dykes (data from Stephenson & Cook 1992).

Lake. They have been described in detail by Stephenson & Cook (1992), who recognised three petrographic variants. East to east-southeast-trending *clinopyroxene±olivine-phyric dykes* and a single *aphyric dyke* (D49) intrude Permian sediments. They cut Bainmedart Coal Measures and Radok Conglomerate, but none is known to intrude the Triassic Flagstone Bench Formation, so a Late Permian to Early Triassic age is tentatively assigned to these dykes. Northeast-trending *plagioclase±olivine-phyric dykes* have only been found cutting Neoproterozoic basement rocks, and could therefore be older. Clinopyroxene-phyric dykes contain phenocrysts with Ti-bearing aluminous augite (or rare diopside) cores ($\text{Ca}_{38-46}\text{Mg}_{30-48}\text{Fe}_{10-28}$) and Ti-rich diopside rims of similar composition to groundmass clinopyroxene. Plagioclase-phyric dykes contain labradorite (An_{57-61}) phenocrysts, whereas groundmass plagioclase is more sodic: An_{44-60} in the aphyric and plagioclase-phyric dykes and An_{40-53} in the clinopyroxene-phyric. Olivine 'phenocrysts' in clinopyroxene-phyric dyke D35, which range from Fo_{89} cores to Fo_{80} rims, similar in composition to groundmass olivine, may be mantle xenocrysts. Sanidine is a major groundmass phase in all dykes, and titanomagnetite (ilmenite in D49), biotite, apatite and, in two dykes, analcite are minor phases. Carbonate±quartz±chlorite±clay amygdaloids suggest shallow emplacement, and some dykes contain slightly resorbed quartz xenocrysts. In some intensely altered dykes, ferromagnesian phases are replaced by reddish-brown iron hydroxides(?) and/or carbonate.

Clinopyroxene-phyric dykes are Ne-normative basanites or basaltic trachyandesites in terms of the total alkalis vs SiO_2 plot (Le Bas et al. 1986: Fig. 142), although D45A is

Hy-normative. The aphyric basaltic trachyandesite dyke (D49) is slightly Q and strongly Hy-normative (Table 19). The clinopyroxene-phyric and aphyric dykes have some common compositional features (Fig. 141), although the latter is lower in most incompatible elements, apart from Y and Zr (Fig. 143). Many incompatible element ratios are similar, however, and not unlike those of the Jetty Peninsula groups 1c-d and 2 dykes, albeit with some scatter (Fig. 144). The main exceptions are the lower P/Zr, Nb/Zr and Y/Zr of most of the Radok Lake dykes, although one clinopyroxene-phyric dyke (D35) has relatively high LILE/Zr and Ce/Zr, and its P/Zr and Nb/Zr are similar to those of the Jetty Peninsula dykes. Spidergrams of two of the clinopyroxene-phyric dykes and the aphyric dyke are very similar (apart from the low U of the aphyric dyke) sharing small negative Nb and Sr anomalies (Fig. 146). The generally similar Jetty Peninsula group 2 dykes (Fig. 145) do not have Nb anomalies.

Plagioclase-phyric dykes are Ne-normative basanites (Fig. 142). They are much more evolved than the other Radok Lake dykes (mg^* 39–45), but have slightly lower SiO_2 , which, combined with somewhat different trace element characteristics (higher LILE/Zr, P/Zr and Nb/Zr: Figs 143, 144), means they cannot be genetically related. Incompatible element ratios are quite similar to those of subgroups 1c and 1d from Jetty Peninsula, although LILE/Zr is slightly higher. Spidergrams differ mainly in the more variable LILE contents of the Jetty Peninsula dykes (Figs 145, 146). The age of these plagioclase-phyric dykes is unknown, so it is possible that they could be co-eval with the Carboniferous Jetty Peninsula dykes, although their orientations are somewhat different.



FIGURE 147
Olivine-clinopyroxene-phyric basanite dyke; Mount Kirkby.

Many of the Radok Lake dykes (plagioclase-phyric and one clinopyroxene-phyric) were thus derived from a generally similar, but even more LILE-enriched, source to that of the Carboniferous alkaline dolerites and camptonites of the Jetty Peninsula area and Palaeozoic basaltic dykes from elsewhere in the NPCM. However, most of the clinopyroxene-phyric and the aphyric Radok Lake dykes differ from all these groups in having much lower Nb/Zr, P/Zr, Ti/Zr and Y/Zr, and thus form a compositionally distinct group derived from a somewhat different enriched mantle source. This provides further evidence that they may be significantly younger (Permian or Triassic) than the plagioclase-phyric Radok Lake dykes.

Other mafic dykes

Mafic dykes with a variety of compositions crop out at a few other places in the NPCM (Fig. 147), but are much less abundant than those at Jetty Peninsula. Those dated have given Palaeozoic ages (Table 25), but it is possible that others may be older or younger.

An altered *basalt* (using the total alkalis–SiO₂ classification of Le Bas et al. 1986) dyke (70280296) from northern **Amery Peaks** (Mount Seaton) contains salite (Ca₄₇Mg₄₀Fe₁₃; 5%) and altered ferromagnesian (calcite + chlorite + ?talc; 15%) phenocrysts. The latter pseudomorphs may be altered orthopyroxene, as the rock is strongly Hy and only slightly Ol normative. Alternatively, if the dyke has been significantly altered in composition (it has unusually low Na₂O and its SiO₂ content is only 45.7%), they may be altered olivine. The groundmass comprises andesine, clinopyroxene, altered ?orthopyroxene, and ilmenite, and chlorite + anthophyllite + calcite ocelli are present. In a petrographically similar dyke at Neill Peak near Mawson, serpentine + iddingsite + talc pseudomorphs are apparently after olivine.

Basaltic andesite (71280126) from **Taylor Platform** has given a Permo–Triassic K–Ar plagioclase age of 246±6 Ma (Sheraton 1983). It consists of andesine–labradorite (11%) and clinopyroxene (with cores of orthopyroxene, 4%) phenocrysts in a relatively fresh, well-crystallised groundmass of clinopyroxene (30%), plagioclase (44%), Fe–Ti oxides (3%), and carbonate (in ocelli, 3%) (Fig. 139B).

All the other analysed dykes are more alkaline olivine basalts. *Trachybasalt* (69280217) from **New Year Nunatak** contains zoned phenocrysts of clinopyroxene (15%) and chloritic pseudomorphs after olivine (5%) in a groundmass of altered feldspar, clinopyroxene, Fe–Ti oxides (3–4%), and minor reddish-brown amphibole and carbonate. Petrographically similar, but Ne normative, *basanite* dykes crop out at **Fox Ridge** (69280225) and **Mount Kirkby** (71280007; Fig. 139C). Clinopyroxene from the former has given a Cambrian K–Ar age of 504±20 Ma (Sheraton 1983), although this may be suspect in view of the altered nature of the dyke. Both contain altered olivine (~10%) and zoned augite–salite (near Ca₄₅Mg₄₃Fe₁₂; 5–15%) phenocrysts in a partly altered groundmass of clinopyroxene, plagioclase (An₄₇ in 69280225), alkali feldspar, reddish-brown amphibole (10% kaersutite in 69290225), and minor ilmenite (2–3%). Olivine in 71280007 is about Fo₈₂, but that in 69280225 is pseudomorphed by serpentine, carbonate, chlorite and talc. Petrographically similar basanite dykes crop out at

Hunt Nunataks. Rare alkaline dolerite dykes (phonotephrite or basanite) crop out at **Fisher Massif** (Table 19). A few olivine-bearing dolerite dykes also crop out to the west of **Beaver Lake**.

Most of these dykes are of alkaline affinities, and have high K/Na (Table 19). Only the Amery Peaks basalt plots in the tholeiitic field on the FMA diagram (Fig. 141), but is marginally alkaline in terms of the alkalis–SiO₂ plot (Fig. 142). The Taylor Platform basaltic andesite plots in the calc-alkaline field in the former diagram (resulting from its much higher Na₂O content), but is subalkaline (just) on the latter. Nevertheless, in terms of trace element characteristics, both these dykes are similar to alkaline dykes in the NPCM—particularly subgroups 1a and 1b dolerites from Jetty Peninsula (Figs 143, 144). The Taylor Platform dyke differs from these dykes mainly in its lower TiO₂ and higher SiO₂. Both are quite different in composition to the tholeiitic metadolerite dykes of the Ruker and Fisher Terranes, having much higher Sr, LILE/Zr, LREE/Zr, Nb/Zr, P/Zr and Ce/Y, and lower Y/Zr. Spidergrams of the two dykes are very similar, and only differ from those of subgroups 1a and 1b from Jetty Peninsula in that they do not have much Th and U

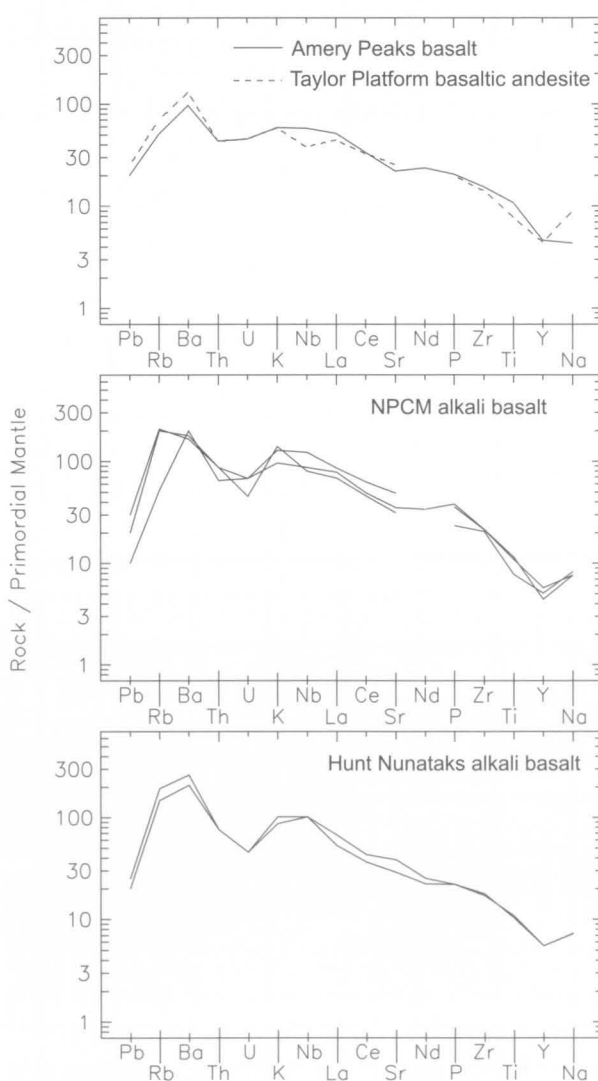


FIGURE 148
Spidergrams for basaltic dykes from the NPCM.

depletion (Figs 145, 148). The data thus suggest derivation of both these dykes from a similarly enriched mantle source, but whether or not they could be co-eval depends on the reliability of the K–Ar age data.

The trachybasalt dyke from New Year Nunatak is slightly Hy-normative, whereas the various basanites are all strongly Ne-normative (Table 19). They are even more strongly enriched in most incompatible elements (LILE, LREE and HFSE), and are quite similar in this regard to group 2 trachydolerites from Jetty Peninsula (Figs 143, 144). The main differences are: the Mount Kirkby dyke has relatively low TiO_2 and P/Zr; the Fox Ridge dyke has high Sr/Zr; and the two Hunt Nunatak dykes have high Ba/Zr. Spidergrams (Figs 145, 146, 148) confirm this general similarity, which suggests that all the Palaeozoic mafic dykes were derived from a broadly similar enriched mantle source, characterised by the presence of a Nb-rich OIB-type (within-plate) component. Much of the variation in incompatible element abundances probably resulted from various degrees of partial melting, which decreased from the tholeiitic to the most strongly alkaline magmas. However, the compositional heterogeneity and range of isotopic ages (if taken at face value) of the dykes mean that they cannot be genetically related. Their geochemistry has been described in more detail by Sheraton (1983) and Mikhalsky & Sheraton (1993), who suggested that the emplacement of some may have been associated with rifting processes before, or during, the breakup of Gondwana.

MESOZOIC ALKALINE ULTRAMAFIC ROCKS

Jetty Peninsula intrusions

Alkaline ultramafic rocks occur mostly as small stock-like bodies or plugs (termed stocks below), dykes on Jetty Peninsula, and sills to the south of Beaver Lake (Fig. 149). They intrude Proterozoic metamorphic rocks and Permo–Triassic continental sediments in the northern and



FIGURE 149

Lower and Upper Northern (Severnøe) alkaline ultramafic stocks; Jetty Peninsula, on eastern side of Beaver Lake. The truck between the bodies gives the scale.

southern parts of Jetty Peninsula, respectively (Fig. 150). Their age was determined by K–Ar whole-rock and mineral dating as Late Jurassic to Early Cretaceous (150 ± 5 to 113 ± 5 Ma; Laiba et al. 1987; 110 ± 3 ; Sheraton 1983). The bodies contain a variety of mantle-derived nodules, mainly peridotite (garnet and spinel lherzolite, harzburgite, and subordinate wehrlite and dunite), that are described in detail below. Metamorphic basement rocks, Permo–Triassic sedimentary rocks, and quartz porphyry inclusions are also present. The latter has not been found in situ in the Beaver Lake area.

The alkaline ultramafic bodies were probably emplaced in two stages. The oldest (140–150 Ma) stocks are dominated by biotite–pyroxene alkali picrite, whereas younger (110–123 Ma) stocks consist of polzenite and/or melanephelinite. Most stocks were formed during two or three intrusion phases. The first intrusive phase in all bodies is represented by tuffisite, which is compositionally similar to the petrographically diverse second intrusive phase. Tuffisite is a mixture of angular and rounded fragments of mantle-derived rocks, metamorphic and sedimentary rocks, and autoliths (lapilli of rushayite, alkali picrite, or melanephelinite) cemented with altered volcanic ash. The proportions of xenoliths and autoliths vary between the intrusions, which probably reflects different erosion levels. These rocks were described as monchiquite breccias by Ravich et al. (1978).

Alkali picrite contains olivine (25–40%) and clinopyroxene (up to 60%) in various proportions, with minor melilite, nepheline, opaque minerals, volcanic glass, and secondary phlogopite. The predominant texture is seriate olivine-phyric, but clinopyroxene and nepheline phenocrysts were also found. Primary igneous olivine (Fo_{88-92}) occurs along with xenogenic mantle-derived olivine (Fo_{94-95}). Olivine crystals in some rocks are mantled by secondary phlogopite. The cryptocrystalline groundmass consists of pyroxene microlites (30–50%), phlogopite (up to 12%), magnetite (up to 10%), perovskite, and secondary minerals (carbonate, natrolite and analcime) replacing glass. Some rocks contain anhedral nepheline (up to 10%) or melilite (up to 20%), altered to carbonate, serpentine and juanite. All contain ocelli composed of late-stage hydrothermal minerals (dolomite, natrolite and analcime) in association with nepheline, clinopyroxene, apatite, phlogopite and andradite. Some bodies contain phlogopite–melilite–pyroxene picrite, nepheline picrite, and nepheline–melilite–pyroxene picrite, with gradational contacts.

Polzenite is an olivine-phyric (20–30%; Fo_{90-92}) rock with a fine-grained matrix of melilite (20–30%), phlogopite (10–20%), nepheline (20%), and Ti-magnetite (up to 10%). It contains various amounts of disintegrated mantle nodules represented by fragments of olivine (Fo_{94-95}) and chrome spinel, and chromite grains. The groundmass texture is microlitic, formed by melilite microlites enclosed in aggregates of secondary minerals after glassy matrix and nepheline. Poikiloblasts of secondary phlogopite, euhedral titanomagnetite grains, perovskite, and apatite occur in the groundmass. Polzenite sills contain olivine (10–35%), phlogopite (10–55%), melilite (15–40%), and nepheline (up to 10%); smaller amounts of clinopyroxene, ilmenite, magnetite, pyrite, perovskite, apatite, and

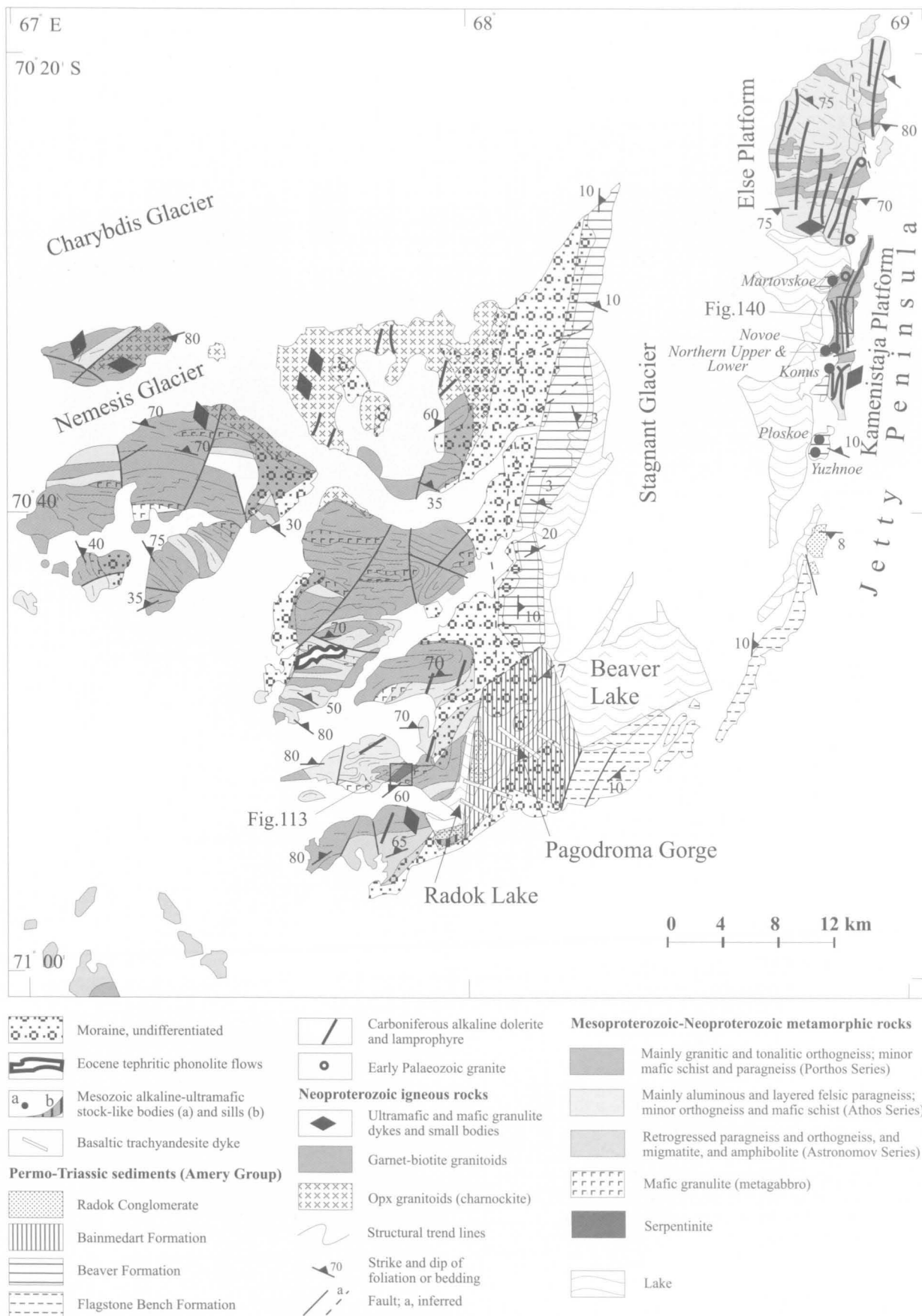


FIGURE 150

Geological map of the Amery Peaks–Beaver Lake–Jetty Peninsula area (Amery Oasis), showing the locations of Figures 113 and 140.

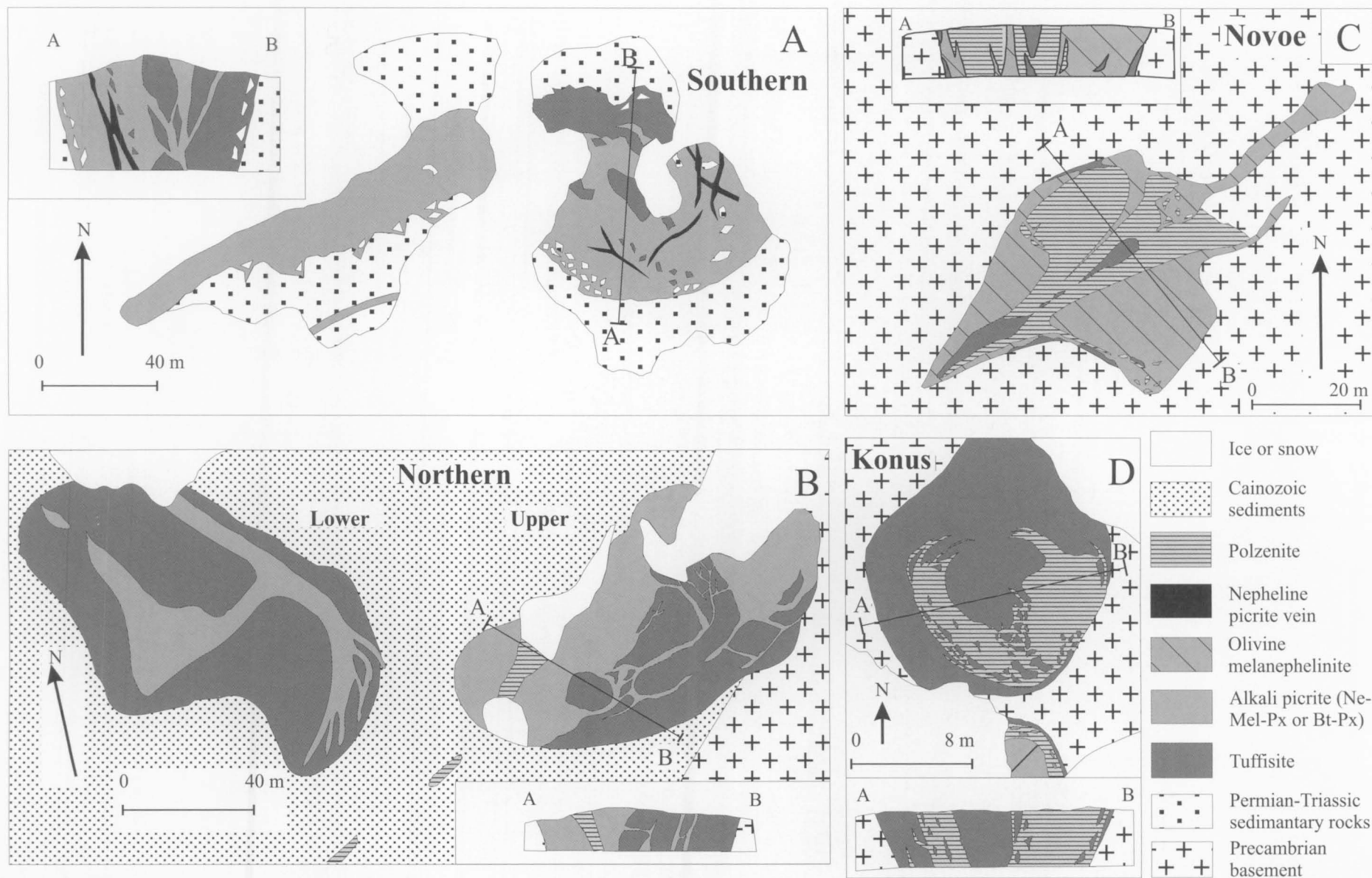


FIGURE 151

Geological sketch maps of Mesozoic alkaline ultramafic stocks; Jetty Peninsula.

carbonate are also present (Fig. 139D). Olivine, which forms phenocrysts up to seven millimetres across, is commonly altered to serpentine, talc and carbonate. Melilite is largely replaced by cebolite and juanite.

Olivine melanephelinite contains phenocrysts (15–30%) of olivine, clinopyroxene, phlogopite and nepheline, with microlites of clinopyroxene (15–25%) and rare melilite, enclosed in a matrix of nepheline (up to 35%), magnetite (3–10%), phlogopite (5–15%), K-feldspar (2–7%), and perovskite.

Rushayite (a glassy variety of olivine melilite) is composed of altered melilite (30–60%), nepheline (8–20%), and minor phlogopite and diopside enclosed in an altered glassy groundmass (30–50%).

Seven stock-like bodies crop out in a north–south-trending chain some 18 kilometres long, and geophysical data suggest that several more such bodies may be covered by moraine or snow within the same linear zone. The location of the bodies is mainly controlled by the intersection of a north–south-trending fault zone, detected by geophysical studies (Ravich et al. 1978; Kurinin & Grikurov 1980, 1982), with northeast to east-trending faults commonly marked by thin dykes of similar alkaline ultramafic composition. The stock-like bodies and plugs

are of oval or rarely isometric shape. They range from 25 to 180 metres along their long axis, which strikes mainly northeast, and have length to width ratios between 1.5:1 and 8:1.

Southern (Yuzhnoe) stock was formed in three phases (Fig. 151A). Eruptive breccia (tuffisite) of the earliest intrusive phase forms the subordinate northeastern part of the intrusion. The clastic material is composed of the host sedimentary rocks, mantle peridotite nodules up to 0.5 metres across, lapilli of alkali picritic composition, and a few fragments of basement metamorphic rocks. The matrix is mainly composed of secondary dolomite. The second and most voluminous intrusive phase is represented by pyroxene alkali picrite, dated at 144 ± 5 Ma (matrix) and 150 ± 5 Ma (phlogopite). Alkali picrite is massive or globular and olivine-phyric. It also contains abundant deep-seated nodules (dominated by lherzolite) and rare sedimentary and tuffisite xenoliths. In the eastern part of the stock, alkali picrite is cut by thin (5–50 cm) veins of nepheline picrite, which represents the third intrusive phase.

Upper Northern (Severnoe Verhnee) and Lower Northern (Severnoe Nizhnee) stocks were formed in two intrusive phases (Fig. 151B). The earlier phase comprises alkali

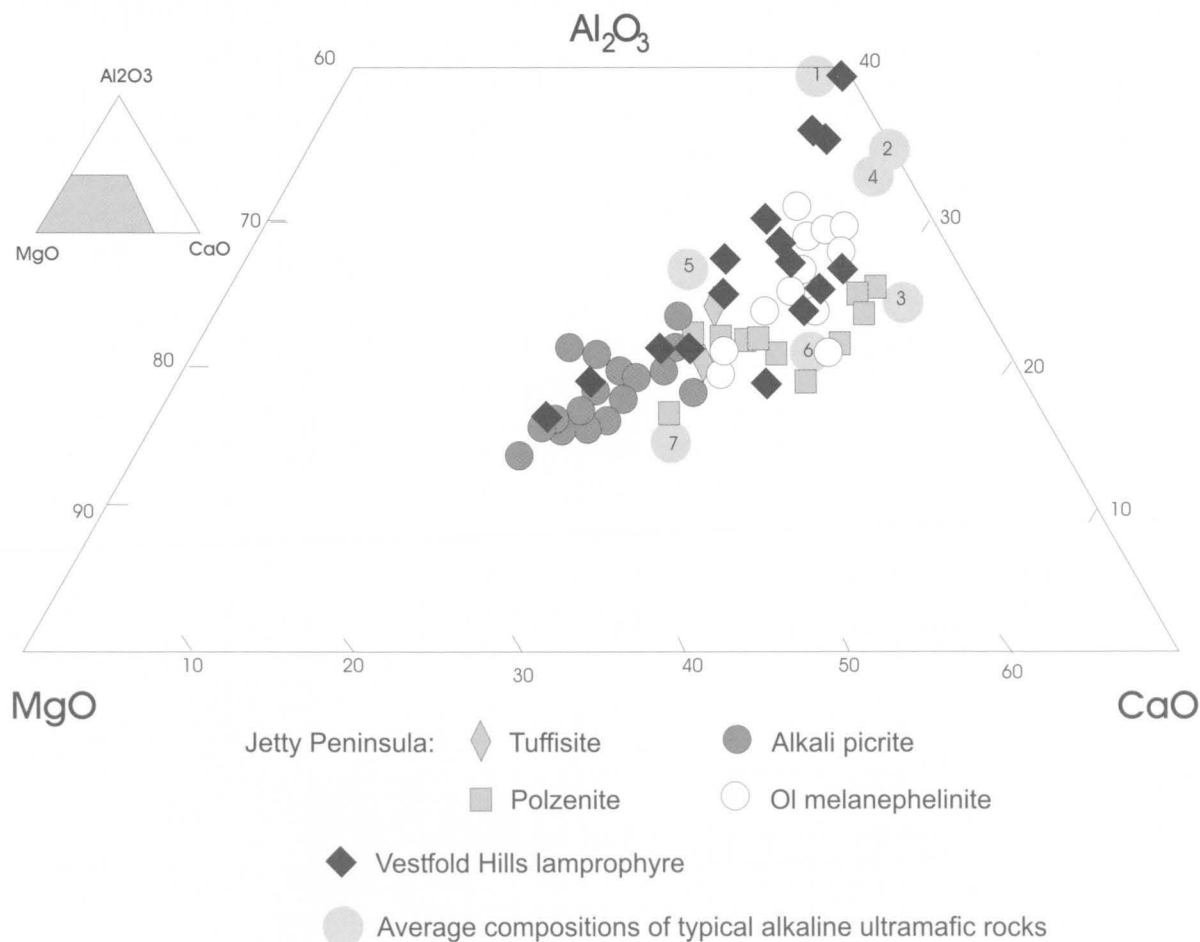


FIGURE 152

$\text{MgO}-\text{Al}_2\text{O}_3-\text{CaO}$ diagram for Mesozoic alkaline ultramafic rocks. The average compositions shown for comparison are: (1) nephelinite, Transbaikalia, (2) melanephelinite, Mongolia, (3) melanephelinite, Kuznetsk Ala Tau, (4) alkali picrite, Czech Republic, (5) alkali picrite, Kuznetsk Ala Tau, (6) olivine turjaite (melilitolite), Maimecha-Kotui Province, and (7) alkaline rocks, Karelia-Kola and Guli Complexes. Data sources: Egorov (1969), Andreeva et al. (1984), Lazarenkov (1988), and A.V. Andronikov (unpublished).

picrite tuffisite, consisting of rounded xenoliths of crustal rocks, autolith lapilli, and bombs (up to 15 cm across). Massive olivine-phyric alkali nepheline-melilite-pyroxene picrite intrudes the breccia. It contains abundant xenoliths and small lithoclasts of upper mantle or crustal origin. The matrix was dated by the K-Ar method at 142 ± 5 Ma (Laiba et al. 1987). Several alkali picrite veins, 0.3 to 1.5 metres thick, occur within tuffisite in the southern parts of both intrusions. The veins are parallel to the stock boundaries and dip toward the centre at 70° to 80° . In the western part of the Upper Northern intrusion, alkali picrite is apparently cut by polzenite. Similar polzenite forms a northeast-trending dyke cutting the host rocks near the intrusive body.

Novoe stock (Fig. 151C) is situated 0.5 kilometres to the northeast of the Upper Northern stock. Emplacement of both bodies was controlled by a fault zone. The stock consists mainly of polzenite, but two lenticular blocks (xenoliths) of rushayite tuffisite occur in the central or axial part of the intrusion. Polzenite contains small rounded dunite inclusions and scattered olivine and chrome spinel xenocrysts. The polzenite has given a K-Ar age of 113 ± 5 Ma (Laiba et al. 1987). The exposures of polzenite are surrounded by a wide zone of melilite-olivine melanephelinite, which represents the last intrusive phase.

Konus stock (Fig. 151D) is composed of rushayite tuffisite (the earliest phase), which accounts for two-thirds of the volume, and alnöite to polzenite (the second phase). The latter form an incomplete ring in the core of the intrusion, which dips steeply (70 – 80°) towards the centre of the body. The polzenite contains numerous xenoliths of breccia and locally intrudes the latter as a stockwork of branching veins.

Ploskoe stock comprises olivine melanephelinite (123 ± 5 Ma: Laiba et al. 1987) and tuffisite of nephelinite composition. The orientation of primary layering, which dips at 75° to 80° toward the centre of the body, suggests that its shape is close to cylindrical. The stock contains abundant xenoliths and large rafts of the host sandstone, which suggests emplacement at a high crustal level.

Martovskoe stock consists of rushayite breccia and melilite-bearing olivine melanephelinite. Secondary carbonate is a major constituent.

Sills of polzenite (alnöite of Walker and Mond 1971) crop out in Permian sedimentary rocks on the southern side of Beaver Lake. They are from five to 11–13 metres thick, and are conformable with the country rocks, dipping at 5° to 15° to the east-southeast. Both sills show vertical zoning which is symmetrical about the central axis. The boundary zones (0.3–0.9 m) consist of intensely altered fine-grained polzenite, which grades into massive varieties. The sills contain uniformly distributed rounded and angular dunite xenoliths and olivine xenocrysts throughout the section. Phlogopite from these rocks has given K-Ar ages of 110 ± 3 Ma (Sheraton 1983) and 117 ± 5 Ma (Laiba et al. 1987).

Dykes of polzenite or biotite-pyroxene alkali picrite strike north or east-northeast. They are near-vertical and 0.5 to 1.0 metres thick.

The alkaline ultramafic rocks show a wide range of strongly SiO_2 -undersaturated compositions (Table 20; Fig. 152). Despite extensive alteration, the lapilli material from

the tuffisite breccia is chemically similar to the alkali picrite or polzenite magma. Alkali picrites are chemically variable. Potassium usually dominates over sodium with $\text{Na}_2\text{O}/\text{K}_2\text{O}$ from 0.6 to 1.1, but rarely up to 1.58. Compared to typical compositions of alkali picrites from other areas, those from Jetty Peninsula are moderately magnesian, low in TiO_2 and FeO (total), high in Al_2O_3 , and relatively high in alkalis (Fig. 152). Compared to average compositions of alkaline and alkaline ultramafic

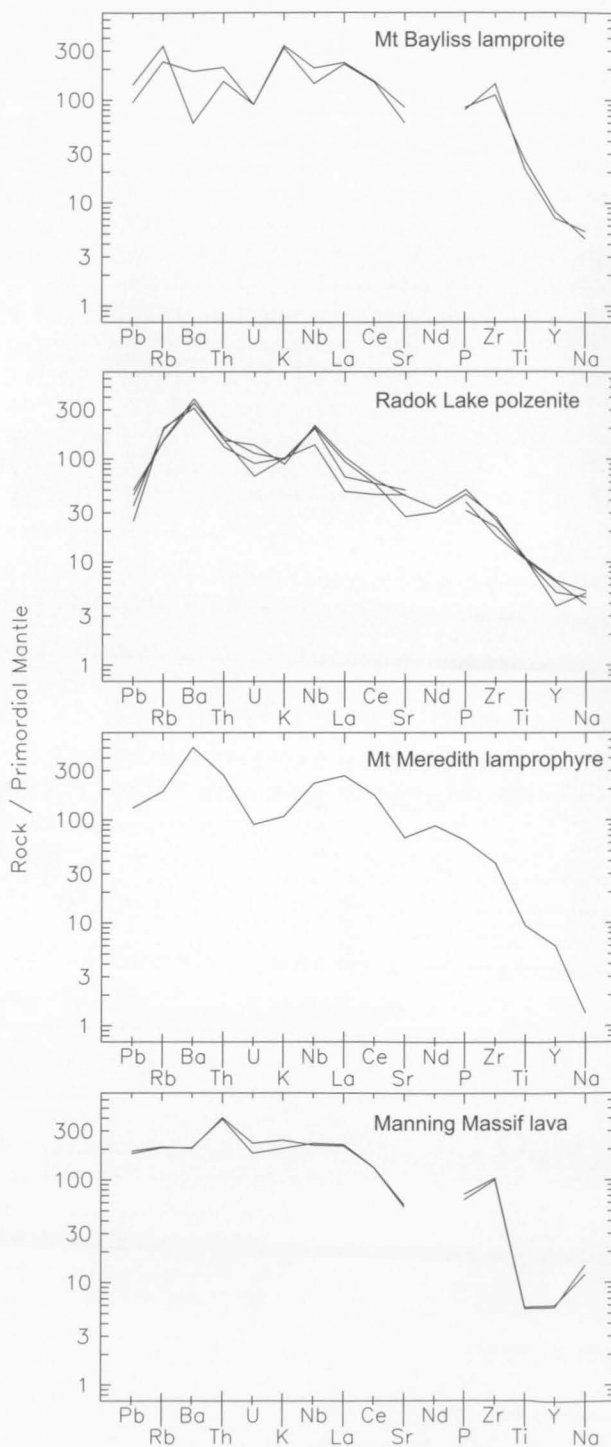


FIGURE 153
Spidergrams for Mount Bayliss lamproites, NPCM
lamprophyres and Manning Massif lavas.

carbonatite-bearing associations (Lazarenkov 1988), the most magnesian alkali picrites are lower in CaO, which may reflect the absence of carbonatite in the Jetty Peninsula association. The Jetty Peninsula rocks also differ from typical kimberlites (Ilupin et al. 1978), mainly in their higher Na₂O and, to lesser extents, higher SiO₂ and Al₂O₃, and lower MgO and CaO. However, they are generally similar in composition to the Dutoitspen pipe in South Africa (Table 20).

Polzenites are characterised by high alkalis (Na₂O + K₂O 2.8–5.7%), with SiO₂ ranging from 32 to 36 percent. The alkali picrites of the stock-like bodies and dykes are moderately potassic (Na₂O/K₂O 0.6–1.1, rarely up to 1.6), whereas polzenite sills are strongly potassic (Na₂O/K₂O 0.4–0.7), possibly related to intense autometamorphic processes (Egorov 1994). The alkaline ultramafic magmas have near-primary compositions, and show only small decreases in SiO₂ and MgO with increasing CaO, Al₂O₃ and TiO₂. These trends suggest variations in the degree of partial melting of the mantle source, but may also indicate the influence of other petrogenetic factors, such as increasing pressure in the source region. Crystal fractionation is unlikely to have had a significant effect on melt composition, because the rocks contain abundant mantle inclusions, which is inconsistent with prolonged evolution of the melt during its ascent to high crustal levels. It is noteworthy that the compositional field of the Jetty Peninsula alkaline ultramafic rocks almost completely overlaps that of ultramafic to alkaline lamprophyres of the Vestfold Hills (Fig. 152; Delor & Rock 1991, Mikhalsky et al. 1994a).

Polzenite sills have strongly fractionated spidergrams that show large enrichments in most incompatible elements from Pb to Zr, particularly Ba, Nb and P (Fig. 153). However, other polzenites have much lower Nb and Zr, being comparable to the alkali picrites in this regard (Table 20). Such variations in trace-element contents could reflect a whole range of processes, such as compositional variations in the mantle source, small degree melting in the presence of residual minor or accessory phases, the presence of LILE-rich metasomatic veins or fluids in the source region, liquid immiscibility in the magma (as evidenced by the presence of ocelli in some rocks), or deuteric alteration.

Mantle nodules comprising lherzolite (including spinel–garnet lherzolite and chrome spinel lherzolite), harzburgite, dunite and wehrlite were found among deep-seated xenoliths from the Southern, Northern (Fig. 154), and Novoe stocks (Andronikov 1987). The composition of mantle olivine ranges from Fo₈₈ to Fo₉₅, with NiO contents of 0.16–0.50 percent. Orthopyroxene contains up to 0.15 percent TiO₂ and up to 1.0 percent Al₂O₃. The two-pyroxene thermometer of Wells (1977) indicates that the garnet-bearing lherzolites were formed at 875–1150°C, whereas assemblages in garnet-free nodules equilibrated at 825–1050°C (Andronikov 1990, 1992). Compositions of the deep-seated nodules provide evidence for upper mantle heterogeneity beneath the Jetty Peninsula area.

Three groups of peridotite nodules were distinguished on the basis of their REE patterns (Andronikov & Egorov 1993): (1) rocks having characteristics similar to primitive mantle, with near-chondritic REE patterns and relatively high SiO₂, Al₂O₃ and CaO; (2) rocks depleted in LREE

during partial melting, with refractory restite features (e.g., lower CaO and Al₂O₃, higher *mg*, and high Cr/(Cr+Al) in spinel); and (3) rocks enriched in LREE by 'cryptic' metasomatism of a previously depleted mantle source region. The timing of metasomatic processes can be roughly assessed by TNd_{DM} model ages of the nodules, which fall into two groups (Andronikov & Belitsky 1995): Mesoproterozoic (1300–1000 Ma) and Neoproterozoic to early Palaeozoic (700–450 Ma).

The Northern and Southern stocks contain quite different mantle nodule assemblages, which also differ in their composition. The Southern stock contains mainly lherzolite nodules (90%) and subordinate harzburgite and dunite. Lherzolite includes chrome spinel and spinel–garnet lherzolite (Andronikov 1990) derived from depths corresponding to about 20 kilobars (Andronikov 1992). The Northern stock contains mainly harzburgite (50%), lherzolite (25%), and subordinate wehrlite and dunite nodules, which indicate a highly depleted mantle composition. The lack of garnet-bearing xenoliths suggests that the Northern stock sampled shallower mantle levels, probably corresponding to about 12 or 15 kilobars (Andronikov 1990, 1992; Andronikov & Sheraton 1996).

Nodules from the Southern and Northern stocks also contain glass of different composition. Those from the Southern stock contain traces of relatively Na-rich glass,



FIGURE 154

Mantle peridotite nodules in the Upper Northern (Severnoe) alkaline ultramafic stock. The hammer points to the largest nodule; smaller nodules are at upper left. The light-coloured xenolith at the top right is a crystalline basement rock. The hammer head is 18 cm long.

TABLE 20. Chemical analyses of representative Mesozoic alkaline ultramafic rocks from the Radok Lake and Fisher Massif areas. Data from Egorov et al. (1993) and A.V. Andronikov, unpublished, with Dutoitspen kimberlite from Milashev (1974).

Sample no.	91286458	R-34	SD-14	KN-3	SV-24	U-22	U-6	PL-17	91286414	34107a	34107-19	34107-9	Dutoitspen
Locality	Radok Lake	Radok Lake	Severnoe stock	Konus stock	Severnoe stock	Yuzhnoe stock	Yuzhnoe stock	Ploskoe stock	Mount Meredith	Fisher Massif	Fisher Massif	Fisher Massif	Dutoitspen
Lithology	Polzenite sill	Polzenite sill	Polzenite dyke	Polzenite	Alkali picrite	Alkali picrite	Alkali picrite	Ol mela-nephelinite	Lamprophyre dyke	Kimberlite dyke	Carbonate kimberlite dyke	Globular carbonate kimb. dyke	Kimberlite
SiO ₂	34.87	32.79	34.50	35.24	39.96	35.76	42.07	38.94	24.19	20.54	14.14	8.28	39.00
TiO ₂	2.21	2.20	2.47	2.38	1.95	1.50	1.72	2.38	2.00	1.25	2.13	0.71	0.95
Al ₂ O ₃	9.14	7.58	8.22	10.55	8.59	5.34	8.24	9.81	4.70	2.24	5.17	2.25	5.52
Fe ₂ O ₃	3.28	4.79	4.67	4.03	3.20	2.31	0.88	2.14	2.66	*12.40	*15.75	*3.31	*10.29
FeO	7.48	5.30	6.01	6.18	6.25	6.70	7.01	7.43	5.41	-	-	-	-
MnO	0.17	0.16	0.20	0.21	0.19	0.17	0.18	0.19	0.14	0.19	0.31	0.19	0.50
MgO	13.80	14.35	17.35	13.61	18.24	23.73	18.21	11.93	15.17	17.06	8.64	4.00	22.65
CaO	13.48	16.02	10.66	15.05	10.67	8.69	7.57	11.91	15.56	22.10	26.89	42.96	6.30
Na ₂ O	1.51	1.91	1.78	1.84	2.34	1.42	2.50	2.62	0.52	0.28	0.23	0.20	1.59
K ₂ O	2.81	2.52	2.32	1.96	1.48	1.80	1.76	2.10	3.01	0.58	0.65	0.53	1.22
P ₂ O ₅	0.99	0.73	0.93	1.00	0.63	0.63	0.78	0.64	1.38	1.56	3.30	2.42	0.45
H ₂ O ⁺	-	-	-	-	-	-	-	-	-	6.26	3.78	2.14	-
CO ₂	-	-	4.10	2.84	3.66	8.90	5.11	6.71	-	15.54	18.70	32.58	-
LOI	8.88	11.83	10.41	6.83	6.74	12.18	8.60	9.69	23.45	-	-	-	11.76
Rest	0.83	0.46	0.64	0.56	0.50	0.45	0.51	0.40	1.02	0.33	0.44	0.57	0.00
Total	99.45	100.64	100.16	99.44	100.74	100.68	100.03	100.18	99.21	100.33	100.13	100.14	100.23
O=F,S,Cl	0.10	0.00	0.00	0.00	0.00	0.00	0.00	0.00	0.03	0.00	0.00	0.00	0.00
Total	99.35	100.64	#100.16	#99.44	#100.74	#100.68	#100.03	#100.18	99.18	100.33	100.13	100.14	100.23
Q	-	-	-	-	-	-	-	-	-	-	-	-	-
C	-	-	-	-	-	1.06	2.17	-	-	-	-	-	-
Or	-	-	10.02	-	8.75	10.64	10.40	12.41	-	3.43	3.84	3.13	7.21
Ab	-	-	-	-	10.12	12.02	21.15	21.22	-	2.37	1.84	1.69	4.08
An	9.86	4.67	7.59	14.74	8.56	-	0.16	8.80	1.60	1.21	-	-	4.32
Lc	13.02	11.68	2.89	9.08	-	-	-	-	-	-	-	-	-
Ne	6.92	8.76	8.16	8.43	5.24	-	-	0.51	2.38	-	0.06	-	5.08
Kp	-	-	-	-	-	-	-	-	10.11	-	-	-	-
Di	7.98	0.17	10.59	14.70	13.60	-	-	2.95	-	-	-	-	19.07
Hy	-	-	-	-	-	2.05	18.12	-	-	0.80	-	4.72	-
Ol	30.23	32.92	34.98	26.73	34.97	47.87	25.45	27.30	32.58	40.15	28.39	6.24	42.76
Cs	12.57	21.62	-	5.28	-	-	-	-	20.61	-	-	-	-
Mt	2.52	2.32	2.47	2.37	2.21	2.12	1.89	2.26	1.87	2.70	3.43	0.72	2.24
Il	4.20	4.18	4.69	4.52	3.70	2.85	3.27	4.52	3.80	2.37	4.04	1.35	1.80
Ap	2.34	1.73	2.20	2.37	1.49	1.49	1.85	1.52	3.27	3.70	7.82	5.73	1.07
Cc	-	-	9.32	6.46	8.32	14.03	11.62	15.26	-	35.34	40.24	70.99	-
S	2000	-	-	-	-	-	-	-	700	-	-	-	-
Sc	34	17	28	22	25	14	14	17	28	-	-	-	-
V	283	191	278	227	199	119	127	182	209	-	-	-	-
Cr	406	547	531	211	796	658	713	247	704	-	-	-	-
Ni	313	238	275	207	570	488	569	163	410	481	66	93	-
Cu	67	-	-	-	-	-	-	-	54	-	-	-	-
Zn	105	-	-	-	-	-	-	-	85	-	-	-	-
Ga	16	-	-	-	-	-	-	-	9	-	-	-	-
Rb	95	125	81	38	36	78	58	107	119	-	-	-	-
Sr	578	1119	994	1674	697	668	783	848	1407	1997	1502	1703	-
Y	29	21	29	29	24	19	19	24	27	22	33	34	-
Zr	303	39	74	185	59	62	169	200	423	151	141	177	-
Nb	144	21	24	30	16	12	40	44	161	-	219	243	-
Ba	2419	1062	2590	1654	1308	1233	1293	1149	3489	-	1090	1570	-
La	66	89	96	88	72	64	71	60	188	-	340	530	-
Ce	103	154	158	152	123	120	132	111	313	-	320	480	-
Nd	41	69	68	66	50	50	54	46	119	-	-	-	-
Pb	10	5	9	10	7	15	12	14	26	-	-	-	-
Th	14	22	23	20	12	22	20	19	25	-	-	-	-
U	1.5	2.1	3.6	3.4	2.9	2.8	2.9	2.8	2.0	-	-	-	-
K/Rb	246	168	238	431	346	192	254	163	210	-	-	-	-
(Ce/Y) _n	8.9	18.0	13.6	13.3	12.7	15.6	17.0	11.8	29.0	-	24.2	35.3	-
Ba/Zr	8.0	27.3	34.9	8.9	22.0	20.0	7.7	5.8	8.3	-	7.7	8.9	-
Ce/Zr	0.34	3.97	2.13	0.82	2.06	1.95	0.78	0.56	0.74	-	2.27	2.71	-
Nb/Zr	0.48	0.54	0.32	0.16	0.27	0.19	0.24	0.22	0.38	-	1.55	1.37	-
Nb/Nb*	2.07	0.27	0.31	0.43	0.29	0.21	0.68	0.76	1.20	-	1.21	0.88	-
Sr/Sr*	0.63	0.79	0.69	1.20	0.64	0.62	0.66	0.85	0.52	-	-	-	-
mg*	73.5	75.8	78.1	74.4	80.7	85.0	83.0	72.8	80.4	76.2	56.1	73.7	83.7

mg* = atomic 100Mg/(Mg + 0.85Fe(total)); * total Fe as Fe₂O₃; # totals exclude CO₂.

while the Northern stock contains K-rich (up to 15% K_2O) or Na-K glass (Andronikov 1997). These glasses are believed to represent partial fusion within the mantle, and thus their composition should partly reflect a varying mantle source composition. More sodic glasses of the Southern stock presumably resulted from partial melting of an amphibole-bearing assemblage, whereas K-rich glasses of the Northern stock represent melting of a phlogopite-bearing assemblage (Andronikov 1997).

Mineral (olivine-spinel) compositions of the nodule suites have revealed different redox states for the mantle beneath the Jetty Peninsula area. The calculated oxygen fugacity relative to the fayalite-magnetite-quartz buffer ($\Delta\log(f_{O_2})$) for Southern stock nodules ranges from FMQ -2.5 to about FMQ (mainly in the graphite stability field), whereas nodules from Northern stocks are more oxidised, ranging from FMQ to FMQ +2 (Andronikov & Sheraton 1996). Virtually all f_{O_2} values are above the C-H₂O buffer, that is, in the stability field of CO₂-bearing fluid. The data suggest that increasing oxidation state was associated with mantle heating, but not with metasomatism (Andronikov & Sheraton 1996).

Marked differences in the composition of mantle nodules from the Southern and Northern stocks indicate derivation from distinct mantle domains or layers, although the stocks are only some 10 kilometres apart (Andronikov & Sheraton 1996). The mantle domain sampled by the Northern stock represents relatively shallow mantle that has undergone extensive melt depletion and subsequent metasomatism and oxidation, possibly at least partly in a subduction zone associated with a Proterozoic continental margin. In contrast, the deeper mantle domain sampled by the Southern stock was more reduced and less refractory (more fertile), but was apparently involved in much less extensive melt extraction and metasomatism, probably (on isotopic evidence) during production of alkaline intra-plate magmas in Palaeozoic times.

The alkaline ultramafic parent magmas of the Jetty Peninsula rocks are likely to be primary melts, which allows estimation of pressure during mantle partial melting and magma segregation using the equation of Ballhaus (1995). This equation gave pressures of about 38–40 kilobars (equivalent to depths of 125–130 km) for the rocks of the Northern and Southern stocks, and 32–34 kilobars (100–110 km) for the Novoe and Konus stocks (A.V. Andronikov, personal communication). Taken at face value, this would suggest that the mantle nodules were derived from well above the actual partial melting (source) zones. One of the main petrogenetic factors controlling the character of partial melting is likely to have been fluid conditions in the mantle. Methane-rich fluid probably ascended from a reduced asthenosphere and entered a strongly oxidised lithosphere, which resulted in the formation of large amounts of water and elementary carbon. Carbon should have been rapidly oxidised, forming large volumes of H₂O and CO₂ in the reaction zone between the methane fluid and lithospheric rocks, and resulting in a considerable decrease in the liquidus temperature of the mantle rocks. Water-rich fluids would have penetrated overlying layers and formed metasomatic hydrous phases (Foley 1992). Partial melting under CO₂-dominant conditions would have produced melts

chemically similar to ultramafic lamprophyres. The mode of occurrence and structure of the small bodies at Jetty Peninsula are consistent with excess fluid contents in the lamprophyric magmas (Rock 1987). The intrusion of such magmas resulted in the formation of a 'piston' of compressed gas in the upper part of the magma column that would have caused a decrease in the strength of the crustal rocks and a rapid ascent to the zone of open fissures, two to three kilometres below the surface.

It is noteworthy that the two stocks intrude different host country rocks: Permo-Triassic Amery Group strata by the Southern stock, and Proterozoic metamorphic rocks by the Northern stock. Assuming that the Permo-Triassic sediments were deposited under tectonic control in a graben or half graben, it is thus possible that a major, long-lived tectonic zone separates two crustal and corresponding lithospheric mantle blocks or domains in the southern Jetty Peninsula area. Mesoproterozoic ultramafic lamprophyre dykes of the Vestfold hills also contain deep-seated nodules very similar to those from the Northern stock of Jetty Peninsula (Andronikov et al. 1994; Andronikov & Mikhalsky 1997), which indicates a prolonged history of the northern Jetty Peninsula-Vestfold Hills mantle domain from at least the Mesoproterozoic.

It has been suggested that the alkaline ultramafic bodies of Jetty Peninsula are diatremes, and some researchers have even attempted to identify them as kimberlite pipes (Ravich et al. 1978; Laiba et al. 1987). The latter hypothesis was based on the occurrence of pyrope garnet in the Southern stock (Andronikov 1987). However, in contrast to kimberlite, the main rock type of this intrusion, nepheline picrite, belongs to the alkali picrite family (Egorov 1994). The wide occurrence of polzenite in the stock-like bodies at Jetty Peninsula suggests a transitional character for this rock suite between the tinguaitite-alnöite-alkali picrite and kimberlite associations. The complicated polyphase structure of the stock-like bodies is of particular significance, and is comparable to the lamproite diatremes of northwestern Australia. With respect to morphology, structure and polyphase development (tuffisite of the first phase is followed by two or three injections of massive lava), the lamproite diatremes are completely homologous to the alkali picrite-polzenite stocks of Jetty Peninsula (Egorov 1994). Diamonds have been found in some nonkimberlitic rocks of similar age: Kakanui nephelinite breccia (New Zealand), Eli-Ness basanite breccia (Scotland), alnöite breccia of Malaita Island (Solomon Islands), alkali picrites of the Urals, and mildly alkaline basalts of the Sahara (Chaika & Uzhgalis 1976; Dawson 1980; and Jaques et al. 1985; cited by Egorov 1994). Egorov & Andronikov (1993) emphasised the potential for the occurrence of diamond in the Jetty Peninsula alkaline ultramafic rocks. Detailed field and mineralogical studies were carried out, and a few diamond grains were recovered from a bulk-rock sample from the Southern stock (VNIIOkeangeologia, unpublished report).



FIGURE 155

Thin kimberlite dyke; centre of southeastern slope of Fisher Massif (photo by A.Yu. Melnik).



FIGURE 156

Magmatic layering in kimberlite dyke; centre of southeastern slope of Fisher Massif.

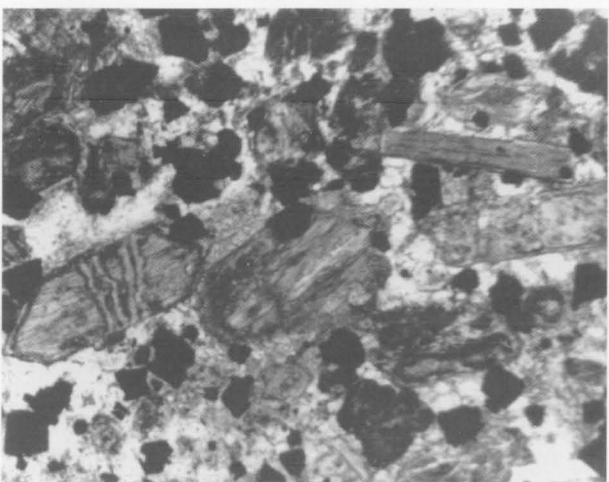


FIGURE 157

Kimberlite dyke containing olivine (replaced by iddingsite), phlogopite and ilmenite, in a carbonate-rich matrix; Fisher Massif. Sample 34107-10; width of field: 1 mm.

Kimberlites of the Fisher Massif area

Kimberlite dykes containing carbonatite globules crop out at **Fisher Massif** (Egorov et al. 1993). They are up to 25 centimetre thick (Fig. 155), dip northwest (300°) at 40 to 70° , and have a layered structure (Fig. 156). The kimberlites are assumed to be of similar Late Jurassic to Early Cretaceous age to the alkaline ultramafic rocks of Jetty Peninsula. The rocks show lenticular banded and globular structures and a porphyritic texture, with phenocrysts of phlogopite and pseudomorphs after olivine (Fig. 157). The groundmass consists of olivine (15–50%, completely replaced by serpentine, chlorite, iddingsite and carbonate aggregates), calcite (25–60%), magnetite (up to 10–15%), apatite (3–5%), phlogopite, and serphopite (a variety of serpentine: 3–5%). Chromite occurs as an accessory phase. Calcite in the groundmass is represented by granoblastic and micropoikiloblastic aggregates or elongated needle-like dendrites of metasomatic origin. The globules are of primary carbonate composition and retain their tabular-grained texture. Egorov et al. (1993) proposed that the banded structure of the dykes reflects igneous layering due to the high concentration of carbonate components in the parental melt, and the calcite globules represent an immiscible carbonate-rich melt. The kimberlitic rocks have very high CaO, and typically high Sr, Ba, Nb and LREE (Table 20).

A possibly related lamprophyric (?monchiquite) dyke of unknown age which crops out at nearby **Mount Meredith** contains altered olivine phenocrysts in an altered fine-grained groundmass with phlogopite, pale brown amphibole, carbonate, and opaque minerals (Fig. 139E). Like the kimberlitic rocks, it is SiO_2 -poor and carbonate-rich (Table 20), with a strongly fractionated spidergram showing particularly strong enrichment in Ba, Nb, LREE, P and Zr, and very low Na (Fig. 153). It is chemically quite similar to the Fisher Massif kimberlites, differing mainly in its lower total FeO and CaO, and higher K_2O and Ba.

EOCENE TEPHRITIC PHONOLITE LAVA OF MANNING MASSIF

Tephritic phonolite (using the volcanic rock classification of Le Bas et al. 1986, but termed leucite tristanite by Sheraton 1983, and alkaline trachybasalt by Andronikov et al. 1998) makes up the surviving part of a lava sequence, which covers an area of 0.2 to 0.6 by 3.8 kilometres at Manning Massif. The sequence includes four lava sheets with a total thickness of up to 20 metres, and appears to have subsided along normal faults (Andronikov & Egorov 1992). The rocks have been dated at 50 ± 2 Ma (K–Ar whole-rock age: Sheraton 1983) and 40 ± 11 Ma (Rb–Sr: Andronikov & Belitsky 1995); $T_{\text{DM}}^{\text{Nd}}$ model ages are 910–990 Ma, with ϵ_{Nd} of -8 to -11 (Andronikov & Belitsky 1995).

The relatively small proportion of scoria (20–40% of sheet thickness) suggests that the magma was relatively dry. Amygdales in the highly vesicular zones commonly contain phillipsite. Glassy rocks at the base of the sheets are porphyritic, with olivine (Fo_{70-80}) phenocrysts. Cataclastic olivine also occurs as xenocrysts (Fo_{85-90}), probably derived from disintegrated mantle nodules. The

lavas consist of plagioclase laths (An_{55-65}), small rounded leucite grains (up to 20%), augite microlites, olivine microphenocrysts and xenocrysts, and a groundmass composed of devitrified glass, rare anhedral alkali feldspar, and opaque grains (including ilmenite). A relatively coarse-grained sample contains olivine microphenocrysts, clinopyroxene, alkali feldspar, reddish-brown biotite, and Fe-Ti oxides (Fig. 139F).

These rocks differ from typical trachybasalt in their relatively high SiO_2 (50–52.3%) and alkalis ($Na_2O + K_2O = 9\text{--}11\%$). Na_2O/K_2O ranges from 0.51 to 1.03. The lavas are strongly Ne-normative (Table 19), and compositionally distinct from any of the other alkaline mafic rocks in the

PCM (Figs 141, 142). The main K-bearing phase is primary igneous leucite. In contrast, the high K of the alkaline ultramafic rocks of Jetty Peninsula is related mainly to secondary(?) phlogopite (Egorov 1994). There is some similarity, particularly in trace-element contents (e.g., very high Zr and Nb), to early Palaeozoic lamproites of the SPCM, but these have much higher TiO_2 and K_2O and lower Al_2O_3 and Na_2O . Spidergrams show positive Th and Zr anomalies, but negative Sr, Ti and Y anomalies (Fig. 153). The negative anomalies may reflect the relatively evolved compositions of the rocks (mg^* 59–60, Cr 60–68 ppm, Ni 61–66 ppm), which imply significant crystal fractionation.

PERMO-TRIASSIC SEDIMENTARY ROCKS (AMERY GROUP)

Permian to Triassic sedimentary rocks crop out in an area about 50 kilometres long and 25 kilometres wide (Fig. 150) around Beaver Lake and Stagnant Glacier (Crohn 1959). The sediments fill a north-south trending rift graben that contains a younger trough, over 450 metres deep, occupied by Beaver Lake. They abut Proterozoic metamorphic rocks to the west along the Amery Fault (McKelvey & Stephenson 1990). No other Palaeozoic to Mesozoic sedimentary rocks crop out in the PCM, but such rocks occur as erratics in moraine in the SPCM, with *Glossopteris*-bearing siltstone at Mounts Rymill and Maguire (Ruker 1963; D.D. Kolobov, unpublished data). Lithologically similar sedimentary rocks have also been reported from Ocean Drilling Program hole 740 in Prydz Bay (Turner 1991, 1993).

In the Beaver Lake area the sedimentary rocks dip gently to the southeast at 10 to 18°, and are locally cut by predominantly east-west-trending normal faults with relative displacements of up to some hundred metres. Mond (1972) assigned the rocks to the Amery Group, which was subdivided into three units (formations), from bottom to top: Radok Conglomerate, Bainmedart Coal Measures, and Flagstone Bench Formation. Detailed descriptions of the stratigraphy are given by Mond (1972), Ravich (1974), Ravich et al. (1977), McKelvey & Stephenson (1990), Aleksashin & Laiba (1993), Webb & Fielding (1993), and McLoughlin & Drinnan (1997a, b). Aleksashin & Laiba (1993) distinguished two separate formations (Bainmedart and Beaver Formations) within the Bainmedart Coal Measures (Fig. 158).

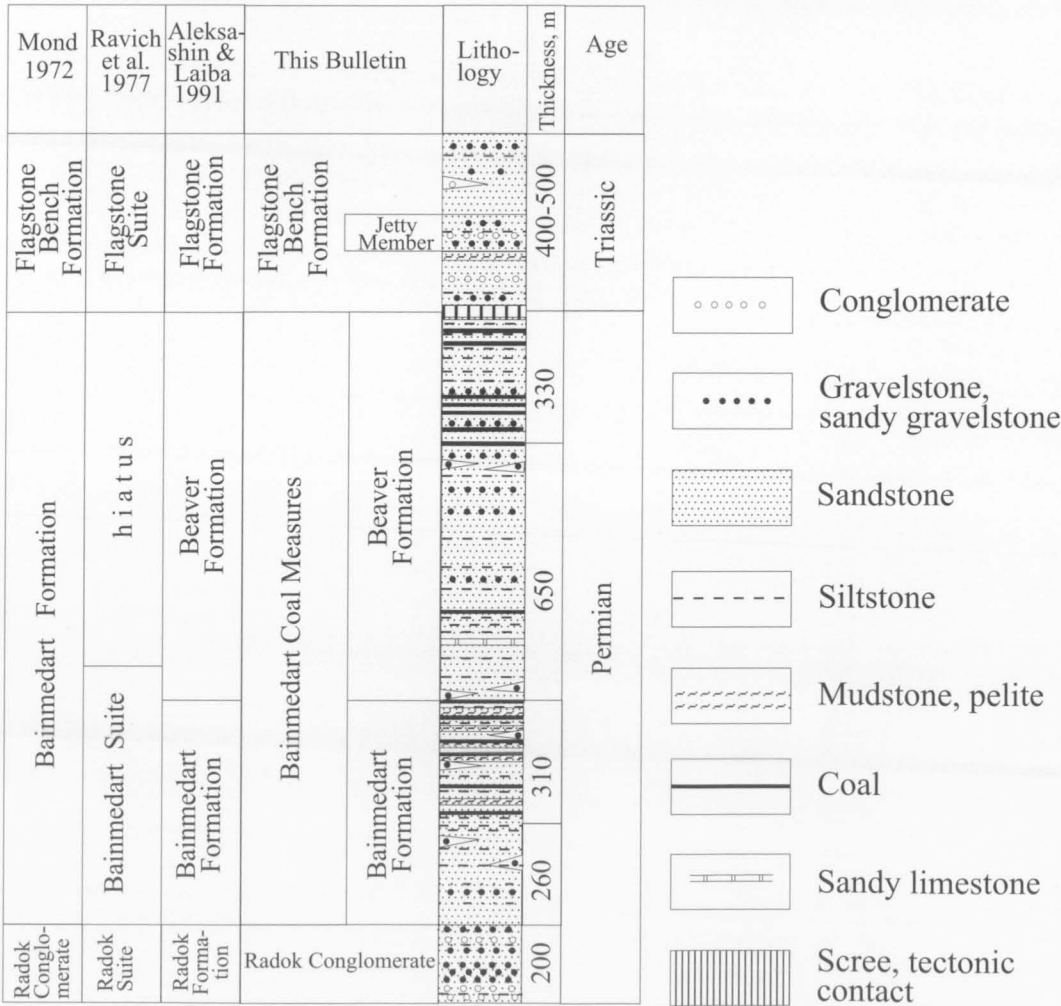


Figure 158
Stratigraphy of Amery Group sedimentary rocks.



FIGURE 159

Radok Conglomerate and Bainmedart Coal Measures cut by a thin alkaline basaltic dyke (above figure); east of Radok Lake.

RADOK CONGLOMERATE

The Radok Conglomerate crops out on the eastern side of Radok Lake and is thought to lie unconformably on Proterozoic metamorphic rocks, though the contact is not exposed and may be faulted. This formation consists of greenish-grey and reddish-brown or purple conglomerate and gravelstone with minor sandstone, siltstone and shale (Fig. 159). The reddish-brown strata are most characteristic of the basal 60 metres, which show irregular stratification with abundant local erosion surfaces. All rock types are intercalated forming cycles two to eight metres thick. Conglomerate pebbles and cobbles up to 20 centimetres across and boulders up to 1.5 metres across consist of metamorphic rocks, and are enclosed in a poorly sorted coarse-grained matrix of quartz, feldspar and rock fragments. They are angular to sub-angular and poorly sorted. Sandstones are very immature arkoses composed mainly of K-feldspar, various amounts of quartz, and minor mica. The better sorted arkoses are more quartz-rich, and are cemented by quartz overgrowths, calcite, and crystalline clay minerals (McKelvey & Stephenson 1990). Mafic minerals and plagioclase are lacking, and garnet is rare. The formation is up to 220 metres thick, and generally fines upwards. The upper part consists of medium-grained sandstone, interbedded with subordinate pebble conglomerate.

Cross-bedding and immature sediment compositions provide evidence for rapid fluvial deposition close to the source region. Textural, petrographic and palaeocurrent data suggest local derivation from Precambrian crystalline source regions to the immediate west during a period of

faulting. Soft-sedimentary features (oversteepening and folding of cross-beds) were reported by McKelvey & Stephenson (1990). Stream-flow, sheet-flow, and sediment gravity-flow facies, suspension fallout in shallow standing water, and organic sediment accumulation in peat-forming wetlands were common depositional conditions. McKelvey & Stephenson (1990) described delta-front interdistributary-bay sediments (22 m thick), termed the Panorama Point Beds, which were separated from the Radok Conglomerate that was deposited in a coarse alluvial fan setting. The middle and upper parts of the Radok Conglomerate contain plant fossils (*Neoggerathiopsis history* Feistm., *Gangamopteris obovata* Carrythers, and *Glossopteris* cf. *communis* Feistm.) which suggest an Early Permian age (Ravich 1974). However, spores of Late Permian age were recovered from this unit (Kemp 1969), and Fielding & Webb (1995) described the Radok Conglomerate as Middle to Upper Permian.

BAINMEDART COAL MEASURES

This unit crops out on the western side of the Beaver Lake–Stagnant Glacier area, and rests disconformably on the Radok Conglomerate and probably the Panorama Point Beds. The basal strata consist of conglomerate ranging from 10 centimetres to three metres in thickness, the Dart Fields Conglomerate of McKelvey & Stephenson (1990). The Bainmedart Coal Measures represent cyclic intercalations of sandstone, siltstone, argillites, mudstone and coal. Most cycles are asymmetric and include three beds, but symmetrical cycles composed of four or rarely five beds were found. The lowermost beds in each cycle

are the most voluminous (1–46 m) and are composed of coarse-grained cross-bedded sandstone of feldspar-quartz or arkosic composition which locally contain gravelstone lenses and seams. The middle beds (0.5–10 m) consist of intercalated finer-graded rocks ranging from sandstone to argillite, with different lithologies grading into one another. The upper beds (0.1–8 m) are composed of coal and coaly siltstone to mudstone. The roofs of the upper beds commonly display washout structures. The formation is 1800 metres (Mond 1972) or 1550 metres (Aleksashin & Laiba 1993) thick, and is compositionally heterogeneous. Different intervals (members) differ in the volume and proportion of the three cyclic components, which may, in part, be absent. The uppermost coal-bearing component is the most variable one.

Aleksashin & Laiba (1993) subdivided the Bainmedart Coal Measures into a lower Bainmedart Formation and an upper Beaver Formation, 570 and 980 metres thick, respectively. These formations differ in the proportion and thickness of the cyclic components. The Beaver Formation contains only subordinate thin siltstone and mudstone beds and layers; it comprises thick coal-free intervals (up to 170 m), and contains rare sandy calcareous beds and well-rounded quartzite pebbles in some layers. Miospore assemblages also differ between the two formations: monosaccate and monosulcate miospores respectively predominate in the Bainmedart and Beaver Formations. The miospore assemblages in both formations correspond with upper Permian Gondwanide assemblages known from India, Australia and Africa (Dibner 1976). Leaf and stem impressions are abundant throughout the strata. Plant microfossils were first described by White (1969), Balme & Playford (1967), and Kemp (1969), and provide evidence for a Late Permian age of the sediments. The lower part the Bainmedart Coal Measures (i.e., the Bainmedart Formation) contains *Glossopteris communis* Feistm., *G. funchsii* Plumst., *G. indica* scm., *G. ampla* Dana, *G. logcuolis* Feistm., *Gangamopteris angustifolia* McCoy, *Dietyopteridium sporiferum* Feistm., *Palaeovittaria* sp., and *Taenioipitius scotli* Krause (petrified wood) characteristic of Upper Permian Gondwana sequences (Mond 1972). Growth-ring analysis indicates a markedly seasonal climate with low to moderate interseasonal variations in wood production (Weaver et al. 1997). Fielding & Webb (1996) assigned the Bainmedart Coal Measures to a high-energy alluvial system, with the sediments forming part of a narrow, corridor-like basin fill that may represent a remnant graben or half-graben.

About 100 coal seams are enclosed within, and restricted to, the Bainmedart Coal Measures. Individual seams are mostly between 0.2 and 1.5 metres thick, with about half exceeding 0.7 metres and a few reaching three or eight metres (Fig. 160). Coal beds have a near-constant thickness and may be traced for many hundreds of metres. The total thickness of coal is up to 80 metres, and is mostly concentrated in the uppermost unit of the Beaver Formation (Fig. 158). Coal beds have a uniform structure, commonly containing pyrite and marcasite-bearing layers and calcareous or ferruginous material near the base; underlying clay or soil beds are very rare. Coal mostly has an attrital texture, layered structure and black colour. Four main coal types may be distinguished on the basis of predominant coal-forming components: (1) gelitic,

composed of gelite (57–75%), fusite (16–40%), and liptite (3–9%); (2) vitrainitic, composed of vitrinite (81–87%), fusite (6–12%), and liptite (1–7%); (3) fusainitic, composed of fusite (40–60%), vitrinite (32–46%), and liptite (3–14%); and (4) a mixed type formed of roughly equal proportions of different coal microlithotypes (Kameneva & Mikhalsky 1985). The coals are of long-flame to gas high-volatile bituminous quality. In a few places, where intruded by mafic dykes, they have been severely baked. The coals contain: moisture 3–6 percent, volatile components 29–54 percent, fixed carbon 28–52 percent, and ash 15–30 percent (Bennett & Taylor 1972; Kameneva & Mikhalsky 1985). Coal comprises C 73–83 percent, O 10–21 percent, H 4.2–5.7 percent, N 1.8–2.2 percent, and S 0.6–1.2 percent, and specific energies (d.m.m.f.) range between 27 and 34 megajoules per kilogram (Bennett & Taylor 1972; Aleksashin & Laiba 1993).

FLAGSTONE BENCH FORMATION

The Flagstone Bench Formation crops out on the southern and eastern banks of Beaver Lake, and is composed of gravelly arkosic sandstone and finer grained rocks. It is over 550 metres thick, and conformably overlies the Middle to Late Permian Bainmedart Coal Measures. The formation comprises cyclic intercalations of coarse-grained, light grey quartzo-feldspathic and very rarely arkosic sandstone, and multi-coloured (magenta, rusty, reddish and yellowish) fine-grained sandstone, siltstone and mudstone containing horizontal and trough cross-bedding structures; conglomerate lenses and layers occur sporadically. In a few places angular felsic volcanic rock fragments constitute a minor part of the clastic material, and altered ash probably contributes to the rock matrix (Argutin 1989). Sandstone sporadically contains accessory garnet, ilmenite, zircon, apatite, monazite, tourmaline, rutile, staurolite, and rare carnotite ($K(UO_2)_2(VO_4)_2 \cdot 3(H_2O)$, rautite ($Ca(UO_2)_2V_{10}O_{28} \cdot 16H_2O$), and other U-bearing phases (Argutin 1989). Ferriferous concretions are abundant in some arkosic sandstone beds.

Traube (1991) described a 70-metre thick member (defined as the Jetty Formation) containing olistoliths (exotic blocks) and conglomerate and breccia with exceptionally coarse debris material in the middle part of the Flagstone Bench Formation, which indicates major tectonic activity in this area. A 60 metre-thick member (the Jetty Member), composed of red weakly lithified sand, gravel and mud-cracked palaeosols, was also reported by Webb & Fielding (1993) from broadly the same stratigraphic position. The underlying and overlying sandstone-dominated members were described as the Ritchie and McKelvey members, respectively, by McLoughlin & Drinnan (1997b). These authors showed that deposition of the Ritchie member took place during a transition from consistently hydric to seasonally dry conditions. Major channel, crevasse/fan and flood-basin facies associations were recognised within the formation. The Flagstone Bench Formation was deposited in a continental environment, under fluctuating discharge conditions chiefly within the channel tracts of axially (between northwest and northeast) flowing, low-sinuosity braided rivers (McLoughlin & Drinnan 1997b); it is locally characterised by landsliding, fluviallacustrine, high-energy alluvial facies with a predominant



FIGURE 160

3.5 m thick coal seam in Bainmedart Coal Measures; east of Radok Lake.

palaeocurrent direction in the Jetty Formation to the east (Traube 1991).

A Triassic age for the uppermost Amery Group sediments on Jetty Peninsula was postulated by Ravich et al. (1977), and was later confirmed by megaflora (leaf fossil) data (Webb & Fielding 1993). The contact between the Flagstone Bench Formation and underlying Bainmedart Coal Measures straddles the Permo-Triassic boundary, which is proved by the first regular occurrence of *Lunatisporites pellucidus*, and the first appearance of *Aratrisporites* and *Lepidopteris* species (McLoughlin et al. 1997). The boundary is marked by the extinction of glossopterid and cordaitalean gymnosperms, and by the extreme decline of a range of gymnospermous and peridophytic palynomorph groups. The earliest Triassic macrofloras and palynofloras are dominated by peltasperms and lycophytes (McLoughlin et al. 1997). The uppermost McKelvey member contains Late Triassic megaflora with *Dicroidium zuberi*, *Dicroidium crassinervis* forma *stelznerianum* (Webb & Fielding 1993), and palynoflora assigned to the Late Triassic (Norian) Onslow Microflora by Foster et al. (1994). The megaflora reported from the Flagstone Bench Formation comprises species widespread in Triassic rocks of Gondwana (Webb & Fielding 1993; Cantrill et al. 1995).

PALAEOENVIRONMENT

The replacement of coal-bearing sequences by red-bed deposits is a common feature in Permo-Triassic continental basins worldwide (Frakes 1979). It indicates a change to warmer and drier climatic conditions. Subsequently the climate became more humid, though in

East Antarctica this is not as evident as in other continents. The mud-cracked red beds of the Jetty Member are succeeded by plant-bearing sediments, though plant fossils show features associated with water-limited conditions (Cantrill et al. 1995). Most workers have suggested that in late Palaeozoic to early Mesozoic times a single linear depression or graben controlled movement of sediments across the present-day Beaver Lake area, Amery Ice Shelf and Prydz Bay shelf into an epicontinental depositional palaeobasin subsequently rifted during Gondwana break-up (Cantrill et al. 1995; Fielding & Webb 1996). The easterly palaeocurrents within the Jetty Member may reflect the Middle Triassic tectonism that was widespread throughout Gondwana (Veevers 1993; Cantrill et al. 1995). Thin alkaline mafic to intermediate dykes cut the Permian Radok Conglomerate and Bainmedart Coal Measures, but are not known to intrude the Triassic Flagstone Bench Formation. Taking into account the Early Triassic (c.240 Ma) K-Ar age of a diorite porphyry dyke that cuts Proterozoic metamorphic rocks on Jetty Peninsula (Hofmann 1991), the authors of this bulletin suggest that the alkaline dykes were emplaced near the Palaeozoic-Mesozoic boundary—probably during a time of both tectonic and alkaline to calc-alkaline igneous activity. Sporadic finds of volcanic rocks as clastic material in sandstone support this suggestion. Assuming that the earliest rift-related magmatic activity in this area occurred about 320 Ma ago (Mikhalsky & Sheraton 1993), it is likely that the Amery Group was deposited under tectonic control as a graben fill, rather than a sheet platform cover, consistent with earlier sedimentological studies.

CAINOZOIC GLACIAL-MARINE AND GLACIAL SEDIMENTS

CAINOZOIC GLACIAL-MARINE SEDIMENTS (PAGODROMA GROUP)

Cainozoic (mainly Neogene) glacial-marine sediments are widespread throughout the NPCM (Bardin 1982), and may also occur in the SPCM, though no age dates are available for the Ruker Terrane. Glacigenic sediments of probable Neogene (to Early Pleistocene) age are collectively referred to as the Pagodroma Group (Hambrey & McKelvey 1995; McKelvey et al. 1999). McKelvey et al. (1995) and Hambrey & McKelvey (1999) reported the Pagodroma Group as being cumulatively more than 800 metres thick, making it the thickest onshore Cainozoic glacial sequence in Antarctica. They also reported the sub-Pagodroma Group surface to be one of high relief, consisting of fjord floors and walls eroded by alpine glaciers and associated with deep weathering of the underlying metamorphic rocks.

A 320 metre-thick sequence of lithified coarse sediment of Miocene age was measured on the southeastern slope of **Fisher Massif** (Laiba & Pushina 1997). The sediments crop out on the upper, relatively gentle part of the slope (Fig. 58), and lie almost horizontally on the erosion surface developed in Mesoproterozoic metamorphic rocks. Their total thickness may well reach 450 metres. The erosion surface is uneven and reveals abundant small mounds. It lies 360 metres above sea level on the southern flank of the escarpment, decreasing northwards down to 300 metres. An older (Early Miocene or Oligocene) sequence crops out at up to 1400 metres above sea level on Fisher Massif (McKelvey et al. 1999).

The sedimentary sequence at Fisher Massif consists mainly of two, rhythmically interbedded sediment types: (1) diamictite, composed of locally derived detritus (low-grade mafic to felsic metamorphic rock fragments), with equal proportions of large, angular rock fragments and coarse-grained matrix; and (2) tillite, containing rounded boulders of distantly derived rock fragments, enclosed in a fine- to coarse-grained matrix in the proportion of about 1:3. The sediments comprise at least four rhythmic sequences, each 30 to 80 metres thick (Fig. 161). Each rhythmic sequence includes one diamictite and one tillite bed. Minor siltstone or sandy siltstone beds one to four metres thick occur in the lower part of the sequence. Thin bands of indurated clay (?nontronite) within a siltstone layer contain fossil marine diatoms.

Diamictite is a dark grey rock that consists of chaotic angular rock fragments, mostly 0.1 to 0.7 metres, but up to 1.2 metres across, enclosed in a coarse-grained sandy matrix. The term 'diamictite' is used here to describe a lithified, poorly sorted deposit, and does not have any genetic connotation. Rock clasts consist of felsic (65%) and mafic (35%) lithologies typical of the Fisher Massif

metavolcanic rocks. There is no evidence of layering, particle sorting, or clast rounding.

Tillite is a grey, poorly stratified rock. It consists of a coarse- to fine-grained matrix enclosing rounded boulders (0.2–0.5 m, up to 2 m across), which comprise 30–35 percent of the rock. The matrix consists of unsorted gravelly, sandy silt with rare, large (5–7 cm) angular fragments. The proportions of different lithologies represented by the boulders varies between different

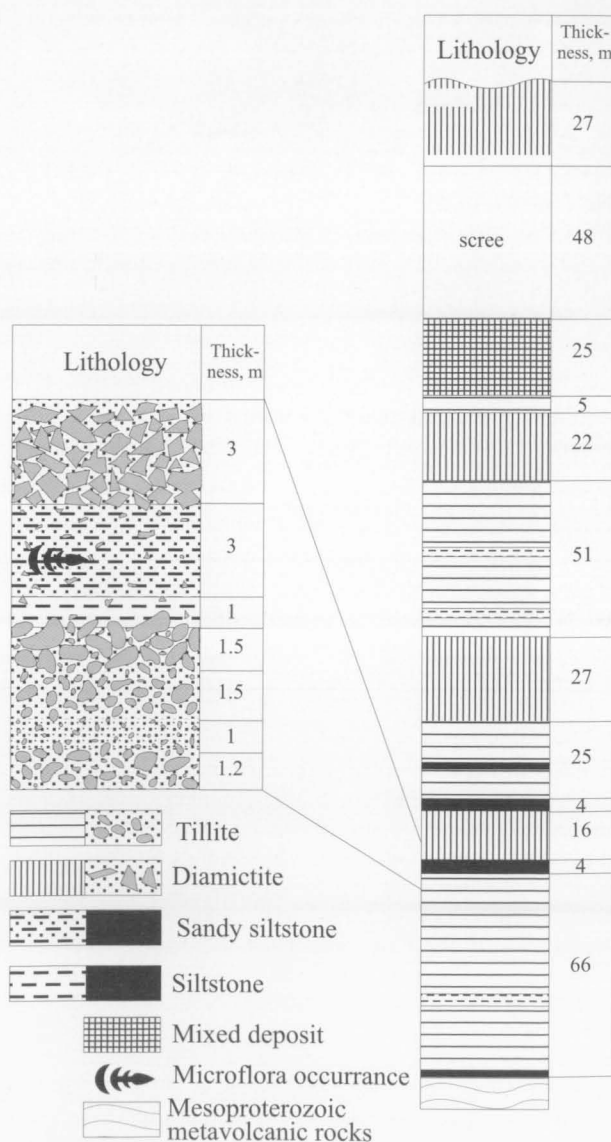


FIGURE 161

Stratigraphy of the Pagodroma Group on southeastern Fisher Massif.

layers. Light-coloured amphibole granite gneiss, pink or white granite, garnet-bearing felsic gneiss, dark green mafic amphibole–chlorite and amphibole–biotite schist, and metagabbro boulders predominate in different beds. Granite gneiss boulders are well rounded, whereas mafic boulders are mostly poorly rounded.

One of the clay bands within a siltstone layer (67m above the base of the sequence) contains fossil diatoms. A total of 27 taxa were recovered (Laiba & Pushina 1997). The diatom assemblage is dominated by benthic species: *Pinnularia quadratarea*, *Rhabdonema* sp., *Rhaphoneis* sp., and *Synedra* sp., among others. Planktonic species (*Actinocyclus ingens*, *Stellarima microtrias*, *Dactyliosolen antarctica*, *Eucampia antarctica*, and *Denticulopsis simonsenii*) are of low abundance. The diatom assemblage suggests a Miocene, most probably Middle to Late Miocene, age for the sediments. The reported planktonic species include deep-sea index zone 1 markers (Schrader 1976; Ciesielski 1983; Harwood & Maruyama 1992). However, the assemblage also includes large numbers of benthic diatoms, suggesting deposition in relatively shallow water less than 50 metres deep.

Granulometric data obtained for siltstones and tillite matrices show that aqueous reworking was an important accumulation factor (Laiba & Pushina 1997). The highly sorted character of the sediments (more than 50% of the sediment volume is composed of one fraction) suggests that the sediments were deposited in active hydrodynamic environments. Thus, tillite and silty deposits are believed to reflect both glacial and aqueous (marine) origins.

Diamictite corresponds to a buried colluvial facies. Particle shape does not indicate extensive reworking, while composition is identical to the Fisher Massif metavolcanic rocks. It is likely that the material fell from steep coastal cliffs. Some compositional differences between diamictite beds may be due to derivation from volcanic sequences of different composition. Some rock material could have been transported by small glaciers.

Different composition and rhythmic structure imply different environments for the origin of the main sediment types: tillite, siltstone and diamictite. Tillite was evidently transported by glaciers and accumulated in a coastal zone with a similar topography to modern Antarctic shore conditions. Siltstone probably also accumulated in the coastal zone, in a warmer environment when glacial transport was not important. Diamictite may represent a shore talus facies, suggesting an open water environment with reduced glacial activity.

The field data and diatom assemblage suggest a primary and continuous sedimentation process. Thus, basal sandy siltstone grades into tillite, which is overlain by a boulder-rich horizon, probably reflecting the end of glacial transport with boulders released from a receding glacier. This horizon is concordantly overlain by siltstone that originated in an aqueous (marine) environment. No scouring is evident on the boulder-rich horizon surface, and only thin bands of indurated clay contain fossil diatoms. Microfossil data also provide evidence for *in situ* primary accumulation, as benthic species are dominant. The limited stratigraphic extent of the centimetre-scale diatom-bearing layer within a four metre-thick siltstone also suggests an *in situ* assemblage. It is most unlikely that this benthic assemblage was transported down to deeper

waters from the edge of the fjord, because other siltstone samples from such redeposited valley wall slump deposits would also contain diatoms.

Since benthic species are predominant in the diatom assemblage, it is likely that these sediments accumulated in a near-shore environment (less than 50 m depth). The basin was free of ice and open for oceanic water penetration, which is evidenced by the presence of oceanic diatom species. The marine basin now occupied by the Lambert Glacier probably had normal salinity and warmer water compared to the modern Antarctic coastal zone. Judging from the small amount of sand in siltstones, the basin was characterised by relatively low hydrodynamic conditions (Laiba & Pushina 1997).

Cainozoic glacial–marine sediments of the Pagodroma Group are also known from the Beaver Lake area (Radok Lake and Pagodroma Gorge), about 80 kilometres north of Fisher Massif. One tillite sequence, up to 150 metres thick, is exposed on the upper part of the western side of **Radok Lake**. The base of the sequence is about 350 metres above sea level. The sequence is mostly covered by scree, and only a 15 metre-thick section of intercalated tillite (up to 4 m thick) and thin (0.1–0.3 m) layered silty sandstone was found. Bardin & Kolosova (1988) reported a boulder-rich tillite and laminated sandstone layers containing small fossil fragments (mollusc shells), but no age estimate could be made. Rock fragments comprise Precambrian metamorphic rocks and granite. The Radok Lake sequence is probably of similar Miocene age to that at Fisher Massif (B.C. McKelvey, personal communication, 1999).

In **Pagodroma Gorge**, nine kilometres farther east (Fig. 5), a semilithified tillite sequence up to 70 metres thick was originally termed the Pagodroma Tillite, but subsequently named the Bardin Bluffs Formation; it is thought to be of Upper Pliocene to Early Pleistocene age (Whitehead & McKelvey 1999). The sequence overlies eroded Permo–Triassic sedimentary strata, and its base ranges from about 160 metres above sea level in the west to below sea level at the mouth of the gorge in the east (Bardin et al. 1976; McKelvey & Stephenson 1990). A lower 15–18 metre-thick grey moraine overlies Permian sediments, and is succeeded by 25–40 metres of brown moraine (Bardin 1982; D.D. Kolobov, unpublished data). The grey moraine consists mainly of Permian sandstone and contains abundant coal dust particles and deuterite limonite, calcite, marcasite and siderite, which may be attributed to a relatively warm, humid environment (Bardin & Kolosova 1988). The brown moraine is more heterogeneous and poorly stratified. It includes granite gneiss fragments, together with Permian sandstone; deuterite matrix minerals are much less abundant and dominated by siderite. These features are consistent with formation near the oscillating glacier margin under reduced conditions. The amount of locally derived fragments decreases upward in the section, whereas the role of more distantly sourced sediment increases. The tillite also contains discontinuous layers and lenses of coarse-grained sandstone and grit–conglomerate, which indicates the influence of water.

Whitehead & McKelvey (1999) distinguished two members separated by a disconformity in the Bardin Bluffs Formation. The nine metre-thick basal Member 1 occurs only near Pagodroma Gorge, and consists of

relatively ice-distal fjordal glaciomarine silt and sand, deposited under marine conditions. The 60 metre-thick Member 2 is more widespread and consists of ice-proximal glaciomarine water-lain tills, with minor sand and conglomerate. It thus records glacial expansion subsequent to the deposition of Member 1.

The Bardin Bluffs Formation contains fossil diatoms of late Neogene age in a thin shell-bearing deposit (Bardin & Belevich 1985). The diatom assemblage is taxonomically and ecologically different from that at Fisher Massif. The tillite contains *Pseudopodosira* sp., benthic species of genera *Diploneis*, *Navicula* and *Amphora*, and planktonic species: *Stephanopixis turris*, *Thalassiosira oestrupii*, *Coscinodiscus oculoides*, *Actinocyclus actinochilus* and others. *Actinocyclus actinochilus* is a Middle Pliocene to Recent species (Harwood & Maruyama, 1992). The abundance, composition and preservation of the diatoms indicate that this sequence accumulated *in situ* in a coastal zone, because Antarctic neritic and glacial-marine species are predominant (Laiba & Pushina 1997). Hambrey & McKelvey (1995) also reported reworked Cretaceous to Lower Pliocene marine microfossils, and suggested sedimentation by wet-based glaciers in a fjordal setting. Diamictite and poorly sorted psammite were the product of deposition close to calving ice cliffs and from icebergs. Lodgement tills formed when the ice grounded on the fjord floor. Sediment facies also provide evidence for subaquatic slumping and gravity flowage. Sand and gravel were deposited from subaquatically discharging streams (Hambrey & McKelvey 1995). Thus, most sediments were deposited on the seaward side of a retreating ice front.

The Pagodroma Group shows broad similarities in age and setting to the Sirius Group of the Transantarctic Mountains (McKelvey et al. 1995; Hambrey & McKelvey 1999). The similarity in topography and the composition of the Fisher Massif and Radok Lake tillites enable a tentative correlation between these sediments, implying that they may be contemporaneous (Miocene) and formed in similar environments. In contrast, the Bardin Bluffs Formation is significantly younger (Pliocene–Early Pleistocene) and differs from the Fisher Massif tillite both lithologically and in its diatom assemblage. The Pagodroma Group records a complex glacial history in the NPCM, dominated by dynamic, sliding glaciers that carried large amounts of both basal and supraglacial debris. It indicates ice recession into the southern part of the Lambert Graben, a distance of several hundred kilometres, implying a highly dynamic Neogene East Antarctic ice sheet (Hambrey & McKelvey 1999). Deposition at Fisher Massif involved at least four major cycles, each with a rapid change of source region from regional to local. The processes driving these changes are not well understood, but are thought to be related to major climatic fluctuations that caused the repeated transformation of the Lambert Glacier depression into an open-water marine embayment. ^{10}Be exposure ages of Pagodroma Group sediments range from 0.01 to 2.33 Ma, consistent with the glacial chronology derived from geomorphological studies. They indicate recession of the East Antarctic ice sheet in the NPCM at about 2.3–1.9, 1.0–0.8, and 0.15 Ma (Fink et al. 1999). Fisher and McLeod Massifs emerged above the ice at least two million years ago.

No direct correlatives of the Fisher Massif sediments are known in Antarctica. Benthic diatom assemblages occur in Upper Pliocene sediments of Cockburn Island (Antarctic Peninsula) and Lower Pliocene sediments of the Vestfold Hills (Harwood et al. 1989; D.M. Harwood, personal communication), but the taxonomic composition of the Fisher Massif diatom assemblage differs from these other assemblages.

QUATERNARY GLACIAL SEDIMENTS

Younger (Late Pleistocene to Holocene) glacial sediments are widespread in the PCM, and moraines partly cover most of the flat tops and gentler slopes of mountains. D.D. Kolobov (unpublished data) suggested that some glacial sediments in the SPCM (Mounts Ruker and Rymill, and elsewhere) may be as old as Neogene, but no direct age indicator was found. Glacial fluctuations and varying bedrock topography have resulted in highly varying moraine thickness. Moraine morphologies indicate that the advance and retreat of alpine-type glaciers in the NPCM were out of phase with those of the larger ice-sheet outlet glaciers (Krebs & Mabin 1997). The distribution of moraines in the PCM indicates two stages of deglaciation since the last maximum, about 18 000 years ago (Bardin & Belevich 1985; D.D. Kolobov, unpublished data). The first stage of deglaciation resulted in thin (up to a few metres) sediment veneers found on the tops of most topographic highs in the SPCM (e.g., Mounts Borland and Maguire, Wilson Bluff and the Mawson Escarpment, within the 1300–1600 m elevation range). Exceptions are Mount Menzies and Cumpston Massif, which were unlikely to have been covered by the ice sheet, and thicker poorly stratified sequences in the NPCM. A few very large erratics occur on the tops of Mounts Maguire, Bayliss and Ruker. The coarse-grained fraction of the moraine comprises locally derived lithologies, even in the extreme south of the area, which suggests that amphibolite-facies rocks underlie the ice sheet south of Mount Borland and Komsomol'skiy Peak. The fine-grained fraction contains reduced pelitic grains, which reflects the aqueous reworking typical of ablation moraine (D.D. Kolobov, unpublished data). The heavy fine-grained fraction comprises epidote, garnet, titanite, apatite, sillimanite, and rare tourmaline, rutile, staurolite and orthopyroxene; scheelite (Mounts Wilson and Dummett, Mawson Escarpment) and molybdenite (Mount Maguire) were also found.

After the second stage of deglaciation, lateral moraines partly covered most of the gentler slopes of mountains throughout the PCM; kame moraines reflect local mountain tongue glacier terminations. Such moraines are most typical of the NPCM, where they locally form veneers, except in the northwestern part (Athos Range) where the snow accumulation rate is very high. Glacial sediments locally fill topographic lows in the bedrock, as in the Reinbolt Hills. The elevation where this generation of moraine occurs decreases northwards: 1500 metres on Blake Nunataks, 1250–1300 metres on Mount Ruker, about 1000 metres on Fisher Massif and Mount Meredith, and 800 metres on Amery Peaks. The moraines are composed of locally derived erratics, and the proportion of large boulders generally decreases northwards. Externally derived *Glossopteris*-bearing sedimentary rocks were found near Mounts Maguire and Rymill, and jaspilite to the west

of Beaver Lake. The fine-grained heavy mineral fraction reflects the country rock composition. In the SPCM it is dominated by amphibole, opaque phases, biotite, epidote, titanite, apatite, garnet, sillimanite and staurolite, with sporadic occurrences of clinopyroxene and orthopyroxene. In the NPCM it is dominated by orthopyroxene, clinopyroxene, biotite, opaque phases and garnet. The light fine-grained fraction is composed predominantly of quartz in the SPCM and feldspar in the NPCM. Scheelite (Mount Ruker) and galena (Reinbolt Hills) have also been found (D.D. Kolobov, unpublished data).

Holocene glacial sediments in the SPCM are confined to abundant lateral moraines (Figs 6–8), which may extend for several tens of kilometres and reach 300 metres in width and 30 metres in height (Mounts Rubin and Stinear, southern Mawson Escarpment: see cover). Kame moraines are typical of the NPCM, where they reach 35 square kilometres on Crohn Massif (D.D. Kolobov, unpublished data). Locally derived erratics predominate (Fig. 10), but an ironstone fragment was found near Mount Maguire. Inverted conical moraines eight to 10 metres high occur throughout the area.

STRUCTURAL GEOLOGY

RUKER TERRANE

There has so far been little detailed structural mapping in the Ruker Terrane, and it is presently impossible to assemble a comprehensive structural history like that proposed for the Beaver-Lambert Terrane by Fitzsimons & Thost (1992). In view of the complex, polymetamorphic nature of the area, its structural evolution is likely to have been at least as complex as that of the Beaver-Lambert Terrane. The oldest recognisable fold structures comprise small intrafolial, generally isoclinal folds in felsic gneisses of the Archaean granitic basement, some of which may have undergone an early granulite-facies metamorphism.

Large-scale, commonly recumbent, folds and thrusts are exposed at a number of places and appear to be the dominant structures in the Ruker Terrane (Figs 162, 163). Metasedimentary rocks are overthrust by basement gneisses at Mounts Rymill and Stinear, and are intensely deformed near the contacts (Hofmann 1982). Various stages of the shearing out of originally discordant mafic intrusions are well exposed on the eastern cliffs of Cumpston Massif (Fig. 164), where the whole stratigraphic

sequence from granitic basement rocks in the north, through quartzite-rich Menzies Series rocks, to Sodrzhestvo Series metasediments in the southeast can be seen. Unfortunately, the strong deformation makes interpretation of the structural relationships of these different units very difficult. Contacts between granitic basement and the Menzies Series at Mount Stinear are marked by thick blastomylonite zones (Hofmann 1982). A major thrust which separates garnet-hornblende-mica schist, quartzite and minor amphibolite from underlying mica quartzite, mica-quartz-plagioclase schist, marble and gypsum at Mount Maguire consists of a 30–50 metre-thick blastomylonite zone (Fig. 165). The mafic rocks are intensely deformed by folds with axial planes parallel to the thrust plane, and a new near-vertical foliation is developed in the underlying metasediments (Hofmann 1982). According to Hofmann (1982), the intensity of folding tends to be greater in Sodrzhestvo Series than in Menzies Series metasediments, where deformation is concentrated near basement contacts. In incompetent beds, disharmonic drag folds, commonly with sheared-out limbs, predominate, whereas in more competent beds,



FIGURE 162

Major recumbent fold in felsic gneiss and minor amphibolite, suggesting south-directed movement; western face of southern Blake Nunataks. The cliffs are about 500 m high.



FIGURE 163

Tight, near-recumbent folds in felsic gneiss and subordinate psammitic to pelitic metasediments and amphibolite, cut by Cambrian pegmatite veins; western side of Mount Twigg. The cliff face about 100 m high.

such as quartzites, boudinage and fracture cleavage are widely developed.

In the southern Mawson Escarpment, relatively flat-lying zones with major recumbent folds are separated by younger steeply dipping high-strain zones (S.D. Boger, University of Melbourne, personal communication, 1999). Prominent zones of tectonic melange as long as seven kilometres and up to four kilometres wide are exposed in the same area. They are of extremely varied composition, and contain rounded blocks, lenses, and boudins of mafic and ultramafic rocks up to 10 metres across, enclosed in strongly folded and sheared felsic to mafic schist.

The predominant structural trend in the Ruker Terrane is east–west, changing to northwest locally (Hofmann 1982; Ravich & Fedorov 1982). Large-scale folds at Blake Nunataks and Mount Menzies trend west to northwest and appear to have a south-directed sense of movement. Although it is by no means certain that all the major recumbent folds belong to the same generation, their similar orientation and style would be consistent with this. At least some (e.g., at Mount Twigg) clearly post-date the emplacement of ?Mesoproterozoic dolerite dykes (Fig. 166), but are older than c.500 Ma felsic intrusives, suggesting that the major folding occurred during the late Mesoproterozoic to early Neoproterozoic (c.1000 Ma) regional metamorphism. It is therefore possible that major folds in the southern part of the Beaver-Lambert Terrane may be of the same generation, which may be equivalent to D_6 in the NPCM (see next section), although the style is somewhat different. For example, a large-scale asymmetric fold at Shaw Massif has a near-vertical limb

and an east–west-trending axis, whereas a major recumbent fold at Mount Johns (Fig. 176) has a southwest-dipping axial plane and northwest-trending axis.

Archaean granite at Mount Ruker contains a few thin gneissose and foliated zones, which strike north to north-northeast. This granite is also cut by much more abundant late brittle to semibrittle zones which strike northwest, generally parallel to the strike of open mesoscopic fold axial planes in the banded ironstone sequence (see below). These structures are thought to reflect two distinct deformational events, only the younger having affected metamorphic rocks of the Ruker Series.

Hofmann (1982) showed that metadolerite dykes intruding granitic basement rocks have quite variable orientations, whereas those in the metasedimentary sequences are mostly controlled by bedding or foliation planes, or joints. The degree of deformation of the dykes is quite variable. Some are relatively undeformed with clearly cross-cutting relations (e.g., southern Mawson Escarpment); others are strongly sheared and concordant (e.g., Cumpston Massif). Most have been amphibolitised, and so have been through a relatively high-grade tectonothermal event, presumably at about 1000 Ma. An earlier deformation is indicated by mafic dykes at Mount Stinear emplaced along blastomylonite zones between granitic basement and metasediments (Hofmann 1982). Metadolerite dykes in the southern Mawson Escarpment are apparently discordant to tight east–west-trending folds which affect both basement orthogneiss and metasediments, as well as an older (?Palaeoproterozoic) generation of high-Mg mafic to ultramafic dykes. A

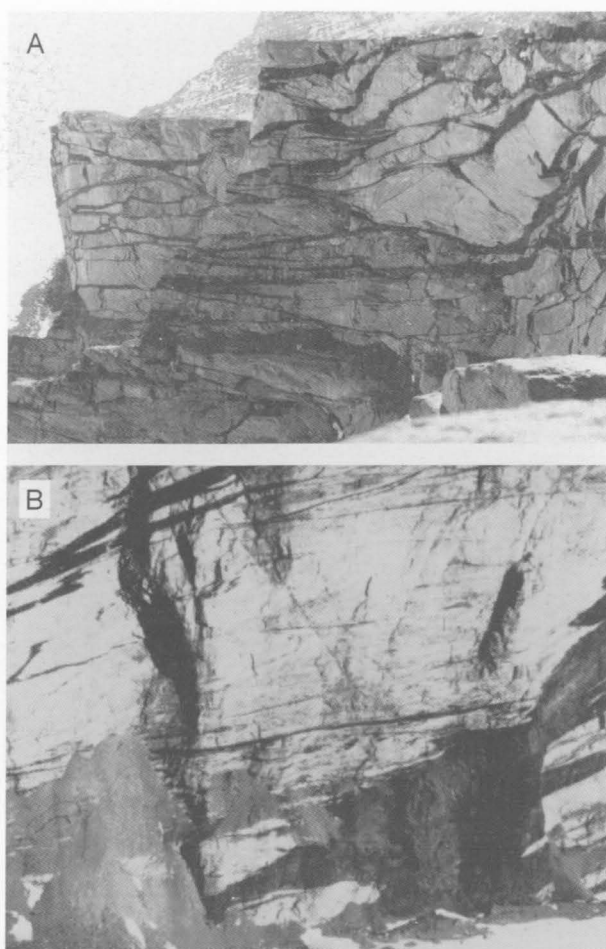


FIGURE 164

Deformation of metadolerite dykes cutting Archaean felsic orthogneiss. (A) Generally concordant, but locally cross-cutting, amphibolite dykes showing only slight shearing; western side of Cumpston Massif. (B) Strongly deformed, but locally discordant dykes; eastern side of Cumpston Massif. The cliffs are about 500 m high.

penetrative lineation in these rocks plunges at about 35° to the northwest.

Several distinct phases of deformation are thus present in the Ruker Terrane, and probably include at least two generations of major fold, one pre-dyke and one post-dyke. However, the ages of the earlier events are unknown, and even correlations between outcrops are highly uncertain. Isoclinal folds are locally common in metasedimentary sequences (e.g., at Mount Twigg), but may well be younger than early isoclinal folds in the granitic basement rocks (e.g., in the southern Mawson Escarpment). Minor folds on the northern side of Mount Menzies have axes plunging north at $20\text{--}40^\circ$, parallel to an associated lineation, and minor folds at Wilson Bluff plunge at about 10° towards 200° . A very large-scale (8 km amplitude) fold on the central Mawson Escarpment, with a near-vertical axis, may belong to the post-dyke generation as discordant mafic dykes appear to be absent from this area. Metasediments at Mounts McCauley and Scherger contain open to tight or isoclinal folds.

A more detailed structural study of the banded ironstone sequence at Mount Ruker was carried out by England & Langworthy (1975). Open concentric mesoscopic folds have axial planes dipping at about 65° towards 240° and axes plunging at about 40° to 190° . Parasitic folds on the limbs of the larger folds are highly flattened and asymmetric (Fig. 167). The folding was attributed to west-northwest-directed shear, in the plane of the contact between banded ironstone and adjacent greywacke. The consistency of fold orientations suggests that they were formed as the result of a single deformation. Metasediments of the Sodruzhestvo Series at Mounts Rubin and Dummett are also deformed by tight concentric folds (Figs 50, 52, 53). Those at Mount Rubin have axial planes dipping at about 60° to the southwest and axes plunging at about 20° to 300° . The similarity of axial planar orientations at Mounts Ruker and Rubin would be consistent with both areas having undergone the same deformation. If this was the case, then either the deformation (and presumably the greenschist-facies metamorphism) occurred during the c.1000 Ma

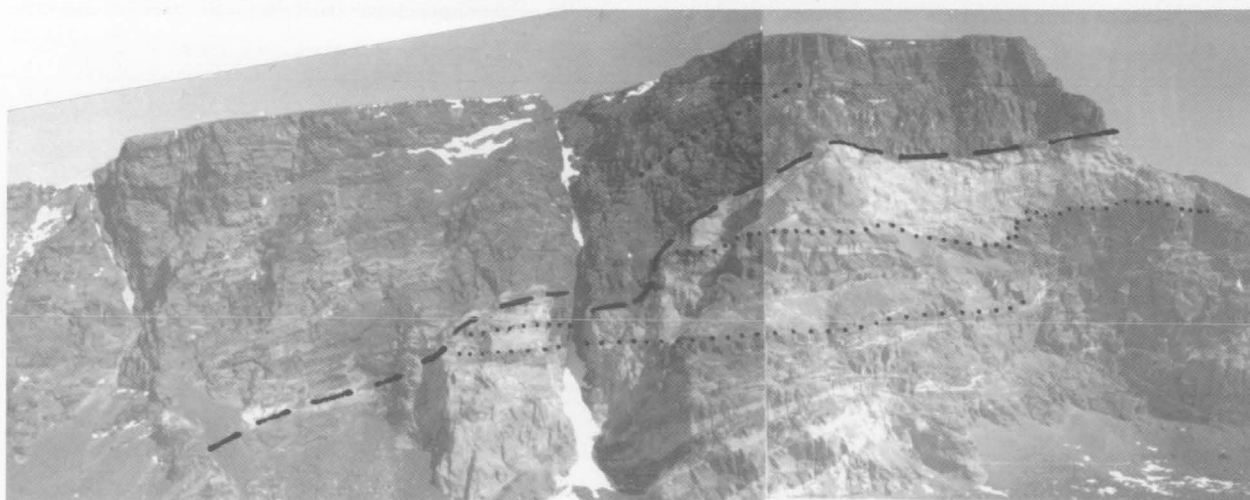


FIGURE 165

Major thrust zone (dashed line); southeastern Mount Maguire. Dark-coloured garnet-hornblende-mica schist, quartzite and minor amphibolite have been thrust over mica quartzite (thick light layer), mica-quartz-plagioclase schist, marble and gypsum. Dotted lines indicate compositional layering.



FIGURE 166

Tightly folded felsic gneiss and subordinate psammitic to pelitic metasediments and amphibolite, cut by Cambrian pegmatite veins (B); western side of Mount Twigg (overlaps left side of Figure 163). Folded, but locally discordant amphibolite bodies (A) may represent Palaeo- to Mesoproterozoic dolerite dykes. Note the helicopter for scale.

tectonothermal event and the Mount Rubin sedimentary rocks must be older than this, or the deformation was younger (e.g., Cambrian), in which case the apparent lack of evidence for the c.1000 Ma event in the Mount Ruker rocks becomes difficult to explain. Alternatively, the folding in the two areas may be unrelated.

Faults have been mapped in some of the larger outcrops, such as Mount Stinear and the Mawson Escarpment, but no systematic analysis has been carried out. Grew (1982) reported the presence of a shallow south-dipping post-metamorphic thrust fault at Mount Maguire. Metasedimentary rocks have been brecciated and locally mineralised with pyrite and hematite to depths of up to 100 metres beneath the thrust, but the rocks above were little affected. The thrust is offset by steeply dipping faults. Other late faults at Mounts McCauley, Ruker and Stinear trend northeast or northwest and have displacements of up to 300 metres (Grew 1982).

FISHER TERRANE

Magnetic anomaly data (Thost et al. 1998) and bedrock topography show that the Fisher Terrane may be about 50 to 55 kilometres wide, with a northeast strike (Fig. 168). Immediately south of Shaw Massif, a subglacial trough separates two domains of different regional magnetic anomalies, which may indicate the boundary between two

different crustal blocks. The magnetic data also suggest that Mount Meredith may be part of the Fisher Terrane, and that Mount Collins is on the boundary with the Beaver-Lambert Terrane.

Metavolcanic rocks at Fisher Massif strike mainly east-northeast and dip northwest at 25–75°. In the southeastern part of the massif, the sequence is thought to be overturned. In the northwestern part metaporphyrries and other rock types are strongly sheared and were probably thrust over the lowermost (oldest), predominantly mafic to intermediate sequence. In a few places metavolcanic rocks dip steeply (75–85°) southeast, which suggests the presence of large open folds with axial planes dipping roughly northwest. Minor folds occur within highly incompetent marble horizons, and very rarely in the metavolcanic rocks. Small (up to 0.5 m amplitude) moderately tight folds in marble (Figs 60, 61) have axial planes dipping 60–70° to the northwest (320°); there is a vague axial plane schistosity, defined by relatively high-temperature mineral assemblages (?M₂). Minor folds in the metavolcanic rocks have axial planes dipping 65–70° to the north, which provides some evidence of multiphase deformation. Broad open folds at Nilsson Rocks are some hundred metres across, with axial planes striking east–west. Small tight to recumbent intrafolial folds, probably representative of an earlier deformation event, were also found. The general strike at Nilsson Rocks

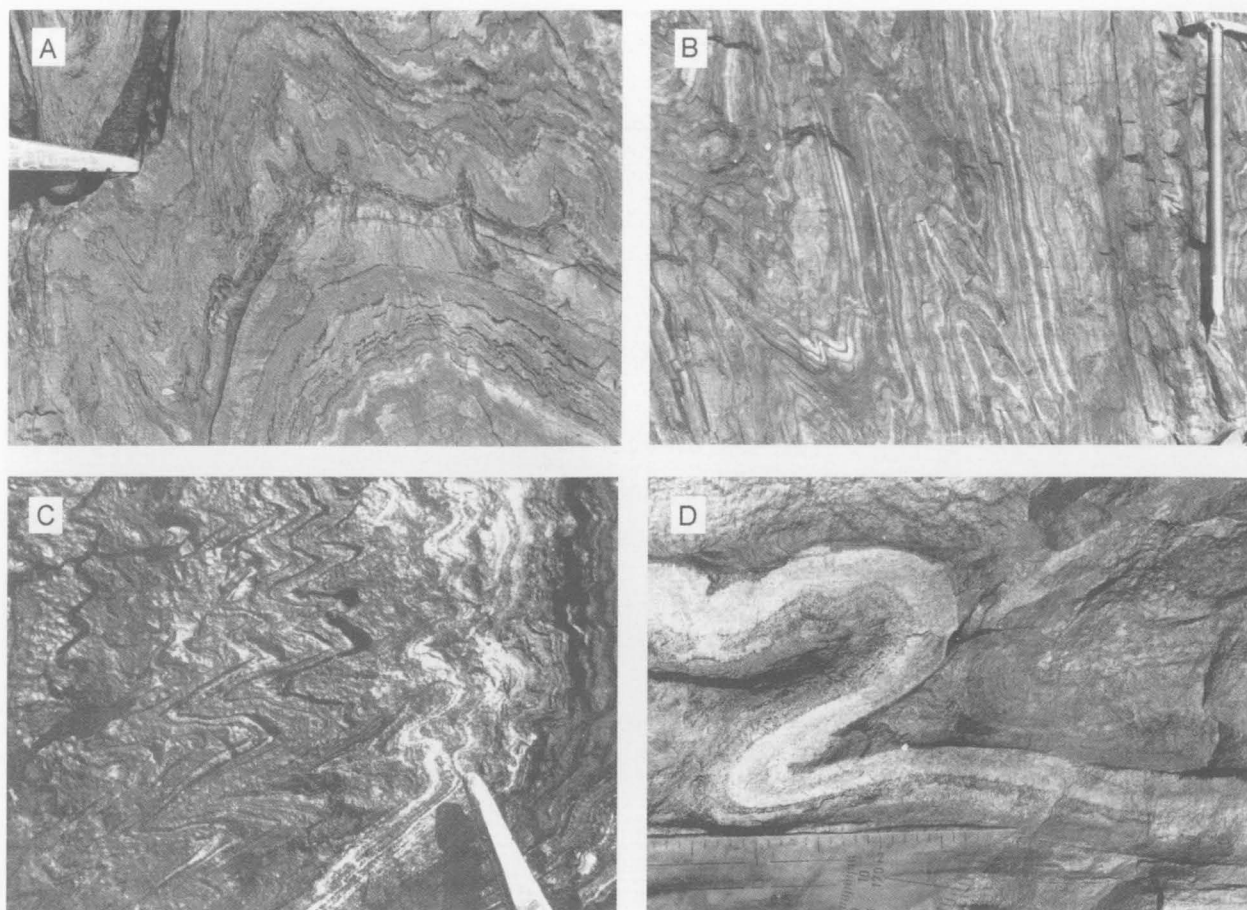


FIGURE 167

Minor folds in banded ironstone; Mount Ruker. (A) Half-wave buckle folds. (B) Highly flattened concentric folds. (C) Small chevron folds. (D) Highly flattened concentric folds in siliceous layer. Note the extent to which ironstone has flowed to accommodate buckling in the more competent siliceous layer.

coincides with that at Fisher Massif, but the rocks mostly dip southeast. Metamorphic rocks at Mount Willing show a wide range of dip and strike that may be attributed to the presence of abundant competent pre- or syn-tectonic intrusive rocks (gabbro and tonalite).

At least three major folding events may be distinguished at Fisher Massif. However age constraints can only be tentative as the age data came mainly from plutonic rocks at Mount Willing, and structural observations came mostly from metavolcanic rocks at Fisher Massif. Small intrafolial folds (F_1) appear to reflect the first deformation (D_1), which also produced the earliest greenschist-facies mineral assemblages and penetrative foliation (S_1). Large tight folds (F_2) reflect a major tectonic event (D_2); they are up to five to 15 kilometres wide and seem to be the dominant structures in the Fisher Terrane. The steeply dipping schistosity (S_2) may be axial planar to F_2 folds. Major thrusts and minor folds with a generally southeastward transport direction were formed during D_3 . This event probably resulted in a secondary schistosity (S_3), which seems to have formed under broadly similar metamorphic conditions to S_2 . Although similar peak metamorphic conditions seem to have been attained during both D_2 and D_3 , it is not clear whether these were two distinct events, or merely two phases of a single tectonic process.

Metamorphic events at Mount Willing were dated at about 1120 Ma (U–Pb zircon ages for metagabbro and a

quartz diorite vein), at about 1020–1010 Ma (resetting of Sm–Nd systems in metagabbro and metatonalite), at 810 Ma (U–Pb zircon age for metagabbro), and at 600–500 Ma (resetting of Rb–Sr systems in metamorphic rocks, and a zircon lower intercept age for a metatonalite). The former age may correlate with epidote-amphibolite-facies metamorphism (M_2) at Fisher Massif. However, it is difficult to correlate D_2 with M_2 at Mount Willing, as apparently little deformed granite is significantly older (c.1190 Ma) than c.1120 Ma quartz diorite veins (which have a migmatitic appearance). The undeformed granite contains metamorphic(?) sillimanite, and amphibolitisation of gabbroic rocks was by no means pervasive, suggesting that the c.1120 Ma (and presumably the c. 1020 Ma) metamorphism at Mount Willing was largely a thermal and hydration event, rather than being associated with a regional deformation. Moreover, the c.1120 quartz diorite veins appear to reflect a magmatic, rather than a regional tectonothermal, event. Thus, it is likely that D_2 (and probably M_2) at least occurred not long before granite emplacement, and may have been contemporaneous with tonalite emplacement at about 1190. D_3 appears to be restricted to the vicinities of thrust zones in certain areas, such as northern Fisher Massif and possibly Nilsson Rocks, and may not have affected Mount Willing, which is mostly composed of relatively competent plutonic rocks. The age of D_3 (still under amphibolite-facies conditions) may be

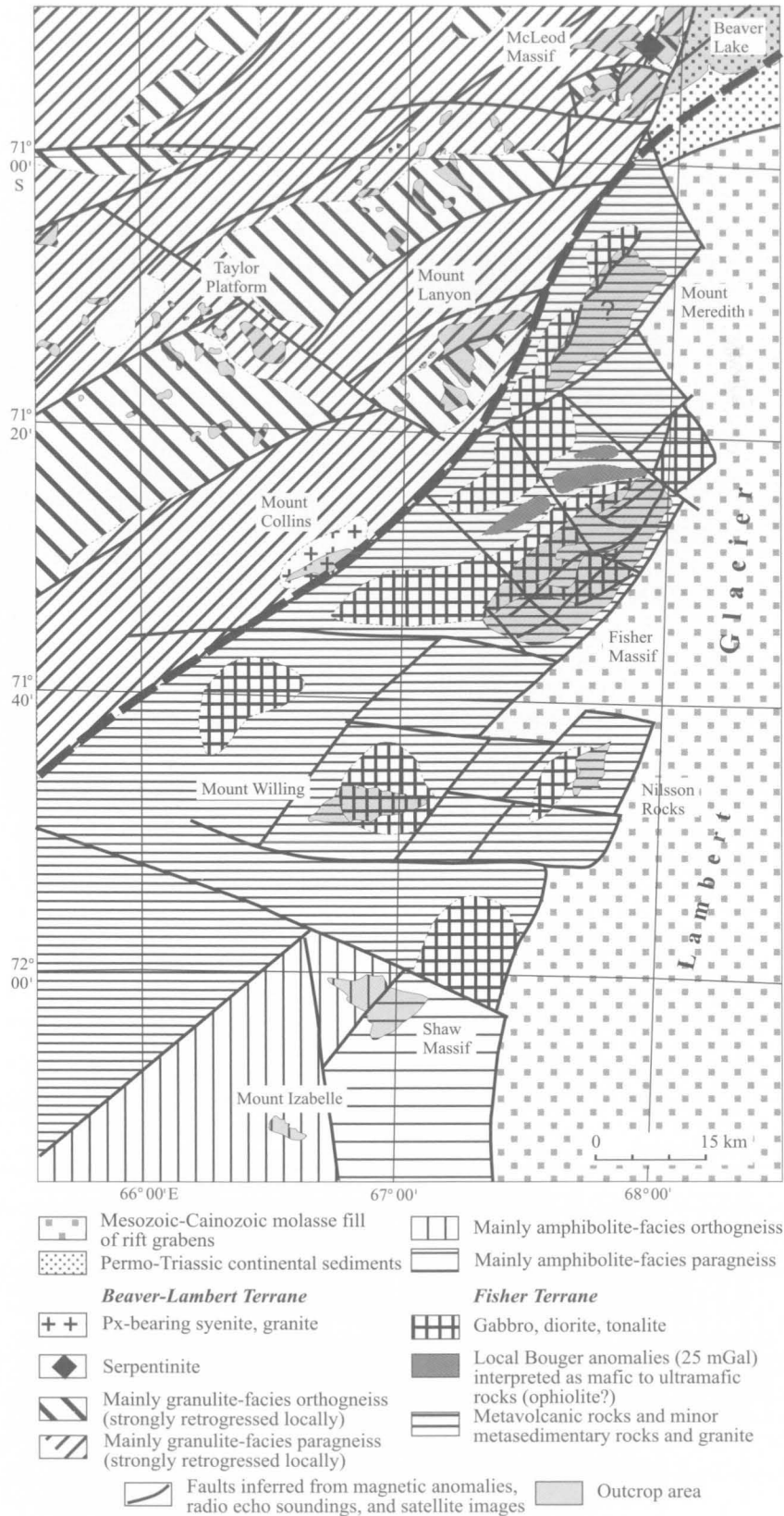


FIGURE 168

Map of the Fisher Terrane and adjacent parts of the Beaver-Lambert Terrane, showing major geological and structural features based on interpretation of magnetic and gravimetric data (Thost et al. 1998; R.G. Kurinin & A.V. Golynsky, unpublished data). Note the inferred continuation of Fisher Terrane rocks, defined by positive magnetic and gravity anomalies, under the ice cover, and the presence of large positive gravity anomalies that may represent ophiolites, near Fisher Massif. A heavy dashed line separates areas of more intense linear magnetic anomalies (to the north) from areas of less intense anomalies of isometric shape (to the south).

tentatively assumed to be about 1120 Ma, although amphibolite-facies metamorphism may have lasted until about 1000 Ma. A further deformation (D_4) is represented by a schistosity (S_4) that is confined to late steeply dipping shear zones. These are from a metre to some hundred metres wide, and mostly strike north-northeast. Low-grade M_3 retrogression may be related to this event. Whether or not these shear zones are related to the c.1020, c.810, or 600–500 Ma thermal events is unknown.

The exposed parts of the Fisher Terrane were subjected to intense faulting, which was most active during Mesozoic to Cainozoic times. Near-vertical faults strike northwest, north or northeast, and display only brittle deformation fabrics (D_5). The youngest structures are numerous thin zones of cataclastic rocks (D_6) that strike predominantly northeast, and commonly enclose abundant secondary quartz. These zones were found cutting an alkaline dolerite of presumed Palaeozoic age. Randomly orientated quartz–calcite veins are likely to be related to these brittle structures.

BEAVER-LAMBERT TERRANE

The most detailed description of the structural history of the Beaver-Lambert Terrane is given by Fitzsimons & Thost (1992), who recognised eight deformational events. Evidence for the two earliest (D_1 and D_2) is preserved only in mafic and ultramafic boudins. D_3 and D_4 produced relatively flat-lying structures that are locally overprinted by upright events (D_5 and D_6)—all of these deformations probably being of late Mesoproterozoic to early Neoproterozoic age. D_7 and D_8 appear to be much younger (c.500 Ma) and resulted in formation of localised, but widespread, shear zones, mylonite and pseudotachylite. Regional structural trends were determined mainly by D_3 and D_6 . Hand et al. (1994a) published a detailed map of Else Platform and identified four phases of deformation (termed D_1 – D_4) there, most of which can be tentatively correlated with some of those (D_3 , D_6 and D_8) of Fitzsimons & Thost (1992). Very similar structural histories have been described by Boger et al. (2000) and Carson et al. (2000) for the Radok lake area and Mount Kirkby, respectively. This section is based largely on the structural history as interpreted by Fitzsimons & Thost (1992).

D_1 deformation

The oldest recognisable structures are moderate to intense millimetre-scale foliation (S_1) and lineation (L_1), defined by composition layering and mineral orientation, respectively. They are preserved only in relatively competent mafic and ultramafic pods and layers (Fig. 169B, C), and are truncated by the pervasive foliation of the enclosing gneiss (S_3). Some coarse-grained orthopyroxene-rich ultramafic bodies may be metacumulates, and their compositional layering may be an original igneous feature (S_0), modified by tectonic flattening (S_1) during D_1 .

D_2 deformation

The S_1 foliation in a few mafic and ultramafic bodies is folded by low-amplitude disharmonic folds (F_2), which do

not show axial-planar fabrics. Wavelengths are less than 0.5 metres and F_2 folds appear to be confined to larger mafic and ultramafic bodies (Fig. 169B). It is possible that S_1 and F_2 are the rotated and folded equivalents of the external S_3 foliation, but S_3 clearly truncates these structures and must therefore be at least partly younger. Moreover, the fact that individual boudins have generally behaved as coherent blocks makes it unlikely that F_2 folds, which are commonly uniformly developed across the boudins, are an early manifestation of the boudinage.

D_3 deformation

The dominant regional foliation and layering in the metamorphic rocks in areas of low D_6 strain, as well as rare intrafolial F_3 folds, were formed during the third deformation (D_3). D_3 appears to have been contemporaneous with the metamorphic peak, and the pervasive, commonly flat-lying S_3 fabric is defined by peak assemblages. S_3 transposed almost all earlier structures, which survive mainly in some mafic and ultramafic bodies, although evidence of an earlier foliation may be preserved in rare F_3 fold hinges. The development of S_3 was associated with boudinage of relatively competent mafic layers (Figs 169A, 170), the internal fabrics of which commonly indicate rotation of individual boudins (Fig. 169C).

In felsic gneisses, the S_3 foliation is defined by lenticular quartz aggregates, elongated aggregates of garnet, orthopyroxene, or other mafic grains, and a preferred orientation of mafic minerals, including biotite in some rocks. Textures are commonly granoblastic inequigranular interlobate, and there is commonly a compositional layering consisting of orthopyroxene or garnet–biotite-rich and quartz–feldspathic layers. Migmatitic structures include locally discordant felsic segregations (leucosome), commonly with garnet–biotite-rich selvages, and discordant leucogneiss sheets and lenses with garnet–biotite schlieren (Fig. 169D). L_3 may be defined by quartz rodding, elongated mineral aggregates or, in metapelitic rocks, sillimanite grains. Typical mafic to ultramafic granulite is more massive, with a granoblastic polygonal texture, although some mafic rocks contain pyroxene aggregates interlayered with diffuse felsic segregations (Hand et al. 1994a).

Hand et al. (1994a) suggested that the earliest deformation recognised at Else Platform (their D_1), which produced the regional gneissic layering, may be equivalent to D_5 – D_6 of Fitzsimons & Thost (1992) in the Porthos Range area. This would be the case if D_1 and D_2 were part of the same progressive deformation, and would imply that older structures at Else Platform have been completely transposed (Hand et al. 1994a). Alternatively, D_1 at Else Platform may be correlated with D_3 in the Porthos Range—that is, the major gneiss-forming events in both areas are equivalent. Either way, the identical orientation and style of D_6 in the Porthos Range area and D_2 at Else Platform (see below) strongly suggest that these two events, at least, are the same (Hand et al. 1994a).

D_4 deformation

Rare isoclinal structures (F_4), which fold S_3 fabrics, have half wavelengths up to about five metres (Figs 171, 172C). Where not reorientated by later deformation, they are

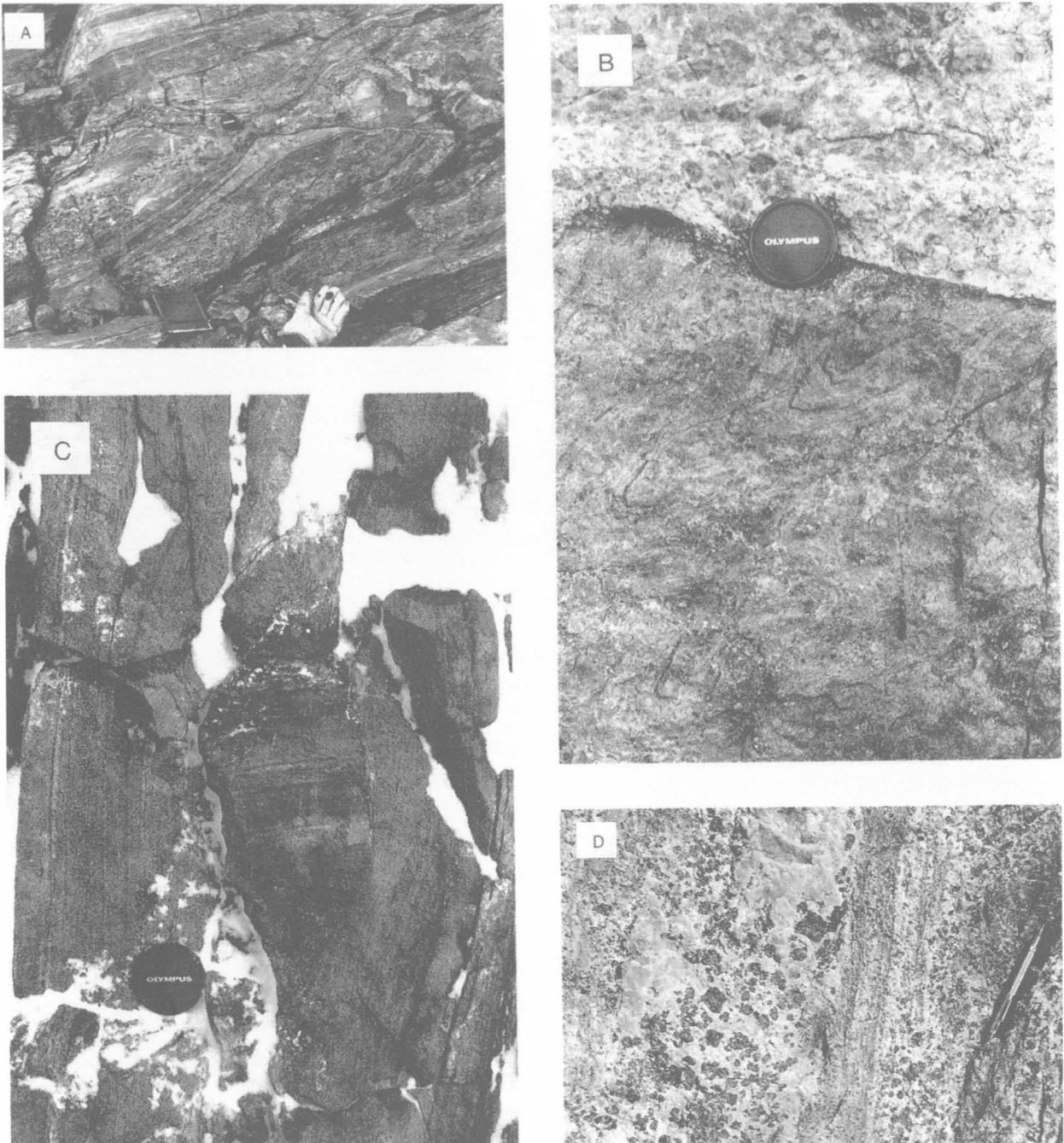


FIGURE 169

Early structural relationships in Beaver-Lambert Terrane gneiss lithologies (Fitzsimons & Thost 1992). (A) Calc-silicate and semi-pelitic layers in paragneiss; Amery Peaks. The foliation and boudinage are D_3 structures. (B) Edge of a block of mafic granulite with S_1 and F_2 folds, which are truncated by the external S_3 foliation; Corry Massif. (C) Boudinaged and rotated pod of ultramafic granulite with an internal foliation (S_1) oblique to that (S_3) of the host layered amphibolite; Corry Massif. (D) Partly migmatitic metapelitic gneiss with garnet porphyroblasts in a quartz-feldspathic matrix containing minor cordierite and sillimanite; Carter Peaks.

recumbent and deform flat-lying S_3 . Generally no S_4 fabric is developed. Although F_4 folds clearly deform S_3 , both D_3 and D_4 are consistent with sub-horizontal shear, and may well have been formed during a single progressive deformation. Possibly equivalent recumbent isoclinal folds in the Reinbolt Hills (F_2 of Nichols & Berry 1991) have an axial-planar foliation and associated lineation, and appear to post-date, or may be synchronous with, orthopyroxene granitoids there. Rootless, isoclinal, intrafolial folds near

Radok Lake (F_2 of McKelvey & Stephenson 1990) may also be equivalent to F_4 of Fitzsimons & Thost (1992), although the presence of a strong associated S_2 or S_2/S_1 foliation suggests they may be equivalent to F_3 of the latter authors.

D_5 deformation

Open to tight upright folds (F_5), mostly with amplitudes of less than 15 centimetres, occur in areas of low D_6 strain

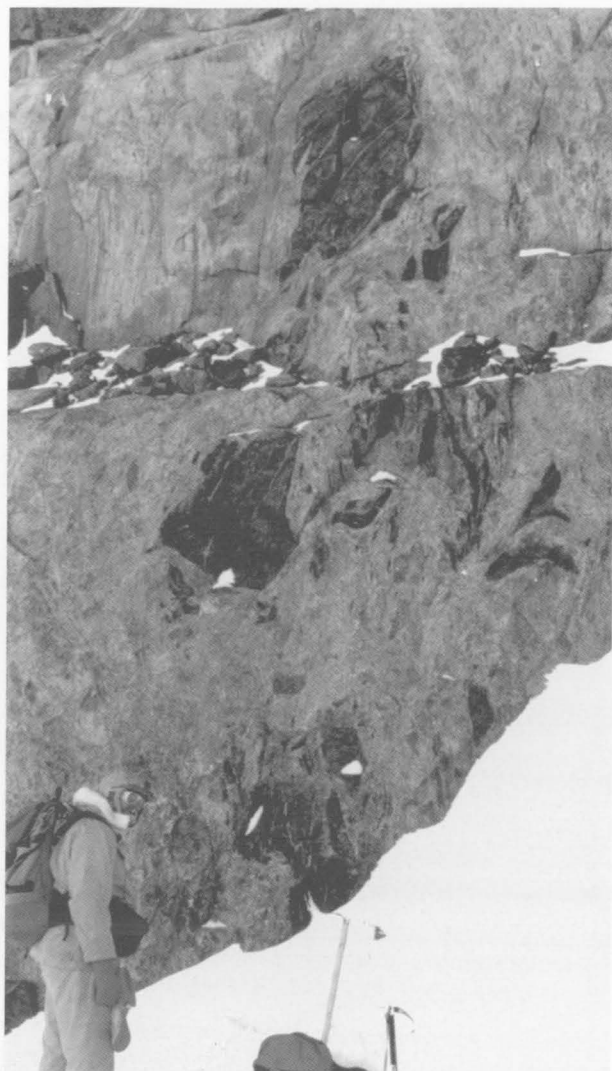


FIGURE 170
Entrained mafic xenoliths in felsic orthogneiss; Mount Kirkby.

(Fig. 172A), whereas F_5 folds in areas of high D_6 strain are commonly isoclinal. They fold S_3 and plunge at low to moderate angles to the east, as does an associated lineation (L_3) defined by quartz ribbons or an orientation of mafic minerals. Similar folds in the Radok Lake area (F_3 of McKelvey & Stephenson 1990) have axial planes striking east-northeast, axes plunging at about 30–40° east–northeast, and amplitudes between a few centimetres and a few metres. An axial-planar foliation, defined by biotite, is developed locally. Larger folds, with amplitudes of tens of metres, may belong to the same generation. D_5 structures have not been found in the orthopyroxene granitoid (charnockite) intrusions, which are therefore either younger or not affected by D_5 . Some granitic leucogneiss bodies are deformed by D_5 folds, whereas others cross-cut them. D_5 structures are coaxial with larger D_6 structures, suggesting that they formed under a similar stress regime during progressive deformation. They were not recognised as a distinct fold phase by Thost & Hensen (1992). However, the truncation of D_5 folds by some leucogneiss bodies suggests an earlier origin than the D_6 folds that post-date all the leucogneisses (Fitzsimons & Thost 1992).

Large-scale open folds at Depot Peak (D_2 of Stüwe & Hand 1992) are overprinted by one to five metre-wide gently north-dipping normal shear zones. If both were formed during a single progressive deformation, as suggested by Stüwe & Hand (1992), they may well be equivalent to D_5 – D_6 of Fitzsimons & Thost (1992)—although on the available evidence, such a correlation can only be tentative. Open to tight upright folds in the Reinbolt Hills (F_3 of Nichols & Berry 1991) are coaxial with F_2 folds in that area, which suggests that both may have formed during progressive rotational deformation. Orthopyroxene granitoids in this area appear to belong to two generations: those at Jennings Promontory being post- D_3 , in contrast to those at Reinbolt Hills, which have an S_2 foliation and may be syn- D_2 (Nichols & Berry 1991).

D_6 deformation

The regional structural trends were largely determined by a heterogeneous deformation which affected all lithological units except for late intrusive rocks (certain granitic rocks, pegmatites and unmetamorphosed mafic dykes). High-strain zones are characterised by development of a strong near-vertical east-trending foliation (S_6) and a moderately east-plunging lineation (L_6), defined by preferred mineral orientation (Figs 172B, D, 173). These fabrics obliterate earlier structures, and originally discordant contacts of granitic bodies and mafic dykes are transposed (Fig. 172B). The high-strain zones are separated by areas in which flat-lying to steep S_3 fabrics are preserved. Such low-strain zones define kilometre-scale F_6 folds (Fig. 174), with central flat-lying sections steepening towards the high-strain zones to define large antiformal, synformal, or monoclinical structures with east–west trending axes (Fig. 175). Similar, but much smaller-scale, structures are exposed at Mount Bunt, where steep east–west zones of intense S_6 foliation, typically one to two metres wide, are separated by two to 10 metre-wide monoclinical zones preserving S_3 fabrics.

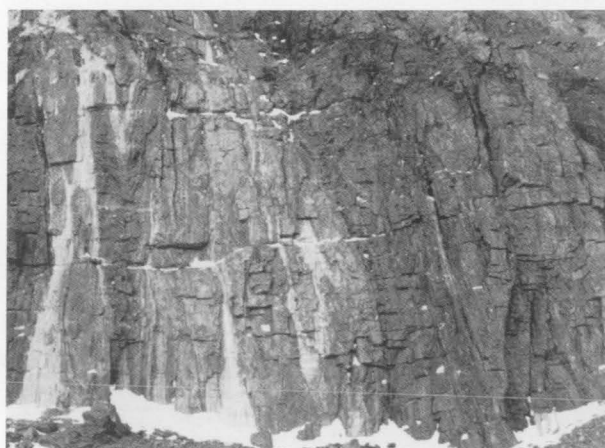


FIGURE 171
Tightly folded (F_4) felsic to mafic gneiss with discontinuous layers of calc-silicate granulite (light colour); Corry Massif. The less competent calc-silicate was locally mobilised during deformation and cross-cuts the S_3 foliation in the host rocks, which is axial planar to the folds. Note the figure (bottom right) for scale.

Parasitic asymmetric F_6 folds in low-strain zones are 0.1–10 metres across, with axes parallel to L_6 , but no consistent vergence was observed in the Porthos Range area.

D_6 is almost certainly equivalent to D_2 of Hand et al. (1994a) at Else Platform. In this area, the high-strain zones trend east to northeast and dip moderately south, although a subordinate group trends north-northeast and

dips southeast. Such shear zones range from five to more than 500 metres across and have diffuse boundaries. Some smaller shear zones are locally highly discordant to the early foliation (termed S_1 by Hand et al. 1994a), but curve along strike into it. Parasitic F_6 folds on the centre of Else Platform are 100–200 metres across and plunge steeply east. Mesoscopic open to isoclinal F_6 folds are common on the limbs of larger structures, and locally have a near-

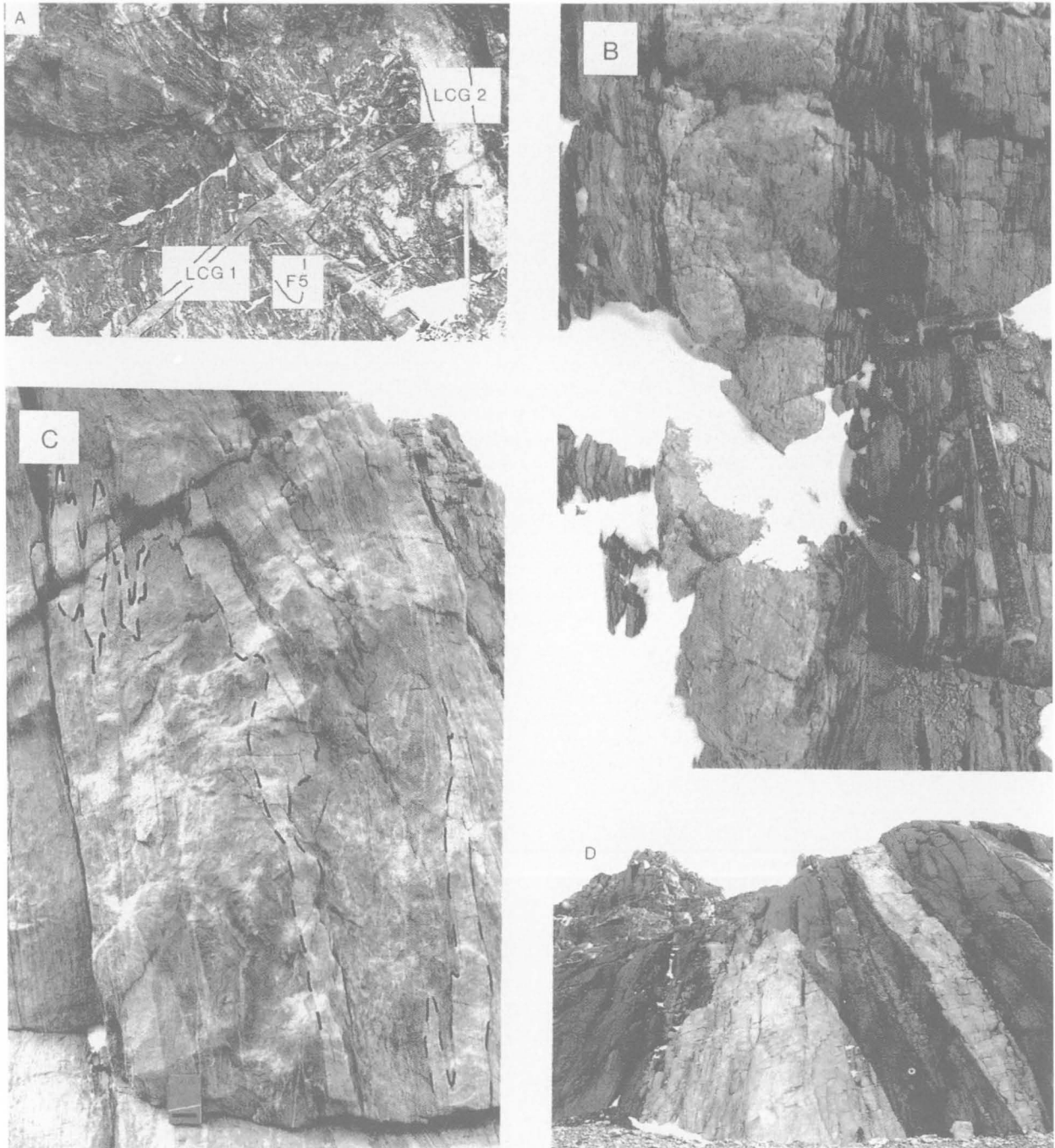


FIGURE 172

Structural relationships involving younger intrusive lithologies of the Beaver-Lambert Terrane (Fitzsimons & Thost 1992). (A) Two generations of granitic leucogneiss cutting garnet-biotite paragneiss in a D_6 low-strain zone; Mount Bunt. The paragneiss has an S_3 foliation and upright symmetrical F_5 folds. (B) D_6 high-strain zone, showing a leucogneiss body and mafic granulite dyke drawn out parallel to S_6 ; Mount Kirkby. (C) Tightly folded (F_4) leucogneiss body in felsic gneiss; Mount Kirkby. (D) Irregular body and dyke of garnet-bearing granitic leucogneiss intruding orthopyroxene-garnet granite ('charnockite') in a D_6 high-strain zone; eastern end of Mount McCarthy. Both leucogneiss and orthopyroxene granite have a well-developed L_6 lineation. Note the figure for scale.

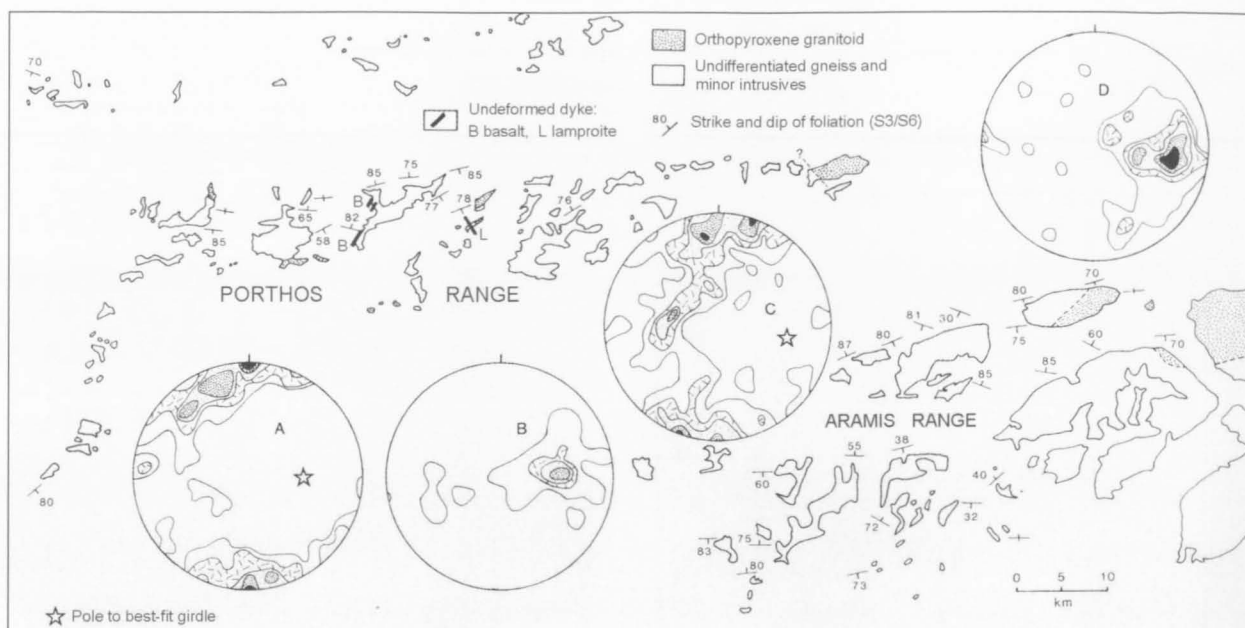


FIGURE 173

Dominant structural trends (S_3/S_6) in the Porthos and Aramis Ranges (Fitzsimons & Thost 1992). A to D are equal-area projections of structural data contoured at various percentages per 1% area. (A) 116 poles to foliations (S_3/S_6) in the Porthos Range, contoured at 0.5, 2, 5, 7 and 10% per 1% area. (B) 36 lineations (L_6) in the Porthos Range, contoured at 3, 10, 15 and 20% per 1% area. (C) 204 poles to foliations (S_3/S_6) in the western Aramis Range, contoured at 1, 2, 3, 4 and 5% per 1% area. (D) 41 lineations (L_6) in the western Aramis Range, contoured at 2, 4, 6, 8 and 10% per 1% area. Note the coincidence of the lineation directions in B and D with the poles to the best-fit girdles in A and C.

vertical axial planar foliation defined by biotite and thin leucosomes. Mylonitic, locally sheath-like folds with axes plunging parallel to L_6 are common in deformed garnet-bearing felsic dykes.

The intense shear foliation is defined by elongated mineral grains and grain aggregates. Biotite, granulated garnet or pyroxene, or stromatic leucosomes define S_6 in felsic rocks, whereas pyroxene-hornblende assemblages characterise mafic rocks (Hand et al. 1994a). The foliation in metapelites comprises a cordierite grain-shape fabric, with aligned biotite, sillimanite and garnet aggregates. Sillimanite may be replaced by cordierite-spinel symplectites. Deformed garnet granite dykes have a homogeneous laminated quartzo-feldspathic matrix

containing garnet porphyroclasts. Fabrics, including porphyroclast textures, indicate south-up movement parallel to a moderate to steep east-southeast-plunging lineation defined by quartz±garnet and biotite. In dykes outside the high-strain zones, S_6 is a moderately developed S-L fabric defined by aligned K-feldspar megacrysts or elongated quartz and garnet aggregates.

Major folds in the northern part of the SPCM may be of the same generation, although their style is rather different. A large-scale asymmetric fold at Shaw Massif has a near-vertical limb and an east-west-trending axis, whereas a major recumbent fold at Mount Johns (Fig. 176) has a southwest-dipping axial plane and northwest-trending axis. An earlier deformation at Shaw Massif is represented by minor folds that plunge at shallow to moderate angles to the southwest, parallel to a prominent lineation. Late, open upright folds at Mount Isabelle also plunge gently southwest.

D₇ deformation

Small, gently dipping shear zones and minor flexures are assigned to D₇. Some have been exploited by pegmatites, which locally have a fabric resulting from reactivation of the shear zones. Northwest-trending, low-angle mylonites and coplanar pseudotachylites in the Radok Lake area may be of the same generation (D₄ of Boger et al. 2000).

D₈ deformation

Mylonite and pseudotachylite are common throughout the NPCM. Sub-horizontal to shallow-dipping planar



FIGURE 174

Major F_6 antiform, plunging to the east; eastern face of Mount Gardner. The cliff is about 150 m high.

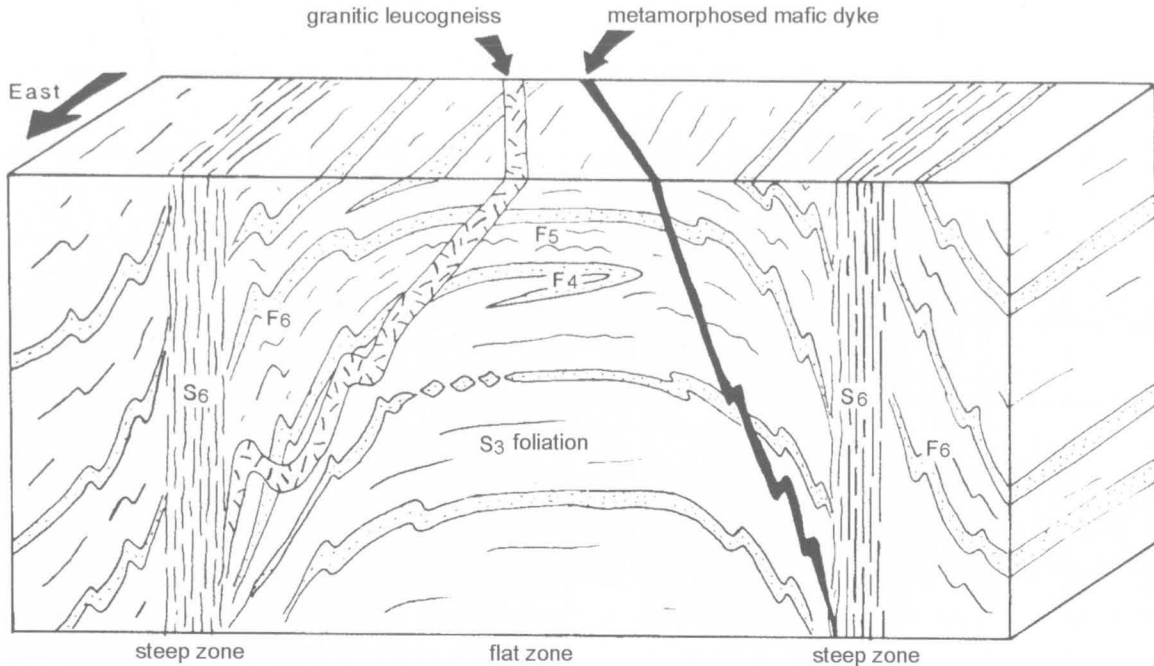


FIGURE 175

Schematic block diagram (after Fitzsimons & Harley 1992) showing regional F_6 folds defined by upright S_6 high-strain zones and flat-lying zones in which S_3 and F_4 structures are preserved. The flat-lying zones are also characterised by mesoscopic F_5 and parasitic F_6 folds, which are of different style but coaxial and closely related, and by discordant contacts between the gneissic rocks and the leucogneiss and metamorphosed mafic dykes.

mylonite zones are typically less than 10 millimetres wide and parallel to nearby pegmatite veins (Fig. 177). Thicker mylonite zones up to 0.5 metres across are commonly steep, and occur in the centres of planar pegmatite bodies at Mount Bunt. Mylonite cross-cuts late granitic bodies at Mount Trott and Thomson Massif, and pegmatite at Mount Creighton. The thickest mylonite zones have displacements up to several metres, but thin zones show little displacement. Anastomosing veins of pseudotachylite are commonly bounded by narrow mylonite zones. Pseudotachylite zones, five to 20 centimetres wide, occur near Radok Lake (McKelvey & Stephenson 1990).



FIGURE 176

Major recumbent fold in migmatitic felsic gneiss, with subordinate amphibolite and paragneiss; southeastern Mount Johns. The cliff is about 600 m high.

Microscopic effects of D_8 include bent twin lamellae in feldspar, kinked biotite, undulose extinction, deformation lamellae, and sub-grain boundaries in quartz, as well as recrystallisation of hornblende and orthopyroxene. More competent ultramafic and mafic rocks, including metamorphosed dykes, tend to be much less affected and largely retain their original granoblastic textures.

Late ductile to brittle-ductile deformation events at Else Platform, termed D_3 and D_4 by Hand et al. (1994a), cannot definitely be correlated with any of those recognised in the Porthos Range area by Fitzsimons & Thost (1992), although at least some may well be equivalent to D_8 . In the former area, north-trending migmatitic granitic dykes contain an S_3 foliation defined by biotite and thin leucosomes, suggesting that the dykes were intruded along active shear zones. The foliation trends 010° , dips steeply east, and is axial planar to isoclinal F_3 folds that plunge gently north with no consistent sense of asymmetry. Annealed quartz and feldspar grains and new garnet growth suggest that extensive recrystallisation occurred after the deformation. They may be related to large north-trending, but undeformed, garnet-biotite pegmatite bodies. A second set of shear zones (D_4 of Hand et al. 1994a) post-dates both migmatitic dykes and most pegmatites. These are small structures of two types: discrete northwest-trending shears, 0.3 to three metres wide, and complex shear and ultramylonite zones, up to 20 metres across. Both types are steeply dipping, and northwest over southeast movement appears to dominate. Small pegmatite veins intrude some D_4 shears that contain greenschist-facies assemblages (biotite, muscovite and chlorite).



FIGURE 177

Pseudotachylite veins in orthopyroxene granitoid, showing a high degree of grainsize reduction and clusters of minute garnet grains (arrowed) in an orthopyroxene-rich matrix. Width of field: 4 mm.

Mylonite zones in the Reinbolt Hills area (assigned to D_4 by Nichols & Berry 1991) contain amphibolite to greenschist-facies assemblages (quartz–K-feldspar–plagioclase–hornblende–biotite–chlorite) and indicate a reverse sense of shear, with a transport direction towards the east (i.e., with the western side overthrusting the eastern) along an average stretching lineation of 084° on planes dipping at $40\text{--}50^\circ$ west.

Late brittle structures

Vertical north-trending quartz and epidote veins occur at Mounts Creighton and Butterworth and a prominent north-trending cleavage is common at many localities. A well-developed near-vertical joint set near Radok Lake strikes south-southeast (McKelvey & Stephenson 1990), and cleavage in the Reinbolt Hills strikes south-southwest (Nichols & Berry 1991). These brittle structures were included in D_8 by Fitzsimons & Thost (1992), as in the Porthos Range area there is little evidence of their age relative to the mylonite or pseudotachylite zones. However, quartz veins cut late pegmatite and mylonite at

Mount Creighton, so at least some may be significantly younger. At Else Platform, vertical north-trending faults are intruded by c.320 Ma alkaline dolerite dykes which are, in turn, displaced by massive quartz veins and lenses (Hand et al. 1994a; Shulyatin 1995). These large (up to 5 m thick and 1.5 km long) quartz veins may well be co-eval with quartz veins in Permo–Triassic sedimentary rocks just to the south and calcite–quartz veins that cut nearby Cretaceous alkaline ultramafic bodies—in which case a late Cretaceous age is likely (Shulyatin 1995). Those at Else Platform contain minor calcite, fluorite, pyrite and chalcopryrite, and traces of gold (Shulyatin 1995).

Hand et al. (1994a) suggested that brittle faulting may have been associated with formation of the north–south-trending basin now occupied by Permo–Triassic sedimentary rocks, extensional deformation during formation of the Lambert Graben, or a combination of these involving re-activation of faults formed in the Permian during breakup of Gondwana. In a more detailed study of fault tectonics in this area, Hofmann (1991) distinguished two major sets of faults: meridional and latitudinal. Meridional faults trend north to northeast and dip at $40\text{--}55^\circ$ west. They include the major, 250–600 metre-wide fault on the western side of Kamenistaja Platform, which has estimated vertical and horizontal displacements of 500–1000 metres and 400–600 metres, respectively, with an oblique downthrow of the western block to the northwest. This fault system is associated with c.320 Ma mafic dykes, c.240 Ma diorite porphyries, and quartz veins, and was apparently repeatedly reactivated during the Mesozoic and Cainozoic. Latitudinal strike-slip faults trend east to east-northeast, and some contain Cretaceous alkali picrite or polzenite dykes. These faults may either be unrelated to the meridional set, or both may represent a single dextral–normal oblique fault system (Hofmann 1991). Together, they reflect a long-lived tectonic evolution extending from the Carboniferous to the Cainozoic and involving mafic dyke emplacement, graben subsidence and deposition of the Permo–Triassic Amery Group, emplacement of alkaline ultramafic rocks, and Cretaceous–late Cainozoic block faulting and uplift.

METAMORPHISM

RUKER TERRANE

The youngest regional metamorphism in the Ruker Terrane post-dates the emplacement of dolerite dykes of probable Mesoproterozoic age, and was therefore attributed to the late Mesoproterozoic–early Neoproterozoic (c.1000 Ma) M_2 event by Tingey (1982a, 1991a). It is thus tentatively correlated with the prograde granulite-facies metamorphism in the Beaver-Lambert and Fisher Terranes, described below. There is also evidence in some areas for at least one earlier high-grade event (all such early events are here termed M_1), as well as a widespread lower grade, commonly retrograde, event (M_3) of probable Cambrian (Ross or Pan-African) age.

Early high-grade metamorphism (M_1)

Archaean granitic basement rocks (Mawson Orthogneiss) show evidence for an early high-grade event (M_1) in their commonly migmatitic nature, which implies partial melting under at least upper amphibolite-facies conditions. The local occurrence of relict igneous textures in the widespread biotite–hornblende granite gneiss suggests that the migmatisation in the associated more strongly foliated orthogneisses pre-dated granite emplacement—that is, the early metamorphism was of Archaean age. There is possible petrographic evidence (relict orthopyroxene + garnet) for an early granulite-facies metamorphism in tonalitic orthogneiss lenses in the southern Mawson Escarpment, but it is unclear whether it represents an earlier metamorphic or magmatic event, or subsequent ‘charnockitisation’.

There is also some evidence for an early high-grade event in the overlying Menzies Series metasediments. Garnet + sillimanite \pm cordierite assemblages in metapelites at Mounts Bird and Newton (Fig. 178A) and orthopyroxene in mafic bodies at Mount Newton indicate transitional upper amphibolite to granulite-facies conditions. This event apparently pre-dated dolerite dyke emplacement (England & Langworthy 1975), but its age is poorly constrained and could be anything from late Archaean to Mesoproterozoic. Relatively high-grade (middle to upper amphibolite-facies) metasediments also occur in the southeast of the SPCM. Sillimanite + biotite + muscovite + plagioclase + quartz, apparently in equilibrium, occurs in a few metapelites at Mount Twigg, and sillimanite + K-feldspar occurs at Mount Borland. Amphibolite contains green to brownish-green hornblende, and garnet is present in amphibolite at Mount Twigg. These assemblages were considered by Tingey (1982b, 1991a) to have formed during M_1 , although their age relationship with the metadolerite dykes is unclear. Upper amphibolite-facies rocks, with co-existing

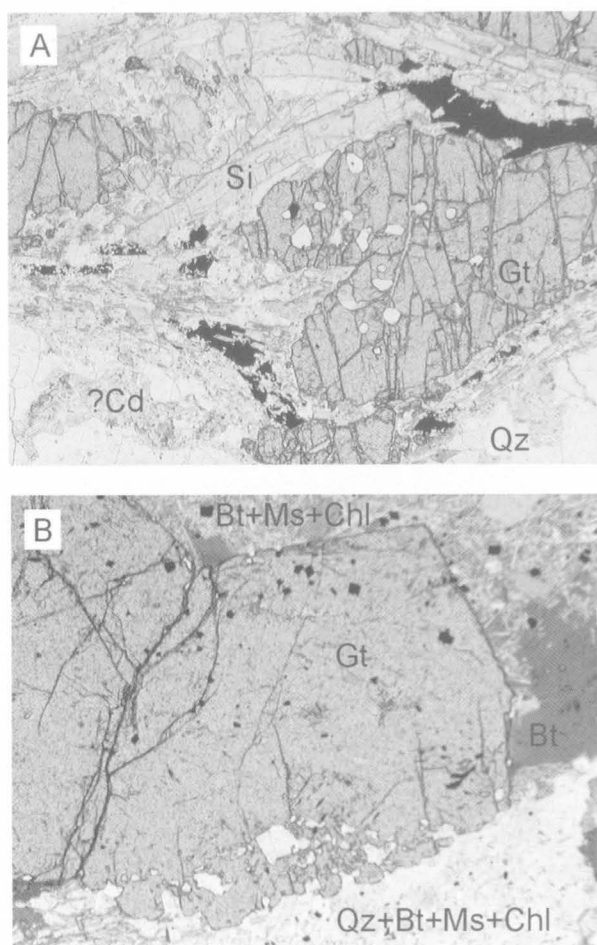


FIGURE 178

Evidence for a possible early high-grade event in the Ruker Terrane. (A) Garnet-sillimanite-biotite-quartz-plagioclase metapelite, with altered ?cordierite (biotite-sericite-chlorite); Mount Newton. Sample 72280728. (B) Part of a discontinuous garnet rim around a felted aggregate of biotite + muscovite + chlorite + minor quartz and chromite in garnet-staurolite-biotite-quartz (-chlorite-muscovite) metapelite; Mount Stinear. The garnet (plus minor staurolite) rim may have formed around an original porphyroblast of ?cordierite + spinel during a relatively high-pressure garnet-staurolite-grade event, with subsequent lower grade alteration of cordierite and some of the biotite; note the euhedral crystal faces of garnet against the original porphyroblast and the irregular external zone, with abundant quartz inclusions, adjacent to the quartz-rich matrix (which also contains a few subhedral garnet grains). Sample 73281447. Width of field: 4 mm.

sillimanite + K-feldspar, that crop out at the isolated Komsomol'skiy Peak 150 kilometres south of the PCM, were also assigned to M_1 by Tingey (1982b, 1991a). Alternatively, variations in pressure-temperature (P-T) conditions during M_2 could account for most of these paragenetic variations.

There is some other evidence, albeit not entirely conclusive, for an early high-grade event. For example, psammo-pelitic rocks in the southern Mawson Escarpment contain aggregates of secondary garnet after coarser primary garnet, and staurolite has grown in fractures in early garnet. England & Langworthy (1975) concluded that an older, higher grade, more magnesian garnet broke down to Fe-Mn-Ca-rich garnet, staurolite, and biotite or chlorite during retrogression, but were uncertain as to the age of this early event relative to that of the dolerite dykes. Two generations of garnet also appear to be present in metapelite at Cumpston Massif. A psammo-pelitic rock from Mount Stinear contains a completely altered (biotite + muscovite + chlorite + minor quartz) porphyroblast with a discontinuous rim of coarse-grained garnet and minor staurolite (Fig. 178B). The original porphyroblast may well have been cordierite, which was then partly overprinted by a high-pressure garnet-staurolite-grade event, and subsequently suffered low-grade alteration. Small grains of chromite in the altered porphyroblast also suggest the original presence of spinel, which would indicate that the early event was possibly of granulite facies (R.N. England, personal communication, 1999). Pelitic schist from Cumpston Massif contains quartz + kyanite + staurolite + garnet + cordierite + biotite + muscovite + plagioclase + chlorite, with biotite and garnet partly replaced by chlorite. Although this assemblage was attributed by Tingey et al. (1981) to kyanite-staurolite grade overprinting of an original garnet-cordierite assemblage, there are no clear reaction relationships, and cordierite-kyanite occurs in different layers to staurolite-kyanite-garnet (Fig. 180B-D). It is thus more likely to be a compositional effect, with cordierite being confined to more magnesian layers and produced during the same lower amphibolite-facies event (presumably M_2) as the staurolite.

Late Mesoproterozoic to early Neoproterozoic(?) metamorphism (M_2)

Tingey (1982b, 1991a) produced a metamorphic map of the SPCM that showed a general increase in the grade of M_2 from lower amphibolite-facies (staurolite-kyanite zone) in the south to upper amphibolite-facies (sillimanite-K-feldspar zone) and locally granulite-facies (two-pyroxene granulite) in the southern part of the Beaver-Lambert Terrane (Fig. 179). Most of the Menzies Series, which occurs throughout much of the Ruker Terrane, contains lower amphibolite-facies (epidote amphibolite-facies) assemblages of relatively high-pressure Barrovian type (Tingey & England 1973). Metapelites typically contain staurolite + kyanite + biotite + muscovite + plagioclase + quartz \pm garnet (Fig. 180A, B), although, as already mentioned, kyanite appears to have coexisted with cordierite in metapelite at Cumpston Massif (Fig. 180C, D). Calcareous metasediments contain blue-green hornblende, diopside, epidote, plagioclase,

quartz, biotite, and/or garnet (Lopatin & Semenov 1982). Compositions of co-existing biotite + garnet and staurolite + garnet indicate metamorphic conditions of 4.2 to 7.5 kilobars and 485 to 610°C (Lopatin & Semenov 1982). The presence of relict andalusite, of probable regional metamorphic origin, as well as kyanite at Mounts Stinear and Maguire suggests relatively low pressures (Grew 1982), but may also indicate a pressure increase during M_2 . Alternatively, it could reflect an as yet unrecognised older metamorphic event in the metasedimentary cover rocks, which would be more difficult to reconcile with an early high-grade metamorphism. Moraine, of possible local derivation, near the summit of Keyser Ridge contains the apparently equilibrium assemblage quartz + biotite + muscovite + chloritoid + staurolite \pm garnet \pm kyanite (Fig. 180E), also suggesting slightly lower grade conditions.

Metadolerite dykes show various stages of recrystallisation, depending on the degree of deformation (Fig. 42). The freshest dolerites retain gabbroic to subophitic textures, with only partial replacement of pyroxene by pale green actinolitic amphibole or chlorite. Others have relict igneous textures, but clinopyroxene is completely altered to pale green actinolite; secondary biotite, epidote and titanite are commonly present. More extensive recrystallisation results in the formation of sieve-like aggregates of dark green hornblende with quartz inclusions and, ultimately, under upper amphibolite-facies conditions, granoblastic-polygonal amphibolites with dark greenish-brown hornblende are formed.

There is some evidence for a slightly higher-grade metamorphic zone (middle amphibolite-facies) in the Mount Cresswell-Binders Nunataks area, as well as near the southern end of the Mawson Escarpment, which thus appears to be transitional to the higher-grade rocks of the Beaver-Lambert Terrane. Amphibolite at Binders Nunataks and Mount Cresswell contains greenish brown hornblende, calcic plagioclase and garnet. The presence of garnet suggests slightly higher-pressure conditions, assuming its stability was not a function of bulk rock composition. However, the presence of hornblende + plagioclase replacing garnet in one rock (Fig. 181) indicates either a subsequent pressure drop (e.g., near-isothermal decompression) or a later low-pressure event. Co-existing sillimanite + muscovite appears to be present in paragneiss in the southern Mawson Escarpment, although many of the rocks there contain polymetamorphic assemblages. It is therefore not entirely clear that these minerals were in equilibrium. Upper amphibolite-facies (almandine amphibolite-facies) conditions, characterised by garnet + sillimanite + K-feldspar \pm cordierite, were attained in the south-central Mawson Escarpment, but the presence of relict staurolite and possibly kyanite in a few metapelites suggests that this relatively high-grade event may have been associated with emplacement of syn- M_3 granitoids. Conversely, middle amphibolite-facies assemblages in the southeastern PCM were considered by Tingey (1982b, 1991a) to have formed during an earlier metamorphic event (M_1), as described above, although the evidence is far from conclusive.

An intermediate zone of greenschist-facies rocks depicted by Tingey (1982b, 1991a) coincides quite closely with the distribution of Sodruzhestvo Series

metasediments, together with the ironstone-bearing Ruker Series. The latter sequence is typified by greenschist-facies phyllite, slate, and calcareous schist containing quartz + biotite + white mica + chlorite \pm carbonate \pm actinolite \pm albite. Metadolerites contain various amounts of

plagioclase (relict igneous), actinolite, epidote, carbonate, biotite, chlorite, titanite, quartz and opaque minerals.

If the Sodruzhestvo Series was deposited in the Mesoproterozoic, which most of the authors consider to be the most likely age, then it may well have been

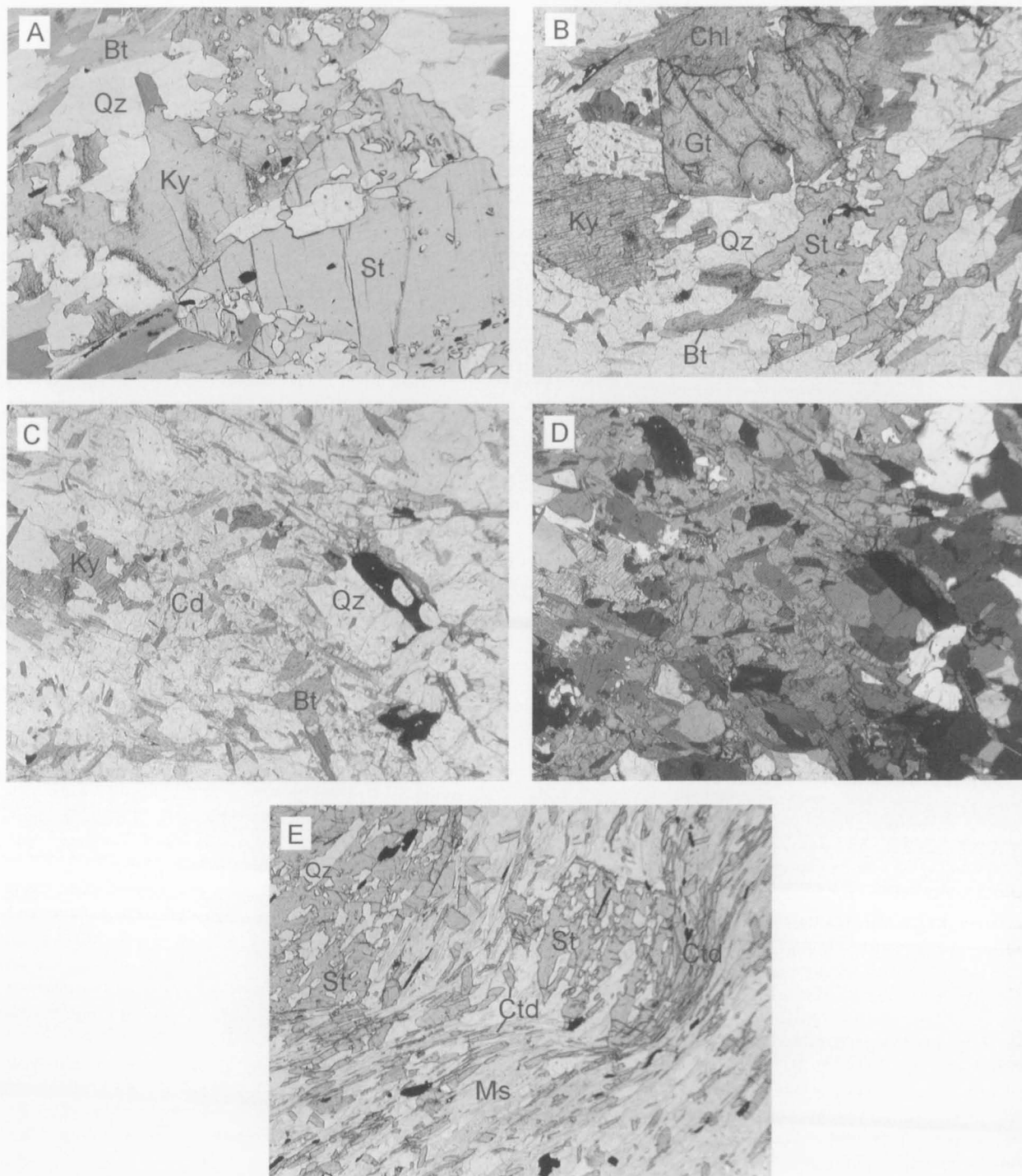


FIGURE 180

Lower amphibolite-facies assemblages in Menzies Series metapelites. (A) Staurolite-kyanite-biotite-chlorite-muscovite-plagioclase-quartz metapelite; Seavers Nunataks. Sample 72280700B. (B) Staurolite-kyanite-garnet-biotite-chlorite-plagioclase-quartz-(muscovite) metapelite; Cumpston Massif. Sample 73281246. (C, D) Cordierite-kyanite-biotite-chlorite-plagioclase-quartz layer; Cumpston Massif. Sample 73281246. (E) Staurolite-garnet-chloritoid-biotite-chlorite-muscovite-quartz metapelite; moraine at Keyser Ridge. Chloritoid appears to be a primary phase, in equilibrium with the other major minerals. Sample 73281274. Cross-polarised light in D; width of field: 4 mm.

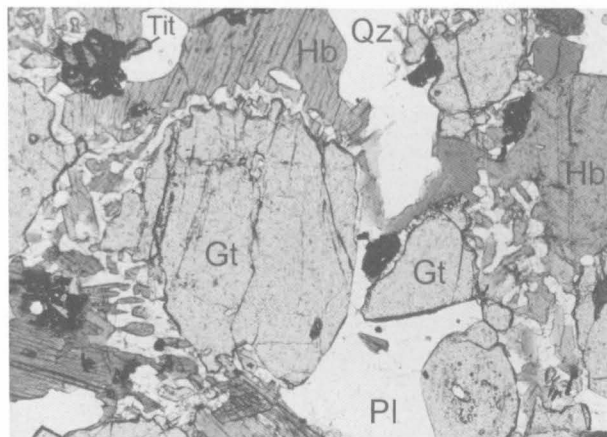


FIGURE 181

Garnet amphibolite containing greenish-brown hornblende, garnet, labradorite, quartz, and minor reddish-brown biotite, titanite (Tit), and opaque minerals; Mount Cresswell. Garnet grains are surrounded by a plagioclase-hornblende symplectite. Sample 73281104; width of field: 2 mm.

metamorphosed during the c.1000 Ma event that presumably affected the Ruker Series (i.e., M_2). Alternatively, if it was deposited in the Neoproterozoic, then its low-grade metamorphism must have occurred during the Cambrian event (M_3), as the rather equivocal Rb-Sr data suggest. A third possibility is that it was deposited in the Mesoproterozoic, but not metamorphosed until the Cambrian event. A further possibility, favoured by one of the authors (ENK), is that the depositional age is as old as early Precambrian, and the isotopic data reflect thermal, rather than metamorphic/deformational, events. Like the Ruker Series, the Sodruzhestvo Series is mainly of greenschist facies, with the assemblage biotite + white mica + chlorite + carbonate + epidote + quartz \pm actinolite \pm plagioclase \pm K-feldspar being typical of calcareous schist and quartzite at Mount Rubin. The metamorphic grade at Goodspeed Nunataks and Mounts Dummett and Seddon is similar, although the rare occurrence of kyanite in schist and quartz veins at northern Goodspeed Nunataks and in pegmatite at Mount Dummett, and of diopside in calcareous rocks at the latter locality suggest a slightly higher metamorphic grade in these areas.

Metasedimentary rocks at Mounts McCauley and Scherger have been tentatively assigned to the Menzies Series, although they are compositionally and petrologically similar to some Sodruzhestvo Series rocks, such as those at Mount Dummett. For example, concordant quartz veins in pelitic schist at Mount Scherger contain kyanite, biotite and muscovite. Secondary fibrolite after kyanite, biotite, or muscovite is common at both Mounts McCauley and Scherger (Fig. 182D). A schist sample from Mount McCauley contains the disequilibrium assemblage quartz + kyanite + staurolite + sillimanite + cordierite + biotite + muscovite + oligoclase (Fig. 182E, F), indicating replacement of staurolite + kyanite by cordierite + sillimanite, probably during emplacement of Cambrian granite and pegmatite veins that are particularly abundant at this locality. It seems probable that the original kyanite + staurolite association in these rocks formed during M_2 , and that there was only one kyanite-staurolite-grade

event in the Ruker Terrane. Although this would be consistent with a Cambrian age for greenschist-facies metamorphism of the Sodruzhestvo Series, it would be equally consistent with an early Neoproterozoic age.

Cambrian metamorphism (M_3)

A Pan-African or Ross (c.500 Ma) metamorphic age for the Sodruzhestvo Series in the Fisher Glacier is quite possible, but in the absence of definitive age data remains uncertain; an M_2 metamorphic age is also possible. Nevertheless, the presence of poikiloblastic cordierite at northern Goodspeed Nunataks and fibrolite (fine-grained sillimanite) at Mount Dummett probably reflects heating associated with emplacement of nearby Cambrian pegmatites. As already mentioned, secondary sillimanite \pm cordierite in metapelite at Mounts McCauley and Scherger is thought to have a similar origin. Garnet \pm relict kyanite + sillimanite \pm cordierite assemblages at Binders Nunataks, staurolite-kyanite schist with secondary sillimanite + cordierite at Mount Stinear (Fig. 182A-C), and garnet-sillimanite-cordierite gneisses with relict staurolite \pm kyanite on the central Mawson Escarpment, as well as hornblende + plagioclase rims on garnet in amphibolite at Mount Cresswell, may also be 'contact-metamorphic' effects.

Some of the metamorphic reactions that occurred in the country rocks during late Neoproterozoic to Cambrian magmatism were described by Lopatin & Semenov (1982), who quote a temperature of about 570°C based on compositions of co-existing garnet and biotite. Replacement of hornblende in concordant amphibolite bodies by cummingtonite and, ultimately, by anthophyllite or gedrite, garnet and cordierite, involved Fe-Mg metasomatism. The common presence of sillimanite, rather than kyanite, shows that M_3 occurred under somewhat lower pressure conditions than M_2 .

Elsewhere in the Ruker Terrane, greenschist-facies retrogression is widespread in both granitic basement rocks and Menzies Series metasediments. Most of this low-grade overprinting is presumed to be of Cambrian age, although not all such retrogression necessarily occurred during this metamorphic episode. However, at least some of the retrogression is clearly associated with mylonite and shear zones, which, by analogy with similar structures in the Beaver-Lambert Terrane, are probably of Pan-African age (Fig. 183A, B). Typical retrograde effects include replacement of biotite by chlorite, and garnet by chlorite, biotite and/or muscovite (Fig. 183A, B, E), and sericitisation and saussuritisation of feldspar. Diopside in calcareous metasediments was partly altered to actinolite and epidote, and secondary actinolite, chlorite, epidote, carbonate, and, less commonly cummingtonite, are present in amphibolite. Chloritoid-chlorite assemblages replace kyanite-staurolite assemblages in quartzite and metapelite near the summit of Mount Menzies (Tingey & England 1973). Staurolite and kyanite are crowded with inclusions of chloritoid and quartz, with minor sericite. Chloritoid was probably produced by the reaction:

$$\text{staurolite} + \text{biotite} + \text{H}_2\text{O} \rightarrow \text{chloritoid} + \text{muscovite} + \text{chlorite} + \text{quartz}.$$

Pyrophyllite partly replaces kyanite in quartzite: $\text{kyanite} + \text{quartz} + \text{H}_2\text{O} \rightarrow \text{pyrophyllite}.$

According to Tingey & England (1973), these reactions probably took place at between 420–440°C and 550°C, at moderate pressure. Similar chloritoid-bearing retrograde rocks at Mounts Bird and Newton (Fig. 183C, D) contain chloritoid, chlorite, sericite, quartz, relict garnet and sillimanite, and rare altered cordierite, indicating

derivation from higher grade (at least upper amphibolite-facies) protoliths. The retrogression was apparently associated with boudinage of dolerite intrusions, and also with deformation of tourmaline-bearing pegmatites (England & Langworthy 1975). It is therefore presumed to be of similar ?Cambrian age to the chloritoid-bearing rocks

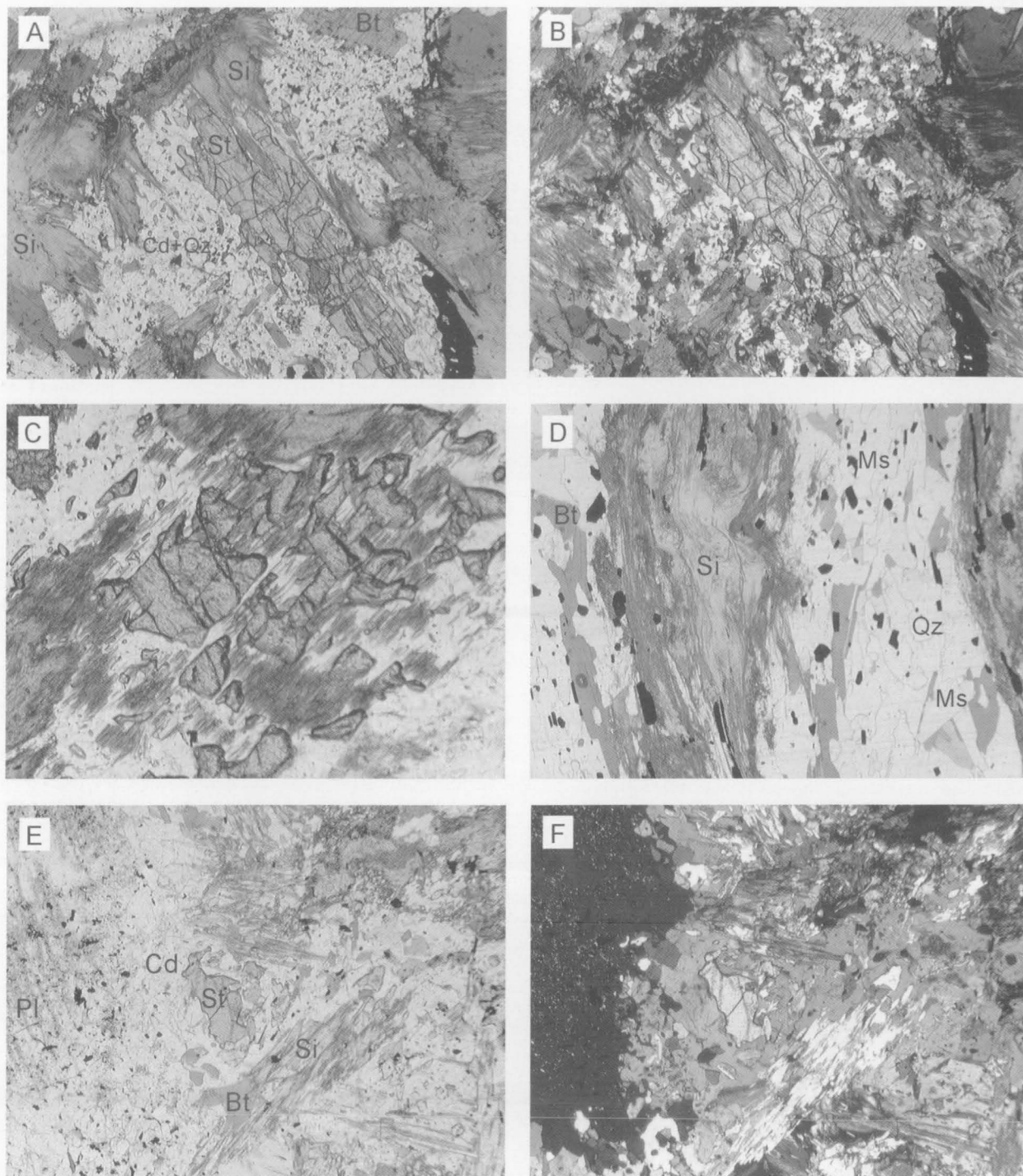


FIGURE 182

High-grade overprinting of low- to medium-grade assemblages in Menzies Series metapelites. (A, B) Fibrous sillimanite (fibrolite) and cordierite overprinting staurolite-kyanite-biotite-chlorite-muscovite-albite-quartz assemblage; Mount Stinear. Sample 73281640; width of field: 4 mm. (C) Detail of above rock, showing replacement of staurolite by sillimanite and cordierite. Width of field: 1.2 mm. (D) Development of fibrolite in biotite-muscovite-quartz(-chlorite) schist; Mount Scherger. Sample 72280836; width of field: 4 mm. (E, F) Secondary fibrolite + cordierite in staurolite-kyanite-biotite-oligoclase-quartz(-muscovite) metapelite; Mount McCauley. Sample 73281347; width of field: 4 mm. Cross-polarised light in B and E.

at Mount Menzies, but, if so, the apparent absence of evidence for a Neoproterozoic metamorphism is puzzling. The reason why chloritoid occurs in only a few restricted areas may well reflect the scarcity of protoliths of suitable bulk composition, with low CaO and *mg*, and high Al_2O_3 .

FISHER TERRANE

Mafic to felsic volcanic rocks of the Fisher Terrane were metamorphosed under greenschist to amphibolite-facies conditions, and thus differ significantly from most Beaver-Lambert Terrane rocks. Metamorphosed volcanic,

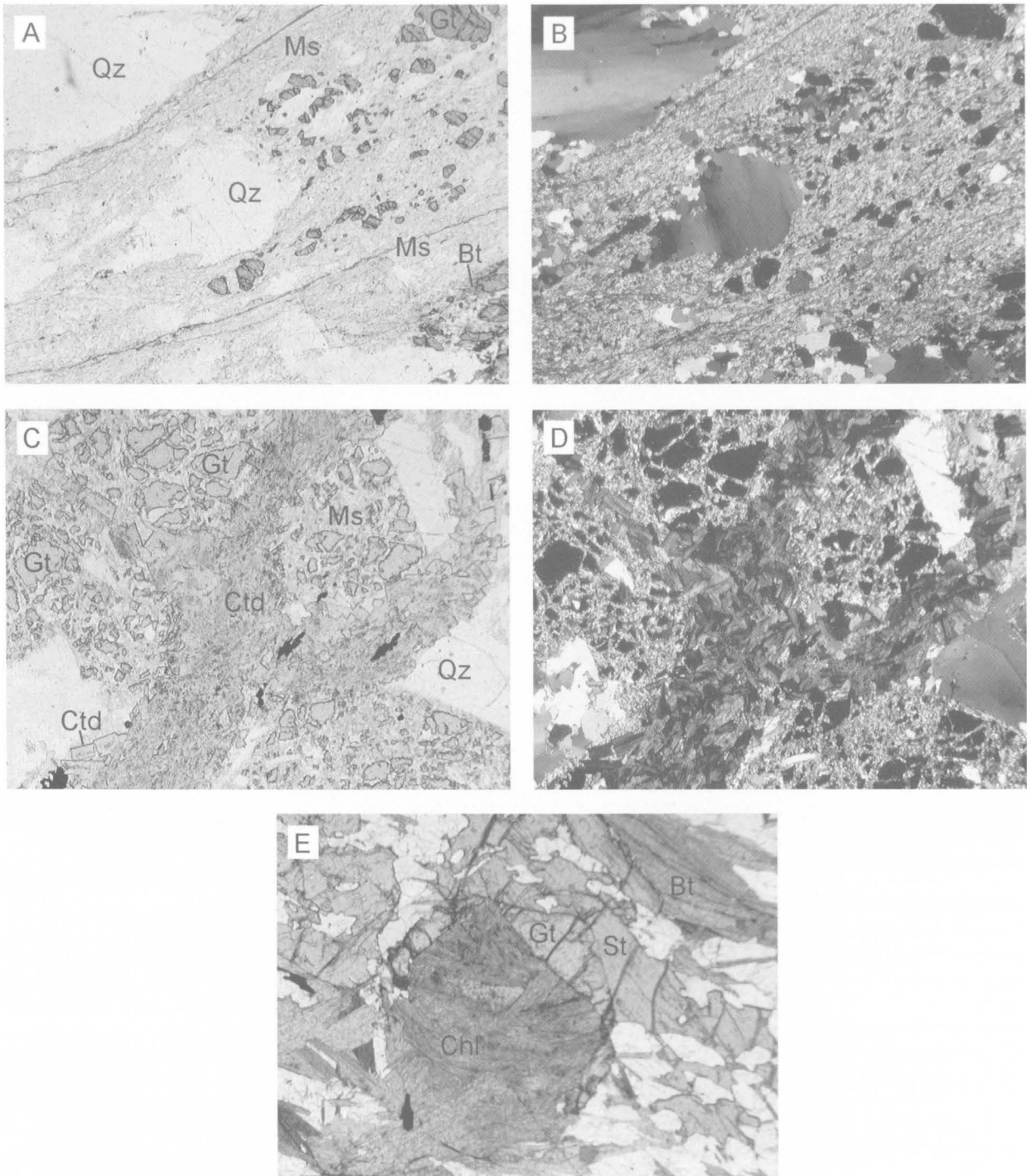


FIGURE 183

Retrograde assemblages in Menzies Series metapelites. (A, B) Replacement of garnet by fine-grained muscovite and biotite in sheared garnet–biotite–quartz (–K-feldspar?) gneiss; Mount Newton. Note undulose extinction in quartz porphyroclasts. Sample 73281461. (C, D) Chloritoid–chlorite–muscovite–quartz schist with relict garnet; Mount Newton. Sample 72280710. (E) Chlorite replacing garnet (atoll garnet) in staurolite–kyanite–garnet–biotite–chlorite–plagioclase–quartz (–muscovite) metapelite; Cumpston Massif. Sample 73281246. Cross-polarised light in B and D; width of field: 4 mm.

tuffaceous and intrusive rocks consist of various amounts of quartz, K-feldspar, plagioclase (mainly oligoclase-andesine), amphibole, biotite, epidote, quartz, opaque minerals, and minor chlorite, titanite, carbonate, sericite and garnet. Pelitic schist contains quartz-plagioclase-biotite-muscovite±garnet assemblages.

Metamorphosed mafic rocks at **Fisher Massif** contain three generations of amphibole: amphibole I (brownish-green or green urtite containing abundant opaque mineral inclusions), amphibole II (pale green fibrous actinolite), and amphibole III (bluish-green hornblende and cummingtonite). Brown biotite I, that formed large flakes, equilibrated with amphiboles I and II. Epidote, calcite, biotite II (green, fine grained), chlorite and pyrite replaced hornblende and biotite I during subsequent events. At least three metamorphic stages may be distinguished: an early greenschist-facies event, an epidote-amphibolite-facies event, and a late retrograde lower greenschist-facies event.

The *early greenschist-facies* assemblages define the northeast trending schistosity (S_1) in the metavolcanic rocks, and corresponding cataclastic structures within plutonic rocks. Uralitic amphibole (after pyroxene, although no relics were found) was replaced by actinolite, plagioclase was recrystallised and became less calcic, and epidote and calcite were formed.

Typical mineral assemblages in mafic metavolcanic rocks are:

albite-oligoclase + actinolite + quartz ± epidote, and
albite-oligoclase + actinolite + biotite + quartz ± epidote ± muscovite;
and in metagabbro:
oligoclase-andesine + actinolite ± biotite ± epidote ± quartz.

Metavolcanic rocks show complete recrystallisation and migmatization within narrow (up to 5 m) contact zones with intrusive rocks (gabbro, diorite and granitoids), which suggests contact metamorphism.

Second stage *epidote-amphibolite-facies* assemblages define a schistosity (S_2) that is steeply dipping and cuts the S_1 foliation and schistosity at low angles. Actinolite was replaced by bluish-green hornblende and cummingtonite. Newly crystallised quartz and biotite contain inclusions of earlier stage minerals.

Typical mineral assemblages in mafic and intermediate metavolcanic rocks are:

oligoclase-andesine + hornblende + epidote ± biotite ± quartz, and
oligoclase + cummingtonite + biotite ± quartz;
in intermediate to felsic metavolcanic rocks:
oligoclase-andesine + biotite + quartz ± epidote ± garnet (almandine);
in metagabbro and metadiorite:
hornblende + oligoclase-andesine ± quartz ± epidote ± biotite;
and in metatonalite and plagiogranite:
oligoclase + epidote + biotite + quartz ± hornblende.

The coexistence of pale bluish-green hornblende, oligoclase and epidote points to relatively high-temperature metamorphic conditions (epidote-amphibolite facies).

Late greenschist-facies assemblages are widespread throughout the area, and are concentrated within numerous cataclastic to high-strain shear zones that are

generally conformable to the foliation. Chlorite, sericite, quartz and green biotite are minor constituents in all lithological types, and reflect relatively low-temperature greenschist-facies conditions.

A study of fluid/liquid inclusions in metamorphic minerals indicated temperature intervals for the three metamorphic events as follows: early greenschist facies at 330–460°C, second epidote-amphibolite facies at 510–590°C, and late greenschist facies at 200–270°C (V.S. Aplonov, unpublished data). Some higher temperature estimates of 620–670°C for metamorphic rocks adjacent to a tonalite pluton reflect the effects of contact metamorphism.

Preliminary estimates, using the garnet-biotite and amphibole-plagioclase geothermometers of Perchuck et al. (1985), suggest metamorphic temperatures between 585° and 640°C, which are in good agreement with the inclusion study. The amphibole-plagioclase geobarometers of Plyusina (1982) and Mishkin (1990), based on An content of plagioclase and Al distribution in amphibole, gave pressure estimates mostly between 1-2 and 2-3 kilobars, supporting the suggestion of a relatively high crustal level for the Fisher Massif metavolcanic rocks.

Somewhat higher-grade peak metamorphic conditions pertained at **Nilsson Rocks**. At least two metamorphic stages were distinguished: earlier amphibolite-facies and later lower greenschist-facies events. The amphibolite-facies metamorphism is reflected in recrystallisation and formation of a northeast-trending penetrative schistosity.

The typical mineral assemblage in felsic gneiss is:

andesine + quartz + biotite ± hornblende ± garnet (almandine) ± K-feldspar;
in mafic schist:
andesine-labradorite + hornblende ± biotite ± diopside;
in metagabbro:
labradorite + quartz + hornblende + cummingtonite ± biotite ± diopside ± garnet (almandine);
in mildly alkaline biotite gabbro:
labradorite + hornblende + biotite ± quartz ± diopside ± K-feldspar;
in metadiorite:
andesine + quartz + biotite ± hornblende ± cummingtonite;
and in metatonalite and plagiogranite:
oligoclase + quartz + biotite ± hornblende.

Diopside is a common constituent in mafic schist and metagabbro, but also occurs in felsic gneiss. Along with the other metamorphic minerals, it has a granoblastic texture. Two generations of hornblende are developed: an earlier dark green variety, and a later light bluish-green variety, probably developed at somewhat lower temperatures during the waning stages of amphibolite-facies metamorphism. Migmatitic veins, mainly of plagiogneiss, are widespread. Retrograde low-temperature greenschist-facies assemblages comprise albite-oligoclase, actinolite, epidote, quartz, late-stage biotite, chlorite and sericite.

Three metamorphic stages were discerned at **Mount Willing**: autometamorphism, prograde amphibolite-facies metamorphism, and retrograde greenschist-facies metamorphism. The autometamorphic stage is represented by replacement of olivine by iddingsite and serpentine, and pyroxene by actinolite and colourless

Fe–Mg amphibole. Grunerite, anthophyllite or cummingtonite form rims around primary ferromagnesian minerals.

Prograde amphibolite-facies metamorphism resulted in the development of a locally penetrative schistosity, generally conformable to magmatic layering. The typical mineral association in metagabbro is:

andesine–labradorite + hornblende + biotite \pm quartz \pm magnetite \pm garnet (almandine).

Metamorphic hornblende is dark green, and ranges from magnesio-hornblende to tschermakitic hornblende and ferrotschermakite. Secondary (outer) rims were formed around colourless Fe–Mg amphibole, probably due to reaction with plagioclase. Actinolite was replaced by, and sometimes grades into, hornblende, which suggests that the auto- and prograde metamorphic processes were co-eval and occurred under similar conditions.

Typical assemblages in felsic gneiss are:

oligoclase + biotite + quartz \pm K-feldspar, and

oligoclase–andesine + cummingtonite + biotite + quartz \pm hornblende \pm garnet.

Mafic schist comprises andesine–labradorite + hornblende + biotite \pm quartz.

Orthopyroxene was also found in one fine-grained relatively leucocratic rock, but a microgabbroic texture indicates a magmatic origin for the orthopyroxene. Two generations of hornblende were developed: one dark green and one bluish green. Bluish-green hornblende replaces cummingtonite.

Retrograde metamorphic assemblages comprise widespread chlorite, a second generation of actinolite, titanite, sericite, quartz, magnetite and calcite. These minerals are abundant in high-strain shear zones.

Biotite–garnet (Ferry & Spear 1978; Ganguly & Saxena 1984) and/or amphibole–plagioclase (Perchuck 1970; Plyusnina 1982; Mishkin 1990) geothermometers were used for two felsic gneisses (samples 39110-15 and 39140-2), and a mafic schist (39146-2). Temperatures were calculated from compositions of apparently equilibrated adjoining amphibole–plagioclase or biotite–garnet cores or edges (Mikhalsky et al. 1999). These methods gave more or less consistent temperatures in the range 530–600°C, with a few estimates as low as 480°C or as high as 670°C. The latter value is consistent with the inferred re-equilibration of the Sm–Nd system at about 1100–1000 Ma (Mikhalsky et al. 1993), thought to have occurred at temperatures of about 600–700°C.

The amphibole–plagioclase geobarometer of Mishkin (1990) gave pressure estimates of 6–9 kilobars. These data support petrographic observations of reaction coronas formed along olivine–plagioclase contacts, which imply crystallisation at pressures above 6–8 kilobars (Green & Hibberson 1970). Thus, a pressure of at least 6 kilobars, which corresponds to a crustal depth of about 20 kilometres, seems to be the best estimate.

The estimated temperature conditions correspond to amphibolite (or almandine-amphibolite) facies. The presence of garnet and rare sillimanite confirm this suggestion. Clinozoisite and epidote are notably lacking from the Mount Willing metamorphic rocks. This implies a higher metamorphic grade than those at nearby Fisher Massif, which were metamorphosed under epidote-amphibolite facies. Anthophyllite rims on orthopyroxene

imply relatively high-temperature hydration, whereas green hornblende rims on anthophyllite indicate retrogressive cooling, possibly during uplift.

Thus, at least three metamorphic events may be distinguished in the Fisher Terrane. Evidence for the earliest greenschist-facies metamorphism (M_1), at about 330–460°C, is only apparent in the Fisher Massif rocks. The higher crustal position of this block is probably the reason that subsequent reworking was at a lower grade than nearby Nilsson Rocks and Mount Willing. Peak metamorphism (M_2) possibly attained temperatures of about 670°C and pressures above 6–8 kilobars at Mount Willing. Retrograde metamorphism (M_3) occurred at low temperatures (200–270°C at Fisher Massif). Many of the exposed rocks at Fisher Massif are highly sheared, so that dynamic and regional metamorphism may have been equally important. Available isotopic data for Mount Willing rocks suggest late Mesoproterozoic metamorphic ages of about 1120 (metagabbro and quartz diorite zircon ages; Laiba & Mikhalsky 1999; Mikhalsky et al. 1999) and about 1020–1010 Ma (resetting of the Sm–Nd system in metagabbro and metatonalite; Mikhalsky et al. 1993, 1999). However, a somewhat older (c.1190) age of apparently undeformed granite at Mount Willing suggests that the peak metamorphic conditions (M_2) were attained just before granite emplacement, at about the time of roughly co-eval tonalite intrusion. Nevertheless, because there is no convincing evidence that thermal and deformational processes were always co-eval, M_2 may have lasted until about 1120 or even 1000 Ma. Retrogression (M_3) appears to have lasted until, or caused overprinting at, about 800 Ma (a thermal event indicated by zircon ages for the Mount Willing layered gabbro) and possibly 600–500 Ma (Rb–Sr mineral ages for mafic schists, and U–Pb zircon lower intercept for a tonalite).

BEAVER-LAMBERT TERRANE

Late Mesoproterozoic–early Neoproterozoic peak metamorphism

The occurrence of the assemblage orthopyroxene–clinopyroxene–plagioclase \pm hornblende \pm quartz in mafic granulite throughout much of the NPCM indicates metamorphism under low- to medium-pressure granulite-facies conditions (Green & Ringwood 1967). Syn- D_3 orthopyroxene-bearing assemblages in felsic and intermediate gneisses, garnet–sillimanite–cordierite in metapelitic rocks, and diopside–wollastonite–scapolite in calc-silicate rocks all indicate similar metamorphic conditions. Granulite-facies conditions appear to have prevailed throughout the time interval D_1 to D_6 , although it is possible that these deformations were separated by periods of lower-grade conditions. However, geochronological data suggest that most or all of these events occurred over a relatively restricted period of time (a few tens of millions of years), so that it is more likely that the rocks remained at depths corresponding to granulite-facies for the whole of that period.

Slightly lower grade conditions (upper amphibolite facies) appear to have prevailed at many outcrops in the southern part of the NPCM, particularly south of the

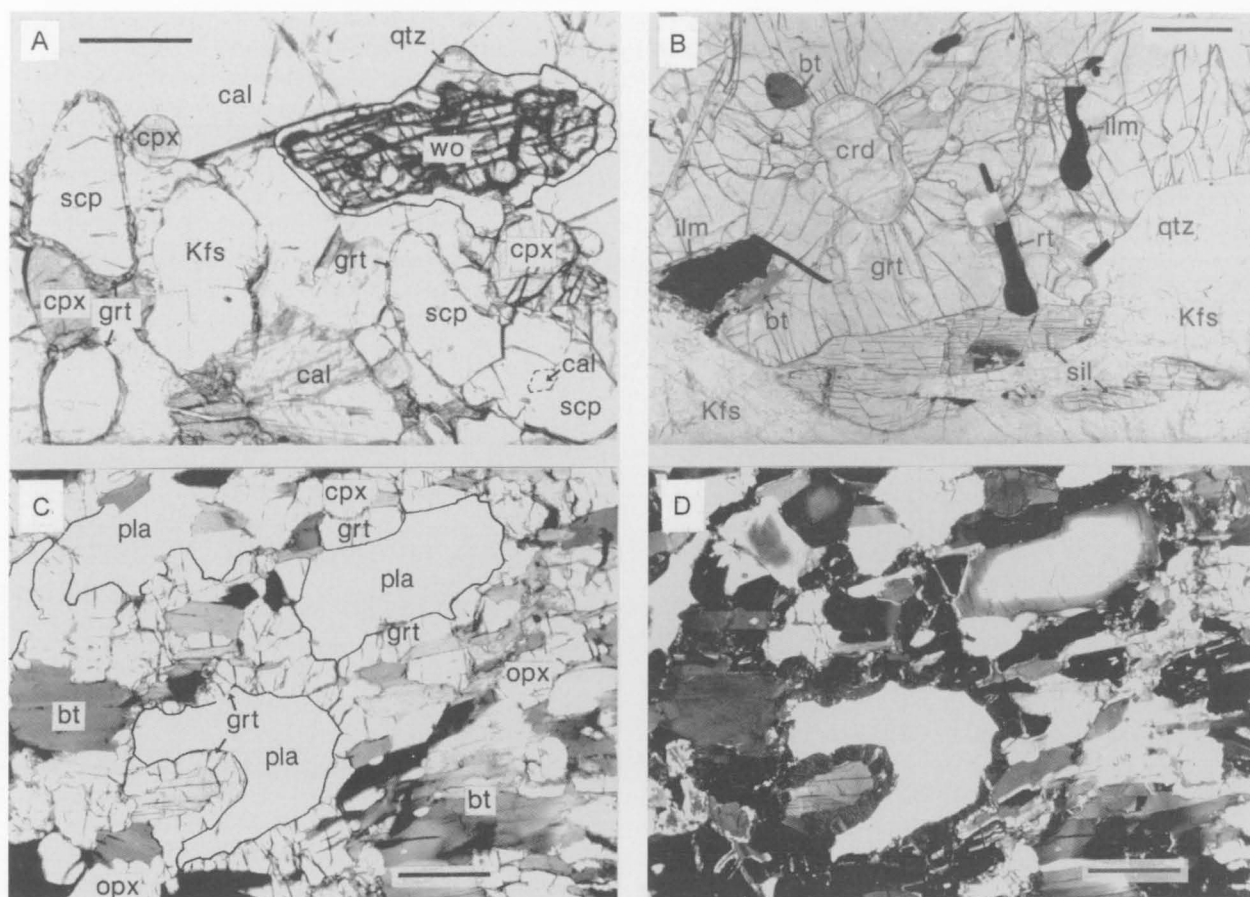


FIGURE 184

Rocks from the Beaver-Lambert Terrane used for P-T estimates (Thost & Hensen 1992). (A) Calc-silicate gneiss, with wollastonite, scapolite, clinopyroxene and K-feldspar (Kfs) in a calcite-rich matrix. Wollastonite contains rounded inclusions of clinopyroxene and calcite, and is rimmed by secondary quartz (qtz, outlined in black). Scapolite is rimmed by secondary garnet (grt). Minerals that occur as aggregates have polygonal grain boundaries. Scale bar: 0.5 mm. (B) Migmatitic metapelite, containing coarse-grained garnet porphyroblasts with inclusions of cordierite (crd), biotite, ilmenite (ilm), and rutile (rt). The matrix comprises coarse-grained sillimanite (sil), K-feldspar and quartz. Scale bar: 1 mm. (C) Mafic granulite, in which large grains and aggregates of plagioclase (pla) are separated from orthopyroxene, clinopyroxene and biotite by secondary garnet coronas. Plagioclase-garnet contacts are outlined in black. Scale bar: 0.5 mm. (D) As for C, with cross-polarised light. Plagioclase grains show pronounced zoning.

Aramis Range, where migmatitic gneisses show evidence for extensive partial melting and granite and pegmatite veins are abundant (Tingey 1972). Tingey (1972) postulated two amphibolite-facies events in this area, one post-dating emplacement of mafic intrusive rocks. Felsic gneiss at Mount Meredith contains biotite ± garnet, but no orthopyroxene, and metapelite contains the assemblage garnet-cordierite-anthophyllite-biotite-spinel-plagioclase.

Metamorphism in the Lambert Series of the northern part of the SPCM was also predominantly of upper amphibolite facies, consistent with a southward decrease in metamorphic grade in the Beaver-Lambert Terrane (Tingey 1972). However, transitional granulite-facies conditions were reached in the northern Mawson Escarpment, where clinopyroxene-orthopyroxene-plagioclase granulite crops out. Brown hornblende is a common additional phase, with some rocks containing up to 50 percent, but hornblende does not generally coexist with quartz. The latter feature is consistent with the prograde reaction:

hornblende + quartz → plagioclase + clinopyroxene + orthopyroxene, which proceeds until one or other of the reactants is consumed. The only recorded occurrence of orthopyroxene in a felsic rock is at Mount Isabelle (hornblende-orthopyroxene-biotite-orthoclase-quartz-plagioclase orthogneiss). Elsewhere, biotite-quartz-feldspar and garnet-biotite-quartz-feldspar assemblages predominate.

High-grade conditions are consistent with the widespread evidence for partial melting. For example, many of the more felsic rocks, such as garnet leucogneisses and metapelites, are migmatitic, with small, locally discordant felsic segregations (leucosome). Various generations of granitic leucogneiss bodies were emplaced between D₃ and D₆, and at least some of the major orthopyroxene granitoid plutons attest to much more extensive crustal melting, albeit at somewhat deeper crustal levels. Orthopyroxene-bearing segregations in mafic granulite may have resulted from limited pre-D₃ fluid-absent melting of hornblende (Thompson 1982; Grant 1985):

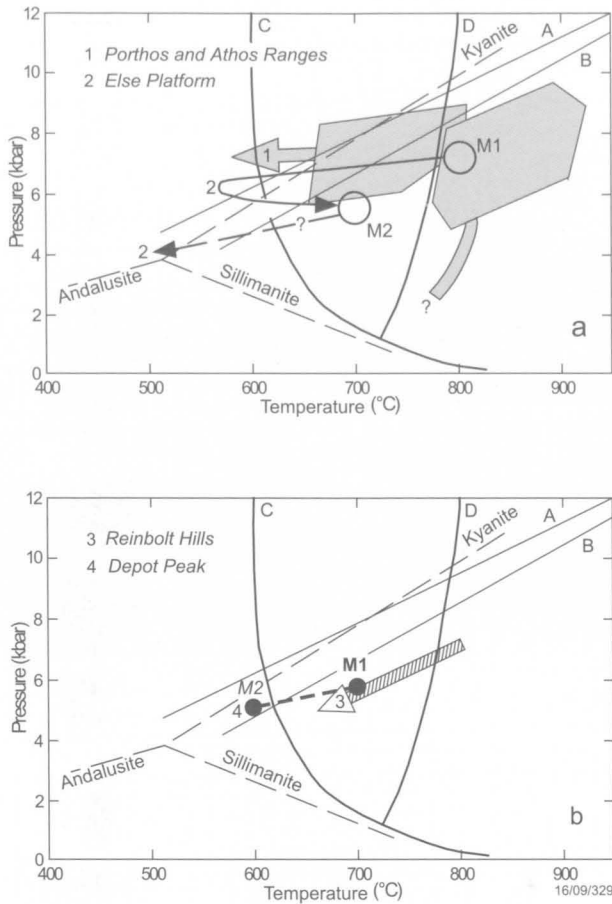


FIGURE 185

P-T diagrams showing estimated peak and retrograde metamorphic conditions (1) in the Porthos and Athos Ranges of the Beaver-Lambert Terrane, and the interpreted anticlockwise P-T path dominated by near-isobaric cooling (Thost & Hensen 1992). Also shown are the interpreted P-T path (2) for Else Platform (Hand et al. 1994a), which involved significant post-peak cooling and decompression; the decompressional P-T path (3) suggested by Nichols & Berry (1991) for the Reinbolt Hills; and the estimated conditions for M_1 and M_2 at Depot Peak (4; Stüwe & Hand 1992). A, Appearance of garnet in quartz tholeiite (Green & Ringwood 1967); B, Appearance of garnet in peridotite (Saxena & Ericson 1985); C, Water-saturated granite solidus (Huang & Wyllie 1973); D, Vapour-absent melting of biotite (Le Breton & Thompson 1988). Aluminium silicate triple point after Holdaway (1971).

hornblende + quartz \rightarrow orthopyroxene + clinopyroxene + plagioclase + melt.

Rare orthopyroxene-bearing leucocratic selvages around mafic bodies also suggest partial melting.

Estimates of the peak metamorphic conditions for the **Porthos Range** area of the NPCM, calculated using a variety of geothermometers and geobarometers, were made by Thost & Hensen (1992) (Figs 184, 185). Samples containing the assemblage garnet-orthopyroxene-plagioclase-quartz are suitable for P-T estimates. Barometers based on the reaction:

plagioclase + orthopyroxene \rightarrow garnet + quartz

(Newton & Perkins 1982; Bohlen et al. 1983a) and on the solubility of Al_2O_3 in orthopyroxene coexisting with garnet (Harley & Green 1982; Harley 1984a) indicate pressures of 7 ± 1 kilobars for felsic gneiss and orthopyroxene granite from the Porthos Range. Corresponding temperatures, based on Fe-Mg exchange between garnet and orthopyroxene (Harley 1984b; Sen & Bhattacharya 1984; Lee & Ganguly 1988), are $750\text{--}850^\circ\text{C}$ (Fitzsimons & Thost 1992; Thost & Hensen 1992). There are no apparent differences in P-T estimates for samples preserving different fabrics (S_3 or S_6). Pressure estimates on metapelites from Carter Peaks using garnet-rutile-ilmenite-sillimanite-quartz and garnet-rutile-ilmenite-plagioclase-quartz equilibria (Bohlen et al. 1983b; Bohlen & Liotta 1986) are very similar (6.5–7 kb at 800°C), and a variety of calibrations using garnet-sillimanite-plagioclase-quartz equilibria (Newton & Haselton 1981; Ganguly & Saxena 1984; Hodges & Crowley 1985) are only slightly lower (5–6 kb at 800°C). Garnet-cordierite (Wells 1979) and garnet-biotite (Ferry & Spear 1978) thermometry gives lower temperatures than those obtained using garnet-orthopyroxene, probably reflecting continued Fe-Mg equilibration during cooling (Thost & Hensen 1992).

Peak metamorphic conditions are also constrained by calc-silicate assemblages, as shown by the petrogenetic

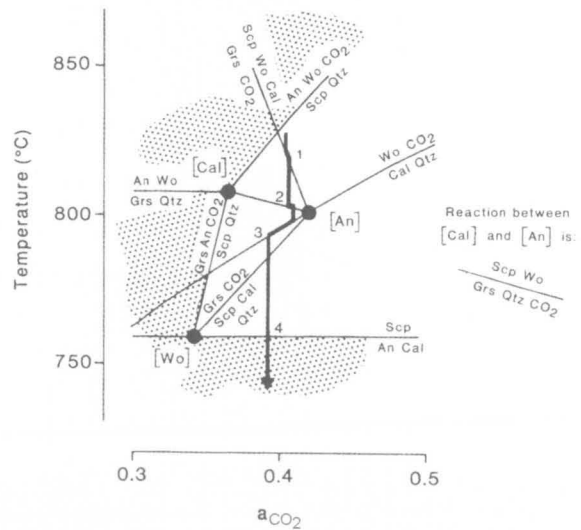


FIGURE 186

Petrogenetic T- a_{CO_2} grid (Fitzsimons & Thost 1992) for the system $CaO-Al_2O_3-SiO_2-CO_2-H_2O$ in the vicinity of the calcite, anorthite and wollastonite-absent invariant points (labelled [Cal], [An], and [Wo], respectively). Numbers 1 to 4 refer to reactions discussed in the text. The shaded area is that part of the grid where scapolite and quartz cannot coexist, which constrains the peak metamorphic conditions since these phases are part of the peak assemblage in many calcite-wollastonite-free calc-silicate layers. The thick line depicts a retrograde path consistent with the observed reaction textures. This path is buffered along the reactions as no volatile fluid was present in sufficient amounts to externally buffer a_{CO_2} to a fixed value. a_{CO_2} is constrained to be low (about 0.4) since the path passes between [Cal] and [An].

T- a_{CO_2} grid of Fitzsimons & Harley (1992) and Fitzsimons & Thost (1992) for the phases garnet, scapolite, wollastonite, plagioclase, calcite, quartz and $\text{H}_2\text{O}-\text{CO}_2$ fluid (Fig. 186). The stability of scapolite-quartz and scapolite-wollastonite-calcite in adjacent layers indicates peak temperatures of 800–830°C.

Peak assemblages at **Else Platform**, which involve garnet-sillimanite-ilmenite \pm rutile and garnet-orthopyroxene (M_1 of Hand et al. 1994a, b), give P-T estimates very similar to those in the Porthos Range: 6.5–7.9 kilobars (Harley & Green 1982; Harley 1984a; Holland & Powell 1990) and 740–820°C (Sen & Bhattacharya 1984; Lee & Ganguly 1988). Fe-Mn exchange between ilmenite and garnet in the cores of M_1 garnets (Pownceby et al. 1987) gives a temperature of $770 \pm 50^\circ\text{C}$. However, in view of the strong M_2 overprint in this area, such conditions are likely to be minimum estimates. Estimated P-T conditions for M_1 at Trost Rocks and Fox Ridge were very similar (Scrimgeour & Hand 1997), as were those in the Reinbolt Hills (Nichols & Berry 1991): 7 ± 1 kilobars (Perkins & Newton 1981; Harley & Green 1982; Bohlen et al. 1983c; Harley 1984a) and $800 \pm 50^\circ\text{C}$ (Sen & Bhattacharya 1984). The lack of compositional differences between minerals defining S_1 , S_2 and S_3 suggests that complete re-equilibration occurred at the end of D_3 . P-T estimates for the metamorphic peak (assigned to M_1) at **Depot Peak**, using the average pressure approach of Powell & Holland (1988) and Holland & Powell (1990) on a garnet-cordierite-sillimanite-spinel-quartz-

feldspar metapelite, are somewhat lower, about 5.6 kilobars at 700°C (Stüwe & Hand 1992).

There is some textural evidence for an earlier prograde P-T path in the form of sillimanite and rounded cordierite inclusions in garnet (Fig. 184B), which suggest that the reaction:

cordierite \rightarrow garnet + sillimanite + quartz

occurred with increasing pressure (Thost & Hensen 1992).

Metapelite at Else Platform contains two types of garnet: (1) an inclusion-rich variety containing oriented inclusions of biotite-sillimanite (\pm spinel, quartz and ilmenite); and (2) subidiomorphic grains, with inclusions of quartz, K-feldspar and ilmenite, which mainly occur in leucosomes (Hand et al. 1994a). The formation of biotite-spinel-free M_1 matrix assemblages and M_1 leucosomes were attributed to reactions such as:

biotite + sillimanite + plagioclase + quartz \rightarrow garnet + K-feldspar + melt,

biotite + spinel + quartz \pm plagioclase \rightarrow cordierite + garnet + melt, or

cordierite + spinel + quartz \rightarrow garnet + sillimanite + ilmenite.

Retrograde metamorphism

Reaction textures in calc-silicate granulites indicate a post-peak period of near-isobaric cooling. Formation of grossularite coronas between scapolite and calcite or

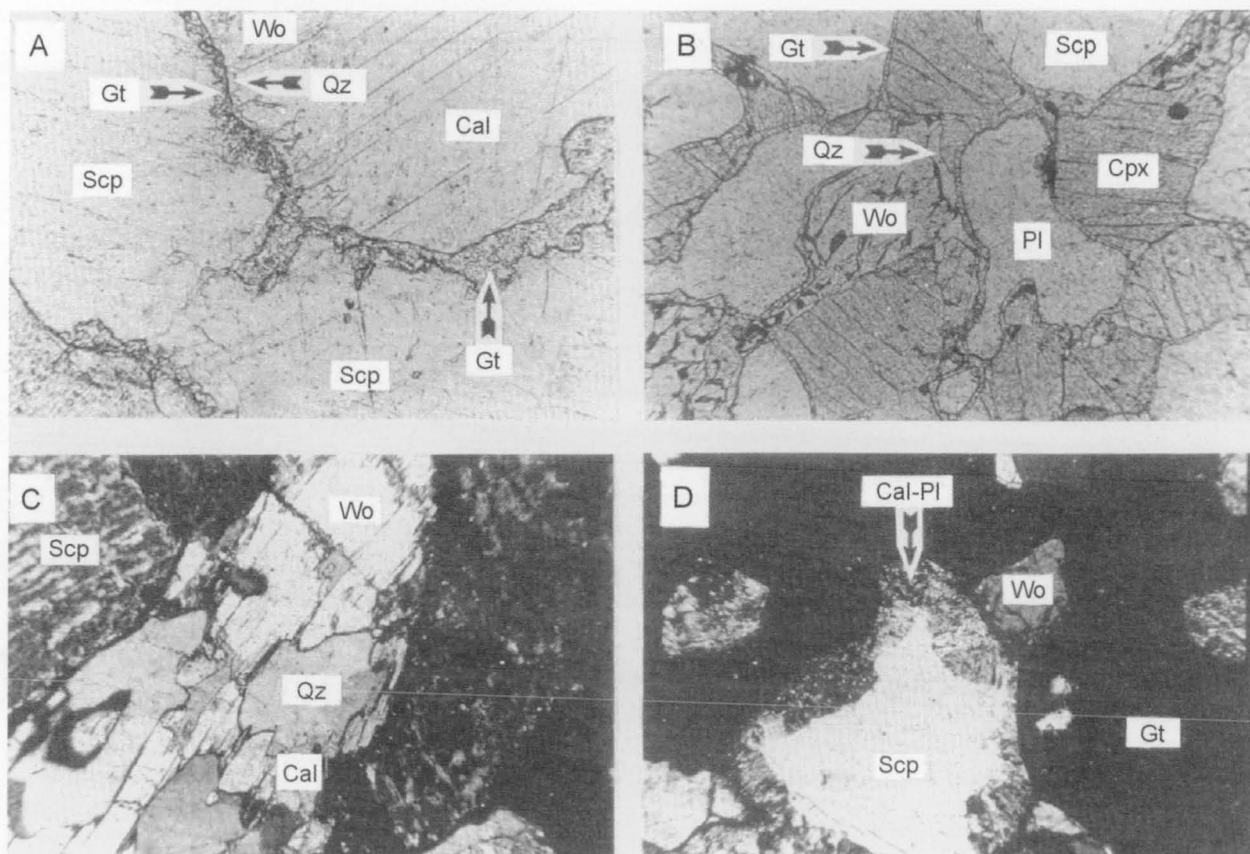


FIGURE 187

Reaction textures in calc-silicate rocks (Fitzsimons & Harley 1992). (A) Garnet corona between scapolite and calcite, and garnet-quartz corona between scapolite and wollastonite. (B) Garnet-quartz coronas between plagioclase and wollastonite. (C) Calcite-quartz intergrowth in wollastonite. (D) Calcite-plagioclase symplectite in scapolite. Fields of view about 1.5 mm.

wollastonite (Fig. 187A, B) can be explained in terms of the reactions:

(1) scapolite + wollastonite + calcite \rightarrow grossularite + CO_2 and

(2) scapolite + wollastonite \rightarrow grossularite + quartz + CO_2 , both of which proceed from left to right on cooling or decreasing a_{CO_2} (Fitzsimons & Harley 1992; Fitzsimons & Thost 1992; Thost & Hensen 1992). Calcite-quartz intergrowths on wollastonite (Fig. 187C) and calcite-anorthite rims on scapolite (Fig. 187D) both post-date the garnet coronas, and can be attributed to the respective reactions:

(3) wollastonite + $\text{CO}_2 \rightarrow$ calcite + quartz, and

(4) scapolite \rightarrow anorthite + calcite,

which also proceed from left to right on cooling. Comparison with the petrogenetic grid (Fig. 186), constrains the retrograde P-T path to one of near-isobaric cooling from about 830 to 750°C. Moreover, the a_{CO_2} during retrogression, and probably also during the metamorphic peak, is constrained to be low (about 0.4). Significantly, interlayered felsic rocks contain the assemblage K-feldspar-quartz-orthopyroxene-biotite, which buffers $a_{\text{H}_2\text{O}}$ to less than 0.35 at 6.5 kilobars and 800°C through the reaction:

biotite + quartz \rightarrow orthopyroxene + K-feldspar + H_2O

(Hansen et al. 1984). Hence, the calc-silicate rocks and orthopyroxene-bearing gneiss cannot have equilibrated with the same volatile fluid phase under high-grade conditions, assuming no other volatile species was present (Fitzsimons & Thost 1992).

Two possible explanations were proposed by Buick et al. (1990): (1) a volatile fluid was present, but its composition was buffered on a local (< 0.5 m) scale, so that orthopyroxene-bearing gneiss equilibrated with CO_2 -rich fluid and calc-silicate rocks with H_2O -rich fluid; or (2) fluid-absent conditions prevailed, and a_{CO_2} and $a_{\text{H}_2\text{O}}$ were buffered within the solid mineral assemblage and were therefore able to vary independently. Estimated low a_{CO_2} (<0.33) and $a_{\text{H}_2\text{O}}$ (0.2) for the Reinbolt Hills area were interpreted in terms of vapour-absent metamorphic conditions by Nichols & Berry (1991).

Development of garnet coronas between plagioclase (zoned from An_{66} to An_{33} near garnet) and pyroxene in mafic granulite from Mount McCarthy (Fig. 184C,D) and elsewhere suggests the reactions:

plagioclase + orthopyroxene \rightarrow garnet + quartz, and

plagioclase + clinopyroxene \rightarrow garnet + quartz.

These reactions can result from either cooling or an increase in pressure, although the presence of strongly zoned plagioclase is probably more consistent with the former (Thost & Hensen 1992). Estimated P-T conditions, based on garnet-clinopyroxene-plagioclase-quartz equilibria (Ellis & Green 1979; Newton & Perkins 1982; Powell 1985; Moecher et al. 1988; Powell & Holland 1988), suggest similar pressures (7 ± 1 kb) and somewhat lower temperatures ($700\text{--}750 \pm 50^\circ\text{C}$) compared to the metamorphic peak, and thus also imply a near-isobaric cooling path (Fig. 185).

In contrast, the presence of andalusite, quartz, chlorite, sericite and carbonate replacing cordierite in metapelite at Mount Meredith (Fig. 188) suggests reactions such as:

cordierite + $\text{CO}_2 \rightarrow$ Mg-Fe carbonate + andalusite + quartz, and

cordierite + $\text{H}_2\text{O} \rightarrow$ chlorite + andalusite + quartz.

These reactions indicate at least some uplift along a clockwise P-T-time path during retrogression, as well as influx of a CO_2 -rich fluid (Ellis & Hiroi 1997).

Stüwe & Hand (1992) used compositions of cordierite rims and garnet rims and small matrix grains in metapelite to estimate P-T conditions during M_2 at Depot Peak: about 5.1 kilobars at 600°C (Fig. 185). Taken at face value, this suggests at least some decompression during cooling, although Stüwe & Hand (1992) pointed out that M_1 and M_2 textures did not necessarily form during a single P-T evolution, but may record entirely separate events.

At Else Platform, M_1 garnet in metapelite is mantled by biotite that is locally deformed by S_2 (probably equivalent to S_6 of Fitzsimons & Thost 1992), suggesting that an influx of fluid occurred between M_1 and M_2 (Hand et al. 1994a). If this fluid was derived from crystallising M_1 melts, then the post-peak conditions may have been dominated by cooling—as is also suggested by reaction textures in calc-silicate rocks (Hand et al. 1994b). Cordierite-bearing M_2 assemblages in biotite-bearing metapelite were interpreted as having formed during a period of increasing temperature through reactions such as:

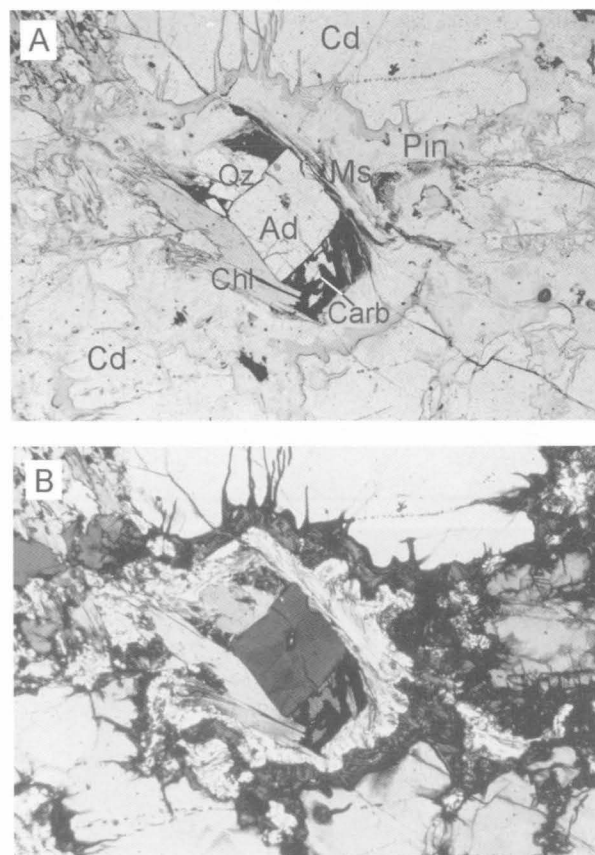


FIGURE 188

Replacement of cordierite by andalusite, quartz, chlorite, carbonate and muscovite in cordierite-anthophyllite-garnet-biotite-plagioclase-quartz lens in felsic gneiss; Mount Meredith. Pinnite (Pin) is a fine-grained mixture of sericite, chlorite, serpentine, Fe oxide, etc. Sample 91286442; cross-polarised light in B; width of field: 2 mm.

biotite + sillimanite + quartz \pm plagioclase \rightarrow spinel + cordierite + ilmenite + K-feldspar + melt, whereas biotite-free rocks show evidence for decompressive reactions, such as:

garnet + sillimanite + ilmenite \rightarrow spinel + cordierite + quartz.

Coronas of cordierite–spinel–ilmenite formed between M_1 garnet and sillimanite, and cordierite rims and symplectites of orthopyroxene formed around garnet in sillimanite-free rocks. Estimated P–T conditions for the M_2 assemblages sillimanite–quartz–cordierite (rim)–spinel (rim) and spinel–quartz–garnet (rim)–cordierite (rim), using the average P–T method of Powell & Holland (1988, 1994), are 5.9 ± 0.4 kilobars at 700°C (Hand et al. 1994b). The corona assemblage garnet–orthopyroxene–cordierite–plagioclase–quartz gives 5.7 ± 0.4 kilobars. Scrimgeour & Hand (1997) give an overall estimate of about 4.5 kilobars at 700°C for M_2 in the western Amery Ice Shelf area. These estimates indicate a broadly decompressional post-peak evolution (Fig. 185), assuming that M_1 and M_2 represent parts of a single evolutionary trend and are not unrelated events (see below). Together with the inferred up-temperature reactions indicated by M_2 assemblages in biotite-rich metapelites, this evolution contrasts with the near-isobaric cooling history and anticlockwise P–T–time path interpreted by Thost & Hensen (1992) for the Porthos Range area. Nevertheless, the inferred post-peak cooling suggests affinities between these areas.

Metapelite in the Reinbolt Hills area shows evidence for a variety of retrograde reactions, which were utilised by Nichols & Berry (1991) to define the post-peak cooling path:

sillimanite + quartz + garnet \rightarrow cordierite,

sillimanite + garnet \rightarrow spinel + cordierite, and
rutile + garnet \rightarrow cordierite + ilmenite + quartz.

The results indicate a decompressional P–T path from 7 kilobars at 800°C to 5 kilobars at 690°C , which is more like that at Else Platform than that in the Porthos Range (Fig. 185).

Metamorphic conditions during the subsequent evolution of the Beaver-Lambert Terrane are more difficult to determine. Mylonite zones in the Porthos Range area are rarely associated with a metamorphic overprint and preserve clasts of garnet and orthopyroxene, suggesting dry conditions. The S_3 foliation in migmatitic granite dykes at Else Platform (possibly structurally equivalent to the c.500 Ma(?) D_8 mylonites of Fitzsimons & Thost 1992) consists of biotite–ilmenite–rutile enveloping garnet, and recrystallised quartz–feldspar leucosomes, so that P–T conditions probably did not exceed those of the water-saturated granite solidus (650 – 700°C at 3–5 kb: Hand et al. 1994a). 'D₄' shear zones at Else Platform contain upper greenschist to lower amphibolite-facies muscovite–biotite–chlorite assemblages; mylonites in the Reinbolt Hills area also contain greenschist to amphibolite-facies assemblages (Nichols & Berry 1991). Similar retrograde effects of uncertain age are common in many parts of the Beaver-Lambert Terrane, with alteration of garnet and biotite to chlorite and saussuritisation and sericitisation of feldspar; secondary muscovite and carbonate may also be present. Retrograde biotite and pale green amphibole rim pyroxene grains in some mafic granulite bodies. A greenschist-facies overprint is also associated with late epidote veins, and hydrothermal alteration, with development of epidote and calcite, affects all the rock types, including mafic dykes, in the southwestern part of Else Platform (Hand et al. 1994a).

DISCUSSION

GEOLOGICAL HISTORY

Ruker Terrane

The geological history of the Prince Charles Mountains area is summarised in Table 21, although it must be emphasised that the exact age and even the sequence of some of these events are by no means conclusively established. Probably the greatest uncertainties are the depositional and metamorphic ages of the various metasedimentary sequences in the Ruker Terrane, which are far from clear. The Ruker Terrane is the only major section of this part of the East Antarctic Shield for which few ion-microprobe U–Pb zircon data are yet available. The first such study of granitic basement rocks from the southern Mawson Escarpment (Boger et al. 2001) has confirmed their Archaean age, but hinted at a complex geological history. Nevertheless, there are now sufficient geochronological data (summarised in Tables 22–25) to allow the construction of a provisional geological history.

The oldest rocks identified in the Ruker Terrane are tonalitic to trondhjemitic orthogneisses of typical Archaean TTG (tonalite–trondhjemite–granodiorite) composition in the southern Mawson Escarpment: Y and HREE-depleted, but Sr-rich, suggesting derivation from a garnet-bearing, but plagioclase-poor mafic source. Such Archaean ‘grey gneisses’ thus appear to represent new felsic crust, possibly generated by melting in a subduction zone or mafic underplate (Tarney et al. 1987; Martin 1993).

Tonalitic rocks containing ?relict orthopyroxene + garnet in the southern Mawson Escarpment, together with granulite-facies rocks at Mount Newton, appear to represent the oldest recognisable metamorphic event. The emplacement age of these tonalitic orthogneisses is unknown, but T_{DM}^{Nd} model ages (3440–3800 Ma) are somewhat older than those of biotite–hornblende granite gneisses (mostly 3340–3510 Ma: V.P. Kovach & B.V. Beliaty, unpublished data). However, T_{DM} (and even T_{CHUR}) model ages tend to overestimate the time of generation of felsic crustal rocks from the mantle, because an additional old, possibly subduction-derived, component is likely to have been involved. For example, a significant part of the LILE and LREE could have been derived from older subducted sedimentary material during magma generation above a subduction zone (Soler & Rotach-Toulhoat, 1990).

A major period of metamorphism, migmatisation and granitic magmatism occurred about 3200–3000 Ma ago. Widespread biotite–hornblende granite gneiss has given U–Pb zircon ages of about 3000 Ma (V.P. Kovach & B.V. Beliaty, unpublished data: Table 22), indistinguishable

from the 3005 ± 57 Ma U–Pb zircon age of biotite granite at Mount Ruker. The former were taken by Kovach & Beliaty (1991) to represent metamorphic ages, but it seems equally likely that they define the time of emplacement. Other U–Pb and Rb–Sr isotopic data (Fig. 26; Halpern & Grikurov 1975; Kovach & Beliaty 1991, and unpublished data; Boger et al. 2001) also suggest major tectonothermal events between 3175 and 2500 Ma. The older ages may reflect the early crust-forming event(s), and the younger ages, high-grade metamorphism and/or igneous activity.

The Mount Ruker granite shows evidence for much younger isotopic disturbance (c.500 Ma), and Rb–Sr isochron ages are significantly younger, in some cases much younger, than U–Pb ages (Tables 22, 24). The biotite–hornblende granite gneiss is unusual among Archaean granitoids in having very high HFSE (Y, Zr and Nb) contents, features typical of late to post-orogenic A-type granitoids which only became common in the Proterozoic. It is not known whether this granite gneiss represents truly anorogenic magmatism, but a broadly similar origin from similar sources to more recent ‘A-type’ granitoids is nevertheless probable.

Formation of granitic basement rocks in the Archaean was followed by a prolonged period or periods of sedimentation and bimodal volcanic activity (Menzies and Ruker Series) that may have extended from the Archaean into the Palaeoproterozoic. The Archaean age assigned to the prominent white to green quartzite-bearing sequences that crop out over much of the Ruker Terrane (event 3 on Table 21) is based mainly on a single Rb–Sr age of 2580 Ma for muscovite in pegmatite cutting quartzite at Mount Stinear (Tingey 1991a). This age may be consistent with the evidence for much younger amphibolite-facies metamorphism (amphibolised dolerite dykes of probable Mesoproterozoic age) in these metasediments, as the blocking temperature for the Rb–Sr system may be as high as 600–650°C for coarse-grained muscovite from pegmatites (Cliff 1985). Other greenschist to amphibolite-facies metasedimentary and metavolcanic sequences (event 6, and possibly further deposition at 8) lack the major quartzite units, but contain more abundant calcareous metasediments and include thick banded ironstone units at Mount Ruker. Like the probable Archaean metasediments, they are cut by metamorphosed ?Mesoproterozoic dolerite dykes, and are therefore considered to be older than about 1400 Ma. However, they are not known to be cut by ?Palaeoproterozoic high-Mg dykes that occur in Archaean granitic rocks at Mount Ruker and elsewhere. These have some geochemical features in common with metamorphosed mafic rocks at Mount Ruker, suggesting that the supracrustal rocks could be of similar age (about 2400 Ma). On the other hand, the

TABLE 21. Summary of the geological history of the Prince Charles Mountains area.

	Ruker Terrane	Fisher Terrane	Beaver-Lambert Terrane	Approx. age (Ma)
1.	Emplacement of tonalite (Mawson Orthogneiss); high-grade metamorphism; ?deposition of sediments.			>3100
2.	Emplacement of granitic rocks, including Hb–Bt granite (Mawson Orthogneiss); upper amphibolite-facies metamorphism and deformation.			3100–3000
3.	Deposition of mainly pelitic and psammitic sediments (Menzies Series).		Emplacement of granitic rocks in source region of metasedimentary rocks (Ruker Terrane?).	2800–2500
4.	?Metamorphism; emplacement of granitic rocks and pegmatites.			c.2500
5.	Intrusion of high-Mg mafic dykes			c.2400
6.	Deposition of pelitic and calcareous sediments, including banded ironstones, and mafic and felsic volcanic rocks (Ruker Series and possibly part of Menzies Series).			
7.	?Metamorphism; pegmatite intrusion.		Emplacement of granitic rocks in source region of metasedimentary rocks (Ruker Terrane?).	2100–1800
8.	?Deposition of sediments.		Emplacement of granitic rocks; deposition of sediments, partly derived from (3) and (7).	
9.	Intrusion of dolerite dykes.		Emplacement of mafic and ultramafic bodies, including dykes, now boudinaged.	1400–1200
10.	?Deposition of calcareous and pelitic sediments (Sodruzhestvo Series): age uncertain.	Mafic to felsic volcanism, deposition of sediments, and emplacement of gabbro and Hb–Bt tonalite, diorite, and granodiorite, probably in a continental margin setting.		c.1300
11.		Intrusion of dolerite dykes.		
12.		Greenschist-facies metamorphism and deformation (D ₁).		
13.		Emplacement of tonalite; deformation (D ₂).		
14.		Emplacement of Bt granite.		1190
15.			?High-grade metamorphism and deformation (?D ₁ and/or D ₂).	1165
16.		Amphibolite-facies metamorphism (?migmatisation) and deformation (D ₃).		1120
17.	Amphibolite-facies metamorphism and deformation; ?emplacement of granitic rocks.	Lower amphibolite-facies metamorphism; emplacement of Bt granite.	Amphibolite to granulite-facies metamorphism (at about 7kb and 750–850°C in the NPCM) and deformation, with development of regional gneissic foliation and associated isoclinal folds (F ₃ and F ₄); emplacement of granitic rocks and migmatisation.	c.1000

TABLE 21. Summary of the geological history of the Prince Charles Mountains area (continued)

Ruker Terrane	Fisher Terrane	Beaver-Lambert Terrane	Approx. age (Ma)	
18.		Emplacement of Px syenite and Hb–Bt granite (Mount Collins) and Opx granitoid plutons; mafic granulite dyke intrusion; formation of open to tight upright folds (F ₅).	980	
19.	Intrusion of dolerite dykes (Fisher Massif, Mount Willing: exact age relations uncertain).	Intrusion of dolerite dykes (Mount Collins: exact age relations uncertain).		
20.		Formation of major east–west-trending upright shear zones (F ₆) under high-grade conditions; emplacement of Gt–Bt granite.	c.940	
21.		Minor flexures and shear zones (F ₇).	900	
22.	Thermal overprint.	Pegmatite intrusion; ?metamorphism.	?c.800–750	
23.	Possible deposition of calcareous and pelitic sediments (Sodruzhestvo Series): age uncertain.			
24.	Greenschist-facies metamorphism and deformation; emplacement of Ms–Bt granite (Mawson Escarpment) and pegmatite bodies.	Thermal overprint.	Greenschist to amphibolite-facies (?locally granulite-facies) metamorphism; formation of shear and mylonite zones (F ₈ , but probably at least two generations); emplacement of Hb–Bt granite (eastern Amery Ice Shelf), Gt–Bt granite and pegmatite bodies.	550–500
25.	Intrusion of lamproite dykes (Mount Rubin: 460 Ma, Mount Bayliss: 420 Ma).	?Intrusion of alkaline mafic dykes.	Intrusion of alkaline mafic dykes, including alkaline dolerite–camptonite dyke swarm (320 Ma) of Jetty Peninsula.	500–250
26.	Major uplift and cooling.	Major uplift and cooling.	Major uplift and cooling.	
27.	?Faulting.	?Faulting.	Brittle faulting, associated with low-grade alteration, mafic dyke intrusion, quartz veins, and graben formation.	c.320–<100
28.	Deposition of siltstone (known only from moraine at Mounts Maquire and Rymill).		Deposition of Amery Group conglomerate, sandstone, shale, and coal measures.	?c.290–220
29.		Intrusion of diorite porphyry dykes (Jetty Peninsula).		240
30.		Intrusion of basanite dykes (Radok Lake).		
31.		Emplacement of alkali picrite stocks (Jetty peninsula).		150–140
32.		Final uplift towards surface.		140–0
33.	Intrusion of kimberlitic dykes.	Emplacement of ultramafic lamprophyre dykes, stocks (Jetty Peninsula) and sills (Radok Lake).		125–110
34.		Extrusion of tephritic phonolite lava (Manning Massif).		50
35.	Formation of glacial deposits.	Formation of Pagodroma Tillite and younger glacial deposits.	Formation of Pagodroma Tillite and younger glacial deposits (Radok Lake).	<10

Main data sources: Tingey (1982a); McKelvey & Stephenson (1990); Nichols & Berry (1991); Fitzsimons & Thost (1992); Arne (1994); Hand et al. (1994a); Mikhalsky et al. (1996), and references given in Tables 22–25.

TABLE 22. U–Pb ages of rocks from the Prince Charles Mountains area (from Sheraton & Black 1988; Manton et al. 1992; Beliatsky et al. 1994; Kinny et al. 1997; Kinny 1998; Laiba & Mikhalsky 1999; Mikhalsky et al. 1999; Carson et al. 2000; Boger et al. 2000; N.N. Krasnikov, E.N. Kamenev, V.P. Kovach, B.V. Beliatsky, unpublished data).

Locality	Lithology	Method	Age (Ma)	Remarks
RUKER TERRANE				
S Mawson Escarpment	Hb–Bt granite gneiss	Z	3070±44	?Metamorphism
S Mawson Escarpment	Hb–Bt granite gneiss	Z–TI	3035±10	?Metamorphism
S Mawson Escarpment	Hb–Bt granite gneiss	Z	2981±27	?Metamorphism
S Mawson Escarpment	Ultramafic schist	Z–TI	2900	?Metamorphism
S Mawson Escarpment	Amphibolite dyke	Z–TI	2375±10	?Emplacement
S Mawson Escarpment	Pegmatite vein	Z–TI	2285±40	Emplacement
S Mawson Escarpment	Bt plagiogneiss	Z–TI	2495±10	?Metamorphism
S Mawson Escarpment	Retrogressed ultramafic schist	Z–TI	1810±25	?Metamorphism
Mount Ruker	Bt granite	Z	3175±50	?Protolith age
Mount Ruker	Bt granite	Z	3005±57	?Emplacement
Mount Ruker	Bt granite	Z	515±20	Metamorphism (lower intercept)
FISHER TERRANE				
Fisher Massif (central)	Bt–Hb metadacite	Z–IM	c.1900	Inheritance
SE Fisher Massif	intermediate–felsic volcanics (A1)	Z	1302±4	Emplacement
SE Fisher Massif	intermediate–felsic volcanics (A2)	Z	1300±3.5	Emplacement
Fisher Massif (central)	Bt–Hb metadacite	Z–IM	1283±21	Emplacement
Fisher Massif (central)	Foliated Bt tonalite	Z–IM	1293±28	Emplacement
NE Fisher Massif	Bt granite	Z–IM	1020±48	Emplacement
NE Fisher Massif	Gabbro–anorthosite	Z–m	940±12	?Metamorphism
Mount Willing	Bt–Hb tonalite gneiss	Z	1289±10	Emplacement
Mount Willing	metatonalite	Z	1176±16	Emplacement
Mount Willing	Bt granite	Z	1194±1	Emplacement
Mount Willing	Quartz diorite vein (?migmatitic)	Z	1113±3	Emplacement (?metamorphism)
Mount Willing	Metagabbro	Z	810±2	Metamorphism or thermal overprint
BEAVER-LAMBERT TERRANE				
C. Mawson Escarpment	felsic gneiss	Z–TI	1310±50	?Metamorphism
C. Mawson Escarpment	felsic gneiss	Z–TI	880±45	?Metamorphism
C. Mawson Escarpment	felsic gneiss	Z–TI	795±40	?Metamorphism
Mount Meredith	Bt–Kf–Pl–Qz paragneiss	Z–IM	2800–2500	Detrital zircons
Mount Meredith	Bt–Kf–Pl–Qz paragneiss	Z–IM	2100–1800	Detrital zircons
Mount McCarthy	Gt leucogranite gneiss	Z–IM	c.1850	Inheritance
McLeod Massif	Prehnite lens in serpentinite	M	1165±13	?Metamorphism
Radok Lake	Cpx–Hb leucosome	Z–IM	1017±31	Emplacement
Radok Lake	Gt–Bt granite (D ₄)	Z–IM	990±18	Emplacement
Radok Lake	Opx leucosome (D ₆)	Z–IM	942±17	Emplacement
Mount Kirkby	Syn–D ₆ pegmatite	Z–IM	991±22	Emplacement
Mount Kirkby	Late–D ₆ pegmatite	Z–IM	910±18	Emplacement
Mount McCarthy	Gt leucogranite gneiss	Z–IM	990±30	Emplacement
Mount McCarthy	Gt leucogranite gneiss	M–IM	950–900	?Emplacement
Loewe Massif	Bt–Hb–Opx quartz monzonite	Z–IM	980±21	Emplacement
Mount Collins	Cpx–Opx quartz syenite	Z–IM	984±12	Emplacement
Mount Collins	Hb–Bt granite	Z–IM	984±7	Emplacement
Mount Collins	Hb–Bt granite	Z–IM	976±25	Emplacement
Carter Peaks	Gt–Si–Cd metapelite	M–IM	950–900	?Metamorphism
Jetty Peninsula	Gt–Bt leucogranite gneiss	Z	940±20	Emplacement
EARLY PALAEOZOIC				
Mount Kirkby	Pegmatite	Z–IM	517±12	Emplacement
Landing Bluff	Hb–Bt granite	Z	c.500	Emplacement
Jetty Peninsula	Pegmatite	Z	507–495	Emplacement

IM, ion-microprobe; TI, thermal ionization; m, model ²⁰⁷Pb/²⁰⁶Pb; M, monazite; Z, zircon.

TABLE 23. Sm–Nd isotopic data for rocks from the Prince Charles Mountains (after Mikhalsky et al. 1992, 1996, 1999; Andronikov & Beliatsky 1995; Andronikov et al. 1998; Laiba & Mikhalsky 1999; V.P. Kovach & B.V. Beliatsky, S-S Sun, unpublished data).

Locality	Lithology	No of samples	Age (Ma)	I.R.	¹⁴⁷ Sm/ ¹⁴⁴ Nd	¹⁴³ Nd/ ¹⁴⁴ Nd	T _{DM} (Ma)
RUKER TERRANE							
Mawson Escarpment (south)	Granitic orthogneiss	12	3176±140		0.13070	0.511279	3431
Mawson Escarpment (south)	Granitic orthogneiss	2(a)	3124±130				
Mawson Escarpment (south)	Tonalitic orthogneiss	3(a)	2942±100		0.12003	0.510976	3528
Mawson Escarpment (south)	Tonalitic orthogneiss	1(a)	1880±68				
Mount Ruker	Biotite granite	3			0.11143	0.510891	3359
Mount Ruker	Felsic mica schist	4			0.104	0.510987	3002
Mawson Escarpment (south)	Dolerite dykes	4			0.1738	0.512496	2530
Mawson Escarpment (south)	Metadolerite dykes	4			0.15201	0.512149	2490
FISHER TERRANE							
Fisher Massif	Metavolcanic rock	3			0.154147	0.512382	1988
NE Fisher Massif	Granodiorite	3			0.112967	0.512063	1658
Fisher Massif	Metatonalite	1			0.114998	0.512066	1687
Mount Willing	Gabbro	Opx, Cpx	1292±67				
Mount Willing	Gabbro and metagabbro	7			0.165978	0.512499	2103
Mount Willing	Metagabbro	Pl, Hb	1023±33				
Mount Willing	Metagabbro	6(a)	994±31		0.16474	0.512523	1981
Mount Willing	Mafic schist	3(a)	1009±54		0.15976	0.512553	1714
BEAVER-LAMBERT TERRANE							
Moore Pyramid	Metapelite	1			0.12304	0.511837	2218
Mount Kirkby	Metagabbro	1			0.14354	0.512213	2053
Radok Lake	Granite gneiss	1			0.09925	0.511558	2127
Mount Gardner	Felsic orthogneiss	1			0.08223	0.511634	1766
EARLY PALAEOZOIC							
Mount Rubin	Lamproite dyke	1			0.07508	0.511879	1408
LATE PALAEOZOIC							
Jetty Peninsula	Alkaline dolerite dykes	8			0.114036	0.512328	1272
MESOZOIC							
Jetty Peninsula	'Enriched' peridotite nodule	4	611±58	0.511942	0.122635	0.512433	1217
Jetty Peninsula	Opx from peridotite nodule	3	1187±62	0.511484	0.13645	0.512554	1196
Jetty Peninsula	Cpx from peridotite nodule	5	374±95	0.512416	0.11096	0.512688	702
CAINOZOIC							
Manning Massif	Tephritic phonolite lava	5			0.083778	0.512212	1113

T_{DM} = (1/λln[1+ [(¹⁴³Nd/¹⁴⁴Nd)_{meas.} - (¹⁴³Nd/¹⁴⁴Nd)_{DM}]/[(¹⁴⁷Sm/¹⁴⁴Nd)_{meas.} - (¹⁴⁷Sm/¹⁴⁴Nd)_{DM}]]], where ¹⁴³Nd/¹⁴⁴Nd_{DM} = 0.51316, ¹⁴⁷Sm/¹⁴⁴Nd_{DM} = 0.2136, λ¹⁴⁷Sm = 6.54 * 10⁻¹² yr⁻¹.

a, whole rock–mineral isochrons, interpreted as metamorphic ages; model ages calculated using whole-rock data.

TABLE 24. Rb–Sr isotopic data for rocks from the Prince Charles Mountains area (after Halpern & Grikurov 1975; Tingey 1991a; Manton et al. 1992; Krasnikov & Fedorov 1992; Mikhalsky et al. 1994, 1999; E.N. Kamenev & B.V. Beliatsky, unpublished data; A.Ya. Krylov & M.G. Ravich, unpublished data).

Locality	Lithology	No. of samples	Age (Ma)	I.R.	⁸⁷ Rb/ ⁸⁶ Sr	⁸⁷ Sr/ ⁸⁶ Sr	T _{UR} (Ma)
RUKER TERRANE							
Mawson Escarpment (south)	Felsic gneiss	8	3036±132	0.7024±0.006	2.0178	0.7953	3223
Mawson Escarpment (south)	Felsic gneiss	7	2762±222	0.7050±0.0008	0.2534	0.7152	4220
Mawson Escarpment (central)	Felsic gneiss	15	2708±90	0.7210±0.0091	7.8911	1.0433	2989
Mount Bayliss	Granitic orthogneiss	9	2750±402	0.7076±0.0153	11.5071	1.1448	2662
Mount Mather	Leucogranite	3	1758±2020	0.7125±0.0106	0.3927	0.7224	3917
Mount Ruker	Granite gneiss	4	1412±152	0.8902±0.0162	8.0993	1.0542	3005
Mount Ruker	Granite gneiss	4	–	–	7.67	1.0203	2870
Mount Rymill	Granite	6	1169±233	1.1139±0.0621	17.8626	1.4303	2817
Mount Stinear	Felsic gneiss	9(6)*	(1042)	(0.875)	4.1750	0.8794	2944
Nunatak 10 km NE of Mount Bird	Felsic gneiss	3	–	–	0.3253	0.7226	5032
Mount Rubin	Granite gneiss and tonalite boulders in metaconglomerate	4	(830)	(0.730)	0.946	0.7414	2932
Mount Rubin	Phyllite	3	(512)	(0.738)	14.5	0.8427	670
Mount Rubin	Mica schist (phyllite)	3	502±69	0.7444±0.0032	8.10	0.8017	846
Mount Rubin	Mica schist (3) and granite gneiss (2)	5	505±40	0.7391±0.0014	–	–	–
FISHER TERRANE							
Fisher Massif	Granite and tonalite	4	1090±297	0.7047±0.0052	1.2547	0.7244	1170
NE Fisher Massif	Biotite granite	5	870±150	0.7068±0.0031	1.0602	0.71939	1046
Mount Willing	Mafic schist	3(a)	636±13	0.7037±0.0001	0.07392	0.704396	2522
Mount Willing	Mafic schist	4(a)	470±28	0.7044±0.0001	0.11269	0.704541	1128
Mount Willing	Garnet–biotite plagiogneiss	–	–	0.7061	0.58603	0.717058	1702
Mount Willing	Biotite–hornblende plagiogneiss (migmatite)	–	–	0.7050	0.30331	0.710684	1873
BEAVER-LAMBERT TERRANE							
Dalton Nunataks	Felsic gneiss	8	941±94	0.7038±0.002	1.9014	0.7298	963
Mount Johns	Felsic gneiss	17	872±69	0.7060±0.0012	1.1641	0.7205	1017
Clemence Massif	Felsic gneiss	9	816±298	0.7104±0.0077	1.8135	0.7315	1079
Mawson Escarpment (north)	Felsic gneiss	5	–	–	0.3534	0.7148	2576
Mawson Escarpment (north)	Felsic gneiss	8	–	–	2.9762	0.7778	1756
Shaw Massif	Felsic gneiss	3	–	–	0.5455	0.7114	1002
Pickering Nunatak	Felsic gneiss	23(5)	1042±347	0.7074±0.0011	1.8975	0.7357	1190
Martin Massif	Felsic gneiss	4	1033±85	0.7086±0.0024	1.8243	0.7342	1180
Mount Gardner	Felsic gneiss	10	974±68	0.7233±0.0147	13.7493	0.9148	1074
Crohn Massif	Granite gneiss	3	973±636	0.7079±0.0198	2.2347	0.7389	1108
Mount Wishart	Garnet leucogneiss	10	925±35	0.7121±0.0007	1.562	0.7328	1322
Mount Bechervaise	Felsic gneiss	7	904±175	0.7429±0.0208	8.8788	0.8575	1212
Moore Pyramid	Felsic gneiss	21(8)	769±36	0.7363±0.0030	6.1171	0.7992	1094
Bond Ridge	Felsic gneiss	6	–	–	5.9601	0.8192	1358
Fox Ridge	Felsic gneiss	2	–	–	20.3366	0.9973	1010
Jetty Peninsula	Felsic gneiss	4	–	–	4.6526	0.7677	963
Jetty Peninsula	Garnet–biotite leucogranite gneiss	3(a)	718±32	0.7611±0.0037	12.54	0.8870	1023
EARLY PALAEOZOIC							
Mawson Escarpment (central)	Muscovite–biotite granite	5	551±74	0.7366±0.0047	4.4811	0.7719	1067
Landing Bluff	Hornblende–biotite granite	8	493±17	0.7184±0.0009	11.1895	0.7972	584
Sansom Island	Hornblende–biotite granite	7	–	–	3.6216	0.7436	768
Jetty Peninsula	Porphyritic biotite granite	4(a)	483±12	0.7240±0.0009	7.333	0.7751	680
Jetty Peninsula	Biotite granite	4(a)	480±13	0.7139±0.0005	3.074	0.7351	709
Mount Rubin	Lamproite dyke	4(a)	461±23	0.71643±0.00015	0.6052	0.720445	2087
CAINOZOIC							
Manning Massif	Tephritic phonolite lava	5	40±1.2	0.70762	0.540318	0.707922	481

T_{UR} = (1/λ)ln{1+ [(⁸⁷Sr/⁸⁶Sr)_{meas.} - 0.7048]/[(⁸⁷Rb/⁸⁶Sr)_{meas.} - 0.085]}, where λ = 1.42 * 10⁻¹¹ yr⁻¹. Numbers in brackets are samples used for isochron.

a, whole rock–mineral isochrons, interpreted as reset ages; model ages calculated using whole-rock data only.

morphology of zircon in the Ruker Series rocks provide some, by no means conclusive, evidence for these rocks having experienced c.2500 Ma metamorphism, and so an Archaean age cannot be discounted.

Mafic metavolcanic rocks from Mount Ruker show some geochemical features (Nb depletion and slightly enriched REE patterns with small Eu anomalies) typical of calc-alkaline basalts of destructive plate margins, although a within-plate origin cannot be entirely ruled out. Wide variations in some trace element abundances suggest that a range of parent melts was involved, although at least some of these variations are probably due to alteration. High-Mg metavolcanic rocks from Mount Ruker appear to have been derived from previously depleted rather than fertile mantle, and thus may be more akin to boninitic than typical komatiitic rocks. It is noteworthy that the Mount Ruker banded ironstones appear to be transitional from the miogeosynclinal Lake Superior type to the eugeosynclinal Algoma type of iron formation. Sedimentation and volcanic activity may thus have occurred in basins, either bordering or within Archaean sialic crustal blocks, perhaps associated with subduction or mafic underplating. Juvenile late Archaean to Palaeoproterozoic volcanic and plutonic rocks are not abundant, and true greenstones may be confined to the southern Mawson Escarpment.

A presumably younger sequence of greenschist-facies calcareous and pelitic metasediments (Sodruzhestvo Series), which crops out mainly around the Fisher Glacier area, is not cut by metadolerite dykes and there is little or no evidence for an earlier metamorphic event. Its age is particularly poorly constrained, as the Rb–Sr isochron ages of 502±69 and 505±40 Ma for granitic boulders and phyllite at Mount Rubin (Table 24) are presumably

metamorphic ages. Although at least some of these metasediments may post-date the c.1000 Ma high-grade event in the Beaver-Lambert Terrane, it is quite likely that others (or even all) may pre-date it—hence the two possible sedimentation events (numbered 10 and 23) on Table 21.

The largely amphibolitised dolerite dyke swarm that provides such a useful stratigraphic marker has not so far proved very amenable to isotopic dating. K–Ar ages of dolerites from Mount Ruker (796±80 and 992±99 Ma: Hofmann et al. 1980; 1040 Ma: A.Ya. Krylov & M.G. Ravich, unpublished data) are almost certainly too young, and are presumably metamorphic ages. Even dating of much fresher dykes may not be straightforward. For example, a dolerite dyke from the Vestfold Hills contains 2483±9 Ma xenocrystic zircon and 1025±56 Ma metamorphic zircon, whereas a felsic segregation in the same dyke contains 1248±4 Ma zircon that is considered to define the emplacement age (Black et al. 1991a). Hence, the age of the dykes in the Ruker Terrane is based mainly on detailed geochemical comparisons with dated dykes in nearby Archaean cratons. Most of the analysed metadolerites are chemically indistinguishable from Group II dolerites in Enderby Land and the Vestfold Hills (Sheraton & Black 1981; Collerson & Sheraton 1986a). Those in the Vestfold Hills have been dated at 1374±125 Ma (Rb–Sr: Collerson & Sheraton 1986a) and 1380±7 Ma (U–Pb zircon ion-microprobe: Lanyon et al. 1993), although other suites have given U–Pb ages of 1754±16 and 1241±5 Ma (Lanyon et al. 1993). Some Ruker Terrane mafic to ultramafic dykes have compositions similar to much older high-Mg dykes in the Vestfold Hills and Enderby Land, although the correlation is less clear. However, a U–Pb zircon age of about 2375 Ma (Mikhalsky

TABLE 25. K–Ar ages of Phanerozoic mafic igneous rocks from the Prince Charles Mountains area (from Sheraton 1983; Laiba et al. 1987; Hofmann 1991; Mikhalsky & Sheraton 1993).

Sample no.	Locality	Lithology	Mineral	Age (Ma)
69280225	Fox Ridge	Basanite dyke	Clinopyroxene	504±20
73281545	Mount Bayliss	Lamproite (melasyenite) dyke	K-arfvedsonite	430±12
			K-richterite	414±10
6 samples	Jetty Peninsula	Dolerite/camptonite dykes	WR isochron	321±10
1872	Jetty Peninsula	Diorite porphyry dyke	Whole rock	245±11
1871	Jetty Peninsula	Diorite porphyry dyke	Whole rock	239±12
71280126	Taylor Platform	Basaltic andesite dyke	Plagioclase	246±6
	Jetty Peninsula	Alkali picrite stock*	Phlogopite	150±5
	Jetty Peninsula	Alkali picrite stock*	Groundmass	142±5
	Jetty Peninsula	Melanephelinite stock*	Whole rock	123±5
	Jetty Peninsula	Polzenite stock*	Whole rock	113±5
6 samples	Jetty Peninsula	'Monchiquite'	WR isochron	119±6
69280152	Radok Lake	Polzenite (alnöite) sill	Phlogopite	110±3
69280153	Radok Lake	Polzenite (alnöite) sill	Phlogopite	110±3
69280334	Radok Lake	Polzenite (alnöite) sill	Phlogopite	108±3
73281594	Manning Massif	Tephritic phonolite lava	Whole rock	51.8±2.0
			Whole rock	49.1±2.0

Constants used: $^{40}\text{K} = 0.0119 \text{ atom \%}$; $\lambda_{\text{p}} = 4.72 \times 10^{-10} \text{ yr}^{-1}$; $\lambda_{\text{e}} = 0.584 \times 10^{-10} \text{ yr}^{-1}$.

* multiphase stock

et al. 1992) is comparable to those of high-Mg dykes in Enderby Land (Rb–Sr age of 2350 ± 48 Ma: Sheraton & Black 1981) and the Vestfold Hills (Rb–Sr age of 2424 ± 72 Ma: Collerson & Sheraton 1986a and U–Pb zircon ages of 2241 ± 4 and 2238 ± 7 Ma: Lanyon et al. 1993). High-Mg dykes from all three Archaean cratons, as well as metagabbros and mafic volcanic rocks at Mount Ruker and mafic to ultramafic schists in the southern Mawson Escarpment, all appear to have been derived from generally similar LILE-rich mantle source regions. This is in marked contrast to the much less enriched source(s) of the younger (probably Mesoproterozoic) dolerites. A few other Ruker Terrane metadolerites have significantly different incompatible element ratios and cannot be correlated with any of the dyke suites so far described from elsewhere. However, the marked overall chemical similarity supports correlation of the Ruker Terrane dykes with those in the other Archaean blocks. Virtually identical dykes (chemically and isotopically) are known to occur in areas as far apart as Enderby Land and the Vestfold Hills. Thus, most Ruker Terrane dykes were probably emplaced about 1380 Ma ago, although some are probably as old as 2240 Ma or more and others could be young as 1240 Ma.

There is evidence for several metamorphic events during the evolution of the Ruker Terrane, but again their absolute ages are poorly defined. As already mentioned, the oldest event seems to have produced the ?relict granulite-facies assemblages found as inclusions in tonalitic orthogneisses of the southern Mawson Escarpment; mafic granulite that pre-dates dolerite dykes at Mount Newton probably reflects the same early high-grade event. The upper amphibolite-facies metamorphism and deformation that affected most of the slightly younger granitic basement rocks (event 2) probably occurred soon after emplacement, as the overlying Menzies Series rocks are of significantly lower grade (mostly lower amphibolite facies). Pervasive isotopic resetting, at least of the Rb–Sr system, took place in the Meso- to Neoproterozoic and the Cambrian. It is likely that some sort of tectonothermal event occurred about 2500 Ma ago (event 4), although the only direct evidence is emplacement of trondhjemite at about 2500 Ma (Kovach & Belitsky 1991) and the 2580 Ma Rb–Sr age of muscovite from pegmatite at Mount Stinear. Similarly, there are somewhat equivocal indications of a metamorphism at about 1800–1900 Ma: 1995 and 1708 Ma muscovite ages from Keyser Ridge (Tingey 1991a), a 1880 ± 68 Ma Sm–Nd mineral isochron age for tonalitic orthogneiss from the southern Mawson Escarpment (V.P. Kovach & B.V. Belitsky, unpublished data), and a 1810 ± 25 Ma TIMS Pb–Pb model age for ?metamorphic zircons from greenschist-facies retrogressed mafic–ultramafic schist of the Menzies Series in the southern Mawson Escarpment (N.N. Krasnikov, unpublished data). Pan-African (550–500 Ma) granites in the south-central Mawson Escarpment contain inherited zircon populations of about 2800, 2150, 1850–1800, and 1600 Ma (ion-microprobe U–Pb data: Boger et al. 2001).

The pervasive regional greenschist to amphibolite-facies metamorphism (commonly relatively high-pressure kyanite–staurolite grade) in the Ruker Terrane (event 17) was attributed by Tingey (1982a, 1991a) to the same late Mesoproterozoic–early Neoproterozoic event that was the dominant prograde one in the Beaver-Lambert Terrane to

the north. The available geochronological data, particularly some of the reset Rb–Sr isochron ages (Table 24), appear to be consistent with this, but are still far from conclusive. A preliminary ion-microprobe U–Pb study of zircons from granitic basement rocks of the southern Mawson Escarpment, while confirming their Archaean age, has so far failed to reveal any evidence for a c.1000 Ma event (Boger et al. 2001). This could reflect the lack of any significant magmatic activity or fluid ingress into the basement rocks at that time. This appears to have been the case for the Archaean orthogneisses of the Rauer Islands, even though they are associated with early Neoproterozoic high-grade rocks (Harley et al. 1998, and see below). An alternative explanation, favoured by Boger et al. (2001), is that the Ruker and Beaver-Lambert Terranes did not amalgamate until Pan-African times. Hence, the age of kyanite-grade metamorphism in the overlying Menzies Series metasediments must remain in doubt, and the possibility that it may be much older (even Archaean) cannot be ruled out.

The fact that rocks of the Beaver-Lambert Terrane in the northern part of the SPCM are juxtaposed with those of the Ruker Terrane (e.g., in the central Mawson Escarpment) implies that the high-grade event probably had some effect on the latter terrane. At least some of the major recumbent folding and thrusting in both the Ruker Terrane and southern part of the Beaver-Lambert Terrane may have occurred during this event. For example, some of the high-strain zones in the Mawson Escarpment may be equivalent to D_6 in the Beaver-Lambert Terrane. The presence of amphibolite-facies assemblages in metadolerite dykes of presumed Mesoproterozoic (c.1380 Ma) emplacement age in much of the Ruker Terrane (event 9) can only be explained if the regional event was younger. C.1000 Ma K–Ar ages of metadolerites from Mount Ruker may well reflect this event. Hence, the authors of this bulletin have tentatively correlated the regional metamorphic events in the two terranes, although there is evidence for at least two earlier medium- to high-grade events in the Ruker Terrane. A number of TIMS Pb–Pb model ages were obtained for zircons from biotite and biotite–hornblende gneisses from the central and northern Mawson Escarpment: 705 ± 5 , 795 ± 40 , 880 ± 45 , and 1310 ± 50 Ma (N.N. Krasnikov, unpublished data). These ages suggest that at least this area was affected by early to late Neoproterozoic metamorphic processes, and therefore it was included in the Beaver-Lambert Terrane.

The last major tectonothermal event (24) to effect the Ruker Terrane was of Pan-African (or Ross, i.e., latest Neoproterozoic to Ordovician) age. This event is recorded in many Rb–Sr ages, mostly between 470 and 530 Ma, for muscovite and biotite from rocks throughout the Ruker Terrane (Tingey 1991a). Muscovite–biotite granite was emplaced in the central Mawson Escarpment 551 ± 74 Ma ago (Rb–Sr isochron age) and many granite and pegmatite veins, which are particularly common in outcrops near the Fisher Glacier, are thought to be of similar age. Their emplacement was associated with development of relatively high-temperature sillimanite ± cordierite assemblages in the metasedimentary country rocks.

Prograde greenschist-facies metamorphism of Sodruzhestvo Series sedimentary rocks in the Fisher

Glacier area may have occurred at this time, but the few geochronological data are equivocal, and it is also quite possible that metamorphism of these rocks occurred during the c.1000 event. Indeed, metamorphism during an even earlier event cannot entirely be ruled out. The presence of kyanite in presumed Sodrzhestvo Series metasediments at northern Goodspeed Nunataks suggests that this metamorphism may locally have attained amphibolite-facies conditions.

The Cambrian event appears to have resulted in development of retrograde chlorite–chloritoid assemblages at Mounts Menzies, Bird and Newton. The lower intercept U–Pb zircon age of c.500 Ma for the Mount Ruker biotite granite attests to extensive isotopic resetting at that time. It is unclear whether or not the Pan-African event in the Ruker Terrane resulted in significant regional deformation, but folding of Sodrzhestvo Series metasediments at Mount Rubin and elsewhere may have occurred at this time. It is also possible that some of the major thrusting may be of similar age.

Further geological activity appears to have been confined to intrusion of ultrapotassic dykes (lamproites) at Mounts Bayliss and Rubin, and subsequent uplift and cooling. Erosion must have reached its present level in at least part of the area by Permian times, when deposition of sedimentary rocks occurred. However, no outcrops are known, and the source of *Glossopteris*-bearing siltstone erratics at Mount Rymill is presumably sub-glacial.

Beaver-Lambert and Fisher Terranes

The oldest identified components of these terranes are represented by 2800–2500 and 2100–1800 detrital zircon populations in paragneiss at Mount Meredith (Kinny et al. 1997; events 3 and 7 of Table 21). Granitic leucogneiss at Mount McCarthy also contains a few c.1850 Ma inherited zircons, and metadacite at Fisher Massif contains a single zircon core of similar age. As discussed above, both these age ranges have been recorded in rocks of the Ruker Terrane, although, apart from the 2500 Ma trondhjemite age reported by Kovach & Belitsky (1991), not as well-defined periods of felsic magmatism—the most likely ultimate source of inherited zircons in younger rocks. No evidence for ages similar to the more widespread c.3000 Ma ages in the Ruker Terrane has yet been found in the Beaver-Lambert Terrane. It is also noteworthy that the rocks at Mount Meredith (and some nearby outcrops) are not entirely typical of most of the Beaver-Lambert Terrane. They are of somewhat lower metamorphic grade, and the dated paragneiss apparently contains no zircon grains of c.1000 Ma age, although a few 1700–1600 Ma rims are present. It is quite possible that these rocks may be more closely related to those of the Fisher Terrane than the rest of the Beaver-Lambert Terrane.

Although many individual Rb–Sr isochron ages (Table 24) have very large error limits, are wholly or partly reset, or may, in some cases, be based on sample sets that were not originally isotopically homogeneous, together they present a very consistent picture. Most of those from the Beaver-Lambert Terrane clearly indicate an early Neoproterozoic age (c.900–1000 Ma), which is confirmed by recent ion-microprobe U–Pb zircon data (Table 22). Moreover, $T_{\text{UR}}^{\text{Sr}}$ model ages are almost entirely late Mesoproterozoic (1000–1300 Ma) in marked contrast to

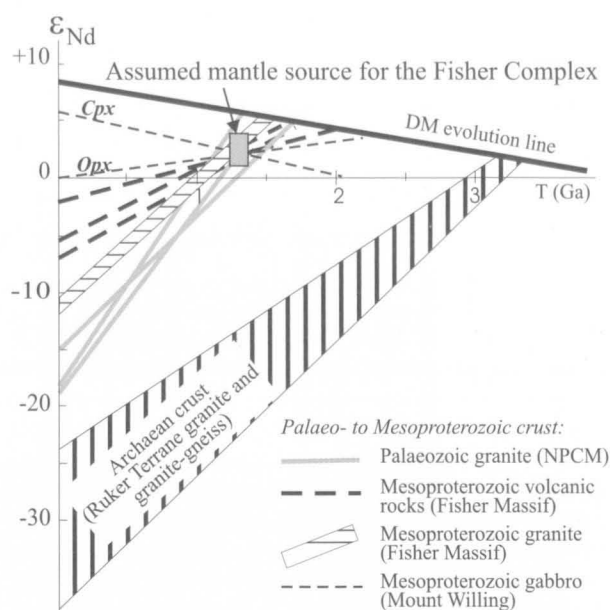


FIGURE 189

ϵ_{Nd} evolution diagram showing probable mantle source composition for rocks of the Mesoproterozoic Fisher Complex (after Mikhalsky et al. 1996). Note the much older depleted mantle (DM) model ages of Archaean granitic basement rocks of the Ruker Terrane. Parameters used for model age calculations: $^{143}\text{Nd}/^{144}\text{Nd}$, 0.51316; $^{147}\text{Sm}/^{144}\text{Nd}$, 0.2136; ^{147}Sm decay constant, λ , $6.54 \times 10^{-12} \text{ yr}^{-1}$.

the Archaean model ages of rocks of the Ruker Terrane. A group of five felsic gneisses from near the northern end of the Mawson Escarpment have a late Archaean $T_{\text{UR}}^{\text{Sr}}$ age, and a Rb–Sr isochron age of $2708 \pm 90 \text{ Ma}$ was obtained from the central Mawson Escarpment (Table 24). However, the Beaver-Lambert Terrane, and probably the Fisher Terrane, apparently includes only a small Archaean component. Its formation could not have involved much reworking of Ruker Terrane protoliths, except presumably where the two terranes are directly juxtaposed, as in the central and northern Mawson Escarpment. The available Sm–Nd isotopic data provide strong support for this interpretation (Fig. 189).

The other important point emphasised by Table 24 is the isotopic similarity of outcrops in the northern part of the SPCM (Clemence and Shaw Massifs, Mount Johns, and the northern Mawson Escarpment) with those in the NPCM. Whole-rock geochemical data also show no significant compositional differences, whereas Mesoproterozoic felsic gneisses from both these areas are compositionally distinct from Archaean felsic gneisses of the Ruker Terrane. The only significant difference between rocks in the northern part of the SPCM and most of those in the NPCM appears to be that the former are of slightly lower metamorphic grade (transitional amphibolite–granulite facies). Hence, they are considered to form an integral part of the Beaver-Lambert Terrane.

If the Beaver-Lambert Terrane extends as far south as the central Mawson Escarpment, then the tectonic significance of the Fisher Terrane becomes more difficult to define, as it cannot merely represent a transitional zone between the Beaver Belt and Ruker Terrane (Mikhalsky et

al. 1996). Several possible tectonic models may be considered for the origin of the mafic to felsic volcanic and intrusive rocks of the Fisher Terrane (the Fisher Complex, FC): (1) a rift structure or aulacogen; (2) a separate microplate; (3) a major suture zone between two continental blocks; or (4) a higher crustal level or less strongly metamorphosed part the Beaver-Lambert Terrane.

Formation of the FC in a rift structure (graben) would be consistent with the previously suggested tectonic structure and evolution of East Antarctica (Grikurov 1980), assuming that the Fisher Terrane was enclosed in an extensive Precambrian granulite terrane. Mikhalsky et al. (1992) suggested a rift-related origin for the Mount Willing layered gabbroic intrusion, with emplacement along a major lithospheric boundary between two different crustal blocks. However, rift-related (within-plate) volcanic sequences are typically of alkaline and/or bimodal type, rather than the tholeiitic to calc-alkaline rocks of the FC that have geochemical features more typical of convergent plate margins. High-grade metamorphic rocks of the Beaver-Lambert Terrane to the north and to the south of the Fisher Terrane appear to have been derived from Palaeo- to Mesoproterozoic protoliths that are not much older than, and may in some cases be younger than, the FC. The presence of higher-grade rocks (migmatites at Nilsson Rocks and orthopyroxene-bearing rocks at Mount Willing) could be taken as evidence for basement-cover relationships in the Fisher Terrane, but most of the authors consider this to be unlikely.

The authors think it unlikely (although not impossible) that the Fisher Terrane represents a distinct microplate (model 2), as its geological history is similar in many respects to that of the Beaver-Lambert Terrane. Its much less intense deformation and metamorphism would be difficult to explain on this basis.

A model implying a major suture between two continental blocks (the Archaean–Mesoproterozoic Ruker Terrane and Meso- to Neoproterozoic Beaver Belt) also seems unlikely, given the compositional and isotopic similarities between the NPCM and northern part of the SPCM. A local suturing between two crustal blocks within a mobile belt might be a more reasonable suggestion. A peculiar feature of the Fisher Terrane is the abundance of mafic volcanic and plutonic rocks, which seems to preclude a direct correlation with the Beaver-Lambert Terrane. Prominent positive gravity anomalies under the ice just north of Fisher Massif (Fig. 168) could possibly be due to the presence of an ophiolite complex. Magnetic anomaly patterns to the north and south of Fisher Massif are quite different (R.G. Kurinin, personal communication). Those to the north are much more intense and show a northeast-trending linear pattern; those to the south have a more isometric pattern lacking high negative values. Although the significance of these differences is far from clear, especially given that rocks in the two areas appear to be of broadly similar age and composition, rather than representing two very different (Archaean *vs* Mesoproterozoic) plates, they do suggest that a suture-zone model cannot be completely discounted. At the same time, no true MORB-type rocks have been found, and most volcanic rocks seem to have originated in continental volcanic arc to island-arc environments. Hence, the Fisher Terrane most probably represents only a part (or sub-terranes) of a much wider

accretionary mobile belt (a suture zone *within* rather than *at the edge of* a terrane). Undepleted (Al-rich) ultramafic rocks in the Beaver-Lambert Terrane could represent oceanic lithosphere (ophiolite) rather than subcontinental lithospheric relics, but their origin remains unclear and they could equally well represent some sort of high-temperature syn-tectonic intrusion.

The Fisher Terrane is much less strongly metamorphosed than the Beaver-Lambert Terrane, and so, in spite of its rather different composition, could represent a higher crustal level equivalent of the latter. Most granitic rocks (including felsic orthogneisses) from the Beaver-Lambert Terrane have volcanic-arc characteristics, and probably formed in a similar subduction-zone environment. Hence, they may at least partly be correlated with the FC. Available Sm–Nd data (see below and Table 23) do not indicate any major differences in T_{DM}^{Nd} model ages between the Beaver-Lambert Terrane and the FC, which suggests that the two terranes may be more or less co-eval. Even the apparent isotopic differences may merely reflect the marked compositional differences, and hence petrogenesis, of rocks in the two terranes. An ϵ_{Nd} evolution diagram suggests derivation of both the FC and the source rocks of early Palaeozoic granites in the Beaver-Lambert Terrane from the mantle in the Mesoproterozoic (Fig. 189). It is unlikely that such a vast mobile belt, which crops out over an area more than 500 kilometres across, was formed entirely in a single active continental margin environment. It is more likely that the Meso- to early Neoproterozoic mobile belt includes a number of distinct components derived in various tectonic environments (new felsic crust formed in volcanic and continental arcs, ophiolite relics, reworked ancient crust, etc.). Continental crust formation may well have occurred over a period of several hundred million years prior to the granulite-facies metamorphism.

Hence, the rift (1), microplate (2), and major suture-zone (3) models are given little support from available geological, chemical and isotopic data, although the last two models cannot be entirely discounted. The Fisher Terrane may simply represent a higher crustal level part of the Beaver-Lambert Terrane, with a much higher proportion of mafic to intermediate volcanic rocks. However, in view of the complex history and composition of the mobile belt itself, no direct correlations between the two terranes are presently possible; detailed isotopic and geochemical studies will be necessary to prove, or disprove, such correlations. Moreover, the outcrops south of Fisher Massif are of somewhat lower grade and are possibly underlain by reworked Ruker Terrane. Archaean relics appear to be present in the northern Mawson Escarpment, but further research is needed to determine the geographical extent of such old components, and the ages of the various protoliths and tectonothermal events. Whatever the relationships, the Fisher Massif volcanic rocks appear to have formed in an active continental margin with an associated island arc about 1300 Ma ago (event 10). Granitic intrusive rocks at Fisher Massif also have volcanic-arc chemical characteristics, consistent with partial melting of a hydrated mafic source, possibly in a subduction environment. Thus, formation of the FC in a specific (compared to the Beaver-Lambert Terrane) tectonic setting with a larger contribution from juvenile mantle-derived melts within a mobile belt is most likely.

The Fisher Massif age data are the only evidence for the precise age of protolith formation in the area. T_{DM}^{Nd} ages are significantly older (mostly between 1640 and 1870 Ma) than the likely time of separation from the upper mantle (c.1300 Ma), and are thus rather misleading (Mikhalsky et al. 1996). Protoliths of the Beaver-Lambert Terrane gneisses (mostly sedimentary and felsic igneous rocks) probably formed at about the same time in the Mesoproterozoic (event 8), consistent with both T_{UR}^{Sr} model ages and inherited zircon ages. There are presently few T_{DM}^{Nd} model ages available, but all indicate Palaeoproterozoic or, more likely in view of their similarity with the Fisher Terrane data, Mesoproterozoic rather than Archaean protolith ages. Five metapelites and felsic gneisses range from 1600 to 2220 Ma (Manton et al. 1992; Zhao et al. 1997; S-S. Sun, unpublished data); orthopyroxene granitoids (1670–1980 Ma) and granitic and syenitic rocks from Mount Collins (1470–1740 Ma: Zhao et al. 1997), as well as leucogranite and biotite granite from Jetty Peninsula (1300–1660 Ma: Manton et al. 1992), are similar or only slightly younger. Like Fisher Massif granitoids, many Beaver-Lambert Terrane orthogneisses, commonly of tonalitic or granodioritic composition, have chemical features (Y and HREE depletion, but little or no Sr depletion) suggesting an origin by melting of a mafic source. They appear to represent new felsic crust, which probably also formed in a subduction environment, and can be looked upon as the Proterozoic equivalent of the Archaean TTG suite. It is noteworthy that the Mount Willing layered gabbro formed under high-pressure conditions (at least 6 kb), and was probably emplaced into an only slightly older metavolcanic sequence. The thickness of this sequence may well reach 20 kilometres, which implies fairly deep trough conditions, or major lithospheric subsidence.

Chemical data are not inconsistent with at least some mafic rocks (amphibolite and granulite) in the Beaver-Lambert Terrane, being the metamorphosed equivalents of the Mesoproterozoic dolerite dyke suite of the Ruker Terrane (event 9). However, the comparison is far from conclusive, and they more probably represent somewhat younger dykes such as those at Fisher Massif (post-1290 Ma: event 11) and Mount Willing (post-1030 Ma). There is a relatively close chemical similarity between a metadolerite dyke from Mount Meredith and metadolerites in the Ruker Terrane, but in view of the likely chemical effects of metamorphism on this dyke (very low Na_2O , and possibly high LILE) a direct correlation is most unlikely. This dyke, like post-980 Ma metadolerites at Mount Collins, was probably emplaced deep in the crust soon after the peak of metamorphism.

The regional high-grade metamorphism peaked about 1000 Ma ago (event 17), with P–T conditions in the Porthos Range area of about 7 kilobars and 750–850°C (Thost & Hensen 1992). The subsequent metamorphic evolution in this area, as evidenced by reaction textures in calc-silicate and other granulites, was apparently one of near-isobaric cooling from about 830 to 750°C. Peak metamorphic conditions further east, in the Jetty Peninsula and Reinbolt Hills areas, were very similar, but seem to have involved a broadly decompressional post-peak evolution, possibly with an intermediate period of cooling and reheating in the former area (Nichols & Berry 1991;

Hand et al. 1994b). The significance of these distinct post-peak metamorphic evolutions will be discussed in the next section. The early Neoproterozoic tectonothermal event was quite long-lived, lasting at least until about 940 Ma, and probably until about 900 Ma (Boger et al. 2000; Carson et al. 2000). It involved several phases of deformation under high-grade conditions, including development of major east–west-trending upright shear zones (event 20). Several phases of felsic magmatism included emplacement of major orthopyroxene granitoid plutons ('charnockites') at 980 Ma (event 18). Syenitic and granitic rocks at Mount Collins are at least partly of similar age, as are biotite granitoids at Fisher Massif, suggesting that the Beaver-Lambert and Fisher Terranes had been juxtaposed by then or possibly much earlier. Felsic magmatism continued until 940 Ma, when garnet–biotite leucogranite was emplaced at Jetty Peninsula.

There is some isotopic evidence for the c.1000 Ma metamorphism in the Fisher Terrane. However, it does not seem to have been accompanied by pervasive schistosity development, and there is also evidence for earlier (c.1120 Ma) amphibolite-facies metamorphism and/or plutonism (event 16), as well as even older tectonothermal events (12–14) in that area. Any structures formed during these older events may have been virtually obliterated by the c.1000 Ma metamorphism in most of the Beaver-Lambert Terrane. Nevertheless, relict D_1 and D_2 structures in mafic and ultramafic boudins may represent such early events. Possible isotopic evidence for an earlier high-grade event, of uncertain significance, in the Beaver-Lambert Terrane comes from a U–Pb age (1165 ± 13 Ma) for monazite from an altered ultramafic body at McLeod Massif.

There is some rather equivocal isotopic evidence for a late Neoproterozoic (c.800–750 Ma) event (22). The 940 Ma (U–Pb zircon age) garnet–biotite leucogranite at Jetty Peninsula has given a Rb–Sr isochron age of 718 ± 32 Ma, and a few other similar Rb–Sr isochron ages have been obtained (Table 24), but it is quite possible that at least some of these ages are due to partial resetting during a c.500 Ma event. Sm–Nd dating of garnet–whole rock samples has given ages of 815–790 Ma, attributed by Zhou & Hensen (1995) to the high-grade event in which the garnet was formed. However, ion-microprobe U–Pb monazite ages for the same rocks give ages of 900–950 Ma, similar to or slightly younger than their U–Pb zircon ages (Kinny 1998). It appears that, like the Rb–Sr ages, the garnet Sm–Nd data reflect re-equilibration during a younger metamorphic event, rather than initial garnet growth. The c.800 Ma age of zircon growth or recrystallisation in the Mount Willing layered gabbro also reflects a thermal rather than a deformational event.

As in the Ruker Terrane, the Ross or Pan-African event (24) is recorded in many muscovite and biotite Rb–Sr ages (mostly 520–480 Ma: Tingey 1991a), as well as Rb–Sr isochron ages for various granitic rocks, including the extensive hornblende–biotite granite plutons on the eastern side of the Amery Ice Shelf (Table 24). Shear and mylonite zones attributed to this event commonly contain greenschist to amphibolite-facies assemblages, so the terrane was still at considerable crustal depths. However, Sm–Nd isochron ages of 631 ± 6 and 555 ± 4 Ma for garnet in leucogranite gneiss from Mount McCarthy (probably of the same generation as that which gave an ion-

TABLE 26. Correlation of major events in the Prince Charles Mountains area with those in adjacent parts of the East Antarctic Shield.

Enderby Land (Napier Complex)	Mawson–Kemp Land Coast (Rayner Complex)	Prince Charles Mountains	Prydz Bay Coast	Vestfold Hills	Approx. age (Ma)
1. Tonalitic magmatism.					3840–3770
2.			Tonalitic, granitic magmatism (<i>RI</i>).		3470, 3270
3. Sedimentation.		Tonalitic magmatism; ?sedimentation (<i>RT</i>).			3150
4. Granulite-facies metamorphism; granitic magmatism.	?Metamorphism; granitic magmatism.	High-grade metamorphism; granitic magmatism (<i>RT</i>).			3000
5. Sedimentation.					
6. Ultra-high-T metamorphism; granitic magmatism.			Gabbroic magmatism; mafic dykes; tonalitic, granitic magmatism (<i>RI</i>).		2850–2800
7.	?Metamorphism; granitic magmatism.	Sedimentation (<i>RT</i>). Felsic and mafic magmatism		Felsic, mafic magmatism; sedimentation.	
8.				Tonalitic magmatism.	2530–2500
9.		?Metamorphism; granitic magmatism (<i>RT</i>).		Granulite-facies metamorphism; gabbroic to granitic magmatism.	2500–2475
10. Amphibolite– granulite-facies metamorphism; granitic magmatism.					2480–2410
11. Dolerite dykes.	?Dolerite dykes; felsic magmatism; sedimentation.	Dolerite dykes; ?metamorphism; ?sedimentation (<i>RT</i>). Felsic magmatism; sedimentation (<i>BT</i>).	Sedimentation . (<i>RI</i> , <i>BB</i>)	Dolerite dykes (2240, 1750); amphibolite-facies mylonite zones.	
12. Dolerite dykes.	Dolerite dykes.	Dolerite dykes; ?sedimentation (<i>RT</i>). Mafic to felsic magmatism (inc. volcanics); sedimentation (<i>FT</i>). Mafic magmatism (?dykes) (<i>BT</i>).	?Dolerite dykes (<i>RI</i>).	Dolerite (1380, 1240) and lamprophyre dykes; mylonite zones.	1400–1200
13.		Metamorphism; dolerite dykes (<i>FT</i>).	Felsic magmatism (<i>RI</i>).		
14. Localised high-P amphibolite– granulite-facies metamorphism, retrograde metamorphism elsewhere.	Granulite-facies metamorphism; granitic magmatism.	Amphibolite (<i>RT</i> , <i>FT</i>) to granulite-facies (<i>BT</i>) metamorphism. Granitic magmatism (<i>FT</i> , <i>BT</i>). Dolerite dykes (<i>BT</i>).	Granulite-facies metamorphism; granitic magmatism; mafic dykes (<i>RI</i> , <i>BB</i>)	Localised high-P amphibolite-facies metamorphism; pegmatites.	1000–900
15.	?Pegmatites.	?Metamorphism; ?pegmatites (<i>BT</i>).			c.750

TABLE 26. Correlation of major events in the Prince Charles Mountains area with those in adjacent parts of the East Antarctic Shield (continued)

Enderby Land (Napier Complex)	Mawson–Kemp Land Coast (Rayner Complex)	Prince Charles Mountains	Prydz Bay Coast	Vestfold Hills	Approx. age (Ma)
16.		?Sedimentation (<i>RT</i>).	?Sedimentation (<i>BB</i>).		
17. Amphibolite- facies mylonite zones; pegmatites.	Amphibolite– granulite-facies mylonite zones.	Greenschist– amphibolite-facies mylonite zones; granitic magmatism.	Greenschist– amphibolite-facies mylonite zones; pegmatites (<i>RI</i>). Granulite-facies metamorphism; granitic magmatism (<i>BB</i>).	Mylonite zones.	550–500
18. Lamproite dykes.		Lamproite (<i>RT</i>) and alkali basalt/dolerite (<i>BT</i>) dykes.	Lamprophyre dykes (<i>RI</i>).	?Alkaline dolerite dykes.	500–250
19.		Amery Group sediments.			c.290–220
20.		Alkaline ultramafic bodies.			150–110
21.		Alkaline mafic lavas.			50

RT, Ruker Terrane; *FT*, Fisher Terrane; *BT*, Beaver Terrane; *RI*, Rauer Islands; *BB*, Bolingen Islands–Larsemann Hills–Brattstrand Bluffs sector of Prydz Bay Coast.

Main data sources: *Enderby Land*, Sheraton et al. (1987b), Harley & Black (1997); *Mawson–Kemp Land Coast*, Clarke (1988), Grew et al. (1988), Young & Black (1991), White & Clarke (1993), Dunkley et al. (1995); *Prydz Bay Coast*, Sheraton et al. (1984), Harley (1988), Zhao et al. (1992, 1995b), Dirks et al. (1993), Kinny et al. (1993), Sims et al. (1994), Carson et al. (1995, 1996), Dirks & Hand (1995), Fitzsimons & Harley (1995), Harley et al. (1995, 1998), Hensen & Zhou (1995), Tong & Liu (1995), Kinny (1998); *Vestfold Hills*, Collerson & Sheraton (1986b), Black et al. (1991b), Passchier et al. (1991), Lanyon et al. (1993), Dirks et al. (1993), Snape & Harley (1997).

microprobe U–Pb zircon age of 990 ± 30 Ma) are more likely to reflect isotopic resetting (Kinny 1998) than garnet growth (Zhou & Hensen 1995; Hensen et al. 1997).

The c.500 Ma event was apparently responsible for the subsequent uplift and cooling of the Beaver–Lambert Terrane. Apatite fission-track data indicate that at least part of the NPCM had cooled below the annealing temperature of about 110°C by the Carboniferous (Arne 1994). Clearly, at least part of the metamorphic basement must have reached the surface by the time the Permo–Triassic Amery Group was deposited, with several kilometres of erosion apparently being involved; the basement rocks would have provided a source of sediments for the Amery Group (Arne 1994). This uplift was accompanied by extensive faulting, which may well have been associated with the initial formation of the Lambert Graben. The Palaeozoic tectonic evolution also involved intrusion of alkaline mafic dykes (alkaline dolerites, camptonites and basanites) in much of the Beaver–Lambert Terrane, but particularly in the Jetty Peninsula area. These dykes have quite different compositions to Proterozoic tholeiitic dolerites, and appear to have been derived from much more enriched mantle source regions. T_{DM}^{Nd} model ages (mostly 1200–900 Ma) of the Jetty Peninsula dykes and stock-like bodies, and the Manning Massif tephritic phonolite lava suggest that mantle enrichment may have been roughly co-eval with felsic crust formation in the area—a phenomenon previously reported from other areas, including the Bunger Hills (Sheraton et al. 1990).

However, younger T_{DM}^{Nd} model ages (700–450 Ma) have also been reported for mantle-derived xenoliths (Andronikov & Belitsky 1995), which suggests that some sort of (?post-collisional) mantle activity lasted until the early Palaeozoic, and resulted in lamproite dyke intrusion into the Ruker and Beaver–Lambert Terranes.

A second period of cooling and uplift began during the late Jurassic and continued into the early Cretaceous. Both apatite fission track and vitrinite reflectance measurements indicate cooling of the Amery Group from more than 80°C since the early Cretaceous, implying removal of about three kilometres of sedimentary material (Arne 1994). This exhumation was probably related to renewed extension of the Lambert Graben, as well as to the beginning of rifting between East Antarctica and India (Veevers et al. 1991). It was accompanied by intrusion of alkaline ultramafic bodies (alkaline picrite at 150–140 Ma, and ultramafic lamprophyre and melanephelinite at 123–110 Ma) in the Jetty Peninsula–Radok Lake area. Further alkaline mafic activity took place in the Eocene, when tephritic phonolite lavas were extruded. A final period of isostatic uplift of about 0.8 kilometres may have resulted from unusually extensive glacial erosion in the Lambert Glacier system (Wellman & Tingey 1981).

REGIONAL CORRELATIONS

A comparison of the geological evolution of the Prince Charles Mountains area with those of adjacent parts of the

East Antarctic Shield (Figs 1, 2) is shown in Table 26. In terms of timing, the Archaean geological histories are generally quite different, suggesting that each Archaean cratonic block represents a distinct microplate. It is noteworthy that in each Archaean block one of the earliest recognisable events is emplacement of tonalitic intrusive (and possibly extrusive) rocks. Rocks of the TTG suite are characteristic of many Archaean high-grade metamorphic and granite–greenstone terranes (Martin 1993) and their Y-depleted, Sr-undepleted compositions indicate partial melting of a garnet-bearing mafic source, either in a subduction environment or mafic underplate. Such rocks are likely to represent juvenile felsic crust, consistent with their emplacement at an early stage in the geological evolution of each block.

The Napier Complex of Enderby Land (Sheraton et al. 1987b) is the largest known Archaean craton in Antarctica. It includes some of the oldest known terrestrial rocks, although the tonalitic orthogneiss dated at 3927 ± 10 Ma by Black et al. (1986a) has since been re-analysed and the age determined to be about 3800 Ma (ion-microprobe U–Pb zircon age: Harley & Black 1997). Emplacement of orthopyroxene granite under granulite-facies conditions at Proclamation Island was dated at 2980 ± 9 Ma, but the ultra-high temperature metamorphism further south in the Tula and Scott Mountains was apparently somewhat younger (2837 ± 15 Ma); a third major high-grade event occurred 2480–2450 Ma ago (Harley & Black 1997). Emplacement of biotite granite took place at 2410 ± 130 Ma (Rb–Sr isochron age: Black et al. 1986b). The geological evolution of the Napier Complex is thus quite complex, and it is possible that different parts experienced different histories. For example, paragneiss in the southwest of the complex at Casey Bay contains no zircons older than 2840 Ma, suggesting that pre-3000 Ma crust was not exposed in the area at the time of sedimentation.

Tonalitic magmatism in the Rauer Islands of the Prydz Bay coast occurred at 3470 ± 30 Ma, granitic magmatism at 3269 ± 9 Ma, a layered mafic–ultramafic igneous body (the Scherbinina Layered Complex) at 2844 ± 6 Ma, and further granitic magmatism at 2810 ± 14 and 2801 ± 6 Ma (Kinny et al. 1993; Harley et al. 1998). In contrast, the nearby Vestfold Hills appears to be mainly of latest Archaean to earliest Palaeoproterozoic age, the predominantly tonalitic Mossel gneiss having been emplaced between 2526 ± 6 and 2501 ± 4 Ma, with voluminous mafic to felsic magmatism (Crooked Lake gneiss, Grace Lake granodiorite) continuing until 2481 ± 14 Ma (ion-microprobe U–Pb zircon ages: Black et al. 1991b). The two principal deformation events have been dated at 2496.3 ± 0.7 Ma (D_1 – M_1) and 2475.3 ± 0.7 Ma (D_2 – M_2) (Snape et al. 1997). Nevertheless, there is evidence from inherited zircon cores and Nd model age data for crust as old as 2800 Ma, and some units (the predominantly mafic Tryne metavolcanics, and the Chelnok supracrustals) appear to pre-date the Mossel orthogneisses (Collerson & Sheraton 1986b).

The Napier Complex and Ruker Terrane are two of the largest Archaean blocks in Antarctica. The former, with the Vestfold Hills, is one of the least modified by Proterozoic or younger events. Archaean rocks are known in many other parts of the East Antarctic Shield, and others may well remain to be identified. For example, granitic magmatism occurred about 2950–3100 Ma ago (Pb–Pb

whole-rock data) at Annandagstoppane in western Dronning Maud Land (Barton et al. 1987). To the east of the PCM, in Queen Mary Land, tonalitic orthogneisses have given ion-microprobe U–Pb zircon ages of 3003 ± 8 and 2889 ± 9 Ma (Cape Charcot, interpreted as emplacement and metamorphic ages, respectively: Black et al. 1992b), and 2641 ± 15 Ma (Obruchev Hills: Sheraton et al. 1992). 2500–3000 Ma detrital zircons occur in paragneisses from the Windmill Islands of Wilkes Land (Oliver et al. 1983; Williams et al. 1983), and orthopyroxene granitoids from Madigan Nunatak, George V Land, have given U–Pb zircon ages of 2350–2700 Ma (Oliver & Fanning 1998). Cambrian muscovite–biotite granite from the Daniels Range in northern Victoria Land contains inherited zircons of 2825 ± 100 , c.2500, c.2000, and 1130 ± 50 Ma (Black & Sheraton 1990), attesting to a long and complex Precambrian geological history near the eastern margin of the East Antarctic Shield in the Transantarctic Mountains area. Similarly, Adams et al. (1982) reported c.2800 Ma U–Pb ages for detrital zircons in paragneisses of the late Neoproterozoic Nimrod Group in the Central Transantarctic Mountains. It thus appears that Archaean rocks are quite widespread in East Antarctica, even though many are covered by the ice sheet.

None of the other Archaean geological histories summarised in Table 26 appears to have much in common with that of the Ruker Terrane. There is evidence that both this and at least part of the Napier Complex underwent a major tectonothermal event about 3000 Ma ago, but their subsequent evolutions seem to have been rather different, even though, given the paucity of modern geochronological (especially ion-microprobe) data, the exact timing of the various late Archaean–Mesoproterozoic events in the Ruker Terrane remains uncertain. There are no obvious correlations for the ages of sedimentary protoliths in the various Archaean blocks, and only in the Ruker Terrane does sedimentation appear to have continued well into the Proterozoic. This is not surprising as this terrane is made up of much lower grade rocks than the other Archaean blocks, and clearly represents a much higher crustal level. Up to several tens of kilometres of overlying crust must have been removed from the high-grade terranes since the Archaean, and this could have provided a source for some of the Proterozoic sedimentary sequences. However, other metasedimentary sequences appear to have been derived from dominantly Mesoproterozoic protoliths. For example, those in the Prydz Bay coast area form part of a much younger association that is unrelated to the predominantly orthogneissic Archaean rocks (see below, and Harley et al. 1995, 1998).

There is some evidence for the occurrence of events common to several of these Archaean cratonic blocks by Mesoproterozoic times. In particular, as discussed above, similar dolerite dyke swarms were emplaced in Enderby Land and the Vestfold Hills between 2240 and 1240 Ma ago, with the most abundant suite at about 1380 Ma. Although there is no isotopic evidence to support it, representatives of at least some of these suites (in particular, the 1380 Ma group) are almost certainly present in the Ruker Terrane, albeit mostly amphibolitised, and possibly also in the Rauer Islands (Sims et al. 1994; Harley et al. 1995, 1998). It is unlikely that such a correlation

means that these Archaean cratons had been assembled into a single crustal block by that time, as they are presently separated by at least 300 kilometres of Neoproterozoic high-grade metamorphic rocks, mostly derived from Proterozoic rather than Archaean protoliths (see below). The dolerite dyke swarms presumably represent major regional mantle melting events, similar to some of the even more extensive periods of tholeiitic magmatism of Phanerozoic times, such as the Jurassic Ferrar tholeiites (Tingey 1991b).

All the Archaean terranes in this part of the East Antarctic Shield show evidence, though not everywhere unequivocal, for medium- to high-grade metamorphism in the earliest Neoproterozoic (1000–920 Ma). In the eastern part of the Napier Complex in Kemp Land, high-pressure garnet-bearing assemblages are extensively developed in both dolerite dykes and country rocks, but elsewhere in the complex such assemblages are mainly confined to discrete shear zones (Sheraton et al. 1987b). Zircon in rocks of the southwestern part of the Napier Complex, where the effects of this shearing are relatively intense, lost Pb at about this time (Grew et al. 1982; Black et al. 1983). Undeformed mafic dykes in the southwestern part of the Vestfold Hills were also recrystallised to garnet–hornblende–clinopyroxene–orthopyroxene–plagioclase assemblages, probably during the same Neoproterozoic metamorphic event that affected the nearby Rauer Islands (Sheraton & Collerson 1983; Collerson & Sheraton 1986b), which would be consistent with an ion-microprobe U–Pb age of 1025 ± 56 Ma for metamorphic zircons in a relatively unaltered 1250 Ma dolerite from the eastern Vestfold Hills (Black et al. 1991a).

The Rauer Islands consist of two distinct components: the Archaean felsic and mafic orthogneisses referred to above, which are cut by several generations of metabasite dykes, and a group of orthogneisses and metasediments derived from Proterozoic protoliths, which are cut by only a few post-1000 Ma metabasite dykes (Harley & Fitzsimons 1991; Harley et al. 1998). P–T conditions in the younger group were estimated from assemblages in metapelitic and calc-silicate rocks to have been 8–9 kilobars at 850°C, followed by decompression to 5–6 kilobars at more than 750–800°C (Harley et al. 1992). This group includes a leuconorite melt phase (1057^{+22}_{-10} Ma), granitic orthogneiss (1027 ± 27 Ma), quartz monzodiorite gneiss (1000^{+57}_{-37} Ma), and late garnet leucogneisses (1004 ± 52 , 998 ± 18 Ma; all ion-microprobe U–Pb zircon ages: Kinny et al. 1993). Ion-microprobe U–Pb ages of monazites from metapelites are also about 1000 Ma (Kinny 1998). However, no isotopic evidence for a c.1000 Ma event has yet been found in the Archaean rocks, which nevertheless show evidence for extensive resetting of the U–Pb system, probably reflecting Pb loss due to fluid infiltration, at about 520 Ma (Harley et al. 1998).

Granulite-facies rocks which crop out along the Mawson and Kemp Land coasts (termed the Rayner Complex in the latter area: Sheraton et al. 1987b) clearly form the extension of the Beaver-Lambert Terrane to the north and west. They are compositionally similar, consisting mainly of intermediate to felsic orthogneiss, layered paragneiss and mafic granulite (including deformed dykes: Trail 1970; Clarke 1988; White & Clarke 1993; Kelly et al. 2000), all cut by large plutons of

orthopyroxene granitoid (Mawson Charnockite: Sheraton 1982; Young & Ellis 1991; Young et al. 1997). Tingey (1991a) gave a summary of Rb–Sr isochron ages for felsic gneisses and orthopyroxene granitoids from the Mawson Coast, mostly based on unpublished data of P.A. Arriens (Australian National University). These range from 1254 ± 31 to 622 ± 25 Ma, with most being between 900 and 1060 Ma. Dunkley et al. (1995) and Dunkley (1998) used ion-microprobe U–Pb zircon dating to obtain much more precise estimates of the ages of the various metamorphic and magmatic events that occurred during the Rayner structural episode at Cape Bruce: granulite-facies metamorphism (D_1 – M_1) at about 995 Ma, granitic orthogneiss at 990 Ma, retrograde metamorphism (D_2 – M_2) between 990 and 960 Ma, felsic dyke intrusion at about 960 and 940 Ma, and metamorphism (M_3) at about 910 Ma. Young & Black (1991) obtained ion-microprobe zircon ages of 985 ± 29 and 954 ± 12 Ma for different phases of the Mawson Charnockite, with growth of zircon rims, probably during D_3 , at 921 ± 19 Ma. Pegmatite at Fold Island in Kemp Land has given a conventional U–Pb zircon age of 940 ± 80 Ma (Grew et al. 1988). These ages cover a very similar range to those obtained for the Beaver-Lambert Terrane (Table 22).

The structural histories of the Beaver-Lambert Terrane and the Rayner Complex are complex, making correlations difficult. Nevertheless, the major east–west-trending upright shear zones in the Beaver-Lambert Terrane (F_6) may be equivalent to open to isoclinal east–northeast-trending folds (F_3) in the Colbeck Archipelago (White & Clarke 1993) and steeply south-dipping D_{3b} shear zones in the Oygarden Islands (Kelly et al. 2000). Similar open to isoclinal F_2 folds with moderately to steeply dipping east-striking axial planes are present in the Stillwell Hills of Kemp Land (Clarke 1988), and a major southeast to east-trending fold (F_4) is the dominant structure at nearby Fold Island (James et al. 1991). This common orientation is consistent with development of all these structures during the same tectonic event (Dunkley 1998). P–T conditions in the Colbeck Archipelago were estimated to have been 5.1 ± 0.8 kilobars at $>700^\circ\text{C}$ during D_1 by White & Clarke (1993), although this was interpreted to have been an Archaean event. It seems just as likely that this estimate reflects an early phase of the regionally penetrative c.1000 Ma event. In any case, a very similar pressure was inferred for the Rayner structural event (5.6 ± 0.4 kb), and the pressure during emplacement of the Mawson Charnockite was estimated to have been 3.9 ± 1.0 kilobars (White & Clarke 1993). All these pressures are somewhat lower than those obtained for the Beaver-Lambert Terrane. However, higher-pressure conditions (9 kb at 800 – 850°) pertained in the Oygarden Islands to the west (Kelly et al. 2000).

The isolated Grove Mountains, about 200 kilometres east of the Mawson Escarpment, have been little studied. They consist of layered grey migmatitic biotite–hornblende, biotite, and leucocratic granite gneiss and plagiogneiss, quartzite and biotite–garnet paragneiss, with rare mafic schist and calc-silicate rocks (McLeod 1959; Tingey & England 1973; England & Langworthy 1975; D.S. Soloviev, unpublished data). Granite and granodiorite bodies crop out at a few localities and orthopyroxene granite (charnockite) at Mount Harding. Preliminary U–Pb

mineral data for paragneiss (Mikhalsky et al. 2001) indicate derivation from Palaeoproterozoic (c.1900–1700 Ma) sedimentary protoliths or, more likely, their felsic igneous source regions, and possibly a metamorphic event at about 800–750 Ma; charnockite was emplaced at about 504 Ma (eastern Grove Mountains), and metamorphism occurred at about 510 Ma (western Grove Mountains). In spite of being much younger, the charnockite has a very similar chemical composition to some of the abundant early Neoproterozoic (c.980 Ma) charnockite plutons in the Beaver-Lambert Terrane and Mawson Coast, having low SiO₂ and high Ti, Nb and Y contents. These older charnockites are believed to have originated in a late-orogenic, rather than anorogenic, tectonic environment, so that the Grove Mountains area was apparently affected by major Pan-African (c.500 Ma) tectonic activity. The Grove Mountains cannot be correlated with the Ruker Terrane, but neither are there clear geochronological similarities with the Beaver-Lambert Terrane. The intensity of the Pan-African event suggests some affinities with the Prydz Bay coast area (see below), but it is possible that the Grove Mountains represent a distinct terrane or microplate.

In contrast to the Beaver-Lambert Terrane, isotopic data have shown that there was significant remetamorphism of Archaean rocks in that part of the Rayner Complex adjacent to the Napier Complex in Kemp Land. Grew et al. (1988) report a U–Pb zircon age of 3081±170 Ma for felsic gneisses from Fold Island, and Clarke (1988) cites a 2692±48 Ma Rb–Sr isochron age for orthopyroxene-bearing felsic gneisses from the Stillwell Hills. Mafic granulite bodies, probably the metamorphosed equivalents of the Mesoproterozoic dolerite dykes in the Napier Complex (Amundsen dykes of Sheraton & Black 1981), crop out along much of the Kemp Land coast, but become increasingly deformed and boudinaged towards the east (Sheraton et al. 1987b; Clarke 1988; James et al. 1991; White & Clarke 1993). Zircon cores from a felsic gneiss xenolith in the Mawson Charnockite include a single 2500 Ma grain, although most grains are 1700–2000 or 1000–1500 Ma old (Young & Black 1991). T_{DM}Nd model ages for the Mawson Charnockite range from 1678 to 2173 Ma, and for gneissic country rocks from 1753 to 2259 Ma (Young et al. 1997), similar to that of a metapelite from Lucas Nunatak (2030 Ma: S-s Sun, AGSO, unpublished data), showing that protoliths of both the exposed country rocks and the source rocks of the orthopyroxene granitoids in that area were largely of Proterozoic age. Some of the older Rb–Sr isochron ages from the Mawson Coast (1254±31, 1153±47; Tingey 1991a) may give an approximate indication of the ages of some orthogneiss protoliths, but relatively high initial ⁸⁷Sr/⁸⁶Sr ratios (0.7447±0.0045 and 0.7409±0.0004, respectively) suggest partial resetting.

In the western part of the Rayner Complex, in western Enderby Land, there is currently little evidence for incorporation of much Archaean material into Mesoproterozoic to early Neoproterozoic metamorphic rocks. Black et al. (1987) reported U–Pb zircon ages of 1488⁺¹⁹_{–16} Ma for anorthosite emplacement and 1465⁺²⁵_{–20} Ma for granite emplacement, as well as T_{DM}Nd model ages of 1290 to 2180 Ma for a range of rock types. Even a Y-depleted tonalitic orthogneiss, chemically similar to

tonalitic rocks in the Napier Complex, has a model age of 1940 Ma and presumably represents a more recent phase of felsic crust generation. The age of granulite-facies metamorphism in this area is indicated by a Rb–Sr isochron age of 1022±62 Ma for granitic orthogneiss (Grew 1978), with a minimum of 923±7 Ma given by a lower intercept U–Pb zircon age for felsic gneiss (Black et al. 1987). Similar ion-microprobe U–Pb zircon ages have been obtained from the Nye Mountains and Sandercock Nunataks, although gneisses from some of the coastal outcrops have given Pan-African (c.520–540 Ma) ages (Shiraishi et al. 1997). This is the only area from which good isotopic evidence for a c.750 Ma magmatic event has been obtained: 766⁺¹⁵_{–11} and 761⁺⁸_{–4} Ma U–Pb zircon ages for biotite granite and pegmatite, respectively (Black et al. 1987), although Clarke (1988) quoted a 718±10 Ma Rb–Sr age for biotite from pegmatite in the Stillwell Hills, Kemp Land.

Unlike the Rauer Islands, there is only limited isotopic evidence from the central Prydz Bay coast for an early Neoproterozoic tectonothermal event, with most isotopic data indicating Pan-African (Cambrian to Ordovician) high-grade metamorphism (Zhao et al. 1992; Carson et al. 1996; Kinny 1998). However, Zhao et al. (1995b) quoted ²⁰⁷Pb/²⁰⁶Pb ages for four zircon grains of 940±6 Ma and a Rb–Sr isochron age of 1024±47 Ma for garnet–biotite leucogranite gneiss from the Larsemann Hills, interpreted to approximate the emplacement age. The former age is identical to that (940±20 Ma) obtained for leucogranite gneiss from Jetty Peninsula by Manton et al. (1992). At Søstrene Island to the southwest, garnet–whole rock Sm–Nd dating of mafic granulite has given an age of 988±12 Ma (Hensen & Zhou 1995). Ion-microprobe U–Pb monazite ages for paragneiss from nearby Bolingen Islands range from 800 to 1000 Ma (Kinny 1998), whereas zircon ages are 550 to 750 Ma and the garnet–whole rock Sm–Nd age is 510±7 Ma, suggesting strong Pan-African overprinting of a Neoproterozoic metasediment. Rocks from both these areas show petrographic evidence for an early high-pressure granulite-facies event that may well be of early Neoproterozoic age (Thost et al. 1991; Dirks & Hand 1995). Ren et al. (1992) reported similar evidence from the Larsemann Hills, where Tong & Liu (1995) inferred that the early high-grade event (at 6.3±0.5 kb and 747±48°C) involved an anticlockwise P–T–time path, which contrasted with the clockwise path that characterised the younger lower pressure event (about 4.5 kb at 750°C). Thost et al. (1991) estimated P–T conditions for the early event at Søstrene Island to be as high as 10 kilobars and 980°C.

Outcrops in the southwestern part of the Prydz Bay coast include abundant orthopyroxene-bearing orthogneiss and mafic granulite, which are lithologically quite distinct from the paragneiss-dominated outcrops in the Bolingen Islands–Larsemann Hills–Brattstrand Bluffs area, and which may represent the basement on which the sedimentary sequences were deposited (Sheraton et al. 1984). Two structurally and lithologically distinct domains, one dominated by felsic to mafic gneiss and the other by metasediments, in the Bolingen Islands may also represent basement and cover (Dirks & Hand 1995). Similarly, Fitzsimons & Harley (1991) and Carson et al. (1995) recognised felsic orthogneiss and mafic granulite

basement rocks, overlain by a metapelite-dominated cover sequence in the Larsemann Hills.

The depositional age of the metasedimentary cover sequences is uncertain. Limited T_{DM}^{Nd} model age data (Sheraton et al. 1984; Zhao et al. 1995b) are consistent with a Proterozoic origin: 1760–2100 Ma for Larsemann Hills metasediments, similar to 1700–1820 Ma for garnet or orthopyroxene-bearing felsic gneisses from the Rauer Islands, metamorphosed during the c.1000 Ma event (Kinny et al. 1993; Harley et al. 1995). However, in view of the tendency for T_{DM} model ages to overestimate the time of felsic crust generation, deposition was unlikely to have been earlier than the Mesoproterozoic. In any case, the model ages only imply derivation of the sedimentary protoliths from Mesoproterozoic source rocks, such as those in the Rauer Islands. Carson et al. (1995) suggested that, although geochronological data are inconclusive, the interleaving of basement and cover (D_1), and at least the next major high-grade tectonothermal event (D_2) in the Larsemann Hills, were most probably of early Neoproterozoic age. Dirks & Hand (1995) suggested a similar timing for equivalent events in the Bolingen Islands, where paragneiss contains 800–1000 Ma monazites (Kinny 1998). On the other hand, $^{207}Pb/^{206}Pb$ ages for detrital zircons from paragneisses in the Larsemann Hills range from 1200 ± 6 to 766 ± 12 Ma (Zhao et al. 1995b). Taken at face value, these data would indicate that at least some of the sedimentary protoliths were deposited during the Neoproterozoic. However, these are minimum ages, and it is possible that Pb loss has occurred, as has been demonstrated for zircons from orthogneisses in the Rauer Islands (Harley et al. 1998) and from paragneiss in the Bolingen Islands (Kinny 1998). Nevertheless, the high degrees of partial melting in metapelitic migmatites at Brattstrand Bluffs was taken by Fitzsimons & Harley (1995) to be more consistent with only one high-grade event, inferred by Fitzsimons (1996) to have been at about 500 Ma. On balance, it seems likely that at least some of the central Prydz Bay coast metasediments were deposited in the Mesoproterozoic and can be correlated with metasedimentary sequences in the Rauer Islands. It is quite possible that others could be Neoproterozoic, and may be of similar age to the low-grade Sodruzhestvo Series metasediments of the Ruker Terrane.

The Pan-African event in the central Prydz Bay coast involved regional penetrative deformation and extensive partial melting under granulite-facies conditions (Dirks et al. 1993; Carson et al. 1996). P–T conditions in this area have been estimated at between 4.5 kilobars at 750°C in the Larsemann Hills (Stüwe & Powell 1989) and 6 kilobars at 860°C at Brattstrand Bluffs (Fitzsimons 1996); decompression reaction textures indicate considerable uplift after the metamorphic peak (Dirks & Hand 1995; Fitzsimons & Harley 1995; Fitzsimons 1996). Isotopic evidence for the age of this event in the Larsemann Hills includes $^{207}Pb/^{206}Pb$ zircon ages of 556 ± 7 and 547 ± 9 Ma for a syn-metamorphic garnet–biotite granite dyke and 531 ± 8 Ma for a granitic pegmatite (Zhao et al. 1992), and ion-microprobe U–Pb zircon ages of 516 ± 7 and 514 ± 7 Ma for a larger body of garnet–biotite granite (Carson et al. 1996). Ion-microprobe U–Pb zircon (536 ± 35 and 535 ± 13 Ma) and monazite (528 ± 4 to 512 ± 13 Ma) ages for anatectic leucogneisses from Brattstrand Bluffs were obtained by

Fitzsimons et al. (1997), who considered the zircon age to best define the metamorphic peak. Most garnet–whole rock Sm–Nd ages of paragneisses and granitic leucogneisses from the Bolingen Islands, Larsemann Hills and Brattstrand Bluffs are between 517 ± 4 and 467 ± 8 Ma, although Kinny's (1998) monazite U–Pb data showed that at least some of these ages are reset. The predominance of c.500 Ma ages led some authors (Dirks & Wilson 1995; Hensen & Zhou 1995; Zhao et al. 1995b) to suggest that the only high-grade metamorphic event in the central Prydz Bay coast was of this age. However, the isotopic evidence given earlier for a c.1000 Ma tectonothermal event, together with petrographic evidence for an early high-pressure granulite-facies event at many localities, make it more likely that there were two distinct periods of high-grade metamorphism. Only some of the granitic and perhaps the metapelitic rocks may post-date the earlier event. The Pan-African event in this area was terminated by emplacement of pegmatite bodies and formation of shear and mylonite zones (Fitzsimons & Harley 1991; Carson et al. 1995; Dirks & Wilson 1995).

As in the PCM, the effects of the Pan-African tectonothermal event in other nearby parts of the East Antarctic Shield (the Grove Mountains excepted) were largely confined to development of shear and mylonite zones and emplacement of granite and pegmatite bodies, accompanied by extensive resetting of various isotopic systems. Nevertheless, P–T conditions during formation of late garnet-bearing mylonite zones and pseudotachylite veins in the Mawson Coast were apparently as high as 6–7 kilobars and 700–800°C (Clarke & Norman 1993; White & Clarke 1994). A pegmatite in the western Napier Complex gave a Rb–Sr isochron age of 522 ± 10 Ma (Black et al. 1983). Minerals in various granitic rocks and pegmatites in the same area and in the adjacent Rayner Complex underwent Pb loss at about the same time (Grew 1978; Grew & Manton 1979; Black et al. 1987). Dolerite dykes in the Vestfold Hills show evidence for resetting of the Rb–Sr system on a mineralogical scale at about 500 Ma (Collerson & Sheraton 1986a). Zircons in orthogneisses in the nearby Rauer Islands underwent Pb loss, associated with fluid infiltration under greenschist to amphibolite-facies conditions, at about 520 Ma (Harley et al. 1998).

NATURE OF THE C.1000 AND C.500 MA EVENTS

The Beaver-Lambert Terrane is only a relatively small part of a complex Mesoproterozoic to early Neoproterozoic mobile belt—albeit with several Archaean cratonic blocks and smaller relics—that extends through much of the East Antarctic coast and once-adjacent parts of Gondwana (Fig. 190). Rocks of generally similar age (1000–1200 Ma) have been documented from Haag Nunataks in West Antarctica (Storey et al. 1994). In East Antarctica, rhyolitic volcanic rocks in Coats Land, about 2500 kilometres west of the PCM, have given a Rb–Sr isochron age of 1076 ± 7 Ma (Storey et al. 1994). Felsic volcanic rocks of the Ritscherflya Supergroup in western Dronning Maud Land have a U–Pb zircon age of 1135 Ma, similar to that of an extensive 1000–1200 Ma orogenic belt in this area (Moyes et al. 1993; Knoper et al. 1995). Magmatic activity and metamorphism occurred between

1130 and 1060 Ma (U–Pb zircon ages) in the Kottas Mountains (Arndt et al. 1989). This late Mesoproterozoic event may be correlated with the Kibaran metamorphics of southern Africa (Weber & Arndt 1991; Groenewald, 1993).

Shiraishi & Kagami (1992) obtained a Sm–Nd isochron age of 961 ± 101 Ma for metamorphic rocks (mainly tonalitic orthogneisses) in the Sør Rondane Mountains of eastern Dronning Maud Land. Comparable Rb–Sr isochron ages (1030–1130 Ma) have been reported for granulite-facies metamorphics in the Lützow-Holm Bay area (Yoshida et al. 1983; Shibata et al. 1986). However, more recent ion-microprobe U–Pb zircon dating has shown that the regional metamorphism in this area was of Pan-African

age (520–550 Ma), although with appreciable 2900–1000 Ma inheritance (Shiraishi et al. 1992, 1994; Fraser et al. 1995). Trondhjemitic orthogneiss from Cape Hinode in the extreme east of Dronning Maud Land has given an ion-microprobe U–Pb zircon age of 1017 ± 13 Ma, suggesting a correlation with the nearby Rayner Complex (Shiraishi et al. 1992, 1994).

High-grade metamorphism in the area to the east of the PCM was somewhat earlier. Granulite-facies metamorphism in the Bunger Hills of Wilkes Land occurred at 1190 ± 15 Ma, followed by emplacement of mafic to felsic plutonic rocks between 1170 and 1150 Ma and dolerite dykes at about 1140 Ma (Sheraton et al. 1995).

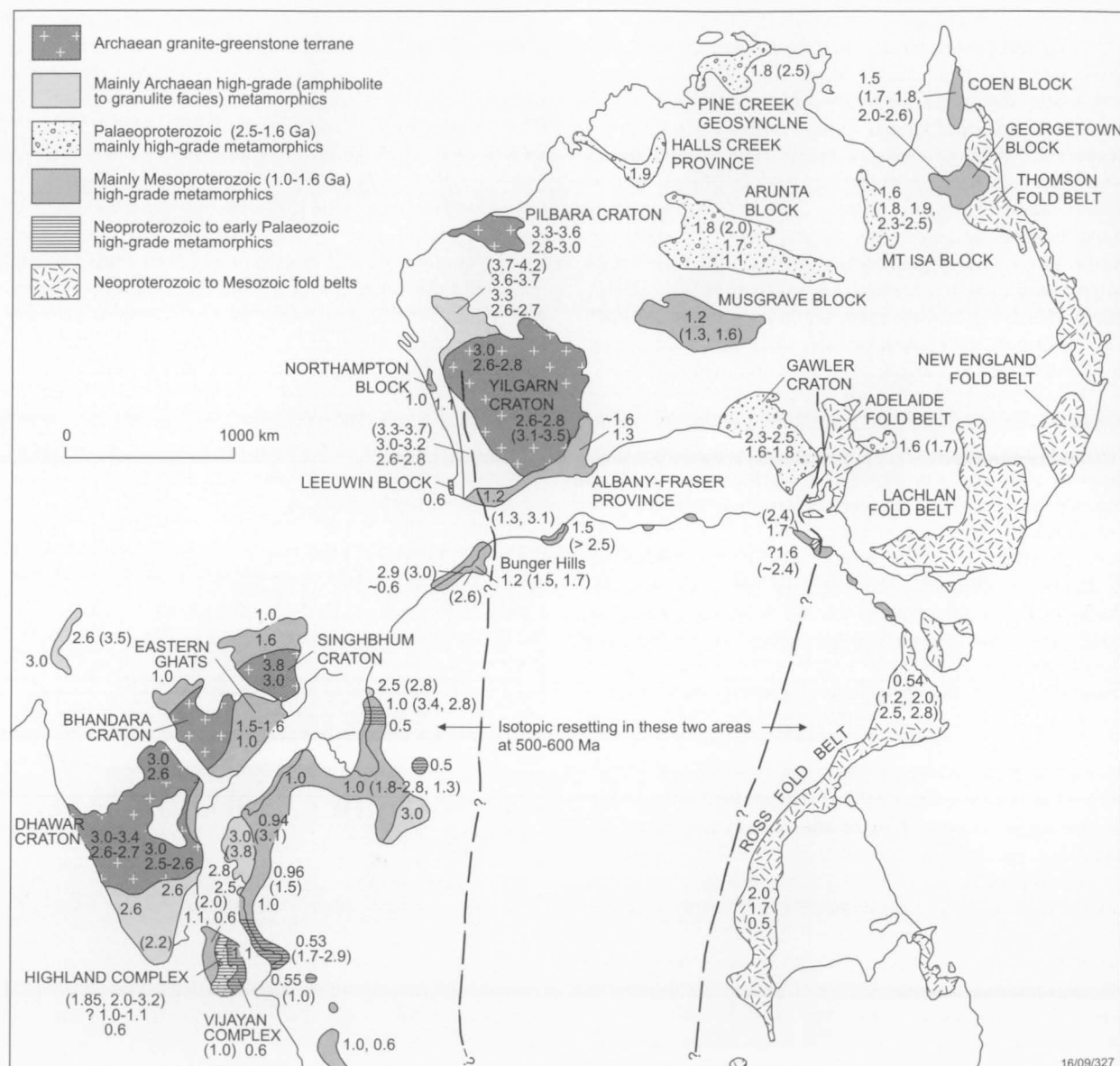


FIGURE 190

Reconstruction of part of Gondwana (using the pre-rifting fit of Veevers & Eittreim 1988), showing major Precambrian metamorphic terranes and Neoproterozoic to Mesozoic fold belts (after Sheraton et al. 1995). Representative isotopic ages (in Ga), as well as provenance ages (in brackets), are shown for the former. Protolith ages and Archaean to Proterozoic provenance ages of metasediments and S-type granitoids in the Ross Fold Belt are also indicated. The Ruker Terrane is of somewhat lower metamorphic grade than other Archaean high-grade terranes, and in part has some features in common with granite-greenstone terranes. Data sources are given by Sheraton et al. (1995), with additional references quoted in the text.

Ion-microprobe U–Pb zircon dating indicates two major phases of metamorphism in the Windmill Islands: an upper amphibolite-facies event at about 1400–1310 Ma and a granulite-facies event at about 1210–1180 Ma; granite at Ford Island was emplaced about 1170 Ma ago, the Ardery Charnockite at about 1160 Ma, and aplite dykes at about 1138 Ma (Post et al. 1995). Biotite Rb–Sr and K–Ar ages are mostly between 1060 and 1160 Ma (Tingey 1991a). There is isotopic evidence in both areas for emplacement of granitic rocks in the Palaeo- to Mesoproterozoic: ion-microprobe U–Pb zircon ages of about 1700 and 1500 Ma for granodiorite in the Bunger Hills (Sheraton et al. 1992) and a Rb–Sr isochron age of 1477 ± 73 Ma for tonalite in the Windmill Islands (Williams et al. 1983). Crust formation and metamorphism at Mount Brown, about 300 kilometres east of the Vestfold Hills, appear to have roughly co-eval with these events (c.1360 Ma: K.D. Collerson, University of Queensland, personal communication, 1998).

Comparable (c.1000 Ma) ages to those of the Beaver-Lambert Terrane and Rayner Complex have been reported from once contiguous parts of Sri Lanka (Kagami et al. 1990) and India (the Eastern Ghats and adjacent areas: Sakar 1968; Grew & Manton 1986) (Fig. 190). Ion-microprobe U–Pb zircon dating of rocks from the western part of the Albany–Fraser Province (the Albany Mobile Belt) in southwestern Australia by Black et al. (1992a) has shown that amphibolite to granulite-facies metamorphism and deformation, as well as several episodes of felsic magmatism, occurred within 10 Ma or so of 1190 Ma—that is, essentially co-eval with metamorphism and deformation in the Bunger Hills and Windmill Islands. A major magmatic event also occurred in the eastern part of the province about 1300 Ma ago (Nelson et al. 1995). Similarly, granulite-facies metamorphism and magmatism occurred in the Musgrave Block of central Australia at about 1300 and 1200 Ma (Gray 1978; Sun & Sheraton 1992; White et al. 1999). The Grenville orogenic belt of North America (Park 1988; Connelly & Heaman 1993) includes both mantle and crust-derived plutonic rocks of very similar age (1130–1160 Ma: Emslie & Hegner 1993) to those in the Bunger Hills. All these data are consistent with Moores' (1991) suggestion that the Grenville orogen once extended around the present coast of East Antarctica into India and Australia in a Neoproterozoic supercontinent (Rodinia) that eventually broke apart, isolating North America (Laurentia) and resulting in formation of the Gondwana supercontinent (Dalziel 1991, 1992).

The fundamental nature of such a global-scale orogenic belt is unclear, but it appears to have been related to assembly of the Rodinia supercontinent, which, on palaeomagnetic evidence, was completed by about 1050 Ma (Powell et al. 1993). Unrug (1996) pointed out that assembly of Rodinia occurred during a series of Mesoproterozoic (1300 to 1000 Ma) orogenies, and depicted the mobile belt in East Antarctica as a collisional or accretionary terrane. According to Powell (1998), Rodinia was assembled between 1300 and 1100 Ma ago, and began to break apart soon after 750 Ma. c. 1000 Ma granulite-facies metamorphism in the Beaver-Lambert Terrane may have been related, either directly or indirectly, to collision of the Archaean to Palaeoproterozoic Indian Shield with East Antarctic plates of similar age (the Ruker Terrane, Napier Complex, and

possibly the Vestfold Hills). Gondwana reconstructions place the Archaean Bhandara and Singbhum Cratons of the Indian Shield adjacent to the NPCM–Amery Ice Shelf area (Sheraton et al. 1995). Similarly, Sheraton et al. (1995) suggested that high-grade metamorphism in the Bunger Hills–Windmill Islands area, some 200 Ma earlier, ultimately resulted from collision of the Archaean Yilgarn Craton of Western Australia with the East Antarctic Shield. However, Gondwana reconstructions and the compositions of syn- to late-metamorphic plutonic rocks suggest that the Bunger Hills rocks may have formed in an Andean-type continental margin, with the actual collision zone having been nearer the present Windmill Islands to the east. The 1000–1200 Ma orogenic belt in western Dronning Maud Land probably resulted from collision of the Kalahari craton of southern Africa with the East Antarctic craton (Knoper et al. 1995).

Formation of the Beaver-Lambert Terrane metamorphic rocks in a convergent tectonic regime is therefore considered to best fit the available geological and geochronological constraints. Stüwe & Hand (1992) contended that the very extensive nature of the c.1000 Ma terrane is difficult to reconcile with a plate tectonic setting, but Phanerozoic convergent margins can be equally wide: up to 800 kilometres in the Palaeozoic Lachlan Fold Belt of southeastern Australia and the Cainozoic central Andes (Fergusson 1998). Moreover, the Andean belt, together with its northward extension as the western Cordillera of North America, is of comparable global extent to the Grenville orogen. Such enormous terranes are, of course, likely to be tectonically and metamorphically highly complex, and may take up to several hundred million years to evolve.

The predominance of Palaeo- to Mesoproterozoic $T_{\text{SR}}^{\text{U-Pb}}$ and $T_{\text{DM}}^{\text{Nd}}$ model ages in the Beaver-Lambert and Fisher Terranes, together with U–Pb zircon data, imply a period of extensive crust generation during the Mesoproterozoic. More direct evidence for a continental margin tectonic setting, probably with an associated island arc, comes from the geochemistry of c.1300 Ma volcanic rocks in the Fisher Terrane. Co-eval tonalites and granodiorites have compositions typical of Andean plate margins. Many orthogneisses in the Beaver-Lambert Terrane also have Y-depleted tonalitic or granodioritic compositions consistent with partial melting of a mafic source: subducted hydrated oceanic crust, a mafic underplate, or both. The most voluminous (mafic to felsic) plutonism in the Andes occurred during periods of compressive deformation associated with active subduction, whereas predominantly mafic magmatic activity took place during periods of extension (Pichowiak et al. 1990; Soler & Bonhomme 1990).

The age of volcanic activity in the Fisher Terrane is quite similar to the emplacement ages of some of the most abundant dolerite dykes suites (1380 and 1250 Ma) in Enderby Land and the Vestfold Hills (Collerson & Sheraton 1986a; Lanyon et al. 1993), indicating widespread magmatism at that time. The older of these dyke groups in the Vestfold Hills trends north–south, and younger ones north-northeast to northeast (similar to the strike of the FC), suggesting anticlockwise rotation of this crustal block, assuming a steady northwest–southeast extension direction. Thus, if the Vestfold Hills block was already *in situ* in the middle–late Mesoproterozoic (which is

suggested by the presence of mantle nodules derived from quite similar subcontinental mantle sources in Mesoproterozoic lamprophyre dykes in the Vestfold Hills and Cretaceous stocks in Jetty Peninsula: Andronikov & Mikhalsky 1997), the compressional and extensional vectors in the central PCM and Vestfold Hills should have been roughly co-eval and co-linear (parallel). The Vestfold Hills dolerites were emplaced in an extensional, presumably rift-related, environment, which could either reflect initial collision of the continental craton with a mid-ocean ridge, or localised extension in a Andean plate margin. The Fisher Terrane may itself have undergone extension at about 1200–1250 Ma when the Mount Willing layered intrusion was formed.

An active continental margin may have existed until some time before 1000 Ma, when closure of the oceanic basin culminated in continental collision with the arrival of the Indian plate. However, earlier accretion of microplates is also possible, and the Indian plate may itself have had an active margin at some stage of its history. A long period of accretion may therefore have involved a mixture of older crustal blocks, continental volcanic arcs, oceanic volcanic arcs, and possibly an oceanic basin component. An earlier island-arc environment, represented by volcanic rocks from Fisher Massif and low-Ti basalts from Mount Willing, appears to have given way to a continental-arc environment. West-northwest-trending post-metamorphic (?Neoproterozoic) mafic dykes at Mount Willing show that the extensional direction had become roughly orthogonal to the Mesoproterozoic extensional event recorded by mafic dyke swarms in the Vestfold Hills. This may be evidence for another tectonothermal cycle, possibly corresponding to late Neoproterozoic magmatic and tectonic activity in the Beaver-Lambert Terrane (see below).

Much of the c.1000 Ma granulite-facies terrane, from the Rayner Complex in Enderby Land to the Rauer Islands, preserves petrographic evidence for substantial (2–4 kb) post-peak decompression (Harley 1988, 1991). Interpreted P–T-time paths are generally clockwise, although only a small, relatively late part of the overall P–T-time path is usually recorded. After decompression the terrane appears to have undergone a prolonged period of near-isobaric cooling at middle crustal levels (3–5 kb: Harley 1988). Such a P–T history can only be explained by major crustal thickening in a convergent tectonic regime, most likely one of continental collision, followed by uplift due to erosion and/or extensional collapse. Clarke (1988) showed that deformation of the Rayner Complex in MacRobertson and Kemp Lands was due to westward thrusting against the stable craton of the Archaean Napier Complex. Two possible tectonic models were proposed by Dunkley (1998) to explain the initial east–west compression followed by north–south contraction implied by the geometry of fold structures in this area. The first was a transition from thrust-type (contraction-dominant) to transcurrent-dominant convergence (i.e., an oblique-collisional setting). The second was a transition from westward convergence to north or northwestward convergence, due to a change in motion of the colliding plates or the late involvement of a north-moving plate, such as the Ruker Terrane of the SPCM. Major south-directed recumbent folding and thrusting in the Ruker Terrane could be of this age. Although a collisional setting is likely, Harley (1988, 1991) has shown that the gradients

of the P–T-time paths commonly also require magmatic underplating to enhance the heat budget. He also suggested that unusually rapid uplift in the Rauer Islands required some degree of extension of the previously thickened crust. Post-peak extension would be consistent with the emplacement of late-orogenic mafic dykes in some parts of the c.1000 Ma terrane.

In contrast to this decompression-dominated retrogression, reaction textures in metamorphic rocks of the Porthos Range area of the Beaver-Lambert Terrane indicate a post-peak period of near-isobaric cooling, with little or no decompression (Fitzsimons & Harley 1992; Fitzsimons & Thost 1992; Thost & Hensen 1992). This near-isobaric cooling was attributed by Fitzsimons & Harley (1992) to the area having been situated near the edge of the orogenic belt which was still undergoing thickening (compression) during the waning stages of the collisional event, when the centre of the belt was undergoing collapse. Metapelites in the Reinbolt Hills contain evidence for significant decompression, from 7 to 5 kilobars (Nichols & Berry 1991). At Jetty Peninsula, a post- M_1 period of near-isobaric cooling was apparently followed by one of post- M_2 decompression associated with some reheating, suggesting a link between the NPCM and Amery Ice Shelf area (Hand et al. 1994b).

The early Neoproterozoic tectonic evolution of the Beaver-Lambert Terrane was clearly complex, although this is not surprising given the size of the terrane: P–T-time paths for a single metamorphic event can range from clockwise to anticlockwise, depending on distance from the heat source (Stüwe & Sandiford 1995). However, as Thost et al. (1991) and Stüwe & Hand (1992) have pointed out, reconstructed P–T-time paths do not necessarily imply a single progressive tectonothermal event, but may reflect two unrelated events. Thus, Scrimgeour & Hand (1997) suggested that the post- M_2 decompression reaction textures in the Jetty Peninsula granulites may be co-eval with similar features which characterise c.500 Ma metamorphics in the central Prydz Bay coast—that is, the low-pressure M_2 assemblages may be of Pan-African age (Carson et al. 1995; Dirks & Hand 1995; Fitzsimons 1996). On the other hand, decompression textures also characterise much of the c.1000 Ma Rayner Complex. Isotopic data do not unambiguously support a c.500 Ma high-grade event in the NPCM, as Sm–Nd garnet–whole rock ages are more likely to reflect isotopic resetting (Kinny 1998) than garnet growth (Zhou & Hensen 1995). Moreover, Scrimgeour & Hand's (1997) correlation of the east–west high-grade shear zones (D_6 of Fitzsimons & Thost 1992), and apparently therefore M_2 , with the c.500 Ma event seems at variance with the evidence of Hand et al. (1994a) that similar structures at Jetty Peninsula are roughly co-eval with 940 ± 20 Ma garnet leucogranite dykes. In the absence of definitive geochronological data, the age of M_2 at Jetty Peninsula remains uncertain, and a relationship to either the c.1000 or the 500 Ma is possible.

Compositions of syn- to late-orogenic orthopyroxene granitoids in the Beaver-Lambert Terrane support a tectonic model involving both mantle-derived additions to the crust and high-temperature crustal melting of overthickened crust. They have a wide range of composition, and comprise low-SiO₂ varieties (quartz monzonite to granite) which were probably derived by fractionation of mantle-derived mafic to intermediate

magmas, and high-SiO₂ granites that have major crustal components—although there may well be a continuum between these two extremes (Sheraton et al. 1996). Syenitic rocks of Mount Collins may have had a similar origin, although fractionation of an alkali basalt, rather than tholeiitic, parent magma is likely. Most high-SiO₂ orthopyroxene granitoids have low Y, suggesting high-pressure melting with residual garnet, although they have very different compositions to the Y-depleted tonalitic orthogneisses. Low-Y compositions of the low-Ti phase of the Mawson Charnockite were taken by Young & Ellis (1991) to imply melting of thickened crust in an Andean or Himalayan-type plate margin. However, Beaver-Lambert Terrane orthopyroxene granitoids show no obvious regional compositional variations that can be correlated with the development of thickened crust in a collisional belt—that is, no particular concentration of Y-depleted granitoids requiring residual garnet. Such granitoids are most common in the NPCM where the country rocks show evidence for near-isobaric cooling, which is more consistent with only limited thickening and therefore little subsequent uplift. This suggests that magmatic underplating may have been at least as important a factor in magma generation as major crustal thickening (cf. Ellis 1987). Both Y-depleted (low-Ti) and Y-undepleted (high-Ti) varieties of the Mawson Charnockite are present in the same area of the Mawson Coast (Young & Ellis 1991). Other granitoids in the Beaver-Lambert Terrane have compositions consistent with intracrustal melting during the granulite event. Garnet granitoids were formed by the melting of predominantly metasedimentary country rocks. The A-type chemical features (high Zr, Nb, Y, REE) of Mount Collins hornblende-biotite granitoids presumably reflect unusually high-temperature, relatively dry melting of igneous precursors during the later part of the high-grade metamorphism, rather than a strictly 'anorogenic' setting.

There is thus some evidence for an evolution of granitoids in the Beaver-Lambert Terrane from early tonalitic to granodioritic continental arc types (low-moderate LILE, low HFSE: Y-depleted orthogneiss and most Fisher Massif granitoids), through mature arc types (higher LILE, low HFSE: some orthopyroxene granitoids), to late-orogenic and 'within-plate' (A-type) granitoids (high LILE and HFSE: some orthopyroxene granitoids, as well as Cambrian A-types). Such a trend would be consistent with a tectonic evolution from an Andean-type plate margin, which existed about 1300 Ma ago, to one of continental collision by 1000 Ma. Development of an extensional regime soon after the emplacement of the plutonic rocks at Mount Collins is suggested by the presence of, as yet undated, metadolerite dykes. A similar evolutionary trend is shown by granitoids in the Bunger Hills, where dolerite dykes were emplaced shortly after major plutonism at 1170–1150 Ma (Sheraton et al. 1995).

The effects of the c.500 Ma Pan-African event are widespread in the East Antarctic Shield. Most areas show evidence for felsic magmatism and isotopic resetting at about 550–500 Ma, with only the sector from east of the Bunger Hills to Adelie Land seemingly lacking such evidence (Sheraton et al. 1995). Farther east, in George V and Oates Lands, c.500 Ma activity was apparently related to the Ross orogeny in the Transantarctic Mountains (Elliot 1975). The Prydz Bay coast and probably the Grove

Mountains area, the Denman Glacier–Mirny area of Queen Mary Land and the Lützow-Holm Complex of eastern Dronning Maud Land appear to have undergone a c.500 Ma regional tectonothermal event. Syenitic plutons were emplaced in the Denman Glacier area at 516±1.5 Ma. New zircon growth and Pb loss from older zircon occurred in nearby tonalitic orthogneiss at 600–500 Ma, although the age of the high-grade metamorphism in this area is not conclusively established (Black et al. 1992b). The Lützow-Holm Complex, and possibly part of the nearby Rayner Complex, underwent amphibolite–granulite-facies metamorphism about 550–520 Ma ago—the first reported Pan-African mobile belt in East Antarctica (Shiraishi et al. 1992, 1994, 1997; Fraser et al. 1995), although there is petrographic and structural evidence for at least one earlier high-grade event (Yoshida 1994). U–Pb zircon dating of biotite gneisses from the Sør Rondane Mountains indicates an early granulite-facies event at about 1110 Ma, with resetting at about 458 Ma during a Pan-African amphibolite-facies event (Grew et al. 1992). Orthopyroxene-bearing syenite in the Humboldt Mountains of central Dronning Maud Land has given a U–Pb zircon age of 512±2.3 Ma (Mikhalsky et al. 1997). In western Dronning Maud Land, Pan-African overprinting was largely confined to discrete shear zones (Jacobs et al. 1995).

Like the c.1000 event, the c.500 Ma Pan-African event appears to have been related to continental assembly, in this case of Gondwana. It probably was not completed until the early to middle Cambrian (Powell et al. 1993; Unrug 1996). The exact nature of this event, at least in the PCM area, is even more enigmatic than that of the earlier one, because the East Antarctica–Australia–India block appears to have behaved as essentially a single unit during the intervening period (Hoffman 1991; Dalziel 1992; Unrug 1996). No suture zone or ophiolite marking the closure of the palaeoceanic basin at that time have been found, and juvenile volcanic rocks are unknown. However, a collisional plate tectonic setting has been proposed for the Pan-African event elsewhere in East Antarctica. For example, Sheraton et al. (1995) suggested a collisional model for the Denman Glacier–Mirny area, which can be correlated with the co-eval Leeuwin Block of the extreme southwest of Australia, to explain the subsequent uplift of the area. The area is separated from the c.1200 Ma Bunger Hills terrane by the Denman Glacier, and the Leeuwin Block is separated from the c.1200 Ma Albany–Fraser Province by the Perth Basin. The Denman Glacier–Perth Basin therefore could be the site of a suture between a Pan-African terrane in the west and a late Mesoproterozoic terrane in the east. Myers (1990) pointed out that assembly of this part of Gondwana was probably not completed until the beginning of the Palaeozoic. A collisional tectonic setting for this area could be consistent with published Rodinia and Gondwana reconstructions, because it is uncertain how far east (i.e., towards Australia) the Indian portion of Gondwana (the Meghalaya Province: Harris 1993) extended at that time (Powell et al. 1988). Hoffman (1991) and Dalziel (1992) showed a Phanerozoic orogen in this northern part of India.

Shiraishi et al. (1987) postulated a tectonic model for the development of the c.500 Ma Lützow-Holm and adjacent Yamato-Belgica Complexes involving southwest-directed collision between the Archaean to Neoproterozoic Napier and Rayner Complexes and a Neoproterozoic block to the west. Shiraishi et al. (1994) suggested that this Pan-African

belt, which also includes the Highland–Southwestern Complex of Sri Lanka, formed during assembly of East and West Gondwana by closure of the ‘Mozambique Ocean’ (Dalziel 1992). Such a model is consistent with the clockwise decompressive P–T–time path interpreted for the Lützow-Holm Complex, and with early high-pressure associations (relict kyanite + staurolite inclusions in garnet: Shiraishi et al. 1987; Motoyoshi, 1990). Kriegsman (1995) interpreted the Pan-African event in Sri Lanka and the Lützow-Holm Complex in terms of collision in the Mozambique Belt causing underthrusting of basement units, followed by high-grade metamorphism and extensional collapse.

In the PCM it is difficult to substantiate a direct relationship between c.500 Ma metamorphism and continental collision, because this part of East Antarctica appears to have been adjacent to India at that time. Boger et al. (2001) proposed that the Beaver-Lambert and Ruker Terranes did not accrete until Pan-African times. However, the limited isotopic data are by no means conclusive, and the presence of Archaean relics in the southern part of the Beaver-Lambert Terrane (the central and northern Mawson Escarpment) is difficult to explain on their model. Similarly, Harley et al. (1998) suggested that the Rauer Islands terrane might not have amalgamated with the c.500 Ma rocks of the Prydz Bay coast, and possibly with the Vestfold Hills, until Pan-African times. Decompressional reaction textures in metapelitic rocks at Brattstrand Bluffs indicate about 11 kilometres of exhumation after the metamorphic peak (Fitzsimons 1996), and similar retrograde reaction textures occur along much of the Prydz Bay coast (Stüwe & Powell 1989; Fitzsimons & Harley 1991; Motoyoshi et al. 1991). Dirks & Hand (1995) and Dirks & Wilson (1995) postulated that exhumation followed an early compressional event involving major crustal thickening, which then gave way to one of extensional collapse. Fitzsimons & Harley (1991) also suggested extensional collapse of overthickened crust. The composition of c.504 Ma orthopyroxene granite in the Grove Mountains suggests late-orogenic magmatism in a collision zone.

In contrast, Stüwe & Powell (1989) considered that peak metamorphic pressures in the Larsemann Hills area (about 4.5 kb) were too low to have been a consequence of thermal relaxation of overthickened crust with normal mantle heat flow, making a collisional model inappropriate. They proposed that an asthenospheric perturbation resulted in extensive magmatic underplating and hence near-isothermal decompression of the terrane. Stüwe & Sandiford (1993) proposed that early Palaeozoic exhumation of the East Antarctic Shield by as much as 10–15 kilometres was caused by substantial basaltic underplating during a period of minor lithospheric thinning. Such a model would explain the lack of an associated pervasive deformation in most of the shield. It would also explain the presence of abundant high-temperature crustal melts (‘A-type’ hornblende–biotite granites) in the eastern Amery Ice Shelf area. Similarly, the presence of voluminous granitoids with A-type affinities and associated lamproitic dykes in western Dronning Maud Land was explained by Groenewald (1995) in terms of underplating by asthenosphere-derived magmas. Moyes et al. (1993) also favoured large-scale underplating over subduction-related processes to explain the effects of the c.500 Ma event in western Dronning Maud Land, which

were largely confined to isotopic resetting, minor felsic magmatism, and open folding, but which may have reached amphibolite to lower granulite-facies (Moyes & Groenewald 1996). These effects are similar to those in most of the Beaver-Lambert Terrane.

A possible tectonic evolutionary model that resolves some of these difficulties, while being consistent with geological evidence, includes both processes. A c.1000 Ma collisional event would have resulted in crustal thickening and relatively high-pressure metamorphism followed by uplift and decompression in much of the terrane, including the Rayner Complex. Magmatic underplating was probably also important. The presence of orthogneissic basement rocks in much of the Prydz Bay coast, as well as a significant amount of isotopic data for a c.1000 event, makes it likely that this area was also involved in the early Neoproterozoic metamorphism. However, if some of the metasedimentary cover sequences post-date this event, then this part of the terrane must have been exhumed to the surface at some stage of the Neoproterozoic. The much younger c.500 Ma event may have been dominated by underplating in the PCM area, but the probability of continental collision in nearby parts of the East Antarctic Shield (Lützow-Holm Bay, Denman Glacier area, and possibly the Grove Mountains) makes it possible that a zone of compressional deformation also existed at that time along the Indo-Antarctic suture—somewhat akin to the model suggested by Kriegsman (1995) for the Lützow-Holm–Sri Lanka area. Formation of retrograde shear zones in the Rayner Complex was apparently a consequence of northward thrusting at this time (Clarke 1988). It is debatable to what extent this zone was part of a Pan-African ‘mobile belt’, as suggested by Carson et al. (1996) and Boger et al. (2001), and it seems premature to dismiss the notion of an originally continuous Grenvillean terrane in the area (Hensen & Zhou 1995). Nevertheless, the Pan-African event was clearly of much greater significance in the geological evolution of East Antarctica than was once believed, but only future work will show which (if any) of the models discussed here is correct.

Whatever the exact nature of the Pan-African event, it was clearly responsible for the final exhumation of the terrane towards the surface—apparently achieved in at least part of the Beaver-Lambert Terrane by the Carboniferous (Arne 1994). This uplift was accompanied by extensive faulting and emplacement of alkaline mafic dykes, probably associated with the initial formation of the Lambert Graben. Eventual breakup of the Gondwana supercontinent occurred during the Jurassic and Cretaceous. India rifted off Antarctica between about 127 and 118 Ma ago (Lawver et al. 1991), which was a time of alkaline igneous activity.

All of the major Mesoproterozoic to Phanerozoic geological events in this part of East Antarctica can thus be related to the assembly and breakup of continental terranes. A felsic magmatic event of unknown extent and significance at c.800–750 Ma may have been related to the breakup of Rodinia that took place at about that time (Powell 1998). The tectonic evolution of the various early Precambrian cratonic blocks, such as the Napier Complex (Harley & Black 1997) and Ruker Terrane, probably involved similar processes, although, in most cases, there are insufficient geological and geochronological data to document their histories in detail.

REFERENCES

- Adams C.J., Gabites J.E. & Grindley G.W. 1982. Orogenic history of the central Transantarctic Mountains: New K–Ar age data on the Precambrian–lower Paleozoic basement. In: Craddock C. (editor). *Antarctic geoscience*. University of Wisconsin Press, Madison; 817–826.
- Aleksashin N.D. & Laiba A.A. 1993. Stratigraphy and lithofacial features of Permian sedimentary sequence of the western coast of Beaver Lake (Prince Charles Mountains, East Antarctica) (in Russian). *The Antarctic*. Russian Committee on Antarctic Research; report 31: 43–51.
- Allègre C.J., Treuill M., Minster J-F., Minster B. & Albarede F. 1977. Systematic use of trace elements in igneous processes, Part 1: Fractional crystallisation processes in volcanic suites. *Contributions to Mineralogy and Petrology*; 60: 57–75.
- Andreeva E.D., Kononova V.A., Sveshnikova E.V. & Yashina R.M. 1984. *Igneous rocks, volume 2* (in Russian). Nauka, Moscow.
- Andronikov A.V. 1987. Deep-seated minerals from alkaline ultramafic rocks of East Antarctica (in Russian). In: *Geologo-geofizicheskie issledovaniya v Antarktike*. Sevmorgeologiya, Leningrad; 48–53.
- Andronikov A.V. 1990. Spinel–garnet lherzolite nodules from alkaline–ultrabasic rocks of Jetty Peninsula (East Antarctica). *Antarctic Science*; 2: 321–330.
- Andronikov A.V. 1992. The first study of mantle inclusions from the Prince Charles Mountains, East Antarctica. In: Yoshida Y. (editor). *Recent progress in Antarctic earth science*. Terra Scientific Publishing Company, Tokyo; 163–171.
- Andronikov A.V. 1997. Varying glass compositions in deep-seated inclusions from alkaline–ultramafic rocks of Jetty Peninsula (East Antarctica): Evidence for mantle metasomatism. In: Ricci C.A. (editor). *The Antarctic region: Geological evolution and processes*. Terra Antarctica Publication, Siena; 901–910.
- Andronikov A.V. & Beliatsky B.V. 1995. Implication of Sm–Nd isotopic systematics to the events recorded in the mantle-derived xenoliths (Jetty Peninsula, East Antarctica). *Terra Antarctica*; 2: 103–110.
- Andronikov A.V. & Egorov L.S. 1992. High-K basaltoids of Manning Massif (in Russian). *The Antarctic*. Soviet Committee on Antarctic Research; report 30: 31–41.
- Andronikov A.V. & Egorov L.S. 1993. Mesozoic alkaline–ultrabasic magmatism of Jetty Peninsula. In: Findley R.H., Unrug R., Banks M.R. & Veevers J.J. (editors). *Gondwana eight: Assembly, evolution and dispersal*. Balkema, Rotterdam; 547–557.
- Andronikov A.V. & Mikhalsky E.V. 1997. Deep-seated xenoliths from Proterozoic ultramafic lamprophyre dykes of the Vestfold Hills (East Antarctica): Evidence for the existence of metasomatized lithosphere. In: Ricci C.A. (editor). *The Antarctic region: Geological evolution and processes*. Terra Antarctica Publication, Siena; 911–921.
- Andronikov A.V. & Sheraton J.W. 1996. The redox state of lithospheric upper mantle beneath the East Antarctic Shield. *Terra Antarctica*; 3: 39–48.
- Andronikov A.V., Mikhalsky E.V. & Beliatsky B.V. 1994. Deep-seated inclusions in alkaline lamprophyres from the Vestfold Hills (East Antarctica). *Petrologiya*; 2: 288–295.
- Andronikov A.V., Foley S.F. & Beliatsky B.V. 1998. Sm–Nd and Rb–Sr isotopic systematics of the East Antarctic Manning Massif alkaline trachybasalts and the development of the mantle beneath the Lambert–Amery rift. *Mineralogy and Petrology*; 63: 243–261.
- Arculus R.J. & Powell R. 1986. Source component mixing in the regions of arc magma generation. *Journal of Geophysical Research*; 91: 5913–5926.
- Argutin A.V. 1989. Geological and geophysical research in Antarctica in the 34th SAE. Unpublished PMGRE open file report, part 3.
- Arndt N.T., Chauvel C., Todt W., Tapfer M. & Weber K. 1989. Granulites in the Koltas Mountains, Antarctica: Geology, geochronology and geochemistry (abstract). *International Workshop on Antarctic Geochronology*, Ludwig-Maximilians University, Munich, Germany; 6.
- Arne D.C. 1994. Phanerozoic exhumation history of northern Prince Charles Mountains (East Antarctica). *Antarctic Science*; 6: 69–84.
- Arriens P.A. 1975. Precambrian geochronology of Antarctica (abstract). 1st Australian Geological Convention, Adelaide. Geological Society of Australia; 97–98.
- Bailey D.K. 1987. Mantle metasomatism—perspective and prospect. In: Fitton J.G. & Upton B.G.J. (editors). *Alkaline igneous rocks*. Geological Society of London; special publication 30: 1–12.
- Ballhaus C. 1995. Platinum-group elements as tracers for mantle redox states. *European Journal of Mineralogy*; 7: 12.
- Balme B.E. & Playford G. 1967. Late Permian plant microfossils from the Prince Charles Mountains, Antarctica. *Revue de Micropaléontologie*; 10: 179–192.
- Bardin V.I. 1982. Composition of East Antarctic moraines and some problems of Cenozoic history. In: Craddock C. (editor). *Antarctic geoscience*. University of Wisconsin Press, Madison; 1069–1076.
- Bardin V.I. & Belevich A.M. 1985. Early glacial deposits in the Prince Charles Mountains (in Russian). *The Antarctic*. Soviet Committee on Antarctic Research; report 24: 76–81.
- Bardin V.I. & Kolosova G.N. 1988. Paleoglacial sediments on the coast of Radok Lake (in Russian). *The Antarctic*. Soviet Committee on Antarctic Research; report 27: 66–75.
- Bardin V.I., Glushankova N.I. & Sudakova N.G. 1976. Lithology of moraine of East Antarctica (in Russian). *The Antarctic*. Soviet Committee on Antarctic Research; report 15: 53–71.
- Barker F. 1979. Trondhjemite: Definition, environment and hypotheses of origin. In: Barker F. (editor). *Trondhjemites, dacites and related rocks*. Elsevier, Amsterdam; 1–12.
- Barton J.M. Jr, Klemd R., Allsopp H.L., Auret S.H. & Copperthwaite Y.E. 1987. The geology and geochronology of the Annandagstoppane granite, western Dronning Maud Land, Antarctica. *Contributions to Mineralogy and Petrology*; 97: 488–496.

- Beard J.S., Lofgren G.E., Sinha A.K. & Tollo R.P. 1994. Partial melting of apatite-bearing charnockite, granulite and diorite: Melt compositions, restite mineralogy and petrologic implications. *Journal of Geophysical Research*; 99: 21591–21603.
- Beliatsky B.V., Laiba A.A. & Mikhalsky E.V. 1994. U–Pb zircon age of the metavolcanic rocks of Fisher Massif (Prince Charles Mountains, East Antarctica). *Antarctic Science*; 6: 355–358.
- Bennett A.J.R. & Taylor G.H. 1972. Coals from the vicinity of the Prince Charles Mountains. In: Adie R.J. (editor). *Antarctic geology and geophysics*. Universitetsforlaget, Oslo; 591–598.
- Bergman S.C. 1987. Lamproites and other potassium-rich igneous rocks: A review of their occurrences, mineralogy and geochemistry. In: Fitton J.G. & Upton B.G.J. (editors). *Alkaline igneous rocks*. Geological Society of London; special publication 30: 103–190.
- Bertrand K.J. 1967. A look at Operation Highjump twenty years later. *Antarctic Journal of the US*; 1: 5.
- Black L.P. & James P.R. 1983. Geological history of the Napier Complex of Enderby Land. In: Oliver R.L., James P.R. & Jago J.B. (editors). *Antarctic earth science*. Australian Academy of Science, Canberra; 11–15.
- Black L.P. & Sheraton J.W. 1990. The influence of Precambrian source components on the U–Pb zircon age of a Palaeozoic granite from northern Victoria Land, Antarctica. *Precambrian Research*; 46: 275–293.
- Black L.P., James P.R. & Harley S.L. 1983. Geochronology and geological evolution of metamorphic rocks in the Field Islands area, East Antarctica. *Journal of Metamorphic Geology*; 1: 277–303.
- Black L.P., Williams I.S. & Compston W. 1986a. Four zircon ages from one rock: The history of a 3930 Ma-old granulite from Mount Sones, Antarctica. *Contributions to Mineralogy and Petrology*; 94: 427–437.
- Black L.P., Sheraton J.W. & James P.R. 1986b. Late Archaean granites of the Napier Complex, Enderby Land, Antarctica: A comparison of Rb–Sr, Sm–Nd and U–Pb isotopic systematics in a complex terrain. *Precambrian Research*; 32: 343–368.
- Black L.P., Harley S.L., Sun S.-S. & McCulloch M.T. 1987. The Rayner Complex of East Antarctica: Complex isotopic systematics within a Proterozoic mobile belt. *Journal of Metamorphic Geology*; 5: 1–26.
- Black L.P., Kinny P.D. & Sheraton J.W. 1991a. The difficulties of dating mafic dykes: An Antarctic example. *Contributions to Mineralogy and Petrology*; 109: 183–194.
- Black L.P., Kinny P.D., Sheraton J.W. & Delor C.P. 1991b. Rapid production and evolution of late Archaean felsic crust in the Vestfold Block of East Antarctica. *Precambrian Research*; 50: 283–310.
- Black L.P., Harris L.B. & Delor C.P. 1992a. Reworking of Archaean and early Proterozoic components during a progressive, middle Proterozoic tectonothermal event in the Albany Mobile Belt, Western Australia. *Precambrian Research*; 59: 95–123.
- Black L.P., Sheraton J.W., Tingey R.J. & McCulloch M.T. 1992b. New U–Pb zircon ages from the Denman Glacier area, East Antarctica, and their significance for Gondwana reconstruction. *Antarctic Science*; 4: 447–460.
- Bogatikov O.A., Bogdanova S.V. & Borsuk A.M. 1987. Magmatic rocks (The evolution of magmatism in Earth history) (in Russian). Nauka, Moscow.
- Boger S.D., Carson C.J., Wilson C.J.L. & Fanning C.M. 2000. Neoproterozoic deformation in the Radok Lake region of the Northern Prince Charles Mountains, East Antarctica; Evidence for a single protracted orogenic event. *Precambrian Research*; 104: 1–24.
- Boger S.D., Wilson C.J.L. & Fanning C.M. 2001. Early Paleozoic tectonism within the East Antarctic craton: the final suture between east and west Gondwana? *Geology*; 29: 463–466.
- Bohlen S.R. & Liotta J.J. 1986. A barometer for garnet amphibolites and garnet granulites. *Journal of Petrology*; 27: 1025–1034.
- Bohlen S.R., Wall V.J. & Boettcher A.L. 1983a. Experimental investigation and application of garnet granulite equilibria. *Contributions to Mineralogy and Petrology*; 83: 52–61.
- Bohlen S.R., Wall V.J. & Boettcher A.L. 1983b. Experimental investigations and geological applications of equilibria in the system $\text{FeO-TiO}_2\text{-Al}_2\text{O}_3\text{-SiO}_2\text{-H}_2\text{O}$. *American Mineralogist*; 68: 1049–1058.
- Bohlen S.R., Wall V.J. & Boettcher A.L. 1983c. Geobarometry in granulites. In: Saxena S.K. (editor). *Kinetics and equilibrium in mineral reactions: Advances in physical geochemistry*, volume 3. Springer-Verlag, New York; 141–172.
- Boyd F.R. 1973. A pyroxene geotherm. *Geochimica et Cosmochimica Acta*; 37: 2533–2546.
- Buick I.S., Harley S.L. & Fitzsimons I.C.W. 1990. Equilibria in granulite facies calc-silicates: Implications for granulite facies metamorphism in East Antarctica. *Geological Society of Australia*; abstracts 25: 254.
- Cantrill D.J., Drinnan A.N. & Webb J.A. 1995. Late Triassic plant fossils from the Prince Charles Mountains, East Antarctica. *Antarctic Science*; 7: 51–62.
- Carmichael I.S.E. 1967. The mineralogy and petrology of the volcanic rocks from the Leucite Hills, Wyoming. *Contributions to Mineralogy and Petrology*; 15: 24–66.
- Carson C.J., Dirks P.G.H.M., Hand M., Sims J.P. & Wilson C.J.L. 1995. Compressional and extensional tectonics in low–medium pressure granulites from the Larsemann Hills, East Antarctica. *Geological Magazine*; 132: 151–170.
- Carson C.J., Fanning C.M. & Wilson C.J.L. 1996. Timing of the Progress Granite, Larsemann Hills: Additional evidence for early Palaeozoic orogenesis within the east Antarctic Shield and implications for Gondwana assembly. *Australian Journal of Earth Sciences*; 43: 539–553.
- Carson C.J., Boger S.D., Fanning C.M., Wilson C.J.L. & Thost D.E. 2000. SHRIMP U–Pb geochronology from Mount Kirkby, Northern Prince Charles Mountains, East Antarctica. *Antarctic Science*; 12: 429–442.
- Chaika V.M. & Uzhgalis E.V. 1976. Orogenic magmatism of Sahara swells and rifts (central part of northern Africa) (in Russian). *Moskovskoe Obschestvo Ispytatelei Prirody*, geological section; bulletin 51: 133–144.
- Champion D.C. & Sheraton J.W. 1997. Geochemistry and Nd isotopic systematics of Archaean granites of the Eastern Goldfields, Yilgarn Craton, Australia: Implications for crustal growth processes. *Precambrian Research*; 83: 109–132.
- Chappell B.W. & White A.J.R. 1974. Two contrasting granite types. *Pacific Geology*; 8: 173–174.
- Ciesielski P.F. 1983. The Neogene and Quaternary diatom biostratigraphy of subantarctic sediments, Deep Sea Drilling Project Leg 71. In: Ludwig W.J., Krashennnikov V.A., et al. (editors). *Initial reports of DSDP 71, part 2*. United States Government Printing Office, Washington; 635–665.
- Clarke G.L. 1988. Structural constraints on the Proterozoic reworking of Archaean crust in the Rayner Complex, MacRobertson and Kemp Land coast, East Antarctica. *Precambrian Research*; 40/41: 137–156.
- Clarke G.L. & Norman A.R. 1993. Generation of pseudotachylite under granulite facies conditions, and its preservation during cooling. *Journal of Metamorphic Geology*; 11: 319–335.
- Cliff R.A. 1985. Isotopic dating in metamorphic belts. *Journal of the Geological Society of London*; 142: 97–110.
- Collerson K.D. & Sheraton J.W. 1986a. Age and geochemical characteristics of a mafic dyke swarm in the Archaean Vestfold Block, Antarctica: Inferences about Proterozoic dyke emplacement in Gondwana. *Journal of Petrology*; 27: 853–886.

- Collerson K.D. & Sheraton J.W. 1986b. Bedrock geology and crustal evolution of the Vestfold Hills. In: Pickard J. (editor). *Antarctic oasis*. Academic Press, Sydney; 21–62.
- Collins W.J., Beams S.D., White A.J.R. & Chappell B.W. 1982. Nature and origin of A-type granites with particular reference to southeastern Australia. *Contributions to Mineralogy and Petrology*; 80: 189–200.
- Connelly J.N. & Heaman L.M. 1993. U–Pb geochronological constraints on the tectonic evolution of the Grenville Province, western Labrador. *Precambrian Research*; 63: 123–142.
- Craddock C.C. 1972. Geological map of Antarctica, scale 1:15 000 000. American Geographical Society, New York.
- Crawford A.R. 1974. Indo-Antarctica, Gondwanaland, and the distortion of a granulite belt. *Tectonophysics*; 22: 141–157.
- Crohn P.W. 1959. A contribution to the geology and glaciology of the western part of Australian Antarctic Territory. Bureau of Mineral Resources, Australia; bulletin 52.
- Dalziel I.W.D. 1991. Pacific margins of Laurentia and East Antarctica–Australia as a conjugate rift pair: Evidence and implications for an Eocambrian supercontinent. *Geology*; 19: 598–601.
- Dalziel I.W.D. 1992. Antarctica; a tale of two supercontinents? *Annual Review of Earth and Planetary Sciences*; 20: 501–526.
- Danchin R.V. 1967. Chromium and nickel in the Fig Tree Shale from South Africa. *Science*; 158: 261.
- Dawson J.B. 1980. *Kimberlites and their xenoliths*. Springer-Verlag, Berlin.
- Delor C.P. & Rock N.M.S. 1991. Alkaline-ultramafic lamprophyre dykes from the Vestfold Hills, Princess Elizabeth Land (East Antarctica): Primitive magmas of deep mantle origin. *Antarctic Science*; 3: 419–432.
- DePaolo D.J. 1981. Trace element and isotopic effects of combined wallrock assimilation and fractional crystallisation. *Earth and Planetary Science Letters*; 53: 189–202.
- DePaolo D.J. & Wasserburg G.J. 1976. Nd isotopic variations and petrogenetic models. *Geophysical Research Letters*; 3: 249–252.
- Dibner A.F. 1976. Late Permian palynofloras from sedimentary rocks from the Beaver Lake area, East Antarctica (in Russian). *The Antarctic. Soviet Committee on Antarctic Research; report 15*: 41–52.
- Dickinson W.R., Beard L.S., Brakenridge G.R., Rejavec J.L., Ferguson R.C., Inman K.F., Knepp R.A., Lindberg F.A. & Ryberg R.T. 1983. Provenance of North American Phanerozoic sandstones in relation to tectonic setting. *Geological Society of America; bulletin 93*: 222–235.
- Dirks P.H.G.M. & Hand M. 1995. Clarifying temperature–pressure paths via structures in granulite from the Bolingen Islands, Antarctica. *Australian Journal of Earth Sciences*; 42: 157–172.
- Dirks P.H.G.M. & Wilson C.J.L. 1995. Crustal evolution of the East Antarctic mobile belt in Prydz Bay: Continental collision at 500 Ma? *Precambrian Research*; 75: 189–207.
- Dirks P.H.G.M., Carson C.J. & Wilson C.J.L. 1993. The deformational history of the Larsemann Hills, Prydz Bay: The importance of the Pan-African (500 Ma) in East Antarctica. *Antarctic Science*; 5: 179–192.
- Dunkley D.J. 1998. The Rayner Complex in MacRobertson Land, East Antarctica. Unpublished PhD thesis, University of Sydney.
- Dunkley D.J., Clarke G.L., Nelson D. & White R.W. 1995. Temporal resolution of complex tectono-metamorphic episodes: A case Proterozoic orogen at Cape Bruce, MacRobertson Land, East Antarctica. VII International Symposium on Antarctic Earth Sciences, Siena, 10–15 September; abstract volume: 116.
- Ebadi A. & Johannes W. 1991. Beginning of melting and composition of first melts in the system Qz–Ab–Or–H₂O–CO₂. *Contributions to Mineralogy and Petrology*; 106: 286–295.
- Eby G.N. 1990. The A-type granitoids: A review of their occurrence and chemical characteristics and speculations on their petrogenesis. *Lithos*; 26: 115–134.
- Egorov L.S. 1969. Melilite rocks of the Maimecha–Kotui province (in Russian). *Trudy Nauchno-Issledovatel'skogo Instituta Geologii Arctiki*; 159.
- Egorov L.S. 1994. Some petrologic, geochemical and genetic peculiarities of the hypabyssal alkaline-ultramafic rocks with the example of the polzenite–alkaline picrite complex of Jetty Peninsula (Prince Charles Mountains, East Antarctica) (in Russian). *Geokhimiya*; 1: 24–39.
- Egorov L.S. & Andronikov A.V. 1993. Prospects of mineral detection associated with alkaline-ultrabasic rocks (Prince Charles Mountains). In: Findlay R.H., Unrug R., Banks M.R. & Veevers J.J. (editors). *Gondwana eight: Assembly, evolution and dispersal*. Balkema, Rotterdam; 559–562.
- Egorov L.S., Melnik A.Yu. & Ukhonov A.V. 1993. First finding of a kimberlite dyke containing syngenetic calcite carbonatite schlieren in Antarctica (in Russian). *Doklady Rossiiskoi Akademii Nauk*; 328: 230–233.
- Ellam R.M. & Cox K.G. 1989. A Proterozoic lithospheric source for Karoo magmatism: Evidence from the Nuanetsi picrites. *Earth and Planetary Science Letters*; 92: 207–218.
- Elliot D.H. 1975. Tectonics of Antarctica: A review. *American Journal of Science*; 275A: 45–106.
- Ellis D.J. 1987. Origin and evolution of granulites in normal and thickened crust. *Geology*; 15: 167–170.
- Ellis D.J. & Green D.H. 1979. An experimental study on the effect of Ca upon garnet–clinopyroxene Fe–Mg exchange equilibria. *Contributions to Mineralogy and Petrology*; 71: 13–22.
- Ellis D.J. & Hiroi Y. 1997. Secondary siderite–oxide–sulphide and carbonate–andalusite assemblages in cordierite granulites from Sri Lanka: Post-granulite facies fluid evolution during uplift. *Contributions to Mineralogy and Petrology*; 127: 315–335.
- Emslie R.F. & Hegner E. 1993. Reconnaissance isotopic geochemistry of anorthosite–mangerite–charnockite–granite (AMCG) complexes, Grenville Province, Canada. *Chemical Geology*; 106: 279–298.
- England R.N. & Langworthy A.P. 1975. Geological work in Antarctica—1974. Bureau of Mineral Resources, Australia; record 1975/30.
- Erlank A.J., Smith H.S., Marchant J.W., Cardoco M.P. & Ahrens L.H. 1978. Zirconium. Abundance in common sediments and sedimentary rock types. In: Wedepohl K.H. (editor). *Handbook of geochemistry*. Springer-Verlag, Berlin; II-4, 40-K1–8.
- Ernst W.G. 1962. Synthesis, stability relations and occurrence of riebeckite and riebeckite–arfvedsonite solid solutions. *Journal of Geology*; 70: 689–736.
- Evensen N.M., Hamilton P.J. & O'Nions R.K. 1978. Rare-earth abundances in chondritic meteorites. *Geochimica et Cosmochimica Acta*; 42: 1199–1212.
- Fedorov L.V., Ravich M.G. & Hofmann J. 1982a. Geologic comparison of southeastern peninsular India and Sri Lanka with a part of East Antarctica (Enderby Land, MacRobertson Land, and Princess Elizabeth Land). In: Craddock C. (editor). *Antarctic geoscience*. University of Wisconsin Press, Madison; 73–78.
- Fedorov L.V., Grikurov G.E., Kurinin R.G. & Masolov V.N. 1982b. Crustal structure of the Lambert Glacier area from geophysical data. In: Craddock C. (editor). *Antarctic geoscience*. University of Wisconsin Press, Madison; 931–936.

- Fergusson C.L. 1998. Comparison of the central Andes with the Silurian–Devonian Lachlan Fold Belt, southeastern Australia. *Geological Society of Australia; Abstracts* 49: 140.
- Ferry J.M. & Spear F.S. 1978. Experimental calibration of the partitioning of Fe and Mg between biotite and garnet. *Contributions to Mineralogy and Petrology*; 66: 113–117.
- Fielding C.R. & Webb J.A. 1995. Sedimentology of the Permian Radok Conglomerate in the Beaver Lake area of MacRobertson Land, east Antarctica. *Geological Magazine*; 132: 51–63.
- Fielding C.R. & Webb J.A. 1996. Facies and cyclicity of the Late Permian Bainmedart Coal Measures in the Northern Prince Charles Mountains, MacRobertson Land, Antarctica. *Sedimentology*; 43: 295–322.
- Fink D., McKelvey B.C., Hambury M.J. & Elliot G. 1999. Surface exposure dating using ^{10}Be in the Prince Charles Mountains (poster). VIII International Symposium on Antarctic Earth Sciences, Wellington, 5–9 July.
- Fitton J.G. & Upton B.G.J. 1987. Alkaline igneous rocks. *Geological Society of London; special publication* 30.
- Fitzsimons I.C.W. 1996. Metapelitic migmatites from Brattstrand Bluffs, East Antarctica—metamorphism, melting and exhumation of the mid-crust. *Journal of Petrology*; 37: 395–413.
- Fitzsimons I.C.W. & Harley S.L. 1991. Geological relationships in high-grade gneiss of the Brattstrand Bluffs coastline, Prydz Bay, East Antarctica. *Australian Journal of Earth Sciences*; 38: 497–519.
- Fitzsimons I.C.W. & Harley S.L. 1992. Mineral reaction textures in high-grade gneisses: Evidence for contrasting pressure–temperature paths in the Proterozoic complex of East Antarctica. In: Yoshida Y., Kaminuma K. & Shiraishi K. (editors). *Recent progress in Antarctic earth science*. Terra Scientific Publishing Company, Tokyo; 103–111.
- Fitzsimons I.C.W. & Harley S.L. 1995. Petrological constraints on the importance of Grenvillian and Pan-African events in the decompressional P–T paths of Prydz Bay. VII International Symposium on Antarctic Earth Sciences, Siena, 10–15 September; abstract volume: 135.
- Fitzsimons I.C.W. & Thost D.E. 1992. Geological relationships in high-grade basement gneiss of the northern Prince Charles Mountains, East Antarctica. *Australian Journal of Earth Sciences*; 39: 173–193.
- Fitzsimons I.C.W., Kinny P.D. & Harley S.L. 1997. Two stages of zircon and monazite growth in anatectic leucogneiss: SHRIMP constraints on the duration and intensity of Pan-African metamorphism in Prydz Bay, East Antarctica. *Terra Nova*; 9: 47–51.
- Foley S.F. 1992. Vein-plus-wall-rock melting mechanisms in the lithosphere and the origin of potassic alkaline magmas. *Lithos*; 28: 435–453.
- Foster C.B., Balme B.E. & Helby R. 1994. First record of Tethyan palynomorphs from the Late Triassic of East Antarctica. *AGSO Journal of Australian Geology and Geophysics*; 15: 239–246.
- Fowler K.F. 1971. Ice thickness measurements in MacRobertson Land. *Bureau of Mineral Resources, Australia; bulletin* 105.
- Frakes L.A. 1979. *Climates through geologic time*. Elsevier, Amsterdam.
- Francis D., Ludden J., Johnstone R. & Davis W. 1999. Picrite evidence for more Fe in Archean mantle reservoirs. *Earth and Planetary Science Letters*; 167: 197–213.
- Fraser G., McDougall I. & Williams I.S. 1995. Field and isotopic constraints on the metamorphic history of Lützow-Holm Bay, East Antarctica. VII International Symposium on Antarctic Earth Sciences, Siena, 10–15 September; abstract volume: 143.
- Ganguly J. & Saxena S.K. 1984. Mixing properties of aluminosilicate garnets: Constraints from natural and experimental data, and applications to geothermobarometry. *American Mineralogist*; 69: 88–97.
- Gill J.B. 1981. *Orogenic andesites and plate tectonics*. Springer-Verlag, Berlin.
- Grant J.A. 1985. Phase equilibria in low-pressure partial melting of pelitic rocks. *American Journal of Science*; 285: 409–435.
- Gray C.M. 1978. Geochronology of granulite-facies gneisses in the western Musgrave Block, central Australia. *Journal of the Geological Society of Australia*; 25: 403–414.
- Green D.H. & Hibberson W.O. 1970. The instability of plagioclase in peridotite at high pressure. *Lithos*; 3: 209–221.
- Green D.H. & Ringwood A.E. 1967. An experimental investigation of the gabbro to eclogite transformation and its petrological applications. *Geochimica et Cosmochimica Acta*; 31: 767–833.
- Grew E.S. 1978. Precambrian basement at Molodezhnaya Station, East Antarctica. *Geological Society of America; bulletin* 89: 801–813.
- Grew E.S. 1982. Geology of the southern Prince Charles Mountains, East Antarctica. In: Craddock C. (editor). *Antarctic geoscience*. University of Wisconsin Press, Madison; 473–478.
- Grew E.S. & Manton W.I. 1979. Archean rocks in Antarctica: 2.5-billion-year uranium–lead ages of pegmatites in Enderby Land. *Science*; 206: 443–445.
- Grew E.S. & Manton W.I. 1986. A new correlation of sapphirine granulites in the Indo-Antarctic metamorphic terrain: Late Proterozoic dates from the Eastern Ghats Province of India. *Precambrian Research*; 33: 123–137.
- Grew E.S., Manton W.I. & Sandiford M. 1982. Geochronologic studies in East Antarctica: age of pegmatites in Casey Bay, Enderby Land. *Antarctic Journal of the United States*; 17(5): 1–2.
- Grew E.S., Manton W.I. & James P.R. 1988. U–Pb data on granulite facies rocks from Fold Island, Kemp Coast, East Antarctica. *Precambrian Research*; 42: 63–75.
- Grew E.S., Manton W.I., Asami M. & Makimoto H. 1992. Reconnaissance geochronologic data on Proterozoic polymetamorphic rocks of the eastern Sør Rondane Mountains, East Antarctica. In: Yoshida Y., Kaminuma K. & Shiraishi K. (editors). *Recent progress in Antarctic earth science*. Terra Scientific Publishing Company, Tokyo; 37–44.
- Grikurov G.E. (editor). 1980. *Tectonic map of Antarctica 1:10 000 000*. Ministry of geology of the USSR, Moscow.
- Grikurov G.E. & Soloviev D.S. 1974. *Geologicheskoe stroenie gornogo obramleniya lednika Lambertova*. Soviet Antarctic Expedition; bulletin 88: 21–29.
- Groenewald P.B. 1993. Correlation of cratonic and orogenic provinces in southeastern Africa and Dronning Maud Land, Antarctica. In: Findlay R.H., Unrug R., Banks M.R. & Veevers J.J. (editors). *Gondwana eight: Assembly, evolution and dispersal*. Balkema, Rotterdam; 111–123.
- Groenewald P.B. 1995. Gondwana underplating at 500 Ma—granites associated with lamproites in Dronning Maud Land, East Antarctica. VII International Symposium on Antarctic Earth Sciences, Siena, 10–15 September; abstract volume: 173.
- Gross G.A. 1970. Nature and occurrence of iron ore deposits. In: *Survey of world iron ore resources—occurrence and appraisal*. United Nations Department of Economic and Social Affairs, New York; 13–31.
- Halpern M. & Grikurov G.E. 1975. Rubidium–strontium data from the southern Prince Charles Mountains. *Antarctic Journal of the United States*; 10: 9–15.
- Hambrey M.J. & McKelvey B.C. 1995. Neogene glacial facies and environments in the northern Prince Charles Mountains, East Antarctica. VII International Symposium on

- Antarctic Earth Sciences, Siena, 10–15 September; abstract volume: 179.
- Hambrey M.J. & McKelvey B.C. 1999. Major Neogene fluctuations of the East Antarctic ice sheet: Evidence from the Lambert Graben. VIII International Symposium on Antarctic Earth Sciences, Wellington, 5–9 July; abstract volume: 131.
- Hand M., Scrimgeour I., Stüwe K., Arne D. & Wilson C.J.L. 1994a. Geological observations in high-grade mid-Proterozoic rocks from Else Platform, northern Prince Charles Mountains region, east Antarctica. *Australian Journal of Earth Sciences*; 41: 311–329.
- Hand M., Scrimgeour I., Powell R., Stüwe K. & Wilson C.J.L. 1994b. Metapelitic granulites from Jetty Peninsula, east Antarctica: Formation during a single event or by polymetamorphism? *Journal of Metamorphic Geology*; 12: 557–573.
- Hansen E.C., Newton R.C. & Janardhan A.S. 1984. Fluid inclusions in rocks from amphibolite-facies gneiss to charnockite progression in southern Karnataka, India: Direct evidence concerning the fluids of granulite metamorphism. *Journal of Metamorphic Geology*; 2: 249–264.
- Harley S.L. 1984a. The solubility of alumina in orthopyroxene coexisting with garnet in $\text{FeO-MgO-Al}_2\text{O}_3\text{-SiO}_2$ and $\text{CaO-FeO-MgO-Al}_2\text{O}_3\text{-SiO}_2$. *Journal of Petrology*; 25: 665–696.
- Harley S.L. 1984b. An experimental study of the partitioning of Fe and Mg between garnet and orthopyroxene. *Contributions to Mineralogy and Petrology*; 86: 359–373.
- Harley S.L. 1988. Proterozoic granulites from the Rauer Group, East Antarctica. I: Decompressional pressure-temperature paths deduced from mafic and felsic gneisses. *Journal of Petrology*; 29: 1059–1095.
- Harley S.L. 1991. Metamorphic evolution of granulites from the Rauer Group, East Antarctica: Evidence for decompression following Proterozoic collision. In: Thomson M.R.A., Crame J.A. & Thomson J.W. (editors). *The geological evolution of Antarctica*. Cambridge University Press; 99–105.
- Harley S.L. & Black L.P. 1997. A revised Archaean chronology for the Napier Complex, Enderby Land, from SHRIMP ion-microprobe studies. *Antarctic Science*; 9: 74–91.
- Harley S.L. & Fitzsimons I.C.W. 1991. Pressure-temperature evolution of metapelitic granulites in a polymetamorphic terrane: the Rauer Group, East Antarctica. *Journal of Metamorphic Geology*; 9: 231–243.
- Harley S.L. & Green D.H. 1982. Garnet-orthopyroxene barometry for granulites and peridotites. *Nature*; 300: 697–701.
- Harley S.L., Fitzsimons I.C.W., Buick I.S. & Watt G. 1992. The significance of reworking, fluids and partial melting in granulite metamorphism, east Prydz Bay, Antarctica. In: Yoshida Y., Kaminuma K. & Shiraishi K. (editors). *Recent progress in Antarctic earth science*. Terra Scientific Publishing Company, Tokyo; 119–127.
- Harley S.L., Snape I. & Fitzsimons I.C.W. 1995. Regional correlations and terrane assembly in east Prydz Bay: Evidence from the Rauer Group and Vestfold Hills. *Terra Antarctica*; 2: 49–60.
- Harley S.L., Snape I. & Black L.P. 1998. The evolution of a layered metaigneous complex in the Rauer Group, East Antarctica: Evidence for a distinct Archaean terrane. *Precambrian Research*; 89: 175–205.
- Harris L.B. 1993. Correlations of tectonothermal events between the Central Indian Tectonic Zone and the Albany Mobile Belt of Western Australia. In: Findlay R.H., Unrug R., Banks M.R. & Veevers J.J. (editors). *Gondwana eight: Assembly, evolution and dispersal*. Balkema, Rotterdam; 165–180.
- Harwood D.M. & Maruyama T. 1992. Middle Eocene to Pleistocene diatom biostratigraphy of Southern Ocean sediments from the Kerguelen Plateau, Leg 120. In: Wise S.M. Jr., Schlich R. et al. (editors). *Proceedings of the Ocean Drilling Project; scientific results* 120: 683–733.
- Harwood D.M., Scherer R.P. & Webb P.-N. 1989. Multiple Miocene marine productivity events in West Antarctica as recorded in Upper Miocene sediments beneath the Ross Ice Shelf (Site J-9). *Marine Micropaleontology*; 15: 91–115.
- Hensen B.J. & Zhou B. 1995. A Pan-African granulite facies metamorphic episode in Prydz Bay, Antarctica: Evidence from Sm-Nd garnet dating. *Australian Journal of Earth Sciences*; 42: 249–258.
- Hensen B.J., Zhou B. & Thost D.E. 1997. Resolution of multiple high grade metamorphic events by garnet Sm-Nd geochronology in the Northern Prince Charles Mountains, Antarctica. In: Ricci C.A. (editor). *The Antarctic region: Geological evolution and processes*. Terra Antarctica Publication, Siena; 97–104.
- Hodges K.V. & Crowley P.D. 1985. Error estimation and empirical geothermobarometry for pelitic systems. *American Mineralogist*; 70: 702–709.
- Hoffman P.F. 1991. Did the breakout of Laurentia turn Gondwanaland inside-out? *Science*; 252: 1409–1412.
- Hofmann J. 1982. Main tectonic features and development of the southern Prince Charles Mountains, East Antarctica. In: Craddock C. (editor). *Antarctic geoscience*. University of Wisconsin Press, Madison; 479–487.
- Hofmann J. 1991. Fault tectonics and magmatic ages in the Jetty Oasis area, MacRobertson Land: A contribution to the Lambert rift development. In: Thomson M.R.A., Crame J.A. & Thomson J.W. (editors). *The geological evolution of Antarctica*. Cambridge University Press; 107–112.
- Hofmann J., Kaiser G. & Klemm W. 1980. K-Ar-Alter präkambrischer Basite der Ostantarktis (Prince Charles Mountains, Oase Vestfold). *Zeitschrift des geologische Wissenschaft*; 8: 1561–1564.
- Holdaway M.J. 1971. Stability of andalusite and the aluminium silicate phase diagram. *American Journal of Science*; 271: 97–131.
- Hole M.J., Saunders A.D., Marriner G.F. & Tarney J. 1984. Subduction of pelagic sediments: Implications for the origin of Ce-anomalous basalts from Mariana Islands. *Journal of the Geological Society, London*; 141: 453–472.
- Holland T.J.B. & Powell R. 1990. An enlarged and updated internally consistent thermodynamic data set with uncertainties and correlations: The system $\text{K}_2\text{O-Na}_2\text{O-CaO-MgO-MnO-FeO-Fe}_2\text{O}_3\text{-Al}_2\text{O}_3\text{-TiO}_2\text{-SiO}_2\text{-C-H}_2\text{-O}_2$. *Journal of Metamorphic Geology*; 8: 89–124.
- Huang W.L. & Wyllie P.J. 1973. Melting relations of muscovite granite to 35 kbar as a model for the fusion of metamorphosed subducted ocean sediments. *Contributions to Mineralogy and Petrology*; 42: 1–14.
- Iltchenko L.N. 1972. Late Precambrian acritarchs of Antarctica. In: Adie R.J. (editor). *Antarctic geology and geophysics*. Universitetsforlaget, Oslo; 599–602.
- Ilupin I.P., Kaminsky F.V. & Frantsesson E.V. 1978. Geochemistry of kimberlites (in Russian). Nedra, Moscow.
- Irvine T.N. & Baragar W.R.A. 1971. A guide to the chemical classification of the common volcanic rocks. *Canadian Journal of Earth Sciences*; 8: 523–548.
- Ivanov V.L. & Kamenev E.N. 1990. The geology and mineral resources of Antarctica (in Russian). Nedra, Moscow.
- Jacobs J., Thomas R.J. & Weber K. 1995. Grenvillian terrains in western Dronning Maud Land and SE Africa and their enigmatic Pan-African overprint. VII International Symposium on Antarctic Earth Sciences, Siena, 10–15 September; abstract volume: 210.
- James R.S. & Hamilton D.L. 1969. Phase relations in the system $\text{NaAlSi}_3\text{O}_8 - \text{KAlSi}_3\text{O}_8 - \text{CaAl}_2\text{Si}_2\text{O}_8 - \text{SiO}_2$ at 1 kilobar water vapour pressure. *Contributions to Mineralogy and Petrology*; 21: 111–141.

- James P.R., Ding P. & Rankin, L. 1991. Structural geology of the early Precambrian gneisses of northern Fold Island, Mawson Coast, East Antarctica. In: Thomson M.R.A., Crame J.A. & Thomson J.W. (editors) *The geological evolution of Antarctica*. Cambridge University Press; 19–23.
- Jaques A.L., Creaser R.A., Ferguson F. & Smith C.B. 1985. A review of the alkaline rocks of Australia. *Transactions of the Geological Society of South Africa*; 88: 311–334.
- Javoy M. & Weis D. 1987. Oxygen isotopic composition of alkaline anorogenic granites as a clue to their origin: the problem of crustal oxygen. *Earth and Planetary Science Letters*; 84: 415–422.
- Jensen L.S. 1976. A new cation plot for classifying subalkaline volcanic rocks. Ontario Division of Mines; miscellaneous paper 66.
- Kadmina I.N., Kurinin R.G., Masolov V.N. & Grikurov G.E. 1983. Antarctic crustal structure from geophysical evidence: A review. In: Oliver R.L., James P.R. & Jago J.B. (editors). *Antarctic earth science*. Australian Academy of Science, Canberra; 498–502.
- Kagami H., Owada M., Osanai Y. & Hiroi Y. 1990. Preliminary geochronological study of Sri Lankan rocks. In: Hiroi Y. & Motoyoshi Y. (editors). *Study of geologic correlation between Sri Lanka and Antarctica (1988–1989)*. Interim Report of Japan–Sri Lanka Joint Research, Chiba University, Japan; 55–70.
- Kamenev E.N. 1982. Regional metamorphism in Antarctica. In: Craddock C. (editor). *Antarctic geoscience*. University of Wisconsin Press, Madison; 429–433.
- Kamenev E.N. 1991. Structure and evolution of Precambrian cratons and metamorphic belts in East Antarctica. Sixth International Symposium on Antarctic Earth Sciences, National Institute of Polar Research, Tokyo, 9–13 September; abstract volume: 261–263.
- Kamenev E.N. 1993. Structure and evolution of the Antarctic shield in Precambrian. In: Findley R.H., Unrug R., Banks M.R. & Veevers J.J. (editors). *Gondwana eight: Assembly, evolution and dispersal*. Balkema, Rotterdam; 141–151.
- Kamenev E.N. & Krasnikov N.N. 1991. The granite–greenstone terrains in the southern Prince Charles Mountains. Sixth International Symposium on Antarctic Earth Sciences, National Institute of Polar Research, Tokyo, 9–13 September; abstract volume: 264–268.
- Kamenev E.N. & Ravich M.G. 1979. *Metamorphic facies map of Antarctica 1:5 000 000*. Ministry of geology of the USSR, Moscow.
- Kamenev E.N., Kameneva G.I., Mikhalsky E.V. & Andronikov A.V. 1990. The Prince Charles Mountains and Mawson Escarpment (in Russian). In: Ivanov V.L. & Kamenev E.N. (editors). *The geology and mineral resources of Antarctica (in Russian)*. Nedra, Moscow; 67–113.
- Kamenev E.N., Andronikov A.V., Mikhalsky E.V., Krasnikov N.N. & Stüwe K. 1993. Soviet geological maps of the Prince Charles Mountains, East Antarctic Shield. *Australian Journal of Earth Sciences*; 40: 501–517.
- Kameneva G.I. & Mikhalsky E.V. 1985. Major features of the distribution of coal-bearing deposits in Antarctica. *Polar Geography and Geology*; 9: 132–145.
- Katchenkov S.M. 1967. Average contents of certain minor chemical elements in the principal types of sedimentary rock. In: Vinogradov A.P. (editor). *Chemistry of the Earth's crust*, volume II; 416.
- Kelly N.M., Clarke G.L., Carson C.J. & White R.W. 2000. Thrusting in the lower crust: evidence from the Oygarden Islands, Kemp Land, East Antarctica. *Geological Magazine*; 137: 219–234.
- Kemp E.M. 1969. Permian flora from the Beaver Lake area, Prince Charles Mountains, Antarctica. 1: Palynological examination of samples. In: *Palaeontological papers*. Bureau of Mineral Resources, Australia; bulletin 126.
- Keppler H. 1993. Influence of fluorine on the enrichment of high field strength trace elements in granitic rocks. *Contributions to Mineralogy and Petrology*; 114: 479–488.
- Kerr A. & Fryer B.J. 1993. Nd isotope evidence for crust–mantle interaction in the generation of A-type granitoid suites in Labrador, Canada. *Chemical Geology*; 104: 39–60.
- Kilpatrick J.A. & Ellis D.J. 1992. C-type magmas: Igneous charnockites and their extrusive equivalents. *Transactions of the Royal Society of Edinburgh: Earth Sciences*; 83: 155–164.
- Kinny P.D. 1998. Monazite U–Pb ages from East Antarctic granulites: Comparisons with zircon U–Pb and garnet Sm–Nd ages. *Geological Society of Australia; abstracts* 49: 250.
- Kinny P.D., Black L.P. & Sheraton J.W. 1993. Zircon ages and the distribution of Archaean and Proterozoic rocks in the Rauer Islands. *Antarctic Science*; 5: 193–206.
- Kinny P.D., Black L.P. & Sheraton J.W. 1997. Zircon U–Pb ages and geochemistry of igneous and metamorphic rocks in the northern Prince Charles Mountains, Antarctica. *AGSO Journal of Australian Geology and Geophysics*; 16: 637–654.
- Knoper M.W., Moyes A.B., Tucker R.D., Amelin Y. & Harris P.D. 1995. Growth of pre-Gondwana crust as indicated by three crustal provinces in western Dronning Maud Land, East Antarctica. VII International Symposium on Antarctic Earth Sciences, Siena, 10–15 September; abstract volume: 230.
- Kovach V.P. & Belitsky B.V. 1991. Geochemistry and age of granitic rocks in the Ruker granite–greenstone terrain, southern Prince Charles Mountains, East Antarctica. Sixth International Symposium on Antarctic Earth Sciences, National Institute of Polar Research, Tokyo, 9–13 September; abstract volume: 321–326.
- Krasnikov N.N. & Fedorov L.V. 1992. Geological structure of Fisher Massif (East Antarctica). *Izvestia Akademii Nauk, earth-science section*; 8: 123–134.
- Krebs K.A. & Mabin M.C.G. 1997. Distribution, activity and characteristics of the alpine-type glaciers of northern Prince Charles Mountains, East Antarctica. *Antarctic Science*; 9: 307–312.
- Kriegsman L.M. 1995. The Pan-African event in East Antarctica: A view from Sri Lanka and the Mozambique Belt. *Precambrian Research*; 75: 263–277.
- Krylov D.P. & Krutikova S.V. 1994. The greenschist rock association of Fisher Massif, Prince Charles Mountains, East Antarctica. *Petrologiya*; 2: 305–310.
- Kurinin R.G. & Grikurov G.E. 1980. The structure of the Lambert Glacier rift zone (in Russian). *Trudy Sovetskoi Antarkticheskoi Ekspeditsii*; 70: 75–86.
- Kurinin R.G. & Grikurov G.E. 1982. Crustal structure of part of East Antarctica from geophysical data. In: Craddock C. (editor). *Antarctic geoscience*. University of Wisconsin Press, Madison; 895–901.
- Laiba A.A. & Mikhalsky E.V. 1995. A layered gabbro intrusion from Willing Massif (Prince Charles Mountains, East Antarctica). VII International Symposium on Antarctic Earth Sciences, Siena, 10–15 September; abstract volume: 233.
- Laiba A.A. & Mikhalsky E.V. 1999. Gabbroids of Willing Massif, East Antarctica, a layered intrusion in a Proterozoic mobile belt: Geologic structure and chemical composition. *Petrologiya*; 7: 32–52.
- Laiba A.A. & Pushina Z.V. 1997. Cenozoic glacial–marine sediments from the Fisher Massif (Prince Charles Mountains). In: Ricci C.A. (editor). *The Antarctic region: Geological evolution and processes*. Terra Antarctica Publication, Siena; 977–984.
- Laiba A.A., Andronikov A.V., Egorov L.S. & Fedorov L.V. 1987. Stock-like bodies and dykes of alkaline ultramafic rocks in Jetty Peninsula (Prince Charles Mountains, East Antarctica) (in Russian). In: *Geologo-geophizicheskie issledovaniya v Antarktike*. Sevmorgeologiya, Leningrad; 35–46.

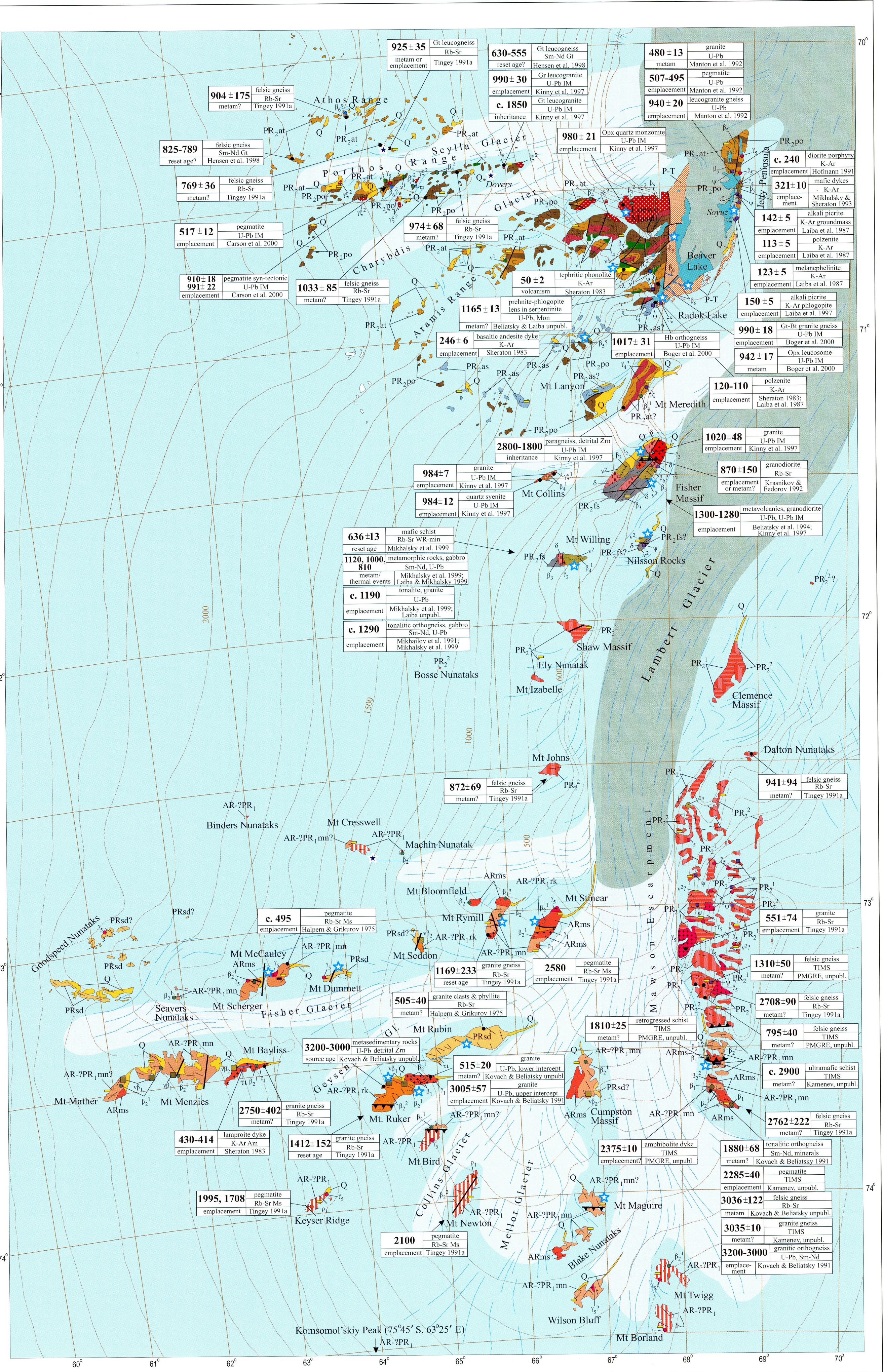
- Lanyon R., Black L.P. & Seitz H.-M. 1993. U–Pb zircon dating of mafic dykes and its application to the Proterozoic geological history of the Vestfold Hills, East Antarctica. *Contributions to Mineralogy and Petrology*; 115: 184–203.
- Lawver L.A., Royer J.-Y., Sandwell D.T. & Scotese C.R. 1991. Evolution of Antarctic continental margins. In: Thomson M.R.A., Crame J.A. & Thomson J.W. (editors). *The geological evolution of Antarctica*. Cambridge University Press; 533–539.
- Lazarenkov V.G. 1988. Formation analysis of continental and oceanic alkaline rocks (in Russian). Nedra, Leningrad.
- Le Bas M.J., Le Maitre R.W., Streckeisen A. & Zanettin B. 1986. A chemical classification of volcanic rocks based on the total alkali–silica diagram. *Journal of Petrology*; 27: 745–750.
- Le Breton N. & Thompson A.B. 1988. Fluid-absent (dehydration) melting of biotite in metapelites in the early stages of crustal anatexis. *Contributions to Mineralogy and Petrology*; 99: 226–237.
- Le Maitre R.W. 1989. A classification of igneous rocks and glossary of terms. Blackwell Scientific Publications, Oxford.
- Lee H.Y. & Ganguly J. 1988. Equilibrium compositions of coexisting garnet and orthopyroxene: Experimental determinations in the system $\text{FeO-MgO-Al}_2\text{O}_3\text{-SiO}_2$ and applications. *Journal of Petrology*; 29: 93–113.
- Lopatin B.G. & Semenov V.S. 1982. Amphibolite facies rocks of the southern Prince Charles Mountains, East Antarctica. In: Craddock C. (editor). *Antarctic geoscience*. University of Wisconsin Press, Madison, 465–471.
- Macpherson H. G. 1958. A chemical and petrographic study of Pre-Cambrian sediments. *Geochimica et Cosmochimica Acta*; 14: 73–92.
- McKelvey B.C. & Stephenson N.C.N. 1990. A geological reconnaissance of the Radok Lake area, Amery Oasis, Prince Charles Mountains. *Antarctic Science*; 2: 53–66.
- McKelvey B.C., Hambrey M.J., Mabin M.C.G., Harwood D.M. & Webb P.-N. 1995. The Neogene Pagodroma Group in the northern Prince Charles Mountains, East Antarctica. VII International Symposium on Antarctic Earth Sciences, Siena, 10–15 September; abstract volume: 262.
- McKelvey B., Hambrey M., Harwood D., Mabin M., Webb P.-N. & Whitehouse J. 1999. The Pagodroma Group: The Neogene record in the northern Prince Charles Mountains of a dynamic Lambert Glacier and East Antarctic ice sheet. VIII International Symposium on Antarctic Earth Sciences, Wellington, 5–9 July; abstract volume: 204.
- McLeod I.R. 1959. Report on geological and glaciological work by the 1958 Australian National Antarctic Research Expedition. Bureau of Mineral Resources, Australia; record 1959/131.
- McLeod I.R. 1964. An outline of the geology of the sector from longitude 45°E to 80°E, Antarctica. In: Adie R.J. (editor). *Antarctic geology*. North Holland, Amsterdam; 237–247.
- McLoughlin S. & Drinnan A.N. 1997a. Revised stratigraphy of the Permian Bainmedart Coal Measures, northern Prince Charles Mountains, East Antarctica. *Geological Magazine*; 134: 335–353.
- McLoughlin S. & Drinnan A.N. 1997b. Fluvial sedimentology and revised stratigraphy of the Triassic Flagstone Bench Formation, northern Prince Charles Mountains, East Antarctica. *Geological Magazine*; 134: 781–806.
- McLoughlin S., Lindström S. & Drinnan A.N. 1997. Gondwanian floristic and sedimentological trends during the Permian–Triassic transition: New evidence from the Amery Group, northern Prince Charles Mountains, East Antarctica. *Antarctic Science*; 9: 281–298.
- Manton W.I., Grew E.S., Hofmann J. & Sheraton J.W. 1992. Granitic rocks of the Jetty Peninsula, Amery Ice Shelf area, East Antarctica. In: Yoshida Y., Kaminuma K. & Shiraishi K. (editors). *Recent progress in Antarctic earth science*. Terra Scientific Publishing Company, Tokyo; 179–189.
- Martin H. 1993. The mechanisms of petrogenesis of the Archaean continental crust—comparison with modern processes. *Lithos*; 30: 373–388.
- Mikhailov V. M. & Sergeyev, M.B. 1997. Main lithological formations of high-grade metamorphic terrane of the northern Prince Charles Mountains, East Antarctica, and their subglacial distribution. In: Ricci C.A. (editor). *The Antarctic region: Geological evolution and processes*. Terra Antarctica Publication, Siena; 89–95.
- Mikhailov V.M., Mikhalsky E.V., Beliatsky B.V. & Semenov V.S. 1991. Layered gabbroid intrusion in the central Prince Charles Mountains (East Antarctica). *Doklady Akademii Nauk SSSR*; 321: 1066–1070.
- Mikhalsky E.V. 1993. Petrochemical characteristics of igneous rocks from Fisher Massif (East Antarctica) (in Russian). The Antarctic. Russian Committee on Antarctic Research; report 32: 41–57.
- Mikhalsky E.V. & Sheraton J.W. 1993. Association of dolerite and lamprophyre dykes, Jetty Peninsula (Prince Charles Mountains, East Antarctica). *Antarctic Science*; 5: 297–307.
- Mikhalsky E.V., Andronikov A.V. & Beliatsky B.V. 1992. Mafic igneous suites in the Lambert rift zone. In: Yoshida Y., Kaminuma, K. & Shiraishi K. (editors). *Recent progress in Antarctic earth sciences*. Terra Scientific Publishing Company, Tokyo; 173–178.
- Mikhalsky E.V., Andronikov A.V., Beliatsky B.V. & Kamenev E.N., 1993. Mafic and ultramafic igneous suites in the Lambert–Amery rift zone. In: Findley R.H., Unrug R., Banks M.R. & Veevers J.J. (editors). *Gondwana eight: Assembly, evolution and dispersal*. A.A. Balkema, Rotterdam; 541–546.
- Mikhalsky E.V., Beliatsky B.V., Andronikov A.V. & Grachev A.F. 1994a. Proterozoic lamprophyre dykes in the Vestfold Hills, East Antarctica. *Petrologiya*; 2: 587–600.
- Mikhalsky E.V., Laiba A.A., Beliatsky B.V., Sosedko T.A. & Andronikov A.V. 1994b. Lamproites from the Rubin Massif, Prince Charles Mountains, East Antarctica. *Petrologiya*; 2: 258–264.
- Mikhalsky E.V., Sheraton J.W., Laiba A.A. & Beliatsky B.V. 1996. Geochemistry and origin of Mesoproterozoic metavolcanic rocks from Fisher Massif, Prince Charles Mountains, East Antarctica. *Antarctic Science*; 8: 85–104.
- Mikhalsky E.V., Beliatsky B.V., Savva E.V., Wetzel H.-U., Fedorov L.V., Weiser T. & Hahne K. 1997. Reconnaissance geochronologic data on polymetamorphic and igneous rocks of the Humboldt Mountains, central Queen Maud Land, East Antarctica. In: Ricci C.A. (editor). *The Antarctic region: Geological evolution and processes*. Terra Antarctica Publication, Siena; 45–53.
- Mikhalsky E.V., Laiba A.A., Beliatsky B.V. & Stüwe K. 1999. Geological structure of Mount Willing (Prince Charles Mountains, East Antarctica), and some implications for metamorphic rock age and origin. *Antarctic Science*; 11: 338–352.
- Mikhalsky E.V., Sheraton J.W. & Beliatsky B.V. 2001. Preliminary U–Pb dating of Grove Mountains rocks: Implications for the Proterozoic to early Palaeozoic tectonic evolution of the Lambert Glacier–Prydz Bay area (East Antarctica). *Terra Antarctica*; 8: 3–10.
- Milashev V.A. 1974. Kimberlite provinces (in Russian). Nedra, Leningrad.
- Mishkin M.A. 1990. Amphibole geothermobarometer for metabasites (in Russian). *Doklady Akademii Nauk SSSR*; 321: 944–946.
- Mitchell R.H. 1985. A review of the mineralogy of lamproites. *Transactions of the Geological Society of South Africa*; 88: 411–437.

- Moecher D.P., Essene E.J. & Anovitz L.M. 1988. Calculation and application of clinopyroxene–garnet–plagioclase–quartz geobarometers. *Contributions to Mineralogy and Petrology*; 100: 92–106.
- Mond A. 1972. Permian sediments of the Beaver Lake area, Prince Charles Mountains. In: Adie R.J. (editor). *Antarctic geology and geophysics*. Universitetsforlaget, Oslo; 585–589.
- Moore E.M. 1991. Southwest U.S.–East Antarctica (SWEAT) connection: A hypothesis. *Geology*; 19: 425–428.
- Motoyoshi Y. 1990. A review of P–T evolution of high-grade metamorphic terranes in East Antarctica. In: Hiroi Y. & Motoyoshi Y. (editors). *Study of geologic correlation between Sri Lanka and Antarctica*. Interim Report of Japan–Sri Lanka Joint Research; 132–139.
- Motoyoshi Y., Thost D.E. & Hensen B.J. 1991. Reaction textures in calc-silicate granulites from the Bolingen Islands, Prydz Bay, East Antarctica: Implications for the retrograde P–T path. *Journal of Metamorphic Geology*; 9: 293–300.
- Moyes A.B. & Groenewald P.B. 1996. Isotopic constraints on Pan-African metamorphism in Dronning Maud Land, Antarctica. *Chemical Geology*; 129: 247–256.
- Moyes A.B., Groenewald P.B. & Brown R.W. 1993. Isotopic constraints on the age and origin of the Brattskarvet intrusive suite, Dronning Maud Land, Antarctica. *Chemical Geology (isotope geoscience section)*; 106: 453–466.
- Mullen E.D. 1983. MnO/TiO₂/P₂O₅: A minor element discriminant for basaltic rocks of oceanic environments and its implications for petrogenesis. *Earth and Planetary Science Letters*; 62: 53–62.
- Munksgaard N.C., Thost D.E. & Hensen B.J. 1992. Geochemistry of Proterozoic granulites from northern Prince Charles Mountains, East Antarctica. *Antarctic Science*; 4: 59–69.
- Myers J.S. 1990. Precambrian tectonic evolution of part of Gondwana, southwestern Australia. *Geology*; 18: 537–540.
- Nakamura N. 1974. Determination of REE, Ba, Fe, Mg, Na and K in carbonaceous and ordinary chondrites. *Geochimica et Cosmochimica Acta*; 38: 757–775.
- Nelson D.R. & McCulloch M.T. 1989. Enriched mantle components and mantle recycling of sediments. In: Ross J. (editor). *Kimberlites and related rocks, volume 1: Their composition, occurrence, origin and emplacement*. Geological Society of Australia; special publication 14: 560–570.
- Nelson D.R., Myers J.S. & Nutman A.P. 1995. Chronology and evolution of the middle Proterozoic Albany–Fraser Orogen, Western Australia. *Australian Journal of Earth Sciences*; 42: 481–495.
- Nesbitt R.W. & Sun S-S. 1980. Geochemical features of some Archaean and post-Archaean high-magnesian–low-alkali liquids. *Philosophical Transactions of the Royal Society of London, series A*; 297: 365–381.
- Newton R.C. & Haselton H.T. 1981. Thermodynamics of the garnet–plagioclase–Al₂SiO₅–quartz geobarometer. In: Newton R.C., Navrotsky A. & Wood B.J. (editors). *Thermodynamics of minerals and melts*. Springer, New York; 131–147.
- Newton R.C. & Perkins D. 1982. Thermodynamic calibrations of geobarometers based on the assemblages garnet–plagioclase–orthopyroxene (clinopyroxene)–quartz. *American Mineralogist*; 67: 203–222.
- Nichols G.T. & Berry R.F. 1991. A decompressional P–T path, Reinbolt Hills, East Antarctica. *Journal of Metamorphic Geology*; 9: 257–266.
- Nixon P.H., Thirlwall M.F., Buckley F. & Davies C.J. 1984. Spanish and Western Australian lamproites: Aspects of whole rock geochemistry. In: Kornprobst J. (editor). *Kimberlites and related rocks*. Elsevier, Amsterdam; 285–296.
- Norrish K. & Chappell B.W. 1977. X-ray fluorescence spectrometry. In: Zussman J. (editor). *Physical methods in determinative mineralogy*. Academic Press, London; 201–272.
- Norrish K. & Hutton J.T. 1969. An accurate X-ray spectrographic method for the analysis of a wide range of geological samples. *Geochimica et Cosmochimica Acta*; 33: 431–453.
- Oliver R.L. & Fanning C.M. 1998. George V Land–Adelie Land–Eyre Peninsula: A tentative correlation. *Geological Society of Australia; abstracts* 49: 341.
- Oliver R.L., Cooper J.A. & Truelove A.J. 1983. Petrology and zircon geochronology of Herring Island and Commonwealth Bay and evidence for Gondwana reconstruction. In: Oliver R.L., James P.R. & Jago J.B. (editors). *Antarctic earth science*. Australian Academy of Science, Canberra; 64–68.
- Park R.G. 1988. *Geological structures and moving plates*. Blackie, Glasgow.
- Passchier C.W., Bekendam R.F., Hoek J.D., Dirks P.G.H.M. & de Boorder H. 1991. Proterozoic geological evolution of the northern Vestfold Hills, Antarctica. *Geological Magazine*; 128: 307–318.
- Pearce J.A. 1982. Trace element characteristics of lavas from destructive plate boundaries. In: Thorpe R.S. (editor). *Andesites: Orogenic andesites and related rocks*. Wiley, Chichester; 525–548.
- Pearce J.A., Harris N.B.W. & Tindle A.G. 1984. Trace element discrimination diagrams for the interpretation of granitic rocks. *Journal of Petrology*; 25: 956–983.
- Perchuck L.L. 1970. Rock-forming mineral equilibria (in Russian). Nauka, Moscow.
- Perchuck L.L., Aranovich L.Ya., Podlesskii K.K., Lavrant'eva I.V., Gerasimov V.Yu., Fed'kin V.V., Kitsul V.I., Karsakov L.P. & Berdnikov N.V. 1985. Precambrian granulites of the Aldan Shield, eastern Siberia, USSR. *Journal of Metamorphic Geology*; 3: 265–310.
- Perkins D. & Newton R.C. 1981. Charnockite geobarometers based on coexisting garnet–pyroxene–plagioclase–quartz. *Nature*; 292: 144–146.
- Pichowiak S., Buchelt M. & Damm K-W. 1990. Magmatic activity and tectonic setting of the early stages of the Andean cycle in northern Chile. In: Kay S.M. & Rapela C.W. (editors). *Plutonism from Antarctica to Alaska*. Geological Society of America; special paper 241: 127–144.
- Plyusnina L.P. 1982. Geothermometry and geobarometry of plagioclase–hornblende-bearing assemblages. *Contributions to Mineralogy and Petrology*; 80: 140–146.
- Post N.J., Kinny P.D. & Hensen B.J. 1995. Geochronological constraints on the tectonothermal history of the Windmill Islands, East Antarctica. VII International Symposium on Antarctic Earth Sciences, Siena, 10–15 September; abstract volume: 313.
- Powell R. 1985. Regression diagnostics and robust regression in geothermometer/geobarometer calibration: The garnet–clinopyroxene geothermometer revisited. *Journal of Metamorphic Geology*; 3: 231–243.
- Powell C.M. 1998. Assembly and break-up of Rodinia. *Geological Society of Australia; abstracts* 49: 360.
- Powell R. & Holland T.J.B. 1988. An internally consistent thermodynamic data set with uncertainties and correlations. 3: Applications to geobarometry, worked examples and a computer program. *Journal of Metamorphic Geology*; 6: 173–204.
- Powell R. & Holland T.J.B. 1994. Optimal geothermometry and geobarometry. *American Mineralogist*; 79: 120–133.
- Powell C.M., Roots S.R. & Veevers J.J. 1988. Pre-breakup continental extension in East Gondwanaland and the early opening of the eastern Indian Ocean. *Tectonophysics*; 155: 261–283.

- Powell C.M., Li Z.X., McElhinny M.W., Meert J.G. & Park J.K. 1993. Paleomagnetic constraints on timing of the Neoproterozoic breakup of Rodinia and the Cambrian formation of Gondwana. *Geology*; 21: 889–892.
- Pownceby M.I., Wall V.J. & O'Neill H.St.O. 1987. Fe–Mn partitioning between garnet and ilmenite: Experimental calibration and applications. *Contributions to Mineralogy and Petrology*; 97: 116–126.
- Prider R.T. 1960. The leucite lamproites of the Fitzroy Basin, Western Australia. *Journal of the Geological Society of Australia*; 6: 71–118.
- Puchelt H. 1972. Barium: Abundance in common sediments and sedimentary rock types. In: Wedepohl K.H. (editor). *Handbook of geochemistry*. Springer-Verlag, Berlin; II-4, 56-K1–8.
- Rapp R.P., Watson E.B. & Miller C.F. 1991. Partial melting of amphibolite/eclogite and the origin of Archean trondhjemites and tonalites. *Precambrian Research*; 51: 1–25.
- Ravich G.M., 1974. The cross-section of Permian coal-bearing strata in the Beaver Lake area (Prince Charles Mountains, East Antarctica) (in Russian). *The Antarctic. Soviet Committee on Antarctic Research*; report 13: 19–35.
- Ravich M.G. 1982. The lower Precambrian of Antarctica. In: Craddock C. (editor). *Antarctic geoscience*. University of Wisconsin Press, Madison; 421–428.
- Ravich M.G. & Fedorov L.V. 1982. Geologic structure of MacRobertson Land and Princess Elizabeth Land, East Antarctica. In: Craddock C. (editor). *Antarctic geoscience*. University of Wisconsin Press, Madison; 499–504.
- Ravich M.G. & Grikurov G.E. 1976. Geological map of Antarctica 1:5 000 000. Kartfabrika ob'edineniia Aereogeologii, Leningrad (now Saint Petersburg).
- Ravich M.G. & Kamenev E.N. 1975. Crystalline basement of the Antarctic platform. Halsted Press, New York.
- Ravich G.M., Gor Yu.I., Dibner A.F. & Lobanova O.V. 1977. The stratigraphy of Upper Palaeozoic Coal Measures (Beaver Lake area, East Antarctica) (in Russian). *The Antarctic. Russian Committee on Antarctic Research*; report 16: 62–75.
- Ravich M.G., Soloviev D.S. & Fedorov L.V. 1978. *Geologicheskoe stroenie zemli Mak-Robertsona (Vostochnaya Antarktida)*. Gidrometeoizdat, Leningrad (now Saint Petersburg).
- Ravich M.G., Fedorov L.V. & Tarutin O.A. 1982. Precambrian iron deposits of the Prince Charles Mountains. In: Craddock C. (editor). *Antarctic geoscience*. University of Wisconsin Press, Madison; 853–858.
- Ravich M.G., Soloviev D.S. & Fedorov L.V. 1984. Geological structure of MacRobertson Land (east Antarctica). Amerind Publishing Co., New Delhi.
- Ren L., Zhao Y., Liu X. & Chen T. 1992. Re-examination of the metamorphic evolution of the Larsemann Hills, East Antarctica. In: Yoshida Y. (editor). *Recent progress in Antarctic earth science*. Terra Scientific Publishing Company, Tokyo; 145–153.
- Ringwood A.E. 1975. *Composition and petrology of the Earth's mantle*. McGraw-Hill, New York.
- Rock N.M.S. 1987. The nature and origin of lamprophyres: An overview. In: Fitton J.G. & Upton B.G.J. (editors). *Alkaline igneous rocks*. Geological Society of London; special publication 30: 191–226.
- Roeder P.L. & Emslie R.F. 1970. Olivine–liquid equilibrium. *Contributions to Mineralogy and Petrology*; 29: 275–289.
- Rogers N.W., Hawkesworth C.J., Matthey D.P. & Harmon R.S. 1987. Sediment subduction and the source of potassium in orogenic leucitites. *Geology*; 15: 451–453.
- Rose L.A. 1980. *Assault on eternity*. Naval Institute Press, Annapolis, Maryland.
- Ruker R.A. 1963. Geological reconnaissance in Enderby Land and southern Prince Charles Mountains. Bureau of Mineral Resources, Australia; record 1963/154.
- Sakar S.N. 1968. *Precambrian stratigraphy and geochronology of Peninsular India*. Dhanbad Publishers, India.
- Sandiford M. 1985. The origin of retrograde shear zones in the Napier Complex: Implications for the tectonic evolution of Enderby Land, Antarctica. *Journal of Structural Geology*; 7: 477–488.
- Saunders A.D., Norry M.J. & Tarney J. 1991. Fluid influence on the trace element compositions of subduction zone magmas. *Philosophical Transactions of the Royal Society of London, series A*; 335: 377–392.
- Saxena S.H. & Eriksson G. 1985. Anhydrous phase equilibria in Earth's upper mantle. *Journal of Petrology*; 26: 378–390.
- Schrader H.J. 1976. Cenozoic planktonic diatom biostratigraphy of the Southern Pacific Ocean. In: Hollister C.D., Craddock C., et al. (editors). *Initial Reports of DSDP 35*. United States Government Printing Office, Washington; 605–672.
- Scrimgeour I. & Hand M. 1997. A metamorphic perspective on the Pan African overprint in the Amery area of MacRobertson Land, East Antarctica. *Antarctic Science*; 9: 313–335.
- Sen S.K. & Bhattacharya A. 1984. An orthopyroxene–garnet thermometer and its application to the Madras charnockites. *Contributions to Mineralogy and Petrology*; 88: 64–71.
- Sharkov E.V. 1983. *Petrology of magmatic processes (in Russian)*. Nedra, Moscow.
- Sheraton J.W. 1980. Geochemistry of Precambrian metapelites of East Antarctica: Secular and metamorphic variations. *BMR Journal of Australian Geology and Geophysics*; 5: 279–288.
- Sheraton J.W. 1982. Origin of charnockitic rocks of MacRobertson Land. In: Craddock C. (editor). *Antarctic geoscience*. University of Wisconsin Press, Madison; 489–497.
- Sheraton J.W. 1983. Geochemistry of mafic igneous rocks of the northern Prince Charles Mountains, Antarctica. *Journal of the Geological Society of Australia*; 30: 295–304.
- Sheraton J.W. 1984. Chemical changes associated with high-grade metamorphism of mafic rocks in the East Antarctic Shield. *Chemical Geology*; 47: 135–157.
- Sheraton J.W. & Black L.P. 1981. Geochemistry and geochronology of Proterozoic tholeiite dykes of East Antarctica: Evidence for mantle metasomatism. *Contributions to Mineralogy and Petrology*; 78: 305–317.
- Sheraton J.W. & Black L.P. 1983. Geochemistry of Precambrian gneisses: Relevance for the evolution of the East Antarctic Shield. *Lithos*; 16: 273–296.
- Sheraton J.W. & Black L.P. 1988. Chemical evolution of granitic rocks in the East Antarctic Shield, with particular reference to post-orogenic granites. *Lithos*; 21: 37–52.
- Sheraton J.W. & Collerson K.D. 1983. Archaean and Proterozoic geological relationships in the Vestfold Hills–Prydz Bay area, Antarctica. *BMR Journal of Australian Geology and Geophysics*; 8: 119–128.
- Sheraton J.W. & Collerson K.D. 1984. Geochemical evolution of Archaean granulite-facies gneisses in the Vestfold Block and comparisons with other Archaean gneiss complexes in the East Antarctic Shield. *Contributions to Mineralogy and Petrology*; 87: 51–64.
- Sheraton J.W. & Cundari A. 1980. Leucites from Gaussberg, Antarctica. *Contributions to Mineralogy and Petrology*; 71: 417–427.
- Sheraton J.W. & England R.N. 1980. Highly potassic mafic dykes from Antarctica. *Journal of the Geological Society of Australia*; 27: 129–135.
- Sheraton J.W., Offe L.A., Tingey R.J. & Ellis D.J. 1980. Enderby Land, Antarctica—an unusual Precambrian high-grade

- metamorphic terrain. *Journal of the Geological Society of Australia*; 27: 1–18.
- Sheraton J.W., Black L.P. & McCulloch M.T. 1984. Regional geochemical and isotopic characteristics of high-grade metamorphics of the Prydz Bay area: The extent of Proterozoic reworking of Archaean continental crust in East Antarctica. *Precambrian Research*; 26: 169–198.
- Sheraton J.W., Ellis D.J. & Kuehner S.M. 1985. Rare-earth element geochemistry of Archaean gneisses and evolution of the East Antarctic Shield. *BMR Journal of Australian Geology and Geophysics*; 9: 207–218.
- Sheraton J.W., Thomson J.W. & Collerson K.D. 1987a. Mafic dyke swarms of Antarctica. In: Halls H.C. & Fahrig W.F. (editors). *Mafic dyke swarms*. Geological Association of Canada; special paper 34: 419–432.
- Sheraton J.W., Tingey R.J., Black L.P., Offe L.A. & Ellis D.J. 1987b. Geology of an unusual Precambrian high-grade metamorphic terrane—Enderby and western Kemp Land, Antarctica. Bureau of Mineral Resources, Australia; bulletin 223.
- Sheraton J.W., Black L.P., McCulloch M.T. & Oliver R.L. 1990. Age and origin of a compositionally varied mafic dyke swarm in the Bunge Hills, East Antarctica. *Chemical Geology*; 85: 215–246.
- Sheraton J.W., Black L.P. & Tindle A.G. 1992. Petrogenesis of plutonic rocks in a Proterozoic granulite-facies terrane—the Bunge Hills, East Antarctica. *Chemical Geology*; 97: 163–198.
- Sheraton J.W., Tingey R.J., Oliver R.L. & Black L.P. 1995. Geology of the Bunge Hills—Denman Glacier region, East Antarctica. Australian Geological Survey Organisation; bulletin 244.
- Sheraton J.W., Tindle A.G. & Tingey R.J. 1996. Geochemistry, origin and tectonic setting of granitic rocks of the Prince Charles Mountains, Antarctica. *AGSO Journal of Australian Geology and Geophysics*; 16: 345–370.
- Shibata K., Yanai K. & Shiraishi K. 1986. Rb–Sr whole-rock ages of metamorphic rocks from eastern Queen Maud Land, East Antarctica. *Memoirs of the National Institute of Polar Research*; special issue 43: 133–148.
- Shiraishi K. & Kagami H. 1992. Sm–Nd and Rb–Sr ages of metamorphic rocks from the Sør Rondane Mountains, East Antarctica. In: Yoshida Y. (editor). *Recent progress in Antarctic earth science*. Terra Scientific Publishing Company, Tokyo; 29–35.
- Shiraishi K., Hiroi Y., Motoyoshi Y. & Yanai K. 1987. Plate tectonic development of late Proterozoic paired metamorphic complexes in eastern Queen Maud Land, East Antarctica. In: McKenzie G.W. (editor). *Gondwana six: Structure, tectonics and geophysics*. American Geophysical Union Monograph 40; 309–318.
- Shiraishi K., Hiroi Y., Ellis D.J., Fanning C.M., Motoyoshi Y. & Nakai Y. 1992. The first report of a Cambrian orogenic belt in East Antarctica—an ion microprobe study of the Lützow-Holm Complex. In: Yoshida Y. (editor). *Recent progress in Antarctic earth science*. Terra Scientific Publishing Company, Tokyo; 67–73.
- Shiraishi K., Ellis D.J., Hiroi Y., Fanning C.M., Motoyoshi Y. & Nakai Y. 1994. Cambrian orogenic belt in East Antarctica and Sri Lanka: Implications for Gondwana assembly. *Journal of Geology*; 102: 47–65.
- Shiraishi K., Ellis D.J., Fanning C.M., Hiroi Y., Kagami H. & Motoyoshi Y. 1997. Re-examination of the metamorphic and protolith ages of the Rayner Complex, Antarctica: Evidence for the Cambrian (Pan-African) regional metamorphic event. In: Ricci C.A. (editor). *The Antarctic region: Geological evolution and processes*. Terra Antarctica Publication, Siena; 79–88.
- Shiraki K. 1975. Chromium: Abundance in common sediments and sedimentary rock types. In: Wedepohl K.H. (editor). *Handbook of geochemistry*. Springer-Verlag, Berlin; II-3, 24-K1–7.
- Shulyatin O.G. 1995. The quartz vein system of the Else Platform (East Antarctica). VII International Symposium on Antarctic Earth Sciences, Siena, 10–15 September; abstract volume: 349.
- Silver L.T. & Chappell B.W. 1988. The Peninsular Ranges Batholith: An insight into the evolution of the Cordilleran batholiths of southwestern North America. *Transactions of the Royal Society of Edinburgh: earth sciences*; 79: 105–121.
- Sims J.P., Dirks P.H.G.M., Carson C.J. & Wilson C.J.L. 1994. The structural evolution of the Rauer Group, East Antarctica: Mafic dykes as passive markers in a composite Proterozoic terrain. *Antarctic Science*; 6: 379–394.
- Snape I. & Harley S.L. 1996. Magmatic history and the high-grade geological evolution of the Vestfold Hills, East Antarctica. *Terra Antarctica*; 3: 23–38.
- Snape I., Black L.P. & Harley S.L. 1997. Refinement of the timing of magmatism, high-grade metamorphism and deformation in the Vestfold Hills, East Antarctica, from new SHRIMP U–Pb zircon geochronology. In: Ricci C.A. (editor). *The Antarctic region: Geological evolution and processes*. Terra Antarctica Publications, Siena; 139–148.
- Soler P. & Bonhomme M.G. 1990. Relation of magmatic activity to plate dynamics in central Peru from Late Cretaceous to present. In: Kay S.M. & Rapela C.W. (editors). *Plutonism from Antarctica to Alaska*. Geological Society of America; special paper 241: 173–191.
- Soler P. & Rotach-Toulhoat N. 1990. Implications of the time-dependent evolution of Pb- and Sr-isotopic compositions of Cretaceous and Cenozoic granitoids from the coastal region on the lower Pacific slope of the Andes of central Peru. In: Kay S.M. & Rapela C.W. (editors). *Plutonism from Antarctica to Alaska*. Geological Society of America; special paper 241: 161–172.
- Soloviev D.S. 1971. Geological structure of the mountain fringe of the Lambert and Amery Glaciers (in Russian). The Antarctic. Soviet Committee on Antarctic Research; report 10: 89–101.
- Soloviev D.S. 1972. Geological structure of the mountain fringe of the Lambert Glacier and the Amery Ice Shelf. In: Adie R.J. (editor). *Antarctic geology and geophysics*. Universitetsforlaget, Oslo; 573–577.
- Stephenson N.C.N. & Cook N.D.J. 1992. High K/Na alkaline mafic dykes near Radok Lake, northern Prince Charles Mountains, East Antarctica. *Lithos*; 29: 87–105.
- Stern R.A. & Hanson G.N. 1991. Archean high-Mg granodiorite: A derivative of light rare earth element-enriched monzodiorite of mantle origin. *Journal of Petrology*; 32: 201–238.
- Stinear B.H. 1956. Preliminary report on operations from Mawson base, Australian National Antarctic Research Expedition 1954–55. Bureau of Mineral Resources, Australia; record 1956/44.
- Storey B.C., Pankhurst R.J. & Johnson A.C. 1994. The Grenville Province within Antarctica: A test of the SWEAT hypothesis. *Journal of the Geological Society, London*; 151: 1–4.
- Stüwe K. & Hand M. 1992. Geology and structure of Depot Peak, MacRobertson Land: More evidence for the continuous extent of the 1000 Ma event of East Antarctica. *Australian Journal of Earth Sciences*; 39: 211–222.
- Stüwe K. & Powell R. 1989. Low-pressure granulite facies metamorphism in the Larsemann Hills area, East Antarctica: Petrology and tectonic implications for the evolution of the Prydz Bay area. *Journal of Metamorphic Geology*; 7: 465–483.
- Stüwe K. & Sandiford M. 1993. A preliminary model for the 500 Ma event in the East Antarctic Shield. In: Findlay R.H., Unrug R., Banks M.R. & Veivers J.J. (editors). *Gondwana eight: Assembly, evolution and dispersal*. Balkema, Rotterdam; 125–130.

GEOLOGY OF THE PRINCE CHARLES MOUNTAINS, ANTARCTICA



Localities mentioned in AGSO Bulletin 247 but not shown on map

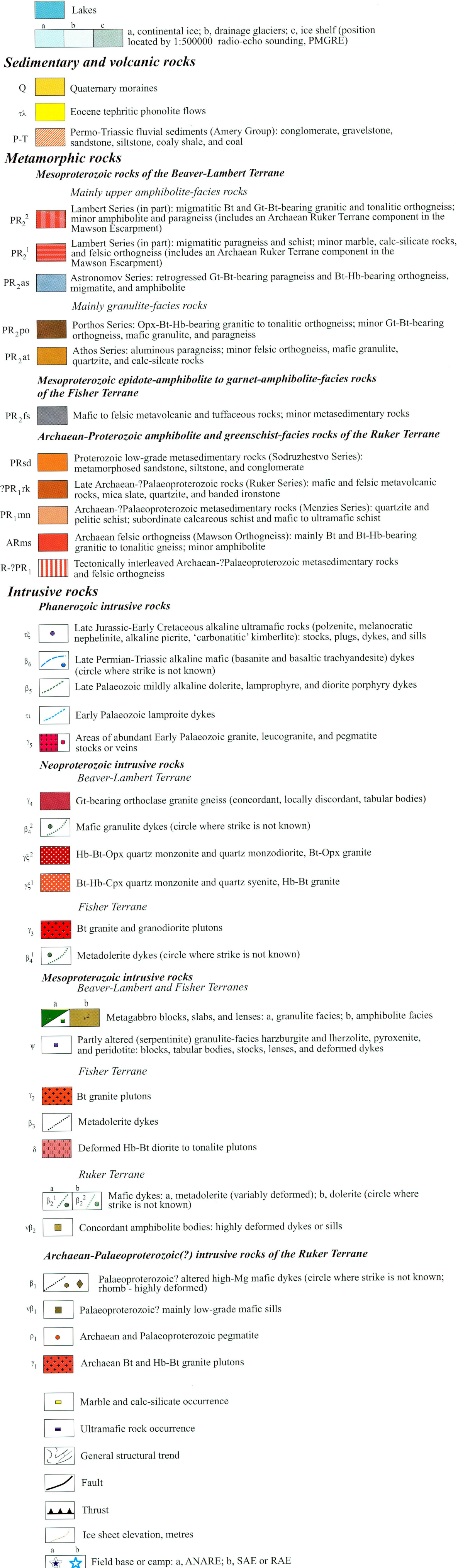
Locality	Lat (S)	Long (E)
Amery Peaks	70°38'	67°23'
Ammonit Nunatak	71°10'	65°50'
Carter Peak	70°20'	64°13'
Corn Massif	70°26'	64°38'
Doppel Peak	69°03'	64°36'
Fox Ridge	70°47'	67°52'
Hunt Nunataks	70°11'	64°52'
Manning Massif	70°43'	67°45'
McKaskle Hills	70°01'	72°58'
McLeod Massif	70°46'	68°00'
Moore Pyramid	70°18'	65°50'
Mount Beck	71°03'	67°03'
Mount Bewsher	70°54'	65°26'
Mount Bunt	70°47'	66°21'
Mount Butterworth	70°42'	66°44'
Mount Creighton	70°25'	65°38'
Mount Gasson	70°28'	65°47'
Mount Gavaghan	70°26'	65°29'
Mount Gleason	71°14'	66°06'
Mount Kirkby	70°26'	65°12'
Mount McCarthy	70°24'	66°33'
Mount Tarr	70°25'	65°45'
Mount Thomas	71°02'	64°39'
Mount Trotter	70°43'	66°26'
Mount Wishart	70°19'	65°13'
New Year Nunatak	71°04'	71°30'
Pickering Nunatak	71°25'	71°00'
Reinbolt Hills	70°30'	72°30'
Silence Nunataks	69°40'	64°50'
Taylor Platform	71°00'	67°10'
Thomas Nunataks	70°32'	65°11'
Thorn Massif	70°35'	66°52'
Trost Rocks	69°46'	68°59'
Webster Peaks	70°28'	65°25'

Compiled by Mikhalsky, E.V., Laiba, A.A., & Sheraton, J.W.
Mostly from unpublished data of the authors, and the following references.

Ravich, M.G., Soloviev, D.S. & Fedorov, L.V., 1978. Geologicheskoe sroenie zemli Mak-Robertdona (Vostochnaya Antarktika).Gidrometeoizdat, Leningrad (now St Petersburg).
Tingey, R.J., 1982b. Geological map of the Southern Prince Charles Mountains, Antarctica, 1:500 000. Bureau of Mineral Resources, Canberra, Australia.
Thost, D.E., Leitchenkov, G.L., O'Brien, P.E., Tingey, R.J., Wellman, P. & Golynsky, A.V., 1998. Geology of the Lambert Glacier-Prydz Bay region, East Antarctica, 1:1 000 000 map. Australian Geological Survey Organisation, Canberra, Australia

Topographic base Antarctic Digital Database (Version 1.0) 1:1 000 000 Sheets SS43-45, SR41-42

To accompany AGSO Bulletin 247: *Geology of the Prince Charles Mountains, Antarctica*, Canberra 2001



GEOLOGY OF THE PRINCE CHARLES MOUNTAINS, ANTARCTICA
May 2001

- Turner B.R. 1993. Palaeosols in Permo–Triassic continental sediments from Prydz Bay, East Antarctica. *Journal of Sedimentary Petrology*; 63: 694–706.
- Turner S.P., Foden J.D. & Morrison R.S. 1992. Derivation of some A-type magmas by fractionation of basaltic magma: An example from the Padthaway Ridge, South Australia. *Lithos*: 28: 151–179.
- Tuttle O.F. & Bowen N.L. 1958. Origin of granite in the light of experimental studies in the system $\text{NaAlSi}_3\text{O}_8 - \text{KAlSi}_3\text{O}_8 - \text{SiO}_2 - \text{H}_2\text{O}$. Geological Society of America; memoir 74.
- Unrug R. 1996. The assembly of Gondwanaland. *Episodes*; 19: 11–20.
- Veevers J.J. 1993. Gondwana facies of the Pangean supersequence: A review. In: Findley R.H., Unrug R., Banks M.R. & Veevers J.J. (editors). *Gondwana eight: Assembly, evolution and dispersal*. Balkema, Rotterdam; 513–520.
- Veevers J.J. & Eittreim S.L. 1988. Reconstruction of Antarctica and Australia at breakup (95 ± 5 Ma) and before rifting (160 Ma). *Australian Journal of Earth Sciences*; 35: 355–362.
- Veevers J.J., Powell C.M. & Roots S.R. 1991. Review of seafloor spreading around Australia. I: Synthesis of the patterns of spreading. *Australian Journal of Earth Sciences*; 38: 373–389.
- Walker K.R. & Mond A. 1971. Mica lamprophyre (alnöite) from Radok Lake, Prince Charles Mountains, Antarctica. Bureau of Mineral Resources, Australia; record 1971/108.
- Watson E.B. & Harrison T.M. 1983. Zircon saturation revisited: Temperature and composition effects in a variety of crustal magma types. *Earth and Planetary Science Letters*; 64: 295–304.
- Weaver B.L. & Tarney J. 1980. Rare earth geochemistry of Lewisian granulite-facies gneisses, northwest Scotland: Implications for the petrogenesis of the Archaean lower continental crust. *Earth and Planetary Science Letters*; 51: 279–296.
- Weaver L., McLoughlin S. & Drinnan A.N. 1997. Fossil woods from the Upper Permian Bainmedart Coal Measures, northern Prince Charles Mountains, East Antarctica. *AGSO Journal of Australian Geology and Geophysics*; 16: 655–676.
- Webb J.A. & Fielding C.R. 1993. Permo–Triassic sedimentation within the Lambert Graben, northern Prince Charles Mountains, East Antarctica. In: Findley R.H., Unrug R., Banks M.R. & Veevers, J.J. (editors). *Gondwana eight: Assembly, evolution and dispersal*. Balkema, Rotterdam; 357–369.
- Weber K. & Arndt N.T. 1991. Proterozoic link between Africa and Antarctica (abstract). Eighth International Symposium on Gondwana, Hobart, Tasmania; 90–91.
- Wellman P. & Tingey R.J. 1976. Gravity evidence for a major crustal fracture in eastern Antarctica. *BMR Journal of Australian Geology and Geophysics*; 1: 105–108.
- Wellman P. & Tingey R.J. 1981. Glaciation, erosion and uplift over part of East Antarctica. *Nature*; 291: 142–144.
- Wells P.R.A. 1977. Pyroxene thermometry in simple and complex system. *Contributions to Mineralogy and Petrology*; 62: 129–139.
- Wells P.R.A. 1979. Chemical and thermal evolution of Archaean sialic crust, southern West Greenland. *Journal of Petrology*; 20: 187–226.
- Whalen J.B., Currie K.L. & Chappell B.W. 1987. A-type granites: Geochemical characteristics, discrimination and petrogenesis. *Contributions to Mineralogy and Petrology*; 95: 407–419.
- White M.E. 1969. Permian flora from the Beaver Lake area, Prince Charles Mountains, Antarctica. 2: Plant fossils. In: Palaeontological papers. Bureau of Mineral Resources, Australia; bulletin 126: 13–18.
- White R.W. & Clarke G.L. 1993. Timing of Proterozoic deformation and magmatism in a tectonically reworked orogen, Rayner Complex, Colbeck Archipelago, East Antarctica. *Precambrian Research*; 63: 1–26.
- White R.W. & Clarke G.L. 1994. Garnet-forming reactions and recrystallisation in high-grade mylonite zones, MacRobertson Land, East Antarctica. *Journal of Metamorphic Geology*; 12: 853–865.
- White R.W., Clarke G.L. & Nelson D.R. 1999. SHRIMP U–Pb zircon dating of Grenville-age events in the western part of the Musgrave Block, central Australia. *Journal of Metamorphic Geology*; 17: 465–481.
- Whitehead J. & McKelvey B. 1999. Stratigraphy of the Plio–Pleistocene Bardin Bluffs Formation, Amery Oasis, northern Prince Charles Mountains, Antarctica. VIII International Symposium on Antarctic Earth Sciences, Wellington, 5–9 July; abstract volume: 317.
- Williams I.S., Compston W., Collerson K.D., Arriens P.A. & Lovering J.F. 1983. A reassessment of the age of the Windmill Metamorphics, Casey area. In: Oliver R.L., James P.R. & Jago J.B. (editors). *Antarctic earth science*. Australian Academy of Science, Canberra; 73–76.
- Wilson M. 1989. *Igneous petrogenesis*. Chapman and Hall, London.
- Windley B.F. 1998. Tectonic development of early Precambrian orogens. In: Motoyoshi Y. & Shiraishi K. (editors). *Origin and evolution of continents*. Memoirs of the National Institute of Polar Research; special issue 53: 8–28.
- Winkler H.J.F. 1974. *Petrogenesis of metamorphic rocks*. Springer-Verlag, Berlin.
- Yanagi T. & Yamashita K. 1994. Genesis of continental crust under island arc conditions. *Lithos*; 33: 209–223.
- Yoshida M. 1994. Tectonothermal history and tectonics of Lützow-Holm Bay area, East Antarctica: A re-interpretation. *Journal of the Geological Society of Sri Lanka*; 5: 81–93.
- Yoshida M., Suzuki M., Shirahata H., Jokima H. & Kizaki K. 1983. A review of the tectonic and metamorphic history of the Lützow-Holm Bay region, East Antarctica. In: Oliver R.L., James P.R. & Jago J.B. (editors). *Antarctic earth science*. Australian Academy of Science, Canberra; 44–47.
- Young D.N. & Black L.P. 1991. U–Pb zircon dating of Proterozoic igneous charnockites from the Mawson coast, East Antarctica. *Antarctic Science*; 3: 205–216.
- Young D.N. & Ellis D.J. 1991. The intrusive Mawson Charnockites: Evidence for a compressional plate margin setting of the Proterozoic mobile belt of East Antarctica. In: Thomson M.R.A., Crame J.A. & Thomson J.W. (editors). *The geological evolution of Antarctica*. Cambridge University Press; 25–31.
- Young D.N., Zhao J-X., Ellis D.J. & McCulloch M.T. 1997. Geochemical and Sr–Nd isotopic mapping of source provinces for the Mawson charnockites, East Antarctica: Implications for Proterozoic tectonics and Gondwana reconstruction. *Precambrian Research*; 86: 1–19.
- Zhao J-X. & Ellis D.J. 1994. Origin of igneous charnockites. *Geological Society of Australia*; abstracts 37: 486–487.
- Zhao Y., Song B., Wang Y., Ren L., Li J. & Chen T. 1992. Geochronology of the late granite in the Larsemann Hills, East Antarctica. In: Yoshida Y. (editor). *Recent progress in Antarctic earth science*. Terra Scientific Publishing Company, Tokyo; 155–161.
- Zhao J-X., Shiraishi K., Ellis D.J. & Sheraton J.W. 1995a. Geochemical and isotopic studies of syenites from the Yamato Mountains, East Antarctica: Implications for the origin of syenitic magmas. *Geochimica et Cosmochimica Acta*; 59: 1363–1382.

Zhao Y., Liu X., Song B., Zhang Z., Li J., Yao Y. & Wang Y. 1995b. Constraints on the stratigraphic age of metasedimentary rocks from the Larsemann Hills, East Antarctica: Possible implications for Neoproterozoic tectonics. *Precambrian Research*; 75: 175–188.

Zhao J-X., Ellis D.J., Kilpatrick J.A. & McCulloch M.T. 1997. Geochemical and Sr–Nd isotopic study of charnockites and related rocks in the northern Prince Charles Mountains, East

Antarctica: Implications for charnockite petrogenesis and Proterozoic crustal evolution. *Precambrian Research*; 81: 37–66.

Zhou B. & Hensen B.J. 1995. Inherited Sm/Nd isotope components preserved in monazite inclusions within garnets in leucogneiss from East Antarctica and implications for closure temperature studies. *Chemical Geology (isotope geoscience section)*; 121: 317–326.

NOTES



Geological Map of the Khatanga Area

Geological Units and Ages:

- 925 ± 35:** Gt leucogneiss, Rb-Sr, Tingey 1991a
- 630-555:** Gt leucogneiss, Sm-Nd Gt, Hensen et al. 1998
- 990 ± 30:** Gt leucogneiss, U-Pb IM, Kinny et al. 1997
- c. 1850:** Gt leucogranite, U-Pb IM, Kinny et al. 1997
- 480 ± 13:** granite, U-Pb, Manton et al. 1992
- 507-495:** pegmatite, U-Pb, Manton et al. 1992
- 940 ± 20:** leucogranite gneiss, U-Pb, Manton et al. 1992
- 904 ± 175:** felsic gneiss, Rb-Sr, Tingey 1991a
- 825-789:** felsic gneiss, Sm-Nd Gt, Hensen et al. 1998
- 769 ± 36:** felsic gneiss, Rb-Sr, Tingey 1991a
- 517 ± 12:** pegmatite, U-Pb IM, Carson et al. 2000
- 910 ± 18:** pegmatite syn-tectonic, U-Pb IM, Carson et al. 2000
- 991 ± 22:** pegmatite, U-Pb IM, Carson et al. 2000
- 1033 ± 85:** felsic gneiss, Rb-Sr, Tingey 1991a
- 974 ± 68:** felsic gneiss, Rb-Sr, Tingey 1991a
- 50 ± 2:** tephritic phonolite, K-Ar, Sheraton 1983
- 1165 ± 13:** prehnite-epidote lens in serpentinite, U-Pb, Mon, Belitsky & Laiba unpubl.
- 246 ± 6:** basaltic andesite dyke, K-Ar, Sheraton 1983
- 1017 ± 31:** Hb orthogneiss, U-Pb IM, Boger et al. 2000
- 984 ± 7:** granite, U-Pb IM, Kinny et al. 1997
- 984 ± 12:** quartz syenite, U-Pb IM, Kinny et al. 1997
- 636 ± 13:** mafic schist, Rb-Sr, WR-mn, reset age, Mikhalsky et al. 1999
- 1120, 1000, 810:** metamorphic rocks, gabbro, Sm-Nd, U-Pb, Mikhalsky et al. 1999; Laiba & Mikhalsky 1999
- c. 1190:** tonalite, granite, U-Pb, Mikhalsky et al. 1999; Laiba unpubl.
- c. 1290:** tonalite orthogneiss, gabbro, Sm-Nd, U-Pb, Mikhailov et al. 1991; Mikhalsky et al. 1999
- 872 ± 69:** felsic gneiss, Rb-Sr, Tingey 1991a
- 870 ± 150:** granodiorite, Rb-Sr, Krasnikov & Fedorov 1992
- 1300-1280:** metavolcanics, granodiorite, U-Pb, U-Pb IM, Belitsky et al. 1994; Kinny et al. 1997
- 1020-48:** granite, U-Pb IM, Kinny et al. 1997
- 990 ± 18:** U-Pb IM, Boger et al. 2000
- 942 ± 17:** Opx leucosome, U-Pb IM, Boger et al. 2000
- 120-110:** polzenite, K-Ar, Laiba et al. 1987
- 150 ± 5:** alkali picrite, K-Ar, Laiba et al. 1987
- 123 ± 5:** melange, K-Ar, Laiba et al. 1987
- 321 ± 10:** mafic dykes, K-Ar, Hofmann 1991
- c. 240:** diorite porphyry, K-Ar, Hofmann 1991
- 142 ± 5:** K-Ar groundmass, K-Ar, Laiba et al. 1987
- 113 ± 5:** polzenite, K-Ar, Laiba et al. 1987
- 123 ± 5:** melange, K-Ar, Laiba et al. 1987
- 150 ± 5:** alkali picrite, K-Ar, Laiba et al. 1987
- 990 ± 18:** U-Pb IM, Boger et al. 2000
- 942 ± 17:** Opx leucosome, U-Pb IM, Boger et al. 2000
- 120-110:** polzenite, K-Ar, Laiba et al. 1987
- 1020-48:** granite, U-Pb IM, Kinny et al. 1997
- 990 ± 18:** U-Pb IM, Boger et al. 2000
- 942 ± 17:** Opx leucosome, U-Pb IM, Boger et al. 2000
- 120-110:** polzenite, K-Ar, Laiba et al. 1987
- 150 ± 5:** alkali picrite, K-Ar, Laiba et al. 1987
- 123 ± 5:** melange, K-Ar, Laiba et al. 1987
- 321 ± 10:** mafic dykes, K-Ar, Hofmann 1991
- c. 240:** diorite porphyry, K-Ar, Hofmann 1991
- 142 ± 5:** K-Ar groundmass, K-Ar, Laiba et al. 1987
- 113 ± 5:** polzenite, K-Ar, Laiba et al. 1987
- 123 ± 5:** melange, K-Ar, Laiba et al. 1987
- 150 ± 5:** alkali picrite, K-Ar, Laiba et al. 1987
- 990 ± 18:** U-Pb IM, Boger et al. 2000
- 942 ± 17:** Opx leucosome, U-Pb IM, Boger et al. 2000
- 120-110:** polzenite, K-Ar, Laiba et al. 1987
- 1020-48:** granite, U-Pb IM, Kinny et al. 1997
- 990 ± 18:** U-Pb IM, Boger et al. 2000
- 942 ± 17:** Opx leucosome, U-Pb IM, Boger et al. 2000
- 120-110:** polzenite, K-Ar, Laiba et al. 1987
- 150 ± 5:** alkali picrite, K-Ar, Laiba et al. 1987
- 123 ± 5:** melange, K-Ar, Laiba et al. 1987
- 321 ± 10:** mafic dykes, K-Ar, Hofmann 1991
- c. 240:** diorite porphyry, K-Ar, Hofmann 1991
- 142 ± 5:** K-Ar groundmass, K-Ar, Laiba et al. 1987
- 113 ± 5:** polzenite, K-Ar, Laiba et al. 1987
- 123 ± 5:** melange, K-Ar, Laiba et al. 1987
- 150 ± 5:** alkali picrite, K-Ar, Laiba et al. 1987
- 990 ± 18:** U-Pb IM, Boger et al. 2000
- 942 ± 17:** Opx leucosome, U-Pb IM, Boger et al. 2000
- 120-110:** polzenite, K-Ar, Laiba et al. 1987
- 1020-48:** granite, U-Pb IM, Kinny et al. 1997
- 990 ± 18:** U-Pb IM, Boger et al. 2000
- 942 ± 17:** Opx leucosome, U-Pb IM, Boger et al. 2000
- 120-110:** polzenite, K-Ar, Laiba et al. 1987
- 150 ± 5:** alkali picrite, K-Ar, Laiba et al. 1987
- 123 ± 5:** melange, K-Ar, Laiba et al. 1987
- 321 ± 10:** mafic dykes, K-Ar, Hofmann 1991
- c. 240:** diorite porphyry, K-Ar, Hofmann 1991
- 142 ± 5:** K-Ar groundmass, K-Ar, Laiba et al. 1987
- 113 ± 5:** polzenite, K-Ar, Laiba et al. 1987
- 123 ± 5:** melange, K-Ar, Laiba et al. 1987
- 150 ± 5:** alkali picrite, K-Ar, Laiba et al. 1987
- 990 ± 18:** U-Pb IM, Boger et al. 2000
- 942 ± 17:** Opx leucosome, U-Pb IM, Boger et al. 2000
- 120-110:** polzenite, K-Ar, Laiba et al. 1987
- 1020-48:** granite, U-Pb IM, Kinny et al. 1997
- 990 ± 18:** U-Pb IM, Boger et al. 2000
- 942 ± 17:** Opx leucosome, U-Pb IM, Boger et al. 2000
- 120-110:** polzenite, K-Ar, Laiba et al. 1987
- 150 ± 5:** alkali picrite, K-Ar, Laiba et al. 1987
- 123 ± 5:** melange, K-Ar, Laiba et al. 1987
- 321 ± 10:** mafic dykes, K-Ar, Hofmann 1991
- c. 240:** diorite porphyry, K-Ar, Hofmann 1991
- 142 ± 5:** K-Ar groundmass, K-Ar, Laiba et al. 1987
- 113 ± 5:** polzenite, K-Ar, Laiba et al. 1987
- 123 ± 5:** melange, K-Ar, Laiba et al. 1987
- 150 ± 5:** alkali picrite, K-Ar, Laiba et al. 1987
- 990 ± 18:** U-Pb IM, Boger et al. 2000
- 942 ± 17:**

Locality	Lat (S)	Long (E)
Ampy Peaks	70°38'	67°13'
Carbery Peaks	70°38'	67°23'
Cornwall Nunatak	70°39'	67°23'
Carter Peaks	70°20'	64°23'
Cory Massif	70°26'	64°38'
Depol Peak	70°26'	64°38'
Fox Nunatak	70°47'	67°52'
Hunt Nunataks	70°11'	64°52'
Manning Massif	70°43'	67°45'
McClintock Nunatak	70°43'	67°58'
McLeod Massif	70°46'	68°00'
Moore Pyramid	70°18'	65°08'
North Nunatak	70°13'	65°03'
Mount Bewsher	70°54'	65°25'
Mount Bunt	70°47'	66°21'
Mount Bentworth	70°42'	66°44'
Mount Buntin	70°42'	66°44'
Mount Gaston	70°26'	65°47'
Mount Gaghavan	70°26'	65°29'
Mount Gough	70°26'	65°29'
Mount Kirkby	70°26'	65°12'
Mount McCarthy	70°24'	64°38'
Mount Tarr	70°22'	64°38'
Mount Tarr	70°22'	64°39'
Mount Trott	70°19'	65°13'
Mount Wishart	70°43'	66°23'
North Nunatak	71°03'	70°10'
Pickering Nunatak	71°25'	71°10'
Reinbolt Hills	70°30'	72°30'
Shear Nunataks	70°30'	72°30'
Sign Nunatak	71°00'	70°10'
Thomas Nunataks	71°30'	67°10'
Thomson Massif	70°35'	66°52'
Ward Nunatak	69°59'	67°10'
Webster Peaks	70°28'	65°25'



Ravich, M.G., Soloviev, D.S. & Fedorov, L.V., 1978. Geologicheskoe sroenie zemli Mak-Robertdona (Vostochnaya Antarktida).Gidrometeoizdat, Leningrad (now St Petersburg).

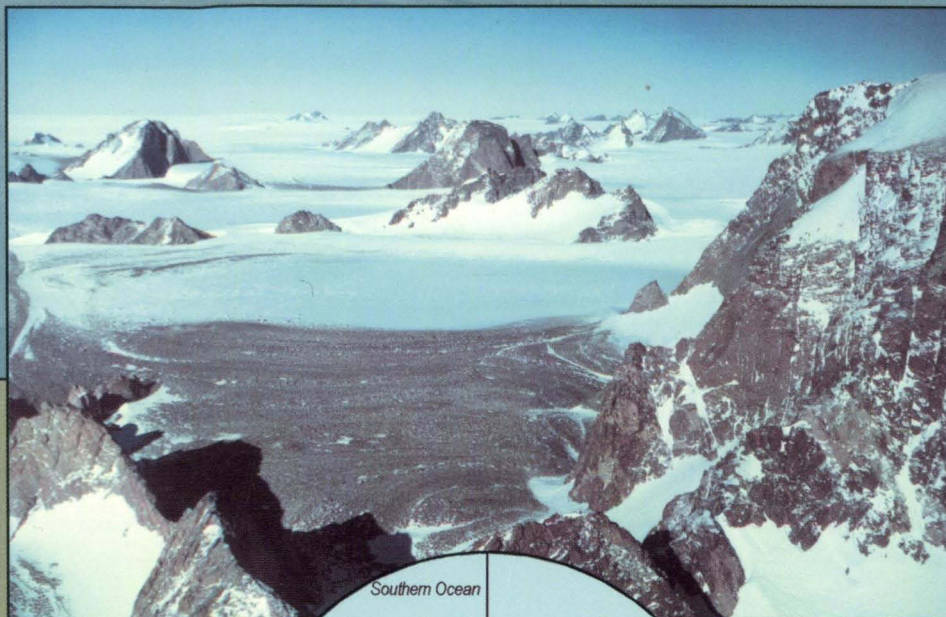
Tingey, R.J., 1982b. Geological map of the Southern Prince Charles Mountains, Antarctica, 1:500 000. Bureau of Mineral Resources, Canberra, Australia.

Thost, D.E., Leitchnikov, G.L., O'Brien, P.E., Tingey, R.J., Wellman, P. & Golynsky, A.V., 1998. Geology of the Lambert Glacier-Prydz Bay region, East Antarctica, 1:1 000 000 map. Australian Geological Survey Organisation, Canberra, Australia

To accompany AGSO Bulletin 247: *Geology of the Prince Charles Mountains, Antarctica*, Canberra 2001



**GEOLOGY OF THE PRINCE CHARLES MOUNTAINS,
ANTARCTICA**
May 2001



The Prince Charles Mountains of MacRobertson Land constitute a 600-kilometre cross section through the metamorphic rocks of the Precambrian East Antarctic Shield, and comprise three distinct geological terranes of Archaean to Neoproterozoic age. Also present are Palaeozoic granites and mafic dykes (including lamproites), Permo-Triassic sediments with coal measures, and Mesozoic and Cainozoic mafic and alkaline ultramafic igneous rocks.

The Precambrian rocks and their Phanerozoic structures are related to the assembly and breakup of the ancient continents of Rodinia and Gondwana. Equivalent continental terranes are found in Western Australia, India and Madagascar.

This Bulletin is a consolidation of the results of investigations by Australian and Soviet/Russian geologists and geophysicists in the Prince Charles Mountains over the last 40 years. It is a significant addition to Antarctic geoscience literature, and substantially increases understanding of the geological evolution of the Prince Charles Mountains.



VNII Okeangeologia



AUSTRALIAN
ANTARCTIC DIVISION

